

# LENS DESIGN

FOURTH EDITION

# OPTICAL SCIENCE AND ENGINEERING

*Founding Editor*

**Brian J. Thompson**

*University of Rochester*

*Rochester, New York*

1. Electron and Ion Microscopy and Microanalysis: Principles and Applications, *Lawrence E. Murr*
2. Acousto-Optic Signal Processing: Theory and Implementation, *edited by Norman J. Berg and John N. Lee*
3. Electro-Optic and Acousto-Optic Scanning and Deflection, *Milton Gottlieb, Clive L. M. Ireland, and John Martin Ley*
4. Single-Mode Fiber Optics: Principles and Applications, *Luc B. Jeunhomme*
5. Pulse Code Formats for Fiber Optical Data Communication: Basic Principles and Applications, *David J. Morris*
6. Optical Materials: An Introduction to Selection and Application, *Solomon Musikant*
7. Infrared Methods for Gaseous Measurements: Theory and Practice, *edited by Joda Wormhoudt*
8. Laser Beam Scanning: Opto-Mechanical Devices, Systems, and Data Storage Optics, *edited by Gerald F. Marshall*
9. Opto-Mechanical Systems Design, *Paul R. Yoder, Jr.*
10. Optical Fiber Splices and Connectors: Theory and Methods, *Calvin M. Miller with Stephen C. Mettler and Ian A. White*
11. Laser Spectroscopy and Its Applications, *edited by Leon J. Radziemski, Richard W. Solarz, and Jeffrey A. Paisner*
12. Infrared Optoelectronics: Devices and Applications, *William Nunley and J. Scott Bechtel*
13. Integrated Optical Circuits and Components: Design and Applications, *edited by Lynn D. Hutcheson*
14. Handbook of Molecular Lasers, *edited by Peter K. Cheo*
15. Handbook of Optical Fibers and Cables, *Hiroshi Murata*
16. Acousto-Optics, *Adrian Korpel*
17. Procedures in Applied Optics, *John Strong*
18. Handbook of Solid-State Lasers, *edited by Peter K. Cheo*
19. Optical Computing: Digital and Symbolic, *edited by Raymond Arrathoon*
20. Laser Applications in Physical Chemistry, *edited by D. K. Evans*

21. Laser-Induced Plasmas and Applications, *edited by Leon J. Radziemski and David A. Cremers*
22. Infrared Technology Fundamentals, *Irving J. Spiro and Monroe Schlessinger*
23. Single-Mode Fiber Optics: Principles and Applications, Second Edition, Revised and Expanded, *Luc B. Jeunhomme*
24. Image Analysis Applications, *edited by Rangachar Kasturi and Mohan M. Trivedi*
25. Photoconductivity: Art, Science, and Technology, *N. V. Joshi*
26. Principles of Optical Circuit Engineering, *Mark A. Mentzer*
27. Lens Design, *Milton Laikin*
28. Optical Components, Systems, and Measurement Techniques, *Rajpal S. Sirohi and M. P. Kothiyal*
29. Electron and Ion Microscopy and Microanalysis: Principles and Applications, Second Edition, Revised and Expanded, *Lawrence E. Murr*
30. Handbook of Infrared Optical Materials, *edited by Paul Klocek*
31. Optical Scanning, *edited by Gerald F. Marshall*
32. Polymers for Lightwave and Integrated Optics: Technology and Applications, *edited by Lawrence A. Hornak*
33. Electro-Optical Displays, *edited by Mohammad A. Karim*
34. Mathematical Morphology in Image Processing, *edited by Edward R. Dougherty*
35. Opto-Mechanical Systems Design: Second Edition, Revised and Expanded, *Paul R. Yoder, Jr.*
36. Polarized Light: Fundamentals and Applications, *Edward Collett*
37. Rare Earth Doped Fiber Lasers and Amplifiers, *edited by Michel J. F. Digonnet*
38. Speckle Metrology, *edited by Rajpal S. Sirohi*
39. Organic Photoreceptors for Imaging Systems, *Paul M. Borsenberger and David S. Weiss*
40. Photonic Switching and Interconnects, *edited by Abdellatif Marrakchi*
41. Design and Fabrication of Acousto-Optic Devices, *edited by Akis P. Goutzoulis and Dennis R. Pape*
42. Digital Image Processing Methods, *edited by Edward R. Dougherty*
43. Visual Science and Engineering: Models and Applications, *edited by D. H. Kelly*
44. Handbook of Lens Design, *Daniel Malacara and Zacarias Malacara*
45. Photonic Devices and Systems, *edited by Robert G. Hunsberger*
46. Infrared Technology Fundamentals: Second Edition, Revised and Expanded, *edited by Monroe Schlessinger*
47. Spatial Light Modulator Technology: Materials, Devices, and Applications, *edited by Uzi Efron*
48. Lens Design: Second Edition, Revised and Expanded, *Milton Laikin*

49. Thin Films for Optical Systems, *edited by Francoise R. Flory*
50. Tunable Laser Applications, *edited by F. J. Duarte*
51. Acousto-Optic Signal Processing: Theory and Implementation, Second Edition, *edited by Norman J. Berg and John M. Pellegrino*
52. Handbook of Nonlinear Optics, *Richard L. Sutherland*
53. Handbook of Optical Fibers and Cables: Second Edition, *Hiroshi Murata*
54. Optical Storage and Retrieval: Memory, Neural Networks, and Fractals, *edited by Francis T. S. Yu and Suganda Jutamulia*
55. Devices for Optoelectronics, *Wallace B. Leigh*
56. Practical Design and Production of Optical Thin Films, *Ronald R. Willey*
57. Acousto-Optics: Second Edition, *Adrian Korpel*
58. Diffraction Gratings and Applications, *Erwin G. Loewen and Evgeny Popov*
59. Organic Photoreceptors for Xerography, *Paul M. Borsenberger and David S. Weiss*
60. Characterization Techniques and Tabulations for Organic Nonlinear Optical Materials, *edited by Mark G. Kuzyk and Carl W. Dirk*
61. Interferogram Analysis for Optical Testing, *Daniel Malacara, Manuel Servin, and Zacarias Malacara*
62. Computational Modeling of Vision: The Role of Combination, *William R. Uttal, Ramakrishna Kakarala, Spiram Dayanand, Thomas Shepherd, Jagadeesh Kalki, Charles F. Lunskis, Jr., and Ning Liu*
63. Microoptics Technology: Fabrication and Applications of Lens Arrays and Devices, *Nicholas Borrelli*
64. Visual Information Representation, Communication, and Image Processing, *edited by Chang Wen Chen and Ya-Qin Zhang*
65. Optical Methods of Measurement, *Rajpal S. Sirohi and F. S. Chau*
66. Integrated Optical Circuits and Components: Design and Applications, *edited by Edmond J. Murphy*
67. Adaptive Optics Engineering Handbook, *edited by Robert K. Tyson*
68. Entropy and Information Optics, *Francis T. S. Yu*
69. Computational Methods for Electromagnetic and Optical Systems, *John M. Jarem and Partha P. Banerjee*
70. Laser Beam Shaping, *Fred M. Dickey and Scott C. Holswade*
71. Rare-Earth-Doped Fiber Lasers and Amplifiers: Second Edition, Revised and Expanded, *edited by Michel J. F. Digonnet*
72. Lens Design: Third Edition, Revised and Expanded, *Milton Laikin*
73. Handbook of Optical Engineering, *edited by Daniel Malacara and Brian J. Thompson*

74. Handbook of Imaging Materials: Second Edition, Revised and Expanded, *edited by Arthur S. Diamond and David S. Weiss*
75. Handbook of Image Quality: Characterization and Prediction, *Brian W. Keelan*
76. Fiber Optic Sensors, *edited by Francis T. S. Yu and Shizhuo Yin*
77. Optical Switching/Networking and Computing for Multimedia Systems, *edited by Mohsen Guizani and Abdella Battou*
78. Image Recognition and Classification: Algorithms, Systems, and Applications, *edited by Bahram Javidi*
79. Practical Design and Production of Optical Thin Films: Second Edition, Revised and Expanded, *Ronald R. Willey*
80. Ultrafast Lasers: Technology and Applications, *edited by Martin E. Fermann, Almantas Galvanauskas, and Gregg Sucha*
81. Light Propagation in Periodic Media: Differential Theory and Design, *Michel Nevière and Evgeny Popov*
82. Handbook of Nonlinear Optics, Second Edition, Revised and Expanded, *Richard L. Sutherland*
83. Polarized Light: Second Edition, Revised and Expanded, *Dennis Goldstein*
84. Optical Remote Sensing: Science and Technology, *Walter Egan*
85. Handbook of Optical Design: Second Edition, *Daniel Malacara and Zacarias Malacara*
86. Nonlinear Optics: Theory, Numerical Modeling, and Applications, *Partha P. Banerjee*
87. Semiconductor and Metal Nanocrystals: Synthesis and Electronic and Optical Properties, *edited by Victor I. Klimov*
88. High-Performance Backbone Network Technology, *edited by Naoaki Yamanaka*
89. Semiconductor Laser Fundamentals, *Toshiaki Suhara*
90. Handbook of Optical and Laser Scanning, *edited by Gerald F. Marshall*
91. Organic Light-Emitting Diodes: Principles, Characteristics, and Processes, *Jan Kalinowski*
92. Micro-Optomechanics, *Hiroshi Hosaka, Yoshitada Katagiri, Terunao Hirota, and Kiyoshi Itao*
93. Microoptics Technology: Second Edition, *Nicholas F. Borrelli*
94. Organic Electroluminescence, *edited by Zakya Kafafi*
95. Engineering Thin Films and Nanostructures with Ion Beams, *Emile Knystautas*
96. Interferogram Analysis for Optical Testing, Second Edition, *Daniel Malacara, Manuel Sercin, and Zacarias Malacara*
97. Laser Remote Sensing, *edited by Takashi Fujii and Tetsuo Fukuchi*
98. Passive Micro-Optical Alignment Methods, *edited by Robert A. Boudreau and Sharon M. Boudreau*

99. Organic Photovoltaics: Mechanism, Materials, and Devices, *edited by Sam-Shajing Sun and Niyazi Serdar Saracftci*
100. Handbook of Optical Interconnects, *edited by Shigeru Kawai*
101. GMPLS Technologies: Broadband Backbone Networks and Systems, *Naoaki Yamanaka, Kohei Shiimoto, and Eiji Oki*
102. Laser Beam Shaping Applications, *edited by Fred M. Dickey, Scott C. Holswade and David L. Shealy*
103. Electromagnetic Theory and Applications for Photonic Crystals, *Kiyotoshi Yasumoto*
104. Physics of Optoelectronics, *Michael A. Parker*
105. Opto-Mechanical Systems Design: Third Edition, *Paul R. Yoder, Jr.*
106. Color Desktop Printer Technology, *edited by Mitchell Rosen and Noboru Ohta*
107. Laser Safety Management, *Ken Barat*
108. Optics in Magnetic Multilayers and Nanostructures, *Štefan Višňovský*
109. Optical Inspection of Microsystems, *edited by Wolfgang Osten*
110. Applied Microphotonics, *edited by Wes R. Jamroz, Roman Kruzelecky, and Emile I. Haddad*
111. Organic Light-Emitting Materials and Devices, *edited by Zhigang Li and Hong Meng*
112. Silicon Nanoelectronics, *edited by Shunri Oda and David Ferry*
113. Image Sensors and Signal Processor for Digital Still Cameras, *Junichi Nakamura*
114. Encyclopedic Handbook of Integrated Circuits, *edited by Kenichi Iga and Yasuo Kokubun*
115. Quantum Communications and Cryptography, *edited by Alexander V. Sergienko*
116. Optical Code Division Multiple Access: Fundamentals and Applications, *edited by Paul R. Prucnal*
117. Polymer Fiber Optics: Materials, Physics, and Applications, *Mark G. Kuzyk*
118. Smart Biosensor Technology, *edited by George K. Knopf and Amarjeet S. Bassi*
119. Solid-State Lasers and Applications, *edited by Alphan Sennaroglu*
120. Optical Waveguides: From Theory to Applied Technologies , *edited by Maria L. Calvo and Vasudevan Lakshminarayanan*
121. Gas Lasers, *edited by Masamori Endo and Robert F. Walker*
122. Lens Design, Fourth Edition, *Milton Laikin*
123. Photonics: Principles and Practices, *Abdul Al-Azzawi*
124. Microwave Photonics, *edited by Chi H. Lee*

# LENS DESIGN

FOURTH EDITION

MILTON LAIKIN



**CRC Press**

Taylor & Francis Group

Boca Raton London New York

---

CRC Press is an imprint of the  
Taylor & Francis Group, an informa business

CRC Press  
Taylor & Francis Group  
6000 Broken Sound Parkway NW, Suite 300  
Boca Raton, FL 33487-2742

© 2007 by Taylor & Francis Group, LLC  
CRC Press is an imprint of Taylor & Francis Group, an Informa business

No claim to original U.S. Government works  
Printed in the United States of America on acid-free paper  
10 9 8 7 6 5 4 3 2 1

International Standard Book Number-10: 0-8493-8278-5 (Hardcover)  
International Standard Book Number-13: 978-0-8493-8278-9 (Hardcover)

This book contains information obtained from authentic and highly regarded sources. Reprinted material is quoted with permission, and sources are indicated. A wide variety of references are listed. Reasonable efforts have been made to publish reliable data and information, but the author and the publisher cannot assume responsibility for the validity of all materials or for the consequences of their use.

No part of this book may be reprinted, reproduced, transmitted, or utilized in any form by any electronic, mechanical, or other means, now known or hereafter invented, including photocopying, microfilming, and recording, or in any information storage or retrieval system, without written permission from the publishers.

For permission to photocopy or use material electronically from this work, please access [www.copyright.com](http://www.copyright.com) (<http://www.copyright.com/>) or contact the Copyright Clearance Center, Inc. (CCC) 222 Rosewood Drive, Danvers, MA 01923, 978-750-8400. CCC is a not-for-profit organization that provides licenses and registration for a variety of users. For organizations that have been granted a photocopy license by the CCC, a separate system of payment has been arranged.

**Trademark Notice:** Product or corporate names may be trademarks or registered trademarks, and are used only for identification and explanation without intent to infringe.

---

**Library of Congress Cataloging-in-Publication Data**

---

Laikin, Milton, 1930-  
Lens design / by Milton Laikin. -- 4th ed.  
p. cm. -- (Optical science and engineering series ; 121)  
Includes bibliographical references and index.  
ISBN 0-8493-8278-5  
1. Lenses--Design and construction. I. Title.

QC385.2.D47L35 2007  
681'.423--dc22

2006050460

---

Visit the Taylor & Francis Web site at  
<http://www.taylorandfrancis.com>

and the CRC Press Web site at  
<http://www.crcpress.com>



# *Dedication*

---

*This revised  
and expanded edition  
is dedicated to my wife, Pat*



---

# Preface

Of the several very fine texts on optical engineering, none gives detailed design information or design procedures for a wide variety of optical systems. This text is written as an aid for the practicing optical designer as well as for those aspiring to be optical designers.

It is assumed that the reader is familiar with ray-tracing procedures, paraxial data, and third-order aberrations. It is also assumed that the reader has access to a computer lens design and analysis program. (See [Appendix D](#) for a list of commercially available lens design programs.) As the personal computer has increased in popularity and computing power, it exceeds, in its scientific computing ability, the large computers of the 1960–1980 era. Many excellent programs are now available for lens optimization, ray-trace analysis, lens plotting, modulation transfer function (MTF) computations, etc. All of these programs, however, are optimization programs; the designer must input a starting solution.

I have taught Introduction to Optical Engineering at the University of California at Los Angeles for several years. I am often asked how I arrive at the starting design. One of the purposes of this text is to answer just that question.

All optical glass listed in the designs are from the Schott glass catalog. (This does not include the Ohara S-FPL53 element used in the designs shown in [Figure 2.4](#) and [Figure 7.5](#); the Ohara S-LAL18 ([Figure 2.5](#)) as well as the gradient index materials of [Chapter 39](#).) Other glass manufacturers (Ohara, Hoya, Chance, Corning, Chengdu, etc.) make nearly equivalent types of glass. This was done for convenience; I do not endorse any one glass manufacturer. In some of the prescriptions, the material listed is SILICA. This is  $\text{SiO}_2$ .  $\text{CaF}_2$  is calcium fluoride.

All lens prescription data, except for the human eye in [Chapter 41](#), are given full size in inches. This allows a practical system for presenting a particular application (perhaps for a 35 mm reflex camera). The lens diameters have reasonable values of edge thickness. The usual sign convention applies; thickness is an axial dimension to the next surface and radius is  $+$  if the center of curvature is to the right of the surface. Light travels left to right and from the long conjugate to the short. Lens diameters are not necessarily clear apertures, but rather, the actual lens diameters as shown in the lens diagrams.

All data for the visual region are centered at the e line and cover  $F'$  to  $C'$ . Two infrared regions are considered; 8–14  $\mu\text{m}$  (center at 10.2) and 3.2–4.2  $\mu\text{m}$  (center at 3.63) that correspond to atmospheric windows. All data for the ultra-violet are centered at 0.27  $\mu\text{m}$  and cover 0.2–0.4  $\mu\text{m}$ . (One needs to exercise caution here because both calcium fluoride and fused silica show some absorption at these short wavelengths. It is very important to select the correct grade.) Field of view (FOV) is quoted in degrees and applies to the full field.

In the first edition of this book, all calculations for the fixed focal length designs were performed using David Grey's optical design and analysis programs. The orthonormalization technique is described by Grey (1966) and the program by Walters (1966). The use of orthogonal polynomials as aberration coefficients was later described by Grey (1980). In this edition, all designs were re-optimized using the ZEMAX

program (Moore 2006). This was necessary because there are now many changes to the glasses that are available because of environmental requirements to remove lead, cadmium, and arsenic. Perhaps most important, the ZEMAX program (like other modern computer design programs listed in [Appendix D](#)) is a more comprehensive program than the earlier GREY versions in that it can perform calculations on decentered and tilted systems and gradient index as well as zoom systems in addition to providing extensive graphical analysis.

In this edition, a CD containing two directories is included.

**Lens.** This contains all the lens prescriptions the same as listed in the text. By using data directly from the computer, some of the prescription errors found in earlier editions are eliminated. This is in a format RADIUS, THICKNESS, MATERIAL, DIAMETER. Files correspond to the figures in the text (not table numbers).

**Optics.** This contains executable ZEMAX files corresponding to the figures in the text. In the preliminary design of these systems, three wavelengths (except, of course, for laser systems) and only a few rays were traced whereas more rays were added to the merit function and, in most cases, five wavelengths were used. In the presence of secondary color, the extra wavelengths give a realistic assessment of MTF for the lens. Therefore, the prescriptions on the disk contain the added rays and wavelengths. Under glass catalogs, PREFERRED (note spelling error) is listed for many of the designs. This is simply a list of Schott optical glass selected for its reasonable price, availability, transmission, and stain resistance that the author often uses. Simply substitute Schott\_2000 for this catalog or load the file PREFERRED.AGF from the included disk into your glass catalogs. Unfortunately, glass availability is changing as well as new glasses are sometimes developed. For example, N-LLF6 used in design 4-1 as well as some other designs, is no longer readily available, so OHARA S-TIL6 should be substituted. Likewise, for SK-18 in design 14-4 is no longer readily available, so OHARA S-BSM 18 should be substituted.

All plots in the figures were done with the ZEMAX program except for plots for the zoom lens movements, secondary color chart, and anti-reflection films. Regarding the zoom lens movement plots, the three curves on these plots represent first-order relative movements of the two moving lens groups. Therefore, the crossing of the curves (as in [Figure 35.9b](#)) does not mean that the moving groups are interfering with each other. The crossing is simply a result of the presentation on the plot. These plots are first-order calculations per the equations in [Chapter 33](#) and [Chapter 34](#). Ten values were first computed and then fitted by a cubic spline equation to do the actual plots.

For most of the systems, four plots for each lens are presented on a page containing MTF, optical layout, ray fans, and RMS spot size. On the MTF plots, the angle quoted is semi-field in degrees as seen from the first lens surface. (Or in some cases, object or image heights.) The data are diffraction included MTF and weighted as indicated in [Table 1.2](#).

Distortion is defined as

$$D = \frac{Y_c - Y_g}{Y_g},$$

where  $Y_c$  is the actual image height at full field and  $Y_g$  is the corresponding paraxial image height. For a focal systems,

$$D = \frac{\tan \theta' / \tan \theta - m}{m},$$

where  $\theta'$  is the emerging angle at full field, and  $m$  is the paraxial magnification (Kingslake 1965).

Although I have taken a great deal of effort to assure accuracy, the user of any of these designs should

- Carefully analyze the prescription to be sure that it meets his or her particular requirements.
- Check the patent literature for possible infringement. Copies of patents are available (\$3.00 each) from Commissioner of Patents, P.O. Box 1450, Alexandria, VA 22313-1450 (<http://www.uspto.gov>). Patent literature is a valuable source of detail design data. Because patents are valid for 20 years after the application has been received by the patent office, (previously 17 years after the patent was granted) older patents are now in the public domain and may be freely used (US Patent Office 1999). The Internet may be utilized to perform a search of the patent literature. The patent office site is <http://www.uspto.gov>. Patents may be searched by number or subject. Text and lens prescription are given (only for patents issued after 1976), but no lens diagram or other illustrations are provided. These illustrations are only available in the printed version of the patent. In *Optics and Photonics News*, Brian Caldwell discusses a patent design each month. There are also patent reviews in Applied Optics.
- All data for the lens prescriptions (in this text, not on the CD) are rounded. A very slight adjustment in back focal length (BFL) may be necessary (particularly with lenses of low f number) if the reader desires to verify the optical data.

This edition contains minor corrections to the previous editions as well as presenting several new designs and sections on stabilized systems, the human eye, spectrographic systems, and diffractive systems. Also, some of the glasses used in the previous designs are now considered obsolete and were replaced.

**Milton Laikin**

## REFERENCES

- Grey, D. S. (1966) Recent developments in orthonormalization of parameter space. In *Lens Design with Large Computers, Proceedings of the Conference*, Institute of Optics, Rochester, New York.
- Grey, D. S. (1980) Orthogonal polynomials as lens aberration coefficients, *International Lens Design Conference, SPIE*, Volume 237, p. 85.
- Kidger, M. (2002) *Fundamental Optical Design*, SPIE Press, Bellingham, WA.
- Kidger, M. (2004) *Intermediate Optical Design*, SPIE Press, Bellingham, WA.
- Kingslake, R. (1965) *Applied Optics and Optical Engineering*, Volume 1, Academic Press, New York.
- Moore, K. (2006) *ZEMAX Optical Design Program, User's Guide*, Zemax Development Corporation, Bellevue, WA.
- US Patent Office (1999) *General Information Concerning Patents*, Available from US Govt. Printing Office, Supt of Documents, Washington DC 20402.
- Walters, R. M. (1966) Odds and ends from a Grey box. In *Lens Design with Large Computers, Proceedings of the Conference*, Institute of Optics, Government Superintendent, Rochester, New York.

---

# Contents

## **Chapter 1**

The Method of Lens Design ..... 1

## **Chapter 2**

The Achromatic Doublet ..... 41

## **Chapter 3**

The Air-Spaced Triplet ..... 51

## **Chapter 4**

Triplet Modifications ..... 61

## **Chapter 5**

Petzval Lenses ..... 73

## **Chapter 6**

Double Gauss and Near Symmetric Types ..... 79

## **Chapter 7**

Telephoto Lenses ..... 87

## **Chapter 8**

Inverted Telephoto Lens ..... 99

## **Chapter 9**

Very-Wide-Angle Lenses ..... 105

## **Chapter 10**

Eyepieces ..... 119

## **Chapter 11**

Microscope Objectives ..... 131

## **Chapter 12**

In-Water Lenses ..... 143

## **Chapter 13**

Afocal Optical Systems ..... 155

<b>Chapter 14</b>	
Relay Lenses .....	169
<b>Chapter 15</b>	
Catadioptric and Mirror Optical Systems.....	183
<b>Chapter 16</b>	
Periscope Systems .....	211
<b>Chapter 17</b>	
IR Lenses.....	219
<b>Chapter 18</b>	
Ultraviolet Lenses and Optical Lithography .....	233
<b>Chapter 19</b>	
F-Theta Scan Lenses .....	245
<b>Chapter 20</b>	
Endoscope .....	253
<b>Chapter 21</b>	
Enlarging and Copying Lenses .....	259
<b>Chapter 22</b>	
Projection Lenses .....	265
<b>Chapter 23</b>	
Telecentric Systems.....	283
<b>Chapter 24</b>	
Laser-Focusing Lenses (Optical Disc).....	291
<b>Chapter 25</b>	
Heads-Up Display Lenses .....	299
<b>Chapter 26</b>	
The Achromatic Wedge .....	305
<b>Chapter 27</b>	
Wedge-Plate and Rotary-Prism Cameras .....	309



<b>Chapter 28</b>	
Anamorphic Attachments.....	317
<b>Chapter 29</b>	
Illumination Systems.....	325
<b>Chapter 30</b>	
Lenses for Aerial Photography.....	333
<b>Chapter 31</b>	
Radiation-Resistant Lenses .....	343
<b>Chapter 32</b>	
Lenses for Microprojection .....	347
<b>Chapter 33</b>	
First-Order Theory, Mechanically Compensated Zoom .....	351
<b>Chapter 34</b>	
First Order Theory, Optically Compensated Zoom Lenses .....	355
<b>Chapter 35</b>	
Mechanically Compensated Zoom Lenses.....	359
<b>Chapter 36</b>	
Optically Compensated Zoom Lenses.....	403
<b>Chapter 37</b>	
Copy Lenses with Variable Magnification.....	415
<b>Chapter 38</b>	
Variable Focal Length Lenses .....	423
<b>Chapter 39</b>	
Gradient-Index Lenses .....	431
<b>Chapter 40</b>	
Stabilized Optical Systems .....	443
<b>Chapter 41</b>	
The Human Emmetropic Eye.....	447

<b>Chapter 42</b>	
Spectrographic Systems .....	451
<b>Chapter 43</b>	
Diffraction Systems .....	459
<b>Appendix A</b>	
Film and CCD Formats.....	465
<b>Appendix B</b>	
Flange Distances .....	467
<b>Appendix C</b>	
Thermal and Mechanical Properties.....	469
<b>Appendix D</b>	
Commercially Available Lens Design Programs.....	471

---

# LIST OF DESIGNS

2-1	48 in. Focal Length Achromat
2-2	Cemented Achromat, 20 in. Focal Length
2-3	Cemented Achromat, 10 in. Focal Length
2-4	Cemented Apochromat
2-5	48 in. Focal Length Telescope Objective
3-2	5 in. Focal Length $f/3.5$ Triplet
3-3	IR Triplet 8-14 Micron
3-4	4 in. IR Triplet 3.2-4.2 Micron
3-5	50 in., $f/8$ Triplet
3-6	18 in., $f/9$ Triplet
4-1	Heliar $f/5$
4-2	Tessar Lens 4 in., $f/4.5$
4-3	Slide Projector Lens
4-4	Triplet with Corrector
4-5	100 mm $f/2.8$
4-6	10 mm $f/2.8$
5-1	Petzval Lens $f/1.4$
5-2	Petzval Lens with Field Flatteners
6-1	Double Gauss $f/2.5$
6-2	50 mm $f/1.8$ SLR Camera Lens
6-3	$f/1$ 5 deg. FOV Double Gauss
6-4	25 mm $f/1.85$ Double Gauss
7-2	Telephoto $f/5.6$
7-3	$f/2.8$ 180 mm Telephoto
7-4	400 mm $f/4$ Telephoto
7-5	1000 mm $f/11$ Telephoto
7-6	Cemented Achromat with 2X Extender
8-1	Inverted Telephoto $f/3.5$
8-2	10 mm Cinegon
8-3	Inverted Telephoto for Camera
9-1	100 deg. FOV Camera Lens
9-2	120 deg. $f/2$ Projection
9-3	160 deg. $f/2$ Projection
9-4	170 deg. $f/1.8$ Camera Lens
9-5	210 deg. Projection
9-6	Panoramic Camera

10-2	10 X Eyepiece
10-3	10 X Eyepiece, Long Eyerelief
10-4	Plossl Eyepiece
10-5	Erfle Eyepiece
10-6	25 mm Eyepiece with Internal Image
11-1	10X Microscope Objective
11-2	20X Microscope Objective
11-3	4 mm Apochromatic Microscope Objective
11-4	UV Reflecting Microscope Objective
11-5	98 X Oil Immersion Microscope Objective
12-3	Flat Port, 70 mm Camera Lens
12-5	Water Dome Corrector
12-6	In-water Lens with Dome
12-7	In-water Corrector for Zoom Lens
13-1	5 X Laser Beam Expander
13-2	5 X Gallean Beam Expander
13-3	50 X Laser Beam Expander
13-4	4 X Galilean Plastic Telescope
13-5	Power Changer
13-6	Albada View Finder
13-7	Door Scope
14-1	1 to 1 Relay
14-2	Unit Power Copy Lens
14-3	.6 X Copy Lens
14-4	Rifle Sight
14-5	Eyepiece Relay
14-6	1:5 Relay
15-2	Cassegrain Lens 3.2-4.2 $\mu\text{m}$
15-3	Starlight Scope Objective $f/1.57$
15-4	1000 mm Focal Length Cassegrain
15-5	50 in. Focal Length Telescope Objective
15-6	10 in. fl $f/1.23$ Cassegrain
15-7	Schmidt Objective
15-8	Reflecting Objective
15-9	250 in., $f/10$ Cassegrain
15-10	Ritchey-Chretien
15-11	Hubble Space Telescope
15-12	Unit Power Concentric Mirrors
15-13	Tilted Mirrors

15-14	Compact Telescope
15-15	Unobscured, All Reflective Lens
16-1	25-mm Focal Length Periscope
16-2	65 mm Format Periscope
17-2	Dual Focal Length IR Lens System
17-3	IR Lens, 3.2 to 4.2 Micro
17-4	10X Beam Expander
17-5	Doublet, 1.8-2.2 $\mu\text{m}$
17-6	Long Wavelength IR Camera
18-1	UV Lens Silica, $\text{CaF}_2$
18-2	Cassegrain Objective, All Fused Silica
18-3	Lithograph Projection
19-1	Document Scanner
19-2	Argon Laser Scanner Lens
19-3	Scan Lens 0.6328 $\mu\text{m}$
20-1	$f/3$ . Endoscope, Rod Lens
20-2	Endoscope, Fiber Optic
21-1	65 mm $f/4$ 10 X Enlarging Lens
21-3	Unit Magnification Copy Lens
22-1	$f/1.8$ Projection Lens
22-3	Projection Lens, 70 mm Film
22-4	70 deg. FOV Projection Lens, $f/2$
22-5	Plastic Projection Lens
22-7	2 in. FL LCD Projection
22-8	Wide Angle LCD Projection Lens
22-9	DLP Projection Lens
23-1	Profile Projector, 20 X
23-2	Telecentric Lens $f/2.8$
23-3	F/2 Telecentric
23-5	3 Chip CCD Camera Lens
24-1	Video Disk $f/1$
24-3	Laser Focusing Lens 0.308 $\mu\text{m}$
24-4	Laser Focus Lens 0.6328 $\mu\text{m}$
25-1	Heads Up Display
25-2	BI-Ocular Lens
27-2	Wedge Plate
27-4	Lens for Rotary Prism Camera
28-1	2X Anamorphic Attachment, 35 mm Film
28-2	2X Anamorphic Attachment, 70 mm Film

28-3	1.5X Anamorphic Expander
28-4	Anamorphic Prism Assembly
29-1	Fused Silica Condenser, 1 X
29-2	Fused Silica Condenser, 0.2 X
29-3	Pyrex Condenser
29-4	Condensor System For 10 X Projection
29-5	Xenon Arc Reflector
30-1	5 in. <i>f</i> /4 Aerial Camera Lens
30-2	12 in. <i>f</i> /4 Aerial Lens
30-3	18 in. <i>f</i> /3 Aerial Lens
30-4	24 in. <i>f</i> /6 Aerial Lens
31-1	Radiation Resistant Lens 25mm <i>f</i> /2.8
32-1	24×Micro-Projection
35-1	10X Zoom Lens
35-2	Afocal Zoom for Microscope
35-3	Zoom Cassegrain
35-4	Zoom Rifle Scope
35-5	Stereo Zoom Microscope
35-6	Zoom Microscope
35-7	20 to 110 mm Zoom Lens
35-8	25 to 125 mm with Three Moving Groups
35-9	Zoom Lens for SLR Camera
35-10	12-234 mm TV Zoom Lens
35-11	40 to 20 mm Zoom Eyepiece
35-12	20 to 40 mm Focal Length Periscope
36-1	Optical Zoom, 100 to 200 mm EFL
36-2	SLR Optical Zoom 72 to 145 mm EFL
36-3	6.25 to 12.5X Optically Compensated Projection Lens
37-1	Xerographic Zoom
37-2	Copy Lens
38-1	Variable Focal Length Projection for SLR Camera
38-2	Variable Focal Length Motion Picture Projection Lens
39-3	3.0 in. <i>f</i> /1.8 Projection Lens, Axial Gradient
39-4	Laser Focusing Lens, Axial Gradient
39-5	Radial Gradient, 50 in. Focal Length
39-6	Selfoc Lens
39-7	Corning-GRIN Laser Focusing Lens
40-2	Stabilized Lens System
41-1	The Human Emmetropic Eye

42-2	Fery Prism
42-3	Littrow Prism
42-5	Littrow Diffraction Grating
43-1	The Achromatic Singlet
43-2	Hybrid Night Vision Lens





---

# 1 The Method of Lens Design

Given an object and image distance, the wavelength region and the degree of correction for the optical system, it would at first appear that with the great progress in computers and applied mathematics it would be possible to analytically determine the radius, thickness, and other constants for the optical system. Neglecting very primitive systems, such as a one- or two-mirror system, or a single-element lens, such a technique is presently not possible.

The systematic method of lens design in use today is an iterative technique. By this procedure, based upon the experience of the designer, a basic lens type is first chosen. A paraxial thin lens and then a thick lens solution is next developed. In the early days of computer optimization, the next step was often correcting for the third-order aberrations (Hopkins et al. 1955). Now, with the relatively fast speed of ray-tracing, this step is often skipped and one goes directly to optimization by ray-trace.

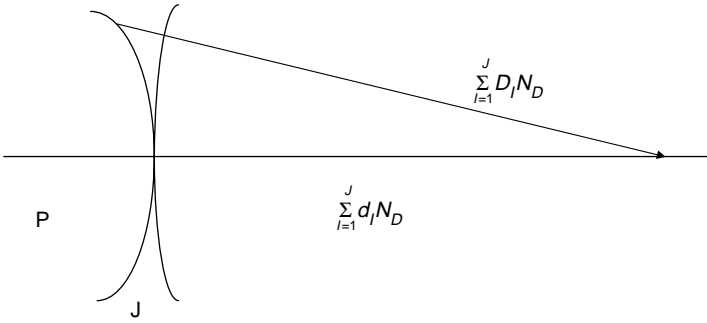
In any automatic (these are really semi-automatic programs because the designer must still exercise control) computer-optimization program, there must be a single number that represents the quality of the lens. Because the concept of a good lens vs. a bad lens is always open to discussion, there are thus several techniques for creating this merit function (Feder 1957a, 1957b; Brixner 1978). The ideal situation is a merit function that considers the boundary conditions for the lens as well as the image defects. These boundary conditions include such items as maintaining the effective focal length (or magnification),  $f$ -number, center and edge spacings, overall length, pupil location, element diameters, location on the glass map, paraxial angle controls, paraxial height controls, etc. There should also be a means to change the weights of these defects so that the axial image quality may be weighted differently than the off-axis image, as well as means for changing the basic structure of the image (core vs. flare, distortion, chromatic errors, etc.) (Palmer 1971). Some merit functions also contain derivative data (Feder 1968).

Most optimization and analysis programs in use today evaluate the optical system by means of ray tracing (Jamieson 1971). However, some compute the aberration coefficients (third and higher orders) at each surface and then form the sum (Buchdahl 1968).

In the early days of optical design, when the cost of tracing a ray was high (as compared to today), a common technique to reduce the number of rays traced was to only trace rays at the central wavelength and carry thru, at each surface, information regarding path-length differences multiplied by the difference in dispersion (Feder 1952; Conrady 1960; Ginter 1990).

Let  $d_I$  be the distance along the axis from surface  $I$  to surface  $I+1$  and let  $D_I$  be the distance for an arbitrary ray from surface  $I$  to surface  $I+1$ . Then for a system of  $J$

surfaces, and  $(N_D)_I$  as the refractive index for the central wavelength following surface  $I$ ,



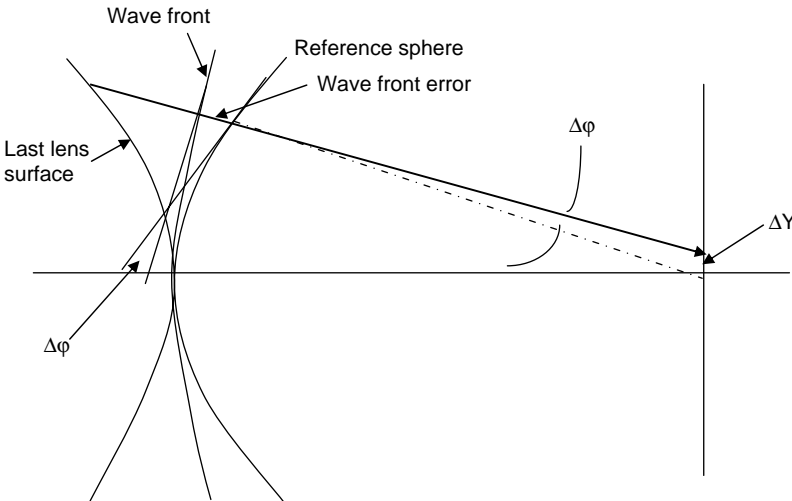
For a spherical wavefront centered at  $P$ ,

$$\sum_{I=1}^J (D - d)_I (N_D)_I = 0,$$

and likewise for the extreme wavelengths,  $F$  and  $C$ , to be united at  $P$ . To be achromatic,

$$\sum_{I=1}^J (D - d)_I (N_F - N_C)_I = 0.$$

As an example of a merit function, let  $d$  be a defect item—the departure on the image surface between the traced rays and its idealistic or Gaussian value (or other means for determining the center of the image). Alternatively, one may use path-length errors as a defect item. The ideal situation is to use a combination of both intercept and path-length errors in the merit function because path-length errors may be obtained with only a small amount of extra computing time, while the rays will be traced.



$\Delta Y \approx k\Delta\phi = k \times (\text{slope difference between the wavefront and the reference sphere}),$

where  $k$  is a proportionally constant. The intercept errors are then approximately proportional to the derivative of the path-length errors. It is also sometimes helpful to add differential errors to the merit function. For example, if  $J$  rays are traced at a particular field angle and wavelength, then

$$\text{Differential error} = \frac{Pl(J) - Pl(J-1)}{Pl(J-1)},$$

where  $Pl(J)$  is the path-length for the  $J$  ray. Because the major load in optimization is the tracing of rays, these extra items improve the image while adding only slightly to computer time. These defect items will be weighted by a factor  $W$  to permit us to control the type of image we desire. If there are  $N$  defect items, then

$$\text{Merit function} = \sum_{i=1}^{i=n} W_i d_i^2.$$

Most merit functions are really “demerit” functions, i.e., they represent the sum of squares of various image errors. Therefore, the larger the number, the worse the image. The input system is ray traced, and the merit function is computed. One of the permitted parameters is then changed, and a new value of the merit function is calculated. A table is then created of merit function changes vs. parameter changes. Then, usually by a technique of damped least-squares (or sometimes by orthonormalization of aberrations) an improved system is created. There are four important characteristics about this process that one should keep in mind:

1. The process finds a local minimum, i.e., a local minimum is reached in respect to a multidimensional plot of all the permitted variables. Only by past experience can one be certain that they have found a global minimum. There are various “tricks” that designers have used to get out of this local minimum and move the solution into a region where there is a smaller local minimum of the merit function. This includes making a few small changes to the lens parameters, changing merit-function weights, and switching from ray-intercept to path-length errors in the merit function (Bociort 2002). A trend in optimization programs is the inclusion of a feature in which the program tries to find this global minimum (Jones 1992, 1994). It does this by making many perturbations of the original system (Forbes 1991; Forbes and Jones 1992).

The orthonormalization process appears to sometimes penetrate these potential barriers. A good procedure then is to first optimize in damped least-squares mode, followed by orthonormalization.

2. The process finds an improvement, however small, wherever it may find it. Thus, if one does not carefully provide bounds on lens thickness, thin lenses of 1/50 lens diameter, or thick lenses (to solve for Petzval sum) of 12 in. could result. Likewise, when glasses are varied, a very small improvement may result in a glass that is either very expensive, not readily available, or has undesirable stain or transmission characteristics.

These computer programs can trace rays through lenses with negative lens thicknesses. Or, the lens system may be so long that it cannot fit into the “box” that has been allocated to it. Therefore, a carefully thought boundary control is vital.

3. Computer time is proportional to the product of the number of rays traced and the number of parameters being varied. Inexperienced designer tend to believe that they will obtain a better lens if they trace more rays; instead, they achieve longer computer runs. The ideal situation is to trace the minimum number of rays in the early stages. The number of rays and field angles should only be increased at the end. Likewise, the image errors should, in the early stages, be referenced to the chief ray for computational speed. As the design progresses, the reference to centroid may be changed. Due to the presence of coma, there is a difference in image evaluation between the chief ray and the image centroid. In most of the designs presented here, three wavelengths were used at the beginning and five wavelengths were used at the end.
4. The program neither adds nor subtracts elements. Therefore, if one starts with a six-element lens, it will always be a six-element lens. It is the art of lens design to know when to add or remove elements.

The use of sine-wave response considering diffraction effects (MTF) is now common in all lens evaluations. The main difficulty in using a sine-wave response as a means of forming a merit function is the very large number of rays that need to be traced, as well as the additional computation necessary to evaluate sine-wave response. This would result in an excessively long computational run. The net result is that diffraction-based criteria, particularly sine-wave response, have not been used as a means of optimizing a lens, but has rather been limited to lens evaluation.

## OPTIMIZATION METHODS

In the least-squares method, the above merit function is differentiated with respect to the independent variables (construction parameters) and equated to zero. The derivative is determined by actually incrementing a parameter and noting the change in merit function. This results in  $N$  equations of the parameter increments. A matrix method for solving these equations for the parameter increments is employed (Rosen and Eldert 1954; Meiron 1959).

It has long been known that the least-squares method suffers from very slow convergence (Feder 1957a, 1957b). To speed convergence, the concept of a metric,  $M$ , is introduced (Lavi and Vogl 1966:15). The gradient obtained from a least squares technique is multiplied by  $M$  to speed convergence, although this is an oversimplification of the technique. This step length computed on the basis of linearity is usually too large, causing the process to oscillate. A damping factor is then introduced into  $M$  that is large when the nonlinearity is large (Jamieson 1971).

The above method will rapidly improve a crude design. After a while, a balance of aberrations will be reached. These residual aberrations vary only slowly when their construction parameters are changed (Grey 1963). Thus, the construction parameters have to be given an infinitesimal increment, which of course reduces the rate of

convergence of the merit function. To avoid this problem, one must consider the rate of change of each of the defect items with respect to the construction parameters. The main difficulty in any automatic differential correction method lies not in the fact that optical systems are nonlinear, but in the fact that every construction parameter affects every defect item.

In the orthonormal method, a set of parameters are constructed that are orthonormal to the construction parameters. This transformation matrix relating the classical aberrations to its orthonormal counterpart is constructed at the beginning of each pass. The merit function then is expressed as the sum of squares of certain quantities, each of which is a linear combination of the classical aberration coefficients. These are orthonormal aberration coefficients because the reduction of any one of these reduces the value of the merit function no matter what the other coefficients may be (Unvala 1966).

## BOUNDARY VIOLATIONS

There are many physical constraints that must be imposed upon the optical system: lens thickness, overall length of the assembly, maximum diameters, refractive index range, minimum BFL, clearance between lens elements, etc. These are entered as boundary controls by the designer and deviations from these bounds are entered into the merit function. Therefore, if the lens is too long and will not fit into the required envelope, this defect is added into the sum of image errors to be corrected. There are several ways to handle these boundary errors:

1. *Absolute control.* With absolute control, a boundary error is not permitted. If a parameter is changed such that it causes a boundary violation, that parameter change is then not allowed. A problem with this method is that it restricts optimization in that a better solution is often found when other parameters are allowed to vary and thus remove this boundary violation.
2. *Penalty control.* With penalty control, a boundary violation is assigned a penalty based upon the weightings that the designer has invoked. This boundary violation is added into the merit function containing the image errors. This is the most common method used in optimization programs.
3. *Variable bounds.* Variable bounds are a more complex method of boundary control. Here, upper and lower bounds are assigned to all the boundary items. As long as the bounded item remains within these bounds, no penalty is added to the merit function. When the bounded item gets very close to the edge of a bound, a penalty is added to the merit function, the bounds are moved in slightly, and the penalty weight increased. Finally, when the bounded item goes beyond the bounds, the weight is substantially increased. This has a tendency to dampen the system and prevent large boundary violations.

## RAY PATTERN

Because a ray may be regarded as the centroid of an energy bundle, it is convenient to divide the entrance pupil into equal areas and to place a ray in the center of each area (Table 1.1). For a centered optical system, one need only trace in one half of the

**TABLE 1.1**  
**Entrance Pupil Fractions, Based on Equal Areas**

<i>N</i> =	2	3	4	5	6	7	8
	0.866	0.913	0.935	0.948	0.957	0.964	0.968
	0.500	0.707	0.791	0.837	0.866	0.886	0.901
		0.408	0.612	0.707	0.764	0.802	0.829
		0.353	0.548	0.645	0.707	0.750	
		0.316	0.500	0.598	0.661		
			0.289	0.463	0.559		
						0.267	0.433
							0.250

entrance pupil. Likewise, for an axial object, only one quadrant need be traced. For systems that lack symmetry, the full pupil needs to be traced.

When starting the design, always trace the minimum number of rays. A reasonable value for the number of rays, *N*, might be equal to 3.

In general, the value for the *J*th value is  $\sqrt{(2(N - J) + 1)/2N}$ .

Today, most lens design programs automate this process. Generally, the pupil (or in some cases the aperture stop) is divided into rings and the number of rays per ring. Thus, the designer simply specifies the number of rings and the number of rays per ring.

For off-axis objects, a chief ray also needs to be traced as well as tracing to both sides of the pupil. For systems that lack symmetry, the full pupil must be traced at all fields. Most modern lens design programs today automate this process of ray selection. The entrance pupil is divided into rings and each ring into sections. Therefore, the designer only needs to specify the number of rings and the number of rays in each ring. As the design progresses, the ray intercept plots should be carefully monitored. If there is considerable flare, then additional rays should be added. Likewise, if there are problems in the skew orientation, some skew rays should be added. In a similar manner, the field angles should be such as to divide the image into equal areas. The image height fractions are (the first field angle is axial, *N* = 1)

$$H(J) = \sqrt{\frac{J}{N - 1}}$$

<i>N</i> =	2	3	4	5	6
<i>H</i> (1)	1.0	0.7071	0.5774	0.5	0.4472
<i>H</i> (2)		1.0	0.8165	0.7071	0.6325
<i>H</i> (3)			1.0	0.8660	0.7746
<i>H</i> (4)				1.0	0.8944
<i>H</i> (5)					1.0

## ASPHERIC SURFACES

Most modern computer programs have the ability to handle aspheric surfaces. For mathematical convenience, surfaces are generally divided into three classes: spheres, conic sections, and general aspheric. The aspheric is usually represented as a tenth-order (or higher order) polynomial. Let  $X$  be the surface sag,  $Y$  the ray height, and  $C$  the curvature of the surface at the optical axis; then

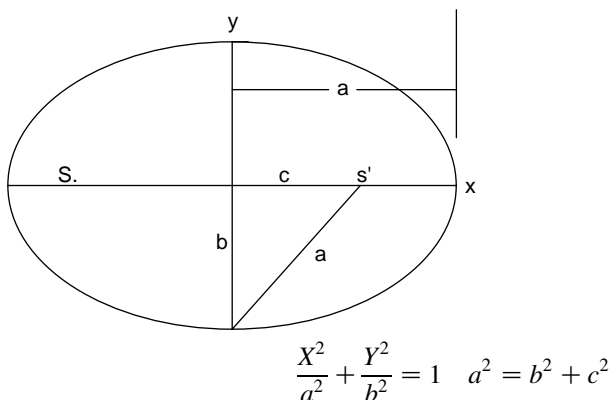
$$X = \frac{CY^2}{1 + \sqrt{1 - Y^2 C^2 (1 + A_2)}} + AY^4 + A_6 Y^6 + A_8 Y^8 + A_{10} Y^{10}.$$

This then represents the surface as a deviation from a conic section.  $A_2$  is the conic coefficient and is equal to  $-\varepsilon^2$ , where  $\varepsilon$  is the eccentricity as given in most geometry texts.

$A_2 = 0$	sphere
$A_2 < -1$	hyperbola
$A_2 = -1$	parabola
$-1 < A_2 < 0$	ellipse with foci on the optical axis
$A_2 > 0$	ellipse with foci on a line normal to optic axis

## CONIC SECTIONS

*Ellipse.*

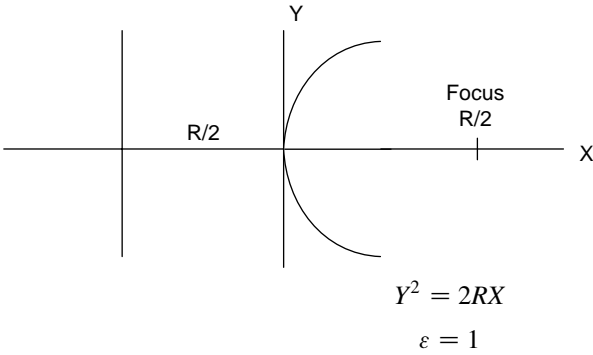


$$R \text{ at } y = 0 = \frac{b^2}{a} \quad M = \frac{S'}{S} = \frac{a+c}{a-c} \quad b = \sqrt{aR}$$

Let  $V$  be the distance from the origin to the ellipse and  $\theta$  the angle measured with respect to the  $X$  axis:

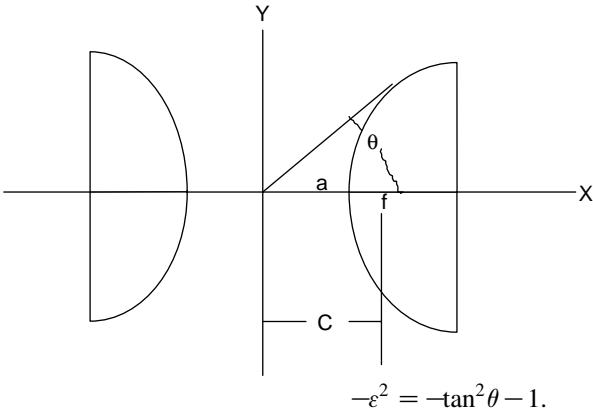
$$\frac{\cos^2 \theta}{a^2} + \frac{\sin^2 \theta}{b^2} = \frac{1}{V^2}.$$

*Parabola.*



$$\text{Radius of curvature} = \frac{(Y^2 + R^2)^{3/2}}{R^2} = R \text{ at } Y = 0$$

*Hyperbola.*



$$\frac{X^2}{A^2} - \frac{Y^2}{B^2} = 1.$$

$$\frac{(x + A)^2}{A^2} - \frac{Y^2}{B^2} = 1.$$

$$C^2 = B^2 + A^2$$

$$\varepsilon = C/A$$

$$R = \frac{B^2}{A} \text{ at } Y = 0.$$



With present technology, it is possible to turn an aspheric surface with single point diamond tooling. This is done with a numerical control system and is being increasingly used for long wavelength infrared systems. In the visual and UV regions, aspherics must be individually polished. The problem is twofold:

1. Most optical polishing machines have motions which tend to generate a spherical surface. (Recently LOH Optical Machinery in Germantown, WI, has made available machines to grind, polish, and test aspheric surfaces.)
2. Aspheric surfaces are very difficult to test.

The best advice concerning aspherics is: unless absolutely necessary, do not use an aspheric surface. Of course, if the lens is to be injection molded, then an aspheric surface is a practical possibility. This is often done in the case of video disc lenses as well as for low cost digital camera lenses (Yamaguchi et al. 2005).

As an aid in manufacturing and testing aspheric surfaces, the author has written a computer program to calculate the surface coordinates as well as the coordinates of a cutter to generate this surface. Let the aspheric surface have coordinates  $X, Y$  and be generated by a cutter of diameter  $D$ . The coordinates of the center of this cutter are  $U, V$ . The cutter is always tangent to the aspheric surface. Referring to Figure 1.1:

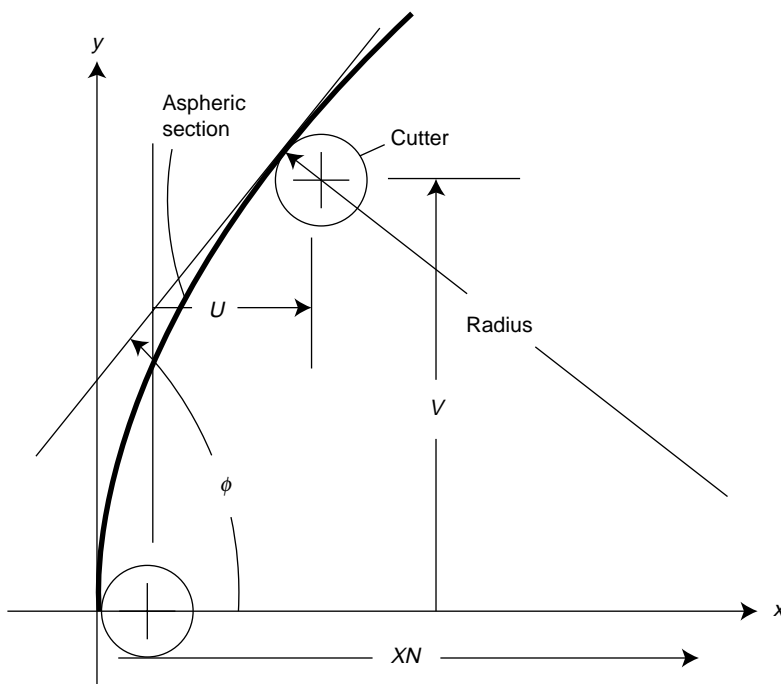


**FIGURE 1.1** Aspheric generation.

$$\tan \phi = \left| \frac{2CY}{1 + \sqrt{1 - C^2 Y^2} (1 + A_2)} + \frac{(1 + A_2) C^3 Y^3}{\left[1 + \sqrt{1 - C^2 Y^2} (1 + A_2)\right]^2 \sqrt{1 - C^2 Y^2} (1 + A_2)} + 4A_4 Y^3 + 6A_6 Y^5 + 8A_8 Y^7 + 10A_{10} Y^9; \right|$$

$$X = \frac{CY^2}{1 + \sqrt{1 - Y^2 C^2} (1 + A_2)} + A_4 Y^4 + A_6 Y^6 + A_8 Y^8 + A_{10} Y^{10};$$

$$U = X + 0.5D \cos \phi - 0.5D;$$

$$V = Y - 0.5D \sin \phi;$$

$$XN = X + \frac{Y}{\tan \phi};$$

$$\text{radius} = \sqrt{Y^2 + (XN - X)^2},$$

where  $XN$  is the radius of curvature of the aspheric surface at the optical axis (the paraxial radius of curvature).

## REFRACTIIVE INDEX CALCULATIONS

The spectral region of interest should be divided such as to achieve nearly equal refractive index increments. Due to the manner in which refractive index varies for typical optical materials, it is preferable to divide the spectral region in equal frequency regions rather than by wavelength; i.e., it is divided into nearly equal reciprocal wavelength increments.

For MTF calculations, five wavelengths are used ([Table 1.2](#)).

Glass catalogs contain index-of-refraction values only at the various spectral and selected laser lines. Calculation at an arbitrary wavelength is performed by using a six-term interpolation formula. The coefficients for this formula for the various glasses are given in the glass catalog. This author (as well as most designers) have the coefficients for the entire glass catalog in addition to those of various other optical materials, stored in a personal computer. It is then only necessary to input the desired wavelengths.

A typical interpolation formula (Schott equation) is

$$N^2 = F_1 + F_2 \lambda^2 + F_3 \lambda^{-2} + F_4 \lambda^{-4} + F_5 \lambda^{-6} + F_6 \lambda^{-8},$$

**TABLE 1.2**  
**Wavelengths and Weights**

Weight	Visual	UV	3.2–4.2 $\mu\text{m}$	8–14 $\mu\text{m}$
0.3	0.48	0.20	3.2	8.0
0.6	0.51	0.23	3.4	8.96
1.0	0.546	0.27	3.63	10.2
0.6	0.59	0.32	3.89	11.8
0.3	0.644	0.40	4.2	14.0

where  $F_1, F_2, \dots, F_6$  are the coefficients for this particular glass and  $\lambda$  the wavelength in  $\mu\text{m}$ . Another formula is the Sellmeier equation (Tatian 1984):

$$N^2 - 1 = \frac{F_1 \lambda^2}{\lambda^2 - F_4} + \frac{F_2 \lambda^2}{\lambda^2 - F_5} + \frac{F_3 \lambda^2}{\lambda^2 - F_6},$$

where the coefficients  $F_4$ ,  $F_5$ , and  $F_6$  represent absorption bands for that particular material.

A simple formula used where there is either a limited wavelength region or lack of data is the Cauchy formula:

$$N = A + \frac{B}{\lambda^2}.$$

## SOLVES

Because most optical systems are defined by first-order parameters—focal length for infinite conjugate lenses, and magnification for finite conjugates—a solve on a surface is generally more efficient (as far as computer time is concerned) than bounds in the merit function. As an example, consider a lens used at an infinite conjugate with desired focal length ( $F$ ) and  $f$ -number ( $\#$ ). If the system is defined with a fixed entrance-pupil diameter ( $D = F/\#$ ), then a marginal ray angle solve may be placed on the last surface (equal to  $-0.5/\#$ ). Likewise, for a finite conjugate system, one may set the object NA and then use the marginal angle solve on the last surface to obtain an approximate control of the magnification (NA is trigonometric whereas the angle solve is paraxial).

There are several things to remember about the use of solves:

1. They are (for most programs) executed sequentially from the first surface to the last.
2. Solves prior to the aperture stop may cause a conflict depending on the system and the particular solve.
3. Avoid solves (particularly curvature solves to control focal length) if this surface is very close to an image.
4. The solves and the aperture definitions must be such that the solve yields a unique solution.

In some of the examples in this text, bounds were placed on the focal length whereas a solve on the last surface would probably have been a better choice.

## GLASS VARIATION

Most modern lens optimization computer programs have the ability to vary the index and dispersion of the material. This assumes a continuum of the so-called *glass map*. This then generally precludes this variation in the UV or infrared regions. However, in the visual region, it is a very powerful variable and should be utilized wherever possible.

To be effective at glass variation, the computer program must be able to bound the glasses to the actual regions of the map; i.e., if refractive index would be left as an unfettered variable, a prescription with refractive index values of 10 would be obtained.

However, not only must the designer carefully bound values of refractive index and dispersion, the designer must also be careful as to the glass he or she chooses. Consider, for example, N-LAK7 vs. N-SK15 (which are fairly close to each other on the glass map). The former, in a grade-A slab, costs \$63/pound whereas the latter costs \$29/pound (2002 prices). Therefore, for a large diameter lens, the price has been greatly increased. Selecting an LASF-type glass can cost from \$111/pound (N-LASF45) to \$648/pound (N-LASF31) for a grade-A slab.

Price is only the beginning. The designer must also check the catalog for:

- *Availability.* Some glasses are more available than others. These so-called *preferred glasses* are indicated in the catalog. Due to environmental pressures, particularly in Europe and Japan, some glasses (such as LAK6) have been discontinued and others have been reformulated. Lead oxide is being substituted with titanium oxide. This reduces the density and these glasses have nearly the same index and dispersion as their predecessor (SF6 and SFL6). Likewise, arsenic oxide and cadmium have been eliminated.
- *Transmission.* Some glasses are very yellow, particularly the dense flints. This is due to the lead oxide content. With the new versions of these glasses, it is worse. For example, the old SF6 containing lead oxide has a transmission of 73% for a 25-mm thickness at 0.4  $\mu\text{m}$ , whereas SFL6 has a transmission of 67%. Catalogs give transmission values at the various wavelengths. In the so-called *mini-catalog*, a value for transmission at 0.4  $\mu\text{m}$  thru a 25-mm path is given.
- *Staining and weathering.* Glass is affected in various ways when contacted by aqueous solutions. Under certain conditions, the glass may be leached. At first, when thin, it forms an interference coating. As it thickens, it slowly turns white. Interactions with aqueous solutions, particularly during the polishing operations, may cause surface staining. Glasses that are particularly susceptible are listed in these glass catalogs. Glasses that are susceptible to water vapor in the air (listed as *climatic resistance*) should never be used as an exterior lens element.

- *Bubble*. Some glasses, due to their chemical composition, are prone to containing small bubbles. These glasses cannot be used near an image surface.
- *Striae*. A few glass types are prone to fine striae (index of refraction variations). These glasses should not be used in prisms or in thick lenses.

When the glass is finally selected, the actual catalog values are then substituted for the “fictitious glass” values. This is done by changing the surface curvatures to maintain surface powers. Let  $\Phi$  be the surface power at the  $J$ th surface with curvature  $C$ , and a fictitious refractive index  $N$ ; then

$$\Phi = (N_J - N_{J-1})CJ = (N' - N_{J-1})C'J,$$

where  $N'$  is the catalog value of the refractive index and  $C'$  is the adjusted value of the curvature.

## GLASS CATALOGS

All refractive index data was taken from the manufacturers’ catalogs. These catalogs are included in most optical design programs and are kept current. As explained above, many of these glasses, when used in the visual region, have poor transmission in the blue region, are prone to staining, have striae or bubbles, or are very expensive. Consequently, for these designs, the glass selection, where appropriate, has been limited to some “preferred” glasses.

Material catalogs may be readily be obtained via the Internet. The following is a listing for some of these materials.

---

Company	Internet Address	Material
Hoya optics	<a href="http://www.hoyaoptics.com">http://www.hoyaoptics.com</a>	Optical glass
Schott glass technologies	<a href="http://www.us.schott.com">http://www.us.schott.com</a>	Optical glass
Ohara glass	<a href="http://www.oharacorp.com">http://www.oharacorp.com</a>	Optical glass
Hikari glass	<a href="http://www.hikariglass.com">http://www.hikariglass.com</a>	Optical glass
Heraeus	<a href="http://www.heraeus-quarzglas.com">http://www.heraeus-quarzglas.com</a>	Fused silica
	See also <a href="http://www.heraeus-optics.com">http://www.heraeus-optics.com</a>	Fused silica
Corning	<a href="http://www.corning.com">http://www.corning.com</a>	Fused silica, Vycor, Pyrex
Morton	<a href="http://www.rohmhaas.com">http://www.rohmhaas.com</a>	Infrared materials
Dynasil	<a href="http://www.dynasil.com">http://www.dynasil.com</a>	Fused silica
Dow	<a href="http://www.dow.com/styron">http://www.dow.com/styron</a>	Polystyrene

---

## CEMENTED SURFACES

Cement thickness is generally less than 0.001 in. Therefore, this cement layer is generally ignored in the lens design process. Modern cements can withstand temperature extremes from  $-62^{\circ}\text{C}$  to greater than  $100^{\circ}\text{C}$  (Summers 1991; Norland 1999). Because these cements have an index of refraction of about 1.55, there will be some reflection loss at the interface. Nevertheless, the cement–glass interface is rarely antireflection coated. For certain critical applications, a  $\lambda/4$  coating at each glass surface prior to cementing will greatly reduce this reflection loss (Willey 1990).

Due to transmission problems with cements, their use is limited to the visual region.

## ANTIREFLECTION FILMS

For light striking at normal incidence on an uncoated surface, the reflectivity,  $R$ , is given by

$$R = \left[ \frac{N_0 - N_s}{N_0 + N_s} \right]^2,$$

where light is in media  $N_0$  and is reflected from media of refractive index  $N_1$ . For air,  $N_0$  is 1; if  $N_s = 1.5$ , then  $R = 4\%$ .

Considering films whose optical thickness is  $\lambda/4$ , then the reflectivity for a single film of index  $N_1$  on a substrate of  $N_s$  is

$$R = \frac{\left[ 1 - \frac{N_1^2}{N_s} \right]^2}{\left[ 1 + \frac{N_1^2}{N_s} \right]^2},$$

which becomes zero when  $N_1 = \sqrt{N_s}$ .

One of the earliest antireflection coatings was a single layer of  $\lambda/4$  optical thickness of magnesium fluoride. This material has an index of refraction of 1.37 (at  $\lambda = 0.55 \mu\text{m}$ ).

For magnesium fluoride and N-LASF31,  $N_e = 1.88577$ ; this is an ideal antireflection coating (see curve A in Figure 1.2 and compare to curve D for N-BK7.)

Consider a two-layer coating (a V-coat) useful for laser systems and devices where only one wavelength is to be considered. For zero reflectivity,  $N_1^2 N_s = N_2^2 N_m$ . Curve B in Figure 1.2 shows such a V-coating using magnesium fluoride as  $N_1$  and  $\text{Al}_2\text{O}_3$  as  $N_2$  on N-BK7 glass ( $N_s$ ), and in air ( $N_m = 1$ ) (see Figure 1.3).

To obtain a very low reflectivity over the visual region, a three-layer coating is required. This has less than 0.5% reflectivity over the region. Such a coating can be achieved with

- $\lambda/4$  of  $\text{MgF}_2$  as the first coating
- $\lambda/2$  of  $\text{ZrO}_2$  as the middle coating
- $\lambda/4$  of  $\text{CeF}_3$  next to the substrate

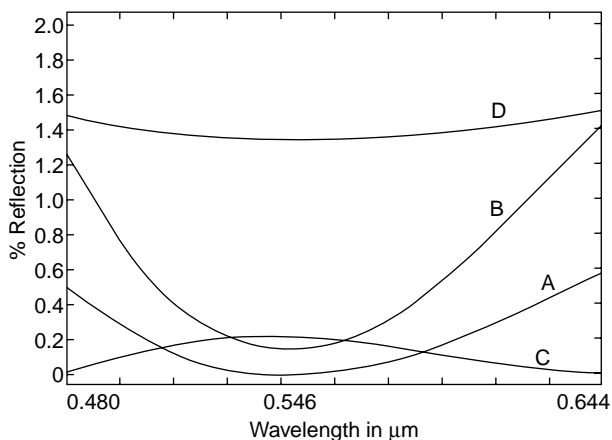


**FIGURE 1.2** Antireflection coatings.

Curve C in Figure 1.2 shows such coating on BK7 glass. For an excellent discussion on thin films, see Rancourt (1996).

It is generally not necessary for the lens designer to specify the details of the antireflection coating. All that is necessary is the wavelength region and the maximum reflectivity. This is because all optical shops have their own proprietary coating formulas.

## VIGNETTING AND PUPIL SHIFT

Vignetting is a reduction in the size of the entrance pupil for off-axis objects due to physical constraints of lens diameters. By this definition, there is no vignetting on-axis. The size of the axial entrance pupil is determined by the system f-number or numeric aperture.

Let the entrance pupil for off-axis objects be defined as perpendicular to the chief ray. Because the entrance pupil is an aberrated image of the aperture stop, the first step is to determine the aperture-stop diameter by tracing an upper-rim axial ray.

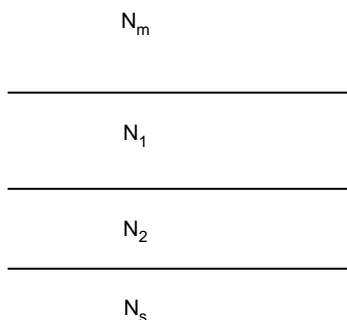


**FIGURE 1.3** A two-layer antireflection coating.

For this off-axis object, the size of the vignetted entrance pupil is determined by iteratively tracing upper, lower, and chief rays to the aperture stop. For certain systems, the full, unvignetted entrance pupil may not be traceable. In these situations, this vignetting and pupil shift to the aperture stop; i.e., the ray coordinate data is shifted and vignetted onto the aperture stop.

Vignetting is nearly the same for all wavelengths (at any particular field angle). Therefore, for convenience, the above procedure only needs to be carried out at the central wavelength. However, there is, in general, a different vignetting and pupil shift for all off-axis field points and configurations (a zoom lens). In a typical computer program, vignetting and pupil shift are handled as follows:

- $VTT(J)$  is the vignetting for a particular field and configuration. It is expressed as a fraction of the aberrated entrance-pupil diameter. It applies only in the meridional direction (see Figure 1.4).
- $VTS(J)$  is the same but in the sagittal direction. For a centered optical system with rotational symmetry, these items are one.
- $PST(J)$  is pupil shift for the vignetted pupil corresponding to the above.
- $PSS(J)$  is the same but in the sagittal direction. For a centered optical system with rotational symmetry, these items are zero.
- In the absence of any pupil shift or vignetting, all  $VTT(J)$  and  $VTS(J)$  items are set equal to 1 and all  $PST(J)$  and  $PSS(J)$  are set equal to zero.
- To trace to the top of the pupil:  $PST(J) + VTT(J) = 1$ .

Entrance pupil coordinates are then shifted and multiplied by the appropriate vignetting coefficient. This applies to all raytracing: MTF data, spot diagram, lens drawings, etc. By this technique, accuracy in MTF and spot-diagram computations is not compromised because the full number of rays is being traced in the presence of vignetting. It also allows the designer to deliberately introduce vignetting into the system when it is necessary to constrain lens diameters.

The lens designer must be cautioned that in systems with considerable vignetting, care must be taken that there are lens diameters to limit the upper and lower rim rays of the vignetted pupil. The aperture stop is now not the limiting surface. Only rays that were traced in optimization must be able to pass through the optical system.

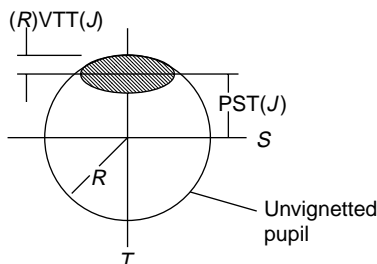


**FIGURE 1.4** The vignetted entrance pupil.



## CHANGING THE NUMBER OF ELEMENTS

Sometimes during the course of the design, the designer will note that an element is becoming very thin and of very low power. In this case, the program's curvature bounds and thickness bounds are invoked to make it a nearly zero-power element. The element is then removed from the prescription.

A tougher case is when the lens image quality is not adequate. The usual advice is to add an element. But where should such an element be added, and how? There are several choices:

1. In front or behind the lens. This is easy: just add a plane plate, guessing at the material type. First vary only the curvatures of this new element along with the curvature and thickness parameters of the remaining elements. Then vary the index and dispersion of the new element. (Obviously not possible if in the infrared or UV regions.)
2. Insert a plate in a large air space in the lens. Remember to readjust the air spaces such that if  $D$  was the original air space and  $D_1$  and  $D_2$  are the new air spaces, and if the plate has a thickness  $T$  and refractive index  $N$ , then  $D = D_1 + D_2 + T/N$ .
3. Split a very thick lens into a cemented doublet. This might be a logical choice if there is considerable chromatic aberration. Vary refractive index and dispersion of both of the new elements.
4. Split a very thick lens into two elements separated by a very small airspace. This could lead to ray-trace difficulties in regions of large angles of incidence. Keep in mind that with today's coating technology, the cost of two air-spaced elements is nearly the same as a cemented doublet. The splitting is generally performed with two plane surfaces separated by a small air gap.

## VARIABLE PARAMETERS

The beginning designer often asks, "What lens parameters should I vary?" The answer, of course, is that one should vary them all—but not right away. The author's general procedure is as follows:

1. First series of runs. Vary all the radii, large airspaces, and positive lens thicknesses. If there is an aspheric surface, then these coefficients should be varied. Radii and aspheric coefficients represent the most powerful lens parameters and so should be varied from the very beginning of the design phase. Positive lens thickness should be varied because it is necessary to control lens edge thickness. Review all the bounds to ensure that the lens is buildable and that it will fit your requirements as to diameter, overall length, back focus, etc.
2. Second series of runs. Add to the above parameters thickness of negative lenses as well as the remaining air spaces. If some of these spacings are giving problems (going to their maximum or minimum values), it is best to just fix this parameter (at least for the time being).

3. Third series of runs. Add to the above parameters index and dispersion of glasses. Obviously, this is skipped if in the UV or IR regions. Then fix the glasses. The author finds this the most “soul searching” part of lens design because he must now make value decisions regarding glass prices and availability, stain and bubble codes, and, of course, performance.
4. Fourth series of runs. With the glasses fixed, again vary all the parameters (except obviously index and dispersion).

At several stages in the design process, it is wise to

1. Run MTF calculations to be sure that the design is meeting your image quality requirements.
2. Check distortion.
3. Plot the lens to be sure that it is buildable.
4. Examine intercept and path-length error plots as well as third-order surface aberration contributions. This often gives the designer an insight into their design problems. Based upon this, the designer might want to split a lens, add a lens, etc. (For a discussion on third-order aberrations, see Born and Wolf (1965)).

## BOUNDS ON EDGE AND CENTER THICKNESS

For the economical production of a lens element:

- Negative elements should have a diameter-to-center thickness ratio of less than 10. This ratio is necessary to prevent the lens from distorting when removed from the polishing block. Diameter-to-thickness ratios as high as 30 are possible, but production costs increase. In the IR region, where material is expensive and there is considerable absorption and scattering, high thickness ratios are common.
- Positive elements should have at least 0.04-in. edge thickness on small lenses less than 1 in. in diameter and at least 0.06-in. edge thickness for larger lenses. This is necessary to prevent the lens from chipping while being processed.

## TEST GLASS FITTING

During the polishing process, all spherical surfaces are compared under a monochromatic light source with a test glass (Malacara 1978:14). A test glass consists of a pair of concave/convex spheres, generally made from Pyrex or sometimes fused silica. When compared to the work in process, Newton rings are seen that represent contours of half-wavelength deviations of the work from a sphere. This is a crude, but yet very practical way to determine the accuracy and irregularity of the work. One-fourth and one-eighth fringe deviations are readily discernible. This technique has two disadvantages:

1. The work surface is being contacted by the test glass and may be scratched. Today, with the availability of the HeNe laser, various interferometers are available (Zygo, for example) in which no surface contact is made.
2. For every value of radius, one needs a pair of test glasses.

All optical shops have an extensive test-glass inventory. These lists are made available to the designer in the hope that he will select values of radii from this list. Cost of a test glass is approximately \$400 per radius value. Therefore, total cost of a prototype optic is vastly reduced if the designer can fit his design to the optical shop's list. It is unfortunate that all shops have a different list, and that there is no such thing as a standardized list.

As a basis for such a list, one might consider a system where all radii are a constant multiplier of the next smallest value, i.e.,  $R_j = cR_{j-1}$ ; for 100 values between 1 and 10,  $c = 1.02329$ .

However, a rationalized system will never happen, and thus the designer must contend with fitting his design to the irrational values of test glasses that are available within his or her shop. The author uses a rather crude technique, as follows:

1. The third-order aberration contributions at each surface are scanned and a radius tolerance is estimated.
2. Any surface that lies within this tolerance limit of a test-glass value is then actually set to the test-glass value.
3. The system is then optimized, of course keeping the test-glass-fitted surfaces constant. (The other radii and thicknesses are varied.)
4. Steps 2 and 3 are then repeated. Values of radii that did not at first lie within its tolerance for a test glass will often move to a new value with the subsequent optimization and now can be fitted.

Other designers have advocated a different technique. They try to fit the most sensitive radii first. They feel that the least-sensitive radii can always be fitted.

Regardless of the method, do not worry if you cannot fit every radius to the test list. If you fit most of them, you will still have saved your client a substantial sum.

## MELT DATA FITTING

Some lenses, particularly long-focal-length, high-resolution types, are sensitive to small changes in refractive index and dispersion of the actual material used as compared to the nominal or catalog value. For materials such as quartz (fused silica), calcium fluoride, silicon, germanium, etc., refractive index is an intrinsic property of these compounds. However, for mixtures such as optical glass, there are slight variations in refractive index from batch to batch. Refractive index is carefully controlled by the glass manufacturer. Typical tolerances for glass as supplied are  $N_d \pm 0.001$  and  $V_d \pm 0.8\%$ .

The glass manufacturer generally supplies to the optical shop a melt datasheet for each supplied batch of glass. These sheets contain the actual measured refractive indices at several spectral lines for that particular batch of glass. In the event that the measured values depart by more than the tolerance limit for the lens, then values of radii, lens thickness, or air spaces must be adjusted. This process is called *melt data fitting* and, fortunately, only needs to be performed on a few types of lenses.

The process becomes complex if the lens designer used refractive index values at wavelengths other than those that the glass manufacturer measured. For example, if data is supplied at the spectral lines *e*, *f*, *c*, and *g*, but the designer requires data at 0.52  $\mu\text{m}$ , then an interpolation technique is needed. A method that seems very effective (private communication from D. Grey) is to fit by least-squares the difference between the melt index of refraction and the corresponding calculated value to an equation of the form

$$R(\lambda) = A\lambda^{-3} + B\delta\lambda^{-2} + C\lambda^{-1} + D.$$

This value of  $R(\lambda)$  is then added to the calculated value of the refractive index. (This calculated value is computed from the polynomial coefficients given in the glass catalog, as previously discussed.)

## THERMAL PROBLEMS

Thermal problems may be divided into two classes:

- The entire lens or mirror has been raised (or lowered) to a uniform temperature.
- There are temperature gradients across the lens or mirror.

If an optical system has its temperature uniformly changed, then the main problem is a shift in the image surface location. Of course, the effective focal length changes and there will be some loss in image quality. These changes may be reduced by various thermal compensation techniques.

In Cassegrain systems, a favored technique is to control the spacing between primary and secondary mirrors with Invar rods. Although the entire system is in an aluminum housing that exhibits considerable dimensional changes with temperature, the most critical spacing—primary to secondary mirror—is now held constant with temperature.

Another technique is to fabricate the entire system out of the same material. For an all-mirror system, this may be conveniently carried out because metal mirror fabrication is now commonplace. Aluminum mirrors are often made by first roughly shaping the mirror, chemically depositing nickel, and then polishing this surface to the desired figure. It is then vacuum-coated with aluminum.

For a lens system, fabricating all of the spacers out of Invar does not help because the radii, lens thicknesses, and refractive indices of the elements are changing with temperature. Fortunately, most optical glass catalogs now give the

change in refractive index,  $dn/dt$ , as well as the thermal expansion coefficient,  $\alpha$ . This data is then used to create a new prescription in which all radii, thicknesses, and refractive indices have now been changed as a result of the temperature change. It is a complex process because an axial spacing change is a result of how the spacer contacts the edge of the lenses. The system is then analyzed and if there are image quality or back-focal-length changes (most likely), then one substitutes a different spacer material. For example, if two elements are spaced with an aluminum alloy (6061) spacer ( $\alpha = 216 \times 10^{-7}/^{\circ}\text{C}$ ), then the space between the elements may be reduced if brass is substituted ( $\alpha = 189 \times 10^{-7}/^{\circ}\text{C}$ ) or increased with a magnesium spacer ( $\alpha = 258 \times 10^{-7}/^{\circ}\text{C}$ ). This, unfortunately, is a very tedious procedure. Computer programs have been written to perform these thermal perturbations.

The second case of temperature gradients causes the lens that formerly had rotational symmetry to be deformed and therefore lack this symmetry. There is very little the lens designer can do about this except to use fused silica where possible and use a very low-expansion material for mirrors, such as titanium silicate (Corning 7971, see [Appendix C](#)). The change in optical path length resulting from a temperature variation  $\Delta T$  is (Reitmayer and Schroder 1975):

$$\Delta W = d[\alpha(n-1) + dn/dt]\Delta T,$$

where  $n$  is the index of refraction,  $d$  is the thickness of the element, and  $\alpha$  is the coefficient of thermal expansion.

Unfortunately, for nearly all materials,  $dn/dt$  is a positive number; i.e., the refractive index increases with temperature. There are a few materials that have a negative  $dn/dt$ . These are the FK series of glasses: PK53, PK54, SK51, LAKN12, and LAKN13.

## OPTICAL TOLERANCES

Perhaps the most neglected portion of the lens design process is the tolerancing and subsequent drawing preparation. Conceivably, this is because it is the least creative portion of the task. However, without proper tolerancing and proper drawings, all of the work of the lens design process may produce an inferior or even an unacceptable product.

Perhaps the simplest method is to use of the merit function from the lens optimization program. That is, if the merit function, as constructed, is adequate for optimization, then why should it not be used to tolerance the lens? For tolerances on curvature, thickness, refractive index, and dispersion, this is a simple task: one makes a series of computer runs in which these parameters are changed by small amounts. Then, by estimating a permitted increase in the merit function, one can arrive at the tolerances for the above parameters.

However, this technique becomes complex when one tries to introduce tilts, decentrations, and surface irregularities into the lens system. There are several additional considerations when tolerancing a lens system:

1. Tolerances must be assigned to each parameter by some statistical method (Koch 1978; Smith 1990). Everything subject to manufacture will depart from the nominal design.
2. In addition to actual image-quality changes as a result of manufacture, certain first-order parameters must often be maintained: effective focal length (or magnification) and back focal length. In this regard, it is helpful to have a printed table of the variation of these first-order parameters vs. the lens parameters of curvature, thickness, and refractive index.
3. There is often a parameter that may be used to compensate for image or first-order errors. The simplest case is a variation in back focal length. This is often compensated by adjusting the mounting flange as the last step in manufacture. Also, in telephoto lenses, the large air space between the front and rear groups may be used to maintain effective focal length.
4. Accuracy and irregularity tolerances: *Accuracy* represents the total number of fringes that the surface deviates from the test glass. *Irregularity* is the difference in fringes as seen in two mutually perpendicular directions. This irregularity causes astigmatism for an axial object. To detect irregularity, the accuracy should not be greater than 4–6 times the irregularity. However, the accuracy also is related to the radius tolerance, particularly in cases where the radius is greater than 10 times the diameter.

Let  $Y$  be the semi-diameter, and  $Z$  the sag at the surface. Then, approximately,  $Z = -Y^2/2R$ . Taking the derivative,  $\Delta Z = -Y^2/2R^2 \Delta R$ . As an example, for an accuracy of four fringes,  $R = 100$  mm,  $Y = 5$  mm, and  $\Delta Z = 1.1 \times 10^{-3}$  mm.  $\Delta R$  then is 0.88 mm, which is probably greater than the radius tolerance (which might be 0.2 mm).

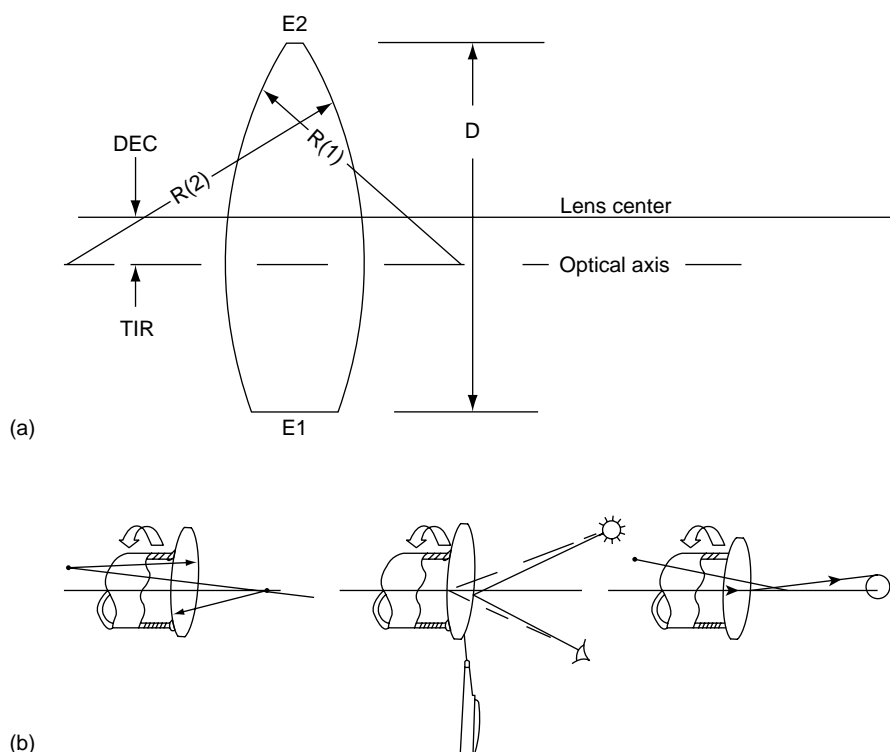
As discussed previously, should the lens be subject to refractive index or dispersion variations of less than catalog values, then melt data fitting is employed. When the designer prepares the lens drawings, the actual tolerances are a blend of tolerances to maintain image quality and tolerances to maintain first-order properties. Ginsberg (1981) discusses this overall tolerancing concept.

Figure 1.5a shows a decentered lens element of focal length  $F$  and refractive index  $N$ . The optical axis contains the centers of curvatures of the lens surfaces. However, the lens is actually centered about an axis indicated as the lens center. *Decenter* (DEC) is the distance between the optical center and the center of the lens. *Image runoff* is the diameter of the circle made by the mutating image as the lens is rotated (see Chapter 6 of Kimmel and Parks (1995)):

$$\text{Image runoff} = 2\text{DEC};$$

$$\text{DEC} = F \text{ deviation};$$

$$\text{Edge variation} = E1 - E2 = \frac{D(\text{deviation})}{N - 1} = \text{TIR}(\text{total indicator runoff}).$$



**FIGURE 1.5** (a) Lens decentration and (b) centering (edging) an element.

This assumes that the part runs true on surface 2 and rotates about the lens center axis.  $D$  is the clear aperture diameter of surface 1, and this is where the dial indicator is placed to read TIR. As the lens is rotated, the image of a distant object will rotate about a circle of diameter  $2DEC$ .

Wedge (in radians) is the edge thickness difference divided by the lens diameter. Figure 1.5b shows how a lens is setup for edging. On the left, a lens is waxed to a true running spindle in preparation for edging (centering). Notice that the center of curvature of the surface in contact with the spindle lies on the center of rotation of the spindle. In the center figure, a bright object is seen as reflected from the external surface of the lens. As the lens is rotated, the image tracks out a circle in space. With the wax still soft (a little heat might be needed), the lens is pushed closer to the centered position and the circle becomes smaller until no movement of the image can be discerned. Alternatively, a dial indicator may be placed near the edge of the external surface. (With this method, there is the possibility of scratching the polished lens surface.) In the figure on the right, a beam of light (perhaps a laser) is transmitted thru the lens and the deviation is noted. Again, the lens is adjusted until no deviation can be detected. With the lens so centered on the spindle, a diamond wheel then edges the lens to the proper diameter.

It is important to try to create a design that is not too sensitive to the construction parameters. The usual method of optimization creates a lens that is in a local

minimum with respect to the “centered” parameters: thickness, curvature, refractive index, and dispersion (assuming that all these parameters were varied). However, optimization does not create a system that is a minimum with respect to tilt and decentrations. As a means of reducing these effects, the designer should try to avoid large angles of incidence and large third-order surface contributions.

In POP, there is a bound (Grey 1970, 1978) whereby sensitivity to tilt and decentration may be reduced. This, however, must be used with caution. The item bounded is the RMS OPD (optical path difference) path-length error induced by tilt or decentration (see the following discussion on wave front perturbations). In addition, at the end of a computer run, there is a printout of lens tolerance data for each surface and for each lens. This is RMS OPD (in  $\mu\text{m}$ ) per 0.001-in. lateral displacement, as well as TIR of 0.001-in. at the edge of the clear aperture. This alerts the designer as to potential sensitive surfaces. Other lens optimization programs have a similar feature.

MTF (modulation transfer function), or OTF (optical transfer function) is presently regarded as the “best” way to evaluate an optical system. Therefore, although most merit functions are not based on diffraction MTF, final analysis of the lens is by diffraction-based MTF. Consequently, some tolerancing programs (for example Code V, [Appendix D](#)) utilize a procedure for calculating the variation of OTF with the construction parameters (Stark and Wise 1980). To reduce ray-trace time, one procedure (Rimmer 1978) is to expand the OTF in a power series in the parameters of interest. Another technique is to consider wavefront perturbations as a function of parameter variations (Hopkins and Tiziani 1966). Let  $\tau$  be the path length error produced by a perturbation:

$$\tau = (N \cos I - N' \cos R)\Omega,$$

where  $N$  and  $N'$  are refractive indices,  $I$  is the angle of incidence,  $R$  is the angle of refraction, and  $\Omega$  is the motion of surface normal to ray propagation.

Consider a lens of refractive index  $N$  in air with a surface irregularity thickness of  $t$ . Then, at near-normal incidence,  $\tau = (N - 1)t$ , whereas for a mirror surface,  $\tau = 2t$ .

Comparing a mirror system to a lens system of refractive index 1.5, the mirror is four times as sensitive to effects of surface irregularity as the equivalent lens. One starts by uniformly assigning tolerances, i.e.,

$$\text{Wavefront error for each parameter} = 0.25\lambda\sqrt{M},$$

where  $M$  is the number of parameters that are subject to manufacturing errors. The total wavefront error then will be

$$\sqrt{\sum_{i=1}^M T_i^2} = \frac{\lambda}{4},$$

where  $T_i$  is the wavefront error for the  $i$ th parameter. Most optical systems are not diffraction limited and so the wavefront error for each parameter may be accordingly increased.



These tolerances should be changed to reflect manufacturing charges. That is, if a lens thickness tolerance becomes  $\pm 0.020$  in., it should be changed to  $\pm 0.005$  in. because there is no price change. This will help relieve the burden for those tolerances that become extremely tight.

Likewise, the designer should consider the cost of tighter part tolerances vs. assembly, adjustment, and test times. In this regard, the author designed and fabricated several complex lenses for undersea use. It was a motor driven lens and had an extensive assembly and test procedure. After fabricating several lenses, the author realized that this assembly and adjustment time was excessive. By tightening many of the lens and mechanical part tolerances, the assembly and adjustment times were greatly reduced. The increase in part cost was substantially less than the cost of labor saved.

## LENS DRAWINGS

Upon completion of lens tolerancing, drawings for all the lens elements are prepared. The designer should keep in mind that drawings are often prepared by a draftsman. The designer should always check that the drawings are accurate and toleranced properly. As an aid to someone else preparing the optical drawings, the author has found it helpful to submit, as part of the design package, the lens prescription in a form in which all columns are clearly labeled. This is illustrated in Table 1.3, which is the lens prescription for the inverted telephoto lens of Figure 8.1. This is also an aid to the mechanical engineer in preparation of lens spacers and housings. All data is in inches, (use millimeters when submitting lens data to other countries). *Sum* is a running sum of axial thickness, starting at the first surface, and *edge* is the edge thickness to the next surface.

Figure 1.6 shows a typical drawing for a cemented element. It is the cemented achromat of Figure 2.2 and is a cross-sectional view as accepted in the optical

**TABLE 1.3**  
**Lens Prescription for Inverted Telephoto,  $f/3.5$**

	Radius	Thickness	Sum	Diameter	Sag	Glass	Edge
1	4.5569	0.100	0.000	0.940	0.024	N-PK51	0.222
2	0.7040	0.825	0.100	0.860	0.147	AIR	0.912
3	0.5900	0.120	0.925	0.940	0.233	SF1	0.079
4	0.5329	0.592	1.045	0.820	0.192	AIR	0.428
5	3.8106	0.302	1.637	0.940	0.029	LF5	0.227
6	-2.4206	0.438	1.939	0.940	-0.046	AIR	0.484
7	Stop	0.015	2.378	0.646	0.000	AIR	0.037
8	5.0596	0.070	2.393	0.940	0.022	SF1	0.167
9	0.7648	0.241	2.462	0.820	0.119	N-LAK21	0.070
10	-1.6496	2.225	2.703	0.820	-0.052	AIR	2.280

Effective focal length = 1.18 in., distance of first lens surface to image is 4.928 in.

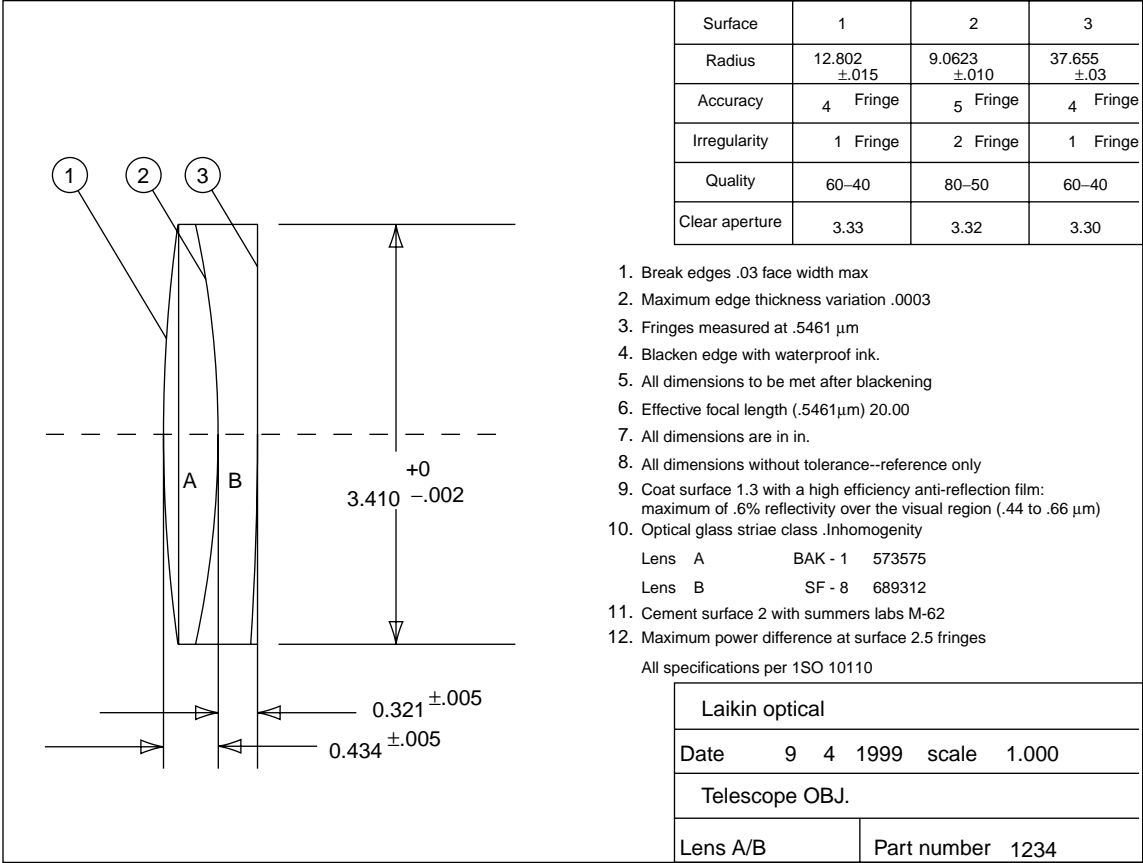


FIGURE 1.6 Lens drawing.

industry, (MIL-STD-34 and ISO standard 10110) not a true view as a mechanical engineer would create.

A few comments concerning this drawing are in order. Some companies would make this into three drawings: lens A, lens B, and a cemented assembly drawing. However, most optical shops would prefer to work with the single drawing. Diameter, center thickness, and radii are toleranced. *Accuracy* represents the total number of fringes seen when a test glass is applied to the surface. *Irregularity* is the difference in fringes between two perpendicular directions. All optical specifications apply only within the clear aperture.

With a cemented assembly, some designers prefer to have the positive element (the crown) somewhat smaller in diameter (perhaps 0.005–0.010) than the negative element. The smaller crown lens can then be moved during the cementing process to assure centration. The lens assembly is then located by the negative element. For this illustration, both elements were made the same diameter. Several points should be made concerning lens drawings:

1. All edges should have some break. This prevents chipping during manufacture and subsequent assembly.
2. Maximum deviation in minutes of arc is sometimes given, or minutes of arc maximum wedge.
3. Often, lenses are used at wavelengths other than the visual region (the IR), and it is therefore important to define the wavelength at which the accuracy and irregularity specification apply. Also, many shops are using the HeNe laser (0.6328  $\mu\text{m}$ ) in their testing.
4. Edges are often blackened to reduce stray light (veiling glare) in the system and prevent any edge build-up. For very high-energy laser systems, this is often deleted.
5. This is to prevent any edge buildup, not necessary if an ink is used.
6. EFL is a handy bit of information. It is an aid in testing of the completed element. It is a reference only, and is therefore not toleranced.
7. Most shops in the United States are on the inch system. If the lens is to be made elsewhere, millimeters would probably be the correct choice.
8. Reference dimensions are very convenient for test and manufacturing purposes. Sometimes lens edge thickness is indicated.
9. Coatings must be specified as to maximum reflectivity over some spectral region. With modern coating technology, the single-layer antireflection coating of a quarter wavelength of magnesium fluoride is now obsolete.
10. The six-digit code is per MIL-G174. Per this code, the first three digits indicate refractive index and the next three indicate dispersion. For the A lens,  $N_d = 1.573$  and  $V_d = 57.5$ . If not an optical glass (quartz, calcium fluoride, silicon, germanium, etc.) then more information as to the material specification must be given. (See also ANSI (1980) for an equivalent specification to MIL-O-13830.)
11. This is a thermosetting cement made by Summers Labs and Norland Products.
12. A large power difference is to be avoided at the cemented interface.

## COMPUTER USAGE

In 1965, I was in charge of a lens design group at EOS (a division of Xerox) in Pasadena. We were using Grey's programs on a CDC 6600. Because the machine was some distance (in El Segundo) from us, we key-punched our data decks and submitted them by overnight courier service. The next morning, our computer runs were brought in, along with punched cards giving the new prescription. Because we could get in only one computer run per day, we carefully thought out each run.

In 1968, I had an office in a computer facility and was then self-employed. Because all I had to do was turn in a data deck to the computer operator, I was able to submit many runs each day. Although my productivity increased, my computer bill also vastly increased.

Now, with a personal computer at my desk, I can get in many more computer runs than I had previously dreamed as possible. Being older and wiser, I now see the value of carefully analyzing a computer run before submitting another one. Most lens design programs print out a lot of very useful data in addition to the lens prescription: first-order data, third-order aberration contributions, tilt and decentration sensitivity data, intercept and path-length data, MTF, etc.

The designer should spend some time analyzing the results of his computer run before forging ahead and submitting another computer run. In this respect, a plot of the lens system is very helpful. Potential problems should be noted. Some of these are

- Large angles of incidence at a surface
- Very thick lenses
- Very thin lens edge
- Length of lens too long to meet system requirements
- Back focal length too short

However, there are occasions when many computer runs with very little thinking is justified. Two such cases are when one has difficulty ray-tracing due either to f-number or field angle. In such a situation, a method that works is to trace at the maximum aperture and field angle possible using all the curvatures, most of the air spaces (the large ones) and the positive lens thickness as variables. Then, for the next optimization run, simply increase the field angle or aperture. In this manner, the lens is "opened up" so that it traces to maximum aperture and field.

## PHOTOGRAPHIC LENSES

Below are some design considerations for photographic lenses. Keep in mind that this represents a generalization and is indicative of photographic lenses for single-lens reflex (SLR)-type cameras (see also Betensky (1980)).

1. Distortion. Distortion should usually be less than 2%. Distortion as high as 3% is tolerable for nonarchitectural scenes.
2. Focus. Since most lenses are focused at full aperture, shift should be less than 0.02 mm when going from wide-open to smallest aperture.

3. Vignetting. Vignetting of 20% can be tolerated at full aperture. There should be no vignetting at half the maximum aperture.
4. Veiling glare. Veiling glare of less than 1% is good, 3% is acceptable, and 6% is poor.
5. Spectral region. Due to the blue sensitivity of most films, it is important to trace from the  $h$  line ( $0.4046\ \mu\text{m}$ ), to the long wavelength at  $C$  ( $0.6563\ \mu\text{m}$ ) (Noffke et al. 2001). However, lenses for the graphic arts industries are generally used with orthochromatic emulsion films (Kodak #2556). A good choice would be  $h$  of  $0.4047\ \mu\text{m}$ ,  $F'$  of  $0.48\ \mu\text{m}$ , and  $e$  of  $0.5461\ \mu\text{m}$ .
6. High contrast for the spatial frequencies of 10–40 cycles/mm.
7. Acceptable image quality when focused from infinity to 10 focal lengths.

Although MTF data for all “visual” lenses (as used in this text) have weights and wavelengths as given previously (see Table 1.2), a better choice for strictly photographic use (considering the blue sensitivity) would be those in Table 1.4 (Betensky 1980).

- Iris. All photographic lenses are fitted with an iris (in contrast to projection lenses that have no iris). Sufficient clearance must be allowed: generally about 0.12 in. on both sides.
- High contrast for spatial frequencies of 10 to 40 cycles/mm.
- Capable of focus (and maintaining a satisfactory image) from infinity to 12 focal lengths. For low  $f$ -number lenses, one often uses a “macro” system in which a moving or “floating” element moves as the lens is focused to reduce spherical and coma aberrations.

## LENSES FOR USE WITH TV-TYPE SYSTEMS

These detectors are generally vidicon or charge-coupled devices. Because their spectral response curves are often different than a “visual” or photographic system, the designer should adjust the wavelength region accordingly.

Resolution for these types of systems are generally lower than for a photographic system. Also note that in electronic datasheets, resolution is often

---

**TABLE 1.4**  
**Wavelength vs. Weight for Photographic Lens**

Wavelength ( $\mu\text{m}$ )	Weight
0.4358	0.3
0.474	0.6
0.52	1.0
0.575	0.6
0.6438	0.3

---

expressed as “TV lines.” This represents the actual number of scan lines, not line pairs/mm, as in optical references. For example, consider a typical 1-in. vidicon (so called because the outside portion of the tube is 1 in. in diameter). It has a vertical height of 0.375 in. At 525 TV lines, its resolution would be

$$\frac{525}{(0.375)^2} \text{ lp/in.} = 28 \text{ lp/mm.}$$

Therefore, one wants high MTF response at low spatial frequencies. This is accomplished by reducing image flare. The ray pattern is then adjusted to trace more rays at the outer portion of the pupil.

Sometimes a system with a large dynamic range is required. Such lenses are generally fitted with an iris. Sometimes this iris is coupled to the photocathode to maintain a constant response as the ambient is changed. Unfortunately, the minimum practical diameter for an iris is about 1 mm. To increase the dynamic range, a neutral density spot is placed in close proximity to this iris (Busby 1972). In a typical system, this spot may only obscure 1% of the area at the aperture stop. If its transmittance is 0.5%, then the dynamic range has been increased by a factor of 200.

## LENSES FOR USE WITH A CCD

Both motion picture and still cameras are now available for film or with a charge-coupled device (CCD) as a detector. CCD as a detector has several advantages over film:

- Large dynamic range. This is the range of the largest to the smallest measurable signal. Typical ranges are greater than 65,000.
- Sensitive over a large wavelength region. This is generally from 0.3 to 0.9  $\mu$ .
- The output is digital and so is adaptable to instant viewing, digital editing, and processing.

## INFRARED SYSTEMS

Several computer programs consider both intercept error and path-length errors in their merit functions. These errors are weighted to achieve a balance between these types of errors. However, such a balance is generally based on visual correction. At much longer wavelengths, it is important to be able to manipulate the merit function to decrease the weight on path-length errors.

Narcissus is an important consideration in infrared systems (see [Chapter 17](#)). Following Howard and Abel (1982) and referring to [Figure 1.7](#), two unrelated paraxial rays are traced: a ray reflected from the detector, and a forward ray going toward the detector. The Lagrange invariant,  $\psi$ , is then

$$\Psi = H_r N' U - H N' U_r,$$

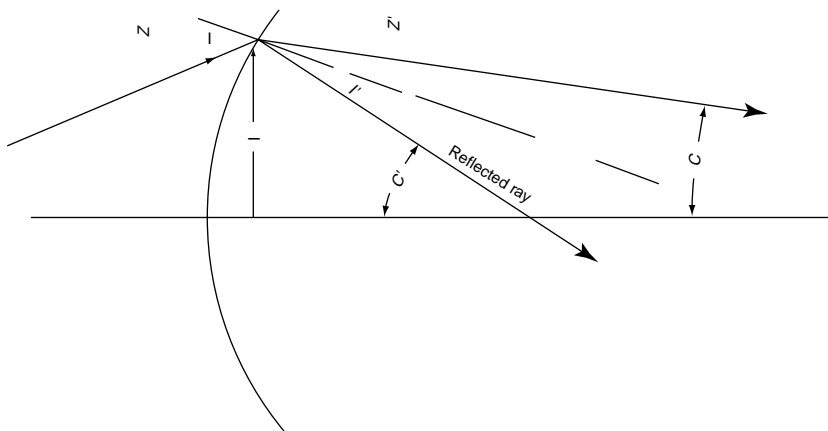


**FIGURE 1.7** Reflected ray in narcissus.

and because  $H_r = H$ , then  $\psi = HN'[U - U_r]$ , and

$$U_r = U + 2I' \quad \Psi = -HN'2I' = HN2I.$$

At the detector plane,  $\psi = H_r N' U'$ . Thus, the radius of the circular ghost at the detector plane,  $H_r$ , is

$$H_r = \frac{2HNI}{N'U'}.$$

It is helpful to have the value of  $HNI$  printed out, on a surface-by-surface basis, to determine if any surfaces will contribute to narcissus. This narcissus effect—the reflection of the detector back upon itself—is only of importance for surfaces prior to the scanning mirror. That is, a scanned reflection from a surface in front of the scanning mirror causes an AC signal, whereas reflections from surfaces past the scanner only cause a DC signal to be impressed upon the detector.

## UV SYSTEMS

The comments above concerning path-length errors vs. intercept errors apply here, as well. In this case, the weight on path-length errors should be increased (see [Chapter 18](#)).

## SECONDARY COLOR

Perhaps the most difficult aberration to control is secondary color. This becomes acute in long-focal-length, large- $f\#$  systems. In a typical visual system correction, the  $F'$  and  $C'$  foci are united behind the  $e$  focus. This longitudinal distance is approximately (focal length)/2000. The 2000 is a consequence of glass chemistry.

$$V = \frac{N_e - 1}{N_{f'} - N_{c'}},$$

$$P = \frac{N_{f'} - N_c}{N_{f'} - N_{c'}}.$$

If one plots all optical glasses for values of  $V$  vs.  $P$ , a near-straight line is obtained. This is shown in Figure 1.8, which is a plot of the readily available optical glasses along with some additional optical materials. To reduce secondary color, Conrady (1960:158) showed that it is necessary to use a material that departs from this “glass line.”

Unfortunately, there are only a few materials that depart from this glass line:

KZFS type glasses: N-KZFS4  
 FK type glasses: N-FK51 (Schott), S-FPL51, S-FPL52, S-FPL53 (Ohara), FCD1, FCD10 (Hoya), and calcium fluoride (actually not a glass but a cubic crystal)

Be careful when selecting some of these materials because they are not always readily available, are fairly expensive, subject to stain, and have high thermal expansion. To reduce secondary color with N-KZFS4 glass, it, like all materials to the left of the glass line, should be a negative lens. Unfortunately, its departure from the glass line is not great enough to be very effective in secondary color reduction.

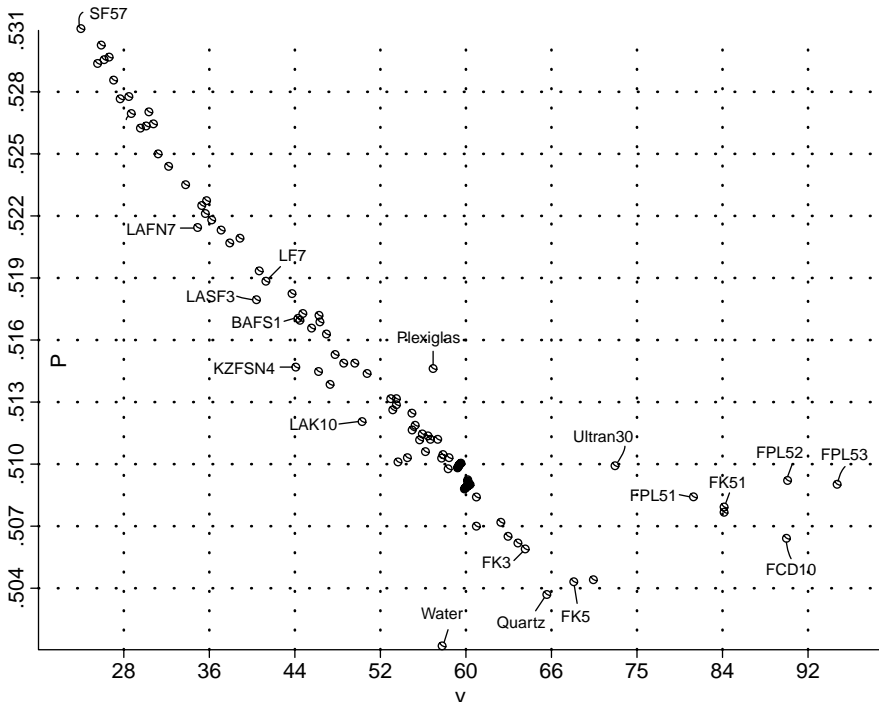


**FIGURE 1.8** Secondary color chart.



As can be seen from [Figure 1.8](#), some of the FK materials and calcium fluoride greatly depart from the glass line. Calcium fluoride is a very transparent cubic crystal, expensive (in comparison to optical glasses), fragile, soft, very slightly hygroscopic, and has a very high thermal expansion coefficient. It is used extensively in microscope objectives (fluorite) because the material costs in small diameters becomes insignificant. N-FK51, S-FPL51, S-FPL52, S-FPL53, FCD1, FCD10, and FCD100 are glasses with a high expansion coefficient and therefore some optical shops feel it is difficult to polish. Some of these FK materials are prone to striae. None of these materials should be used as an exterior element in an optical system. Because they lie to the right of the glass line, they become positive lenses when used for secondary color correction. S-FPL53 is a relatively new material and it promises to be the most effective way to reduce secondary color. Its values of  $V$  and  $P$  are very close to those of  $\text{CaF}_2$ .

## THE DIFFRACTION LIMIT

For an optical system with a uniformly (incoherent) illuminated, circular entrance pupil:

$$\text{Depth of Focus} = 2\lambda(f\#)^2(1 + m)^2,$$

$$\text{Resolution} = \frac{1000 \text{ lp/mm}}{\lambda f\#(1 + m)} = \frac{1818 \text{ lp/mm}}{f\#(1 + m)} \text{ at } \lambda = 0.55 \text{ } \mu\text{m},$$

$$\text{Radius of Airy disc} = 1.22 \lambda f\#(1 + m),$$

where  $\lambda$  is wavelength in  $\mu\text{m}$ ,  $m$  is the absolute value of the magnification (equal to zero for an object at infinity),  $f$  is the ratio of focal length/entrance-pupil diameter.

This is the basis of the Raleigh criterion of resolution. Raleigh felt that he could resolve two objects that were an Airy disc-radius apart. According to the Sparrows criterion, a designer can achieve results somewhat better than this. Using this criterion:

$$\text{Least linear separation resolvable} = \lambda f\#(1 + m).$$

If the system is not diffraction limited and has a resolution of  $R$  in lp/mm, then

$$\text{Depth of focus} = 2f\#(1 + m)/R.$$

## DEPTH OF FIELD

Consider a lens of focal length  $F$ , with an entrance-pupil diameter of  $A$ , and focused at an object a distance  $D$  away; then the hyperfocal distance,  $H$ , is given by

$$H = \frac{F^2}{F\#B}.$$

This assumes that  $H \gg F$ , where  $F\# = F/A$ , and  $B$  is the spot-size diameter of an acceptable image. For most cinematography cases,  $B = 0.025 \text{ mm}$ .

The near distance at which the lens is acceptably sharp is (Smith 2000):

$$\frac{HD}{H + D - F} \cong \frac{F^2 D}{F^2 + f^{\#} BD} \text{ for } D \gg F,$$

and the far limit is

$$\frac{HD}{H - D + F} \cong \frac{F^2 D}{F^2 - f^{\#} BD} \text{ for } D \gg F.$$

For  $H \gg F$  and  $D = H$  (the hyperfocal distance), then it is acceptably sharp from  $H/2$  to infinity. In the usual photographic lens, values of these near and far limits are engraved on the lens housing such that the photographer may note these limits for the various settings of his iris.

## DIFFRACTION-LIMITED MTF

Consider a lens with a uniformly illuminated entrance pupil in incoherent light. The MTF response,  $T$ , is then

$$T = \frac{2 [\arccos(K) - K(1 - K^2)^{1/2}]}{\pi},$$

where  $K$  is the normalized spatial frequency ( $K = S\lambda f^{\#}$ ) and  $S$  is the spatial frequency in lp/mm for which one wants to find the response.  $K$  then lies between 0 and 1.

For easy computation of MTF diffraction-limited response, [Table 1.5](#) gives values of  $K$  vs.  $T$ . Consider, for example, a 50-mm  $f/2.8$  photographic lens ( $\lambda = 0.55 \mu\text{m}$ ); then,

$$\frac{1.0}{\lambda f^{\#}} = 649 \text{ lp/mm},$$

which is the diffraction limit. Therefore, at  $S = 100 \text{ lp/mm}$ ,  $K = 0.15$ . Referring to the table, the response is 0.81 (of course, most photographic lenses are not diffraction limited at  $f/2.8$ ).

## LASER OPTICS

A strictly Gaussian beam in its fundamental transverse mode has a beam profile given by (O'Shea 1985; Siegman 1971):

$$I = I_0 e^{-2R^2/W^2},$$

where  $I_0$  is intensity at the center of the beam,  $R$  is a distance measured from the beam center, and  $W$  is the beam radius where the intensity is reduced to  $1/e^2 I_0$ . This beam profile is shown in [Figure 1.9](#).

Most gas laser systems have such a Gaussian beam profile. When the laser manufacturer lists the beam diameter as  $d$  ( $d = 2W$ ), it corresponds to the  $1/e^2$  intensity

---

**TABLE 1.5**  
**Diffraction-Limited MTF Response**

<b><i>K</i></b>	<b><i>T</i></b>
0.02	0.97
0.04	0.95
0.06	0.92
0.08	0.90
0.10	0.87
0.12	0.85
0.14	0.82
0.16	0.80
0.18	0.77
0.20	0.75
0.22	0.72
0.24	0.70
0.26	0.67
0.28	0.65
0.30	0.62
0.32	0.60
0.34	0.58
0.36	0.55
0.38	0.53
0.40	0.50
0.42	0.48
0.44	0.46
0.46	0.44
0.48	0.41
0.50	0.39
0.52	0.37
0.54	0.35
0.56	0.33
0.58	0.31
0.60	0.28
0.62	0.26
0.64	0.24
0.66	0.23
0.68	0.21
0.70	0.19
0.72	0.17
0.74	0.15
0.76	0.14
0.78	0.12
0.80	0.10
0.82	0.09
0.84	0.07
0.86	0.06

---

*(continued)*

**Table 1.5** (Continued)

<i>K</i>	<i>T</i>
0.88	0.05
0.90	0.04
0.92	0.03
0.94	0.02
0.96	0.01
0.98	0.00

value (0.135). Within this diameter is 86% of the power. Within a diameter of  $1.5d$  is 99% of the power. It is thus common practice to design laser optical systems (focusing lenses, beam expanders, etc.) to accommodate this  $1.5d$ . (For very high-power systems,  $2d$  is often used; it then contains 99.97% of the total power.)

Within close proximity to the laser is the beam waist. Beyond this waist, the beam expands (hyperbolic). The full angle beam divergence at a distance from this waist is given by  $1.27\lambda/d$  (Kogelnik and Li 1966).

Some common laser lines are given in [Table 1.6](#).

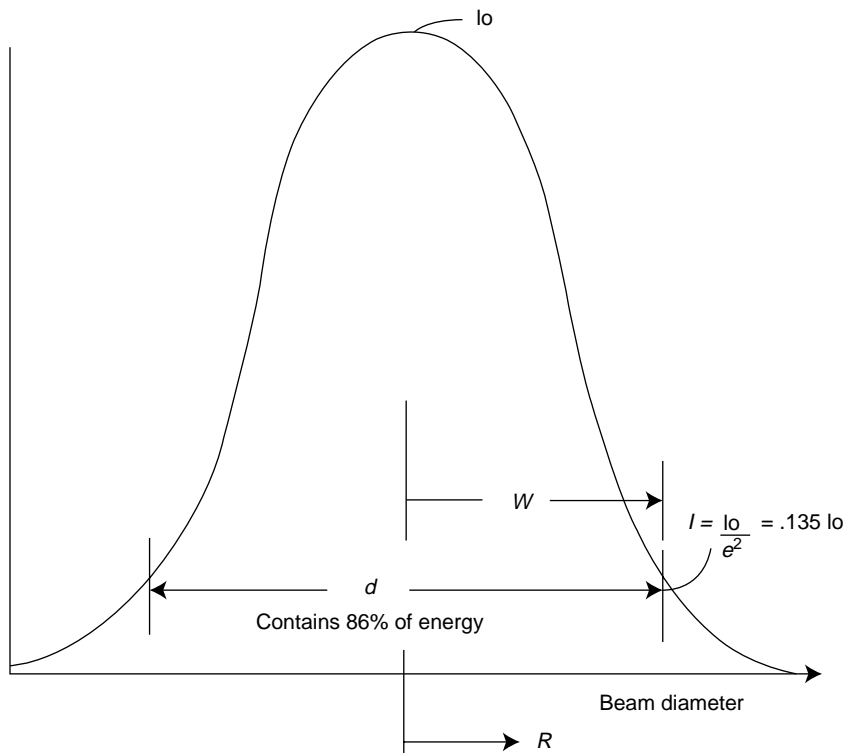


**FIGURE 1.9** Intensity versus beam diameter for a Gaussian beam.

**TABLE 1.6**  
**Some Common Laser Lines**

Laser	Strongest Lines (μm)
F <sub>2</sub>	0.157
Xe <sub>2</sub>	0.172
ArF excimer	0.1934
KrCl	0.222
KrF excimer	0.248
XeCl excimer	0.308
XeF excimer	0.351
Helium cadmium	0.4416
Argon ion	0.4880, 0.5145 (lines from 0.45 to 0.53)
Helium neon	0.6328
Krypton ion	0.6471, 0.6764 (lines from 0.46 to 0.68)
Ruby	0.6943
Nd:YAG	1.064
Erbium fiber	1.550–1.567 tuneable
Erbium/YAG	2.94
Carbon dioxide	10.59

Source: Weber, M. J., *Handbook of Laser Wavelengths*, CRC Press, New York, 1998.

**REFERENCES**

American National Standards Institute (1980) Definitions, methods of testing, and specifications for appearance of imperfections of optical elements and assemblies, PH3.617, American National Standards Institute, New York.

Betensky, E. (1980) Photographic lenses, In *Applied Optics and Optical Engineering*, Volume 8 (R. Shannon and J. Wyant eds.) Academic Press, New York.

Bociort, F., Serebriakov, A., and Braat, J. (2002) Local optimization strategies to escape from poor local minimum, *International Lens Design Conference 2002, SPIE* Volume 4832, p. 218.

Born, M. and Wolf, E. (1965) *Principles of Optics*, Pergamon Press, New York.

Brixner, B. (1978) The merit function in lens design, *Appl. Opt.*, 17: 715.

Buchdahl, H. A. (1968) *Optical Aberration Coefficients*, Dover Publications, New York.

Busby, E. S. (1972) Variable light transmitting filter for cameras, US Patent #3700314.

Conrady, A. E. (1960) *Applied Optics and Optical Design*, Part 2, Dover Publication, New York, p. 659.

Cox, A. (1964) *A System of Optical Design*, Focal Press, London.

Eastman Kodak Co., *Optical Formulas and Their Application*, Kodak Publication AA-26, Eastman Kodak.

Feder, D. (1957a) Automatic lens design methods, *JOSA*, 47: 902.

Feder, D. (1957b) Calculation of an optical merit function and its derivatives, *JOSA*, 47: 913.

Feder, D. (1962) Automatic lens design with a high speed computer, *JOSA*, 58: 1494.

Feder, D. (1968) Differentiation of ray tracing equations, *JOSA*, 52: 1494.

- Fischer, R. E., ed. (1978) *Computer Aided Optical Design, Proc. SPIE*, Volume 147, Bellingham, WA.
- Fischer, R. E., ed. (1980) *International Lens Design Conference, Proc. SPIE*, Volume 237, Bellingham, WA.
- Forbes, G. and Jones, A. (1991) Towards global optimization with adaptive simulated annealing, *SPIE*, 1354: 144.
- Forbes, G. and Jones, A. (1992) Global optimization in lens design, *Opt. Photonics News*, 3: 22.
- Forbes, G. and Jones, A. (1995) An adaptive simulated annealing algorithm for global optimization over continuous variables, *J. Global Optim.*, 6: 1.
- Ginsberg, R. H. (1981) An outline of tolerancing, *Opt. Eng.*, 20: 175.
- Ginter, H. (1990) An enhancement of Conrady's D-d method, *1990 International Lens Design Conference, Proc. SPIE*, volume 1354, p. 97.
- Grey, D. (1963) Aberration theories for semi-automatic lens design by electronic computers, *JOSA*, 53: 672–680.
- Grey, D. (1970) Tolerance sensitivity and optimization, *Appl. Opt.*, 9: 523.
- Grey, D. (1978) The inclusion of tolerance sensitivities in the merit function for lens optimization, *Proc. SPIE*, 147: 63.
- Herman, R. M. (1985) Diffraction and focusing of gaussian beams, *Appl. Opt.*, 24: 1346.
- Hopkins, H. H. and Tiziani, H. J. (1966) A theoretical and experimental study of lens centering errors, *Br. J. Appl. Phys.*, 17: 33.
- Hopkins, R., McCarthy, C. A., and Walters, R. M. (1955) Automatic correction of third order aberrations, *JOSA*, 45: 365.
- Howard, J. W. and Abel, I. R. (1982) Narcissus; reflections on retroreflections in thermal imaging systems, *Appl. Opt.*, 21: 3393.
- Institute of Optics (1967) *Lens Design with Large Computers, Proceedings of the Conference*, Rochester, NY.
- International Lens Design Conference (1985) at Cherry Hill, NJ, Technical Digest SPIE, Bellingham, WA.
- ISO Standard 10110 (1995) American National Standards Institute, 11 West 42nd Street, New York, NY 10036.
- Jamieson, T. H. (1971) *Optimization Techniques in Lens Design*, American Elsevier, New York.
- Kimmel, R. and Parks, R. E. (1995) *ISO 10110, Optics and Optical Instruments*, American National Standards Institute, New York, NY 10036.
- Kingslake, R. (1978) *Lens Design Fundamentals*. Academic Press, New York.
- Kingslake, R. (1983) *Optical System Design*. Academic Press, New York.
- Kingslake, R. (1989) *History of the Photographic Lens*, Academic Press, New York.
- Koch, D. G. (1978) A statistical approach to lens tolerancing, *Proc. SPIE*, 147: 71.
- Kodak, *Optical Formulas and Their Application*, Kodak Publication AA-26.
- Kogelnik, H. and Li, T. (1966) Laser beams and resonators, *Proc IEEE*, 54: 1312; see also *Appl. Opt.*, 5: 1550.
- Lavi, A. and Vogl, T. P. eds. (1966) *Recent Advances in Optimization Techniques*, Wiley, New York.
- Lawson, L. L. and Hanson, R. J. (1974) *Solving Least Squares Problems*, Prentice Hall, Englewood Cliffs, NJ.
- Malacara, D. (1978) *Optical Shop Testing* Wiley, New York.
- Meiron, J. (1959) Automatic lens design by the least squares method, *JOSA*, 49: 293.
- Military Standard, Preparation of Drawings for Optical Elements, MIL-STD-34.
- Military Standardization Handbook, MIL HBK-141 (1962) Govt. Printing Office, Washington, DC 20402.

- Noffke, J. W., Achtner, B., Gangler, D., and Schmidt, E. (2001) The new ultra-primess, *Proc. SPIE*, 4441: 9
- Norland Products Inc. (1999) *Products catalog*. New Brunswick, NJ, Norland Products.
- O'Shea, D. C. (1977) *Introduction to Lasers and Their Application*, Addison-Wesley, New York.
- O'Shea, D. C. (1985) *Elements of Modern Optical Design*, Wiley Interscience, New York.
- O'Shea, D. C. and Thompson, B. J. eds. (1988) *Selected Papers on Optical Mechanical Design Proc. SPIE*, Volume 770, Bellingham, WA.
- Palmer, J. M. (1971) *Lens Aberration Data*, American Elsevier Publishing, New York.
- Rancourt, J. D. (1996) *Optical Thin Films, User Handbook*, SPIE, Bellingham, WA.
- Reitmayer, F. and Schroder, H. (1975) Effect of temperature gradients on the wave aberration in a thermal optical systems, *Appl. Opt.*, 14: 716.
- Rimmer, M. P. (1978) A tolerancing procedure based on modulation transfer function, *Proc. SPIE*, 147: 66.
- Rosen, S. and Eldert, C. (1954) Least squares method for optical correction, *JOSA*, 44: 250–252.
- Siegman, A. E. (1971) *Introduction to Lasers and Masers*, McGraw-Hill, New York.
- Smith, W. (1990) Fundamentals of optical tolerance budget, *1990 International Lens Design Conference, Proc. SPIE*, Volume 1354, p. 474.
- Smith, W. (2000) *Modern Optical Engineering*. McGraw-Hill, New York.
- Starke, J. P. and Wise, C. M. (1980) MTF based optical sensitivity and tolerancing programs, *Appl. Opt.*, 19: 1768.
- Summers Laboratories. (1999) *Summer Laboratories Catalog*, Fort Washington, PA, Summer Laboratories.
- Tamagawa, Y. and Tajime, T. (1996) Expansion of an athermal chart into a multilens system, *Opt. Eng.*, 35: 3001.
- Tamagawa, Y. and Wakabayashi, W. (1994) System with athermal chart, *Appl. Opt.*, 33: 8009.
- Tatian, B. (1984) Fitting refractive index data with the Sellmeier dispersion formula, *Appl. Opt.*, 23: 4477.
- Tuchin, G. D. (1971) Summing of optical systems aberrations caused by decentering, *Sov. J. Opt. Technol.*, 38: 546.
- Unvala, H. A. (1966) The orthonormalization of aberrations AD- 640395, Available from NTIS, Springfield, VA.
- Wang, J. (1972), Tolerance conditions for aberrations, *JOSA*, 62: 598.
- Weber, M. J. (1998) *Handbook of laser wavelengths*, CRC Press, New York.
- Welford, W.T (1986) *Aberrations of Optical Systems*, Adam Hilger, Bristol.
- Wiley, R. R. (1990) Anti-reflection coating for high index cemented doublets, *Appl. Opt.*, 29: 4540.
- Yamaguchi, S., Sato, H., Mori, N., and Kiriki, M. (2005) Recent technology and usage of plastic lenses in image taking objectives, *Proceedings of SPIE*, Volume 5874, p. 58720E.





## 2 The Achromatic Doublet

Consider two thin lenses with a real and distant object with a combined effective focal length of  $F$ . Let  $F_a$  be the focal length of the a lens (facing the long conjugate) with a  $V$  value of  $V_a$ , and likewise for the b lens. Then (Kingslake 1978:80),

$$F_a = \frac{(V_a - V_b)F}{V_a} \quad \text{and} \quad F_b = \frac{(V_b - V_a)F}{V_b}.$$

Using thin-lens  $G$ -sum formulae (Smith 2000:338; Ingalls 1953:208) to obtain a lens system with zero third-order spherical aberration and coma, the following algorithm for a thin lens achromatic doublet is obtained:

- Select materials:  $V_a, N_a, V_b, N_b$ , and system focal length  $F$
- Determine  $F_a$  and  $F_b$  from above equations
- $C_a = \frac{1}{F_a(N_a - 1)}$ ;  $C_b = \frac{1}{F_b(N_b - 1)}$
- $H = (G8b)(C_b^2) - (G8a)C_a^2 - (G7b)C_b/F$
- $XI = (G5a)C_a/4$ ;  $XK = (G5b)C_b/4$
- $A = (G1a)C_a^3 + (G1b)C_b^3 - (G3b)C_b^2/F + (G6b)C_b/F^2$
- $B = -(G2a)C_a^2$ ;  $E = (G4a)C_a$ ;  $XJ = (G4b)C_b$
- $D = (G2b)C_b^2 - (G5b)C_b/F$ ;  $P = A + H(XJ*H/XK - D)/XK$
- $Q = B + XI(2XJ*H/XK - D)/XK$ ;  $R = E + XJ(XI/XK)^2$
- $ROOT = Q^2 - 4P*R$  (Check for negative root)
- $C1 = \frac{-Q + \sqrt{ROOT}}{2R}$  (King 1993)
- $C4 = -(H + XI*C1)/XK$ ;  $C2 = C1 - C_a$ ;  $C3 = C_b + C4$

In the above equations,  $G1a$  is the  $G1$  sum for the a lens,  $G8b$  is the  $G8$  sum for the b lens, etc. (see Smith [2000]); i.e.,  $G8 = N(N - 1)/2$ , etc. The symbol  $*$  denotes multiplication as used in most of the programming languages.  $C1, C2, C3$ , and  $C4$  are the surface curvatures. It is important to realize that various authors (Buchdahl 1985; Robb 1985; Sigler 1986) have provided data on selecting glasses for the paraxial thin lens correction of chromatic aberration at several wavelengths. To achieve this correction, it is required to use materials “off the glass line” such as N-FK51. When one optimizes such solutions to obtain a reasonable correction over a modest field and with actual lens thickness, the apochromatic correction is balanced against the trigonometric aberrations.

This algorithm has been programmed on the author’s computer to rapidly arrive at a thin lens, third-order solution as a start for lens optimization (Table 2.1). A similar program is discussed by Reidl (1981). The ATMOS program by R. Massimo

**TABLE 2.1**  
**Thin-Lens, Third-Order Solution for an Achromat**

<i>Na</i>	<i>Va</i>	<i>Nb</i>	<i>Vb</i>	<i>C1</i>	<i>C2</i>	<i>C3</i>	<i>C4</i>
4.0031	701.4	2.4054	34.20	0.1005	0.0655	−0.0378	−0.0341
1.5187	63.96	1.6522	33.60	0.1646	−0.2415	−0.2404	−0.0707
1.5712	55.70	1.6241	36.11	0.1573	−0.3405	−0.3376	−0.0422
1.5749	57.27	1.6522	33.6	0.1567	−0.2642	−0.2631	−0.0454
1.4610	8.648	1.4980	6.195	0.1726	−0.5921	−0.5835	−0.0764
3.4313	420.2	4.0301	188.4	0.1046	0.0300	0.0241	0.0509
2.2524	233.1	1.3572	29.53	0.1123	0.0209	−0.0500	−0.0094
1.7125	128.53	1.5183	101.24	0.2551	−0.4058	−0.4573	0.2583

(Appendix D) provides a simple way to design a telescope objective. Several examples are now given for a focal length of 10.

The first case is germanium and zinc selenide, 8–14- $\mu\text{m}$  region. Then follows three combinations for the visual region: N-BK7 and SF2 glass; N-BAK4 and F2 glass; N-BAK1 and SF2 glass. Next is a UV doublet with  $\text{CaF}_2$  and quartz (silica). The next two cases are for the infrared region 3.2–4.2  $\mu\text{m}$ ; a silicon–germanium combination, followed by IRTRAN2–IRTRAN1 doublet; last is SF4, N-BAK2 for the 1.8–2.2- $\mu\text{m}$  region. This last case was optimized and shown in Figure 17.5.

The second case was scaled to a focal length of 48 for an  $f/8$  telescope objective with a field of view of  $1.5^\circ$ . It was optimized and is shown as Figure 2.1. The data for this lens follows in Table 2.2.

Figure 2.2 shows a cemented achromat,  $f/6$  of 20-in. focal length. Field of view is  $1.5^\circ$ . The data for this lens is given in Table 2.3.

In both of these designs, the entrance pupil is in contact with the first lens surface. As is typical with such designs, the off-axis sagittal MTF is better than tangential. Due to the small field of view and large  $f$ -number, the main aberrations are secondary color and field curvature. Longitudinal secondary color is approximately equal to focal length divided by 2000.

The radius of the Petzval surface (for a single thin lens) is equal to  $-NF$ . However, in the above doublet case,  $R_p = -1.45F$ . Due to the presence of astigmatism, the best image surface radius is substantially shorter than this, approximately 0.48 focal length.

These same equations may be used to obtain a lens of negative focal length, the so called Barlow Lens (Ingalls 1953). For a focal length achromat of  $-10$ , simply change the sign of the curvatures as given in Table 2.1. Figure 2.3 shows a 10-in. focal length cemented achromat. It is  $f/5$  and covers a  $3^\circ$  field of view. Data for this lens is given in Table 2.4.

As discussed earlier, to reduce secondary color, a material that is off the glass line must be selected. For three thin lenses in contact, the value

$$\sum \frac{\varphi_i P_i}{V_i}$$

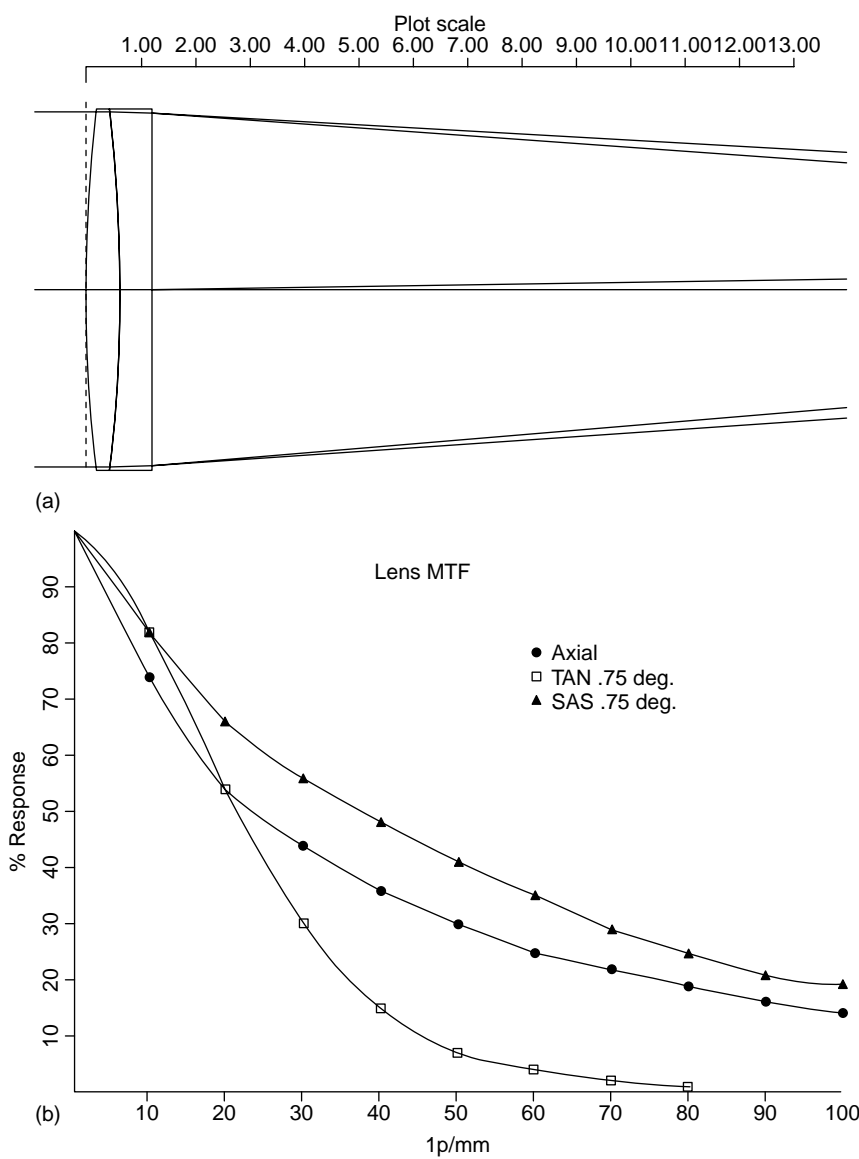


FIGURE 2.1 48-in. focal length achromat.

must be zero, where  $\varphi_i$  is the lens element power, and (Knetsch 1970)

$$V_i = \frac{N_e - 1}{N_f - N_c},$$

$$P_i = \frac{N_f - N_e}{N_f - N_c}.$$

**TABLE 2.2**  
**A 48-in. EFL, f/8 Telescope Objective**

Surface	Radius	Thickness	Material	Diameter
1	29.32908	0.7000	N-BK7	6.100
2	−20.06842	0.0320	Air	6.100
3	−20.08770	0.5780	SF2	6.000
4	−66.54774	47.3562	Air	6.100

Distance from first lens surface to image =48.666.

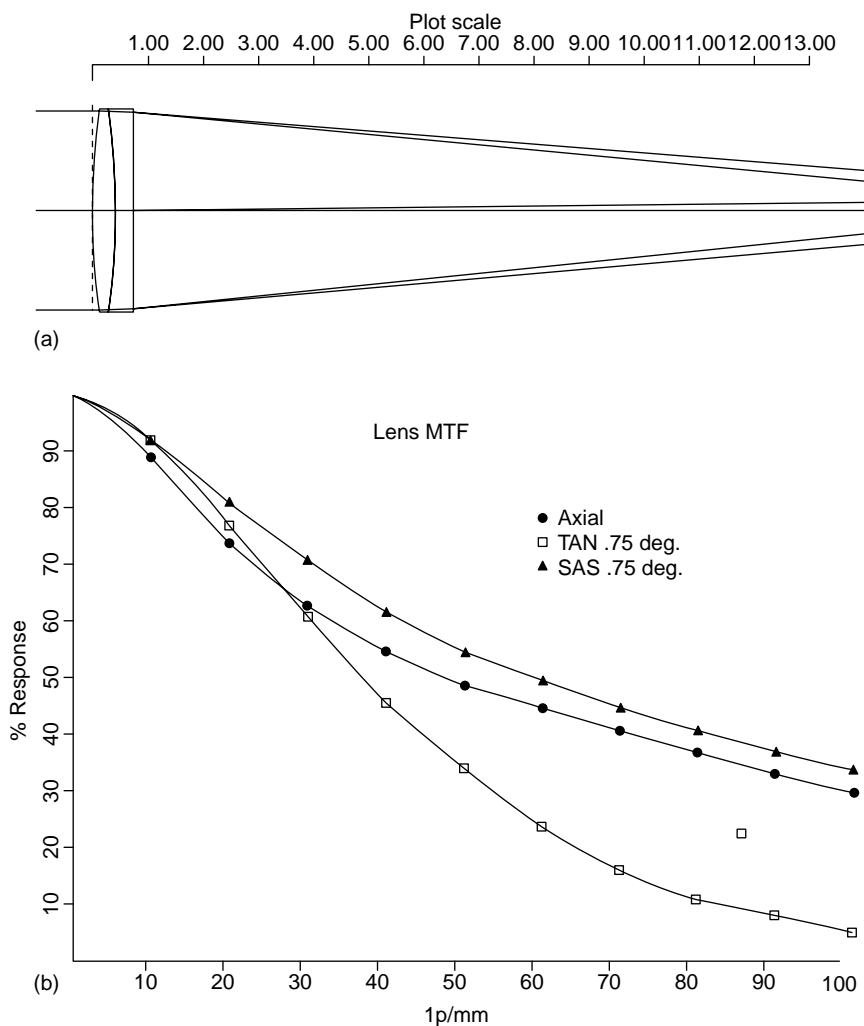


**FIGURE 2.2** Cemented achromat, 20-in. focal length.

**TABLE 2.3**  
**Cemented Achromat,  $f/6$ , 20-in. Focal Length**

Surface	Radius	Thickness	Material	Diameter
1	12.38401	0.4340	N-BAK1	3.410
2	−7.94140	0.3210	SF2	3.410
3	−48.44396	19.6059	Air	3.410

Distance from first lens surface to image = 20.361.

McCarthy (1955) shows an interesting way to greatly reduce secondary color with only two ordinary glass types. The patent shows two cemented doublets (N-BK7 and F4) separated by a large distance. The first doublet is nearly afocal, whereas the second has all of the system power. The separation between the lenses is the focal length of the rear doublet. Blakley (2003) discusses correction of lateral color with dialyte systems.

Figure 2.4 is a cemented, three-element lens with greatly reduced secondary color. The data for this lens is given in Table 2.5.

Entrance pupil is in contact with the first lens surface. Like the above achromat (Figure 2.2), it is  $f/6$ , 20-in. focal length and has a field of view of  $1.5^\circ$ . The longitudinal secondary color is approximately one-third that of the design shown in Figure 2.2. This greatly improves the axial MTF. However, the off-axis is limited by astigmatism, which is about the same as for the above achromat (Figure 2.2).

Figure 2.5 shows a telescope objective suitable for amateur astronomy. It has a 48-in. focal length, is  $f/6$ , has a field of view of  $0.75^\circ$ , and is very nearly diffraction limited. To be useful for photography, it is corrected over the wavelength region 0.436–0.707  $\mu\text{m}$ . The prescription for this is listed in Table 2.6.

Unfortunately, this lens is an expensive lens to build due to the large-diameter calcium fluoride element. Surprisingly, an achromatic lens (actually a “pseudo” achromat) may be made with only one type of glass.

Consider two thin lenses,  $F_1$  and  $F_2$ , separated by a distance  $D$ . The back focal length (BFL) is given by

**TABLE 2.4**  
**Cemented Achromat,  $f/6$ , 10-in. Focal Length**

Surface	Radius	Thickness	Material	Diameter
1	6.4971	0.3500	N-BAK1	2.100
2	−4.9645	0.2000	SF1	2.100
3	−17.2546	9.7267	AIR	2.100

Distance from the first lens surface to image = 10.277.

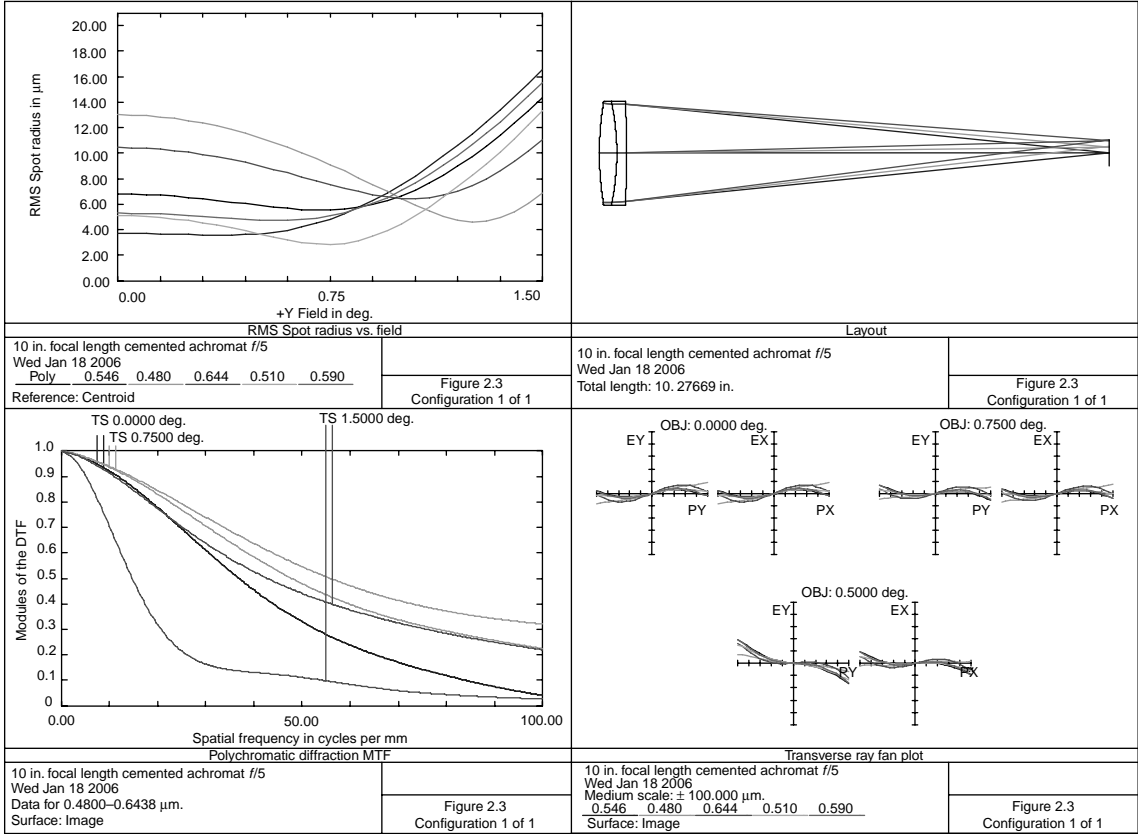


FIGURE 2.3 Cemented achromat, 10-in. focal length.

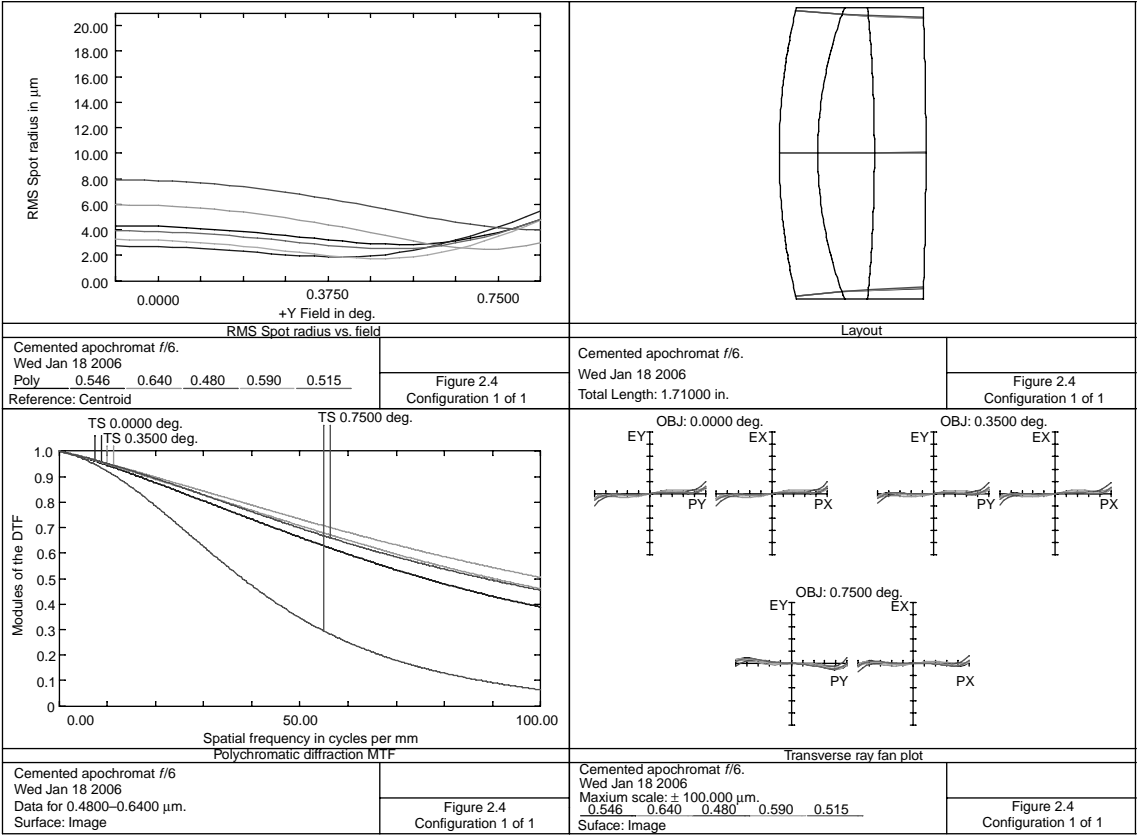


FIGURE 2.4 Cemented achromat.

**TABLE 2.5**  
**Lens with Reduced Secondary Color**

Surface	Radius	Thickness	Material	Diameter
1	7.28125	0.4500	N-SSN5	3.400
2	4.76851	0.6600	S-FPL53	3.400
3	−18.53124	0.6000	N-BAK1	3.400
4	−47.21180	18.7923	Air	3.400

Distance from first lens surface to image = 20.502.

$$\text{BFL} = \frac{(F_1 - D)}{F_1 + F_2 - D}.$$

Differentiating to determine  $\partial \text{BFL} / \partial \lambda$  and setting this to zero:

$$D = F_1 \pm \sqrt{-F_1 F_2}.$$

For example, if  $N=1.5$ ,  $F_1=20$ , and  $F_2=-10$ , then  $D=5.8578$ ,  $\text{EFL}=-48.284$ , and  $\text{BFL}=-34.142$ . Note that this is not a true achromat because two wavelengths are not united at a common focus. The BFL change with wavelength is now a minimum, so this is only of value over a limited wavelength region. Also, the negative EFL and BFL is a problem (see also Malacara and Malacara [1994]).

**TABLE 2.6**  
**A 48-in. Telescope Objective**

Surface	Radius	Thickness	Material	Diameter
0	0.0000	0.100000E+11		0.00
1	−12.7172	0.8000	N-PSK3	7.960
2	−18.5430	0.0148		8.400
3	Stop	0.0150		8.181
4	15.7580	1.6701	CAF2	8.400
5	−13.0390	0.0487		8.400
6	−12.8310	0.8000	S-LAL18	8.240
7	−18.5430	1.1799		8.400
8	9.8197	0.8000	N-SK16	8.400
9	8.0010	44.3502		7.320
10	0.0000	0.0000		0.629

Distance from first lens surface to image = 49.678.



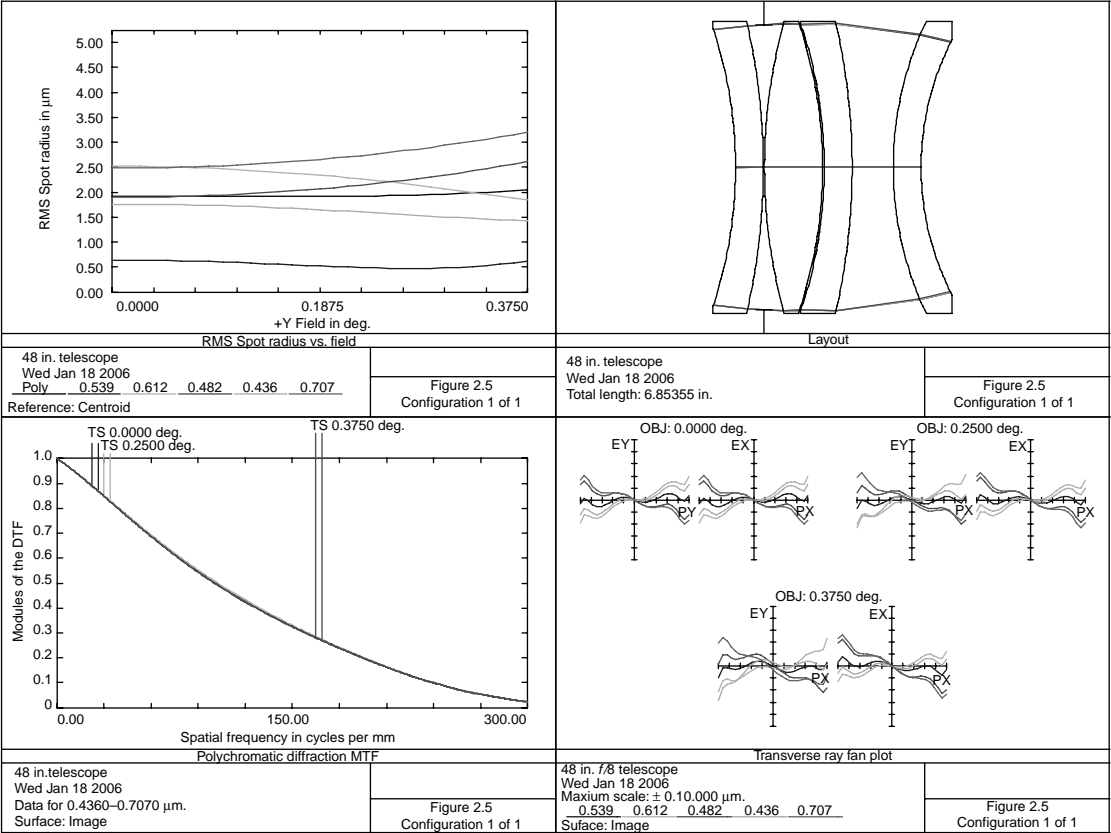


FIGURE 2.5 Forty-eight-in. focal length telescope objective.

## REFERENCES

- Blakley, R. (2003) Dialyte refractor design for self-correcting lateral color, *Opt. Eng.*, 42: 400.
- Buchdahl, H. A. (1985) Many-color correction of thin doublets, *Appl. Opt.*, 24: 1878.
- Hariharan, P. (1997) Apochromatic lens combinations, *Opt. Laser Technol.*, 4: 217.
- Hastings, C. S. (1889) Telescope objective, US Patent #415040.
- Hopkins, R. E. (1955) Automatic design of telescope objectives, *JOSA*, 45: 992.
- Ingalls, A. G., ed., (1953) *Amateur Telescope Making*, Book 3, Scientific American, New York, p. 208.
- King, S. (1993) Personal correspondence. I would like to thank him for pointing out a subtle error in the first edition.
- Kingslake, R. (1978) *Lens Design Fundamentals*, Academic Press, New York.
- Knetsch, G. (1970) Three Lens Objective with good correction of the secondary spectrum, US Patent #3536379.
- Kutsenko, N. I. (1975) The calculation of thin three lens cemented components, *Sov. J. Opt. Technol.*, 45: 82.
- Lessing, N. W. (1957) Selection of optical glasses in apochromats, *JOSA*, 47: 955.
- Malacara, D. and Malacara, Z. (1994) Achromatic aberration correction with only one glass, *Proc. SPIE*, 2263: 81.
- McCarthy, E. L. (1955) Optical system with corrected secondary spectrum, US Patent #2698555.
- Rayces, J. L. and Aguilar, M. R. (1999) Differential equation for normal glass dispersion, *Appl. Opt.*, 38: 2028.
- Rayces, J. L. and Aguilar, M. R. (2001) Selection of glasses for achromatic doublets, *Appl. Opt.*, 40: 5663.
- Reidl, M. (1981) The thin achromat, *Electro-Opt. Syst. Des.*, Sept: 49.
- Robb, P. N. (1985) Selection of optical glasses, 1: two materials, *Appl. Opt.*, 24: 1864.
- Sigler, R. D. (1986) Glass selection for air spaced apochromats using the Buchdahl dispersion equation, *Appl. Opt.*, 25: 4311.
- Smith, W. (2000) *Modern Optical Engineering*, McGraw-Hill, New York.
- Szulc, A. (1996) Improved solution for the cemented doublet, *Appl. Opt.*, 35: 3548.
- Überhagen, F. (1970) Doublet which is partially corrected spherically, US Patent #3511558.

# 3 The Air-Spaced Triplet

The air-spaced triplet is sometimes referred to as a *Cooke triplet*. It was developed by Harold Dennis Taylor in 1894 (he worked for a company in York, England: T. Cooke and Sons). There are enough degrees of freedom to design an anastigmat lens. Referring to [Figure 3.1](#), for a series of three thin lenses (note that although the lenses are thin, the air spaces separating them are appreciable), the Petzval sum, longitudinal chromatic, and lateral color are set to zero as system power is controlled. Assume that the materials for the first and third lenses are the same that the stop is at the second lens, and a distant object.

- $F_a = 1/P_a$ , where  $P_a$  is the power of the first lens, etc.
- $TR = T_2/T_1$
- $T_3 = \frac{[(F_a - T_1)F_b - (F_a + F_b - T_1)T_2]F_c}{(F_a - T_1)F_b + (F_a + F_b - T_1)(F_c - T_2)}$  (3.1)

- $X = T_3PTR$ , where  $P$  is the power of the lens assembly
- $P_b = \frac{1}{F_b} = -P_c N_b \frac{X+1}{N_a}$  (3.2)

- $P_a = XP_c$  (3.3)

- $P = P_a + P_b + P_c - T_1 P_a (P_b + P_c) - T_2 P_c (P_a + P_b) + T_1 T_2 P_a P_b P_c$  (3.4)

- $P_c = \frac{1/X - \sqrt{[(X/TR^2 + 1)V_b N_a / (V_b N_a / (V_a X N_b (X + 1)))]}}{T_1}$  (3.5)

The algorithm becomes an iterative technique. Let  $E$  be a very small number (the error of the iteration). Given values of  $N_a$ ,  $V_a$ ,  $N_b$ ,  $V_b$ ,  $TR$ , and system power  $P$ .

- As a start, let  $T_1 = 0.1/P$ ;  $X = 0.8$
- Then,  $T_2 = TR T_1$
- DO 7J = 1, 10
- From Equation 3.5, calculate  $P_c$
- From Equation 3.2, calculate  $P_b$
- From Equation 3.3, calculate  $P_a$
- From Equation 3.1, calculate  $T_3$
- From Equation 3.4, calculate  $P$
- $X1 = T_3 PTR$

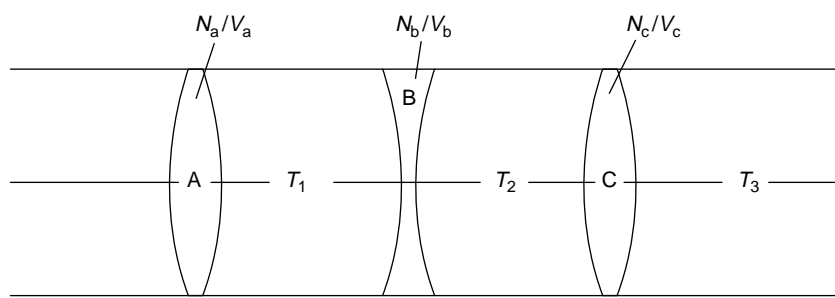


FIGURE 3.1 Triplet lens.

- $IF(ABS(X1 - X) - E)$  if less than 0.0 go to 8 else go to 6
- 6  $X = X1$
- 7 CONTINUE
- 8  $S = P/\phi$
- $P_a = P_a/S$
- $P_b = P_b/S$
- $P_c = P_c/S$
- $T_1 = T_1S$
- $T_3 = T_3S$
- $T_2 = T_1TR$

This algorithm was programmed on the author’s computer and is routinely used for triplet starting solutions.

Table 3.1 gives six such solutions,  $F = 100$ , and assumes that  $T_2 = T_1$  ( $TR = 1$ ).

The first three solutions are for the visual region, the next is for the UV region, and the last two are for the IR region of 3.2–4.2  $\mu\text{m}$ . This algorithm does not converge for materials such as germanium and zinc selenide Vogel (1968). This table illustrates the advantage of using this third order technique as preliminary design tool. Note that by reducing the refractive index of the middle element of the second solution as compared to the first, a more compact system with a longer BFL is obtained.

TABLE 3.1  
Thin-Lens Triplet Starting Solutions

$P_a$	$P_b$	$P_c$	$T_1$	$T_3$	Material
0.02244	−0.04804	0.02556	12.203	87.797	N-SK16, F2
0.03364	−0.06556	0.03495	3.751	96.249	N-SK16, N-LLF1
0.02088	−0.04913	0.02514	16.938	83.062	Plexiglas, polystyrene
0.03505	−0.07391	0.03703	5.327	94.673	CaF <sub>2</sub> , quartz
0.01873	−0.05124	0.02490	24.788	75.212	Silicon, germanium
0.00938	−0.03296	0.04315	78.262	21.737	IRTRAN2, IRTRAN3

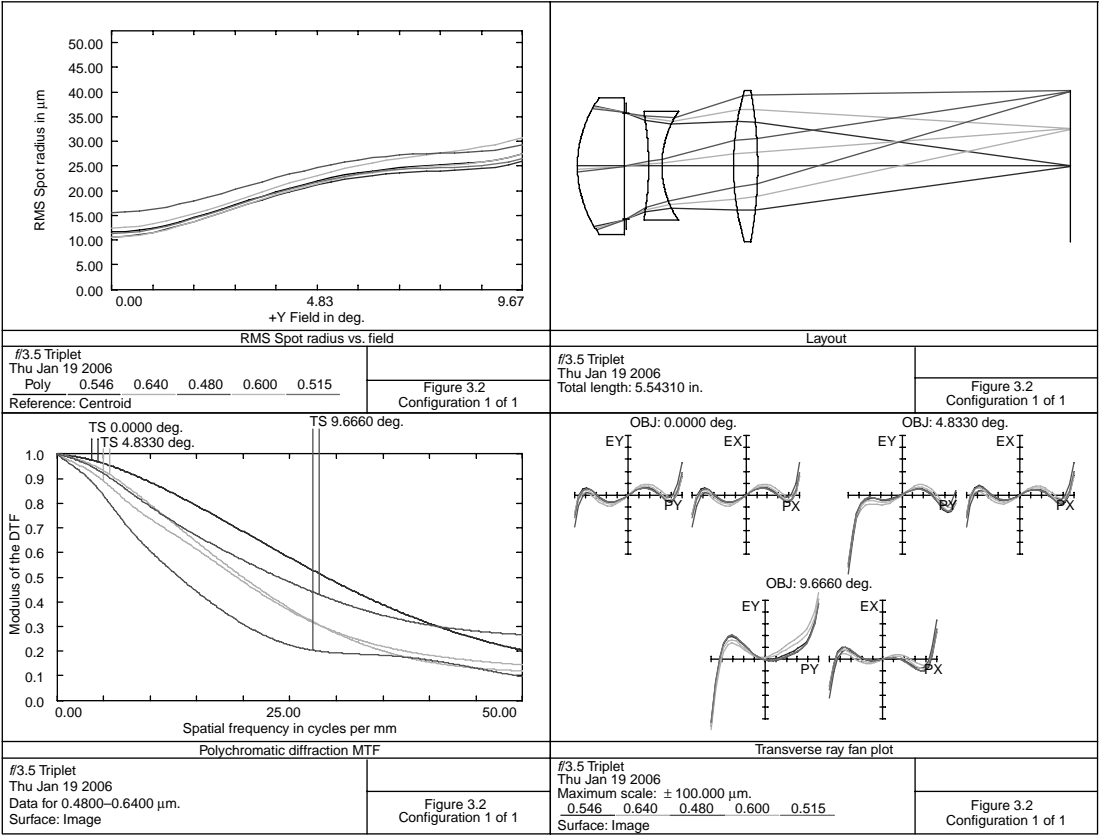


FIGURE 3.2 A 5-in. focal length,  $f/3.5$  triplet.

**TABLE 3.2**  
**An  $f/3.5$  Triplet**

Surface	Radius	Thickness	Material	Diameter
1	1.3214	0.5250	N-SK16	1.540
2	0.0000	0.0200	AIR	1.540
3	Stop	0.2541	AIR	1.197
4	-3.5136	0.1500	F2	1.220
5	1.0975	0.8056	AIR	1.220
6	3.0243	0.2710	N-SK16	1.700
7	-4.5153	3.5174	AIR	1.700

Distance from front lens vertex to image = 5.543, distortion = 0.84%.

As a start in optimization, it is expedient to hold the powers and spacing of the elements while bending the lenses to solve for spherical, coma, and astigmatism. Next, thicken the elements and vary all the parameters. Optimizing the first solution yields a design shown in Figure 3.2. It is  $f/3.5$  and was designed to project  $24 \times 36 \text{ mm}^2$  film (EFL = 5). The prescription for this lens is given in Table 3.2.

To reduce the Petzval sum, designs of this type have glasses such that the front and rear elements are made from a high-index crown, whereas the center element is a low-index flint (Sharma 1982).

After a few small changes in Vogel's prescription, and then an optimization, the solution is obtained for an infrared lens (8–14  $\mu\text{m}$ ) as shown in Figure 3.3. The prescription is given in Table 3.3.

The entrance pupil is in contact with the first lens surface. It is  $f/2$ , has a focal length of 10 and a field of view of  $8^\circ$ . It is interesting to note that the rear lens is actually a negative lens and is therefore acting as a field flattener. Considering the long wavelength, this lens is nearly diffraction limited.

**TABLE 3.3**  
**Infrared Triplet, 8–14  $\mu\text{m}$**

Surface	Radius	Thickness	Material	Diameter
1	10.4578	0.5901	Germanium	5.100 Stop
2	14.1079	4.3909	Air	5.000
3	-15.8842	0.5900	ZnSe	3.800
4	-18.2105	5.6218	Air	3.900
5	2.5319	0.3918	Germanium	2.400
6	2.4308	1.3065	Air	2.100

Distance from first lens surface to image = 12.891, distortion = 0.24%.

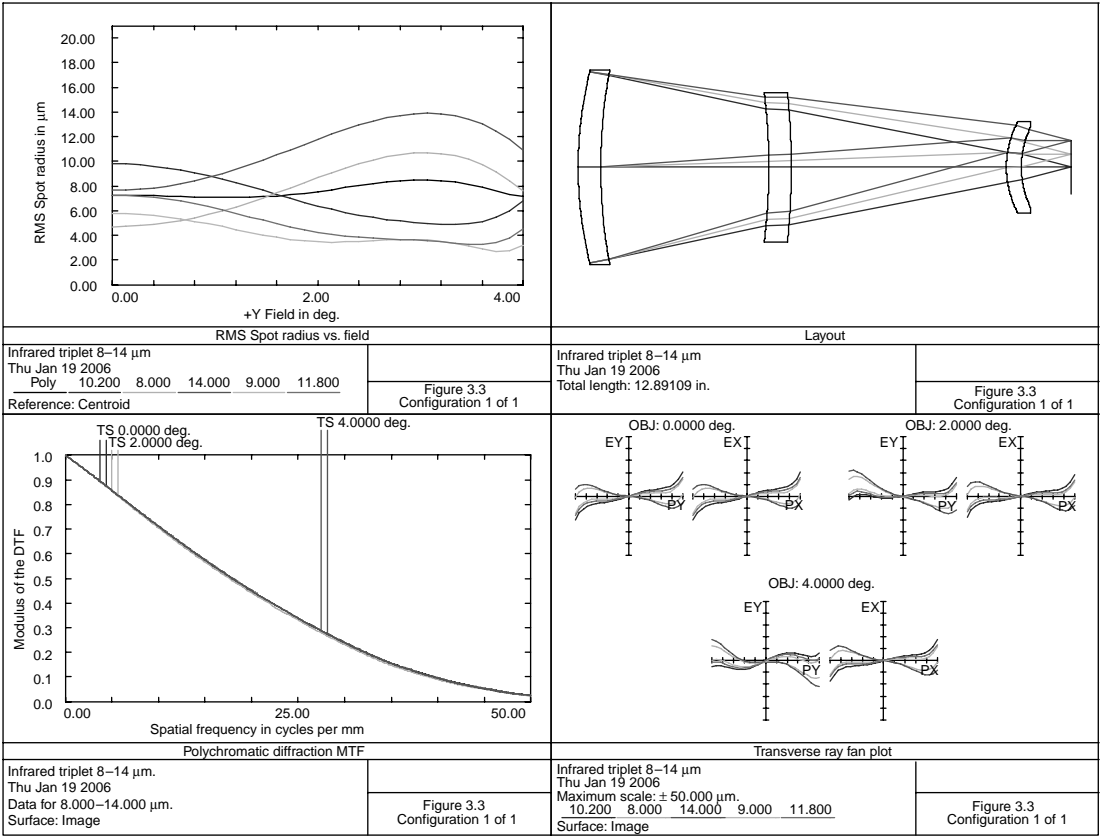


FIGURE 3.3 An IR triplet, 8–14 μm.

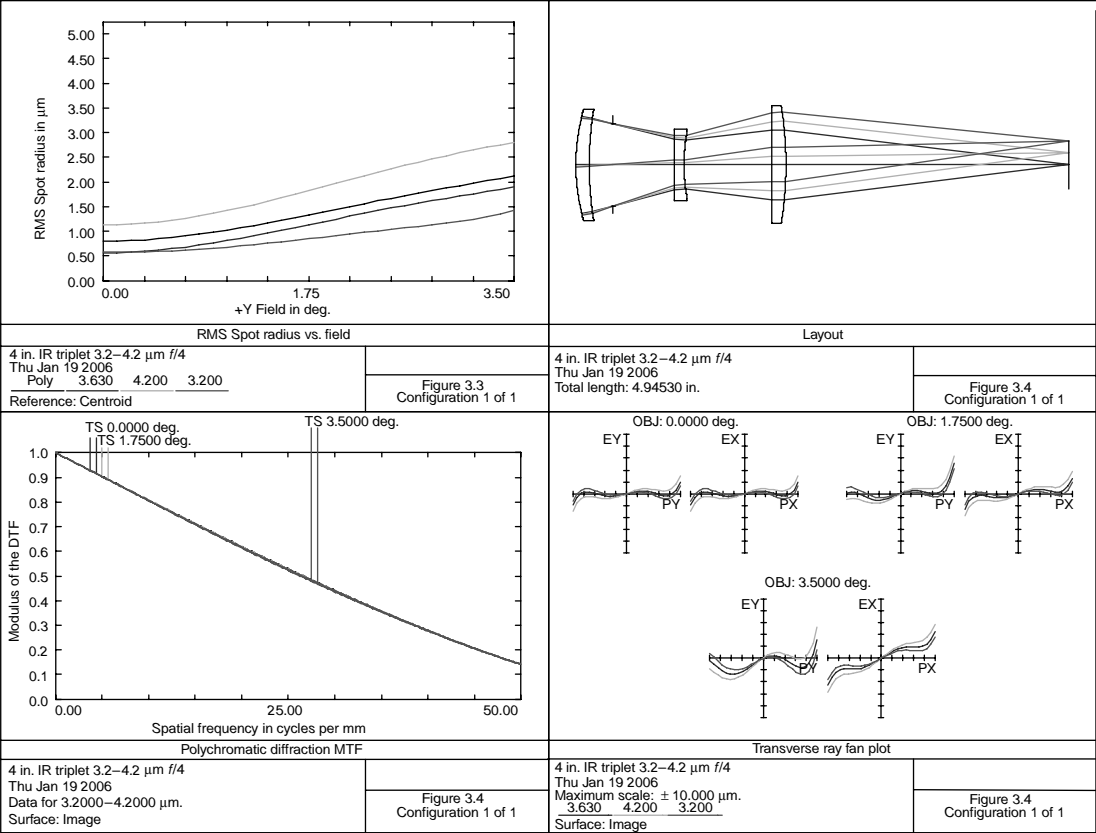


FIGURE 3.4 A 4-in. IR triplet, 3.2–4.2 μm.



**TABLE 3.4**  
**A 4-in. IR Triplet, 3.2–4.2- $\mu\text{m}$ ,  $f/4$**

Surface	Radius	Thickness	Material	Diameter
1	2.0721	0.1340	Silicon	1.120
2	3.5488	0.2392	Air	1.120
3	Stop	0.6105	Air	0.830
4	13.7583	0.1000	Germanium	0.720
5	1.7491	0.8768	Air	0.680
6	0.0000	0.1462	Silicon	1.180
7	−3.5850	2.8386	Air	1.180

Distance from first lens surface to image = 4.945, distortion = <0.17%.

Figure 3.4 is the result of an optimization of the fifth solution (silicon–germanium, 3.2–4.2  $\mu\text{m}$ ), EFL = 4. The lens prescription is given in Table 3.4. This lens is  $f/4$  with a field of view of  $7^\circ$ .

In Figure 3.5 is shown a 50-in. focal length,  $f/8$  triplet that covers a  $2.25 \times 2.25$  (3.18 diagonal) film format. It was designed to be used for photography by amateur astronomers. The lens prescription is given in Table 3.5. Distortion is negligible. The limiting aberration is longitudinal secondary color, which is 1.4 mm.

In Figure 3.6 is shown an  $f/9$ , 18-in. focal length triplet designed to project letter-sized ( $8.5 \times 11$  in.) documents. The specifications are given in Table 3.6.

**TABLE 3.5**  
**A 50-in. EFL Triplet**

Surface	Radius	Thickness	Material	Diameter
1	11.4909	0.7006	N-SK16	6.320
2	51.4450	0.1436	AIR	6.320
3	Stop	2.0023	AIR	6.066
4	−45.4740	0.6000	LF5	5.800
5	12.3302	3.2981	AIR	5.700
6	98.2327	0.6998	N-SK16	6.180
7	−22.9598	45.5079	AIR	6.180

Distance from first lens surface to image = 52.952.

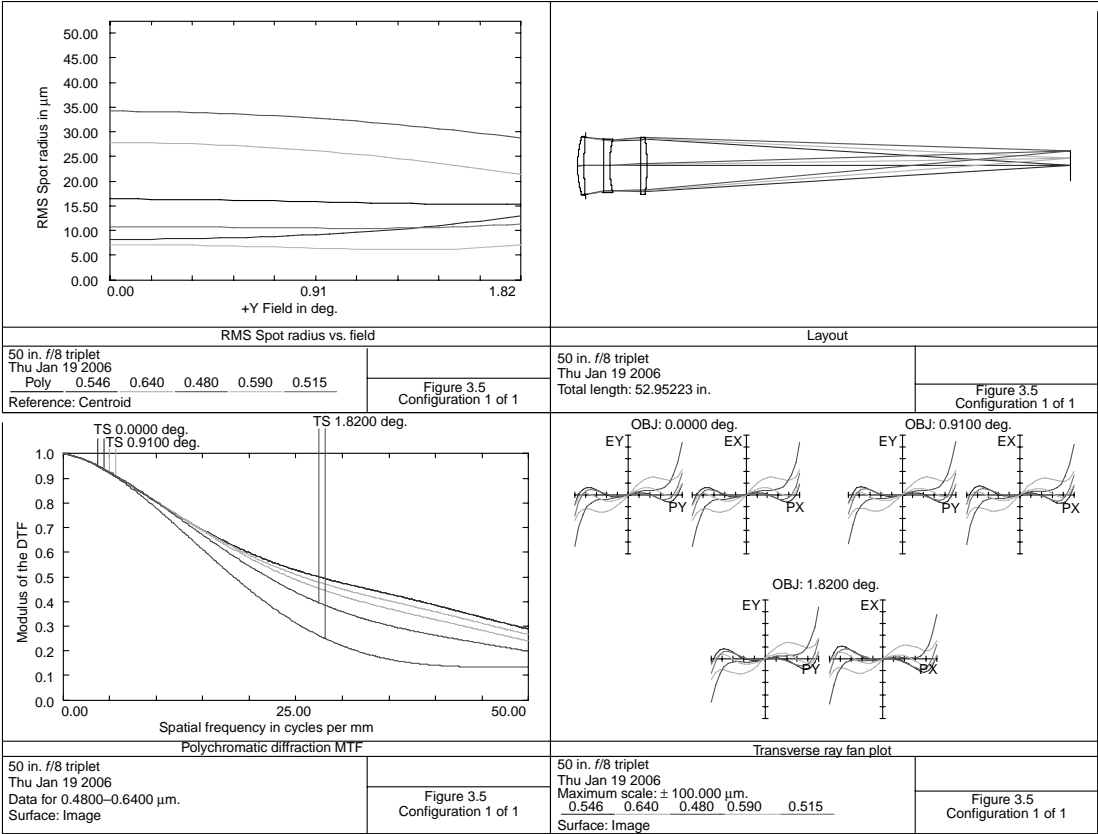


FIGURE 3.5 A 50-in., f/8 triplet.

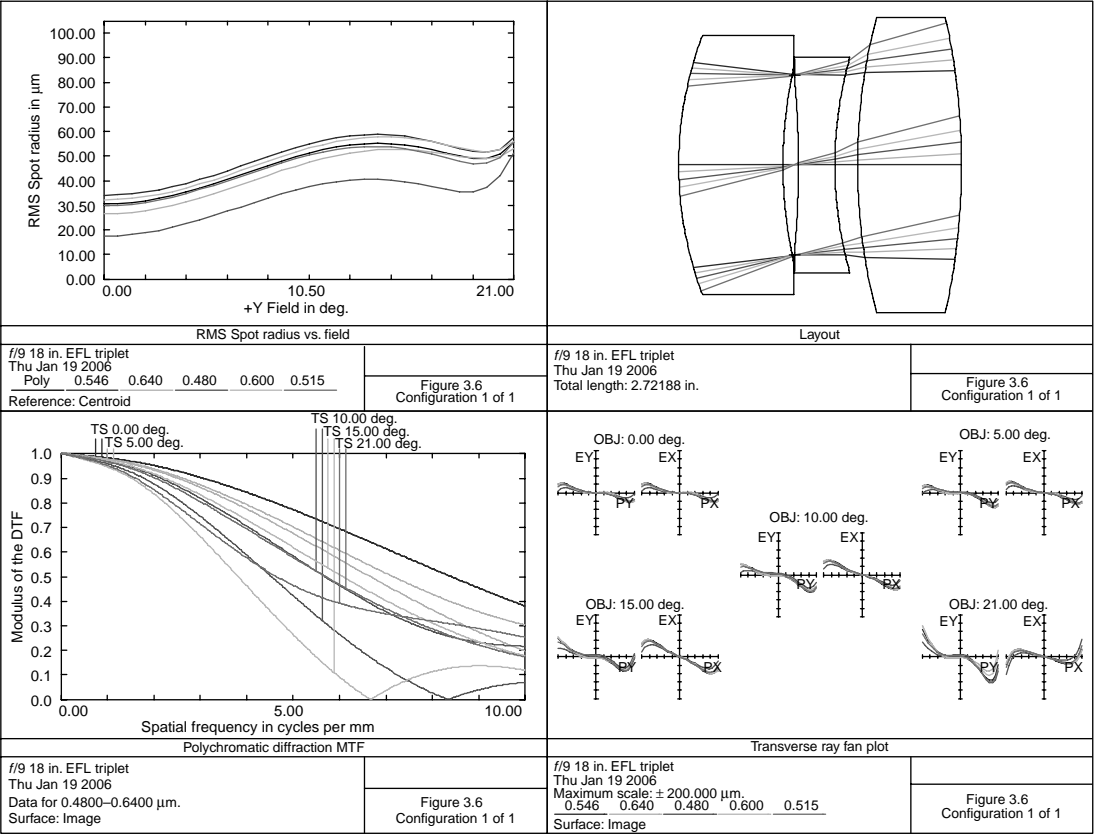


FIGURE 3.6 An 18-in., f/9 triplet.

**TABLE 3.6**  
**An  $f/9$ , 18-in. EFL Triplet**

Surface	Radius	Thickness	Material	Diameter
0	0.0000	0.100000E+11		0.00
1	3.5121	1.0035	N-LAK33A	2.500
2	4.3116	0.1109		1.880
3	Stop	0.0382		1.736
4	-9.0210	0.3500	LF5	1.740
5	3.7834	0.2192		2.080
6	5.6958	1.0001	N-SK16	2.840
7	-6.5950	16.4135		2.840
8	0.0000	0.0000		

Distance from front surface to lens surface = 2.722, distortion = 0.45%.

## REFERENCES

- Ackroyd, M. D. (1968) Wide angle triplets, US Patent #3418040.  
 Ackroyd, M. D. (1969) Triplet type projection lens, US Patent #3443864.  
 Arai, Y. (1980), Achromatic objective lens, US Patent #4190324.  
 Conrad, L. H. (1972) Three element microphotographic objective lens, US Patent #3640606 and #3640607.  
 Eckhardt, S. K. (1997) Fixed focus triplet projection lens for overhead projectors, US Patent #5596455.  
 Kallo, P. and Kovacs, G. (1993) Petzval sum in triplet design, *Opt. Eng.*, 32: 2505.  
 Kingslake, R. (1968) Triplet covering a wide field, US Patent #3418039.  
 Kobayashi, K. (1969) Ultra-achromatic fluorite silica triplet, US Patent #3486805.  
 Sharma, K. D. (1982) Utility of low index high dispersion glasses for Cook triplet design, *Appl. Opt.*, 21: 1320.  
 Sharma, K. D. and Gopal, S. V. (1982) Significance of selection of Petzval curvature in triplet design, *Appl. Opt.*, 21: 4439.  
 Stephens, R. E. (1948) The design of triplet anastigmat lenses, *JOSA*, 38: 1032.  
 Tronnier, E. (1965) Three lens photographic objective, US Patent #3176582.  
 Vogel, T. (1968) Infrared optical System, US Patent #3363962.

---

# 4 Triplet Modifications

To reduce the f-number, the front element is often split into two positive lenses. Another modification involves the splitting of the rear element into a cemented negative–positive lens. The *Tessar* lens is a modification in which both front and rear elements are split into cemented negative–positive assemblies. The *Heliar* lens is still another modification and is shown in [Figure 4.1](#); details are given in [Table 4.1](#). The lens in the figure is  $f/5$  with a  $20^\circ$  field of view (FOV), and has a focal length of 10. Visual region. [Figure 4.2](#) shows a 4-inch focal length,  $f/4.5$  Tessar lens. It covers an image field of 3.0 in diameter; details are given in [Table 4.2](#).

In the above examples, note the use of a high index crown for front and rear elements, and low index flint for the center element. Tessar-type lenses are often used as enlarging lenses. This design is similar to the Velesik (1975) patent. In both cases, the rear cemented assembly has a small  $V_d$  difference and a strong curvature between the elements.

[Figure 4.3](#) shows a lens for use with a slide projector for 35-mm SLR film; the prescription is given in [Table 4.3](#). From [Appendix A](#), this has a diagonal of 1.703. Because this lens has a focal length of 4.0, the FOV is  $24^\circ$ . The lens is  $f/2.8$ .

If a target of 33 lp/mm was projected with this lens, the screen image of these lines would subtend one minute of arc for an observer at the projection lens. Because an observer cannot resolve one minute of arc (probably 2–3 minutes arc would be more realistic) in a darkened room such as that in which slides would be projected, this lens performance is excellent.

In [Figure 4.4](#), a two-element field corrector has been added to the usual triplet design. F-number and FOV are the same as in [Figure 3.2](#); however, the resolution is vastly improved due to the reduction of coma. The prescription is given in [Table 4.4](#).

[Figure 4.5](#) shows a 100-mm  $f/2.8$  lens in which the spacing between the last two elements has been substantially increased; details are given in [Table 4.5](#). It resembles a reversed form of the Tessar lens shown in [Figure 4.2](#). The FOV is  $15.24^\circ$ . It may be used either as a camera lens or as a projection lens for 35-mm cinematography.

[Figure 4.6](#) shows a 10-mm  $f/2.8$  lens suitable as an objective for a CCD camera with a 1/2-in. chip (8-mm diagonal); details are given in [Table 4.6](#).

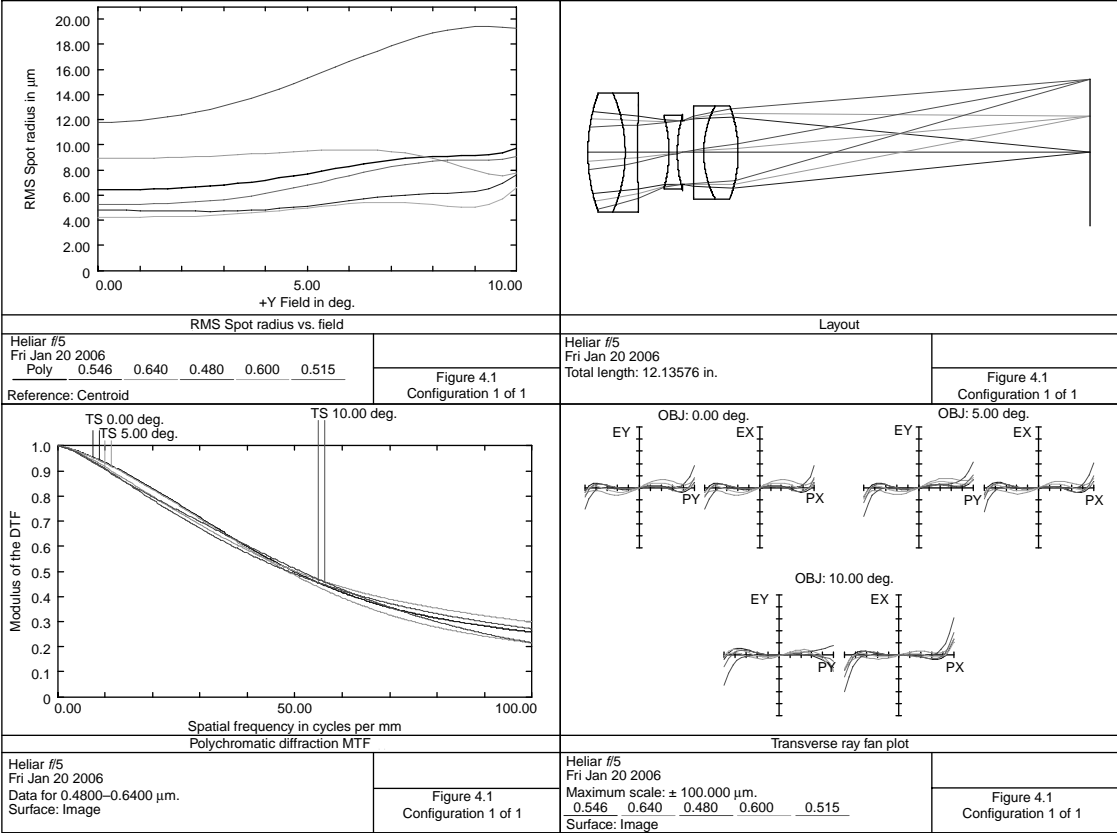


FIGURE 4.1 A Heliar *f*/5 les.

---

**TABLE 4.1**  
**Heliar Lens,  $f/5$**

Surface	Radius	Thickness	Material	Diameter
1	4.2103	0.9004	N-SK16	2.860
2	−3.6208	0.2999	N-LLF6	2.860
3	29.1869	0.7587		2.320
4	−3.1715	0.2000	N-LLF6	1.780
5	3.2083	0.1264		1.660
6	Stop	0.2629		1.555
7	43.0710	0.2500	N-LLF6	2.240
8	2.4494	0.8308	N-SK16	2.240
9	−3.2576	8.5066		2.240

Distance of front lens surface to image = 12.136, distortion = 0.12%.

---



---

**TABLE 4.2**  
**An  $f/4.5$  Tessar Lens**

Surface	Radius	Thickness	Material	Diameter
1	1.3329	0.2791	N-SK15	1.400
2	−9.9754	0.2054		1.400
3	−2.0917	0.0900	F2	0.940
4	1.2123	0.0709		0.820
5	Stop	0.1534		0.715
6	−7.5205	0.0900	K10	1.260
7	1.3010	0.3389	N-SK15	1.260
8	−1.5218	3.4025		1.260

Distance of first lens surface to image = 4.630, distortion = 0.34%.

---

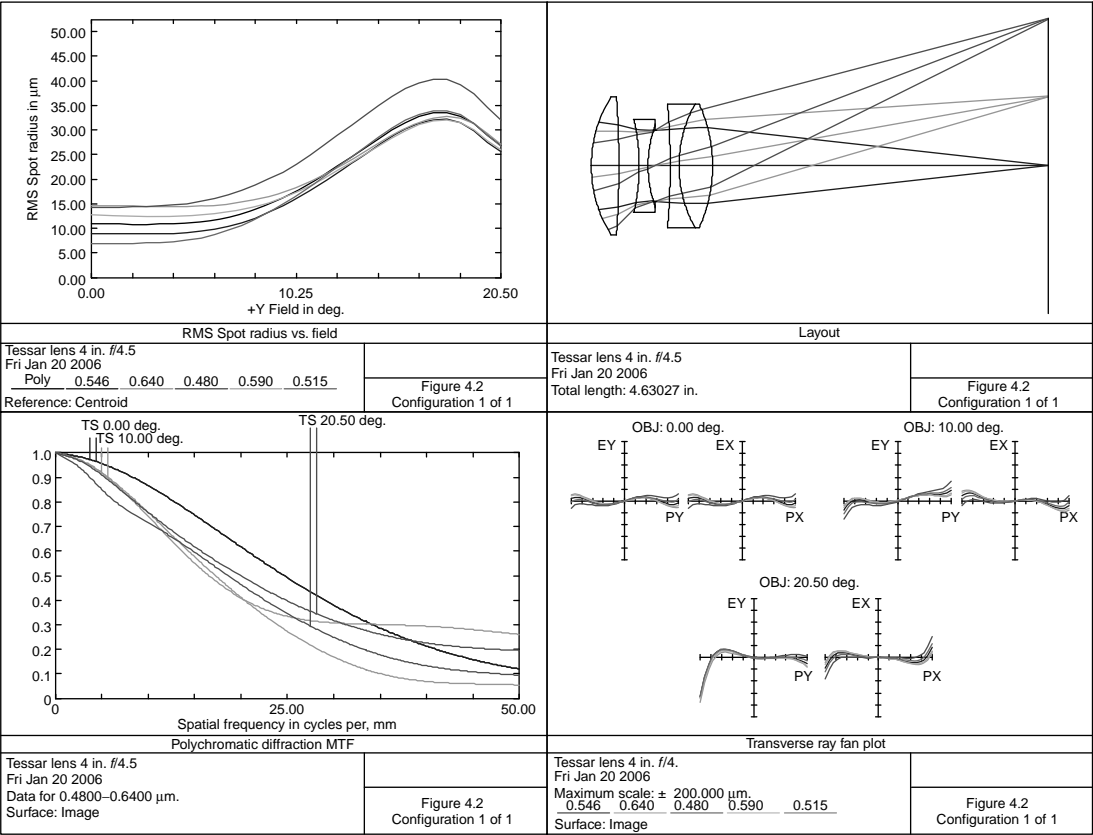


FIGURE 4.2 A Tesseract lens, 4-in., *f*/4.5.



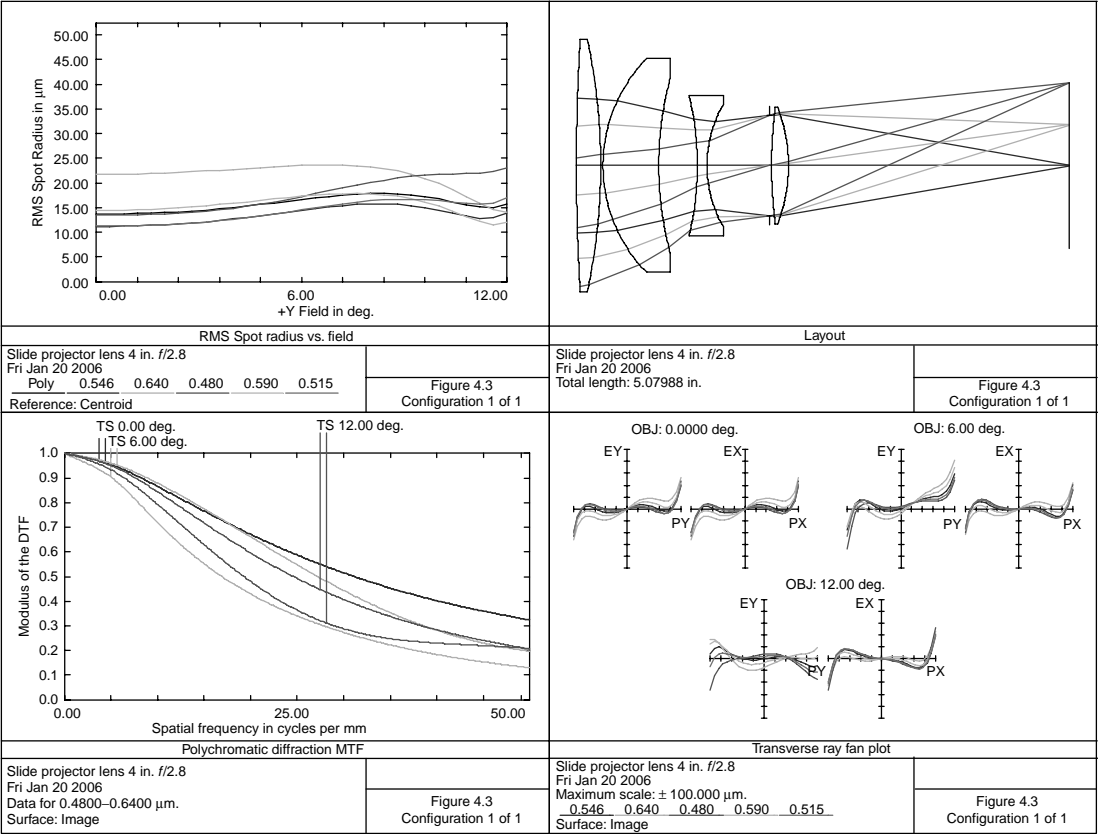


FIGURE 4.3 A slide-projector lens.

**TABLE 4.3**  
**Slide Projector Lens**

Surface	Radius	Thickness	Material	Diameter
1	21.8985	0.2488	N-SK4	2.600
2	−6.2473	0.0239		2.600
3	1.5677	0.5763	N-SK4	2.200
4	3.5212	0.3969		1.800
5	−3.0936	0.1000	SF5	1.440
6	1.2744	0.6424		1.260
7	Stop	0.0222		1.030
8	4.6891	0.1740	N-SK4	1.200
9	−1.6590	2.8954		1.200

Distance of first lens surface to film = 5.080, distortion = 0.08%.

**TABLE 4.4**  
**A 5-in. Focal Length,  $f/3.5$  Lens with Field Corrector**

Surface	Radius	Thickness	Material	Diameter
1	1.9863	0.5000	N-SK16	1.860
2	6.2901	0.4878		1.640
3	Stop	0.1016		1.134
4	−2.5971	0.1843	F5	1.280
5	2.4073	0.0719		1.340
6	5.8147	0.3153	N-SK16	1.460
7	−2.1926	2.6845		1.460
8	1.9071	0.5020	N-SK16	2.000
9	2.3148	0.0150		1.840
10	1.1907	0.2000	N-SK4	2.000
11	0.9911	1.1590		1.680

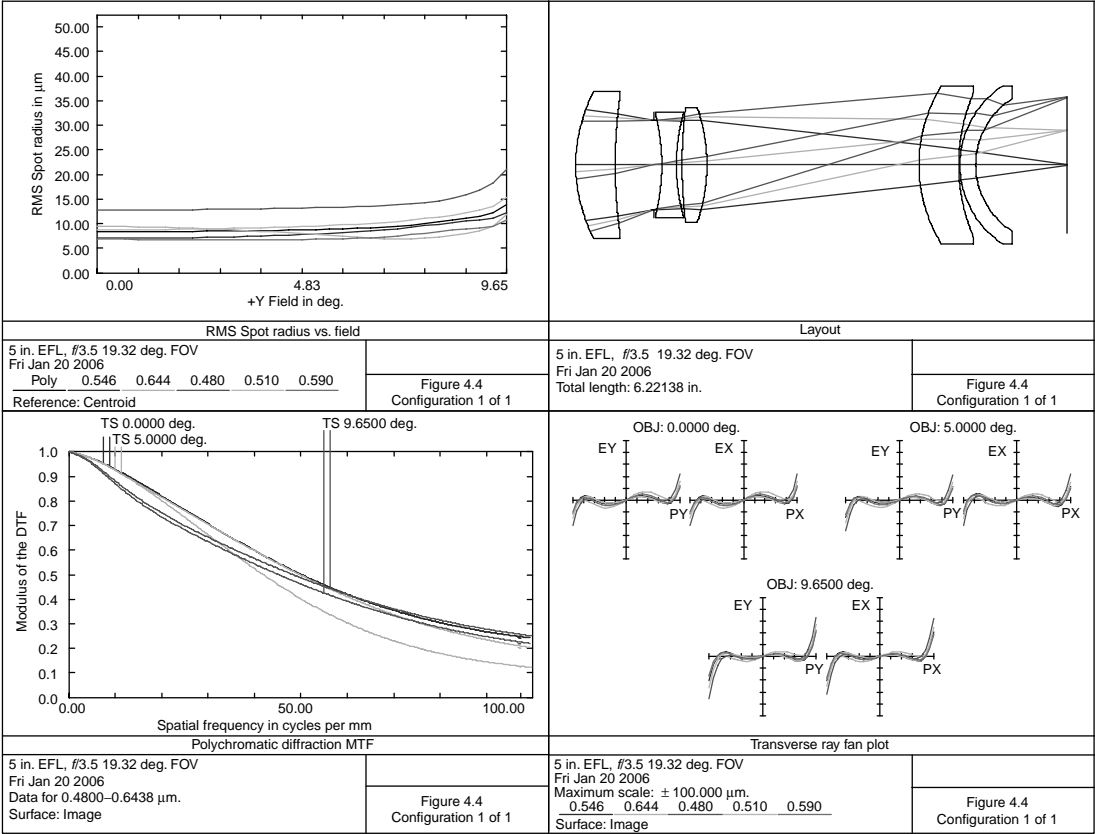


FIGURE 4.4 Triplet with corrector. Distortion is 1.0%. Distance of first lens to image is 6.221.

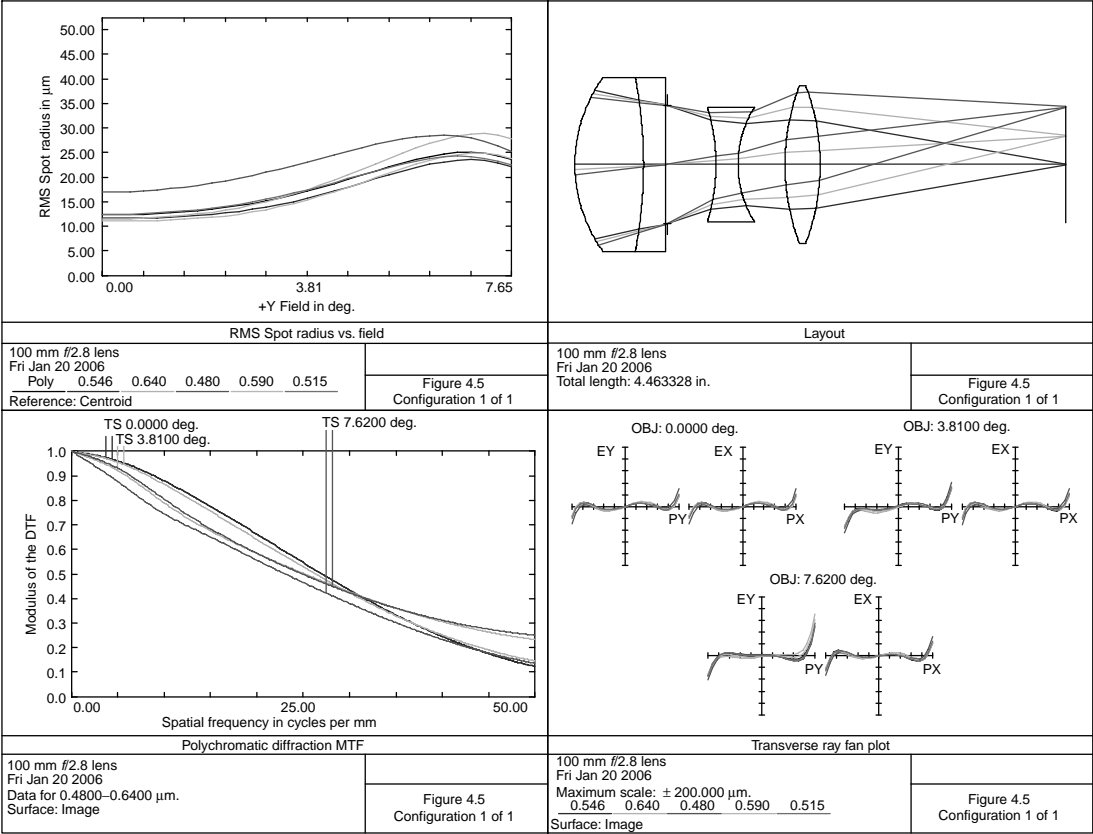


FIGURE 4.5 A 100-mm f/2.8.

---

**TABLE 4.5**  
**A 100-mm  $f/2.8$  Lens**

Surface	Radius	Thickness	Material	Diameter
1	1.3502	0.6245	N-SK4	1.580
2	−4.1565	0.2000	SF1	1.580
3	0.0000	0.0200		1.580
4	Stop	0.4384		1.072
5	−1.7713	0.2000	F5	1.040
6	0.9780	0.4267		1.040
7	2.0072	0.3199	N-SK4	1.440
8	−2.0072	2.2338		1.440

Distance of first lens surface to image=4.463.

---



---

**TABLE 4.6**  
**A 10-mm  $f/2.8$  Camera Lens**

Surface	Radius	Thickness	Material	Diameter
1	0.1664	0.0495	N-LAK33	0.200
2	0.4557	0.0215		0.170
3	−0.3066	0.0200	N-LAK33	0.164
4	−0.1459	0.0200	F5	0.164
5	0.1459	0.0184		0.120
6	Stop	0.0027		0.111
7	0.2829	0.0250	N-LAK33	0.140
8	−0.3529	0.3063		0.140

Distance of first lens surface to image=0.463, distortion=0.95%.

---

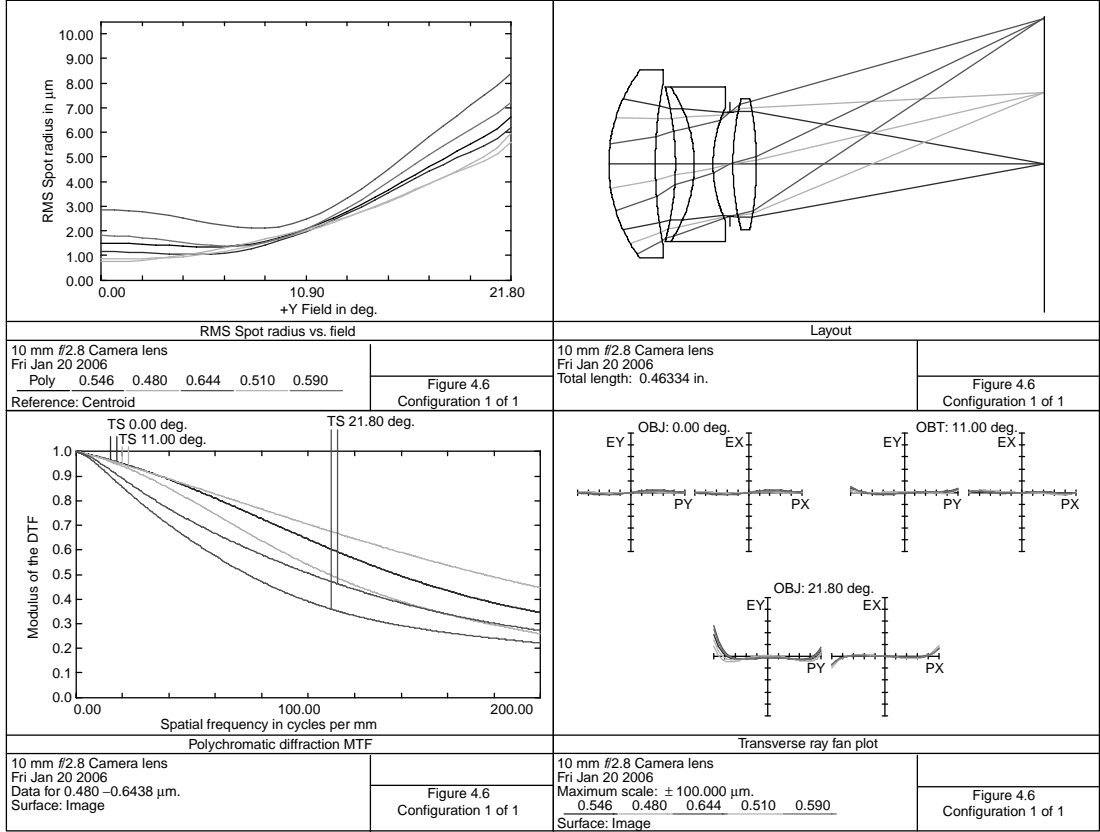


**FIGURE 4.6** A 10-mm  $f/2.8$  lens. Distortion is 0.95%. Distance of first lens surface to the image is 0.463.

## REFERENCES

- Cook, G. H. (1950) Highly corrected three component objectives, US Patent #2502508.
- Doi, Y. (1981) Rear stop lens system, US Patent #4298252.
- Edwards, G. (1972) Four component objective, US Patent #3649104.
- Eggert, J. (1965) Objective lens consisting of four lens units, US Patent #3212400.
- Guenther, R. E. (1970) Four element photographic objective, US Patent #3517987.
- Hopkins, R. E. (1965) Optical lens system design, AD 626844 Defense Documentation Center.
- Mihara, S. (1984) Compact camera lens system with a short overall length, US Patent #4443069.
- Sharma, K. D. (1979) Design of new 5 element Cook triplet derivative, *Applied Optics*, 18: 3933.
- Sharma, K. D. (1980) Four element lens systems of the Cooke triplet family, *Applied Optics*, 19, 698.
- Tateoka, M. (1983) Projection lens, US Patent #4370032.
- Tronnier, A. W. (1937) Unsymmetrical photographic objective, US Patent #2084714.
- Velesik, S. (1975) Reproduction lens system, US Patent #3876292.





---

# 5 Petzval Lenses

This class of lenses consists of two positive members separated by a large airspace of perhaps half of the focal length of the lens. The system exhibits a large negative Petzval sum, has an inward curving field, and so is only useable for small fields of view. It is of economical construction and is capable of low f-number.

Figure 5.1 shows a basic  $f/1.4$  projection lens for 16-mm motion picture film; details are provided in Table 5.1. It has a  $14^\circ$  field of view and a focal length of 2; there is considerable flare at the edge of the pupil.

In Figure 5.2 a modified Petzval-type lens is shown; details are provided in Table 5.2. It is a modification of the Angenieux patent (Angenieux 1953). Because a characteristic of these Petzval-type lenses have a strong inward curving field, a field-flattening lens was placed just in front of the image surface. It is  $f/1.15$  with a focal length of 2.433 and covers a field of  $9.9^\circ$ . This corresponds to an image diagonal of 0.42 in. and thus is suitable for use with a 0.67-in. CCD (11-mm diagonal).

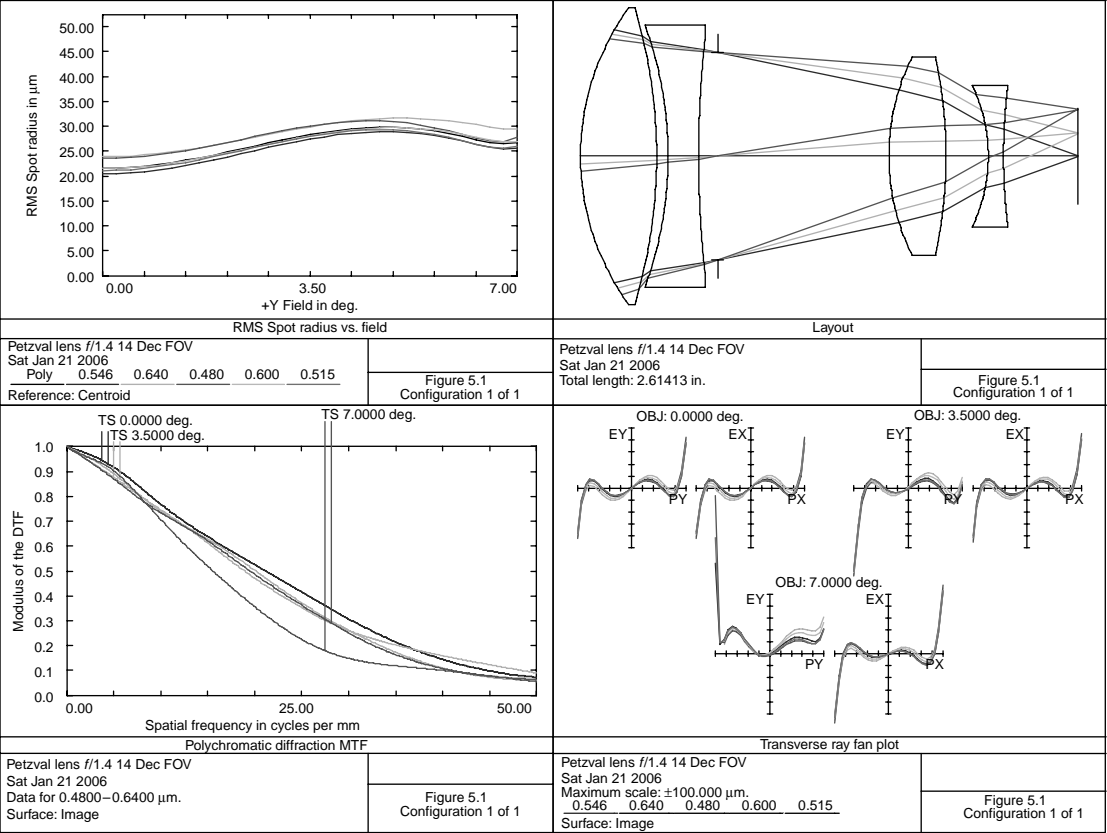


FIGURE 5.1 Petzval lens *f*/1.4.

**TABLE 5.1**  
**An *f*/1.4 Petzval Lens**

Surface	Radius	Thickness	Material	Diameter
1	1.3265	0.4000	N-LAK12	1.560
2	−2.6919	0.0600		1.560
3	−2.0028	0.1600	SF4	1.380
4	5.4499	0.1000		1.220
5	Stop	0.8999		1.087
6	1.1724	0.3000	N-LAK12	1.040
7	−2.4602	0.2221		1.040
8	−0.8615	0.0800	LF5	0.740
9	3.0039	0.3921		0.700

Distance from front lens surface to image=2.614, distortion=0.17%.

**TABLE 5.2**  
**Modified Petzval-Type Lens with Field Flatteners**

Surf	Radius	Thickness	Material	Diameter
1	4.6627	0.3000	N-LAK33	2.380
2	0.0000	0.0150		2.380
3	2.0799	0.5391	N-PSK3	2.140
4	−2.6476	0.1700	F2	2.140
5	2.6476	0.1470		1.760
6	Stop	1.5182		1.663
7	1.1028	0.6000	N-PSK3	1.360
8	−1.1028	0.1300	F2	1.360
9	−3.3330	0.3712		1.360
10	−1.0400	0.0600	SF2	0.600
11	3.8085	0.1000		0.600

Distance from first surface to image=3.95, distortion=0.12%.

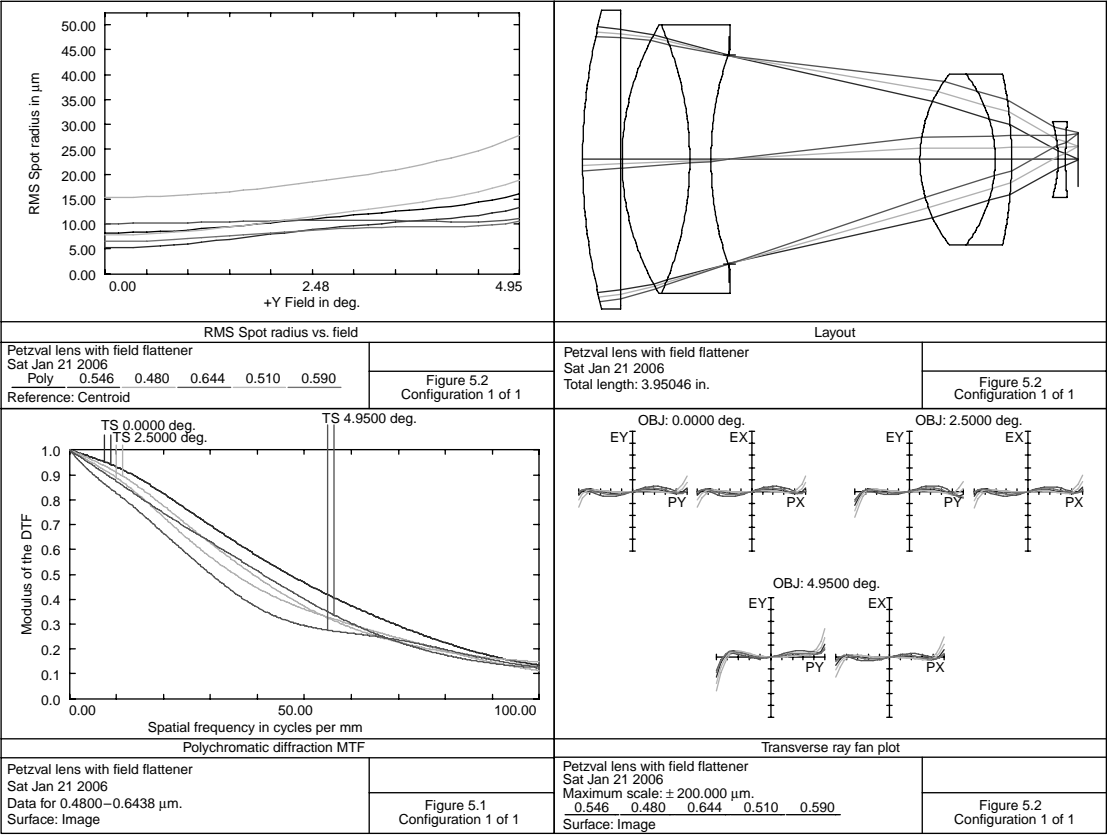


FIGURE 5.2 Petzval lens with field flattener.

## REFERENCES

- Angenieux, P. (1953) Large aperture photographic objective, US Patent #2649021.
- Rogers, P. J. (1980) Modified petzval lens, US Patent #4232943.
- Shade, W. (1951) Objectives of the petzval type with a high index collective lens, US Patent #2541484.
- Smith, W. J. (1966) Objective of the petzval type with field flattener, US Patent #3255664.
- Werfeli, A. (1956) Photographic and projection objective of the petzval type, US Patent #2744445.



---

# 6 Double Gauss and Near Symmetric Types

This type of lens was derived from a telescope objective originally designed by C. F. Gauss (Kingslake 1951). It is one of the basic forms of anastigmatic photographic lenses and consists of a nearly symmetric arrangement of elements about a central stop. Surrounding this stop are two achromats with the flint element facing the stop (Brandt 1956), such that its surface is concave toward the stop. It can be well corrected over a large aperture and moderately large field of view.

Apertures are generally  $f/2.8$  or less, with fields of view of at least  $30^\circ$ , and a *BFL* of 0.5–0.9 *EFL*. It is the basic lens supplied (50-mm focal length) with 35-mm single-lens reflex (SLR) cameras as well as motion-picture cameras. To reduce the *f*-number, additional elements are generally added in the front and rear.

In [Figure 6.1](#) is shown an  $f/2.5$  double Gauss lens of 1.378 (35-mm) focal length for use in a motion-picture camera (35-mm film). The prescription is given in [Table 6.1](#).

The use of the high-index-of-refraction lanthanum crown glass (N-LAK33) in this design helps to reduce spherical aberration. Also note from the layout that there is some vignetting at the full field which reduces the relative illumination at the edge to about 80% (see comments for the lens shown in [Figure 6.2](#)).

Figure 6.2 shows a 50-mm  $f/1.8$  SLR camera lens. It is the basic lens supplied with 35-mm SLR cameras. The large back focal length required is to clear the shutter and reflex mirror mechanism in the camera. A great deal of effort has been spent in developing lenses for these cameras that are compact, lightweight, and have good performance. See, for example, Wakamiya (1984).

This lens has some vignetting such that the relative illumination at  $23^\circ$  off-axis is 66% and 91% at  $16^\circ$  off-axis. There is no vignetting at  $f/4$ . Because focusing is generally done at full aperture in the center of the field, then at the time of exposure the lens is stopped down. Therefore, it is important to have relatively low spherical aberration to prevent a focal shift as the lens is stopped down. The lens data for Figure 6.2 is given in [Table 6.2](#). This lens is a minor modification to Wakimoto (1971). The patent description covers an  $f/1.4$  lens.

Because this lens has vignetting, it is important that the designer adjust lens diameters such that the system is physically realizable. This is because most computer programs consider vignetting by appropriately adjusting the entrance-pupil diameter at the various field positions to satisfy the designers vignetting instruction. The lens diameters must be such that only those rays traced may actually pass thru the lens. It is never a problem if there is no vignetting; the aperture stop

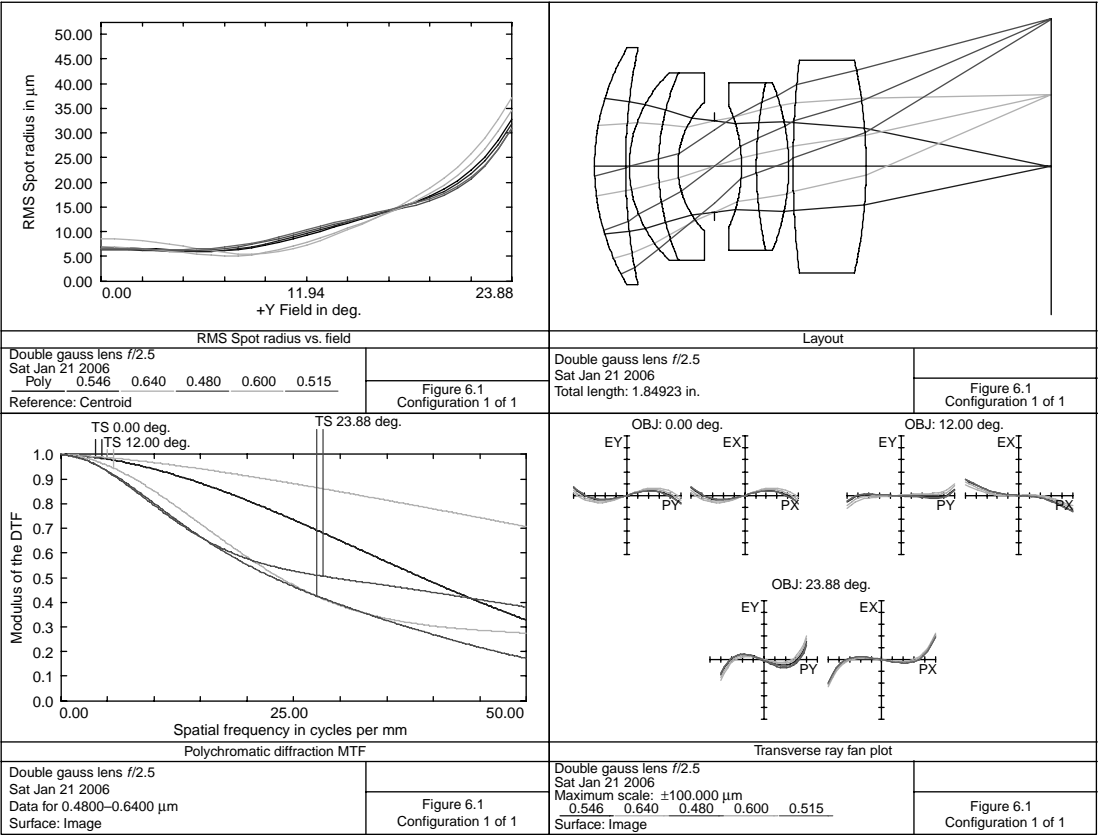


FIGURE 6.1 A double Gauss f/2.5 lens.



**TABLE 6.1**  
**An  $f/2.5$  Double Gauss Lens**

Surface	Radius	Thickness	Material	Diameter
1	0.9377	0.1258	N-LAK33	0.960
2	2.3033	0.0150		0.960
3	0.5241	0.1185	N-LAK33	0.760
4	0.9235	0.0783	SF1	0.760
5	0.3714	0.1466		0.520
6	Stop	0.1109		0.368
7	-0.6206	0.0600	F5	0.500
8	1.5225	0.1311	N-LAK33	0.680
9	-0.9137	0.0175		0.680
10	3.6353	0.2956	N-LAK33	0.860
11	-2.0103	0.7500		0.860

Distance from first lens surface to image = 1.849, distortion = 1.6%.

prevents this. Referring to the lens diagram, note that the first lens limits the lower rim ray at full and mid fields, whereas the last lens and surface 9 limit the upper rim ray.

Figure 6.3 shows an  $f/1$  lens of focal length 4. Field of view is  $5^\circ$ . It is a minor modification to what this author submitted at the 1980 Lens Design Conference. (Juergens, 1980). Following is the lens data for Figure 6.3 (Table 6.3).

**TABLE 6.2**  
**A 50-mm  $f/1.8$  Lens for SLR Cameras**

Surface	Radius	Thickness	Material	Diameter
1	1.3517	0.1746	N-BASF2	1.480
2	3.1073	0.0150		1.420
3	1.0848	0.2934	N-LAK8	1.260
4	23.3464	0.0800	SF2	1.260
5	0.6617	0.2770		0.900
6	Stop	0.3652		0.772
7	-0.6679	0.0800	SF2	0.940
8	2.7336	0.2911	N-LAK33	1.260
9	-1.0096	0.0150		1.260
10	0.0000	0.2358	N-LAK33	1.520
11	-2.3087	0.0150		1.520
12	3.1206	0.1318	N-LAK8	1.620
13	27.5356	1.3006		1.620

Distance from first lens surface to image = 3.275, distortion = 5%.

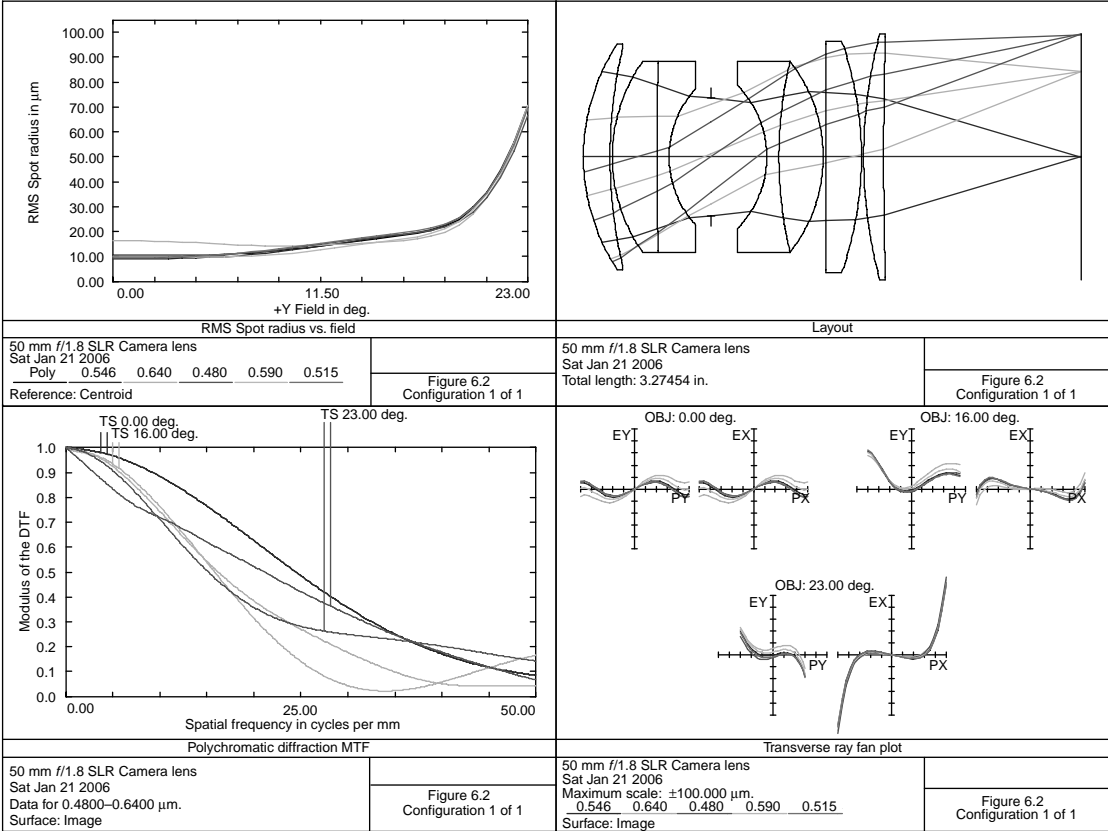


FIGURE 6.2 A 50-mm *f*/1.8 SLR camera lens.

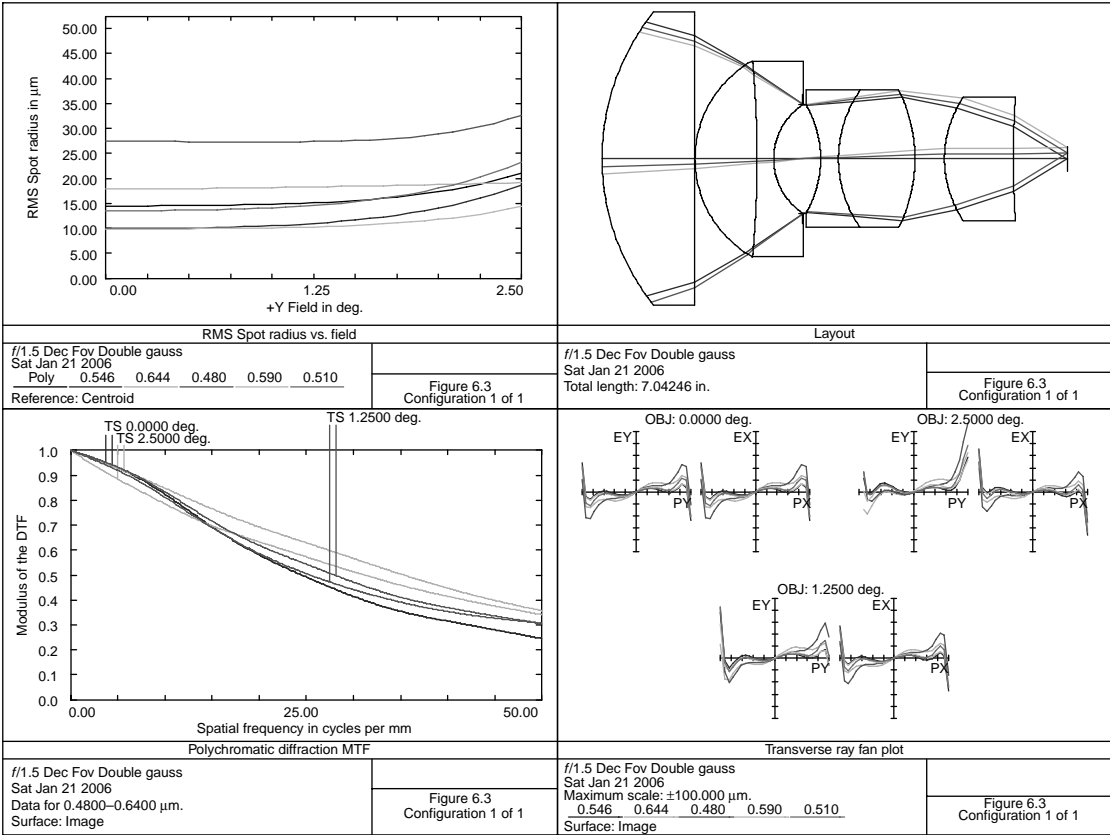


FIGURE 6.3 An  $f/1$ ,  $5^\circ$  FOV double Gauss lens.

**TABLE 6.3**  
**A 4.0 EFL *f*/1 Lens**

Surface	Radius	Thickness	Material	Diameter
1	3.5519	1.3991	N-LAF2	4.440
2	0.0000	0.0088		4.440
3	1.7043	0.9385	N-PSK3	2.960
4	−16.2382	0.2522	SF1	2.960
5	0.9860	0.4336		1.660
6	Stop	0.2777		1.654
7	−1.6424	0.2702	SF1	1.660
8	1.8028	1.1586	N-LAF2	2.080
9	−2.3336	0.4472		2.080
10	1.6593	1.0438	N-LAF2	1.880
11	14.4112	0.8128		1.880

Distance from first lens surface to image = 7.042, distortion = 0.3%.

**TABLE 6.4**  
**A 25-mm *f*/.85 Double Gauss Lens**

Surface	Radius	Thickness	Material	Diameter
1	−1.3208	0.5000	N-LASF45	1.680
2	−1.5870	0.0100		1.920
3	1.9289	0.2672	N-LASF43	1.760
4	−14.4115	0.0208		1.760
5	−13.5126	0.0900	SF6	1.700
6	31.7442	0.0100		1.760
7	0.6799	0.2000	N-LASF43	1.200
8	0.6526	0.0808	SF6	1.040
9	0.4889	0.2791		0.840
10	Stop	0.1576		0.788
11	−1.0226	0.0600	SF57	0.840
12	0.6805	0.4000	N-LASF31	1.080
13	−1.5009	0.0100		1.080
14	0.8688	0.5000	N-LASF31	1.140
15	2.5004	0.0100		1.140
16	1.1817	0.5585	N-LASF43	0.900
17	1.1430	0.0603		0.480

Distance from first lens surface to image = 3.214, distortion = 5.4%.

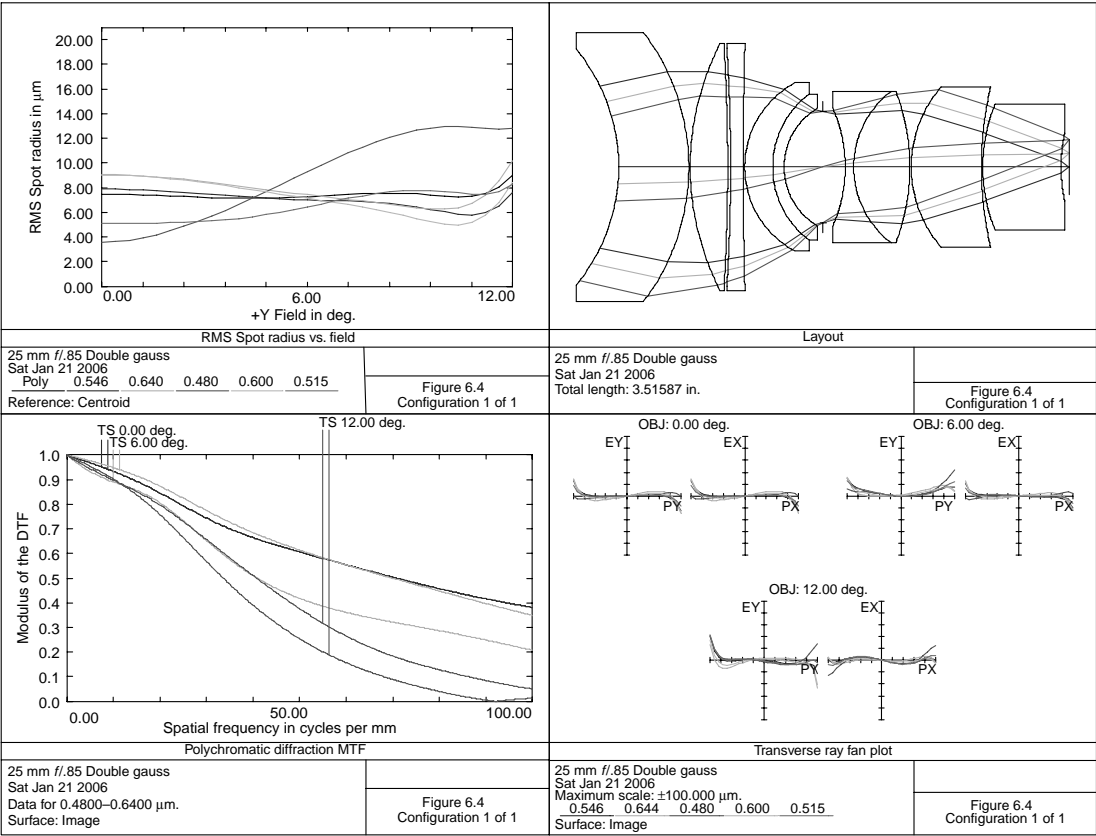


FIGURE 6.4 A 25-mm *f*/0.85 double Gauss lens.

Unfortunately, this lens has a few thick elements, a short back focal length, and no room for an iris mechanism. However, considering its low f-number, it has excellent image quality. See also the projection lens example of [Figure 22.1](#).

[Figure 6.4](#) shows a 25-mm  $f/0.85$  lens. This is a modification of Kitahara (1999) and reviewed by Caldwell (1999). The front meniscus element is acting as a coma corrector to the system. Unfortunately, there is an abundance of high-refractive-index glasses in this design. However, this is required for correction at large numeric apertures. Also, the LASF glasses are expensive and show some absorption in the blue (N-LASF45 has a transmission of 0.68 at  $0.4\ \mu\text{m}$  for a 25-mm thickness). It is important when optimizing lenses of high numeric aperture like this to trace a sufficient number of rays. In ZEMAX, the author used a ray pattern with six rays on-axis covering half of the pupil (due to symmetry, see [Table 1.1](#)). The lens data for this design are detailed in [Table 6.4](#). The distortion of 5.4% is large considering the small field angle.

## REFERENCES

- Brandt, H. M. (1956) *The Photographic Lens*, Focal Press, New York.
- Caldwell, B. (1999) Fast double Gauss lens, *Optics and Photonic News*, 10, 38–39.
- Fujioka, Y. (1984) Camera lens system with long back focal distance, US Patent #4443070.
- Imai, T. (1983) Standard photographic lens system, US Patent #4396255.
- Juergens, R. C. (1980) The sample problem: a comparative study of lens design programs and users, *1980 International Lens Design Conference Proc. SPIE*, 237: 348.
- Kidger, M. J. (1967) Design of double Gauss systems, *Applied Optics*, 6, 553–563.
- Kingslake, R. (1951) *Lenses in Photography*, Garden City Books, Garden City, NY.
- Kitahara, Y. (1999) Fast double gauss lens, US Patent #5920436.
- Mandler, W. (1980) Design of basic double Gauss lenses. *Proc. SPIE*, 237: 222.
- Momiyama, K. (1982) Large aperture ratio photographic lens, US Patent #4364643.
- Mori, I. (1983) Gauss type photographic lens, US Patent #4390252.
- Mori, I. (1984) Gauss type photographic lens, US Patent #4426137.
- Wakamiya, K. (1984) Great aperture ratio lens, US Patent #4448497.
- Wakimoto, Z. and Yoshiyuki, S. (1971) Photographic lens having a large aperture, US Patent #3560079.

# 7 Telephoto Lenses

Telephoto lenses consist of a front positive ( $F_a$ ) and a rear negative ( $F_b$ ) group separated by a distance  $T$  (see [Figure 7.1](#)). The telephoto ratio is defined as  $L/F$  (Cooke 1965). Assuming thin lenses,

$$\frac{1}{F} = \frac{1}{F_a} + \frac{1}{F_b} - \frac{T}{F_a F_b},$$

$$\text{BFL} = \frac{F(F_a - T)}{F_a}.$$

Solving the above equations gives

$$F_a = \frac{TF}{F - L + T}, \quad \text{and} \quad F_b = \frac{T(T - L)}{F - L}.$$

The absolute value of  $F_b$  is maximum at  $T = L/2$ .

[Figure 7.2](#) shows a telephoto lens derived from that of Aklin (1945). It is  $f/5.6$ , with a  $20^\circ$  field of view ( $FOV$ ) and effective focal length ( $EFL$ ) of 5.0. The data for the lens is given in [Table 7.1](#).

[Figure 7.3](#) show an  $f/2.8$  telephoto lens for use with a single-lens reflex (SLR) camera (film size is 1.703 diagonal). The lens prescription is given in [Table 7.2](#).

[Figure 7.4](#) shows a 400-mm focal length  $f/4$  telephoto lens for which the data is given in [Table 7.3](#). It covers an image diameter of 1.07 in. and is therefore useful for 35-mm motion-picture cinematography.

Internal focusing is generally used on relatively long lenses of this type. It has the mechanical advantage of keeping the entire lens fixed to the camera, while only moving an internal element. For examples of this, see Kreitzer (1982) or Sato (1994). In this case, the last two cemented doublets are moved toward the film plane when going from a distant object to a near one. [Table 7.4](#) shows this focusing movement.

This is accomplished with a computer program that can handle multi-configurations. Since the aperture stop diameter should (preferably) remain fixed as we focus, paraxial image height is used instead of field angle and  $f/\#$ . In this case, thickness  $7$  is varied while holding the overall length constant for all the configurations.

[Figure 7.5](#) shows a 1000-mm  $f/11$  telephoto lens for which the data is given in [Table 7.5](#). It covers a diameter of 1.704 in. and so may be used for an SLR camera.

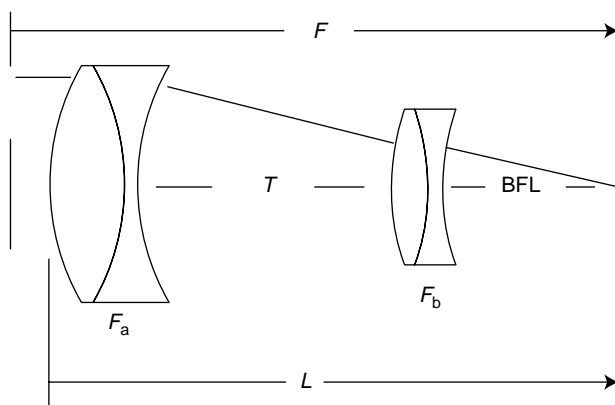


**FIGURE 7.1** Telephoto lens groups.

Overall length is 20.00 and so its telephoto ratio is 0.508. Due to the thickness of the middle element of the front triplet, this lens will be “front heavy.” The reader might find it instructive to compare this design to the Cassegran lens of [Figure 15.4](#).

Focusing is accomplished by moving the rear cemented doublet. As with the previous design the aperture diameter is fixed while focusing at the different object distances. Also, the overall length must be held while focusing. Details of the focusing movement are given in [Table 7.6](#).

Quite frequently, it is desirable to extend the focal length of an existing objective ( $F_a$ ) by adding a negative achromat ( $F_b$ ) a distance  $T$  from this objective. In addition to creating a telephoto lens, it may also be used as a dual-mode system, i.e., by inserting a mirror between the objective and the negative achromat, a dual-focal-length system may be attained. Consider the cemented achromat in [Figure 2.2](#). If one wants to double the focal length of this lens, then from the above equations with  $T=8.0$ , a negative achromat of focal length of  $-24.0$  is required.

Using the same materials, N-BAK1 and SF2 as the objective, the thin-lens achromat equations are used to arrive at a starting solution (refer to [Table 2.1](#)). The system is then optimized by varying only the parameters of the negative lens. [Figure 7.6](#) shows the results of this. Effective focal length is 40 and FOV is  $1.5^\circ$ . The lens data for [Figure 7.6](#) is detailed in [Table 7.7](#). This system has considerable lateral color that results in the nearly horizontal lines in the root mean square (RMS) spot-size plot.



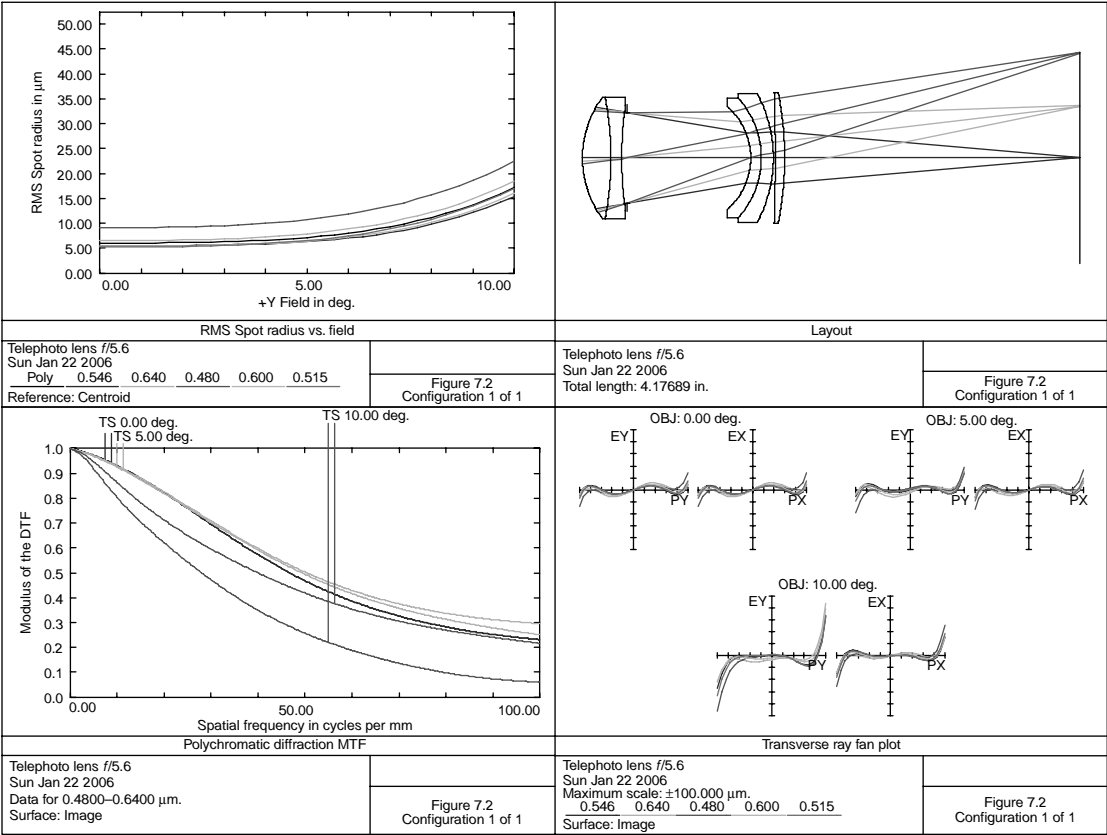


FIGURE 7.2 A telephoto f/5.6 lens.

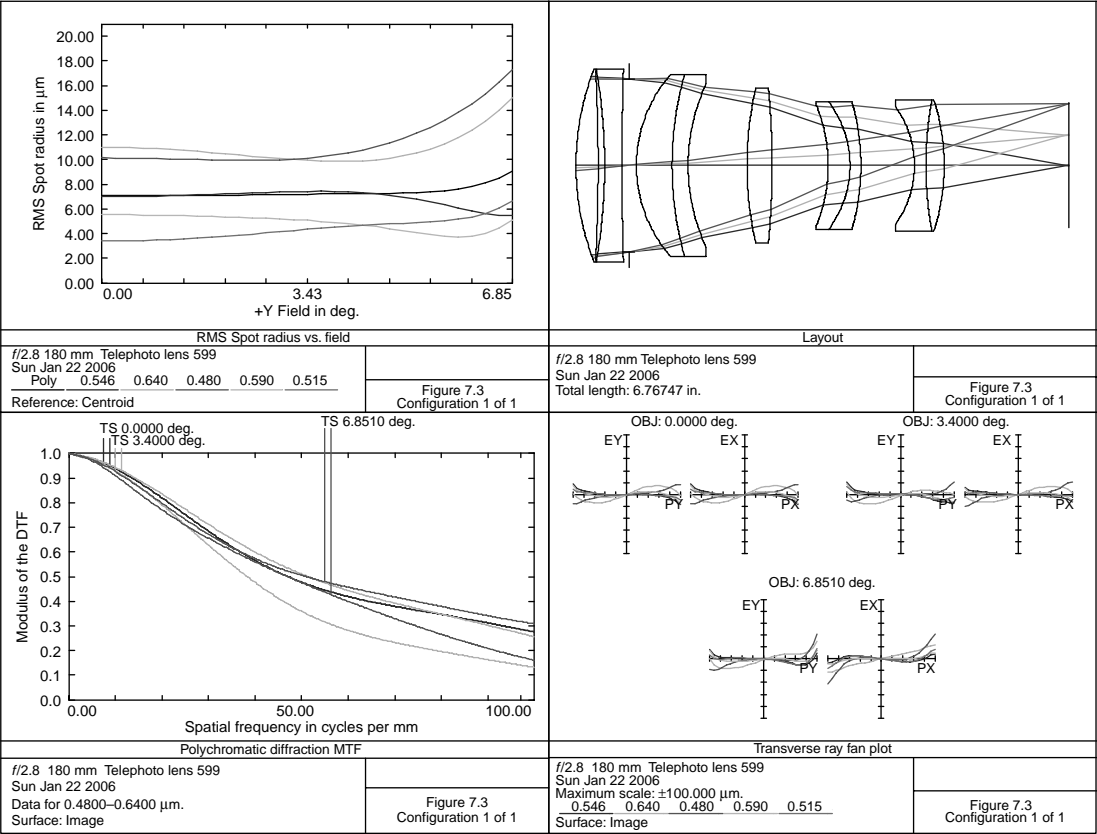


FIGURE 7.3 A *f*/2.8 180-mm telephoto lens.

**TABLE 7.1**  
**An  $f/5.6$  Telephoto Lens with  $EFL$  of 5.0**

Surface	Radius	Thickness	Material	Diameter
1	0.8589	0.2391	N-BK7	1.020
2	-2.6902	0.0900	N-BASF2	1.020
3	3.0318	0.0481		0.880
4	Stop	1.0347		0.766
5	-0.5715	0.0900	N-ZK7	0.860
6	-0.7423	0.1005	N-LAF33	1.000
7	-1.1433	0.0156		1.080
8	-17.0388	0.0793	SF1	1.100
9	-2.7695	2.4796		1.100

Distance from first lens surface to image=4.177, distortion=0.47%  
 (pincushion), telephoto ratio=0.835.

**TABLE 7.2**  
**An  $f/2.8$ , 180-mm Telephoto Lens**

Surface	Radius	Thickness	Material	Diameter
1	3.6349	0.3036	N-BK7	2.640
2	-24.7282	0.0895		2.640
3	-7.6566	0.2374	F5	2.580
4	41.9314	0.1000		2.640
5	Stop	0.1000		2.370
6	1.9097	0.4879	N-BK10	2.500
7	4.5888	0.2200	SF1	2.500
8	2.6494	0.8101		2.240
9	4.8821	0.3426	N-KF9	2.120
10	-11.3966	0.7696		2.120
11	-2.1864	0.2998	K10	1.700
12	-1.4618	0.1500	SF1	1.740
13	-3.1274	0.7330		1.740
14	-1.4059	0.1600	N-K5	1.620
15	5.1640	0.2494	SF5	1.800
16	-2.9315	1.7146		1.800

Distance from first lens surface to image=6.767, distortion=0.57%  
 (pincushion), telephoto ratio=0.955.

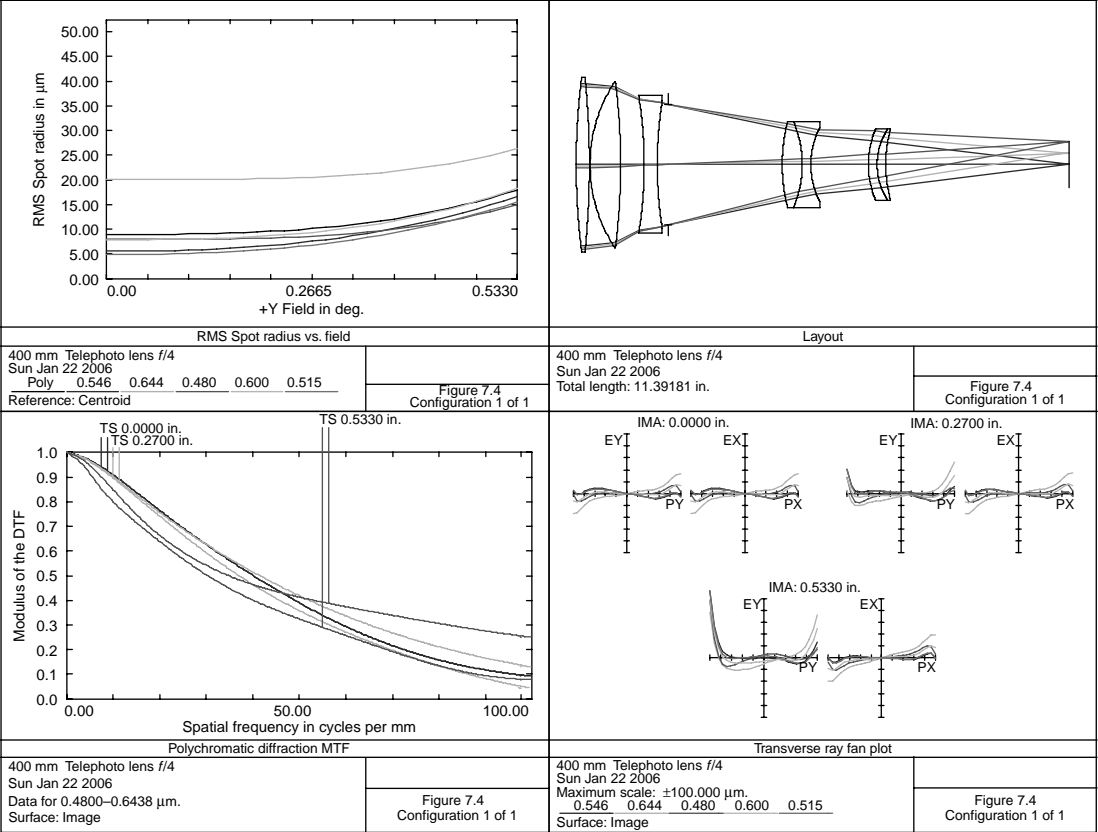


FIGURE 7.4 A 400-mm *f*/4 telephoto lens.

**TABLE 7.3**  
**A 400-mm *f*/4 Telephoto Lens**

Surface	Radius	Thickness	Material	Diameter
1	16.2665	0.3042	N-FK5	4.020
2	−19.9912	0.0150		4.020
3	3.4920	0.7067		3.820
4	−15.0735	0.5468		3.820
5	−9.8613	0.3000	SF1	3.180
6	9.7403	0.2610		2.960
7	Stop	2.6245		2.791
8	4.0679	0.4635	SF1	1.980
9	−2.4971	0.2000	N-LAF3	1.980
10	1.8699	1.3277		1.680
11	2.1187	0.2000	SF1	1.660
12	1.5200	0.2011	N-FK5	1.660
13	3.0828	4.2414		1.560

Distance from first lens surface to image=11.392, distortion=0.35%  
(pincushion), telephoto ratio=0.72.

**TABLE 7.4**  
**Focusing Movement for 400-mm Telephoto Lens**

Object Distance	<i>T</i> (7)	<i>T</i> (13)
Infinity	2.624	4.241
1500	2.706	4.160
750	2.789	4.077
500	2.874	3.992

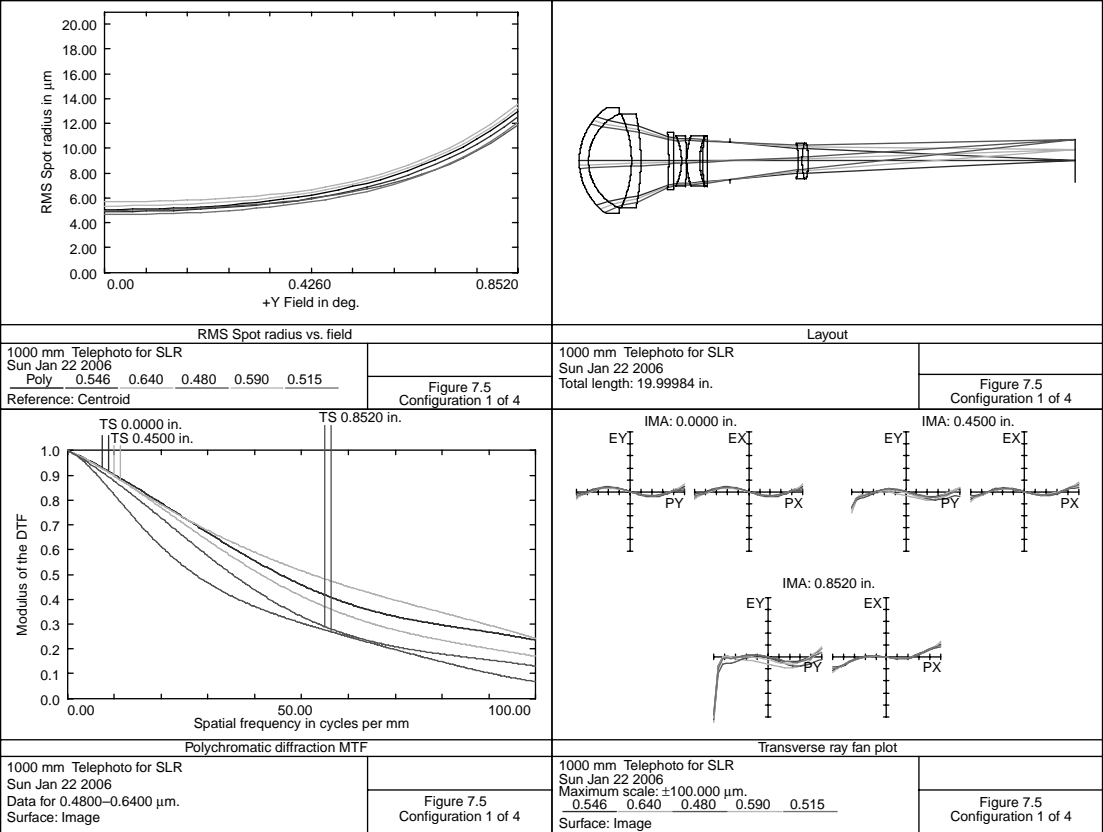


FIGURE 7.5 A 1000-mm f/11 telephoto lens.

**TABLE 7.5**  
**An Apochromat Telephoto for an SLR**

Surface	Radius	Thickness	Material	Diameter
1	2.6332	0.3730	N-LAK12	4.260
2	2.0674	1.7336	S-FPL53	3.800
3	−4.4324	0.3730	N-SK16	3.800
4	−9.5362	1.1269		3.800
5	−13.7333	0.1976	SF1	2.300
6	62.0769	0.3173		2.200
7	−2.3374	0.1980	N-LAK10	2.040
8	−13.6459	0.0150		2.040
9	3.0957	0.5227	S-FPL53	2.040
10	2.6268	0.1092		1.880
11	5.2901	0.1876	SF1	2.040
12	48.8360	0.9234		2.040
13	Stop	2.7584		1.496
14	−2.9733	0.1463	N-LAK10	1.360
15	3.1113	0.2491	F5	1.420
16	−3.4606	10.7685		1.420

Distortion = +0.27% (pincushion).

**TABLE 7.6**  
**Focusing Movement for 1000-mm Telephoto Lens**

Object Distance	<i>T</i> (13)	<i>T</i> (16)
Infinity	2.758	10.768
5000	2.847	10.680
2000	2.983	10.544
1000	3.216	10.311

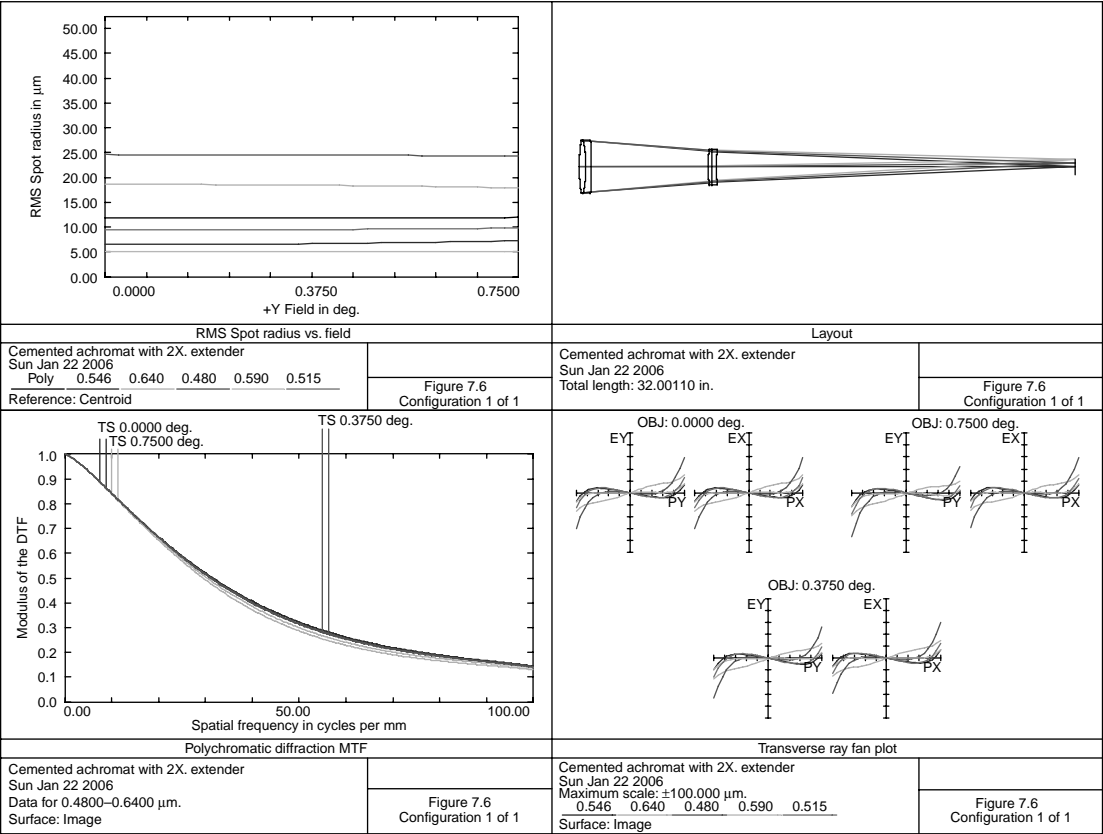


FIGURE 7.6 A cemented achromat with a 2× extender.



**TABLE 7.7**  
**Cemented Achromat with 2× Extender**

Surface	Radius	Thickness	Material	Diameter
1	12.3840	0.4340	N-BAK1	3.410 Stop
2	−7.9414	0.3210	SF2	3.410
3	−48.4440	7.5706		3.410
4	17.9546	0.2500	SF2	2.320
5	−32.0067	0.2500	N-BAK1	2.320
6	6.8946	23.1755		2.240

Distance from first lens surface to image = 32.001, distortion = 0.02%.

## REFERENCES

- Aklin, G. (1945) Telephoto objective, US Patent #2380207.  
 Arai, Y. (1984) Large aperture telephoto lens, US Patent #4447137.  
 Cooke, G. H. (1965) *Photographic Objectives, Applied Optics and Optical Engineering*, (R. Kingslake, ed.) 3: 104 Academic Press, NY.  
 Eggert, J. (1968) Photographic telephoto lenses of high telephoto power, US Patent #3388956.  
 Horikawa, Y. (1984) Telephoto lens system, US Patent #4435049.  
 Kreitzer, M. H. (1982) Internal focusing telephoto lens, US Patent #4359272.  
 Matsui, S. (1982) Telephoto lens system, US Patent #4338001.  
 Sato, S. (1994) Internal focusing telephoto lens, US Patent #5323270.  
 Tanaka, T. (1986) Lens system, US Patent #4575198.



---

# 8 Inverted Telephoto Lens

The inverted telephoto, or retrofocus, lens consists of a negative front lens group and a rear positive lens group. It is characterized by having a long back focal length (BFL) in relation to its effective focal length (EFL). This type of construction is then extensively used in short-focal-length, wide-angle lenses for single-lens reflex (SLR) cameras. Here, a long BFL is required to clear the moving mirror and shutter mechanisms. It is thus important when setting up the merit function in the optimization program to properly limit the minimum allowable back focal length. [Figure 8.1](#) shows an inverted telephoto. The requirements for this lens were that it have a BFL of at least 1.8 F (Laikin 1974). [Table 8.1](#) provides the lens data for [Figure 8.1](#).

Note that the lenses all have the same diameter and they may therefore be readily assembled into a housing with the same inside diameter. Field of view is  $28.5^\circ$ . Note that the second element is meniscus and nearly concentric about the aperture stop. It helps reduce spherical aberration of the assembly.

[Figure 8.2](#) shows a wide angle inverted telephoto lens; the lens data is given in [Table 8.2](#). It is a modification of the Albrecht (1962) patent. It has a focal length of 10 mm, is  $f/2.5$  with a  $70^\circ$  FOV and may therefore be used as a camera lens for 16-mm cinematography (0.500 diagonal).

This lens shows relatively little chromatic aberration. The main aberration is oblique spherical. This causes the drop in tangential MTF response. However, because the entrance pupil is enlarged at the edge of the field, relative illumination is 0.99 of the axial value. Also note that for a lens designed with vignetting, it is important to mechanically limit the off axis bundle. This is accomplished here at surfaces 1 and 12.

[Figure 8.3](#) shows an inverted telephoto lens also suitable as a camera lens for 16-mm cinematography; the data is provided in [Table 8.3](#). This covers a diagonal of 0.5 in. and has a focal length of 0.628 in. (16 mm). Overall length is 3.357. Field of view is  $43.28^\circ$ . This lens is a modification of the Miles (1972) patent.

An interesting variation of the inverted telephoto design is its use as a soft focus photographic lens for portraiture. Since the portrait photographer does not want a lens with extreme resolving power that would show the subjects facial blemishes, a lens with spherical aberration is sometimes used. (Another trick is to use some grease on the front element to soften the image.) Caldwell (1999) discusses such a system in his patent review of the Hirakawa (1999) patent.

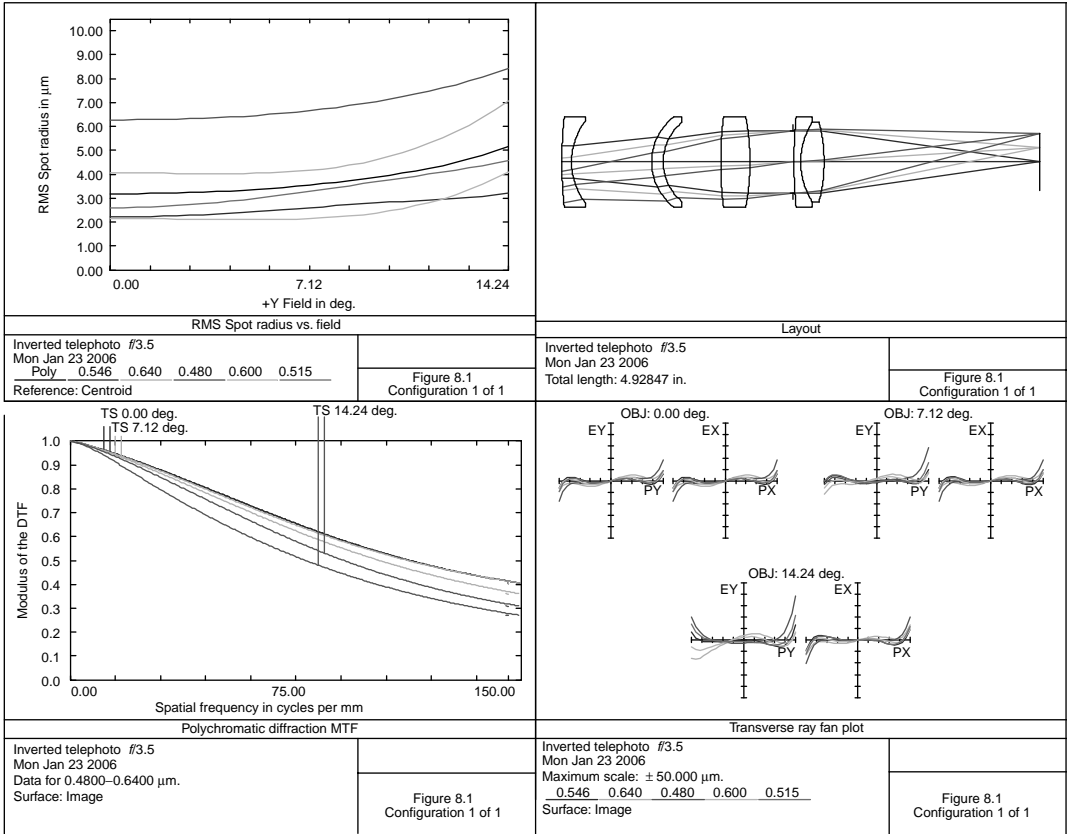


FIGURE 8.1 An inverted telephoto,  $f/3.5$ .

**TABLE 8.1**  
**Inverted  $f/3.5$  Telephoto Lens**

Surface	Radius	Thickness	Material	Diameter
1	4.5569	0.1000	N-PK51	0.940
2	0.7040	0.8254		0.860
3	0.5900	0.1200		0.940
4	0.5329	0.5916	SF1	0.820
5	3.8106	0.3022		0.940
6	− 2.4206	0.4382		0.940
7	Stop	0.0150	SF1	0.647
8	5.0596	0.0695		0.940
9	0.7648	0.2412		0.820
10	− 1.6496	2.2253	N-LAK21	0.820

Distance from front lens to image = 4.928, distortion = 2.39%, lens focal length = 1.181.

**TABLE 8.2**  
**Wide-Angle Inverted Telephoto**

Surface	Radius	Thickness	Material	Diameter
1	− 3.6590	0.0874	N-LAF2	1.520
2	0.8260	0.4851	N-PSK3	1.310
3	− 1.6509	0.2232		1.310
4	1.0609	0.1716		0.840
5	− 1.7274	0.0649	N-BK7	0.840
6	0.2416	0.4439		0.500
7	Stop	0.1263		0.255
8	− 7.2279	0.0604	SF1	0.440
9	0.7971	0.2495	N-SK16	0.610
10	− 0.6222	0.0150		0.610
11	4.3097	0.1058		0.660
12	− 0.9908	0.0150	N-LAK12	0.660
13	0.9191	0.1721		0.660
14	− 0.6616	0.0600		0.660
15	2.8942	0.6069	SF1	0.620

Distance from first lens surface to image = 2.887, distortion = 10.5% (10% vignetting).

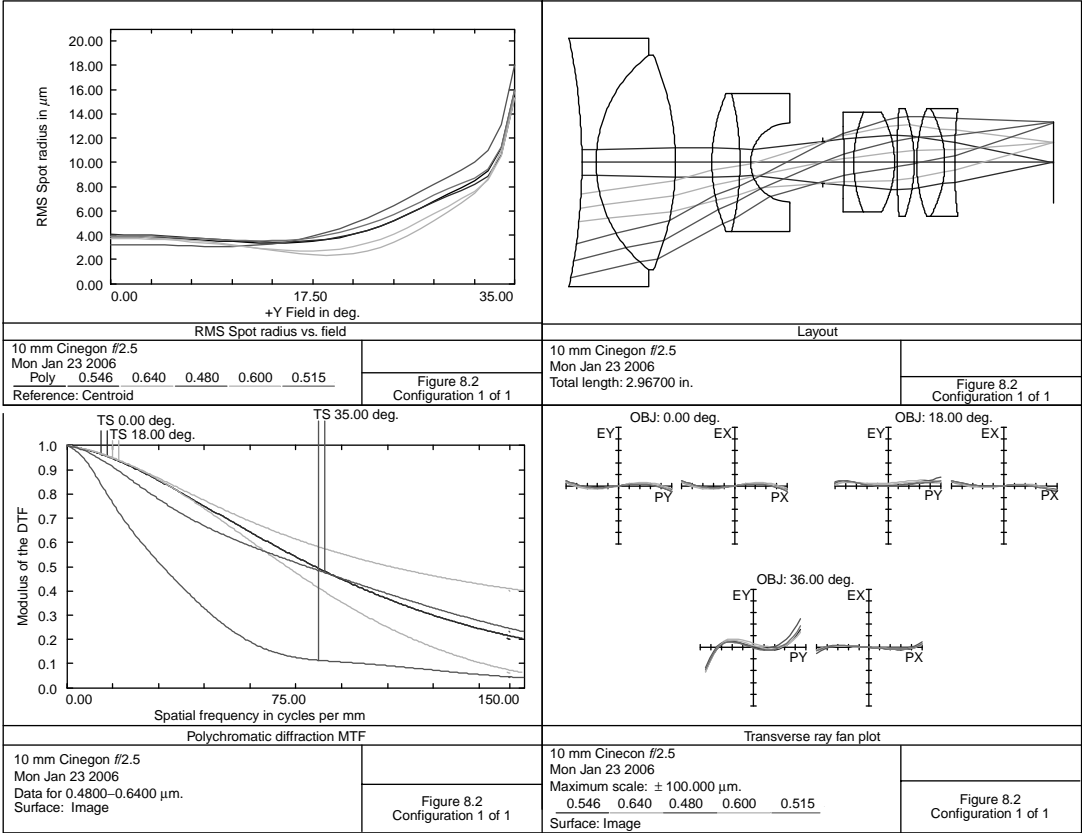


FIGURE 8.2 A 10-mm Cinegon.

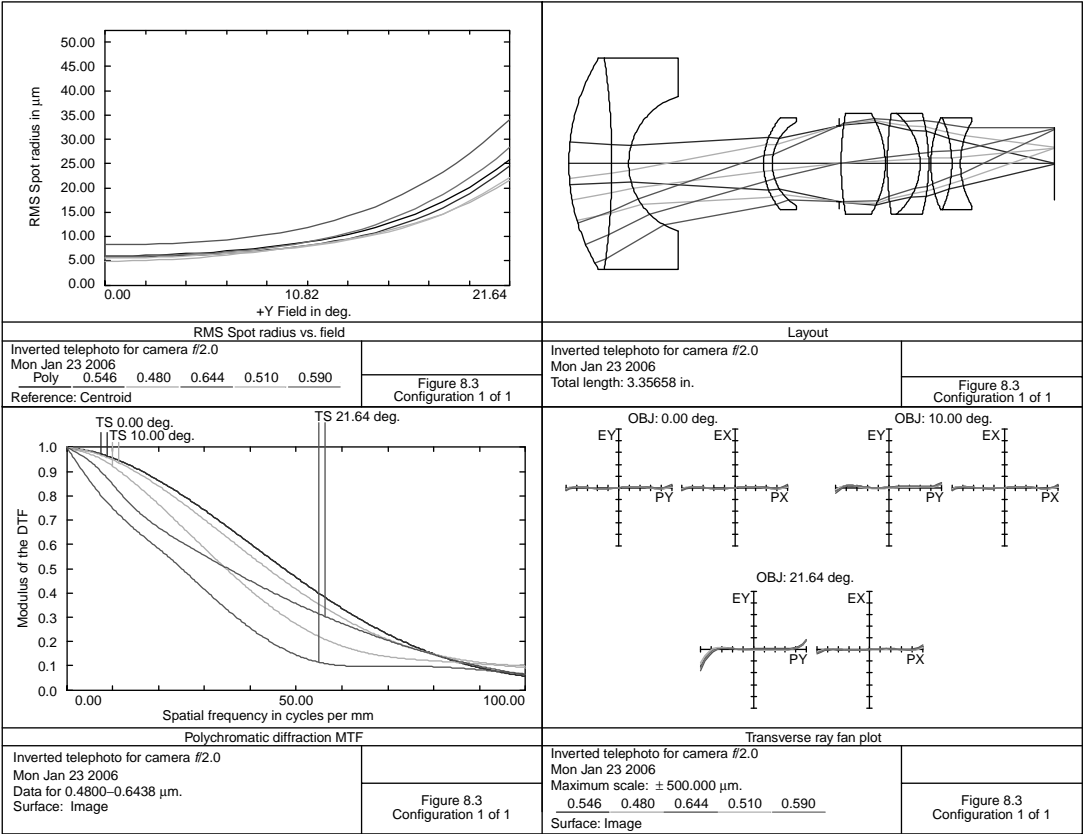


FIGURE 8. 3 An inverted telephoto for a camera.

**TABLE 8.3**  
**Inverted  $f/2.0$  Telephoto for a Camera**

Surface	Radius	Thickness	Material	Diameter
1	1.4027	0.2969	N-LAF2	1.460
2	-5.1486	0.1162	N-LLF6	1.460
3	0.4868	0.9329		0.930
4	0.4912	0.0600	SF5	0.640
5	0.3357	0.4606		0.580
6	Stop	0.0150		0.526
7	2.0683	0.3041	N-LAK10	0.700
8	-0.6738	0.0150		0.700
9	2.2926	0.2256	N-BK7	0.700
10	-0.4527	0.0600	SF1	0.700
11	-1.3877	0.0150		0.700
12	0.7873	0.1445	N-ZK7	0.640
13	-0.7873	0.0600	N-BAF4	0.640
14	0.5847	0.6508		0.580

Distortion = 2.1%.

## REFERENCES

- Albrecht, W. (1962) High speed photographic objective with wide image angle, US Patent #3045547.
- Caldwell, B. (1999) Wide angle soft focus photographic lens, *Opt. Photonics News*, 10: 49.
- Cooke, G. H. (1955) Optical objectives of the inverted telephoto type, US Patent #2724993.
- Fischer, H. (1977) High speed wide angle objective lens system, US Patent #4025169.
- Fujibayashi, K. (1980) Compact retrofocus wide angle objective, US Patent #4235519.
- Hirakawa, J. (1999) Wide angle soft focus photographic lens, US Patent #5822132.
- Hopkins, R. E. (1952) Wide angle photographic objective, US Patent #2594021.
- Hudson, L. M. (1960) Photographic objective, US Patent #3064533.
- Kingslake, R. (1966) The reversed telephoto objective, *SMPTE*, 76: 203.
- Kubota, T. (1979) Small retro-focus wide angle photographic lens, US Patent #4134945.
- Laikin, M. (1974) High resolution reverse telephoto lens, US Patent #3799655.
- Miles, J. R. (1972) Objective lens for short focal length camera, US Patent #3672747.
- Momiyama, K. (1984) Inverted telephoto type wide angle objective, US Patent #4437735.
- Mori, I. (1972) Retrofocus type lens system, US Patent #3635546.
- Tsunashima, T. (1979) Wide angle photographic objective, US Patent #4163603.



---

# 9 Very-Wide-Angle Lenses

Very-wide-angle lenses have fields of view greater than  $100^\circ$  and are of the inverted telephoto design. Such large field angles result in very large distortion—so large that a designer really should not even quote distortion as such. The lens, of course, has focal length, but has little meaning considering the large distortion. According to the  $\cos^4$  law of illumination (Reiss 1945, 1948; Ray 1997), the illumination of optical systems is given by  $E = k \cos^4 \theta$ . However, this assumes no distortion and a constant entrance-pupil diameter with field angle. Therefore, lenses obeying this “law” would have no illumination past semi-field angles of  $90^\circ$ .

If  $Y$  is the image height (measured from the optical axis to image centroid) and  $\theta$  the semi-field angle, then for a distant object  $Y = F \tan \theta$  if there is no distortion. In fisheye lenses,  $Y \approx 0.015F\theta$  (Laikin 1980). That is, image height is nearly a linear function of the field angle.

With increasing field angle, the entrance pupil moves from inside the lens toward the front of the lens and substantially increases in size. This pupil movement is extremely apparent when examining such lenses. Pupil aberration must be considered during the design; ray starting data must be constantly readjusted at the various field angles. During analysis and MTF calculations, this starting data must also be adjusted at the various wavelengths.

During the preliminary design phase, determining the initial pupil shift values is a difficult task. In the ZEMAX program, as in other lens design programs, this determination of pupil shift is done automatically. Also, the computer program should allow the EFL to be varied at will, ignore the distortion, and maintain only the image heights at various field angles.

Due to the very short focal length, axial secondary color will not be a problem. However, the large field angle makes lateral secondary color impossible to eliminate. Large distortion creates a unique problem: lens aberrations are sensitive to object distance changes. For convenience, this author generally designs projection lenses first at an infinite conjugate. Then, for the last few computer runs, finite conjugate and screen curvature is introduced. However, all of the following examples are presented for an infinite conjugate and are corrected over the visual region.

Figure 9.1 shows a  $100^\circ$ -field-of-view (FOV) camera lens for which the data is given in Table 9.1. It was designed to cover the 35-mm academy format (1.069 diagonal). Focal length is 0.656 and it is  $f/2$ .

Note from the ray diagram that this lens has a nearly telecentric exit pupil. As a camera lens, this is immaterial; however, if this is to be used for projection, one must either place a negative field lens between the film gate and the arc source to properly

locate the arc image (see comments about exit-pupil location under [Figure 9.3](#)) or redesign this for proper exit-pupil location.

This is an interesting design because only two common glasses are being used and it does not contain any of the lanthanum types frequently used in some of the other designs in this section.

[Figure 9.2](#) shows an  $f/2$   $120^\circ$ -FOV projection lens for 70-mm cinematography; data is given in [Table 9.2](#). The lens focal length is 1.123. It has the same glass types as the above design, but the exit pupil is properly located for a normal projection system.

The exit pupil is located at a distance of  $-5.32$  from the film plane. This is the position that the lamp source (an arc) should be imaged into.

[Figure 9.3](#) shows an  $f/2$   $160^\circ$ -FOV projection lens for 70-mm cinematography. The lens data is provided in [Table 9.3](#). The lens focal length is 0.943. It is a minor modification of a projection lens designed for Omni Films International (Sarasota, FL) for their Cinema 180 theaters. Notice that the second and third lenses are really the same.

Because this lens was designed for high-power xenon arc projection (as was the lenses shown in [Figure 9.2](#) and [Figure 9.5](#)), the following must be maintained (see also [Chapter 22](#)):

1. A BFL of at least 2 in. is required for film transport mechanism clearance.
2. Special optical cements must be used to withstand the high power densities if cemented surfaces are used.
3. Exit pupil should be about 4–6 in. in front of the film gate. The arc is imaged in this location for most projectors.

The reduced response at  $80^\circ$  off-axis as compared to axial is not really detrimental in wide-field projection systems. The observer's interest is mainly on the center of the screen and his visual acuity is greatly reduced at his peripheral vision. The limits of the normal visual field is  $160^\circ$  horizontal and  $120^\circ$  vertical. Note the large diameters of the front lenses. As a practical matter, it is important to select material that is economical and readily available—thus the choice for N-BK7 glass. Fields of vision greater than this requires the observer to rotate his head (or entire body).

[Figure 9.4](#) shows a  $170^\circ$   $f/1.8$  lens designed as a camera lens for 16-mm film (0.500 diagonal). The data is provided in [Table 9.4](#).

Note that the second surface is nearly a hemisphere. The computer program in use should have a means for preventing this surface from becoming a hyper-hemisphere. In some programs, the bound is the sag at the surface minus the semi-clear aperture at this surface. In ZEMAX, one method to prevent a near hemisphere is to form the product of lens diameter and curvature and then set a limit to this operand.

[Figure 9.5](#) shows a  $210^\circ$ -FOV,  $f/2$  projection lens; lens details are given in [Table 9.5](#). It was designed to be used with a 10-perforation-frame, 70-mm film. From [Appendix A](#), note that this format is  $1.912 \times 1.808$ . The  $210^\circ$  field corresponds

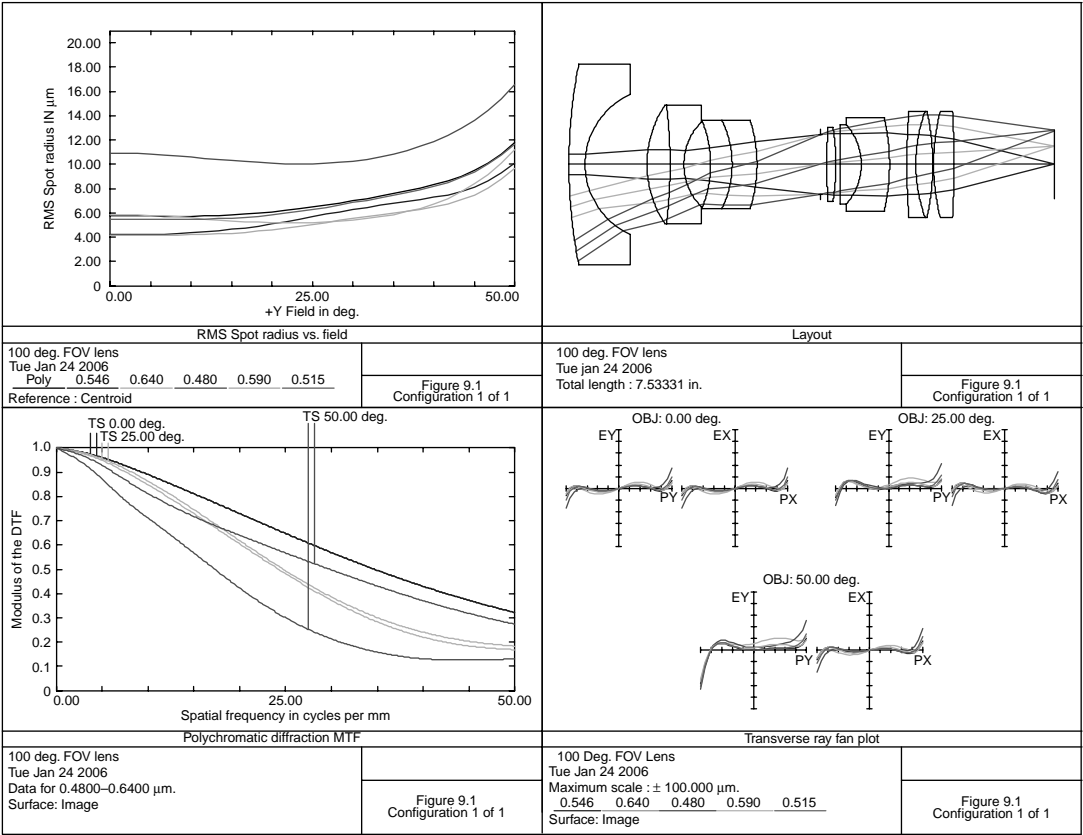


FIGURE 9.1 A 100°-FOV camera lens.

**TABLE 9.1**  
**A 100°-FOV Camera Lens**

Surface	Radius	Thickness	Material	Diameter
1	8.0107	0.2500	N-SK4	3.100
2	1.1856	0.9613		2.160
3	1.6747	0.3578	SF1	1.840
4	−7.5157	0.2136	N-SK4	1.840
5	0.9411	0.4146		1.320
6	−1.7688	0.3333	SF1	1.320
7	−1.5531	0.3863	N-SK4	1.380
8	−2.2281	0.9842		1.380
9	Stop	0.1000		0.917
10	13.6803	0.1400	N-SK4	1.140
11	−3.4279	0.0605		1.140
12	20.0257	0.3332	N-SK4	1.240
13	−0.9258	0.4374	SF1	1.240
14	−3.2233	0.2679		1.460
15	10.3847	0.1400	SF1	1.640
16	2.4272	0.2609	N-SK4	1.640
17	−3.8828	0.0150		1.640
18	3.3650	0.3167	N-SK4	1.640
19	−14.7547	1.5604		1.640

The distance from first lens surface to image = 7.533.

to an image circle of 1.849. It was to be used to project vertically an image into a spherical dome.

To prevent surfaces 2 and 4 from becoming a hyper-hemisphere, bounds were placed on these surfaces as described for the design above. Also due the large diameter of the front lens, an upper bound was placed on the diameter of the front surface. The front two lenses are N-K5, which although not quite as economical as N-BK7, is readily available and moderately priced. Unfortunately, the third lens assembly is a cemented triplet which is used to improve the color correction at the edge of the field.

Figure 9.6 shows a panoramic camera system (see also Powell (1995); Kweon (2005) for similar systems); the details are given in Table 9.6. The first surface shown (surface 2 in the prescription table) is a hyperbolic mirror with a conic coefficient of  $-2.97286$ . The eccentricity,  $\epsilon$ , is  $\sqrt{2.97286} = 1.7242$ .

Surface 1 is a reference surface. This forms a 360° panoramic image in the form of a donut. The outer diameter is 0.94 in., corresponding to objects 60° off-axis. The inner diameter of this donut image is 0.20 in., corresponding to objects 20° off-axis. The effective focal length of this system is 0.3075 in. and it is  $f/6.41$ .

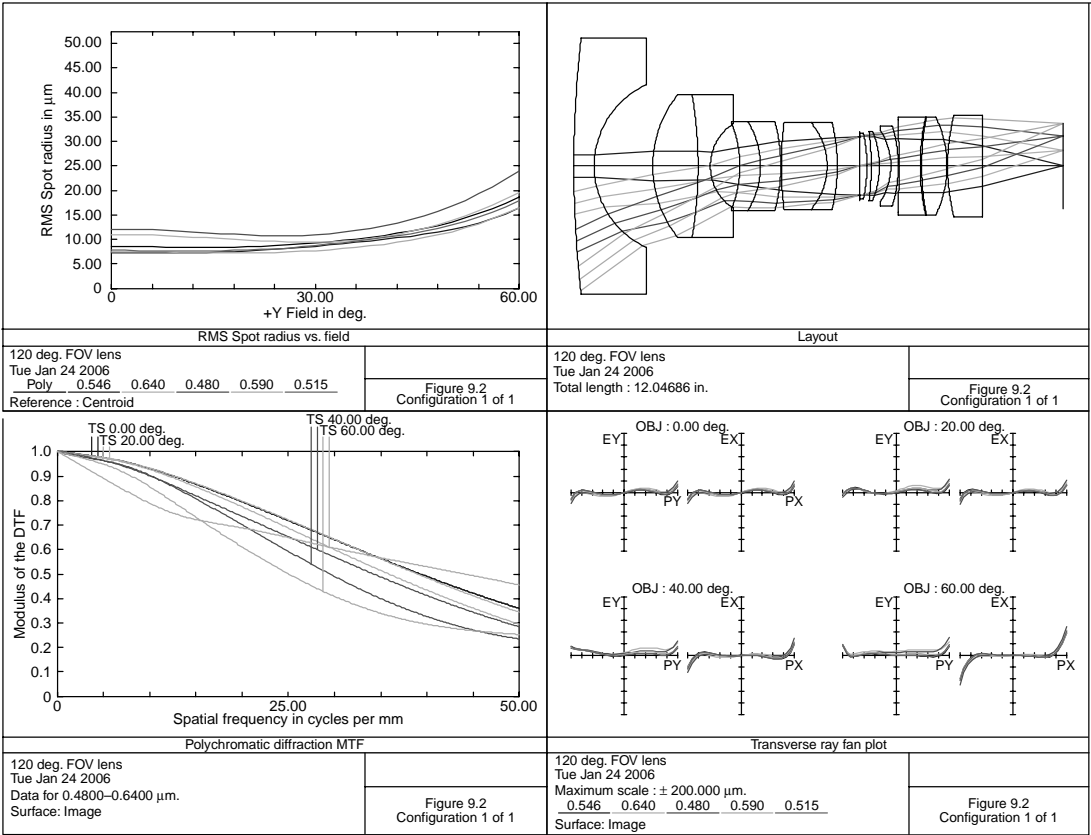


FIGURE 9.2 A 120°-FOV  $f/2$  projection lens.

**TABLE 9.2**  
**A 120°-FOV Projection Lens**

Surface	Radius	Thickness	Material	Diameter
1	28.2482	0.5000	N-SK4	6.300
2	2.2027	1.4379		4.000
3	2.7819	1.1174	SF1	3.500
4	−10.4886	0.3022	N-SK4	3.500
5	1.2417	0.7247		2.080
6	−2.8768	0.5088	SF1	2.080
7	−2.0989	0.4998	N-SK4	2.180
8	−4.2448	0.0150		2.180
9	8.4162	1.1279	N-SK4	2.140
10	−1.6294	0.2486	SF1	2.140
11	−4.5056	0.5412		2.140
12	Stop	0.0200		1.452
13	0.0000	0.1689	N-SK4	1.620
14	−3.8691	0.1065		1.620
15	−6.6827	0.2007	N-SK4	1.720
16	−2.2167	0.2822		1.720
17	−1.6444	0.1827	SF1	1.760
18	−3.3466	0.0149		1.960
19	−36.4599	0.5235	SF1	2.260
20	5.3765	0.0373		2.400
21	6.4204	0.6243	N-SK4	2.400
22	−2.7537	0.0150		.400
23	5.1876	0.8475	N-SK4	2.500
24	0.0000	2.0000		2.500

Distance from first lens surface to image=12.047.

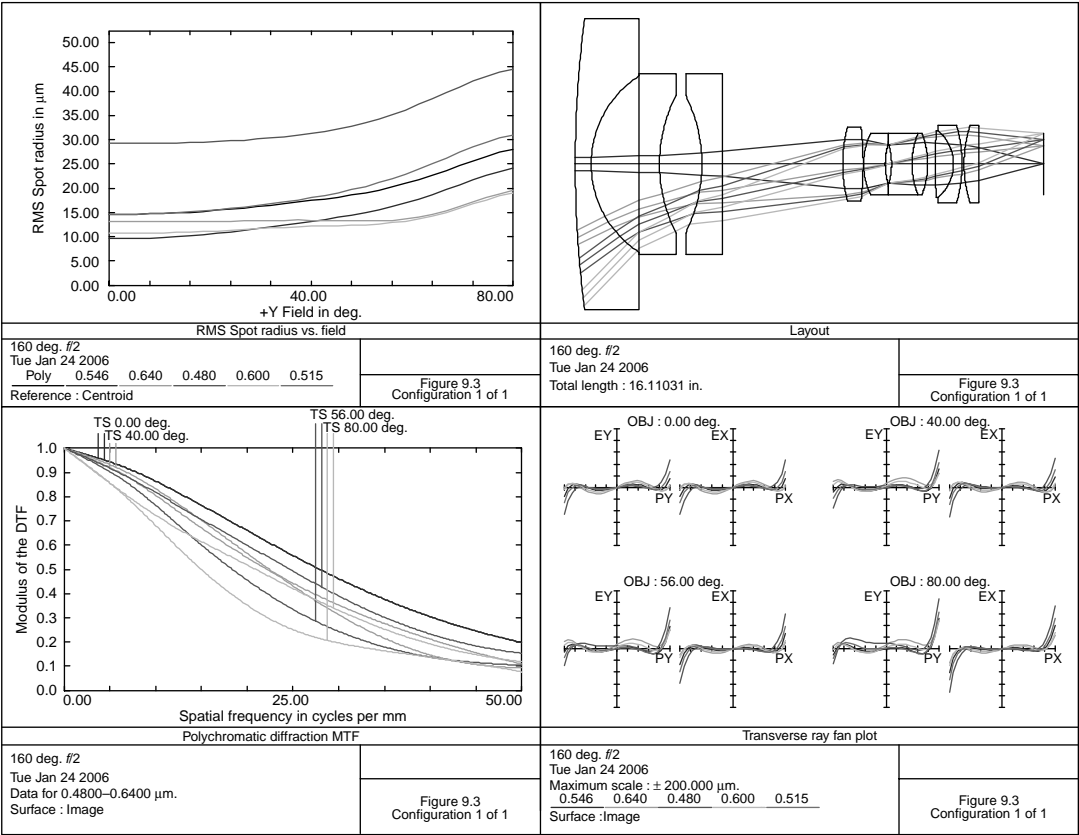


FIGURE 9.3 A 160°-FOV  $f/2$  projection lens.

**TABLE 9.3**  
**An  $f/2$  160°-FOV Projection Lens**

Surface	Radius	Thickness	Material	Diameter
1	38.9150	0.5459	N-BK7	10.000
2	3.6152	1.6595		6.080
3	0.0000	0.6927	N-BK7	6.200
4	5.2515	1.4576		4.720
5	−5.2515	0.6927	N-BK7	4.720
6	0.0000	4.1494		6.200
7	5.1075	0.7000	SF4	2.520
8	−10.8385	0.0162		2.520
9	2.3897	0.7443	SF4	2.100
10	2.2789	0.1136		1.400
11	Stop	0.1040		1.333
12	−2.3536	0.7038	SF1	1.400
13	2.7829	0.5423	N-LAK7	2.100
14	−2.8287	0.2506		2.100
15	13.1578	0.6350	N-LAK7	2.300
16	−1.4944	0.2922	SF4	2.300
17	−4.8082	0.0668		2.680
18	4.3447	0.5059	N-LAK21	2.680
19	72.8673	2.2376		2.580

Distance front lens surface to image= 16.110.



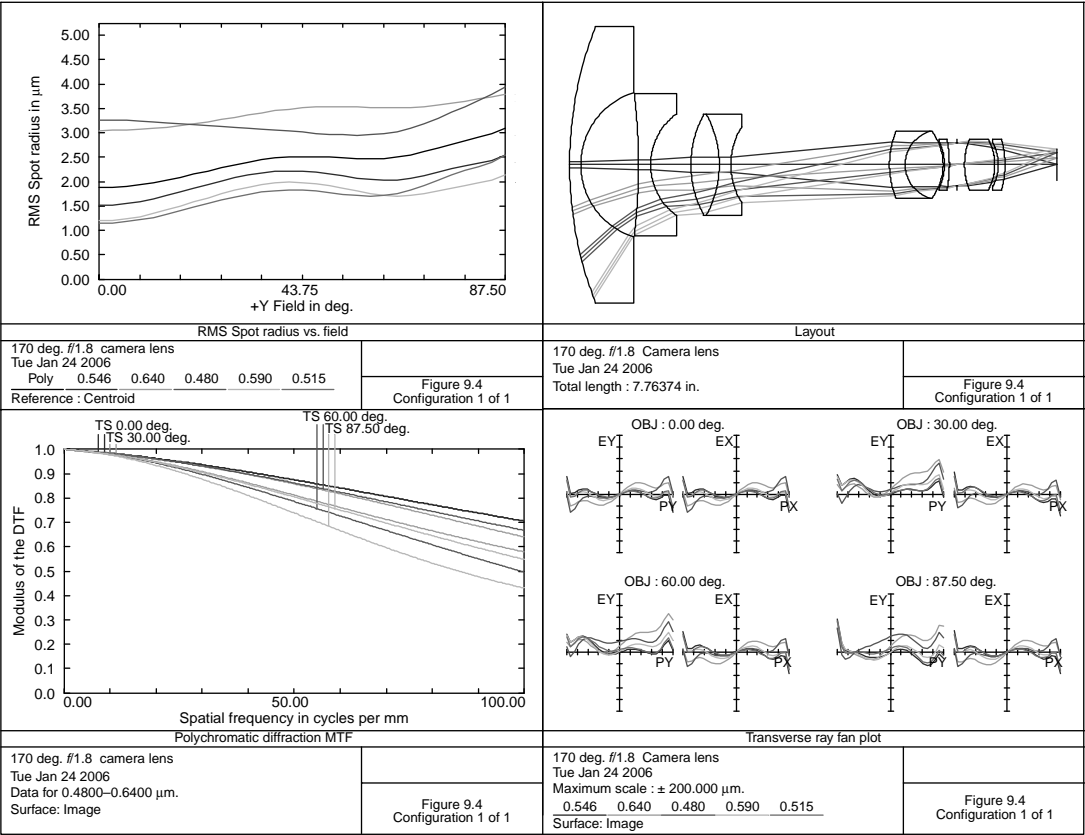


FIGURE 9.4 A 170°-FOV  $f/1.8$  camera lens.

**TABLE 9.4**  
**A 170°-FOV,  $f/1.8$  Camera Lens**

Surface	Radius	Thickness	Material	Diameter
1	6.0515	0.1796	N-BK7	4.400
2	1.2087	0.9182		2.300
3	-9.4697	0.1939	N-SK5	2.260
4	1.0053	0.6402		1.620
5	1.6634	0.4518	SF1	1.600
6	-1.6712	0.1825	N-LAK9	1.600
7	1.1206	2.5272		1.220
8	1.3895	0.2500	N-LAK9	1.060
9	0.5522	0.6047	N-PSK3	1.060
10	-0.8844	0.0196		1.060
11	-0.8804	0.0800	SF1	0.780
12	-2.1545	0.1200		0.820
13	Stop	0.1200		0.684
14	1.0354	0.4830	N-PSK3	0.820
15	-0.8443	0.0546		0.820
16	-0.7386	0.1076	SF1	0.700
17	-1.5285	0.8308		0.820

Distance from first lens surface to image = 7.764, lens focal length = 0.205.

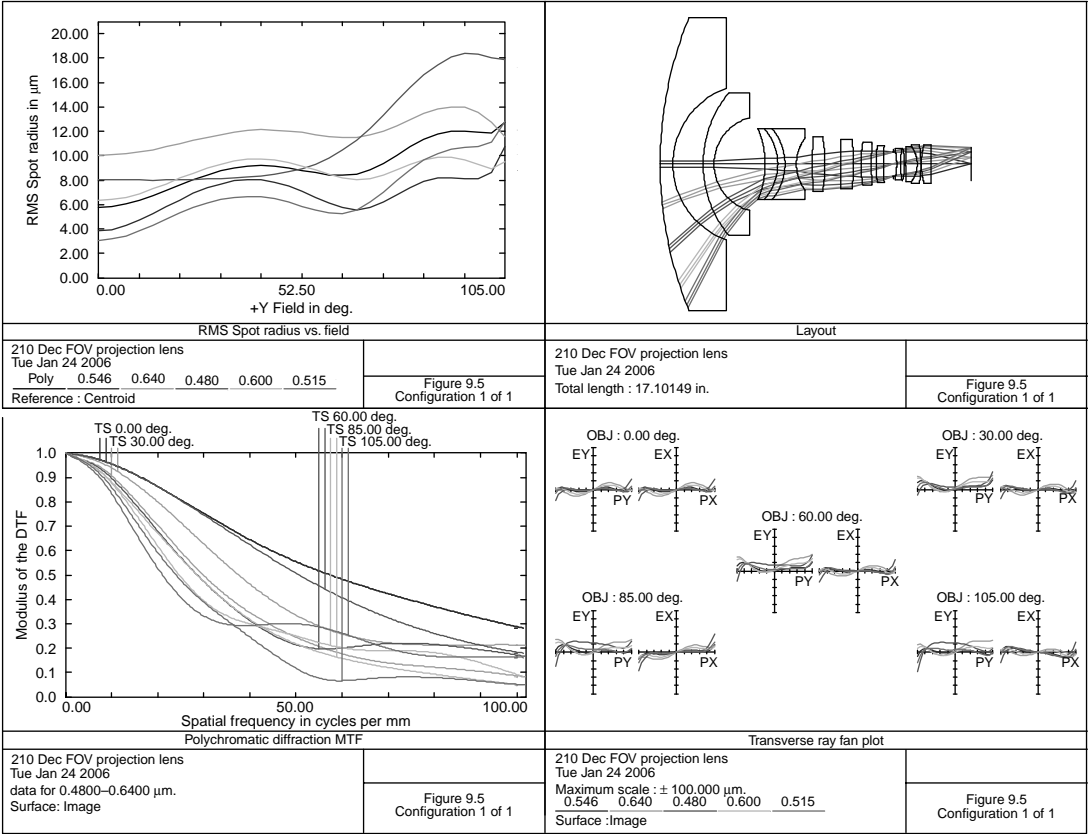


FIGURE 9.5 A 210°-FOV projection lens.

**TABLE 9.5**  
**A 210°-FOV Projection Lens**

Surface	Radius	Thickness	Material	Diameter
1	21.1576	0.7000	N-K5	16.080
2	4.4088	1.6598		8.320
3	6.1240	0.6000	N-K5	7.800
4	2.6351	2.8079		5.080
5	−4.9887	0.6898	N-K5	3.880
6	−2.9312	0.4000	SF4	3.880
7	−3.0217	0.6229	N-PSK3	3.880
8	2.3857	0.8744		2.880
9	22.0209	0.7000	SF4	2.960
10	−8.2506	0.8566		2.960
11	101.6268	0.7000	N-SSK5	2.700
12	−12.9224	0.4212		2.700
13	7.5022	0.5714	SF4	2.360
14	29.4757	0.2557		2.180
15	7.6940	0.4131	SF5	2.000
16	19.1201	0.5462		2.000
17	Stop	0.1681		1.340
18	−3.7912	0.2042	SF5	1.500
19	4.0170	0.2330	N-LAK7	1.720
20	−3.5074	0.0496		1.720
21	9.6933	0.6446	N-LAK7	1.920
22	−1.6179	0.2000	SF4	1.920
23	−6.4878	0.0150		2.140
24	3.5035	0.5518	N-LAK7	2.140
25	−68.3415	2.2162		2.140

Distance from first lens surface to image = 17.101.

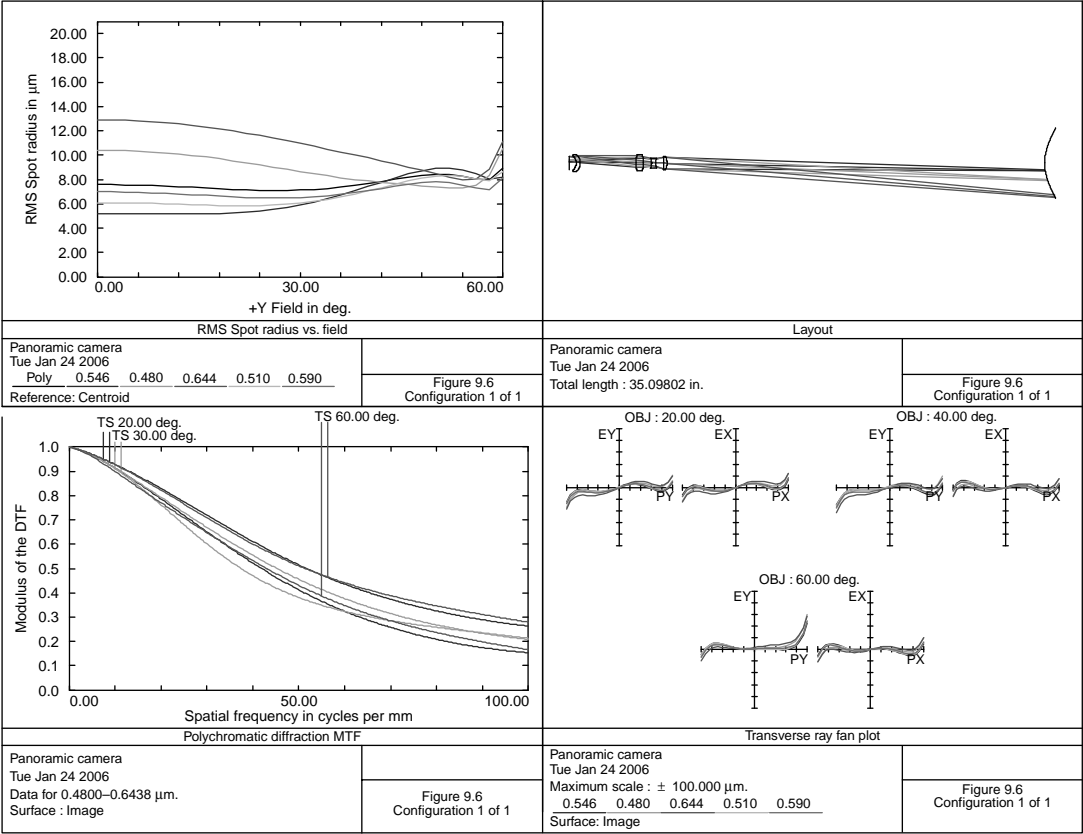


FIGURE 9.6 A panoramic camera lens.

---

**TABLE 9.6**  
**Panoramic Camera**

Surface	Radius	Thickness	Material	Diameter
1	0.0000	23.8353		90.313
2	3.1104	−27.2424	MIRROR	5.040
3	−1.0371	−0.2512	N-LAK7	1.000
4	−7.1456	−0.0157		1.000
5	Stop	−0.5387		0.800
6	1.5402	−0.3000	SF5	0.760
7	−0.9317	−0.6287		0.760
8	−7.5302	−0.5090	N-LAK7	1.160
9	1.7559	−4.0030		1.160
10	−0.7849	−0.3000	N-LAK21	1.220
11	−0.6634	−0.4976		1.040

---

## REFERENCES

- Brewer, S., Harris, T., and Sandback, I. (1962) Wide angle lens system, US Patent #3029699.
- Chahl, J. S. and Srinivasan M. V. (1997) Reflective surfaces for panoramic imaging, *Appl. Opt.*, 36: 8275.
- Horimoto, M. (1981) Fish eye lens system, US Patent #4256373.
- Hugues, E. (1969) Wide angle short photographic objective, US Patent #3468600.
- Kumler, J. and Bauer, M. (2000) Fisheye lens designs and their relative performance, *Proc. SPIE*, 4093: 360.
- Kweon, G., Kim, K. T., Kim, G., and Kim, H. (2005) Folded catadioptric lens with an equidistant projection scheme, *Appl. Opt.*, 44: 2759.
- Laikin, M. (1980) Wide angle lens systems, *Proc. SPIE*, 237:530 (1980 Lens Design Conference).
- Miyamoto, K. (1964) Fish-eye lens, *JOSA*, 54: 1060.
- Momiyama, M. (1983) Retrofocus type large aperture wide angle objective, US Patent #4381888.
- Muller, R. (1987) Fish eye lens system, US Patent #4647161.
- Nakazawa, K. (2000) Super wide angle lens, US Patent #6038085.
- Powel, I. (1995) Panoramic lens, US Patent #5473474.
- Ray, S. F. (1997) *Applied Photographic Optics*, 2nd ed., Focal Press, Oxford, p. 120.
- Reiss, M. (1945) The  $\cos^4$  law of illumination, *JOSA* 35: 283.
- Reiss, M. (1948) Notes on the  $\cos^4$  law of illumination, *JOSA* 38: 980.
- Shimizu, Y. (1973) *Wide angle fisheye lens*, US Patent #3737214.
- Yamada, H. (1998) *Wide angle lens*, US Patent #5812326.

---

# 10 Eyepieces

An eyepiece is a lens system with an external entrance pupil. The eye should be placed at this entrance pupil location. The distance from the entrance pupil to the first lens surface is called *eye relief*. Eye relief should be at least 10 mm (to obtain adequate clearance for eyelashes), 15 mm to provide more comfortable viewing, and 20 mm for people wearing spectacles. In the case of eyepieces used for rifle sights, the eye relief should be at least 3 in. to allow for rifle recoil (see [Figure 14.4](#) and [Figure 35.4](#)). For an example of a zoom eyepiece, see [Figure 35.11](#) that shows an eyepiece that zooms from 40 to 20-mm effective focal length.

The iris of the eye varies from 2-mm diameter (bright sunlight) to 8-mm diameter (dark viewing). Its focal length is approximately 17 mm (Luizov 1984). This iris diameter  $D$  (in mm) is approximated by the empirical expression:  $D = 5.3 - 0.55 \ln B$  (see also Equation 3 of Alpern (1987)), where  $B$  is the scene brightness in ft. Lamberts. Some representative values of  $B$  are given in [Table 10.1](#).

Typical eyepieces are designed to cover 3–6-mm diameter entrance pupil. If the viewer is observing in a moving vehicle (as in military equipment), entrance pupils as large as 10-mm diameter are sometimes used. This is to prevent the observer from losing his field of view as his head moves from side to side.

The human eye can resolve (Ogle 1951) 1 min arc (central foveal cone vision), about 3 min arc at 5° off-axis, and 10 min arc at 20° off-axis (rod vision). This is for relatively high illumination levels—about 100 ft. Lamberts. Visual acuity drops as the illumination level decreases.

When designing a binocular device, be sure to allow sufficient interpupillary adjustment. This is typically 51–77 mm (could be as low as 45 mm for some small children). Difference in binocular magnification (aniseikonia) should be kept to within 0.5%. The two systems should be aligned (disparity) as follows:

---

Horizontal:	8 min arc convergent 4 min arc divergent
Vertical:	4 min arc

---

Eyepieces should have the ability to move longitudinally (focus) thru 4 diopters.

From Newton's formula,  $F^2 = -XX'$ , where  $X$  is the apparent image distance, and  $X'$  is the amount of eyepiece movement in inches (see [Figure 10.1](#)) and  $D$  is the equivalent movement in diopters.

In most eyepieces, the distance from the eye to the principal plane is approximately a focal length. Therefore, the eyepiece forms an image, a distance  $X$ ,

**TABLE 10.1**  
**Scene Brightness vs. Eye Pupil Diameter**

Environment	Scene Brightness (ft. Lamberts)	<i>D</i> (mm)
Clear night	0.01	7.8
Dawn/dusk	1.0	5.3
Office	100.0	2.7
Sunny day	1000.0	1.5

as shown in Figure 10.1, from the eye:

$$F^2 = \frac{39.37}{D} X'.$$

The lens moves away from the eye for negative diopters, forming a virtual image in front of the eye.

Eyepiece magnification, *M*, is the ratio of the apparent image size as viewed thru the eyepiece to the object size. Because this object is generally imaged at a distance of about 10 in. from the eye (the distance of most distinct vision, and thus the distance that one normally holds his reading material),

$$M = \frac{F_e + 10}{F_e},$$

where *F<sub>e</sub>* is the eyepiece effective focal length.

When an eyepiece is combined with a microscope objective (to form a compound microscope) the resultant magnification is the product of objective magnification and eyepiece magnification. Since the smallest object, *Z*, that may be resolved is limited by diffraction (see [chapter 11](#)),

$$Z = \frac{0.61\lambda}{NA}.$$

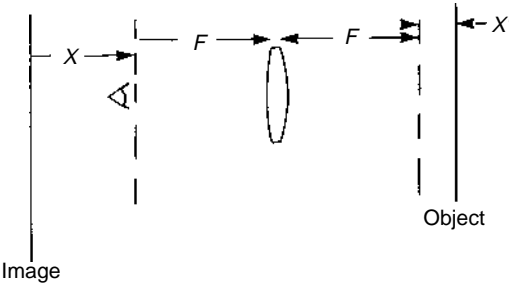


**FIGURE 10.1** A positive diopter with focusing eyepiece.



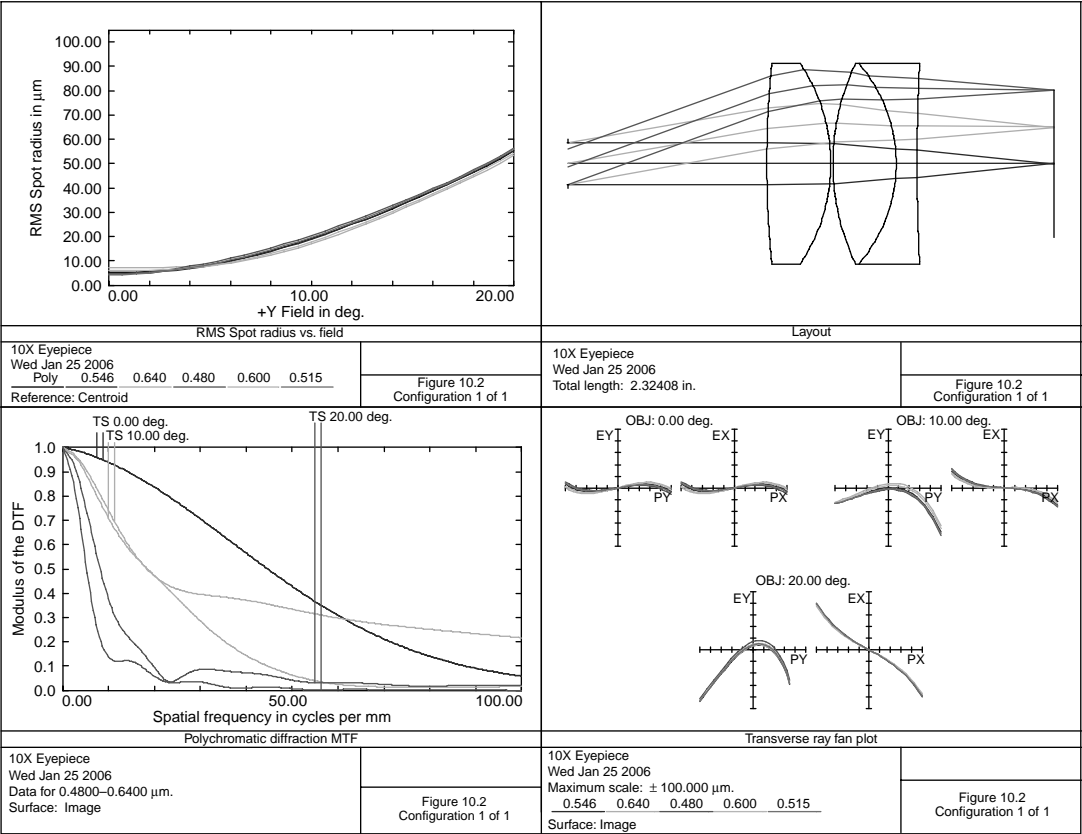


FIGURE 10.2 A 10× eyepiece.

**TABLE 10.2**  
**A 10× Eyepiece**

Surface	Radius	Thickness	Material	Diameter
1	Stop	0.9500		0.197
2	4.7709	0.3058	N-SK5	0.960
3	−0.8585	0.0100		0.960
4	1.1195	0.3024	N-BK7	0.960
5	−0.7329	0.1000	SF1	0.960
6	9.5115	0.6558		0.960

Distance from first lens surface to image=1.374, distortion=3.5%.

The minimum angular resolution as seen by the eyepiece, then, is

$$\frac{ZM_o}{F_e}.$$

Equating this to the limiting resolution of the eye of 1-min arc, note that the system magnification, *M*, should be 216 (at λ=0.55 μm). Most observers usually like to increase this to about 500. However, when used with an objective, *F<sub>o</sub>*, to form an afocal telescope, the angular magnification of this system is *M*=*F<sub>o</sub>*/*F<sub>e</sub>*, and is limited by diffraction such that the angular resolution is

$$\text{Angular resolution} = \frac{4.6 \text{ sec arc}}{D}.$$

This is Dawes’ rule, where *D* is the objective entrance pupil diameter in inches and the wavelength is 0.55 μm (Smith 2000). This angular resolution is then multiplied by the system magnification, *M*, and setting it to the angular resolution of the eye, one determines that the system magnification should be at least 13 times the diameter of the entrance pupil. However, due to sales appeal, low-cost refracting telescope are available with system magnifications many times this value.

Because the general design procedure is to trace from long conjugate to short, what is actually the system exit pupil (where the eye would be) is now called the entrance pupil. The designer must then bound the exit pupil to correspond to the telescope objective, relay, microscope objective, etc., location. This is typically a positive distance of 5–30 in. Some wide-angle systems can have considerable pupil aberration; it is then necessary to locate both the paraxial location of this exit pupil as well as using a chief ray to locate this pupil. Also, one should remember that because the eye-mind system always tries to bring the most important detail into the center of the field, axial resolution then is much more important than off-axis (unlike a photographic camera lens).

Figure 10.2 shows a 10× eyepiece with a 5-mm diameter entrance pupil and a 40° field of view (FOV). It is a modification of the usual Kellner form. Exit pupil is located 25.2 from the image surface. Note from the layout that there is some

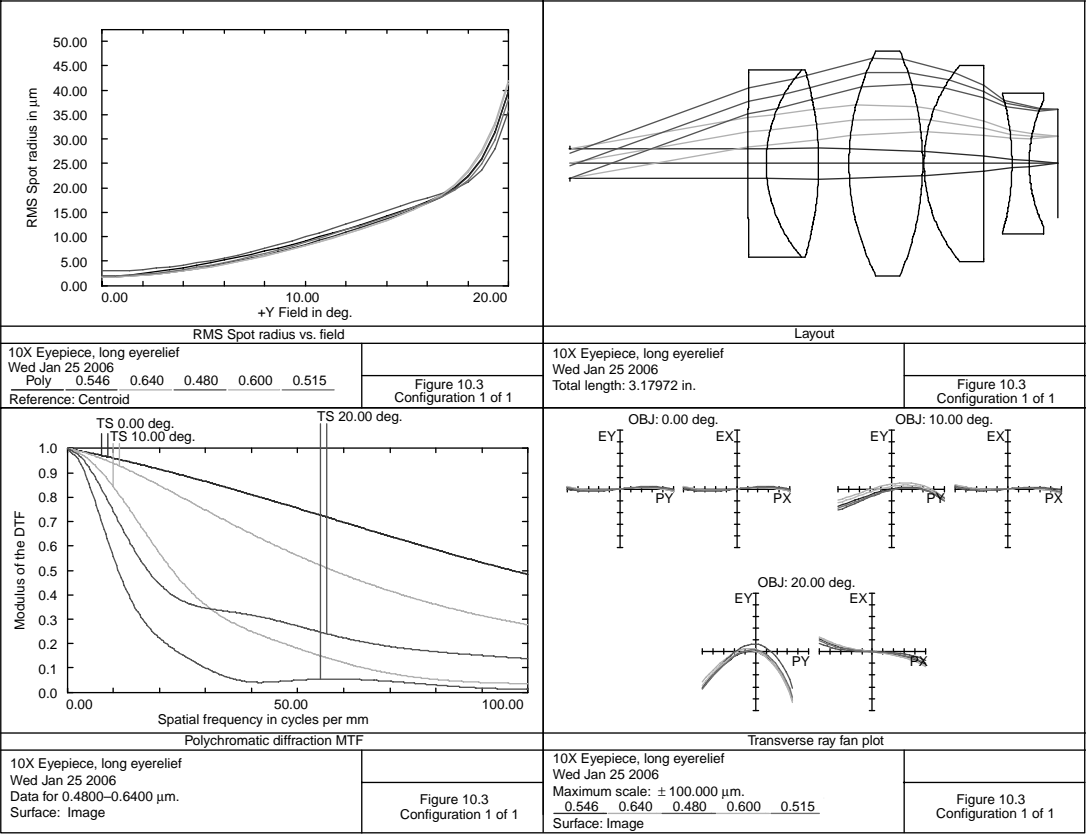


FIGURE 10.3 A 10× eyepiece, long eye relief.

**TABLE 10.3**  
**A 10× Eyepiece with Long Eye Relief**

Surface	Radius	Thickness	Material	Diameter
1	Stop	1.1583		0.197
2	23.9176	0.1197	SF1	1.220
3	0.9233	0.3421	N-SK16	1.220
4	−2.1362	0.1973		1.220
5	1.6039	0.4801	N-PSK3	1.460
6	−1.8755	0.0097		1.460
7	0.9966	0.3906	N-PSK3	1.280
8	0.0000	0.1815		1.280
9	−1.7120	0.1122	SF1	0.920
10	0.9454	0.1883		0.820

Distance first lens surface to image = 2.022, distortion = 5.0%.

vignetting of the pupil at full field. The prescription for this eyepiece is given in Table 10.2.

Figure 10.3 shows a 10× eyepiece with the same pupil diameter and field of view as above, but with an increased eye relief (see Ludewig 1953). The eyepiece details are provided in Table 10.3. Exit pupil is located 50.0 from the image surface. Vignetting is the same as above. The ray intercept plot shows considerable coma at the edge of the field.

This design is slightly superior to the Plossl or symmetric eyepiece that is shown in Figure 10.4; details are given in Table 10.4. This design consists of two identical cemented doublets with the crown elements facing each other. This is an advantage in reducing production costs. It was designed for the same pupil diameter and field of view as the above two designs. The poor sagittal MTF response at full field is due to astigmatism as indicated by the ray fan plot.

**TABLE 10.4**  
**A Plossl Eyepiece**

Surface	Radius	Thickness	Material	Diameter
1	Stop	0.7610		0.197
2	2.1218	0.1182	SF1	0.980
3	0.9042	0.2783	N-SK14	0.980
4	−1.7701	0.0197		0.980
5	1.7701	0.2783	N-SK14	0.980
6	−0.9042	0.1182	SF1	0.980
7	−2.1218	0.7246		0.980

Distance from first lens surface to image = 1.537, distortion = 6.5%, exit pupil is 31.88 from image surface.

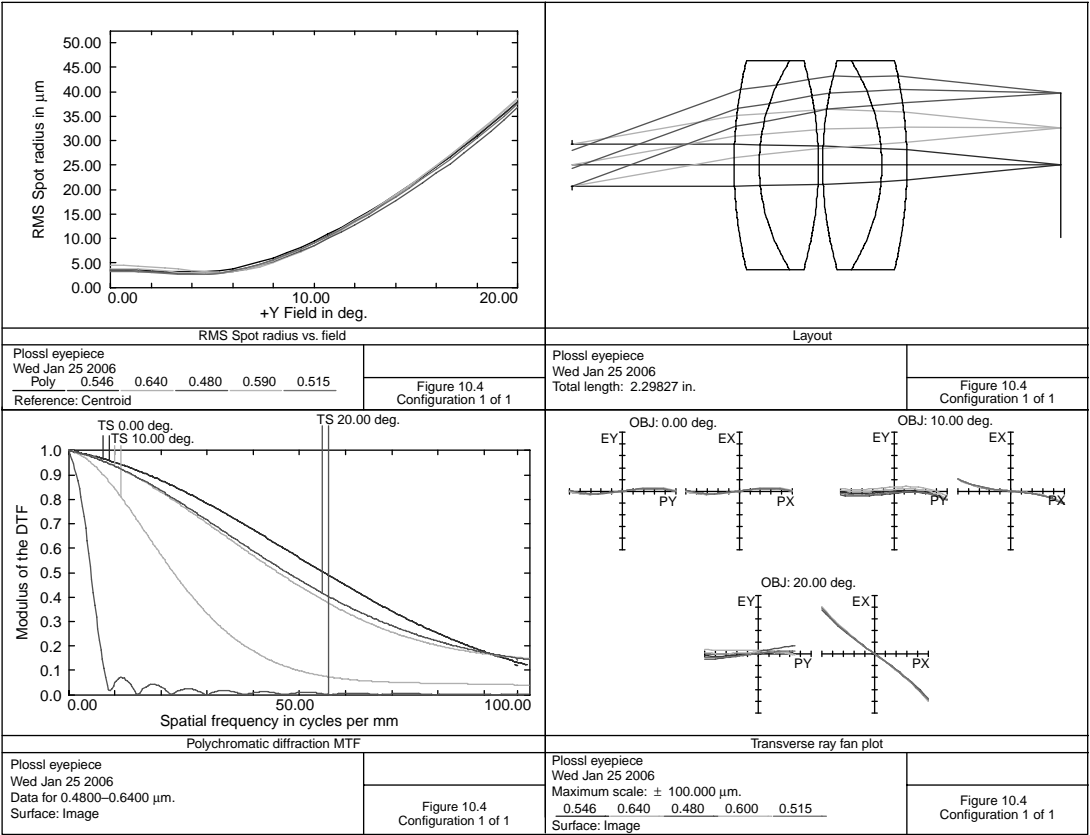


FIGURE 10.4 A Plossl eyepiece.

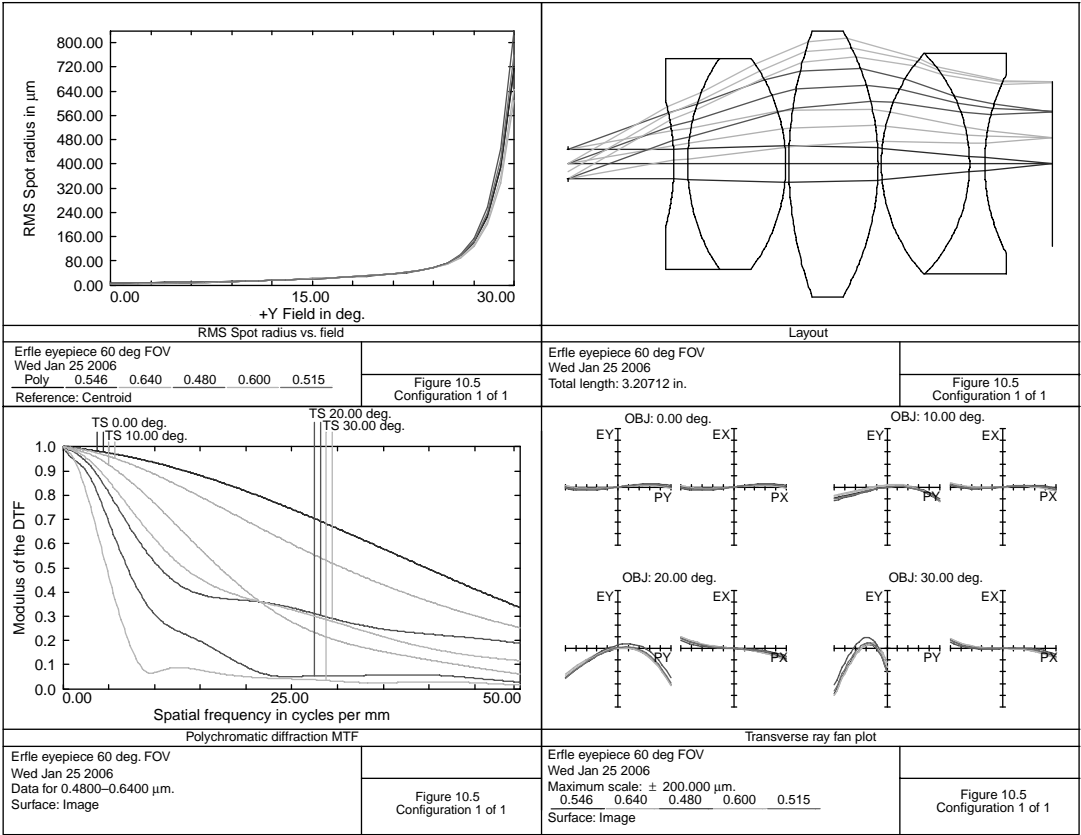


FIGURE 10.5 An Erfle eyepiece.

**TABLE 10.5**  
**Erfle Eyepiece with 60° FOV**

Surface	Radius	Thickness	Material	Diameter
1	Stop	0.7000		0.197
2	−1.6156	0.0900	SF1	0.840
3	1.2630	0.6500	N-SK14	1.400
4	−1.1748	0.0207		1.400
5	2.5770	0.5911	N-LAK10	1.760
6	−1.7677	0.0210		1.760
7	1.0852	0.5843	N-FK5	1.460
8	−1.0511	0.1000	SF1	1.460
9	1.2950	0.4500		1.180

Distance from first lens surface to image = 2.507, distortion = 6.0%.

Figure 10.5 shows an Erfle eyepiece with a 5-mm diameter entrance pupil and 60° FOV; details are given in Table 10.5. The exit pupil is located 10.0 from the image surface.

This lens was optimized using four field angles: axial, 10, 20, and 30°. As can be seen from Figure 10.5, 50% vignetting was introduced and the pupil shifted such that, for the full field case, only the bottom half of the pupil was being traced. The ray fan plot shows considerable coma for this lens.

Figure 10.6 shows an eyepiece with an internal image. This is a modification of the Nagler (1981) patent; details are given in Table 10.6. It has an internal image so

**TABLE 10.6**  
**Eyepiece with Internal Image**

Surface	Radius	Thickness	Material	Diameter
1	Stop	0.7720		0.197
2	−1.4468	0.3691	N-LAK22	0.820
3	−0.6358	0.1979	SF1	0.960
4	−1.2325	0.2145		1.160
5	2.4062	0.4744	N-ZK7	1.440
6	−1.5047	0.2005	SF1	1.440
7	−2.4257	1.5926		1.440
8	0.9430	0.8400	N-LAK22	1.420
9	0.9667	1.3622		1.000
10	−2.5657	0.1500	N-SK16	0.620
11	1.3208	0.1400	SF1	0.660
12	11.2116	−1.3001		0.640

Distance from first lens surface to image = 5.541, distortion = 1.0% (at 15°).

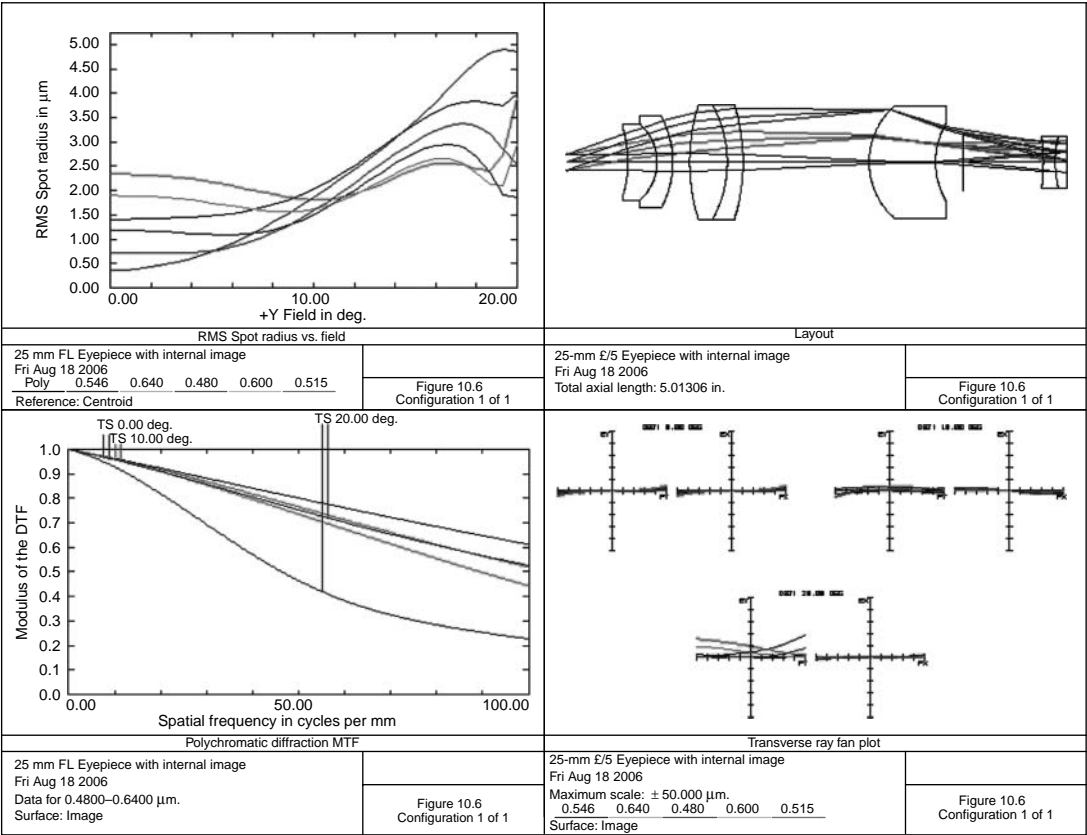


FIGURE 10.6 25-mm *f*/5 eyepiece with an internal image/lens MTF.



use is limited to systems where a reticle or grid is not required. It is also quite long (5.541 from first lens surface to the last lens surface.) Note that this has the same focal length (1.0) and FOV (40°) as the first three designs in this section. However, it exhibits superior performance. Distortion is 1% at 15 deg. and nearly zero at the edge of the field.

## REFERENCES

- Abe, H. (1971) Wide angle eyepiece, US Patent #3586418.
- Alpern, M. (1987) Eyes and vision, *Handbook of Optics*, McGraw Hill and the Optical Society of America, New York.
- Andreyev, L. N. (1968) Symmetric eyepieces with improved correction, *Sov. J. Opt. Tech.*, 5: 303.
- Bertele, L. (1929) Occular, US Patent #1699682.
- Clark, T. L. (1983) Simple flat field eyepiece, *Applied Optics*, 22: 1807.
- Dyer, A. (1993) Choosing eyepieces, *Astronomy*, June, 57.
- Fedorova, N. S. (1980) Relation between MTF and visual resolution of a telescope, *Sov. J. Opt. Tech.*, 47: 1.
- Fukumoto, S. (1996) Eyepiece, US Patent #5546237.
- Giles, M. K. (1977) Aberration tolerances for visual optical systems, *JOSA*, 67: 634–643.
- Kashima, S. (1993) Eyepieces, US Patent #5202795.
- Koizumi, N. (1997) Wide field eyepiece with inside focus, US Patent #5612823.
- König, A. (1940) Telescope eyepiece, US Patent #2206195.
- Ludewig, M. (1953) Eyepiece for optical instruments, US Patent #2637245.
- Luizov, A. V. (1984) Model of reduced eye, *Sov. J. Opt. Tech.*, 51: 325.
- MIL HDBK 141 (1962) Chapter 14, Optical Density, Military Standardization Handbook, Defense Supply Agency.
- Nagler, A. (1981) Ultra wide angle Flft field eyepiece, US Patent #4286844.
- Nagler, A. (1987) Ultra wide angle eyepiece, US Patent #4747675.
- Olge, K. N. (1951) On the resolving power of the human eye, *JOSA*, 41: 517.
- Repinski, G. N. (1978) wide angle five lens eyepiece, *Sov. J. Opt. Tech.*, 45: 287.
- Rosen, S. (1965) Eyepiece and magnifiers, Chapter 9, Volume 3, *Applied Optics and Optical Engineering*, Academic Press.
- Skidmore, W. H. (1967) Eyepiece design providing a large eye relief, *JOSA*, 57: 700.
- Skidmore, W. H. (1968) Wide angle eyepiece, US Patent #3390935.
- Smith, W. (2000) *Modern Optical Engineering*, Section 6.10, McGraw Hill, NY.
- Taylor, E. W. (1945) The evolution of the inverting eyepiece, *J. Scientific. Inst.*, 22: 43.
- Veno, Y. (1996) Eyepiece, US Patent #5557463.
- Wald, G. (1945) The spectral sensitivity of the human eye, *JOSA*, 35: 187.
- Wenz, J. B. (1989) Single eyepiece binocular microscope, US Patent #4818084.



---

# 11 Microscope Objectives

Microscope objective are essentially diffraction-limited optical devices. These lenses are characterized by specimen magnification and NA. The image is generally about 16 mm in diameter.

Most designs are based upon an old concept of 160-mm tube length. That is, the distance from the image to a principal plane in the objective was 160 mm. This corresponds to an object to image distance of about 180 mm. They were designed to be mounted on a precision shoulder 35.68 mm from the specimen that was covered by a 0.18-mm-thick glass. This cover glass is made either from fused silica (UV-type objectives) or a chemically resistant soda lime glass. Because this type of glass is reasonably close to N-K5, it is used in these designs. For an oil-immersion objective, an additional thickness of 0.14 mm of oil is placed between the cover glass and the first lens surface (generally a plane surface).

The objective thread is “Whitworth,” with a 55° included angle, 36 threads/in., 0.796 major diameter. Typical laboratory microscopes have a shoulder-to-specimen distance of 45 mm.

Several manufacturers have instituted infinity-corrected systems. This allows greater flexibility in microscope design. Various beam splitters and other accessories can now be readily inserted into the collimated beam. All designs shown here are for 180 mm object-to-image distance with a 16-mm diameter image. Also note that, although microscope magnification is listed as image diameter/specimen diameter, the usual convention of tracing from the long conjugate is followed here; in this case, it is from the 16-mm image diameter to the specimen. Thus magnification as computed from these prescriptions is the reciprocal of the listed magnification.

According to the Raleigh criterion, the distance between two resolved images is  $Z = 0.61\lambda/\text{NA}$ , where  $Z$  is the separation of the images,  $\lambda$  is the wavelength of light, and  $\text{NA} = N \sin \theta$ .  $N$  is the refractive index of the medium in which is the image. Thus, to increase resolution, one needs to decrease the wavelength of the illumination system (see Design 11.4, a UV objective) or increase the NA beyond 1. This is accomplished by immersing the object in oil (see Design 11.5, a 98× oil-immersion objective). Values of NA given in the following prescriptions are paraxial, that is,

$$\text{NA} = \frac{\text{Entrance pupil diameter}}{2.0(\text{Focal length}) \times (1.0 + 1.0/\text{magnification})}.$$

In [Figure 11.1](#) is shown a 10× microscope objective; details are provided in [Table 11.1](#). It consists of two widely spaced cemented doublets (Lister type).

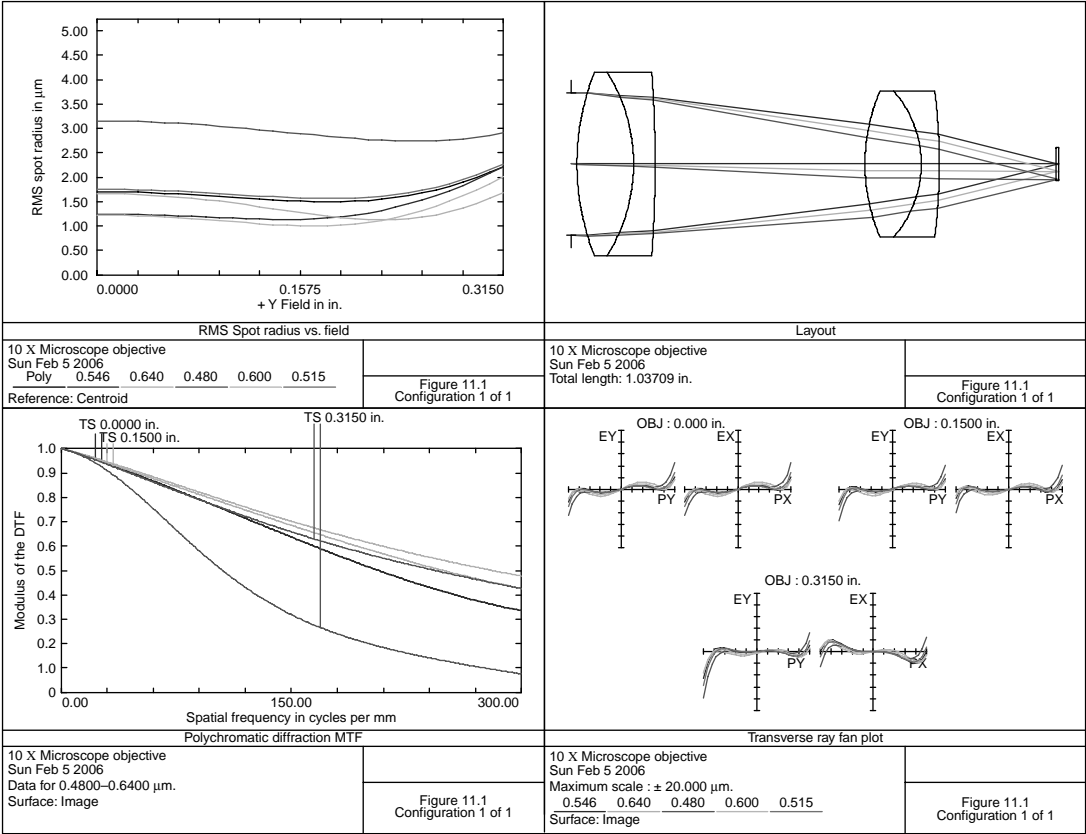


FIGURE 11.1 A 10 $\times$  microscope objective.

**TABLE 11.1**  
**A 10× Microscope Objective**

Surface	Radius	Thickness	Material	Diameter
0	0.0000	6.0503		0.630
1	Stop	0.0120		0.303
2	0.5266	0.1204	N-BK7	0.390
3	−0.3663	0.0459	F5	0.390
4	−2.5909	0.4463		0.390
5	0.3892	0.1197	N-BK7	0.310
6	−0.2326	0.0383	F5	0.310
7	−1.2163	0.2474		0.310
8	0.0000	0.0070	N-K5 cover glass	0.070

Distance from first lens surface to image = 5.013, distortion = 0.15%.

The NA is 0.22; the effective focal length (EFL) is 0.618. The object distance to the aperture stop is 6.050. The last surface represents the protective cover slip.

In Figure 11.2 is shown a 20× microscope objective for which NA is 0.49 and EFL is 0.309; details are provided in Table 11.2. This lens has some primary color. The ray plots show some flare at the edge of the pupil.

Figure 11.3 shows a 4-mm EFL apochromatic objective for which NA is 0.91 (the actual focal length is 3.76 mm). Details are provided in Table 11.3. There is some flare at the edge of the pupil and a very small amount of primary color. Note that the next to last lens surface ( $R = 0.09332$ ) is nearly concentric about the image. The spherical contribution at this surface is then zero. Magnification is 47.5.

Figure 11.4 shows a UV reflecting objective (UV spectral region, 0.2–0.4  $\mu\text{m}$ ) for which NA is 0.72 and magnification is 53. Details are given in Table 11.4. The EFL is 0.129. The aperture stop is located at the secondary mirror which is bonded to the calcium fluoride negative lens.

Near-diffraction-limited performance is obtained in the central portion of the field. At the edge of the field, there is considerable flare. Because chromatic aberration is very small for this type of design, the wavelength region may be extended into the visual region. (Longitudinal chromatic aberration is considerable at wavelengths below 0.24  $\mu\text{m}$ .) The last surface in the above designs corresponds to the protective cover slip. See Figure 15.8 for a reflecting objective design that may be modified for microscope use.

Figure 11.5 shows a 98× oil-immersion microscope objective of NA 1.28 and EFL of 0.0706. Details are provided in Table 11.5.

Note that a glass is listed for the material to the right of the image surface. If, as usual, there is no material listed to the right of the image surface, most computer programs insert  $N = 1.0$  for the refractive index, which can cause ray-trace difficulties for very high numeric aperture systems such as this one. Setting the refractive index to the same value as the previous surface prevents this.

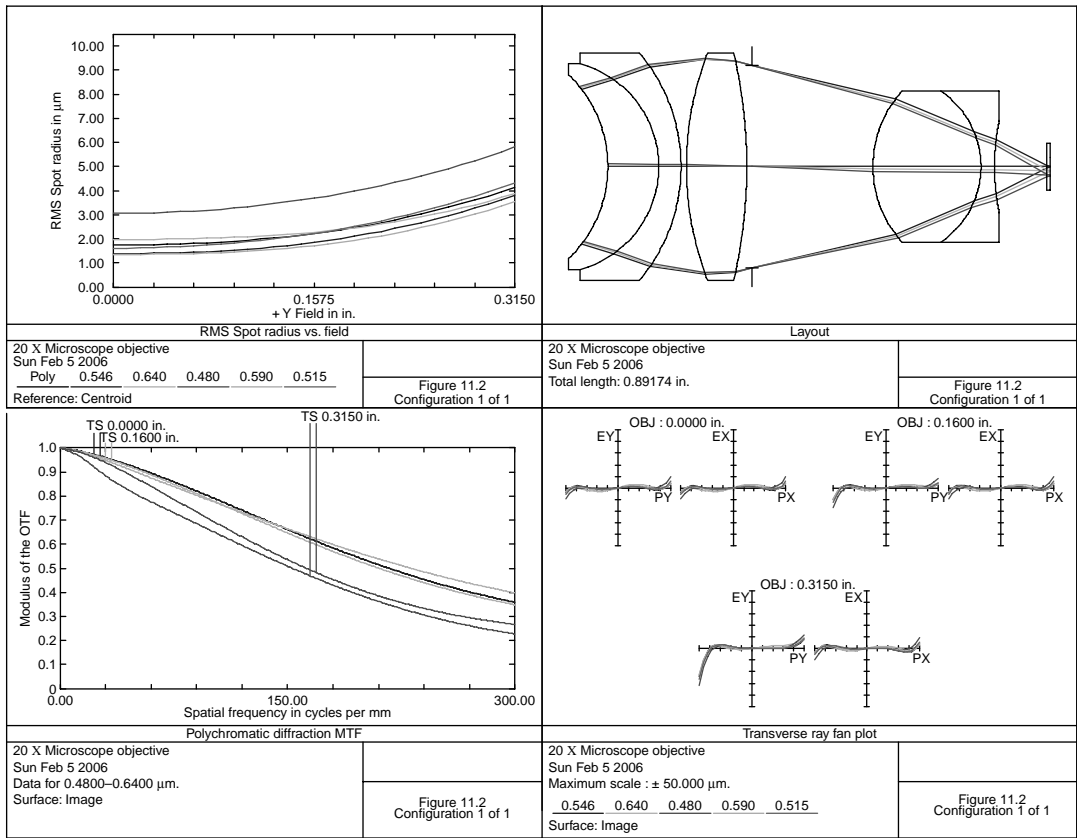


FIGURE 11.2 A 20× microscope objective.

**TABLE 11.2**  
**A 20× Microscope Objective**

Surface	Radius	Thickness	Material	Diameter
0	0.0000	6.2679		0.630
1	−0.2352	0.0941	N-SK16	0.340
2	−0.1968	0.0413	SF4	0.380
3	−0.3251	0.0100		0.420
4	0.5837	0.1115	N-SK16	0.420
5	−0.9401	0.0100		0.420
6	Stop	0.2236		0.375
7	0.2077	0.2000	N-SK16	0.280
8	−0.1686	0.0250	SF4	0.280
9	0.4108	0.0965		0.173
10	0.0000	0.0070	N-K5	0.088
11	0.0000	0.0000		0.034

Distance from object to first lens surface=6.268, distance from first lens surface to image=0.819, distortion=0.21%.

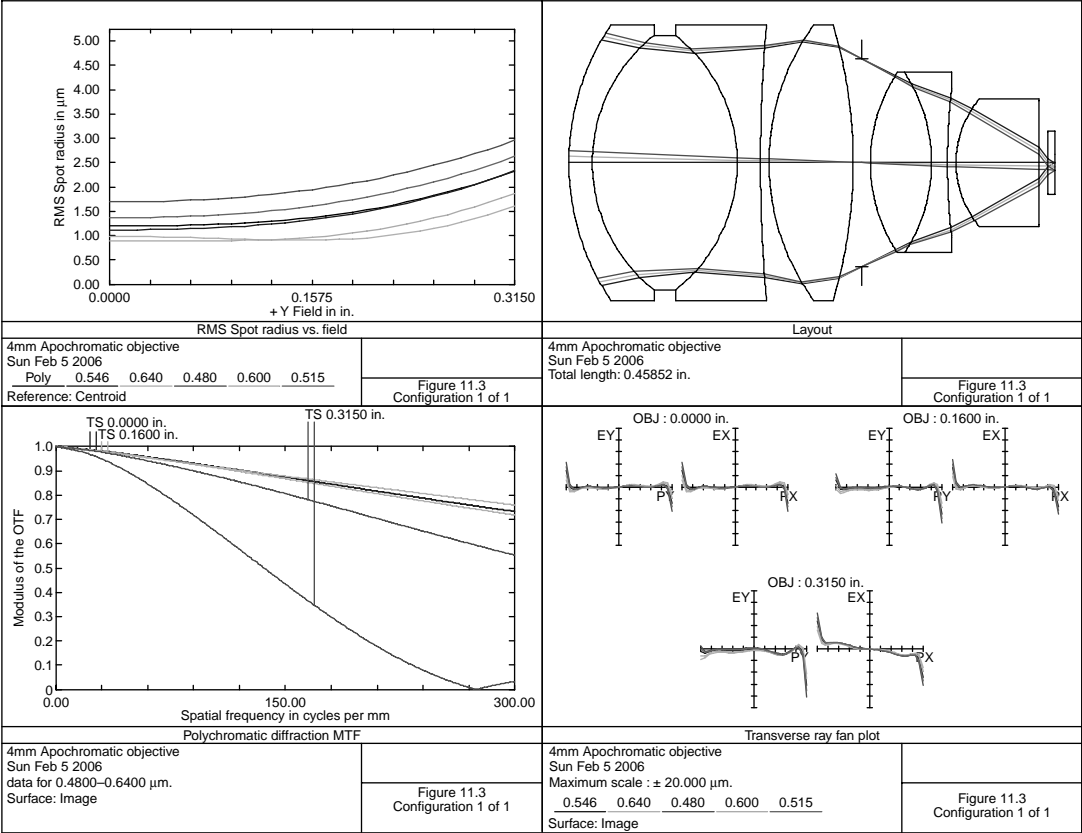


FIGURE 11.3 A 4-mm apochromatic microscope objective.



---

**TABLE 11.3**  
**A 4-mm Apochromatic Objective**

Surface	Radius	Thickness	Material	Diameter
0	0.00000	6.6303		0.630
1	0.23353	0.0220	N-LAK14	0.260
2	0.15292	0.1367	CAF2	0.240
3	−0.15292	0.0220	N-LAK14	0.240
4	1.54185	0.0080		0.260
5	0.22209	0.0795	N-LAK14	0.260
6	−0.44781	0.0080		0.260
7	Stop	0.0080		0.196
8	0.15418	0.0578	CAF2	0.170
9	−0.15418	0.0150	F2	0.170
10	0.62418	0.0080		0.140
11	0.09332	0.0783	N-SK5	0.120
12	0.00000	0.0083		0.120
13	0.00000	0.0070	N-K5	0.060
14	0.00000	0.0000		0.015

Distance from first lens surface to image=0.4585, distortion=0.15%.

---

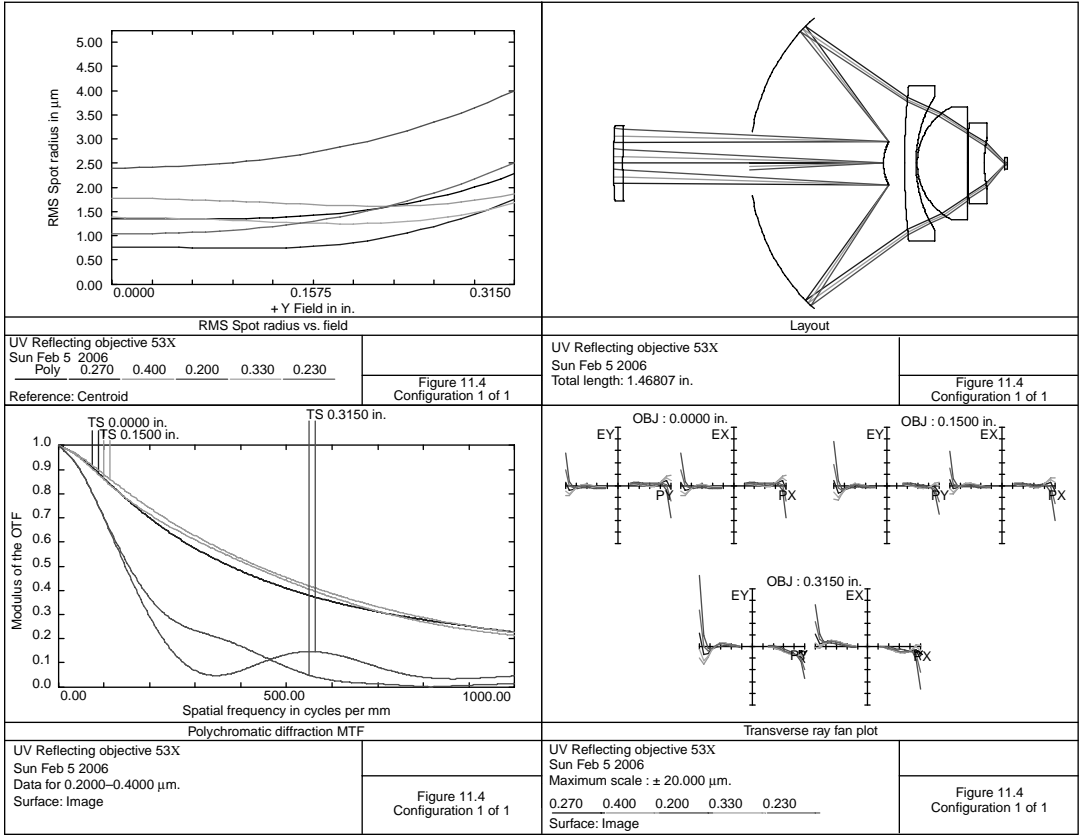


FIGURE 11.4 A UV reflecting microscope objective.

---

**TABLE 11.4**  
**A 53× UV Reflecting Objective**

Surface	Radius	Thickness	Material	Diameter
0	0.0000	5.6198		0.630
1	1.72300	0.0350	SILICA	0.284
2	2.90631	0.9731		0.284
3	0.17783	−0.4995	MIRROR	0.161 Stop
4	0.72913	0.5776	MIRROR	1.082
5	2.66996	0.0427	CAF2	0.580
6	0.48467	0.0050		0.500
7	0.23767	0.1861	CAF2	0.420
8	8.64894	0.0050		0.320
9	7.25758	0.0588	SILICA	0.300
10	0.44435	0.0771		0.196
11	0.00000	0.0071	SILICA	0.042
12	0.00000	0.0000		0.042

Distance from first lens surface to image = 1.468, distortion = 0.17%.

---

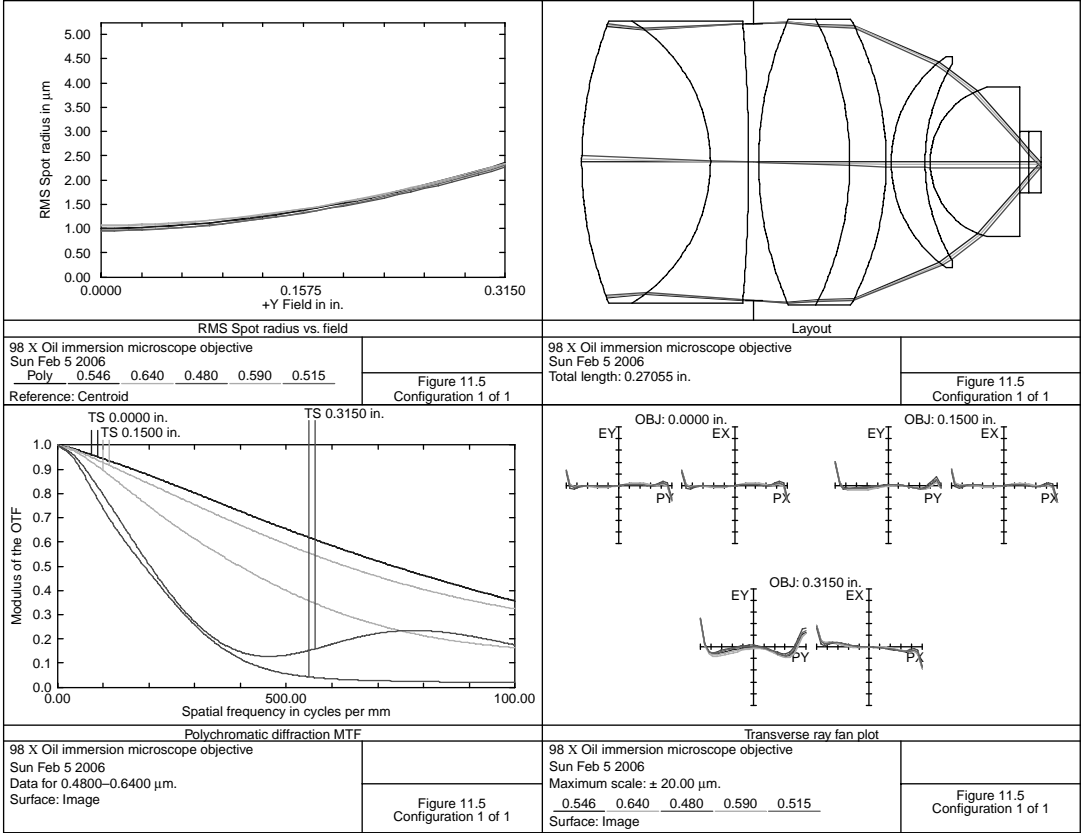


FIGURE 11.5 A 98× oil immersion microscope objective.

**TABLE 11.5**  
**A 98× Oil-Immersion Microscope Objective**

Surface	Radius	Thickness	Material	Diameter
0	0.00000	6.8186		0.630
1	0.22369	0.0759	CAF2	0.166
2	−0.09757	0.0224	F4	0.166
3	−0.99257	0.0030		0.166
4	Stop	0.0030		0.163
5	0.21206	0.0536	CAF2	0.168
6	−0.18691	0.0214	N-PSK53	0.168
7	−0.17955	0.0030		0.168
8	0.07585	0.0200	N-LAK21	0.124
9	0.11369	0.0030		0.116
10	0.04570	0.0527	N-BK7	0.088
11	0.00000	0.0055	TYPEA	0.036
12	0.00000	0.0071	N-K5	0.036
13	0.00000	0.0000	N-K5	0.006

Distance from first lens surface to image = 0.2705, object distance to first lens surface = 6.8186, distortion = 0.26%.

This type of design is sometimes called a *semi-apochromatic* or *fluorite* objective. To be a true apochromat, a triplet should be added in the front. This cemented triplet would have calcium fluoride as a middle element. The oil is a microscope immersion oil (Cargille 1995) and has the following values for index of refraction.

As evident from Table 11.6, this closely approximates the refractive properties of N-BK7 (at the *e* line). The last element then is made of N-BK7 with the front plano side not antireflection coated because it will be in contact with the immersion oil. Such near-hemispheres are sometimes made by a ball-rolling process as are ball bearings. That is, these small parts are not blocked as in conventional lens manufacture, but are rolled between two parallel plates. A near-perfect sphere is

**TABLE 11.6**  
**Refractive Properties of Type-A Immersion Oil**

Wavelength (μm)	Index of Refraction
0.4861	1.5239
0.5461	1.5180
0.5893	1.5150
0.6563	1.5115

then obtained, and then these parts are conventionally blocked and the flat side ground and polished.

The main off-axis aberration is coma, which severely limits performance at the edge of the field. However, for the typical clinical application (examination of blood cells, etc.) the primary interest is in the central portion of the field.

## REFERENCES

- Beck, J. L. (1969) A new reflecting microscope objective, *Applied Optics*, 8: 1503.
- Benford, J. (1965) Microscope objectives, In *Applied Optics and Optical Engineering*, Kingslake, R., ed., Volume 3, Academic Press, New York, pp. 145–182.
- Benford, J. (1967) Microscopes, In *Applied Optics and Optical Engineering*, Volume 4, Academic Press, New York, p. 31.
- Cargille, R. P. (1995) Microscope immersion oils data sheet, IO-1260, Carville Labs, Cedar Grove, NJ.
- Castro-Ramos, J., Cordero-Davila, A., Vazquez-Montiel, S., and Gale, D. (1998) Exact design of aplanatic microscope objectives consisting of two conic mirrors, *Applied Optics*, 37: 5193.
- Esswein, K. (1982) Achromatic objective, US Patent #4362365.
- Grey, D. S. and Lee, P. H. (1949) A new series of microscope objectives, *JOSA*, 39: 727.
- Martin, L. C. (1966) *Theory of the Microscope*, Blackie and Son, London.
- Matsubara, M. (1977) Microscope objective, US Patent #4037934.
- Rybicki, E. (1983) 40 × Microscope objective, US Patent #4379623.
- Sharma, K. (1985a) Medium power micro objective, *Applied Optics*, 24: 299.
- Sharma, K. (1985b) High power micro objective, *Applied Optics*, 24: 2577.
- Suzuki, T. (1997) Ultra high NA microscope objective, US patent #5659425.
- Sussman, M. (1983) Microscope objective, US Patent #4376570.

---

# 12 In-Water Lenses

Visibility in water is limited by scattering. Indeed, there are many places in the world where a bather cannot see his own feet! Twenty feet in seawater could be regarded as the limit of practical seeing. [Figure 12.1](#) gives the transmission of 10 m of seawater (from Smith and Baker 1981). Noting that most optical glasses show considerable absorption at wavelengths below 0.4  $\mu\text{m}$ , a reasonable wavelength region for optimization would be 0.4–0.6  $\mu\text{m}$  (this should also be modified by the illumination and detector system sensitivity). However, designs discussed in this section are for the normal visual region.

Using the Schott (also called a Laurent series formula) equation for refractive index  $N$ :

$$N^2 = F_1 + F_2\lambda^2 + \frac{F_3}{\lambda^2} + \frac{F_4}{\lambda^4} + \frac{F_5}{\lambda^6} + \frac{F_6}{\lambda^8},$$

where  $\lambda$  is the wavelength in microns. Values for  $F_1, F_2$ , etc. for pure water (Centeno 1941) and seawater were fitted by a least squares fit (20°C). Coefficients for pure water and seawater are given in [Table 12.1](#).

This yields the following refractive index values ([Table 12.2](#)):

Mobley (1995) and Huibers (1997) also lists index of refraction values for seawater and pure water.

The increase in refractive index of seawater is due to salt concentration. It increases approximately 0.00185 per 1% salt concentration. The above values assume a salt concentration of 3.5%, which is the average salinity of the world ocean (3.5 g of salt per 100 g water; oceanography texts refer to this concentration as 35%).

Index of refraction of water decreases 0.0001 per °C at the above salt concentration and over the temperature region 10°C–20°C (Quan and Fry 1995).

In general, for in-water systems, if  $F'$  is the distance from the second principal plane to the image of a distant object, and  $F$  a like distance measured from the first principal plane, then for an image in air:  $F' = F/N$ , where  $N$  is the refractive index of the water.

Image height will be (in the absence of distortion) equal to  $NF \tan \theta$ . The actual optical system used depends upon the type of port required—usually a flat plate or concentric dome.

## FLAT PLATE PORT

The simplest type of port is, of course, a flat plate. This is encountered when looking at fish in an aquarium or when using the usual face mask in a pool. Objects in water

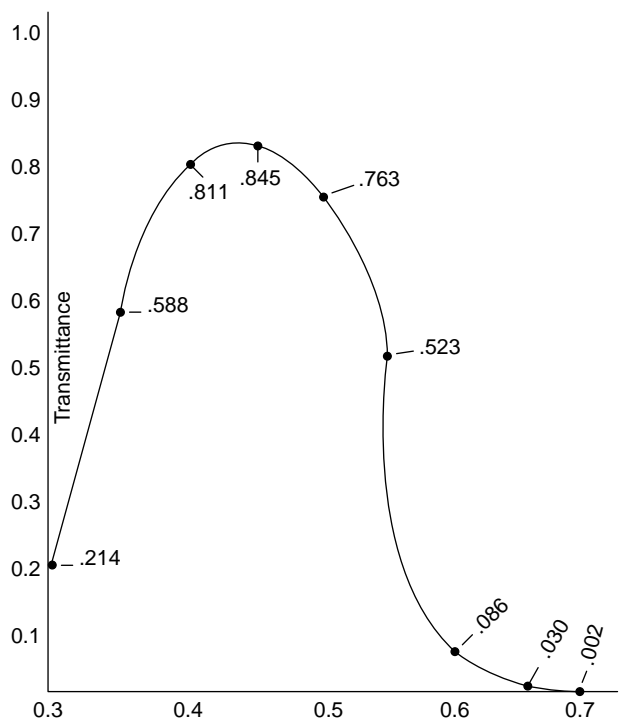


**FIGURE 12.1** The transmission of 10 m of seawater. (From Smith, R. and Baker, K., *Applied Optics*, 20, 177–184, 1981.)

appear larger than they actually are. Figure 12.2 shows the relationship between angle in water and its exit angle in air after passing thru a 0.5-in. thick Pyrex<sup>®</sup> flat port. For small angles, the relationship is nearly linear and there is no distortion, only a change in field of view (FOV). It thus appears that the focal length of the lens has increased by a factor of the refractive index of the water. For large angles, the view in water is compressed and therefore distortion is noted. Because most marine

**TABLE 12.1**  
**Coefficients in Dispersion Formula**

	Pure Water	Sea Water
$F_1$	1.766499	1.7836370
$F_2$	−0.01484022	−0.01494094
$F_3$	0.004454459	0.004305215
$F_4$	$3.904621 \times 10^{-4}$	$4.634989 \times 10^{-4}$
$F_5$	$−1.630518 \times 10^{-5}$	$−2.155772 \times 10^{-5}$
$F_6$	$4.134407 \times 10^{-7}$	$5.164058 \times 10^{-7}$



**TABLE 12.2**  
**Refractive Index Values for Water**

Wavelength (μm)	Pure Water	Sea Water
0.40	1.34308	1.34973
0.45	1.33914	1.34569
0.50	1.33638	1.34287
0.55	1.33434	1.34078
0.60	1.33275	1.33916
0.65	1.33145	1.33785

scenes do not contain straight lines, this should not be a problem. The maximum angle of view,  $\theta$ , in water for a flat port is

$$\theta = \arcsin \frac{1.0}{1.334} = 48.5^\circ.$$

Because all of this is wavelength dependent, considerable lateral color will be seen and will be very noticeable on viewing fish (at large angles of incidence) in an aquarium.

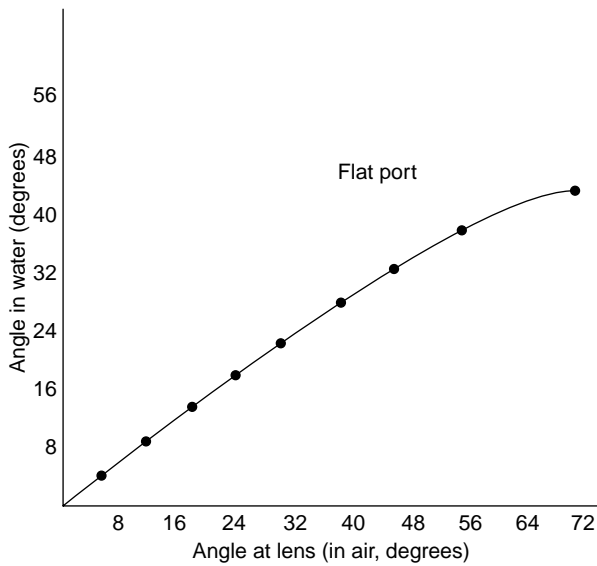


**FIGURE 12.2** The relationship between angle in water and its exit angle in air after passing thru a 0.5-in.-thick Pyrex<sup>®</sup> flat port.

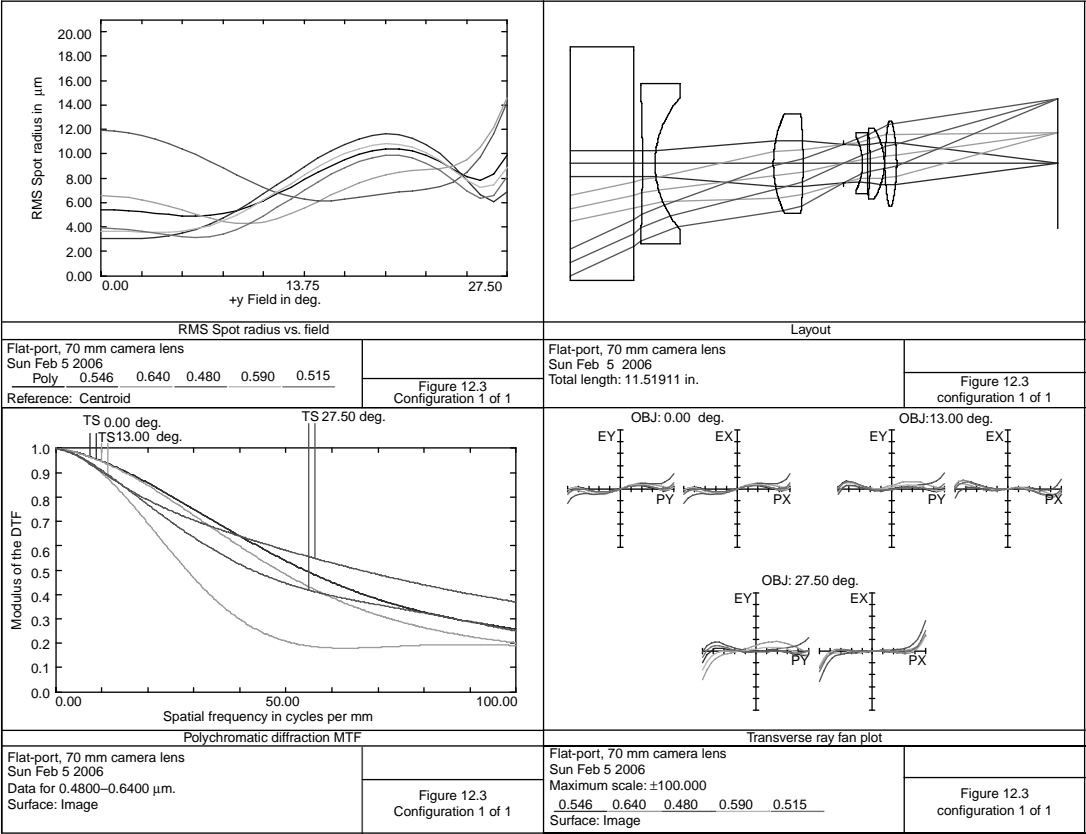


FIGURE 12.3 A flat-port, 70-mm camera lens.

**TABLE 12.3**  
**Flat-Port 70-mm Camera Lens**

Surface	Radius	Thickness	Material	Diameter
0	Infinite	Infinite	SEA WATER	
1	0.0000	1.5000	PYREX	5.500
2	0.0000	0.2000		5.500
3	−41.2230	0.3000	N-SK16	3.800
4	2.3470	2.7953		3.100
5	2.8049	0.7012	N-LAK7	2.340
6	−12.6884	0.9658		2.340
7	Stop	0.4386		0.920
8	−1.3876	0.1200	SF4	1.240
9	25.7448	0.0603		1.440
10	−6.5202	0.3338	N-BAF10	1.480
11	−1.5515	0.0150		1.660
12	5.5285	0.2779	N-LAK14	2.000
13	−4.4786	3.8112		2.000

Distance from front of PYREX® port to image surface = 11.519, distortion is 6.9%.

Figure 12.3 shows an optical system designed for in-water photography using a flat-port camera and 70-mm film. (This is a modification of a design by R. Altman.) Details are given in Table 12.3.

This lens is  $f/3.9$ , has a focal length of 2.371, and was designed for a camera using 70-mm film and having an image diagonal of 3.3. The FOV is  $55^\circ$  in water.

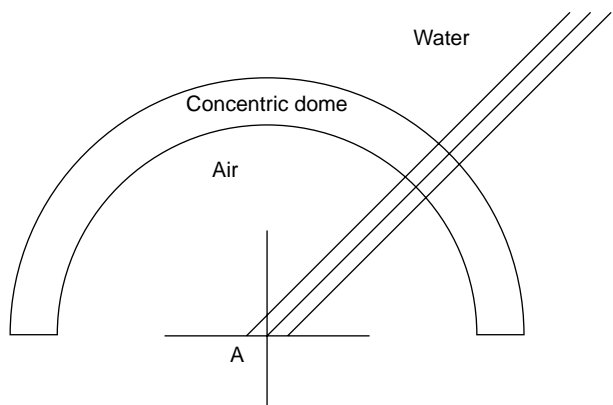


**FIGURE 12.4** A water–dome interface.

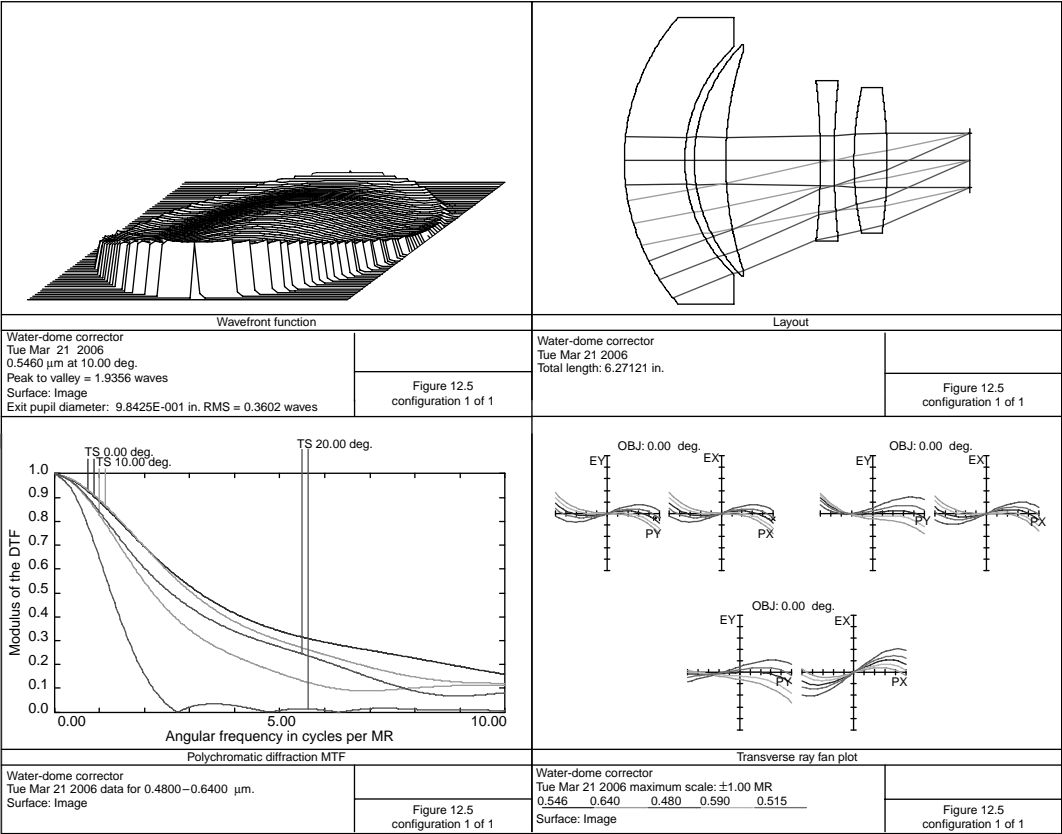


FIGURE 12.5 Water-dome corrector.

## CONCENTRIC DOME

For deep-water exploration, the concentric dome is preferred. This is based upon the enormous pressure requirements that one encounters in deep water (at 5000 ft., for instance, the pressure is 2200 psi). Concentric dome ports of acrylic material are often used, or if glass then N-BK7 is chosen. [Figure 12.4](#) shows a water–dome interface.

If point A is the center of curvature of the dome and is also the entrance pupil of the system, then a chief ray from a distant object will pass through the water–dome interface without refraction. If the entrance pupil is maintained small compared to the radius of curvature of the dome, then upper and lower rim rays will also pass through with only a slight change in their angles.

Because a concentric lens has its principal planes at its center of curvature, and if the lens has its front principal plane also at this location, the net effect is a system with the same FOV in water and in air (Pepke 1967).

To compensate for the aberrations of the water–dome interface and to move the pupil to a more accessible location, a corrector is sometimes used. Because the water–dome interface acts like a strong negative lens, considerable difficulty is also encountered in focusing a standard lens placed behind this water–dome interface. The afocal corrector solves these problems. This will allow a stock lens—designed for infinity in air correction—to be used behind this corrector. The system shown in [Figure 12.5](#) was designed to be used with a 50-mm f/2.0 lens from a 35-mm single-lens reflex (SLR) camera. Details are given in Table 12.4.

Unfortunately, the edge of the first lens surface is too thin and so  $T_3$  should be increased. The FOV in water is  $40^\circ$ . The stock 50 mm lens then should be placed such that its entrance pupil corresponds to the exit pupil (the stop) location.

In [Figure 12.6](#), an f/2.8 lens suitable for a 35 mm SLR camera (43.3 mm diagonal) is shown; details are provided in [Table 12.5](#). This is a modification of

**TABLE 12.4**  
**Water–Dome Corrector**

Surface	Radius	Thickness	Material	Diameter
0	Infinite	Infinite	SEA WATER	
1	3.9400	1.1000	ACRYLIC	5.200
2	2.8400	0.1739		4.140
3	2.9807	0.5702	N-KF9	4.200
4	6.3916	1.7175		4.040
5	−13.8549	0.2500	LAFN7	2.920
6	13.7458	0.3596		2.780
7	6.2722	0.6000	N-ZK7	2.640
8	−9.7417	1.5000		2.640
9	Stop			0.984

Distance from front of acrylic dome to last lens surface = 4.771, distortion = 0.75%.

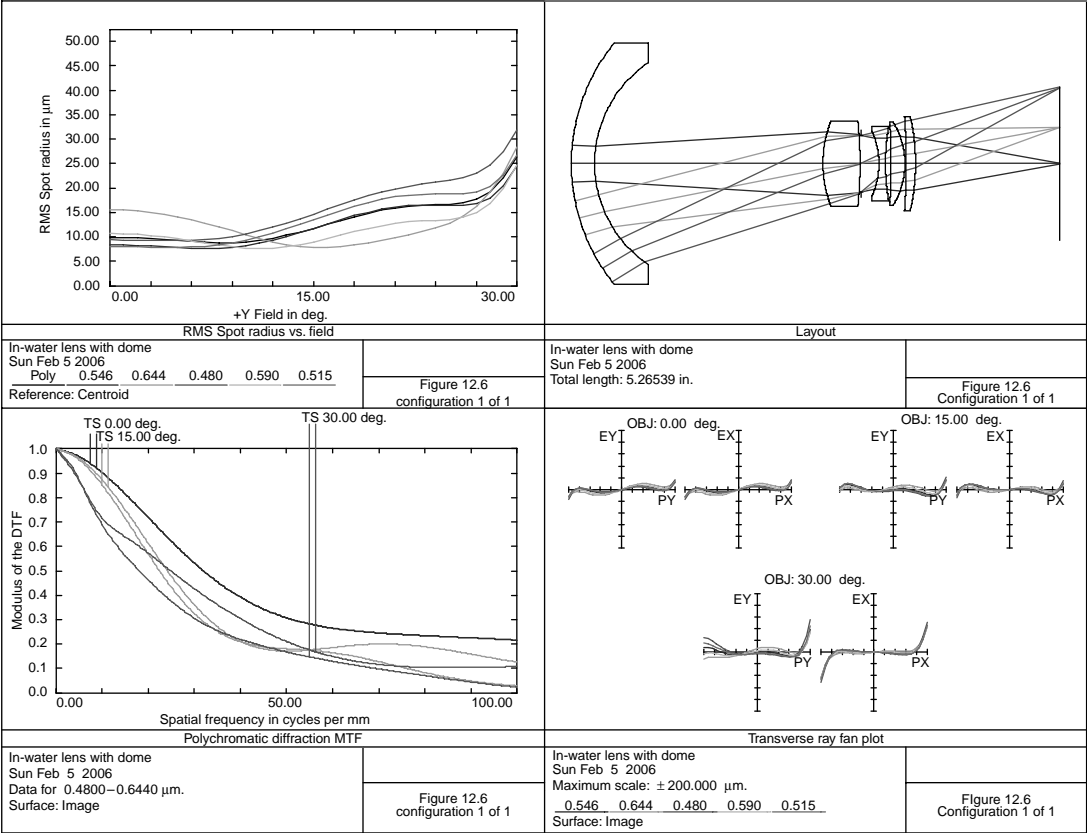


FIGURE 12.6 In-water lens with dome.

**TABLE 12.5**  
**In-Water Lens with Dome**

Surface	Radius	Thickness	Material	Diameter
0	Infinite	Infinite	SEA WATER	
1	2.0638	0.2500	N-BK7	2.600
2	1.3115	2.4606		2.180
3	1.2667	0.4000	N-LAF21	0.920
4	-4.5246	0.0150		0.920
5	Stop	0.1889		0.609
6	-0.8383	0.0700	SF4	0.700
7	2.2706	0.0594		0.800
8	-8.3424	0.1500	N-LAF21	0.840
9	-0.8589	0.0150		0.900
10	-6.7938	0.1000	N-LAF21	1.020
11	-2.2992	1.5565		1.020

Distance from first lens surface to image = 5.265, distortion = 3.7%.

Ohshita (1989). Note that the dome is not strictly concentric because it has some negative power. This forms a retrofocus system, thus allowing a long back focal length in relation to its focal length (1.105). A concentric dome is usually preferred for structural reasons to better withstand the high pressures encountered at great depths. Focusing is accomplished by moving the rear four elements in relation to the dome. Even though N-LAF21 is an expensive glass, the diameters are not very large, so this should not pose a problem.

An afocal, in-water corrector for use with a stock zoom lens is of special interest because it allows for zooming capabilities in a remotely controlled vehicle (Laikin 2002). To accomplish this, one uses the multiconfiguration capability of the optical design program (Figure 12.7). This is necessary because the entrance pupil of the stock zoom lens moves longitudinally with focal length and of course changes its diameter. It is convenient to first create a table of the various first-order parameters for this zoom system. This is shown in Table 12.6a for a 10:1 zoom lens.

Unfortunately, the zoom lens manufacturer is reluctant to provide the necessary pupil distance data. Fortunately, very accurate data for the zoom lens entrance pupil location is not required and so may be determined by looking into the front of the lens with the iris stopped down and illuminated from the rear. The image of the iris (the entrance pupil) is then determined by its location in reference to the lens housing. This system was designed for a zoom lens using a 0.5-in. CCD (8 mm diagonal). Distortion is very low, less than 0.1% over the entire zoom range. The lens system was optimized at the six configurations and listed in Table 12.6b. Note the large amount of astigmatism at the corner of the field. To maintain a compact design, the zoom lens manufacturer increased the f-number at the long focal length positions. Entrance-pupil distances were measured as discussed above.

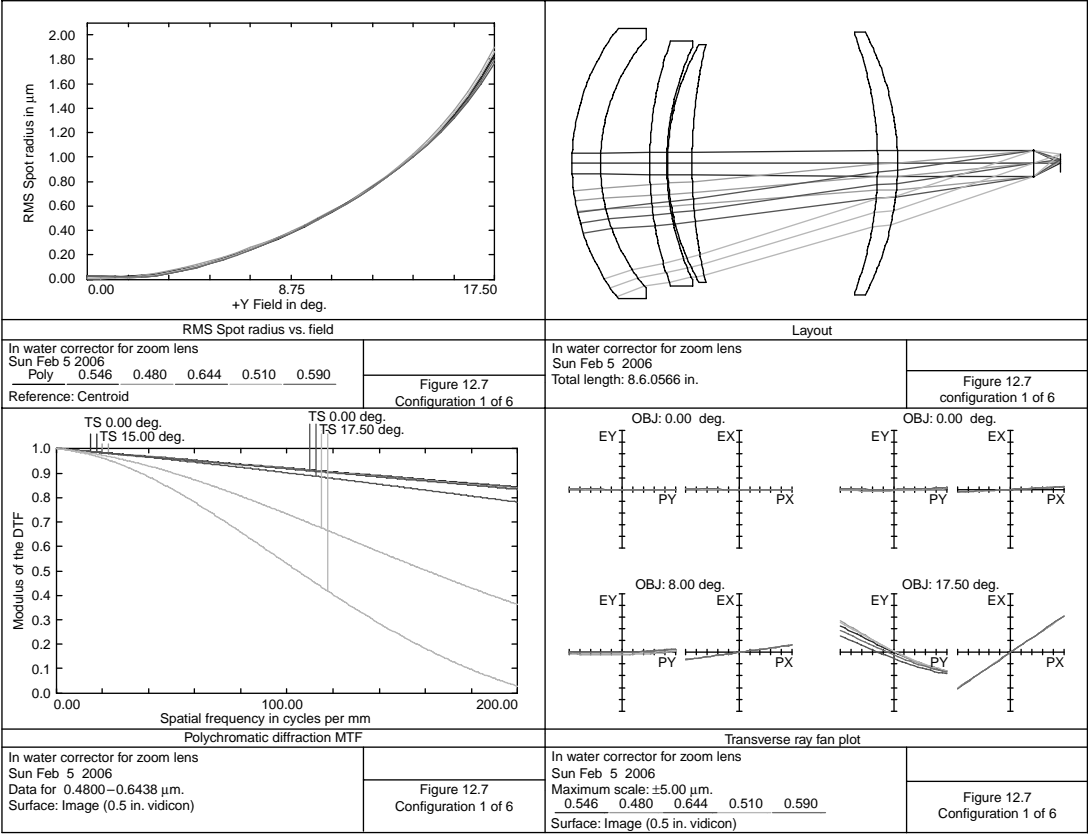


FIGURE 12.7 In-water corrector for zoom lens.



**TABLE 12.6a**  
**First-Order Properties of Zoom Lens with Corrector**

Configurations	EFL	f-Number	Pupil Diameter	Pupil Distance	FOV <sup>a</sup>
1	0.4724	2.0	0.236	2.4	35.0
2	0.7487	2.0	0.374	3.6	22.68
3	1.1867	2.0	0.593	4.8	14.3
4	1.8808	2.0	0.940	6.0	9.0
5	2.9809	2.4	1.242	7.8	5.7
6	4.7244	2.4	1.968	8.4	3.6

<sup>a</sup> FOV is the field of view in seawater in deg.

**TABLE 12.6b**  
**In-Water Corrector for Zoom Lens**

Surface	Radius	Thickness	Material	Diameter
0	Infinity	Infinity	SEA WATER	
1	3.9000	0.5000	N-BK7	4.760
2	3.4000	0.8679		4.380
3	6.5354	0.3000	SF4	4.300
4	4.8577	0.0150		4.100
5	4.2360	0.4300	N-LAK10	4.200
6	9.1016	3.2704		4.200
7	− 6.5863	0.3500	N-LAK10	4.520
8	− 4.9840	2.4000		4.620
9	Stop	0.4724		0.472
10	0.0000	0.0000		0.317

Distance from front vertex of the dome to last lens vertex = 5.733.

**REFERENCES**

Austin, R. W. and Halikas, G. (1976) The index of refraction of seawater, Reference 76-1, Scripps Inst. of Oceanography, San Diego, CA.

Centeno, M. (1941) Refractive index of water, *JOSA*, 31: 245.

Defant, A. (1961) *Physical Oceanography*, Chapter 2 , Vol. 1. Pergamon Press.

Hale, G. M. and Querry, M. R. (1973) Optical constants of water, *Applied Optics*, 12: 555.

Huibers, P. D. T. (1997) Models for the wavelength dependence of the index of refraction of water, *Applied Optics*, 36: 3785.

Hulbert, E. O. (1945) Optics of distilled and natural waters, *JOSA*, 35: 698.

Jerlov, N. G. (1968) *Optical Oceanography* Elsevier Publishing Co, NY.

Jerlov, N. G. and Nielsen, R. S. (1974) *Optical Aspects of Oceanography*, Academic Press, NY.

- Laikin, M. (2002) Design of an in-water corrector system, *Applied Optics*, 41: 3777.
- Mertens, L. (1970) *In-Water Photography*, Wiley Interscience, New York.
- Mobley, C. D. (1995) The optical properties of water, *Handbook of Optics*, Vol. 1, Chapter 3, McGraw Hill, NY.
- Ohshita, K. (1989) Photo taking lens for an underwater camera, US Patent #4856880.
- Padgitt, H. R. (1965) Lens system having ultra-wide angle of view, US Patent #3175037.
- Palmer, K. and Williams, D. (1974) Refractive index of water in the IR, *JOSA*, 64: 1107.
- Pepke, M. H. (1967) Optical system for photographing objects in a liquid medium, US Patent #3320018.
- Quan, X. and Fry, E. S. (1995) Empirical equation for the index of refraction of seawater, *Applied Optics*, 34: 3477.
- Smith, R. and Baker, K. (1981) Optical properties of the clearest natural waters, *Applied Optics*, 20: 177–184.
- SPIE Seminar Proceedings, (1968) *Underwater Photo-Optical Instrumentation*, SPIE 12, Bellingham, WA.
- SPIE Seminar Proceedings, (1968) *Ocean Optics*, SPIE 637, Bellingham, WA.

---

# 13 Afocal Optical Systems

Afocal optical systems are used for a variety of purposes, ranging from power changers in microscopes, IR scanning or FLIR systems, laser beam expanders, and view finders.

Some computer programs simply use a very large image distance for ray-trace evaluation, whereas others use a “perfect lens” at the exit pupil. This converts angular errors to intercept errors so that one may obtain the usual plots of intercept and path-length errors, spot diagrams, and MTF analysis.

Figure 13.1 shows a  $5\times$  laser (HeNe,  $0.6328\text{ }\mu\text{m}$ ) beam expander; details are given in Table 13.1. There is an intermediate image  $0.465\times$  to the right of the first plano surface. A small aperture for mode selection is generally placed at this location. Note that from the wavefront map and the ray plots, there is considerable flare at the edge of the field.

Note that the MTF data presented here in Figure 13.1 through Figure 13.3, as well as the other designs for laser systems, assumes a Gaussian distribution in the entrance pupil. That is, the amplitude  $A$ , at a distance  $R$  from the optical axis is given by  $A_R = e^{-GR^2}$ . In these designs,  $G$  is equal to 1 and so the amplitude ( $A$ ) at the edge of the pupil is reduced to 0.3678 of the peak and the intensity is reduced to 0.135 of peak.

Because this design consists of two essentially thin lenses separated by a large airspace, as a preliminary design, each lens is shaped for minimum spherical aberration. For simplicity, a plano-convex form was chosen. Because the refractive index for minimum spherical aberration is 1.686, N-SF8 glass comes closest to this (1.68448). With this type of all positive lenses, spherical aberration adds.

Using a negative–positive system (a Galilean telescope) greatly reduces spherical aberration and makes a more compact system, as shown in Figure 13.2 and detailed in Table 13.2. However, a mode selection aperture is not possible. On the other hand, for a very-high-power laser (not this HeNe laser), it might be preferred because there is no focused spot and so less chance of ionization of air.

Both of the above systems were designed for a 0.2-in. (5-mm) diameter entrance pupil. Note the superior performance of the Galilean-type system due to spherical aberration canceling with the use of positive and negative components.

Figure 13.3 shows a Galilean-type beam expander of  $50\times$  magnification; details are provided in Table 13.3. It was designed to accommodate a 0.08-in. (2-mm) diameter input HeNe ( $0.6328\text{-}\mu\text{m}$ ) laser beam.

Due to the large amount of spherical aberration present, the positive group was split into two lenses. To provide more negative spherical aberration for the negative component, a glass of lower refractive index was used, N-F2 (1.61656).

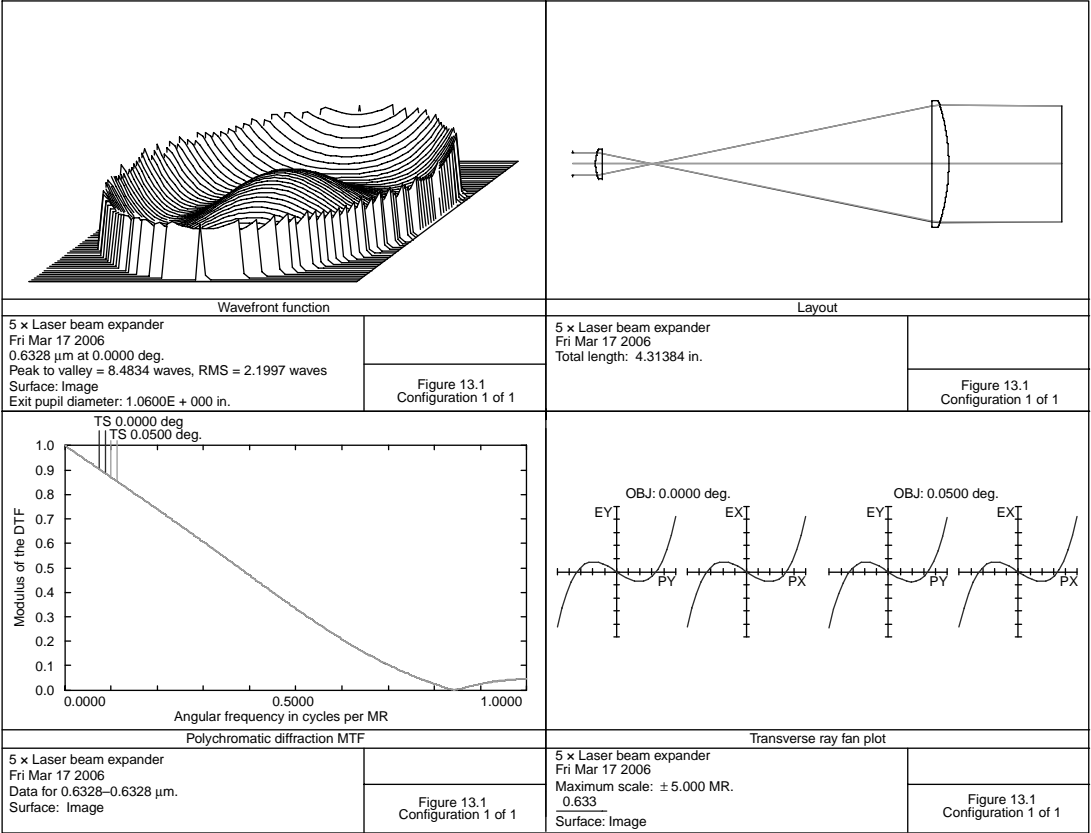


FIGURE 13.1 A 5× laser beam expander.

**TABLE 13.1**  
**A 5× Laser Beam Expander**

Surface	Radius	Thickness	Material	Diameter
1	Stop	0.2000		0.200
2	0.3459	0.0620	N-SF8	0.260
3	0.0000	2.9018		0.260
4	0.0000	0.1500	N-SF8	1.120
5	−1.7518	1.0000		1.120
Overall length of lens = 3.114.				

**TABLE 13.2**  
**A 5× Galilean Beam Expander**

Surface	Radius	Thickness	Material	Diameter
1	Stop	0.2000		0.200
2	−0.3940	0.0300	N-SF8	0.240
3	0.0000	2.1984		0.280
4	0.0000	0.1350	N-SF8	1.100
5	−1.9816	1.0000		1.100
Overall length of lens = 2.363.				

**TABLE 13.3**  
**A 50× Laser Beam Expander**

Surface	Radius	Thickness	Material	Diameter
1	Stop	0.2000		0.080
2	0.1495	0.0590	N-F2	0.130
3	0.0626	11.1143		0.120
4	−15.3924	0.4000	N-SF8	5.600
5	−7.9626	0.0300		5.600
6	0.0000	0.4000	N-SF8	5.600
7	−16.1509	1.0000		5.600
Overall length of lens = 12.0.				

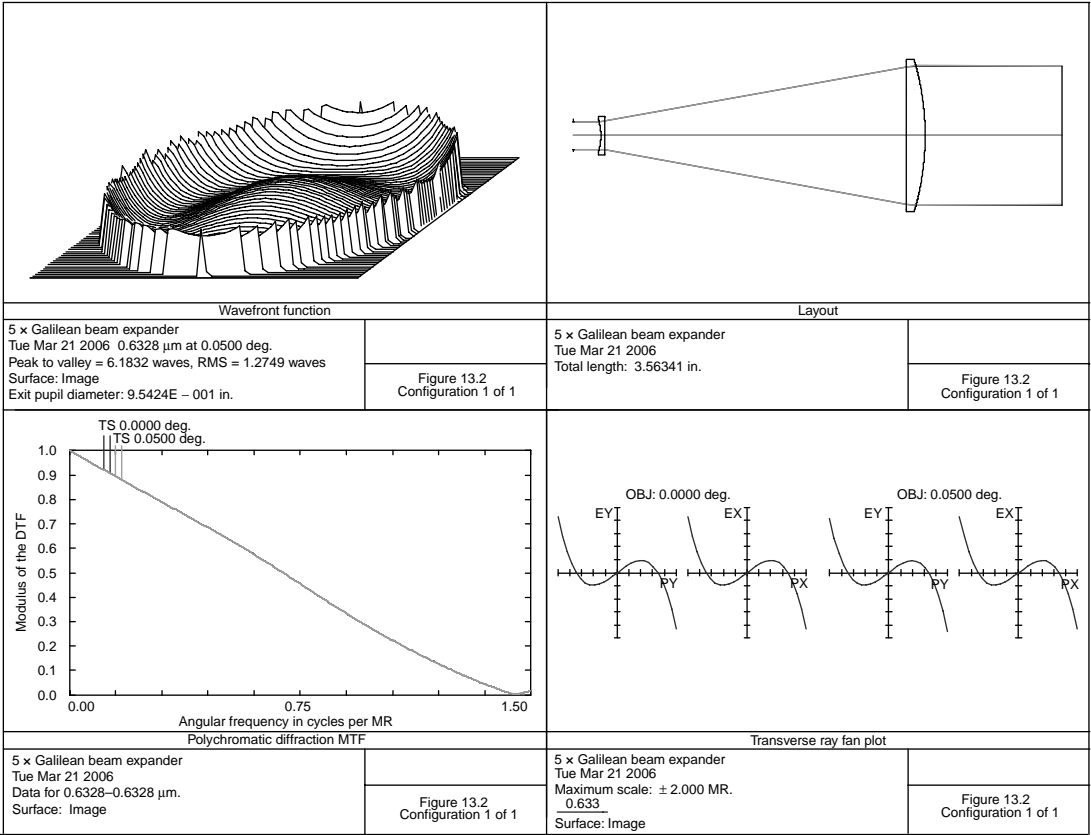


FIGURE 13.2 A 5× Gallean beam expander.

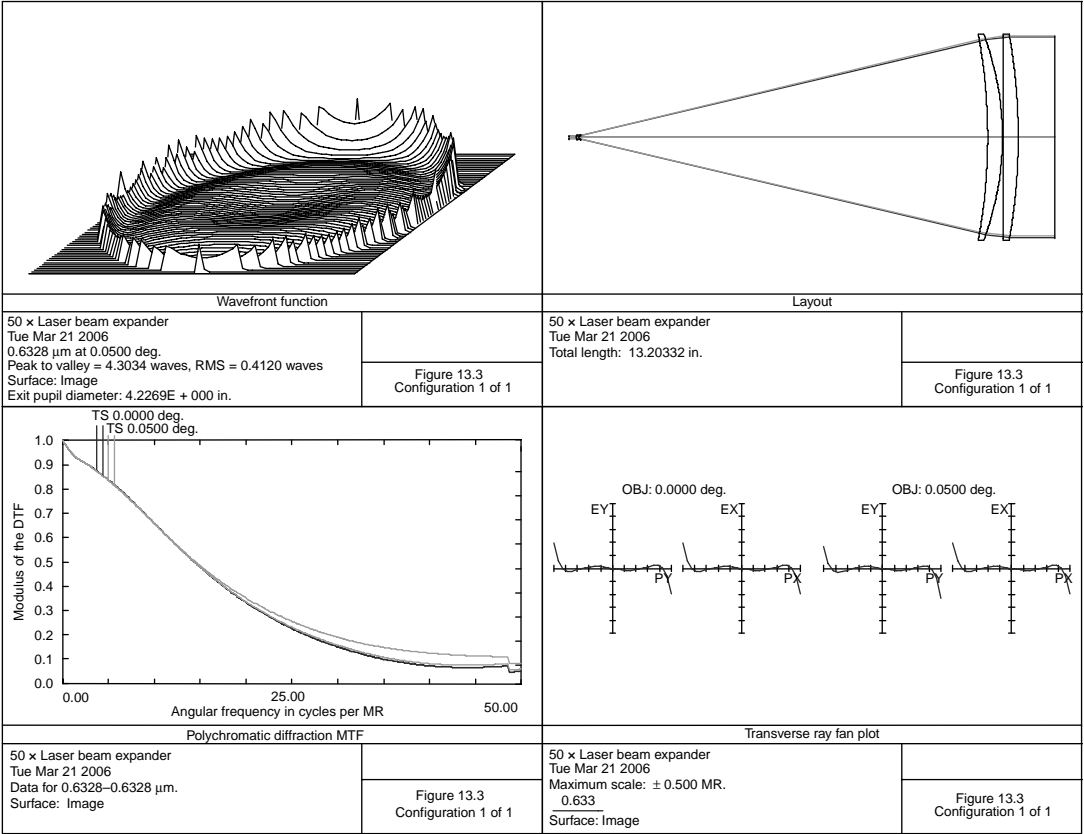


FIGURE 13.3 A 50 $\times$  laser beam expander.

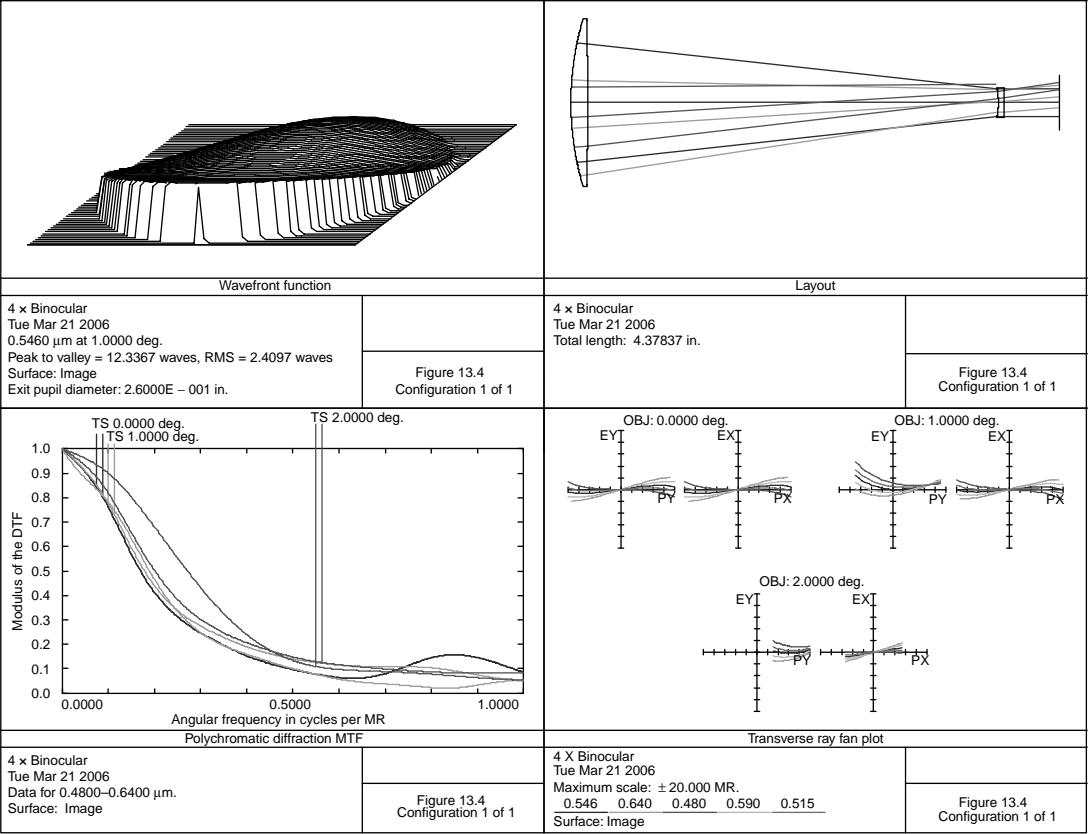


FIGURE 13.4 A 4 $\times$  Galilean plastic telescope.



**TABLE 13.4**  
**Galilean 4× Plastic Telescope**

Surface	Radius	Thickness	Material	Diameter
1	2.6370	0.1500	Acrylic	1.500
2	−36.7252	3.6784		1.500
3	−0.7379	0.0500	Acrylic	0.260
4	2.8057	0.5000		0.260
5	Stop			0.200

Overall length of lens = 3.878.

In Figure 13.4 is shown a simple Galilean 4× plastic telescope. Because the exit pupil for such systems lie inside the telescope a positive value of 0.5 (corresponding to a 12-mm eye relief and 5-mm pupil diameter) was nevertheless used. At 2° off-axis, the pupil is then vignetted by 50% and shifted, while at 1° off-axis, the pupil is vignetted by 20% and also shifted up. Two of these units are often used to form a low-cost binocular. The data for Figure 13.4 is given in Table 13.4. The ray plots show considerable chromatic aberration which substantially contributes to the loss in response at full field.

In Figure 13.5 is shown an afocal power changer for use in a microscope. It is designed to rotate on a turret. A doublet is used with the usual microscope objective such that collimated light emerges. This goes to the power changer and then to another doublet that forms an image of the specimen to be viewed with an eyepiece. The power-changer lenses are arranged such that light may pass through the two lenses (unit power); the lenses may be rotated to the position shown (0.75×) or rotated 180° (1.333×). The lens data for Figure 13.5 is given in Table 13.5.

In Figure 13.6 is shown an Albada viewfinder. This is a simple viewfinder used on some inexpensive cameras and on certain types of photometers. Table 13.6 contains lens data for Figure 13.6.

**TABLE 13.5**  
**A 0.75× Power Changer**

Surface	Radius	Thickness	Material	Diameter
1	Stop	0.1000		0.590
2	−6.8741	0.1400	LF5	0.700
3	−0.9226	0.0600	N-SK16	0.700
4	3.5381	0.7900		0.700
5	−21.1430	0.1100	LF5	0.960
6	1.4217	0.3000	N-SK16	1.060
7	−2.7189	1.0000		1.060

Overall length of lens system = 1.40.

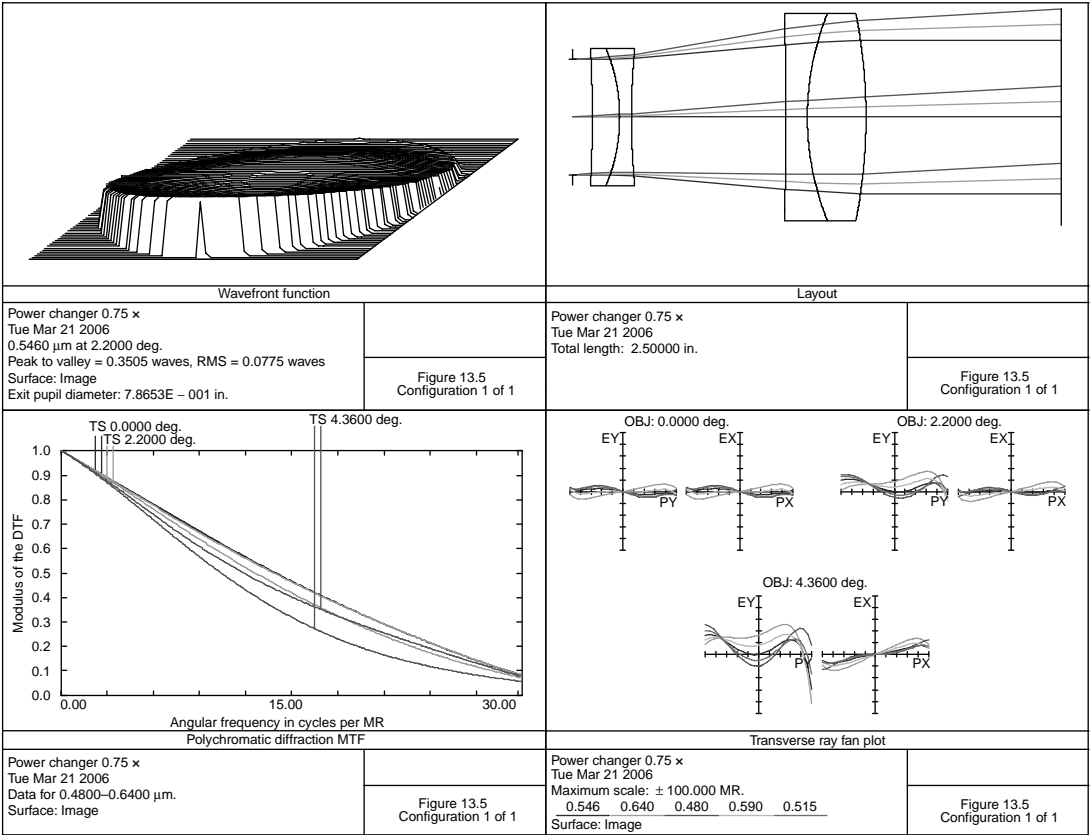


FIGURE 13.5 Power change.

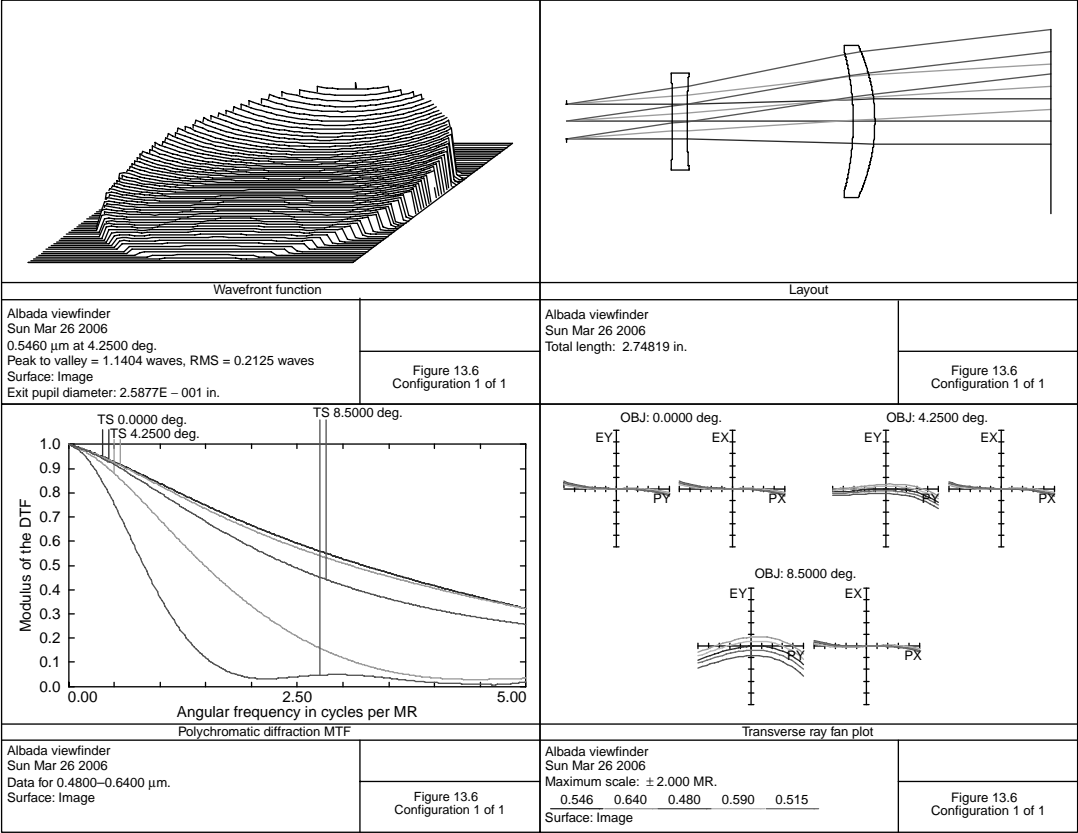


FIGURE 13.6 Albada viewfinder.

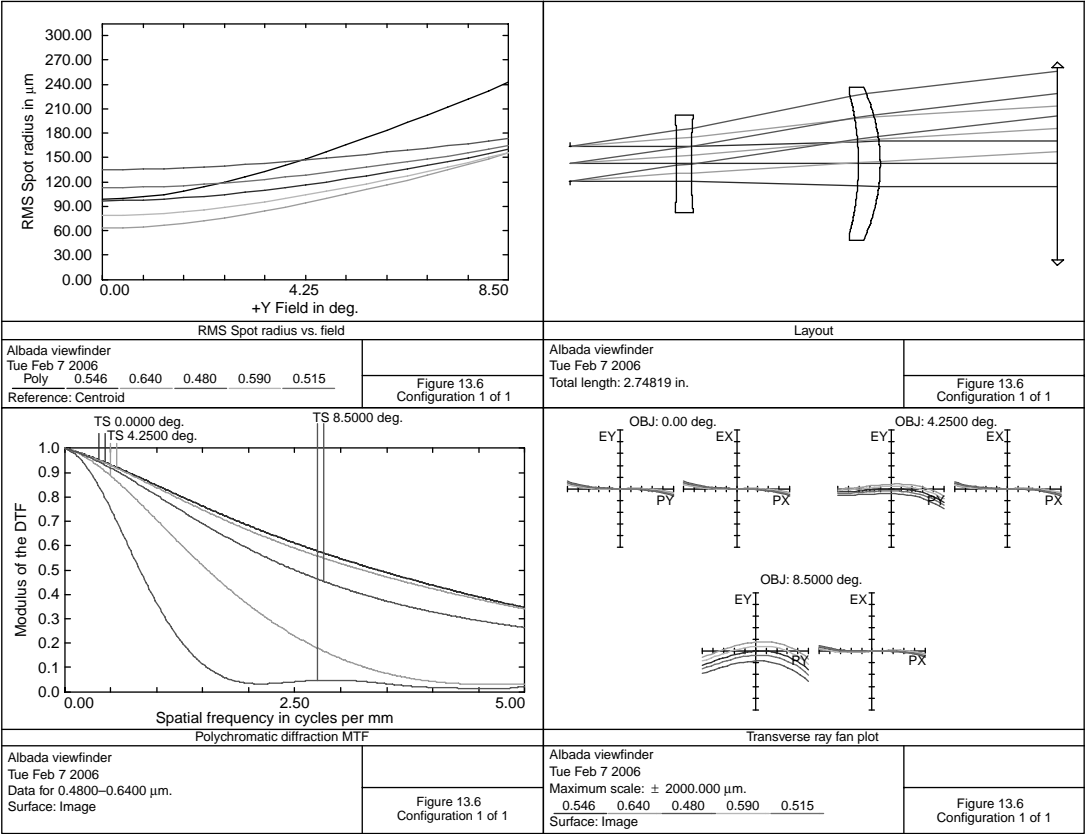


FIGURE 13.6 (continued)

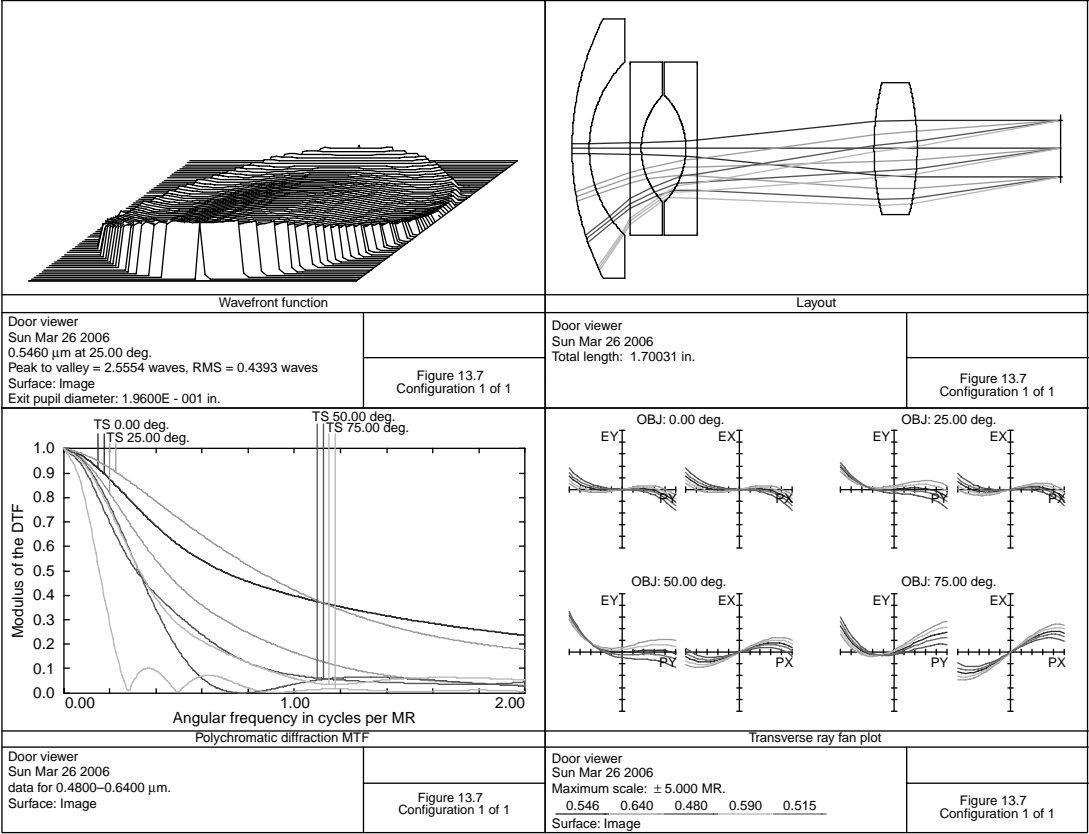


FIGURE 13.7 Door scope.

**TABLE 13.6**  
**Albada Viewfinder**

Surface	Radius	Thickness	Material	Diameter
1	Stop	0.6000		0.200
2	−5.8020	0.0820	N-K5	0.550
3	3.3010	0.9432		0.550
4	−1.5970	0.1230	N-K5	0.780
5	−1.0320	1.0000		0.860

Overall length of lens system = 1.148.

In place of the usual antireflection film, surface 4 ( $R = -1.597$ ) is instead coated with a quarter-wave thickness of ZnS. This has a reflectivity of approximately 30%. The pattern to be projected is evaporated with chrome (or Nichrome) onto surface 3. Looking through this view finder, it acts as a Galilean telescope of 1.29 power. Because the chrome pattern is at the focus (as shown by the dashed lines in Figure 13.6) of the optical system consisting of the first lens and the mirror of surface 3 (EFL = 0.767), this pattern also appears as a bright image at infinity. The MTF plot is for the view through the system. This, then, was designed by successive iterations: optimization of the complete system, tracing from a distant object through the first lens with reflection off surface 4 to the reticle pattern on surface 3, and finally, tracing from the eye to surface 5, 4, and to the reticle pattern on surface 3.

For security reasons, it is desirable for a homeowner to be able to look through a small hole in his door and see a wide field of view. It is obvious that a simple hole in the door provides a narrow field of view. However, a reversed Galilean telescope can provide the viewer with a wide field of view through a small door opening.

**TABLE 13.7**  
**Door Scope**

Surface	Radius	Thickness	Material	Diameter
1	0.9939	0.0600	N-K5	0.900
2	0.4301	0.1407		0.600
3	0.0000	0.0400	N-K5	0.600
4	0.2696	0.1553		0.372
5	−0.2696	0.0400	N-K5	0.372
6	0.0000	0.6143		0.600
7	0.9798	0.1500	N-K5	0.460
8	−0.9798	0.5000		0.460
9	Stop	0.0000		0.196

Distance from first surface to last surface = 1.20.

Such door viewers are sold in hardware stores and are a common door accessory. Figure 13.7 shows such a door viewer for which the data is given in Table 13.7. It has a  $150^\circ$  field of view and a 5-mm exit pupil 0.5 in. from the last lens surface. Of course, if the observer moves his eye sideways, the field of view is thereby increased. Following is lens data for Figure 13.7.

This system, like all wide angle optical systems, exhibits considerable shift of the entrance pupil toward the front of the lens with field angle. It also suffers from primary color, due to this simple construction with only one glass type. (Also see Chapter 9 and design 17.4 for a  $10\times$  beam expander at  $10.6\text{ }\mu\text{m}$ ).

## REFERENCES

- Besenmatter, W. (2000) Recent progress in binocular design, *Optics and Photonics News*, November 30–33.
- Fraser, R. and McGrath, J. (1973) Folding camera viewfinder, US Patent #3710697.
- Itzuka, Y. (1982) Inverted galilean finder, US Patent #4348090.
- Neil, I. A. (1983) Collimation lens system, US Patent #4398786.
- Neil, I. A. (1983) Afocal refractor telescopes, US Patent #4397520.
- Ricco, L. D. (1945) Scanning lens, US Patent #2373815.
- Rogers, P. J. (1983) Infra-red optical systems, US Patent #4383727.
- Wetherell, W. B. (1987) Afocal Lenses, *Applied Optics and Optical Engineering*, Shannon, R. and Wyant, J., eds., Chapter 3, Volume 10, Academic Press, New York.
- Yanagimachi, M. (1979) Door scope, US Patent #4172636.





---

# 14 Relay Lenses

Relays are used to relay an image from one place to another. They are used in rifle sights, periscope systems, microscopes, and military infrared imaging systems. (This type of lens is also used for photocopy work.) Generally, a field lens is required at an image plane to image the exit pupil of the previous group into the entrance pupil of the next group. The designer should keep in mind that a computer program, if allowed to vary the refractive index of this field lens, will select a glass of high index and low dispersion. Very little is gained by using glasses of refractive index greater than that of N-SK5. Also a material must be selected with a low bubble code. Because this field lens is at an intermediate image, dirt, scratches, and other imperfections are imaged onto the final image. It is thus advisable to slightly move the field lens away from the intermediate image.

One to one imaging is desired because a completely symmetric lens may be used. This means that all transverse aberrations (distortion, coma, and lateral color) are zero. (See discussion under [Figure 21.3](#) for a unit magnification copy lens.)

[Figure 14.1](#) shows a symmetric one-to-one relay (without its field lens) for a 1.2-diameter object; details are provided in [Table 14.1](#). It was designed as a copy lens for 35-mm motion-picture film. The numeric aperture (NA) is

$$NA = \frac{0.5}{f^\#(M + 1)} = 0.1.$$

The KZFSN4 elements help to reduce secondary color. Note that the lens is completely symmetric about the stop; however,  $T17$  is not quite the same as the object distance due to field curvature and spherical aberration.

[Figure 14.2](#) shows a lens used in photocopy work; the prescription is given in [Table 14.2](#). It images a 40-in. diameter object at unit magnification. Although, this particular design is in the visual region, some of these lenses are designed to be used with orthochromatic film and are therefore designed for a shorter wavelength region. A general procedure in the graphic arts and printing trades is to create the various articles and pictures as a “paste-up.” This is then photographed to make the actual printing plate. A recent trend in the graphic arts is the use of a computer to directly generate the printing plate.

This design is unusual in that the MTF at full field is better than at mid-field. This is due to large sagittal errors at mid-field. This lens is  $f/11$  and has a focal length of 26.664. Copy lenses are generally fitted with an iris.

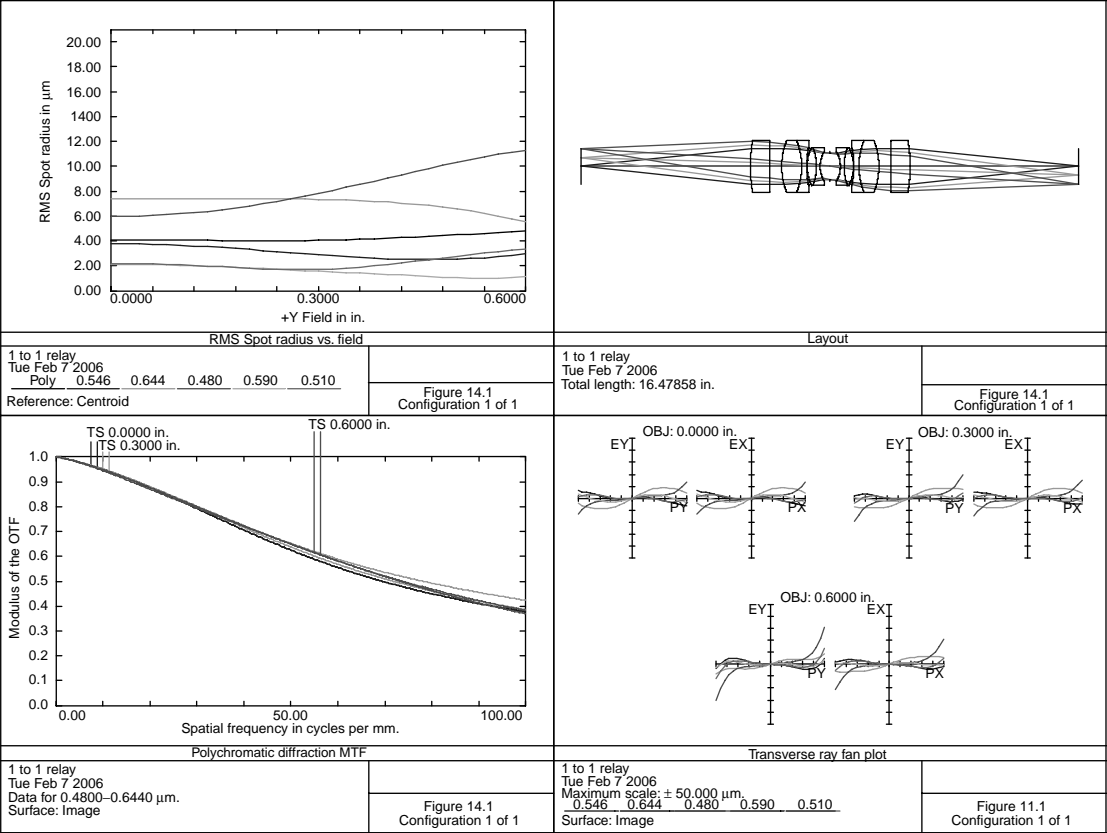


FIGURE 14.1 A 1 to 1 relay.

**TABLE 14.1**  
**A 1 to 1 Relay**

Surface	Radius	Thickness	Material	Diameter
0	0.0000	5.6018		1.200
1	4.8569	0.6499	N-LAK12	1.720
2	0.0000	0.3886		1.720
3	2.3595	0.6586	N-LAK12	1.720
4	−2.3595	0.1675	N-BAF4	1.720
5	2.9401	0.0150		1.260
6	1.4406	0.3092	N-SSK2	1.260
7	−1.7750	0.1209	KZFSN4	1.260
8	0.9580	0.3365		0.980
9	Stop	0.3365		0.863
10	−0.9580	0.1209	KZFSN4	0.980
11	1.7750	0.3092	N-SSK2	1.260
12	−1.4406	0.0150		1.260
13	−2.9401	0.1675	N-BAF4	1.260
14	2.3595	0.6586	N-LAK12	1.720
15	−2.3595	0.3886		1.720
16	0.0000	0.6499	N-LAK12	1.720
17	−4.8569	5.5840		1.720
18	0.0000	0.0000		1.200

Lens focal length = 4.697, distance from first lens surface to image = 10.876.

Figure 14.3 shows a copy lens for  $0.6\times$  magnification. It was designed to image a 10-in. diameter object into a 6-in. diameter image. It is  $f/3.46$  (NA is 0.0879). The lens data for Figure 14.3 is given in Table 14.3.

These elements tend to be rather thick. This helps reduce the Petzval sum. There is some flare at the edge of the pupil. Whenever a lens is to be fitted with an iris, be sure to allow at least 0.12 on both sides of the stop location for this iris mechanism. (In this case, the stop location should be moved a little to the right.)

Figure 14.4 shows a small three-element relay being used to create an erect image in a rifle sight. The prescription is given in Table 14.4. In a rifle sight, unlike a binocular, a long, in-line optical system is desired. This facilitates mounting on the rifle. The front objective forms an image very close to the front surface of the field lens. (This could cause a problem because dust and blemishes on this surface will be visible.) The relay then images this onto the first surface of the field lens (surface 4). At this image location, a cross-line is placed that may take the form of an actual wire stretched over a frame or a photographic pattern on the lens. A more desirable situation is to have this intermediate image on a thin glass plate just in front of the field lens. This cross-line may be adjusted transversely to bore sight the scope to the rifle. The eyepiece then forms a virtual image of this to the eye.

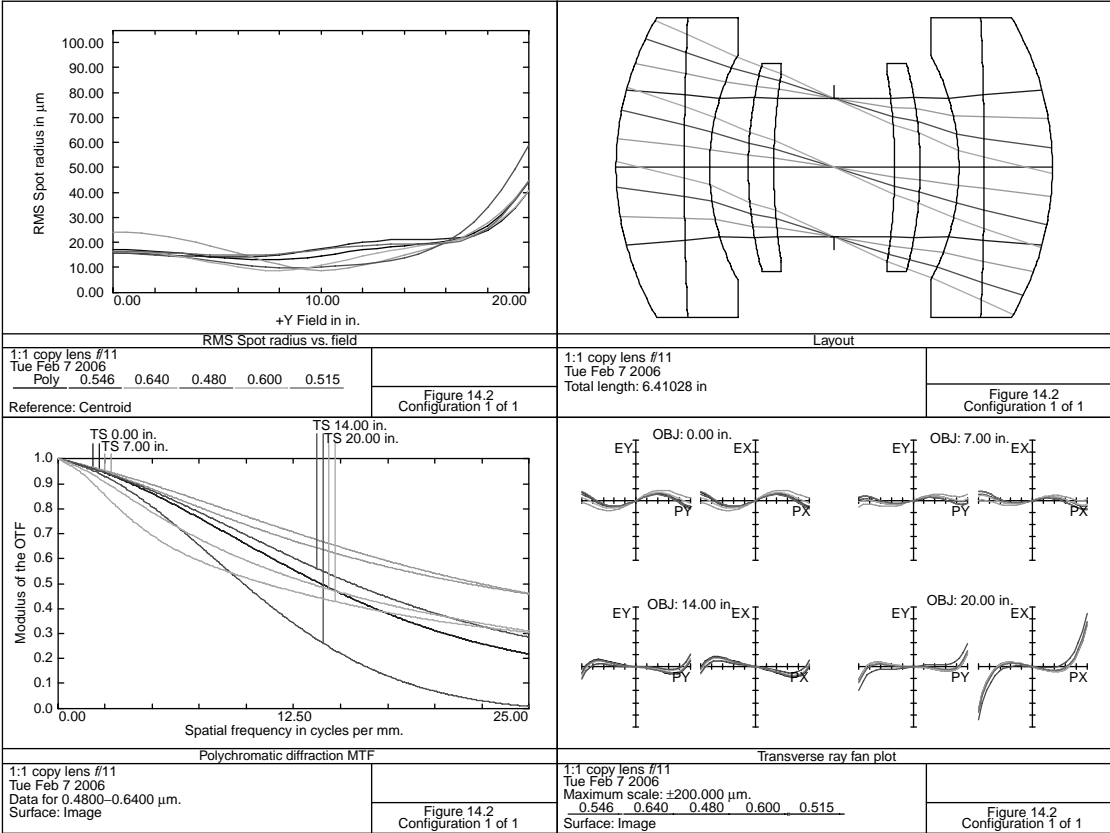


FIGURE 14.2 Unit power copy lens.

**TABLE 14.2**  
**1:1 Copy Lens**

Surface	Radius	Thickness	Material	Diameter
0	0.0000	50.0000		40.000
1	4.3332	1.0025	N-PSK53	4.400
2	48.4668	0.3707	N-BALF4	4.400
3	3.4936	0.5698		3.300
4	5.8676	0.3750	N-FK51	3.060
5	8.8510	0.8872		2.800
6	Stop	0.8872		2.040
7	−8.8510	0.3750	N-FK51	2.800
8	−5.8676	0.5698		3.060
9	−3.4936	0.3707	N-BALF4	3.300
10	−48.4668	1.0025	N-PSK53	4.400
11	−4.3332	49.9925		4.400
12	0.0000	0.0000		40.001

Distance from first lens surface to image is = 56.403.

Note that on the lens MTF plot, the abscissa (like all the afocal systems discussed here) has units of cycles/mil radian. Three cycles/mil radian is approximately 1 arc min, the limit of visual acuity.

Due to rifle recoil, a very large eye relief is required (3.92 in this case). To obtain this long eye relief, the aperture stop of the system is located inside the relay. The image of this by the eyepiece is the exit pupil. Magnification of the system is 4.0, field of view is 5.0°. Entrance pupil diameter is 16 mm.

Because a rifle sight is often exposed to rain, fog, snow, etc. it is important that glass types used for front and rear lens surfaces be selected for high weather and stain resistance. In the usual glass catalogues, the most resistant materials are indicated with low numbers such as 0, 1, or 2, whereas glasses with poor stain and weather resistance have codes of 4 or 5. In some of the glass catalogues, weather resistance is termed *climatic resistance* and is a measure of the effect of water vapor in the air on the glass. Staining is a result of the glass being in contact with slightly acidic water—often due to a fingerprint.

At the edge of the field there is some primary lateral color. [Figure 35.4](#) shows a zoom rifle sight that might be of interest.

[Figure 14.5](#) shows an eyepiece relay, similar to the above rifle sight. The prescription is given in [Table 14.5](#). It was designed to view a 16-mm diameter object with a 4-mm diameter entrance pupil for a 16-mm film camera.

Note that this design features a relay composed of two identical cemented doublets. Although this simple construction is economical to manufacture, it has the usual astigmatism common to cemented doublets. This results in the image degradation at the edge of the field.

[Figure 14.6](#) shows a high numeric aperture (0.4) relay; details are provided in [Table 14.6](#). The object diameter is 0.32 and is imaged at a 1/5 reduction.

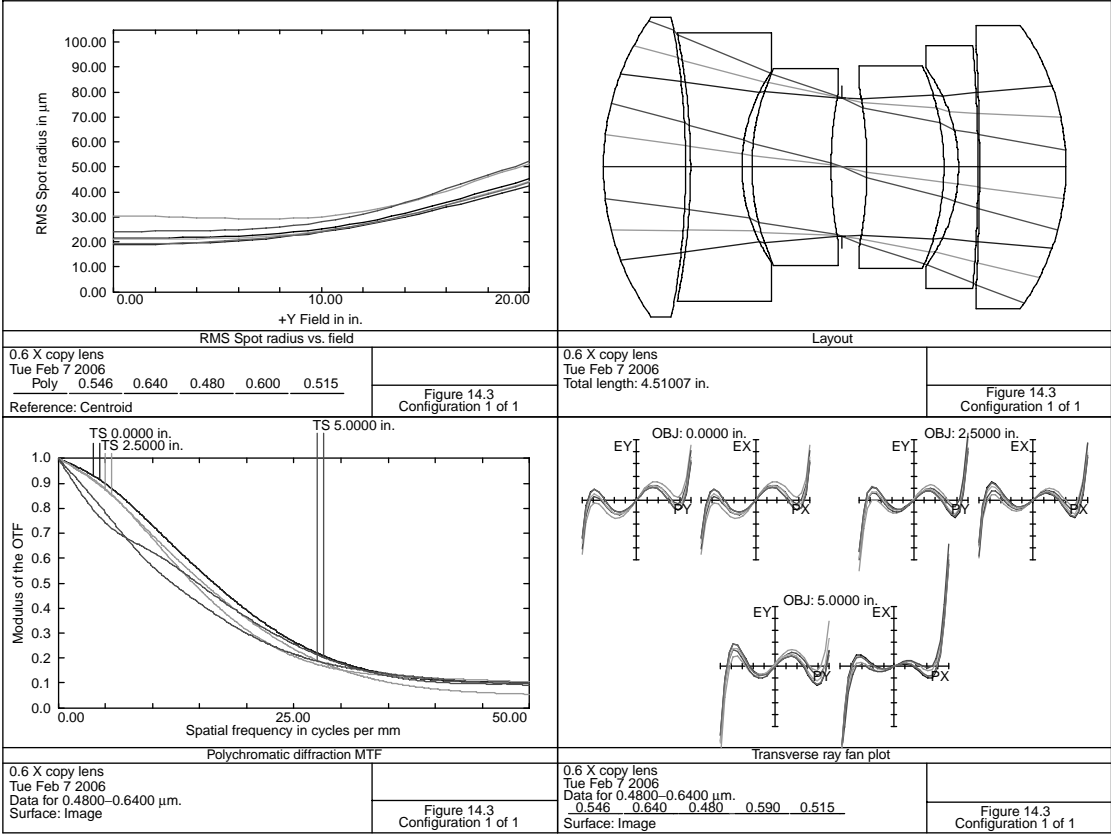


FIGURE 14.3 A 0.6× copy lens.

---

**TABLE 14.3**  
**A 0.6× Copy Lens**

Surface	Radius	Thickness	Material	Diameter
0	0.0000	16.6667		10.000
1	2.5180	0.8022	N-LAK12	2.920
2	−7.7191	0.0481		2.920
3	−6.6004	0.5000	LF5	2.620
4	1.6416	0.0984		1.870
5	2.2888	0.7712	N-LAK7	1.920
6	3.8396	0.1008		1.420
7	Stop	0.2491		1.344
8	−4.0484	0.7500	N-LAK7	1.540
9	−2.4317	0.1424		1.980
10	−1.6226	0.1900	LF5	1.940
11	−13.9145	0.0150		2.360
12	−21.7698	0.8429	N-LAK12	2.360
13	−2.3675	8.7264		2.760
14	0.0000	0.0000		6.093

Distance first lens surface to image=13.236, lens focal length=7.076,  
distortion is 0.5%.

---

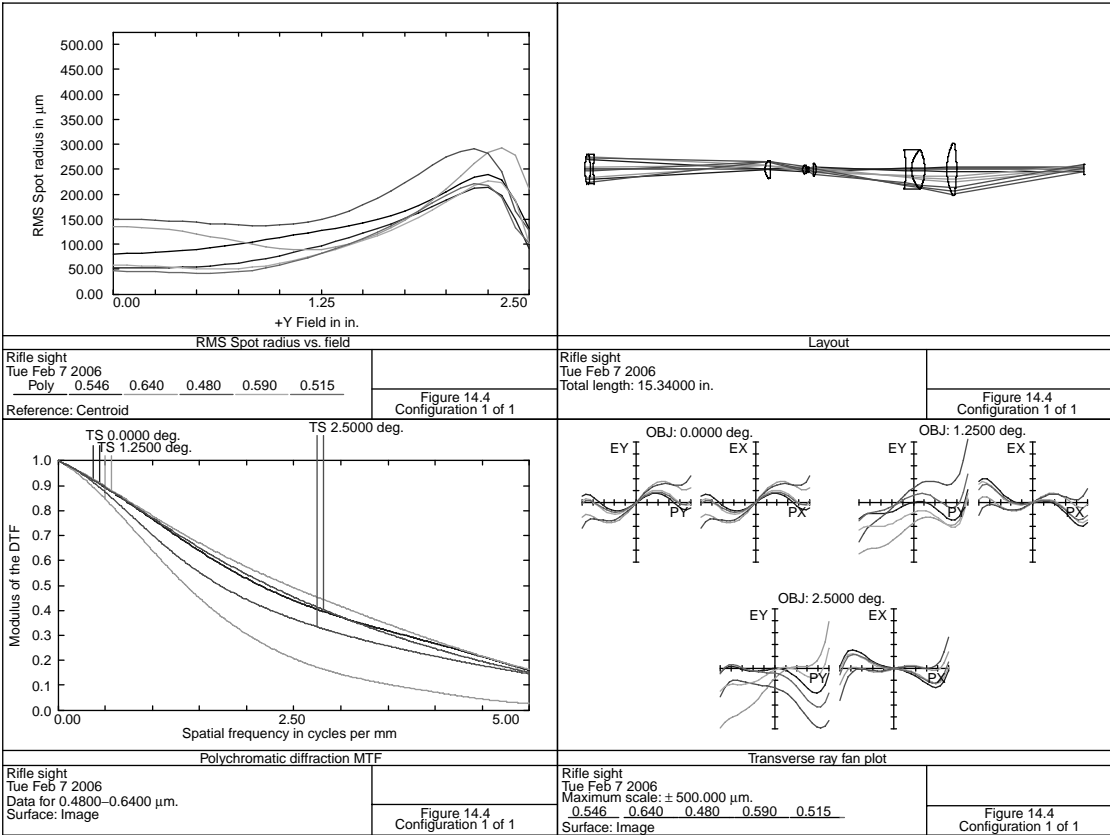


FIGURE 14.4 Rifle sight.



---

**TABLE 14.4**  
**Rifle Sight**

Surface	Radius	Thickness	Material	Diameter
1	1.8860	0.1635	N-BK7	0.900
2	−2.0688	0.1000	F2	0.900
3	13.0679	5.2726		0.900
4	0.4190	0.1500	N-BK7	0.540
5	1.1764	1.0074		0.480
6	0.2109	0.0914	N-SK18	0.240
7	1.4389	0.0293		0.160
8	Stop	0.0211		0.109
9	−0.3619	0.0322	F2	0.140
10	0.1871	0.1471		0.148
11	1.7273	0.0956	N-SK18	0.380
12	−0.3147	2.7496		0.380
13	−3.5888	0.1783	SF4	1.200
14	0.8492	0.4034	N-SK2	1.200
15	−1.4514	0.6778		1.200
16	1.8328	0.3008	N-BAF3	1.580
17	−4.9786	3.9200		1.580

Distance from first surface to last surface = 11.42, distortion = 0.03%.

---

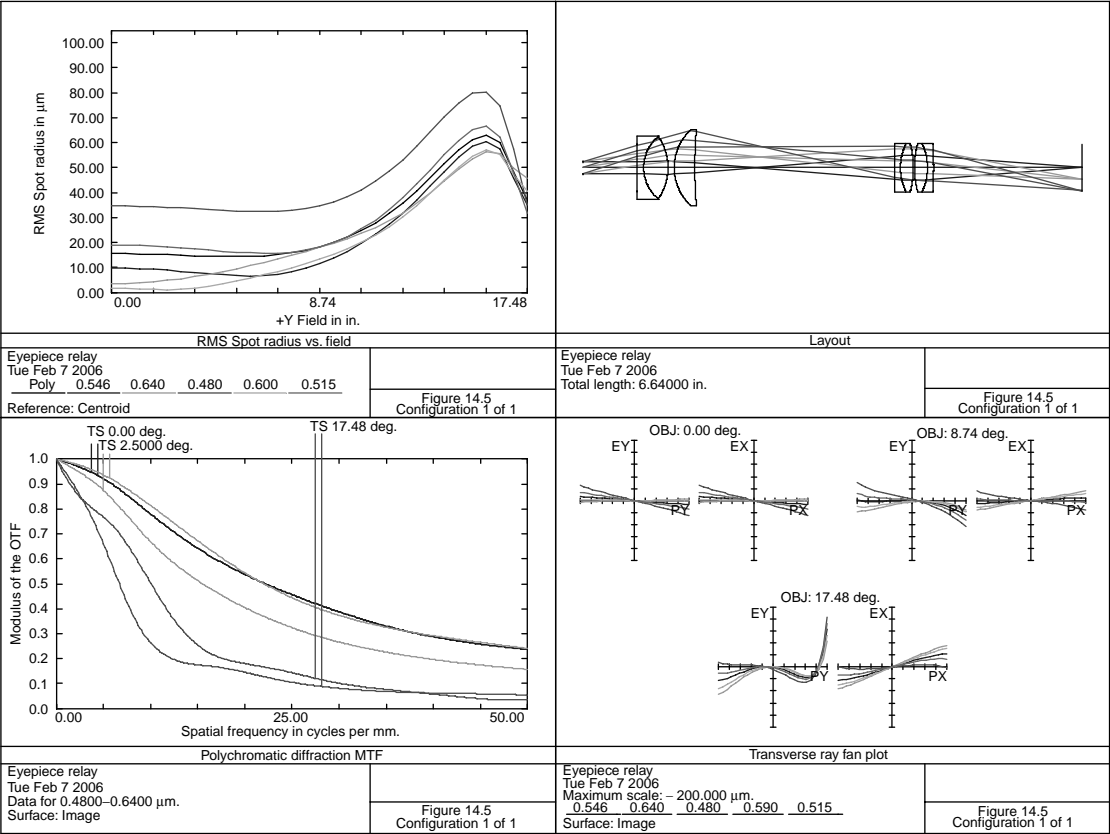


FIGURE 14.5 Eyepiece relay.

---

**TABLE 14.5**  
**Eyepiece Relay**

Surface	Radius	Thickness	Material	Diameter
1	Stop	0.7170		0.157
2	−10.6581	0.0880	SF1	0.640
3	0.5360	0.3246	N-BK7	0.840
4	−0.7199	0.0825		0.840
5	0.6937	0.2735	N-BK7	1.020
6	6.1289	2.6546		1.020
7	6.0463	0.0808	SF2	0.640
8	0.7433	0.1722	N-SK5	0.640
9	−1.2753	0.0150		0.640
10	1.2753	0.1722	N-SK5	0.640
11	−0.7433	0.0808	SF2	0.640
12	−6.0463	1.9787		0.640

Distance from first lens surface to image = 5.923, distortion = 1.73%.

---

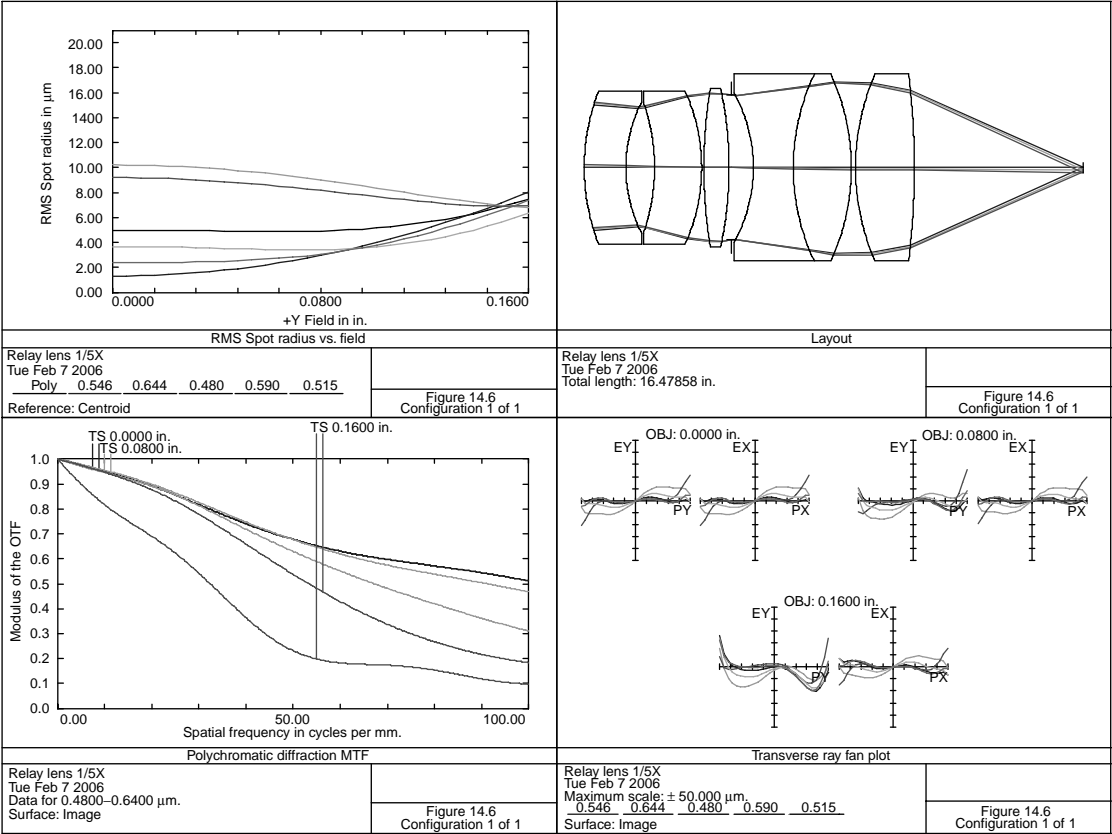


FIGURE 14.6 A 1/5X relay.

**TABLE 14.6**  
**A 1/5X Relay**

Surface	Radius	Thickness	Material	Diameter
0	0.0000	5.1067		0.320
1	1.4554	0.2825	SF4	1.040
2	0.9863	0.1948		0.890
3	−1.3539	0.3207	N-LAF21	0.890
4	−1.2580	0.0150		1.040
5	3.4212	0.1702	N-LAF21	1.080
6	−2.6453	0.0150		1.080
7	Stop	0.1509		0.984
8	−1.0529	0.2720	SF4	1.020
9	1.4860	0.3933	N-LAK10	1.270
10	−1.5321	0.0295		1.270
11	1.5949	0.3996	N-LAF21	1.270
12	−5.2280	1.1497		1.270

Object to image distance=8.500, distortion=0.04% (pincushion).

**REFERENCES**

Cook, G. (1952) Four component optical objective, US Patent #2600207.  
Itoh, T. (1982) Variable power copying lens, US Patent #4359269.  
Kawakami, T. (1976) Symmetrical type four component objective, US Patent #3941457.  
Shade, W. E. (1967) Projection printer lens, US Patent #3320017.  
Terasawa, H. (1985) Projection lens, US Patent #4560243.  
Tibbetts, R. E. (1971) High speed document lens, US Patent #3575495.  
Yonekubo, K. (1982) Afocal relay lens system, US Patent #4353624.



---

# 15 Catadioptric and Mirror Optical Systems

A mirror has substantially less spherical aberration than a lens of equivalent focal length. In addition, the spherical aberration of a concave mirror is opposite in sign to that of a positive lens. Therefore, several researchers (Maksutov 1944; Bowers 1950) have proposed the use of a weak negative lens in conjunction with a concave mirror. Schmidt (Hodges 1953) proposed a weak aspheric corrector at the center of curvature of a spherical mirror.

In the Cassegrain system, two mirrors are required. The primary has a hole in it and the smaller secondary is attached to (or is actually a part of) one of the front corrector lenses. Due to vignetting, fields of view are generally limited to about  $15^\circ$ .

The computer program must have the following features:

1. Surface radii, material, and thickness must be capable of being tied or set equal to another surface.
2. Axial distances from one surface to another must be capable of being bounded.
3. Beam diameter at the secondary mirror has to be limited.
4. Delete tracing of the chief ray and other rays that will ultimately be blocked by the central obscuration. Most computer programs simply have the user trace additional rays that are then deleted at the obscuration. A more efficient way is to adjust the rays in the entrance pupil to allow for this central obscuration.

Figure 15.1 shows a Cassegrain mirror system with a primary and secondary mirror separated by a distance  $T$ , forming an image a distance  $B$  from the secondary. Assuming a sign convention in which  $T$  and  $B$  are positive and  $R_p$  and  $R_s$  are negative as shown, then

$$F = \frac{R_p R_s}{2R_p - 2R_s + 4T} = \text{Effective focal length.}$$

Let  $H$  be the height ratio of a paraxial axial ray at the secondary mirror divided by the height at the primary. If the object is at infinity then

$$H = \frac{R_p 2T}{R_p}$$

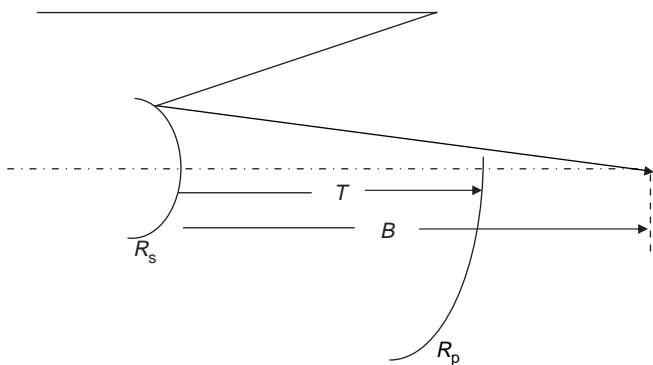


FIGURE 15.1 Cassegrain mirror system.

and

$$B = \frac{2R_sT + R_sR_p}{4T - 2R_s + 2R_p} = HF.$$

Most practical systems require that  $B$  should be at least as large as  $T$  (the image is outside the primary mirror). Also, the obscuration by the secondary needs to be minimized. Assigning a reasonable value for  $H$  of 0.3 and for a focal length,  $F$ , of 100 gives the data in Table 15.1 ( $B$  is obviously 30 for all values in this table).

If only two mirrors are used, then for a flat field (zero Petzval sum),  $R_p=R_s=-140$  with  $T=49$ . However, to correct for other aberrations, it is necessary to add some refractive elements as shown in the following examples. The below table is useful in obtaining a starting solution.

The effect of obscuration must be considered in evaluating the image. Diffraction, as a result of the obscuration, increases the energy in the outer portions

TABLE 15.1 Primary and Secondary Mirror Geometry $F=100$		
$R_p$	$R_s$	$T$
-171.428	-360.000	60.000
-122.449	-94.737	42.857
-95.238	-54.545	33.333
-77.922	-38.298	27.273
-65.934	-29.508	23.077
-57.143	-24.000	20.000
-50.420	-20.225	17.647
-45.113	-17.476	15.789
-40.816	-15.385	14.286
-37.267	-13.740	13.043



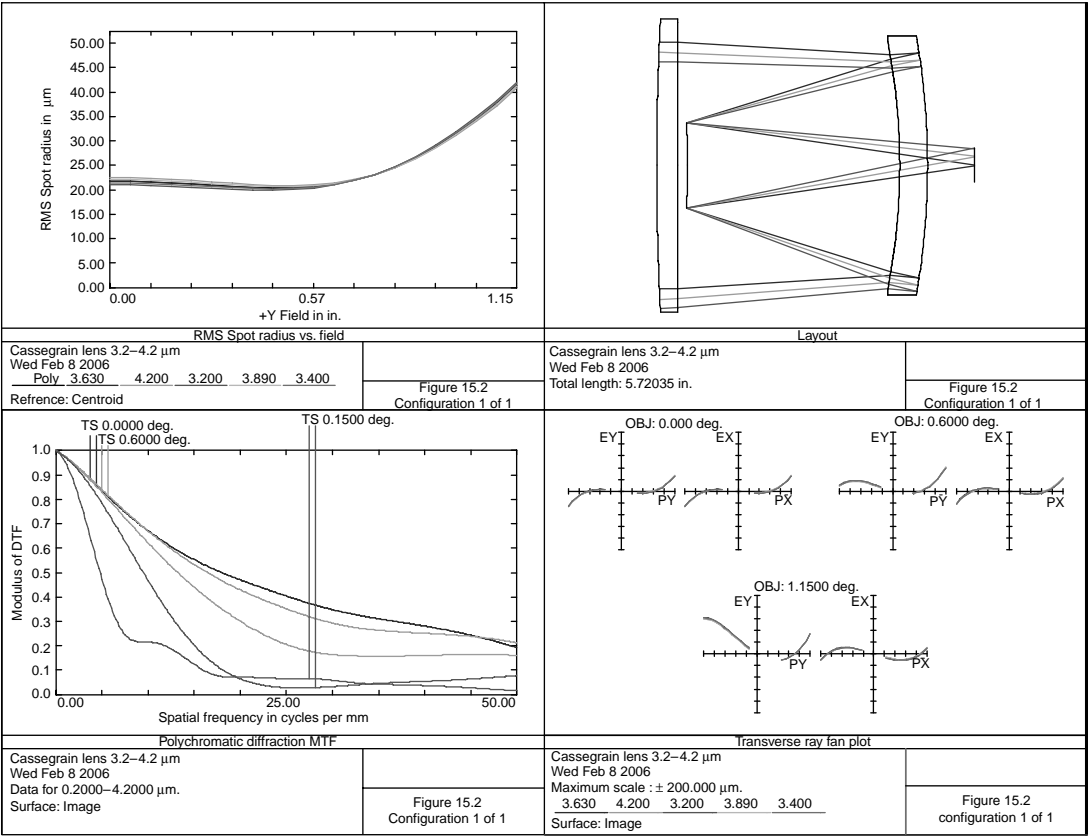


FIGURE 15.2 Cassegrain lens, 3.2–4.2 μm.

of the image at the expense of the central bright spot. This reduces the MTF response at low spatial frequencies, and increases the response at higher spatial frequencies (Mahajan 1977).

For very short wavelength lithography (wavelengths less than 0.2  $\mu\text{m}$ ), mirror systems are being developed. See for example the Wang and Pan patent in the Chapter 18 references.

Figure 15.2 shows a 15-in. focal length,  $f/3.333$  lens that covers the spectral region 3.2–4.2  $\mu\text{m}$ . It has a 2.3° field of view (FOV). Details are provided in Table 15.2.

As an alternate, this design could have used zinc sulfide (ZnS) in place of the zinc selenide (ZnSe). Note that for the system as shown, a ray may pass thru the front corrector and go directly to the image. To prevent this from occurring, baffles are required. This is accomplished with a lens extension tube placed in front of the lens plus a tube in the hole of the primary mirror, as well as a shield at the secondary mirror.

Placing baffles to prevent these unwanted rays is a complex task (Song 2002). Although computer programs are available to help the designer in this specific task, a simple method is to make a large and careful layout showing the limiting rays. Then, trace rays that would penetrate the system without making the necessary reflections at primary and secondary mirrors. From this layout, the required baffles may be determined.

Also note that the front lens is positive. However, in conjunction with the Mangin primary mirror, the refractive elements have negative power.

Figure 15.3 shows a 4.0-in. focal length,  $f/1.57$  Cassegrain with a 15° FOV for the visual region. The prescription is given in Table 15.3. The front corrector is of the usual negative form. Note that the secondary mirror has the same radius as the front refracting surface. This is a manufacturing convenience because, with a mask, a reflecting coating is first applied to the inside diameter (corresponding to the secondary mirror) an antireflection coating applied to the entire surface and then the mirror surface protected with a black paint.

**TABLE 15.2**  
**Cassegrain Lens, 3.2–4.2  $\mu\text{m}$**

Surface	Radius	Thickness	Material	Diameter
1	53.2907	0.3800	ZnSe	5.280
2	0.0000	4.0000		5.280
3	−11.4239	0.5000	ZnSe	4.460
4	−13.5164	−0.5000	Mirror	4.660
5	−11.4239	−3.8200		4.460
6	−10.1885	5.1603	Mirror	1.548 Stop

Distance from first lens surface to image = 5.720, distortion = 0.16%.

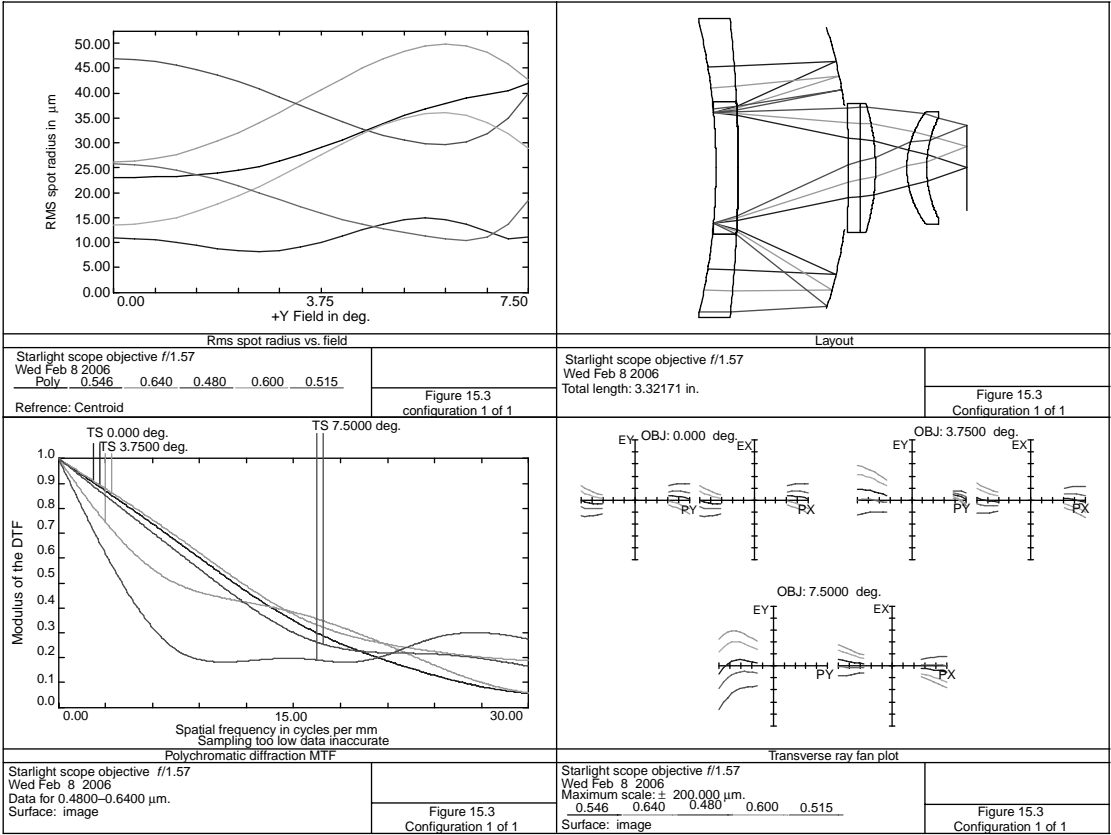


FIGURE 15.3 Starlight scope objective,  $f/1.57$ .

**TABLE 15.3**  
**Starlight Scope Objective**

Surface	Radius	Thickness	Material	Diameter
1	-7.7618	0.2750	N-BK7	3.600
2	-16.8186	1.3662		3.700
3	-5.6768	-1.3662	Mirror	3.440
4	-16.8186	-0.2750	N-BK7	1.640
5	-7.7618	0.2750	Mirror	1.361 Stop
6	-16.8186	1.3662		1.640
7	-15.1741	0.1500	SF2	1.500
8	0.0000	0.1846	N-LAK7	1.540
9	-2.7866	0.3873		1.540
10	1.1320	0.2469	N-SK16	1.400
11	1.4144	0.5000		1.240

Distance from first lens surface to image = 3.110, distortion = negligible.

Due to its compact form and low f-number, a variation of this design was extensively used during the Korean War as a night-vision device. Excellent imagery may be obtained to wavelengths as long as 0.85  $\mu\text{m}$ . With an image intensifier tube

**TABLE 15.4a**  
**A 1000-mm Focal Length Cassegrain**

Surface	Radius	Thickness	Material	Diameter
0	0.0000	0.100000E+11	0.00	
1	-7.4824	0.5000	N-BK7	5.420
2	-10.3064	4.5628		5.660
3	-13.0811	-4.3128	MIRROR	5.900
4	-6.8785	2.9218	MIRROR	2.230 Stop
5	6.8720	0.2250	N-SK16	2.320
6	-37.1174	0.1358		2.320
7	-51.5664	0.2000	SF4	2.260
8	-6.4233	0.2000	N-SK16	2.260
9	-10.0893	0.5185		2.260
10	-8.6473	0.2000	SF4	1.960
11	44.1553	4.2290		1.920
12	-3.3870	0.1300	N-LAK9	1.120
13	1.7302	0.2000	N-BALF4	1.200
14	13.9542	3.2912		1.140
15	0.0000	0.0000		1.705

Distance from first lens surface to image = 13.001, distortion = 1%.

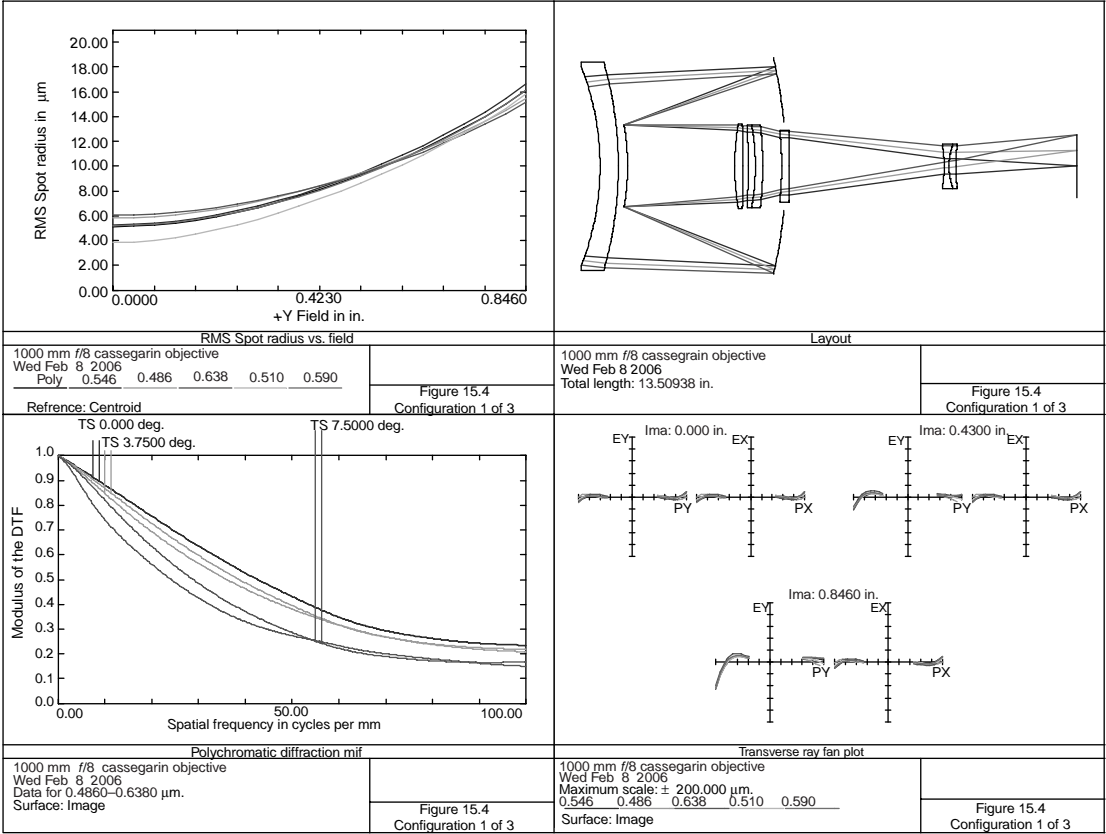


FIGURE 15.4 A 1000-mm focal length Cassegrain.

**TABLE 15.4b**  
**Focus Movement**

Object Distance	<i>T</i> (6)	<i>T</i> (11)
Infinite	0.1358	4.2290
5000	0.3404	4.0245
2500	0.5533	3.8115

and an eyepiece, it was fitted to a rifle to allow a soldier to function at night with the aid only of “starlight.”

Figure 15.4 shows a 1,000-mm focal length, *f*/8.0 Cassegrain for use with a 35-mm single lens reflex (SLR) camera (visual region, 43-mm diagonal image). Details are given in Table 15.4a. To reduce the diameter of the secondary mirror, it was made the stop.

Although the system as shown has no vignetting, there may be a small amount after one introduces the tubular baffle required around the lenses inside the primary mirror. Long lenses like this are generally focused by moving an internal group of lenses inside the lens barrel. Table 15.4b lists this focus movement.

Figure 15.5 shows a Cassegrain telescope objective with a 50-in. focal length. It is *f*/14 with a 2° FOV; details are given in Table 15.5. This is a modification of a very

**TABLE 15.5**  
**A 50-in. Focal Length Telescope Objective**

Surface	Radius	Thickness	Material	Diameter
1	−23.0755 <sup>a</sup>	0.6000	Silica	5.060
2	−22.8578	11.0000		5.140
3	−36.1813	−11.0000	Mirror	4.740
4	−22.8578	−0.6000	Silica	5.140
5	−23.0755 <sup>a</sup>	0.6000	Mirror	1.298 Stop
6	−22.8578	10.5000		5.140
7	3.3580	0.2000	N-BK7	1.460
8	2.1424	0.1968		1.360
9	−3.3739	0.2000	SF1	1.360
10	−3.0195	4.3068		1.460

Distance from the first lens surface to image = 16.0004, distortion is 1.5%.

<sup>a</sup> This is an aspheric surface with the following relationship:  $X = \frac{0.0433361Y^2}{1 + \sqrt{1 + 0.0537045Y^2}} - 0.000302Y^4 + 5.39681 \times 10^{-6}Y^6$ . This represents a surface with a deviation from a hyperbola.

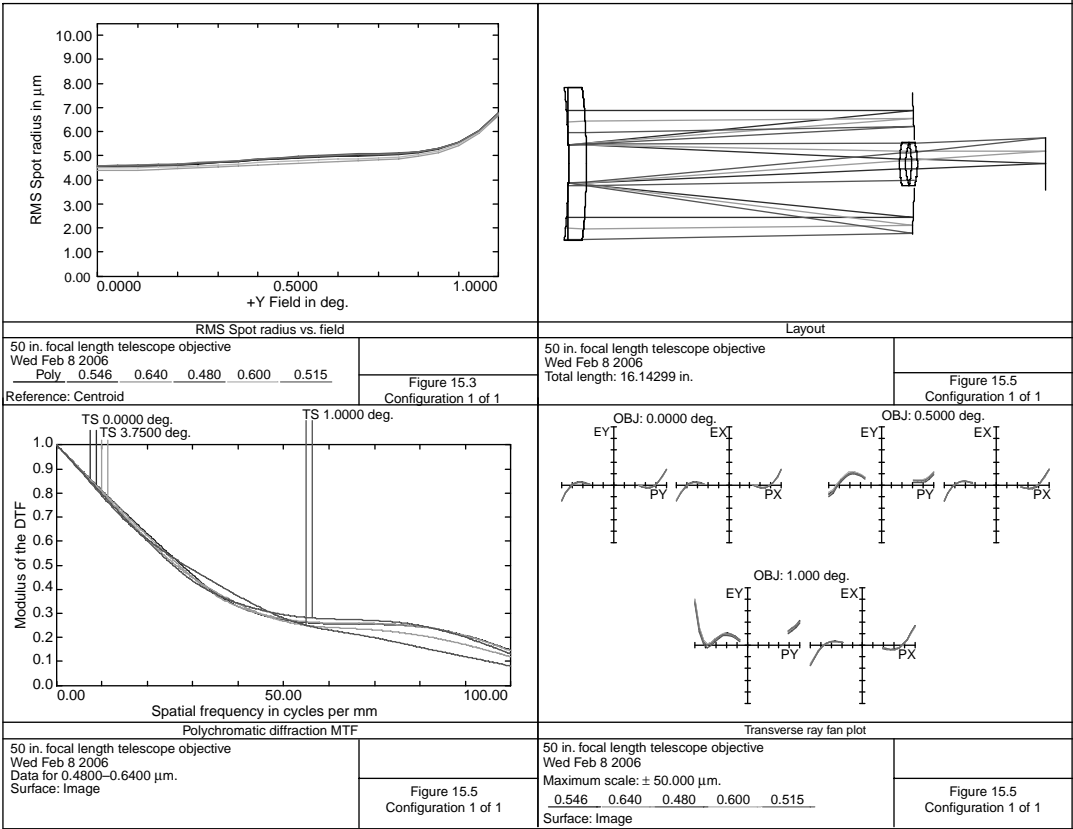


FIGURE 15.5 A 50-in. focal length telescope objective.

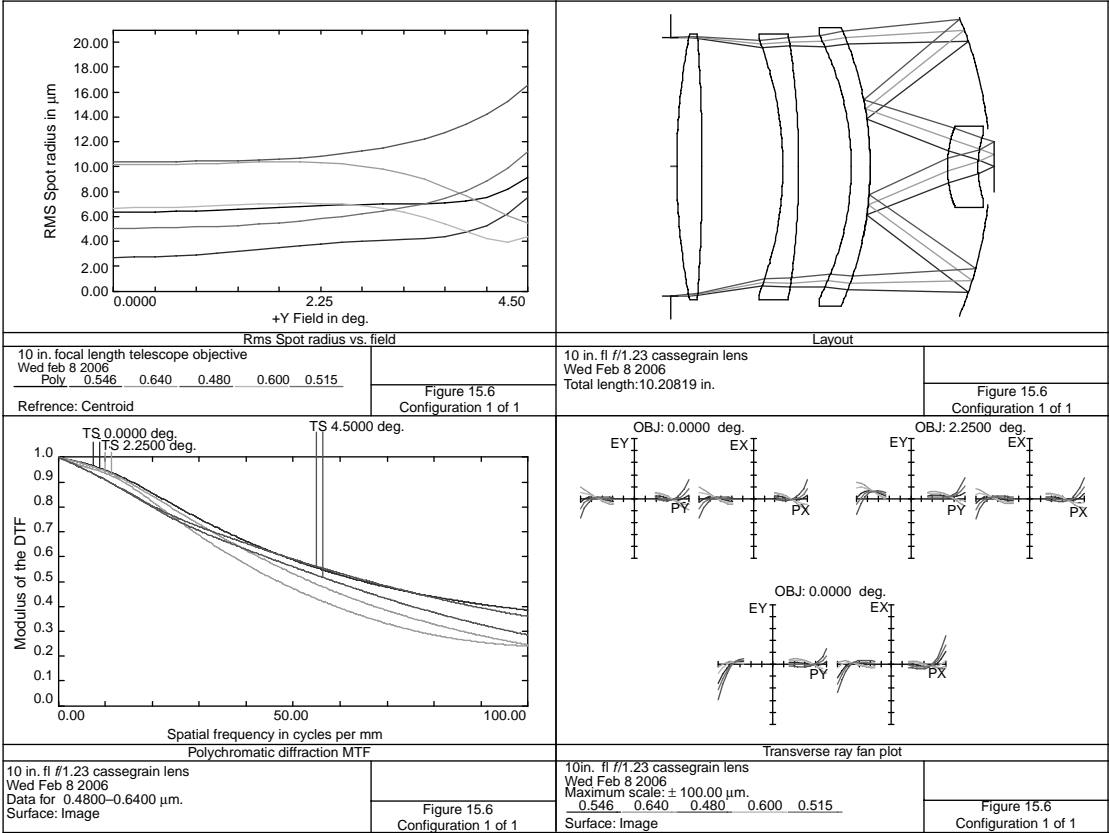


FIGURE 15.6 A 10-in. *f*/1.23 Cassegrain.



**TABLE 15.6**  
**A 10-in. Focal Length  $f/1.23$  Cassegrain**

Surface	Radius	Thickness	Material	Diameter
1	Stop	0.2000		8.129
2	21.8754	0.8000	N-BK7	8.400
3	−58.9582	2.5484		8.400
4	−11.2271	0.5000	N-BK7	8.100
5	−26.6751	1.6572		8.400
6	−9.0986	0.6000	N-BK7	8.360
7	−11.0594	3.7677		8.800
8	−12.0050	−3.7677	Mirror	9.420
9	−11.0594	2.4363	Mirror	4.334
10	3.5312	0.9663	N-BK7	2.540
11	3.2929	0.5000		2.000
12	0.0000	0.0000		1.569

Distance from first lens surface to image = 10.208, distortion < 0.41%.

popular commercially available telescope objective for SLR photography and amateur astronomy.

Figure 15.6 shows a 10-in. focal length,  $f/1.23$  Cassegrain. The prescription is given in Table 15.6. It was designed for a 40-mm diameter image ( $\text{FOV} = 9.0^\circ$ ). The design is remarkable in that only one material is used; it nevertheless has negligible chromatic aberration. Although designed for the visual region, it is useable over an extended wavelength region (Shenker 1966).

Baffling may be accomplished with a cone surrounding the rear lens and a short lens hood. Although the distortion is less than 0.41%, the central obscuration is unfortunately large.

In 1930, Bernard Schmidt completed his famous camera. At the center of curvature of a spherical mirror, he placed an aspheric plate with the flat side facing the mirror. It was a concentric system with the image being formed halfway between the corrector and the mirror. The image surface was spherical and of radius equal to the focal length.

Schmidt manufactured his corrector plate by calculating the elastic deformation of a plate held by a ring of known diameter. Using a vacuum pump, he then deformed this plate the proper amount, ground one surface flat, and then released the vacuum, allowing the plate to assume its proper aspheric shape. Palomar Observatory has two Schmidt cameras, one with an 18-in. and the other with a 48-in. aperture. These are used to map the entire night sky of the northern hemisphere.

Figure 15.7 shows a Schmidt objective. It is  $f/1.8$  and covers a field of  $7^\circ$ . Focal length is 10. Details are given in Table 15.7.

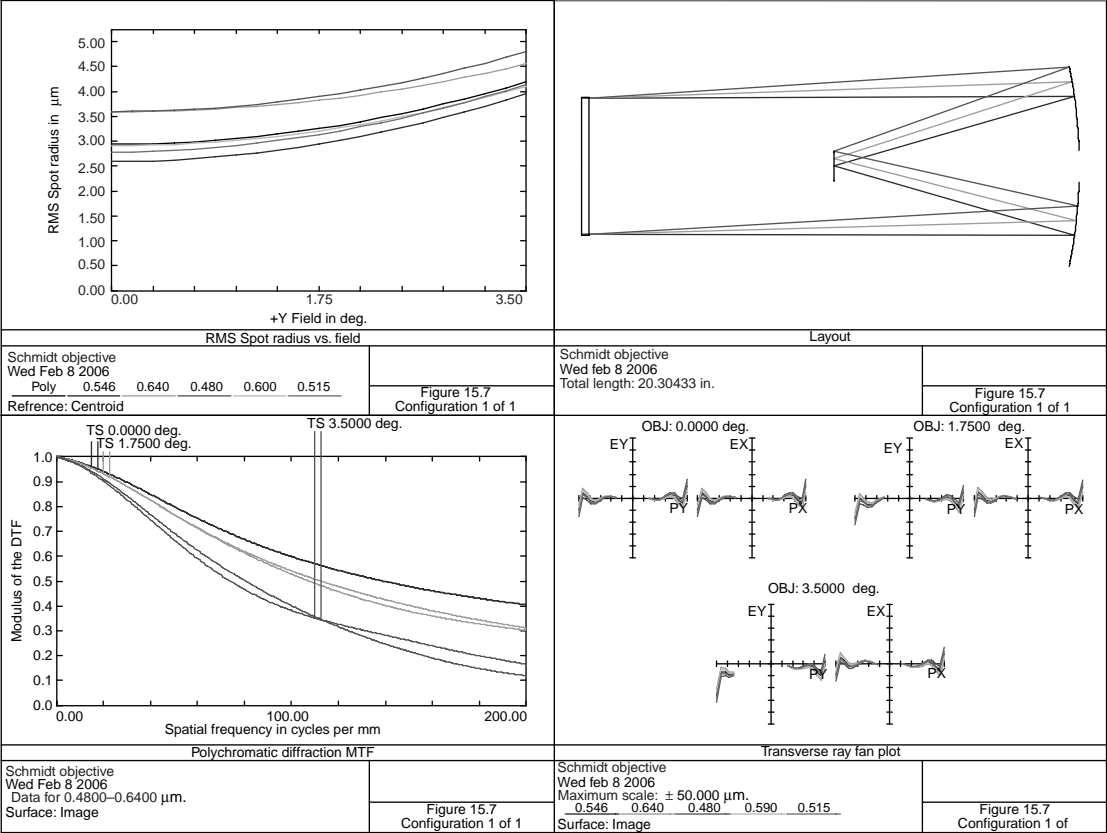


FIGURE 15.7 Schmidt objective.

---

**TABLE 15.7**  
**Schmidt Objective**

Surface	Radius	Thickness	Material	Diameter
1	0.0000	0.3000	Silica	5.660
2	Stop	20.0000		5.556
3	−20.0000	−9.9980	Mirror	8.141
4	−9.8289	0.0000		1.222

---

Because the aspheric surface (surface 2) is plane, there is no conic term. The equation for this surface is

$$X = -4.406904 \times 10^{-5} Y^4 - 9.213268 \times 10^{-6} Y^6 + 1.335688 \times 10^{-6} Y^8 \\ - 6.879200 \times 10^{-8} Y^{10}.$$

The disadvantage of this system is the inconvenient position of the image inside the objective as well as its curvature. Its advantage lies in simplicity of construction and its ability to give excellent resolution over a large wavelength region and field of view. A Cassegrain version has been proposed (Baker 1940). This requires an aspheric primary mirror with a spherical secondary. Radii are the same, and therefore a zero Petzval sum with a flat field is obtained. However, the author's experience with this modification has been disappointing. I found it far better to use one of the all-spherical systems as given above.

All of the above systems (with perhaps the exception of the Schmidt system) are telephoto lenses. That is, the overall length of the lens is much less than the effective focal length. They also have relatively short (as a fraction of their focal length) back

---

**TABLE 15.8**  
**Reflecting Objective,  $f/2.5$** 

Surface	Radius	Thickness	Material	Diameter
1	0.0000	1.7946		1.018
2	2.1332	−1.7946	Mirror	0.802 Stop
3	3.6328	1.7946	Mirror	2.360
4	2.1332	0.3523	N-K5	1.600
5	1.5664	0.4190		1.380
6	0.0000	0.1993	SF4	1.360
7	−23.5725	2.4867		1.360
8	0.0000	0.0000		0.201

---

Distance from the first surface to image = 5.252, distortion = 0.11%.

---

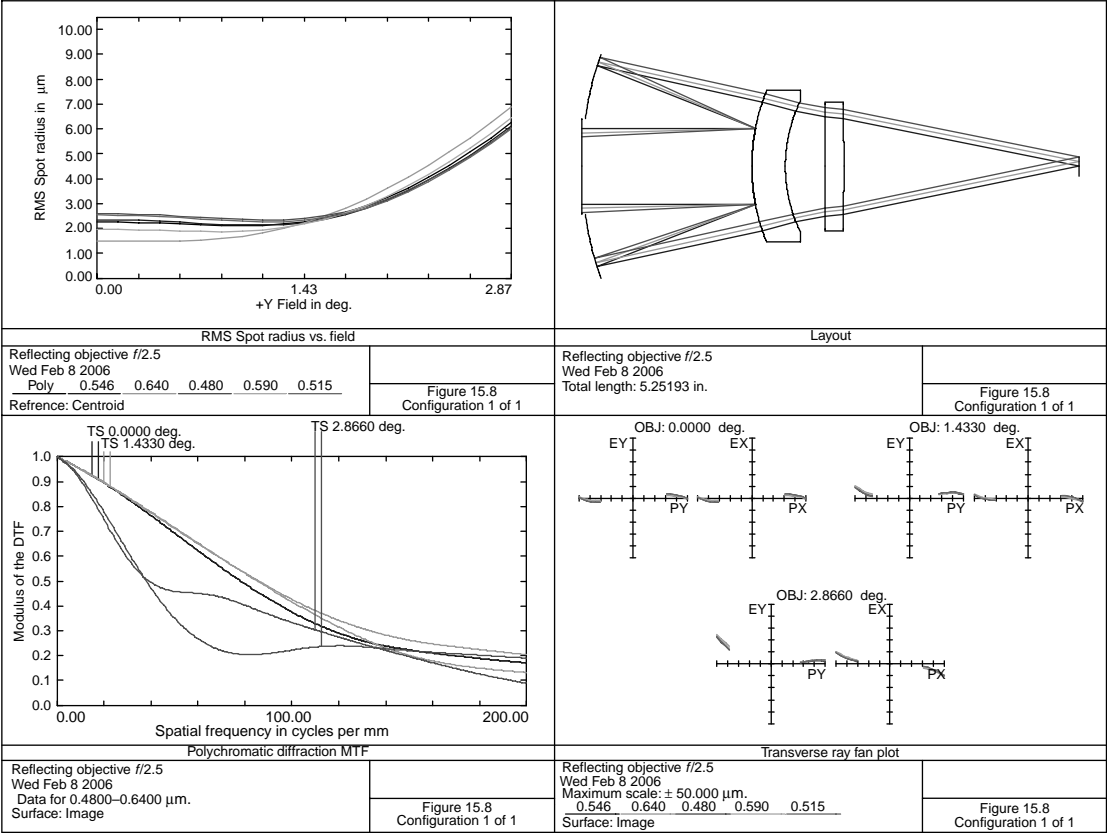


FIGURE 15.8 Reflecting objective.

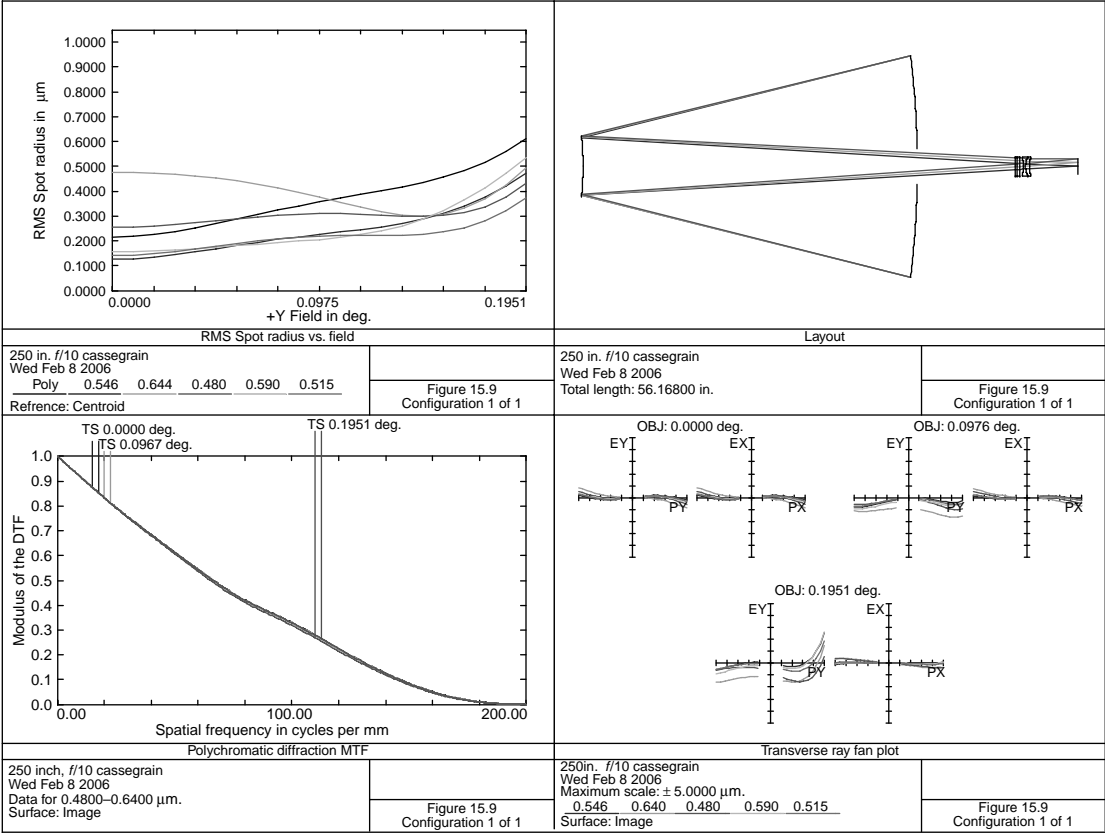


FIGURE 15.9 A 250-in.,  $f/10$  Cassegrain.

focal lengths. By reversing the role of primary and secondary mirrors, one may obtain an inverted telephoto type of design. Here, the overall length will be substantially longer than the effective focal length and the back focal length will be longer than the effective focal length. This is a useful system for lenses of relatively short focal length, where a long working distance is required. Such an inverted telephoto type of design is shown in [Figure 15.8](#). It is  $f/2.5$  and has an image of 0.2 diameter. Details are provided in [Table 15.8](#).

The computer program must have the ability to bound the ray heights at the mirror surfaces. Because there is a hole in the large mirror (surface 2), the first mirror surface must have sufficient curvature to cause the outer rim rays to strike the large mirror outside of this hole. This lens would make an ideal long working distance microscope objective (see [Chapter 11](#)). Surface 1 is a central obscuration to block all rays with a height of less than 0.1.

In [Figure 15.9](#) is shown a long effective focal length (250 in.)  $f/10$  objective; details are given in [Table 15.9](#). Image size is 1.703, so it is suitable for a 35-mm SLR camera. Both mirrors are hyperbolas, so this may be considered as a modified Ritchey–Chretien design (Rutten 1988). The lens data is given in [Table 15.9](#).

It should be noted here that the usual Cassegrain telescope has a paraboloid primary mirror and a hyperboloid secondary. The Dall–Kirkham telescope has a prolate ellipsoid primary mirror and a spherical secondary. The Ritchey–Chretien telescope has a hyperboloid primary mirror and a hyperboloid secondary (Schroeder 2000).

Considerable baffling will be required in this system, as well as a spider mechanism to hold the secondary mirror in place. Diffraction effects for this mechanism are not considered in the MTF plot.

To illustrate the importance of the two cemented doublets in the rear, in [Figure 15.10](#) is shown a Ritchey–Chretien design with the same focal length,

---

**TABLE 15.9**  
**A 250-in. Cassegrain Objective**

Surface	Radius	Thickness	Material	Diameter
1	−102.3640	−37.8137	Mirror	25.060 Stop
2	−35.3325	48.8327	Mirror	6.910
3	23.5556	0.2500	N-SK16	2.140
4	97.0299	0.3600	LF5	2.140
5	−8.4651	0.3492	2.140	
6	−6.0339	0.2500	N-LLF1	1.980
7	2.3002	0.5000	LF5	2.140
8	8.5504	5.4581	1.900	
9	0.0000	0.0000	1.705	

Distance from secondary mirror to image = 56.000 in., conic coefficient,  
Surface 1 = −1.075613, conic coefficient, surface 2 = −3.376732.

---

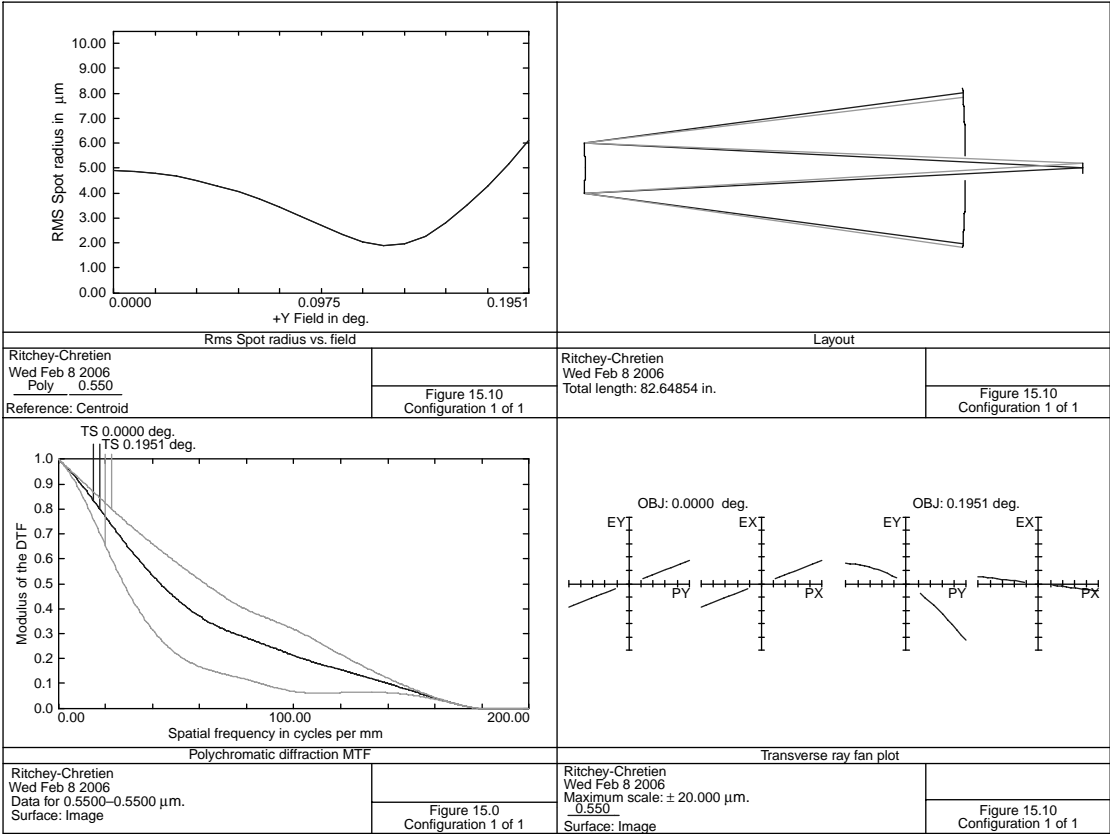


FIGURE 15.10 The Ritchey–Chretien system.

**TABLE 15.10**  
**Ritchey–Chretien Design**

Surface	Radius	Thickness	Material	Diameter
1	−188.3465	−63.0701	Mirror	26.400
2	−99.8005	82.5633	Mirror	8.260 Stop
3	0.0000	0.0000	1.703	

Conic surface coefficient 1 = −1.159739, conic surface coefficient 2 = −6.877339.

f-number and field of view as the above design. However, it consists of only two hyperbolic mirrors (Rutten 1988). The details of this design are given in Table 15.10.

Note that the design in Figure 15.9 has less obscuration by the secondary mirror. The two doublets in the rear help to correct the off-axis aberrations: coma, astigmatism, and field curvature. Another example of a Ritchey–Chretien system is the Hubble Space Telescope (Jones 1979; Smith 1989). This has a 2.4-m diameter primary mirror, an effective focal length of 57.6 m, is  $f/24$ , and has a field of view of  $0.3^\circ$ . Note that this has an inward curving field and is analyzed on this curved surface. It was launched on April 24, 1990. It circles the Earth every 97 min at an altitude of 600 km. This is shown in Figure 15.11. The prescription is given in Table 15.11.

It is often desired to use mirrors in an unobscured mode. To achieve this, the object and image must be either tilted or displaced from each other. In Figure 15.12, two concentric spherical mirrors are used to image a point source (perhaps a fiber). The prescription for this mirror is given in Table 15.12. The object is displaced upward by 3.0 from the optical axis and so the image is located 3.0 below the optical axis. It forms an  $f/4.0$  diffraction limited beam (Offner 1973; Korsch 1991).

Another method is the use of tilted mirrors. Rogers (2002) provides several examples of unobscured mirror systems and compares them with the conventional

**TABLE 15.11**  
**Hubble Space Telescope**

Surface	Radius	Thickness	Material	Diameter
0	0.0000	0.100000E+11		0.00
1	0.0000	193.3071		95.487
2	−434.6457	−193.3071	Mirror	94.488 Stop
3	−53.1224	250.5983	Mirror	11.479
4	−25.0150	0.0000		11.849

Conic surface coefficient 2 = −1.001152, conic surface coefficient 3 = −1.483014.



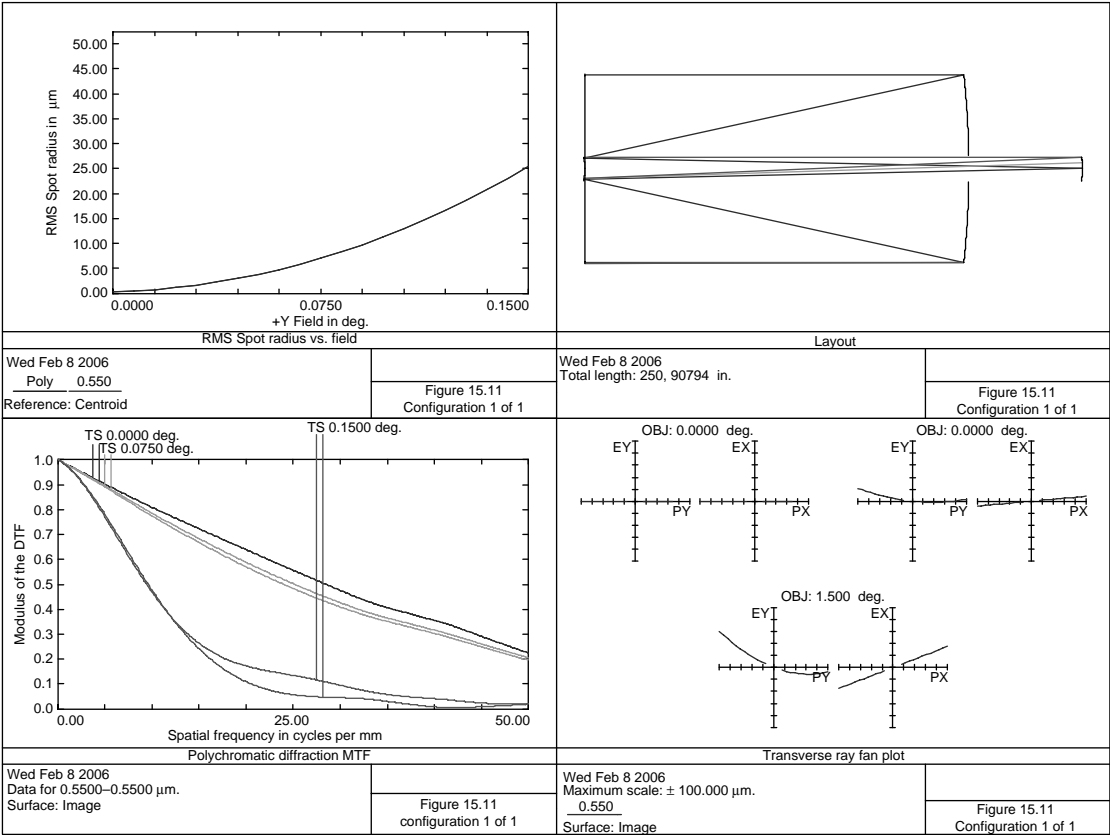


FIGURE 15.11 The Hubble Space Telescope.

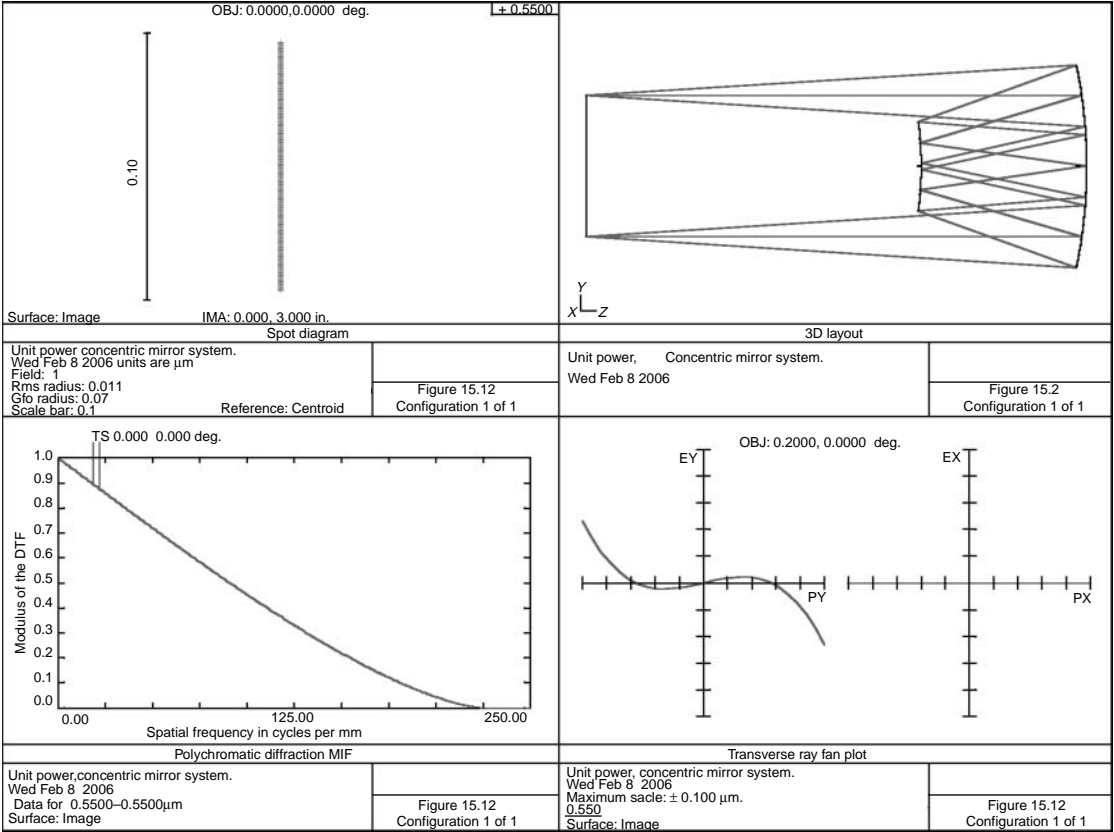


FIGURE 15.12 Unit power concentric mirrors.

**TABLE 15.12**  
**Unit Power Concentric Mirror**

Surface	Radius	Thickness	Material	Diameter
0	0.0000	21.2256	0.000	
1	0.0000	0.0000	0.000	
2	−21.2256	−7.0157	Mirror	8.598
3	−14.2099	7.0157	Mirror	3.774
4	−21.2256	−7.0157	Mirror	2.648 Stop
5	−14.2099	7.0157	Mirror	3.774
6	−21.2256	−21.2256	Mirror	8.598

refractive system. Howard (2002) shows several examples of tilted conic mirrors. This is demonstrated in the following figure. The first mirror is a torroid, the purpose of which is to remove the astigmatism due to the tilted mirrors. Coma is now the dominant aberration as indicated in the spot diagram for configuration 1. In configuration 2, the beam is tilted downward, which nearly eliminates the coma as shown in [Figure 15.13](#). Both configurations are identical except for the tilt of the second mirror:  $10^\circ$  up for configuration 1 and  $10^\circ$  down for configuration 2. Effective focal length is 10.0 and the  $f$ -number is  $f/4$ . Details are provided in Table 15.13.

The above is for configuration 1 that has an RMS spot size of  $112.6\ \mu\text{m}$ . In configuration 2 that has an RMS spot size of  $10.3\ \mu\text{m}$ , all the tilt angles are positive and the  $Y$  displacement of the image is  $-1.07257$ . The reason for this large reduction in coma for this second case is due to the fact that although the image height for both systems after reflecting from the first mirror is positive, after reflection from the second mirror the image height is positive for the first case and negative for the second case.

Referring to the expression for the coma contribution for a thin lens passed centrally by the oblique pencils as given in Conrady (1957):

**TABLE 15.13**  
**Tilted Mirrors**

Surface	Radius	Thickness	Material	Diameter
1	Stop	0.0000		2.500
2	0.0000	0.0000		0.000 $10^\circ$ tilt
3	−32.7249	0.0000	Mirror	2.547 $R_y = -31.36735$
4	0.0000	−6.1767		0.000 $10^\circ$ tilt
5	0.0000	0.0000		0.000 $-10^\circ$ tilt
6	32.0183	6.1767	Mirror	1.573
7	0.0000	0.0000		0.000 $-10^\circ$ tilt
8	0.0000	0.0		$Y\text{ Disp.} = 1.07257$

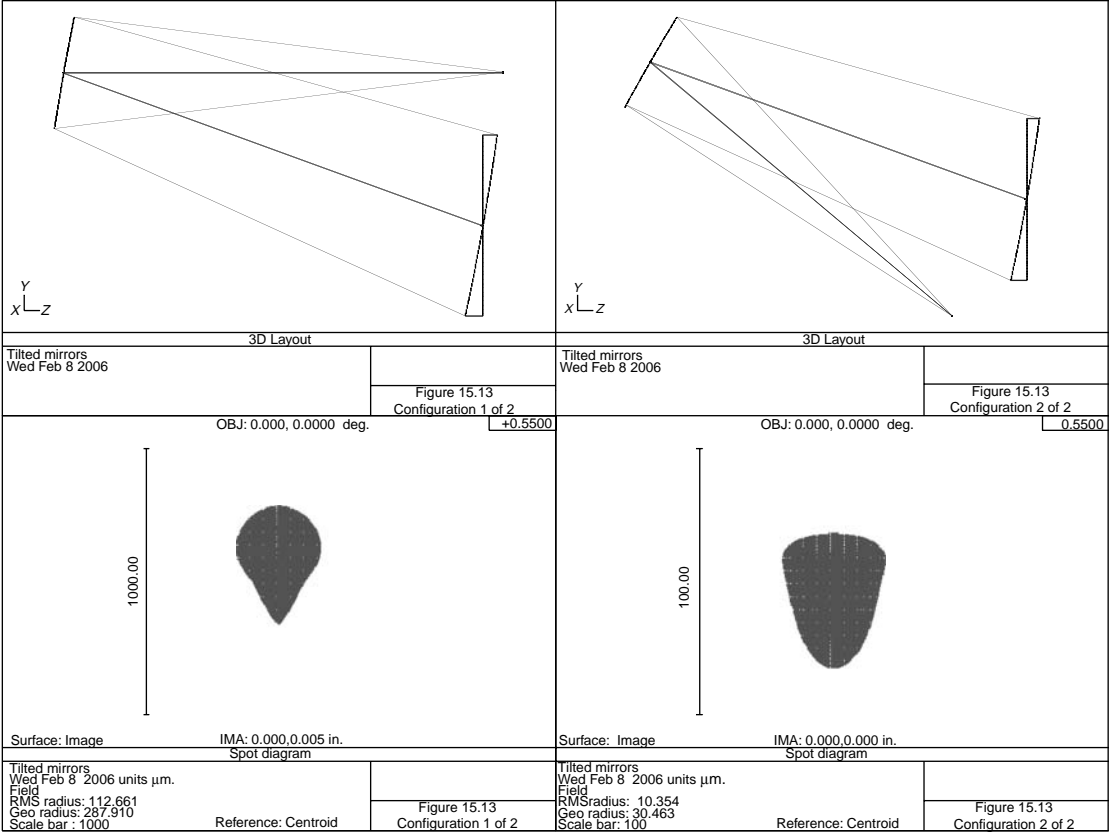


FIGURE 15.13 Tilted mirrors.

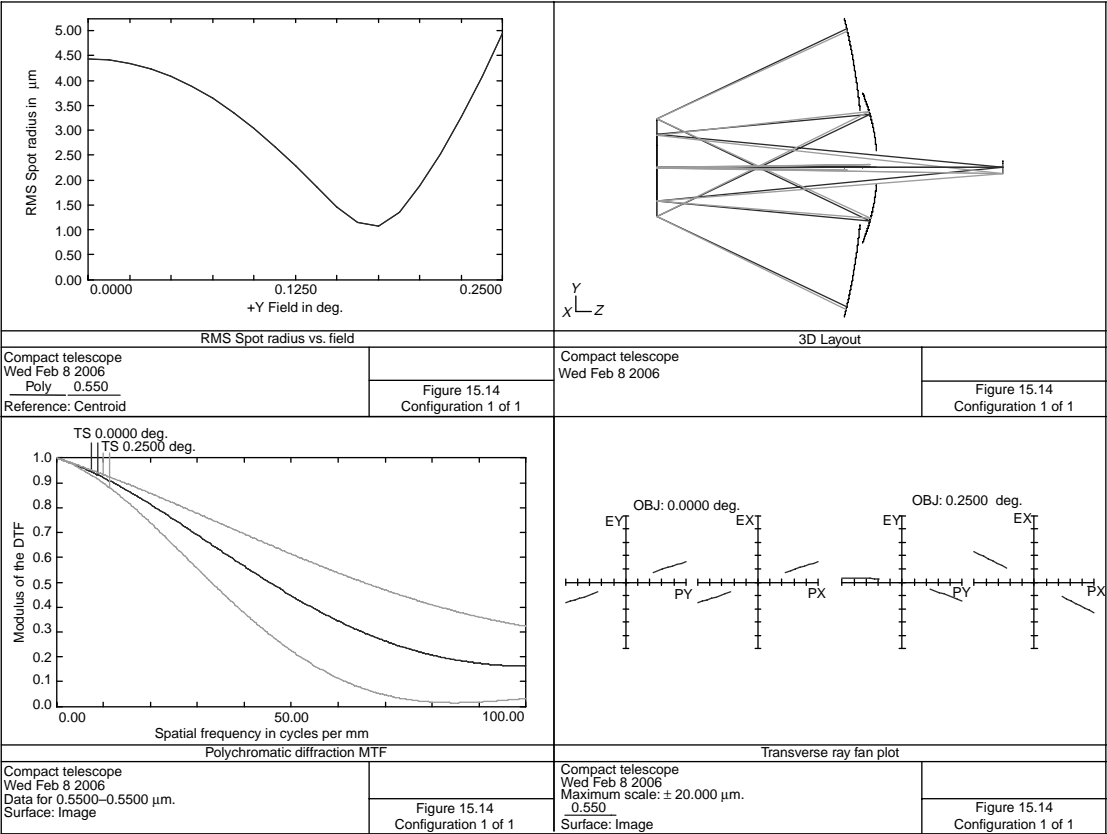


FIGURE 15.14 Compact telescope.

**TABLE 15.14**  
**Compact Telescope**

Surface <sup>a</sup>	Radius	Thickness	Material	Diameter	Conic
0	0.0000	0.100000E+11		0.00	
1	−16.4794	−5.5119	Mirror	7.619	−0.9774823
2	Stop	5.9056		2.607	
3	−5.2556	−5.9056	Mirror	3.014	−0.4605796
4	0.0000	9.2807	Mirror	1.803	
5	0.0000	0.0000		0.344	

<sup>a</sup> Surfaces 1 and 3 are ellipses.

$$CC' = H'_k SA^2 [0.25G_5(C)(C_1) - G_7C(v_1) - G_8C^2],$$

where SA is the spherical aberration contribution of the mirror and noting that the refractive index after reflection from a mirror is  $-1.0$ , thereby making  $G_5=0$  and  $G_8=1.0$ , the coma contributions become proportional to the image heights ( $H'_k$ ) for each mirror. Therefore, in the first case, the coma contributions of the mirrors are additive, whereas in the second case one subtracts from the other.

With regards to systems with tilted or decentered surfaces, it is important to realize that there are essentially two methods of specifying the system: local coordinates and global.

*Local.* In this method, the optical axis is tilted or displaced as required and all subsequent surfaces are now referenced to this new axis. Some programs utilize a dummy surface for this tilt and displacement. This surface does no refraction but instead displaces and tilts the ray and path-length values at the surface. It has the advantage of being generally easier to input the data because optics are generally centered with respect to the new tilted or displaced axis. Bounds are required to limit surface values in the global sense—generally in respect to the original axis.

*Global.* Here, all surface data is referenced to a common optical axis. When lenses are tilted or displaced, the designer must calculate the surface location in respect to the original optical axis to correctly input the system.

In Figure 15.14 is shown a novel version of a Gregorian telescope objective; details are given in Table 15.14. As with all Gregorian systems, it has an intermediate image and a concave secondary mirror, but the path is folded by means of a flat mirror. It is an all-mirror system with an excellent image but a small field of view of  $0.5^\circ$ . This prescription is the same as that given in the patent (Draganov 2004) except for scaling to 1000-mm focal length and a minor adjustment of the conic coefficients and back focal length. The system is  $f/5.0$ .

In Figure 15.15 is shown an all-reflective and unobscured system; details are given in Table 15.15. Focal length is 1.972 with  $f/3.0$  and covers field angles of  $40\text{--}55^\circ$  off-axis. Note that the large mirror (surfaces 3 and 5) is a hyperboloid. This is

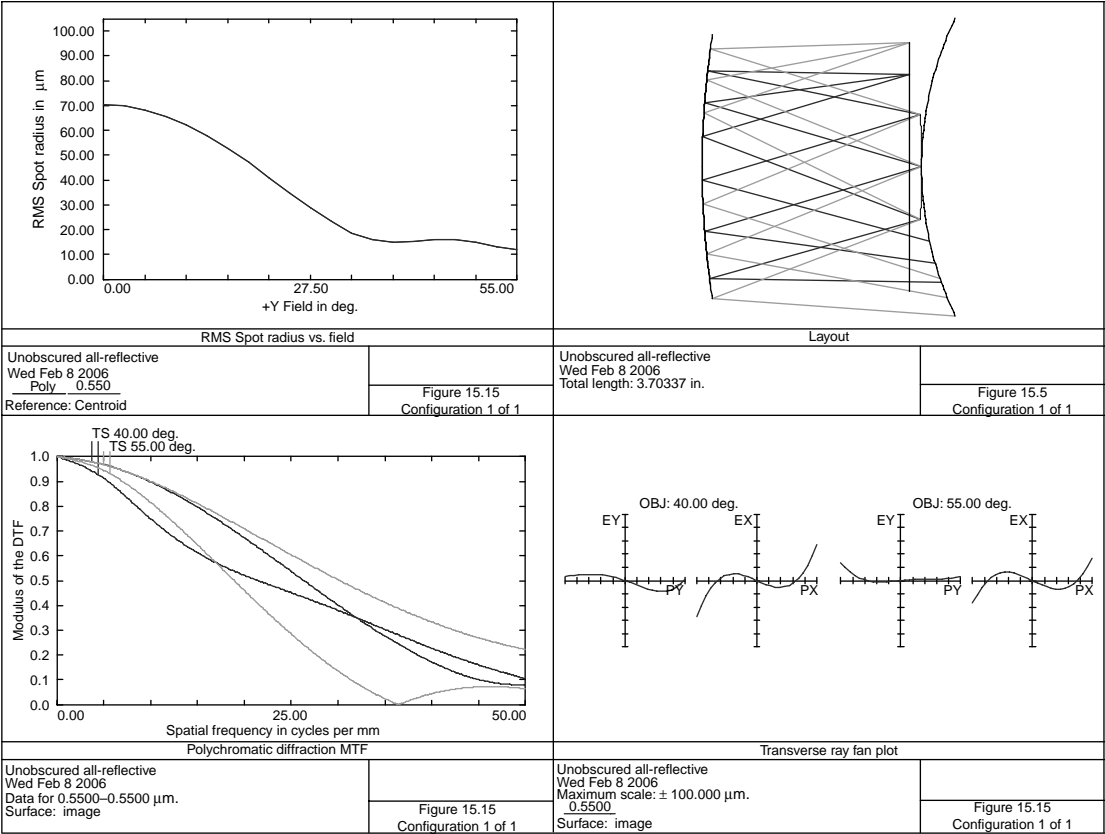


FIGURE 15.15 Unobscured, all-reflective lens.

**TABLE 15.15**  
**Unobscured All-Reflective System**

Surface	Radius	Thickness	Material	Diameter	Conic
0	0.0000	0.100000E+11			
1	0.0000	3.2101		14.934	
2	5.0566	−3.2101	Mirror	4.357	
3	12.2125	3.2101	Mirror	3.864	−6.317378
4	−16.5863	−3.2101	Mirror	1.542 Stop	
5	12.2125	3.0276	Mirror	3.438	−6.317378
6	0.0000	0.0000		3.631	

further described in Owen (1990). No effort was made to control image height or distortion.

## REFERENCES

- Abel, I. R. (1983) Compact optical system, US Patent #4411499.
- Amon, M. (1973) Large catadioptric objective, US Patent #3711184.
- Amon, M., Rosen, S., and Jackson, B. (1971) Large objective for night vision, *Applied Optics*, 10: 490.
- Baker, J. G. (1940) A family of flat field cameras, equivalent in performance to the Schmidt camera, *Proc. Amer. Phil. Soc.*, 82: 339.
- Barnes, W. J. (1979) Optical materials—Reflective, In *Applied Optics and Optical Engineering*, Shannon, R. S. and Wyant, J. eds., Vol. 7, Academic Press, New York.
- Blakley, R. (1995) Modification of the classic Schmidt telescope, *Optical Engineering*, 34: 1471.
- Blakley, R. (1996) Cesarian telescope optical system, *Optical Engineering*, 35: 3338.
- Bouwers, A. (1950) *Achievements in Optics*, Elsevier Publishing, New York.
- Bowen, I. S. (1960) Schmidt cameras, In *Telescopes*, Kuiper, G. P. and Middlehurst, B. M., eds., University of Chicago Press, Chicago.
- Bruggemann, H. P. (1968) *Conic Mirrors*, Focal Press, New York.
- Conrady, A. E. (1957) *Applied Optics and Optical Design*, Dover, New York.
- Draganov, V. (2004) Compact telescope, US Patent #6667831.
- Hodges, P. C. (1953) Bernard Schmidt and his reflector camera, *Amateur Telescope Making*, 3: 365.
- Howard, J. M. and Stone B. D. (2002) Nonanamorphic imaging with three conic mirrors, International Optical Design Conference, 2002, SPIE, 4832: 25.
- Jones, O. J. (1979) Space telescope optics, *Optical Engineering*, 18: 273.
- Korsch, D. (1991) *Reflective Optics*, Academic Press, New York.
- Kuiper, G. P. and Middlehurst, B. M. (1960) *Telescopes*, University of Chicago Press, Chicago.
- Lucy, F. A. (1941) Exact and approximate computation of Schmidt cameras, *JOSA*, 31: 358.
- Lurie, R. (1975) Anastigmatic catadioptric telescope, *JOSA*, 65: 261.
- Mahajan, V. N. (1977) Imaging with obscured pupils, *Optics Letters*, 1: 128.



- Maksutov, D. D. (1944) New catadioptric meniscus system, *JOSA*, 34: 270.
- Maxwell, J. (1971) *Catadioptric Imaging Systems*, American Elsevier Publishing, New York.
- Owen, R. C. (1990) International optical design conference, 1990, SPIE, 1354: 430.
- Offner, A. (1973) Unit power imaging catoptric anastigmat, US patent #3748015.
- Powell, J. (1988) Design of a 300 mm focal length f/3.6 spectrographic objective, *Optical Engineering*, 27: 1042.
- Puryayev, D. T. and Gontcharov, A. V. (1998) Aplanatic four-mirror system for optical telescopes, *Optical Engineering*, 37: 2334.
- Rayces, J. L. (1975) All spherical solid catadioptric system, US Patent #3926505.
- Rogers, J. M. (2002) Unobscured mirror designs, International Optical Design Conference, 2002, SPIE, 4832: 33.
- Rutten, H. and van Venrooij, M. (1988) *Telescope Optics*, Willmann-Bell, Richmond, VA.
- Shimizu, Y. (1972) Catadioptric telephoto objective lens, US Patent #3632190.
- Shenker, M. (1966) High speed catadioptric objective, US Patent #3252373.
- Schroeder, D. J. (2000) *Astronomical Optics*, Academic Press, New York.
- Smith, R. W. (1989) *The Space Telescope*, Cambridge University Press, New York.
- Song, N., Yin, Z., and Hu, F. (2002) Baffles design for an axial two-mirror telescope, *Optical Engineering*, 41: 2353.
- Stephens, R. E. (1948) Reduction of sphero-chromatic aberration in catadioptric systems, *Journal of Research of the National Bureau of Standards*, 40: 467.



---

# 16 Periscope Systems

The periscope systems discussed here are not of the long submarine type; they are instead an extended optical system used in special-effects cinematography. Such an elongated lens system allows the cinematographer to get his very bulky camera into an otherwise inaccessible place. Some cinematographers have erroneously concluded that the depth of field is greater than that obtained from the usual depth-of-field tables given in cinematography manuals (Samuelson 1998). One reason for the apparent discrepancy is that these depth-of-field tables are measured from the lens front principal plane (a nodal point). For periscope systems, this principal plane is usually well within the body of the periscope, giving an apparently short near-depth-of-focus distance. Another reason is that these systems generally have many lens surfaces and a large distance between lens groups. Even with modern high-efficiency antireflection coatings and threads and sand-blasted finishes on the interior walls, there is still substantial veiling glare in the final image. This results in a loss of contrast that gives the appearance of enhanced depth of field.

Such a device is shown in [Figure 16.1](#) and detailed in [Table 16.1a](#). A mirror is placed at the front external entrance pupil. This allows the cinematographer to scan the field in a vertical direction. (This assumes that the periscope tube is vertical and that the axis of the front mirror is horizontal.) Behind the relay is a penta-roof prism that deviates the beam 90° and yields an image of the correct orientation on the film. This replaces the normal camera lens. Lens effective focal length is 1.0 and yet the length from entrance pupil to image is 36.151. See [Figure 35.12](#) for a zoom version of this type of periscope.

The lens  $f$ -number is 4.5. Lens transmittance (considering the aluminized front mirror and the silvered surfaces on the penta-roof prism) is 0.658. Unfortunately, the glasses N-LAF34 and N-FK51 are expensive materials, but these are needed for color correction due to the prism block.

$$T^{\#} = \frac{f^{\#}}{\sqrt{\text{transmittance}}} = 5.6.$$

The rear group of lenses (surface 14.27) moves forward to focus from distant objects to less than 2 in. in front of the front mirror. This mirror is located at the entrance pupil that is 1.162 in. in front of the first lens surface. This type of internal focusing is required when one realizes the large sizes of the periscope and camera. It would be difficult, mechanically, to move the periscope in relation to the camera. It is far simpler to move a lens group inside the periscope housing. This allows the periscope to be rigidly attached to the camera ([Table 16.1b](#)).

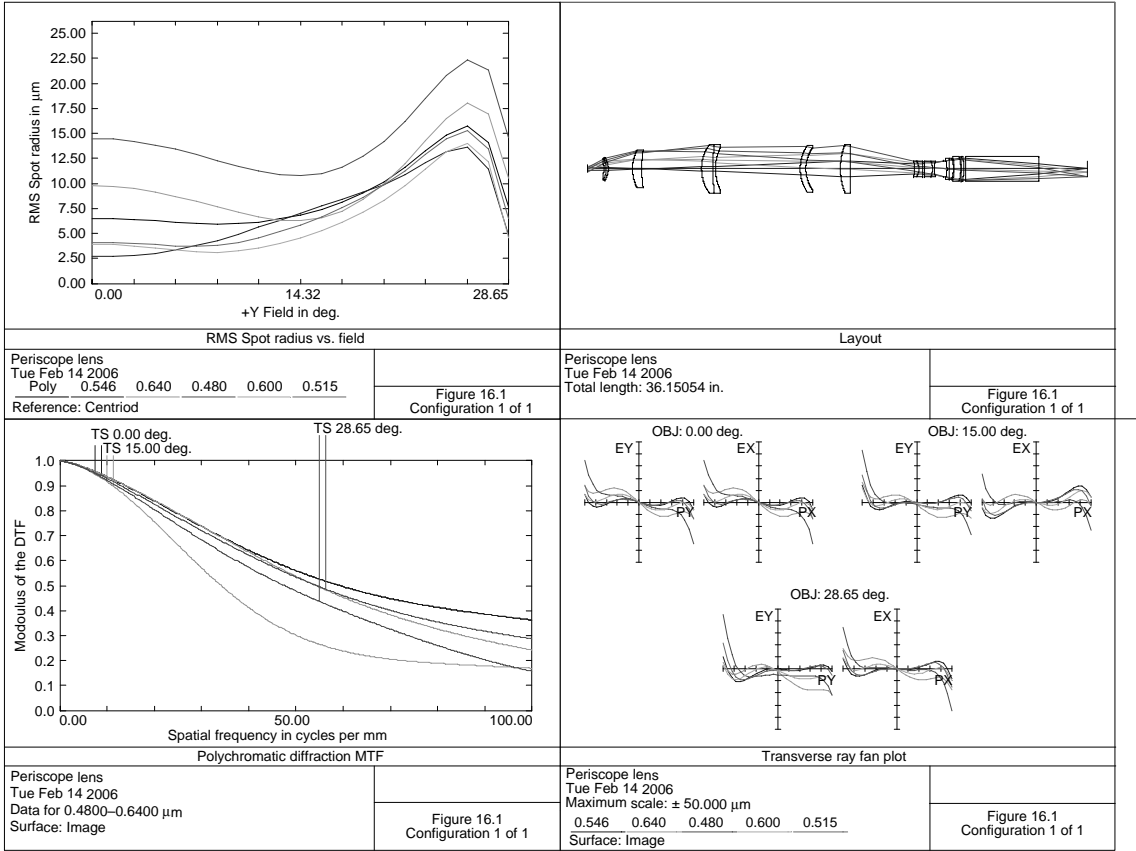


FIGURE 16.1 A 25-mm focal length periscope.

**TABLE 16.1a**  
**A 25-mm Focal Length Periscope**

Surface	Radius	Thickness	Material	Diameter
1	0.0000	1.1621		0.537 Entrance pupil
2	−3.8155	0.1777	N-LAK9	1.480
3	−1.7942	0.1524	N-LAF2	1.540
4	−1.4536	1.7515		1.640
5	3.0089	0.6650	N-LAK7	2.680
6	8.7785	4.3233		2.600
7	2.9643	0.8370	N-SK4	3.520
8	23.2507	0.1814	SF1	3.520
9	3.6454	6.1202		3.180
10	3.0885	0.4000	N-LAF34	3.360
11	2.6251	2.5001		3.120
12	4.7208	0.7399	LAFN7	3.540
13	−47.6360	4.6346		3.540
14	−1.6427	0.3000	N-FK51	1.140
15	−1.1654	0.2769	LLF1	1.180
16	5.1913	0.1000		1.100
17	4.0210	0.6155	N-LAK22	1.140
18	−1.3050	0.1427	SF5	1.140
19	2.9370	0.6588		1.060
20	Stop	0.2371		1.103
21	−2.1993	0.1472	SF5	1.240
22	8.4918	0.3297	N-LAK22	1.540
23	−2.2226	0.0166		1.540
24	−6.5182	0.5078	N-LAF2	1.560
25	−3.4210	0.0153		1.760
26	13.7066	0.2070	N-LAF3	1.840
27	−4.0663	0.1008		1.840
28	0.0000	5.3000	N-SK16	1.760 Penta roof prism
29	0.0000	3.5500		1.760
30	0.0000	0.0000		1.083

Distortion = 1.0%.

In a previous edition of this book, this design had an intermediate image focused very close to surface 9. This causes any scratches or dust on this surface to be in focus. In this design, the intermediate image lies between surfaces 6 and 7. At this location a field stop could be placed to help reduce stray light.

This design was optimized for infinity and then the focus movement determined. As a consequence, performance is considerably degraded when focused at near objects. Instead, one should optimize at various object distances with maximum weight at an intermediate distance; perhaps 50 in.

**TABLE 16.1b**  
**Periscope Focusing for 25-mm Focal Length Periscope**

Object Distance	$T(27)$	$T(13)$
Infinity	0.1008	4.6346
100.0	0.1151	4.6203
50.0	0.1284	4.6070
25.0	0.1545	4.5809
10.0	0.2301	4.5053

The entire unit is fitted on a rotary mount such as to be able to scan  $360^\circ$  in azimuth. These lenses are generally equipped with motors such that the iris, focus, front mirror, and rotary mount may be remotely controlled.

Figure 16.2 shows a periscope for use with 65-mm wide film. Referring to Appendix A, this film format has a diagonal of 2.101. This periscope has a focal length of 1.480, is  $f/8$  and has an FOV of  $71.4^\circ$ . The prescription is given in Table 16.2a.

The entire rear assembly, with the iris included, moves toward the film for focusing. The following table gives the movements in Table 16.2b.

This periscope differs from the previous in that there is no erecting/folding prism. The system is normally used in a vertical position. A mirror at the entrance pupil deviates the beam  $90^\circ$ . As in the above case, this mirror moves under motor control. Between the iris and the film is another mirror to again deviate the beam  $90^\circ$ . The camera is then oriented “upside down” so that an erect image is obtained on the film.

Note that the iris is actually external to the lens system. This causes considerable aberration of the entrance pupil. That is, the computer program must increase the diameter of the entrance pupil (in the tangential orientation) such that the diameter of the beam at the iris location is the same for the off-axis bundle as the axial. The lens element of N-FK51 glass helps to reduce secondary color.

When computing the focusing movements for these periscopes (or any relay systems) it is important to check magnification changes as the lens is focused. That is, if the relay magnification is reduced during focusing from long conjugate to a close distance, the final image may not fill the film frame. One then has to start with a larger format to allow for this reduction in image size during focus.

Another type of cinematography periscope utilizes an available photographic front objective coupled with a field lens and relay system. (Such systems are commercially available from Century Precision, Panaviaion, Cine Magic, and Roessel.) This has the advantage of excellent image quality, a relatively low  $f$ -number, and, most importantly, the ability to use a wide variety of front objectives. The field lens is chosen to operate over a limited range of exit-pupil locations. Although this excludes some lenses (fisheye) there are still many available that fall within the field lens correction. Its disadvantage is the diameter of the photographic objective prevents the periscope from having its entrance pupil very close to the ground.

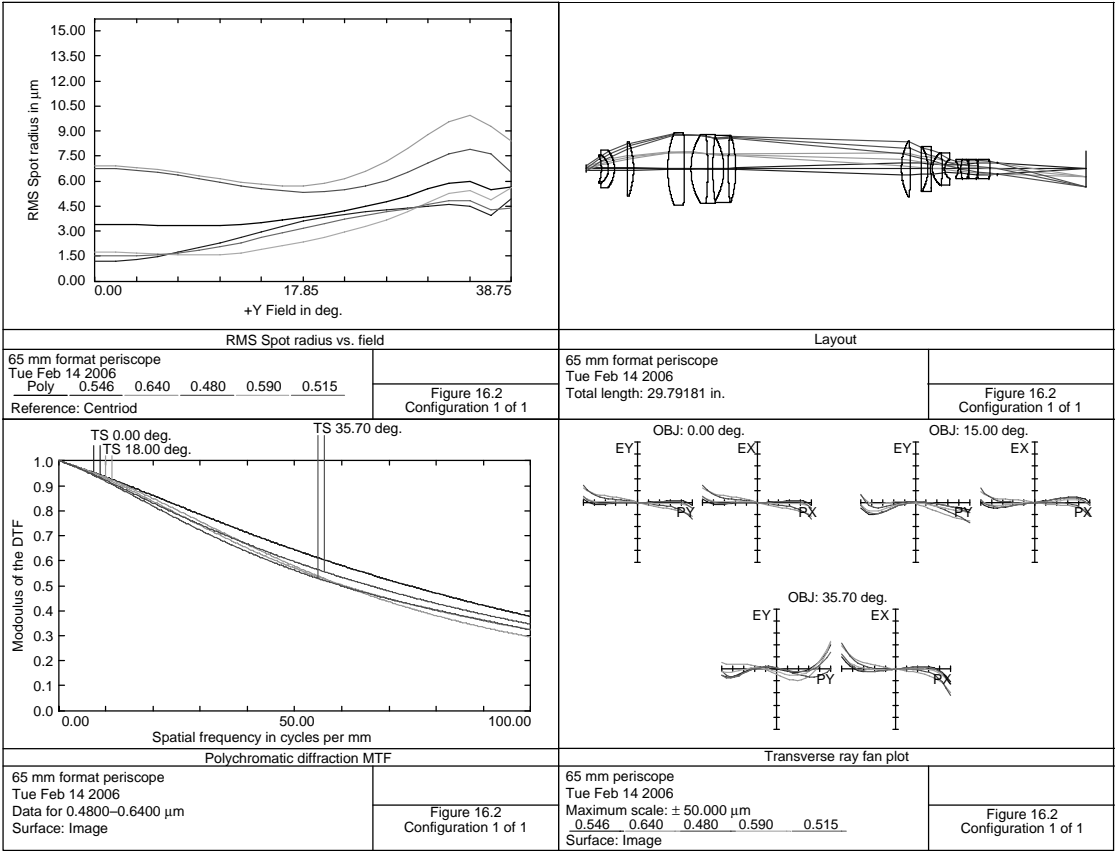


FIGURE 16.2 A 65-mm format periscope.

**TABLE 16.2a**  
**A 65-mm Format Periscope**

Surface	Radius	Thickness	Material	Diameter
1	0.0000	0.9000		0.444 Entrance pupil
2	−2.5413	0.4175	N-LAF3	1.580
3	−1.0119	0.3603	SF1	1.700
4	−1.8235	0.7908		2.200
5	−29.6118	0.3465	N-LAK12	3.080
6	−4.8709	2.0348		3.180
7	6.2988	1.0012	N-LAK12	4.280
8	−44.7760	0.3860		4.280
9	3.9356	1.0011	N-BK7	4.100
10	−20.9124	0.2935	SF1	4.100
11	13.1605	0.6668		3.760
12	−3.7687	0.2617	N-SK4	3.760
13	20.1688	0.4529	SF1	3.980
14	−7.0713	9.8661		3.980
15	3.7174	0.5447	SF5	3.340
16	−17.2857	0.6285		3.340
17	361.2484	0.4070	N-FK51	2.660
18	−2.6962	0.1705	N-ZK7	2.660
19	15.1835	0.0933		2.280
20	1.2340	0.5698	N-LAK22	1.940
21	−24.4095	0.1537	SF5	1.940
22	0.7068	0.8239		1.180
23	−0.8258	0.1545	SF5	0.960
24	2.0745	0.4779	N-LAK22	1.140
25	−1.1643	0.0192		1.140
26	−2.4526	0.5135	N-LAF2	1.080
27	−1.9328	0.0292		1.140
28	−6.0046	0.7011	N-LAF3	1.060
29	−2.7163	0.4280		1.140
30	Stop	5.2979		0.662

Distance from entrance pupil to image = 29.792.



---

**TABLE 16.2b**  
**Periscope Focusing (for 65-mm-Wide Film)**

Object Distance	<i>T</i> (14)	<i>T</i> (30)
Infinity	9.866	5.298
100.0	9.831	5.334
50.0	9.794	5.370
25.0	9.719	5.445
10.0	9.469	5.695

Distortion = 1.3%.

---

## REFERENCES

- Frazier, J. A. (1998) Wide angle, deep field, close focusing optical system, US Patent #5727236.
- Hajnal, S. (1980) Snorkel camera system, US Patent #4195922.
- Hajnal, S. (1986) Snorkel system, US Patent #4375913.
- Hajnal, S. (1986) Rotatable snorkel system, US Patent #4580886.
- Hopp, G. (1969) Periscope, US Patent #3482897.
- Kenworthy, P. (1973) A remote camera system for motion pictures, *Society of Motion Picture and Television Engineers*, 82: 159.
- Kollmorgen, F. L. G. (1911) Periscope, US Patent #1006230.
- Laikin, M. (1980) Periscope lens systems, *American Cinematographer*, 702.
- Latady, W., and Kenworthy, P. (1969) Motion picture camera system, US Patent #3437748.
- Roessel, W. (1995) Snorkel lens system, US Patent #5469236.
- Samuelson, D. (1998) *Hands-On Manual for Cinematographers*, Focal Press, Oxford.
- Taylor, W. (1997) Tri-power periscope head assembly, US Patent #4017148.



---

# 17 IR Lenses

Infrared lenses differ from lenses designed for the visual region in several important aspects:

- There are a lot less materials to choose from. Fortunately, available materials have high index of refraction and low dispersion (germanium, zinc selenide, etc.).
- Due to the high cost of these materials, and their relatively poor transmission, thickness should be kept to a minimum. Many of these materials are polycrystalline and exhibit some scattering; this is another reason to keep the lenses thin.
- The long wavelength means a much lower resolution requirement.
- The walls of the housing are emitting radiation and therefore contribute to the background.
- Detectors are often linear arrays, in contrast to film or the eye. These detectors are usually cooled.
- One must check that the detector is not being imaged back onto itself in a process known as *narcissus*; see Hudson (1969:275) and the discussion in [Chapter 1](#).

Absorption in our atmosphere by  $\text{H}_2\text{O}$ ,  $\text{CO}_2$ , and  $\text{N}_2\text{O}$  causes various “windows” or regions of transmission. Water vapor is the principal absorber in the 1- to 4- $\mu\text{m}$  region whereas carbon dioxide absorbs significantly at 2.7  $\mu\text{m}$  and is also the main absorber between 4 and 5  $\mu\text{m}$ . Therefore, the two main infrared windows are 3.2–4.2  $\mu\text{m}$  and the 8–14  $\mu\text{m}$  region (Wolf 1985). Regarding the refractive index of germanium, there are slight differences between the polycrystalline material and single crystal. The data used here is for the polycrystalline material. Due to slight absorption at 14  $\mu\text{m}$ , there is a little uncertainty as to the refractive index.

Infrared systems are used for a wide variety of industrial and military applications, including cancer detection (mammograms), discovery of electronic problems in circuit boards, military night-vision systems, and detection of hot bearings on railroad car wheels. Various detectors are used, some of which are given below:

Material	Wavelength Region (μm)
InGaAs (indium, gallium, arsenide)	0.9–1.7
Ge (germanium)	0.7–1.85
Si (silicon)	0.32–1.06
PbS (lead sulfide)	1.0–2.5
PbSe (lead selenide)	2.5–4.5
Hg:Cd:Te (mercury, cadmium, telluride)	0.8–2.5

Cooling increases the region of sensitivity for these detectors. These detectors are available as arrays, so a scanning system would not be necessary. For the 8.0–14.0 μm infrared region, a scanning system is usually used as shown in Figure 17.1.

Other than the infrared region, single-element lenses are rarely used by themselves for imaging purposes. (The obvious exception is the meniscus lens used in inexpensive box cameras. See also [Chapter 24](#) for single-element laser focusing lenses.) However, in the IR, the high refractive index of germanium (and the generally lower resolution requirements of the IR) make the simple meniscus lens a useful device.

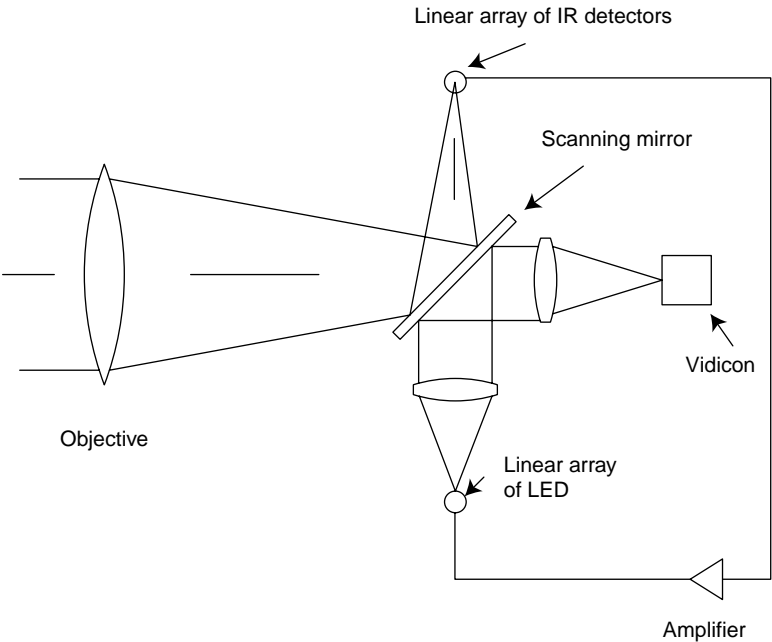


**FIGURE 17.1** Indicates how a FLIR (forward-looking infrared) system operates.

**TABLE 17.1a**  
**Minimum Spherical Aberration Lenses at 3.63  $\mu\text{m}$**

$R_1$	$R_2$	$T$	BFL	Material
9.940	16.640	0.146	9.896	Silicon
8.934	23.994	0.180	9.882	$\text{As}_2\text{S}_3$
8.968	23.645	0.179	9.883	ZnSe
8.640	27.486	0.190	9.878	ZnS
10.213	15.249	0.137	9.899	Germanium

For a distant object and thin lens minimum spherical aberration (Riedl 1974):

$$\frac{R_2}{R_1} = \frac{2N^2 + N}{2N^2 - 4 - N},$$

where  $R_1$  and  $R_2$  are the front and rear lens radii.

In Table 17.1a and Table 17.1b, values of  $R_1$ ,  $R_2$ ,  $T$  (the center thickness), and BFL are given for lenses of various materials. Effective focal length is 10, and diameter is 3.0. Using the above formula,  $R_1$  and  $R_2$  were calculated and then a thickness chosen as to yield a 0.1 edge thickness. (The lens then had to be scaled to 10.0 EFL.)

Figure 17.1 indicates how a forward-looking infrared (FLIR) system operates. This system originated as a sensing system for fighter aircraft. In these early days, they were large devices and were consequently placed in front of the aircraft facing forward, hence *forward looking*. The objective forms an image onto a linear array of IR detectors. The amplified output of each detector drives a corresponding light-emitting diode (LED). This array of LEDs is imaged, after reflection from the back side of the scanning mirror, onto an image tube (vidicon). This, in turn, drives a conventional cathode ray tube display. In this manner, a scanned infrared image is converted into a visual image onto a “TV” screen. The system shown in Figure 17.1 is actually obsolete today because most modern infrared systems incorporate solid-state detectors. There is now a company that manufactures infrared cameras called FLIR Systems.

**TABLE 17.1b**  
**Minimum Spherical Aberration Lenses at 10.2  $\mu\text{m}$**

$R_1$	$R_2$	$T$	BFL	Material
10.203	15.297	0.137	9.899	Germanium
8.920	24.134	0.180	9.882	ZnSe
8.524	29.181	0.194	9.876	ZnS

These systems operate in one of the “atmospheric windows” that are 3–5 or 8–12  $\mu\text{m}$ . At these wavelengths, sun shining on polished metal will appear bright to the eye, but black in infrared. Likewise, black anodized aluminum will appear white on an infrared camera because it absorbs sunlight and becomes warm.

Figure 17.2 is a schematic of an infrared objective. The front four lenses comprise an afocal telescope of magnification 9.357 that covers the spectral region of 8–14  $\mu\text{m}$ . Note from the ray fan plot that, although there is considerable chromatic aberration due to the long wavelength, performance is still adequate. The prescription is given in Table 17.2a.

To keep the diameter of the front lens to a minimum, the entrance pupil is placed in contact with this front element. Pupil diameter is 9.0 and so the  $f$ -number is 2.777. This system was designed to use an array of 160 detectors, 0.004 in. on centers. Thus in the plane of the paper, the field of view is 1.47°.

The vertical to horizontal aspect ratio of typical “TV” displays is 3/4. Horizontal field of view of the objective then is 1.96°. Because the effective focal length of the lenses to the right of the scan mirror is 2.672, the scan mirror moves a total of 9.19°. The last two surfaces in the system represents a window which is used to protect the cooled detector array.

To obtain a wide field of view, the three lenses in front of the scan mirror (surfaces 4–9) are replaced as indicated in Table 17.2b to provide a wide field of view of 3.66°. The operator then may search the field in the wide FOV mode, and when the target is located, switch to narrow FOV (Akram 2003).

Figure 17.3 shows an IR lens to be used in the 3.2–4.2  $\mu\text{m}$  spectral region; details are given in Table 17.3. It is  $f/1.5$  and covers a 5° field. The EFL is 4.5 (at 3.63  $\mu\text{m}$ ). Detectors for the 3.2–4.2  $\mu\text{m}$  region are often protected with a sapphire window. This was not included in the above design.

Sometimes it is desirable to expand a laser beam. This has the additional advantage of reducing the beam divergence by the magnification factor (see Chapter 13 on afocal systems). In Figure 17.4 is shown such a beam expander for use with a CO<sub>2</sub> laser at 10.6  $\mu\text{m}$ ; details are given in Table 17.4. The beam is expanded by a factor of 10.0. Notice the excessive flare at the edge of the aperture.

In this case, the input beam intensity is assumed to have a Gaussian distribution of the form

$$I = I_0 e^{-2}$$

where  $I_0$  is the intensity in the center of the beam,  $I$  is the intensity at the edge of the entrance pupil. The intensity at the edge has fallen to 13.5% of the center.

In the near IR region, 0.7 to 2.5  $\mu\text{m}$ , ordinary glass may be used. Several very dense flints with high refractive index (Schott N-SF57, Ohara S-NPH2, and Hoya E-FDS1 for example) that show considerable absorption in the visual region are very transparent here. In this spectral region, a very interesting thing occurs to the values of  $V$ . At 1.2  $\mu\text{m}$ ,  $V$  values of many crowns and flints are the same, whereas at 2.2  $\mu\text{m}$ ,  $V$  values of flints are often greater than the crowns.

Consider the region 1.8 to 2.2  $\mu\text{m}$ , with center at 2.0  $\mu\text{m}$ ; then,  $N$  and  $V$  values for N-BAK2 are 1.51833 and 101.238, respectively, whereas for SF4,  $N$  and  $V$  are

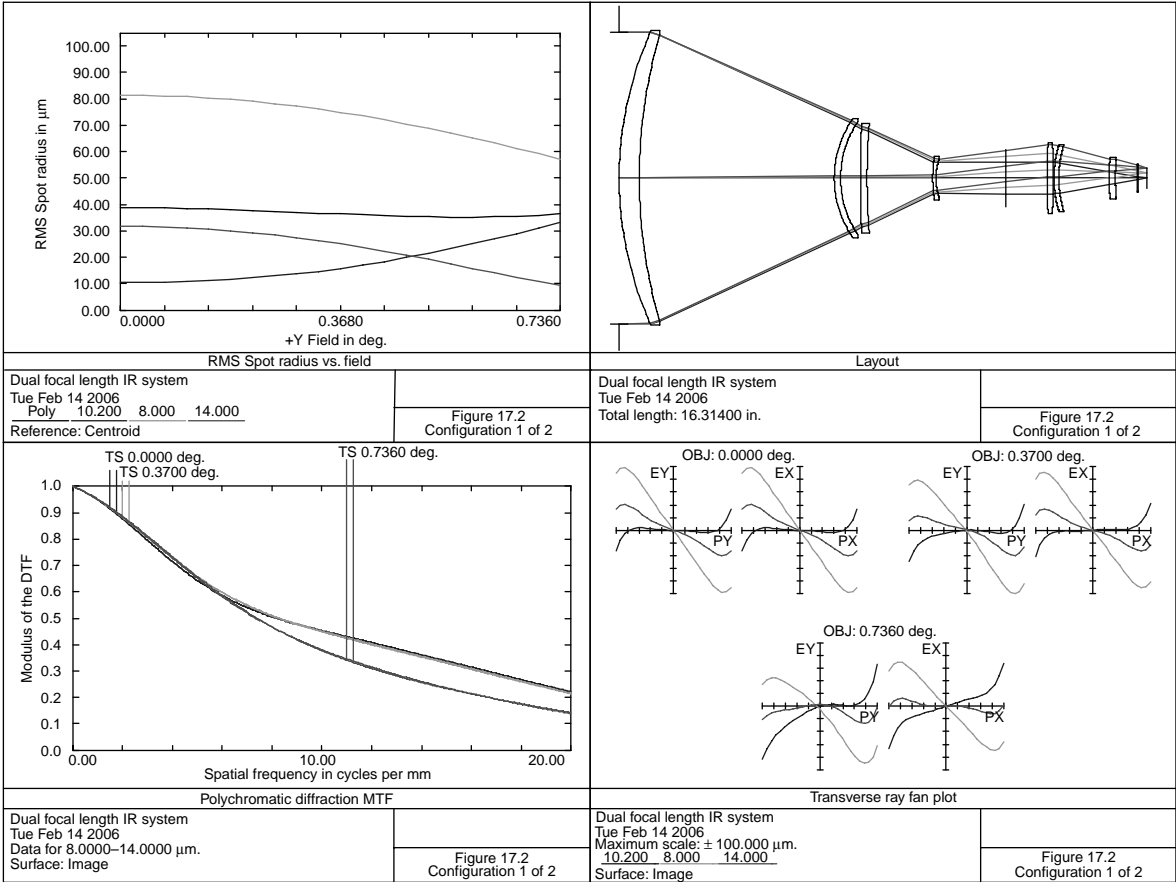


FIGURE 17.2 Dual focal length IR lens system.

**TABLE 17.2a**  
**Dual Focal Length IR Lens System, 25-in. Focal Length**

Surface	Radius	Thickness	Material	Diameter
0	0.0000	$0.100000 \times 10^{11}$		0.00
1	Stop	0.0000		9.000
2	11.0025	0.6227	Germanium	9.100
3	15.8018	6.0193		8.880
4	3.1701	0.2000	Germanium	3.700
5	3.1272	0.6158		3.480
6	47.4227	0.2000	ZnSe	3.380
7	20.9638	2.0310		3.240
8	4.2229	0.1000	Germanium	1.320
9	1.8186	2.1415		1.220
10	0.0000	1.2909		1.780
11	20.1641	0.2000	Germanium	2.180
12	-15.2434	0.0150		2.180
13	3.5941	0.1500	ZnSe	2.080
14	3.5679	1.5531		1.980
15	6.6340	0.1920	Germanium	1.280
16	6.7657	0.6745		1.180
17	0.0000	0.0400	Germanium	0.860
18	0.0000	0.2682		0.860
19	0.0000	0.0000		0.648

Distance from first lens surface to image = 16.314, effective focal length = 25.0  
(at 10.2  $\mu\text{m}$ ), distortion = 0.09%.

**TABLE 17.2b**  
**A 10-in. Focal Length Conversion**

Surface	Radius	Thickness	Material	Diameter
3		6.3916		
4	20.3250	0.2803	Germanium	2.080
5	10.9855	0.5844		2.000
6	7.3959	0.1019	ZnSe	1.860
7	5.8780	1.1364		1.800
8	1.6078	0.2120	Germanium	1.320
9	1.3641	2.1415		1.160

Distortion = 0.43%.



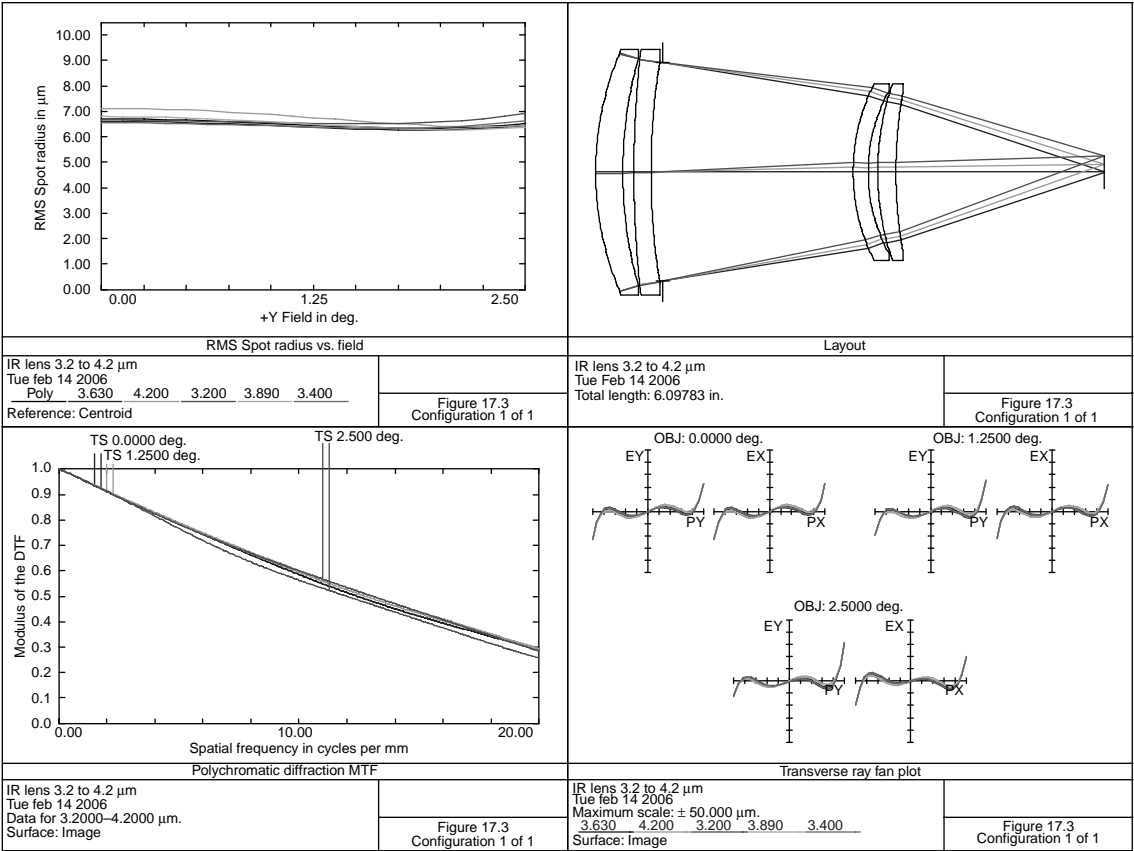


FIGURE 17.3 IR lens, 3.2–4.2  $\mu\text{m}$ .

**TABLE 17.3**  
**IR Lens, 3.2–4.2  $\mu\text{m}$**

Surface	Radius	Thickness	Material	Diameter
1	3.6879	0.3250	Silicon	2.940
2	5.1177	0.1333		2.780
3	13.1607	0.2050	Germanium	2.940
4	8.4938	0.1350		2.680
5	Stop	2.2867		2.620
6	2.3571	0.1800	Germanium	2.120
7	2.0207	0.1148		1.940
8	3.2650	0.2180	Silicon	2.120
9	5.4889	2.5000		1.880

Distance from first lens surface to image = 6.098, distortion = 0.03%.

1.71253 and 128.533, respectively. Preliminary values of curvatures were taken from [Table 2.1](#) and optimized for a focal length of 10.0,  $f/8$ , and a  $1.5^\circ$  FOV. It is shown in [Figure 17.5](#); details are provided in [Table 17.5](#).

Schott Glass (1992) has available a line of infrared transmitting glasses. These glasses exhibit good transmission from 0.4 to 4  $\mu\text{m}$  (5  $\mu\text{m}$  in the case of IRG11).

Riedl (1996) presents a two element (both of germanium) lens for the 8–12  $\mu\text{m}$  region. It is a Petzval type of lens (the two elements have a large separation with the rear element being close to the image). To correct for the residual spherical aberration, the rear surface of the first element has a diffractive surface. This weak diffractive surface also improves the chromatic correction.

In [Figure 17.6](#) is shown a hyperbolic mirror imaging a wide field into a lens system (see the panoramic camera of [Figure 9.6](#)). Details are provided in [Table 17.6](#). Field of view is  $68\text{--}112^\circ$  from the optical axis and is  $f/1.75$ . A “donut-shaped” image is thus formed with diameters of 0.208 on the inside and 0.472 on the outside.

**TABLE 17.4**  
**A 10 $\times$  Laser-Beam Expander**

Surface	Radius	Thickness	Material	Diameter
1	Stop	0.5000		0.300
2	−0.3107	0.0500	ZNSE	0.340
3	0.0000	1.2921		0.400
4	−2.3600	0.5000	ZNSE	2.460
5	−1.7023	0.0200		2.740
6	32.9071	0.3100	ZNSE	3.040
7	−11.6462	1.0000		3.040

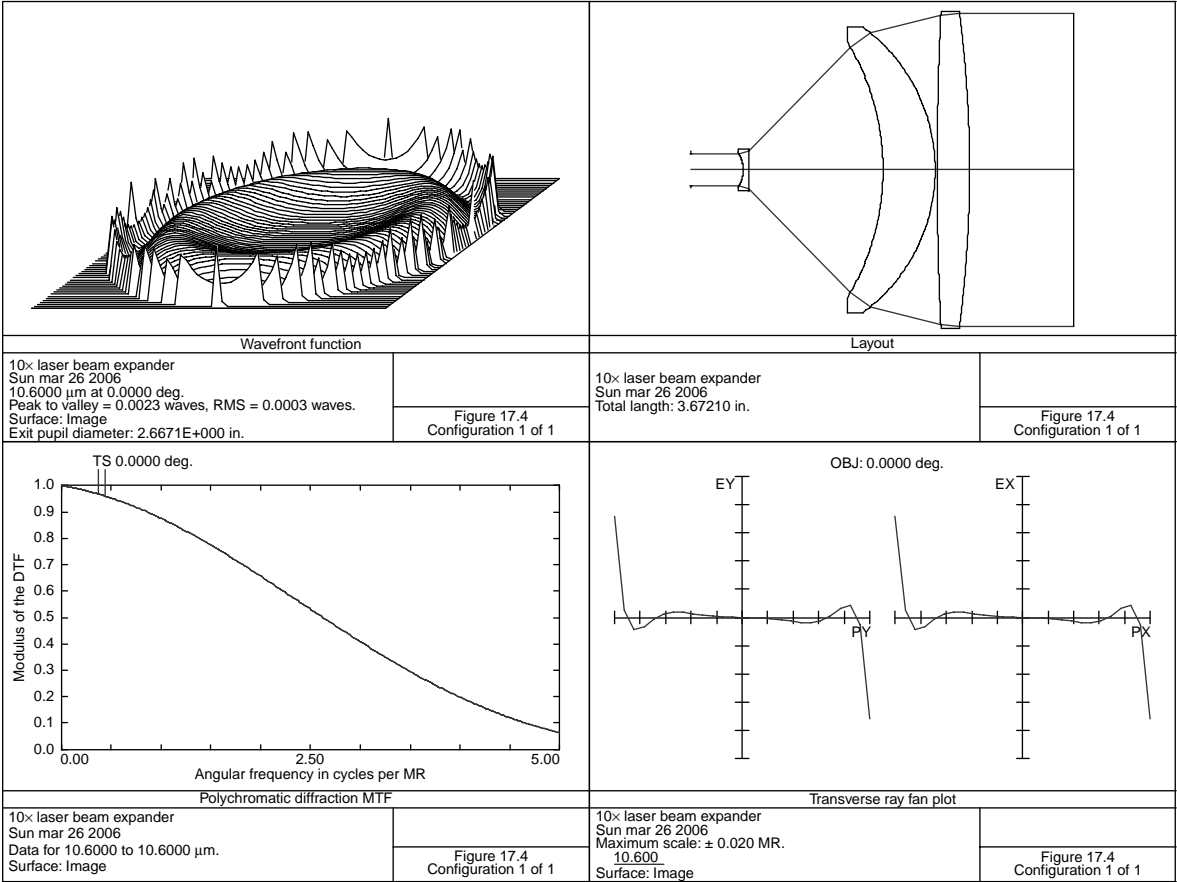


FIGURE 17.4 A 10 $\times$  beam expander.

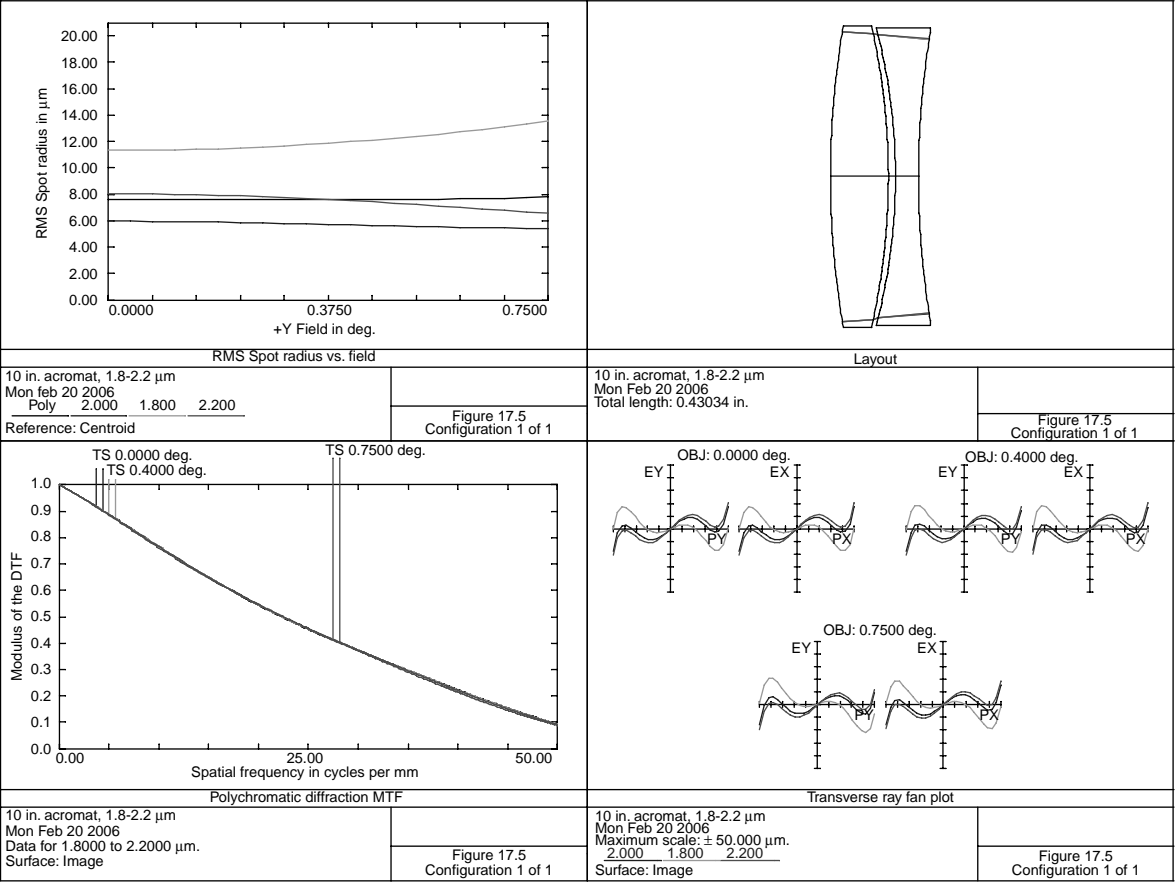


FIGURE 17.5 Doublet, 1.8–2.2 μm.

**TABLE 17.5**  
**A 10.0 Focal Length Achromat, 1.8–2.2 μm**

Surface	Radius	Thickness	Material	Diameter
1	3.8202	0.2500	SF4	1.300 Stop
2	−2.9282	0.0300		1.300
3	−2.5421	0.1000	N-BAK2	1.280
4	3.8430	9.4260		1.240
5	0.0000	0.0000		0.262

**TABLE 17.6**  
**Long-Wavelength Infrared Camera**

Surface	Radius	Thickness	Material	Diameter
0	0.0000	$0.100000 \times 10^{11}$		0.00
1	1.5360	−2.3750	Mirror, conic coefficient = −2.073545	5.140
2	0.4144	−0.1301	Germanium	0.380
3	0.5736	−0.1578		0.460
4	−2.0255	−0.1081	Germanium	0.380
5	5.2922	−0.0640		0.380
6	Stop	−0.3629		0.229
7	0.2631	−0.2428	ZnSe	0.380
8	0.5047	−0.0647		0.700
9	1.3151	−0.1321	Germanium	0.780
10	1.0131	−0.0197		0.880
11	−0.5428	−0.2066	Germanium	0.880
12	−0.6678	−0.1331		0.690
13	0.0000	0.0000		0.472

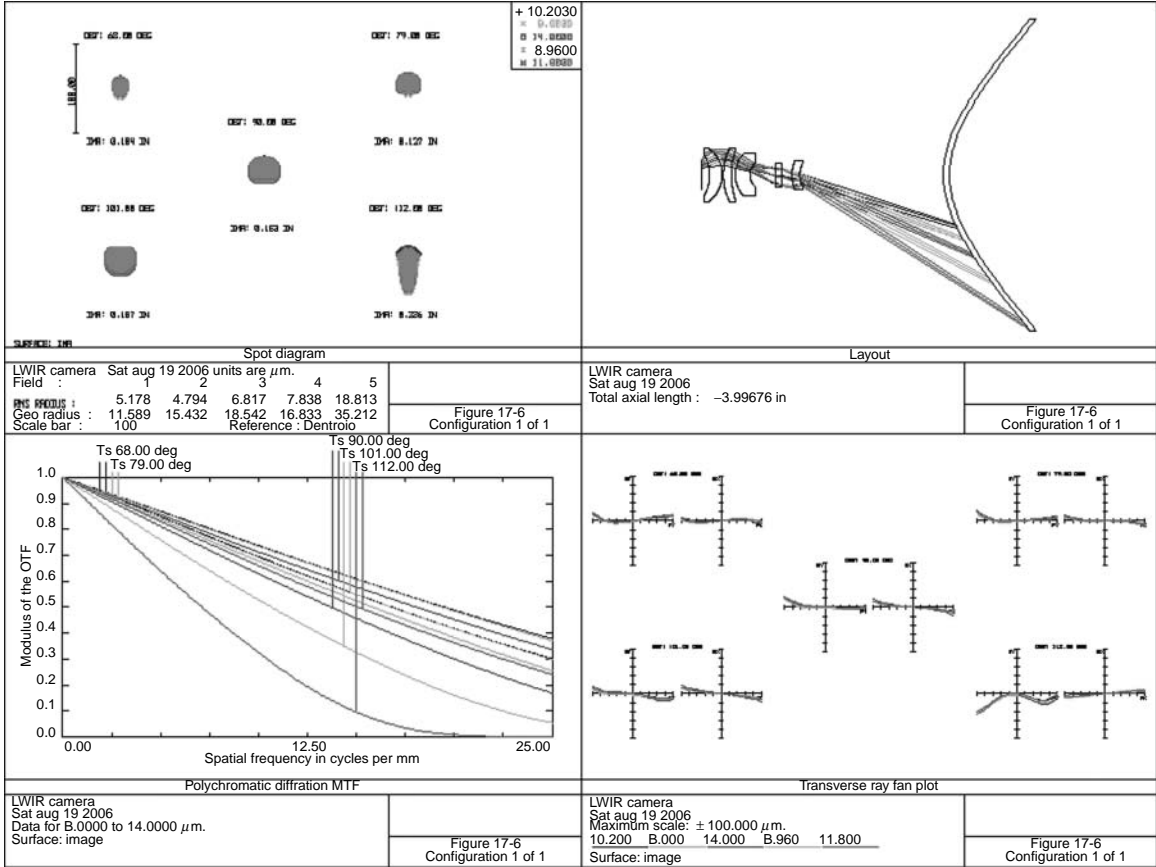


FIGURE 17.6 Long wavelength IR camera.

## REFERENCES

- Akram, M. N. (2003) Design of a multiple field of view optical system for 3 to 5 micron infrared focal plane array, *Optical Engineering*, 42: 1704.
- Fjeldsted, T. P. (1983) Four element infrared objective lens, US Patent #4380363.
- Hudson, R. (1969) *Infrared System Engineering*, Wiley, New York.
- Jamieson, T. H. (1976) Aplanatic anastigmatic two and three element objectives, *Applied Optics*, 15: 2276.
- Kirkpatrick, A. D. (1969) Far infrared lens, US Patent #3439969.
- Kokorina, V. F. (1996) *Glasses for Infrared Optics*, CRC Press, Boca Raton, FL.
- Lloyd, J. M. (1975) *Thermal Imaging Systems*, Plenum Press, New York.
- Neil, I. A. (1985) Infrared objective lens system, US Patent #4505535.
- Norrie, D. G. (1986) Catadioptric afocal telescopes for scanning infrared systems, *Optical Engineering*, 25: 319.
- NTIS, (1971) *Engineering Design Handbook, Infrared Military Systems*, AD 885227, NTIS, Springfield, VA.
- Optical materials for infrared instrumentation, IRIA, (1959) University of Michigan report #2389 also supplement of 1961, Information and Analysis Center, Ann Arbor, MI.
- Riedl, M. J. (1974) The single thin lens as an objective for IR imaging systems, *Electro-Optical Sys Design*, M. S. Kiver Publications, p. 58.
- Riedl, M. J. (1996) Design example for the use of hybrid optical elements in the IR, *OPN Engineering and Laboratory Notes*, SPIE, Bellingham, WA.
- Rogers, P. J. (1977) Infrared lenses, US Patent #4030805.
- Schott Glass, (1992) *Data Sheet #3112e*, Schott Glass Technologies, Durea, PA.
- Sijgers, H. J. (1967) Four element infrared objective, US Patent #3321264.
- Wolf, W., Ed. (1965) *Handbook of Military Infrared Technology*, Office of Naval Research, Washington, DC.
- Wolf, W. and Zissis, G. (1985) *The Infrared Handbook*, Research Institute of Michigan, Ann Arbor, MI.





---

# 18 Ultraviolet Lenses and Optical Lithography

Lenses for the UV spectral region are used in photo-mask printing, printing of reticles onto a material with a photo-resist, microscope objective for fluorescence studies (see [Figure 11.4](#)), forensic photography, optical lithography, etc.

As with the infrared spectral regions, a major problem is finding suitable materials. For the spectral region, 0.2–0.4  $\mu\text{m}$ , the most important materials are fused silica and calcium fluoride. Although several glasses have been developed to have reduced absorption below 0.4  $\mu\text{m}$ , they have limited use because there is considerable absorption even at 0.3  $\mu\text{m}$ . Recently, Schott Glass Technologies (1992) and Ohara Corp. (1993) have announced a new family of UV transmitting glasses called their *i*-line glasses designed for high transmittance at 0.365  $\mu\text{m}$ . These materials have high chemical durability as well as being transparent over a large wavelength region. [Table 18.1](#) lists these new materials.

Schott, Inc. has developed a series of *i*-line glasses. These glasses have nearly the same refractive index values as the regular glasses but are melted and tested to have high transmittance at 0.365  $\mu\text{m}$ . [Table 18.2](#) contains a list of these glasses.

[Table 18.3](#) details some of the properties of UV-transmitting materials. Sapphire and magnesium fluoride are often used as window materials for certain types of detectors. Because these materials are birefringent, they cannot be used as lenses. The first number in the thermal expansion column in the above table for these materials represents the expansion parallel to the optic axis and the next value is perpendicular.

To obtain high transmission at the UV wavelengths, fused silica is made from a purified  $\text{SiCl}_4$ . This is then directed into a hydrogen/oxygen flame to produce  $\text{SiO}_2$ . Due to its high melting temperature, it is difficult to obtain a homogeneous material and also avoid contaminants that would reduce transmission at these short wavelengths.

Antireflection coatings are a problem due to the fact that some commonly used coating materials are absorbing in this spectral region. The usual reflection curves, which the coater presents, are not adequate here. Always insist on a transmission curve as well. For the 0.157- $\mu\text{m}$  lithography, antireflection coatings are a major problem due to the lack of a variety of transparent materials (Chen et al. 2004).

A recent development is the Blu-ray project in which 27 gigabytes of information may be recorded on a single 12-cm CD/DVD disk using a 0.405- $\mu\text{m}$  laser (conventional CDs and DVDs use 0.780- and 0.650- $\mu\text{m}$  lasers, respectively).

[Figure 18.1](#) shows a lens designed for this spectral region (0.2–0.4  $\mu\text{m}$  with center at 0.27  $\mu\text{m}$ ); details are given in [Table 18.4](#). It is  $f/4.0$  with a focal length of

**TABLE 18.1**  
**Ohara New UV-Transmitting Glasses**

Glass	$N_d$	$V_d$	Wavelength <sup>a</sup> (μm)
S-FPL51Y	1.4970	81.1	0.310
S-FSL5Y	1.4875	70.2	0.302
BSL7Y	1.5163	64.1	0.315
BAL15Y	1.5567	58.7	0.323
BAL35Y	1.5891	61.2	0.318
BASM51Y	1.6031	60.7	0.320
PBL1Y	1.5481	45.9	0.319
PBL6Y	1.5317	49.0	0.316
PBL25Y	1.5184	40.8	0.336
PBL26Y	1.5673	42.9	0.337
PBM2Y	1.6200	36.3	0.345
PBM8Y	1.5955	39.3	0.339

<sup>a</sup> For 70% transmittance and 25-mm thickness.

5.0 and a FOV of 10°. It is a modification of Tibbets (1962). The main aberration is primary chromatic color as can be seen from the RMS spot radius plot.

Figure 18.2 shows a Cassegrain lens system used to image an object 2.75 diameter at a magnification of 0.1 (0.2–0.4 μm with center at 0.27 μm). Details are provided in Table 18.5.

**TABLE 18.2**  
**i-Line Glasses from Schott, Inc.**

Glass	$N_d$	$V_d$
FK5HT	1.48756	70.56
BK7HT	1.51633	64.14
K5HT	1.52245	59.53
K7HT	1.51114	60.47
LLF1HT	1.54814	45.89
LLF6HT	1.53174	48.97
LF5HT	1.58148	40.91
LF6HT	1.56732	42.85
F2HT	1.62004	36.37
F8HT	1.59551	39.18
F14HT	1.60139	38.28

**TABLE 18.3**  
**UV-Transmitting Materials**

Material	Transmission Region (μm)	Density (g/cm <sup>3</sup> )	Solubility per 100 g Water at 20°C	Knoop Hardness	Melting Point (°C)	Thermal Expansion 10 <sup>-6</sup> / K at 283 K
LiF	0.12–6.0	2.639	0.27	102	870	37
CaF <sub>2</sub>	0.13–10.0	3.181	0.0016	158.3	1423.	18.85
BaF <sub>2</sub>	0.15–12.5	4.89	0.12	82	1280.	18.1
MgF <sub>2</sub>	0.12–7.0	3.18	0.0002	415	1585	13.7/8.9
Al <sub>2</sub> O <sub>3</sub>	0.17–5.5	3.987	0.	2000	2040	5.6/5.0
SiO <sub>2</sub>	0.18–3.0	2.202	0.	522.	1600	0.55

Note that the secondary mirror ( $R = -2.9890$ ) has a different radius than the second surface of the corrector ( $R = -1.9288$ ). This means that the corrector/secondary must be made in two sections with the secondary being aligned and bonded to the corrector. For manufacturing reasons, this should be changed by tying the curvature of surface 6 to surface 2. To keep the obscuration small, the aperture stop is located at this secondary mirror. The primary mirror is a Mangin type. In the visual region, silver (suitably protected with an overcoat of copper and then painted) is generally used as a second surface mirror because of its higher reflectivity than aluminum. However, in the 0.2–0.4 μm region, aluminum is the preferred coating material because silver has reduced reflectivity below 0.38 μm (Hass 1965).

Optical lithography is used in the production of computer chips (Mack 1996). This typically involves a very high resolution lens operating at a single UV wavelength.

For a circular, uniformly illuminated pupil, the radius of the airy disc is

$$R = \frac{0.61\lambda}{\text{NA}}.$$

Inside this radius is 84% of the energy. Thus, to increase resolving power, the wavelength must be reduced and a high-NA lens system should be used. The depth of focus becomes  $0.5\lambda/(\text{NA})^2$ . To obtain this high resolution, it is helpful to have a single wavelength source. Many years ago, this was accomplished by the use of one of the spectral lines (0.365 μm, 0.405 μm, and 0.436 μm) of a low-pressure mercury arc lamp. To obtain higher resolution, it is necessary to use even shorter wavelengths. Today, the preferred source is an excimer laser. Excimer is short for *excited dimer*—a molecule consisting of two identical atoms such as He<sub>2</sub> or Xe<sub>2</sub> that exist only in the excited state. This term now includes ArF, KrCl, KrF, XeCl, and XeF.

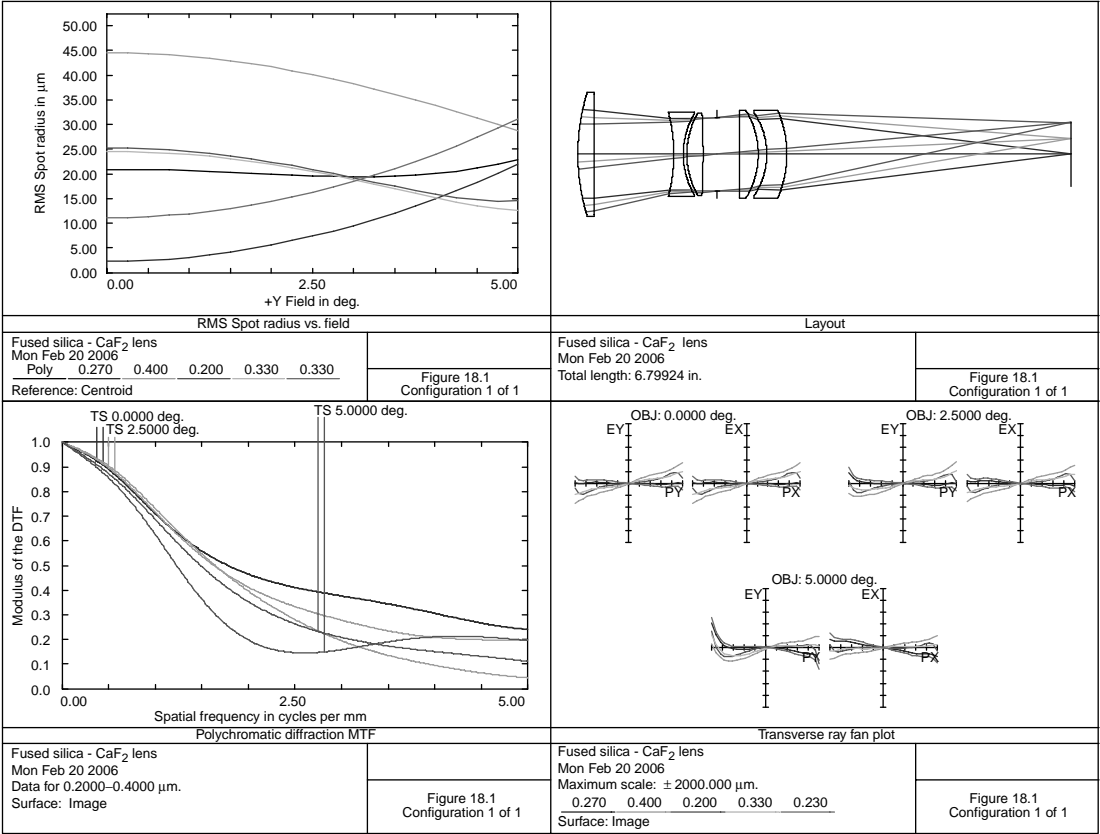


FIGURE 18.1 UV lens silica, CaF<sub>2</sub>.

Laser	Wavelength ( $\mu\text{m}$ )
F <sub>2</sub>	0.15763
ArF	0.19339
KrCl	0.222
KrF	0.248
XeCl	0.308
XeF	0.350

The use of the excimer laser (F<sub>2</sub>) at 0.157  $\mu\text{m}$  is under development. A high-power laser has been used to excite a supersonic stream of xenon gas to emit radiation at 0.13  $\mu\text{m}$ . To go to shorter wavelengths will require direct writing with an electron beam.

Unfortunately, there are only a few materials that are transparent at wavelengths below 0.35  $\mu\text{m}$ . These are calcium fluoride, lithium fluoride, magnesium fluoride, barium fluoride, strontium fluoride, sapphire, diamond, and fused silica. Transmission at these short wavelengths is very dependent on material purity. Damage threshold, index homogeneity, and fluorescence are additional problems. Matsumoto and Takash (1998) discusses irradiation damage at 0.193  $\mu\text{m}$  and shorter wavelengths. Oxide and fluoride materials are usually “grown” in a vacuum and then subsequently annealed to reduce stress birefringence. Calcium fluoride exhibits slight birefringence at 0.157  $\mu\text{m}$  (Burnett, Levine, and Shirley 2001). A catadioptric system minimizes this defect by placing most of the focusing power in the mirror.

**TABLE 18.4**  
**Fused Silica–Calcium Fluoride Lens**

Surface	Radius	Thickness	Material	Diameter
0	0.0000	$0.100000 \times 10^{11}$		0.00
1	2.9298	0.2285	CaF <sub>2</sub>	1.700
2	−46.0249	1.0919		1.700
3	−2.3471	0.1312	Silica	1.157
4	1.0880	0.0496		1.112
5	1.1344	0.2224	CaF <sub>2</sub>	1.140
6	−10.8536	0.1950		1.140
7	Stop	0.3086		1.020
8	44.0565	0.2578	CaF <sub>2</sub>	1.220
9	−1.1589	0.1175		1.220
10	−1.0150	0.2753	Silica	1.140
11	−1.5764	3.9216		1.220
12	0.0000	0.0000		0.883

Distance from first lens surface to image = 6.799, distortion is negligible.

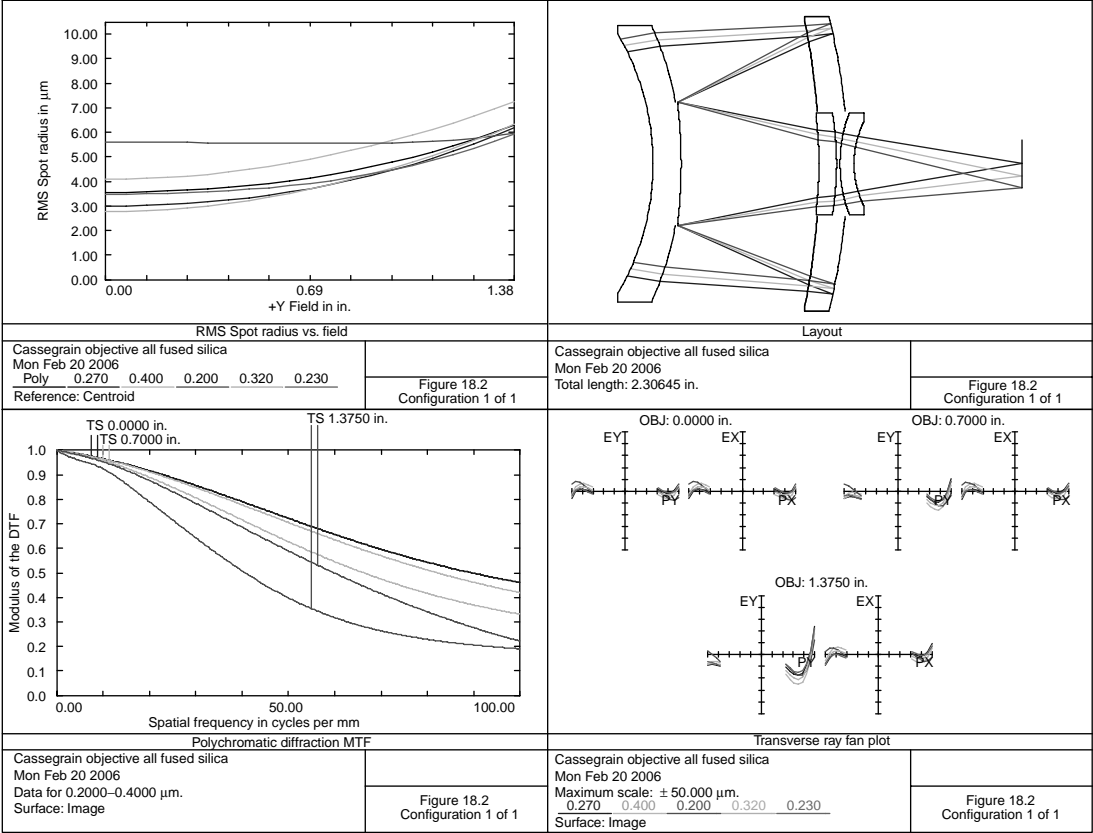


FIGURE 18.2 Cassegrain objective, all fused silica.

**TABLE 18.5**  
**Cassegrain Objective, All Fused Silica**

Surface	Radius	Thickness	Material	Diameter
0	0.0000	39.3700		2.750
1	−1.4667	0.1600	Silica	1.480
2	−1.9288	0.7869		1.580
3	−4.1223	0.1617	Silica	1.620
4	−3.3439	−0.1617	Mirror	1.680
5	−4.1223	−0.7869		1.620
6	−2.9890	0.7869	Mirror	0.700 Stop
7	−2.1435	0.1000	Silica	0.540
8	−1.7957	0.0200		0.580
9	0.8305	0.0800	Silica	0.580
10	0.5479	0.9591		0.480

Distance from first lens surface to image = 2.106, distortion = 0.44%, image space  
 NA = 0.1644, magnification = −0.1.

Extensive development is using optical lithography at the 0.193  $\mu\text{m}$  line using a high-index-refraction liquid immersion techniques to obtain line spacings of 0.03  $\mu\text{m}$ .

To obtain even smaller image sizes, the trend is toward using source wavelengths shorter than 0.193  $\mu\text{m}$  (Kubiak and Kania 1996). Optical absorption by air at these short wavelengths requires that the system be purged with either helium or nitrogen.

Polishing of optics for high energy UV optics is also a problem. A  $\lambda/10$  surface specification at 0.193  $\mu\text{m}$  is nearly three times tighter than the same specification at 0.546  $\mu\text{m}$ . Subsurface damage has also been identified. During the act of polishing the surface, there is a layer of material that “flows” while the material is being worked. This causes microfractures and other surface defects that under high illumination levels eventually cause failure.

The manufacture of integrated circuits on a silicon substrate involves a step and repeat process. This requires an optical system with very low distortion and generally must be telecentric in both object and image space. Such a system is shown in Figure 18.3 and detailed in Table 18.6. It was designed for use with a KrF 0.248 $\mu\text{m}$  source. Object is 0.145 in diameter and the magnification is −0.25 NA is 0.56. This is a minor optimization from the Sasaya, Ushida, and Mercado (1998) patent.

Maximum distortion occurs at about 0.7 of full field and is 0.00014%. The separation between the sagittal and tangential foci indicates that there is some small astigmatism present.

Because resolution in an optical system is given by  $R = k_1 \lambda / \text{NA}$  (Rothschild 2005) and the depth of focus is  $\pm k_2 \lambda / \text{NA}^2$ , where the constants  $k_1$  and  $k_2$  are

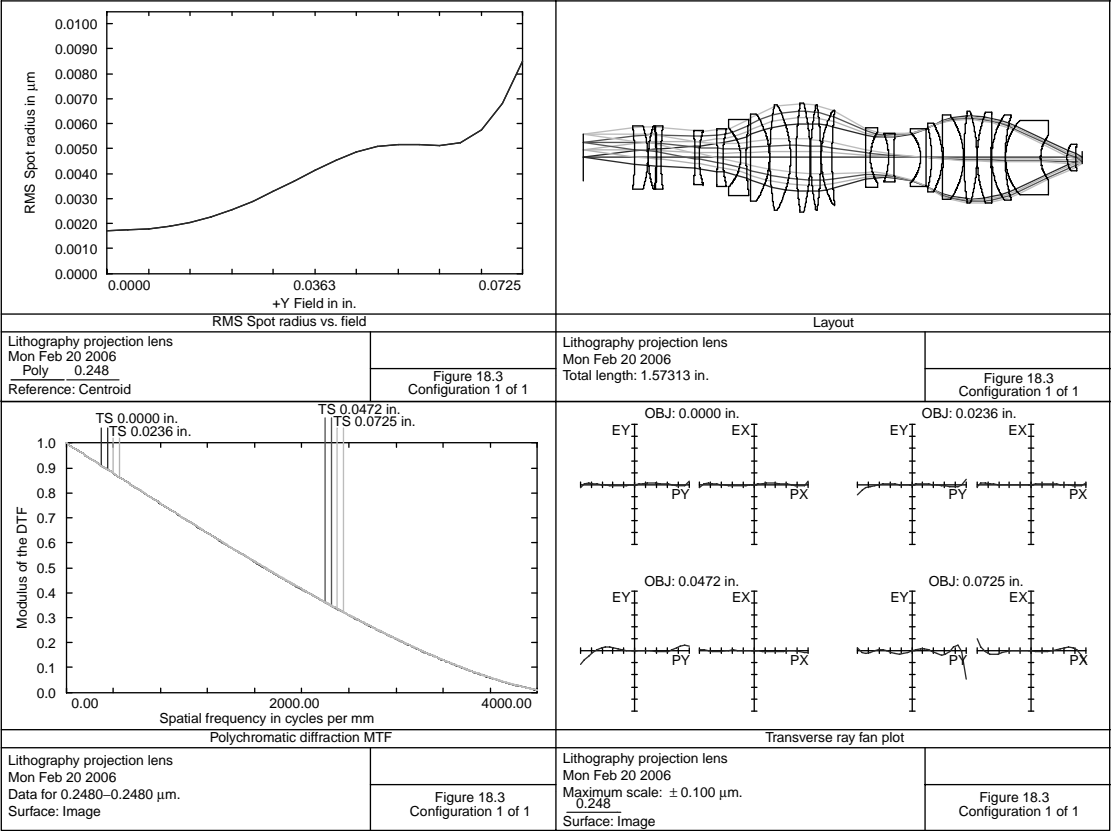


FIGURE 18.3 Lithography projection.



**TABLE 18.6**  
**Lithography Projection Lens**

Surface	Radius	Thickness	Material	Diameter
0	0.0000	0.1615		0.145
1	−0.79639	0.0418	Silica	0.189
2	−0.31776	0.0013		0.197
3	0.31768	0.0247	Silica	0.198
4	−0.90519	0.0014		0.198
5	−1.53140	0.0138	Silica	0.196
6	0.86996	0.1068		0.199
7	−0.96937	0.0138	Silica	0.171
8	0.30419	0.0567		0.169
9	−4.54831	0.0179	Silica	0.176
10	0.36328	0.0559		0.180
11	−0.13317	0.0179	Silica	0.185
12	0.83902	0.0148		0.240
13	0.0000	0.0581	Silica	0.273
14	−0.24698	0.0014		0.273
15	0.97362	0.0653	Silica	0.330
16	−0.34739	0.0176		0.330
17	1.12092	0.0447	Silica	0.342
18	−0.71734	0.0009		0.342
19	0.82256	0.0323	Silica	0.332
20	−1.18244	0.0009		0.332
21	0.31346	0.0345	Silica	0.300
22	1.42431	0.1071		0.296
23	−2.67307	0.0138	Silica	0.187
24	0.15590	0.0569		0.162
25	−0.21770	0.0171	Silica	0.154
26	1.01511	0.0839		0.154
27	−0.11720	0.0176	Silica	0.161
28	3.98510	0.0171		0.183 Stop
29	−0.40426	0.0339	Silica	0.193
30	−0.21818	0.0019		0.214
31	−7.96203	0.0650	Silica	0.246
32	−0.23180	0.0014		0.265
33	1.01215	0.0411	Silica	0.289
34	−0.50372	0.0008		0.289
35	0.40042	0.0441	Silica	0.287
36	3.75600	0.0014		0.281
37	0.24527	0.0429	Silica	0.267
38	0.49356	0.0013		0.267
39	0.17401	0.1101	Silica	0.233
40	0.11185	0.0832		0.139
41	0.07661	0.0263	Silica	0.082
42	0.18719	0.0223		0.065
43	0.0000	0.0000		0.036

Effective focal length=10.644, object to image distance=1.573.

**TABLE 18.7**  
**Future Lithography Lens Requirements**

Wavelength	0.157 $\mu\text{m}$
(For extreme UV lithography, see the Kubiak and Kania (1996) and Wang and Pan (2001)	
NA	0.85
Resolution	0.075 $\mu\text{m}$ (assumes a value of $k_1=0.4$ )
Magnification	5
Image size	31-mm diameter

functions of the lithography resist process (Levenson 2001), it is seen that increasing the numeric aperture, although improving the resolution, also greatly reduces the depth of focus. Therefore, the recent trend in lithography is to reduce the wavelength (Hudyma 2002). Typical requirements for future lens development are listed in Table 18.7 (additional future improvements would be in illumination systems and phase shift masks).

REFERENCES

Betensky, E. I. (1967) Modified gauss type of optical objective, US Patent #3348896.

Burnett, J., Levine, Z., and Shirley, E. (2001) *Photonics Spectra*, December, 88.

Burnett, J., Levine, Z., and Shirley, E. (2002) The trouble with calcium fluoride, *SPIE oe Magazine*, March, 23.

Chen, H.-L., Fan, W., Wang, T. J., Ko, F. H., Zhai, R. S., Hsu, C. K., and Chuang, T. J. (2004) Optical-gradient antireflection coatings for the 157-nm optical lithography applications, *Applied Optics*, 43: 2141–2145.

Elliott, D. J. and Shafer, D. (1996) Deep ultraviolet microlithography system, US Patent #5488229.

Gupta, R., Burnett, J., Griesmann, U., and Walhout, M. (1998) Absolute refractive indices and thermal coefficients of fused silica and calcium fluoride near 193 nm, *Applied Optics*, 37: 5964–5968.

Hass, G. (1965) Mirror Coatings, In *Applied Optics and Optical Engineering*, Volume 3, Chapter 8, (R. Kingslake ed.) Academic Press, Newyork, p. 309.

Hudyma, R. (2002) An overview of optical systems for 30 nm resolution lithography at EUV wavelengths, *International Optical Design Conference, 2002, SPIE*, Volume 4832, pp. 137–148.

Hwang, S. (1994) Optimizing distortion for a large field submicron lens, *Proceedings of SPIE*, 2197: 882.

Kubiak, G. D. and Kania, D. R., Eds., (1996) *Extreme Ultraviolet Lithography, Vol. 4 of OSA Trends in Optics and Photonics*, Optical Society of America, Washington, DC.

Levenson, H. J. (2001) *Principles of Lithography*, SPIE Press, Bellingham, WA.

Lowenthal, H. (1970) Lens system for use in the near ultraviolet, US Patent #3517979.

Mack, C. A. (1996) Trends in optical lithography, *Optics and Photonics News*, April 29–33.

Matsumoto, K. and Takash, M. (1998) *International Optical Design Conference, 1998, SPIE*, Volume 3482, p. 362.

Ohara Corp. (1993) *i-Line Glasses*. Ohara Corp., Somerville, NJ.

Rothschild, M. (2005) Projection optical lithography, *Materials Today*, February 18–24.

- Sasaya, T., Ushida, K., and Mercado, R. (1998) All fused silica 0.248 nm lithographic projection lens, US Patent #5805344, This patent is reviewed by Caldwell in Optics and Photonics News, November 40.
- Schott Glass Technologies (1993) *Schott Glass Catalog*, Schott Glass Technologies, Durea, PA.
- Sheats, J. R. and Smith, B. W., Eds., (1992) *Microlithography: Science and Technology*, Marcel Dekker, New York.
- Tibbetts, R. E. (1962) Ultra-violet lens, US Patent #3035490.
- Wang, Z. and Pan, J. (2001) Reflective optical system for EUV lithography, US Patent #6331710.



---

# 19 F-Theta Scan Lenses

F-theta scan lenses are used to scan a document for either printing or reading. A scanning device is situated an external entrance pupil; it may be a rotating polygon, rotating mirror, mirror galvanometer, piezoelectric deflector, etc. The document to be scanned is usually flat. In the case of the rotating polygon that is rotating at a high, uniform angular velocity, for the image positions to be uniformly spaced it is necessary that the image height be proportional to the scan angle (not to the tangent of the angle as in a photographic lens). This linear requirement is generally true for the other scanning devices.

$$\text{Image height} = KF\theta,$$

where  $F$  is lens focal length and  $\theta$  is the scan angle. If  $\theta$  is in degrees, then  $K \approx 0.0175$ .

In [Figure 19.1](#) is shown a document scan lens with a 24-in. focal length, a 2.0-in. diameter entrance pupil, visual correction; it is designed to scan a 14-in. wide document for a scan angle of  $33.4^\circ$ . Details are given in [Table 19.1a](#). As one would expect, resolution at the edge of the field is limited by lateral secondary color ([Table 19.1b](#)).

[Figure 19.2](#) shows a scan lens for use with an argon laser ( $0.488 \mu\text{m}$ ); details are given in [Table 19.2a](#). Focal length is 20 in. and the f-number is  $f/30$ . The scan angle is  $30^\circ$  ([Table 19.2b](#)).

In [Figure 19.3](#) is shown a scan lens for use at the  $0.6328 \mu\text{m}$  (HeNe) laser line. Details are given in [Table 19.3a](#). The effective focal length (EFL) is 20.

This system, as well as the previous, is diffraction limited over the full field. Apodization of the entrance pupil was not used in the systems of this section. However, because the last two are for use with a laser, the entrance pupil should have been apodized to allow for the usual  $1.0/e$  amplitude variation of Gaussian beams. Also note that the lenses in this section all have a Back Focal Lengths (BFLs) slightly longer than the EFLs. This inverted type is necessary to obtain a linear scan ([Table 19.3b](#)).

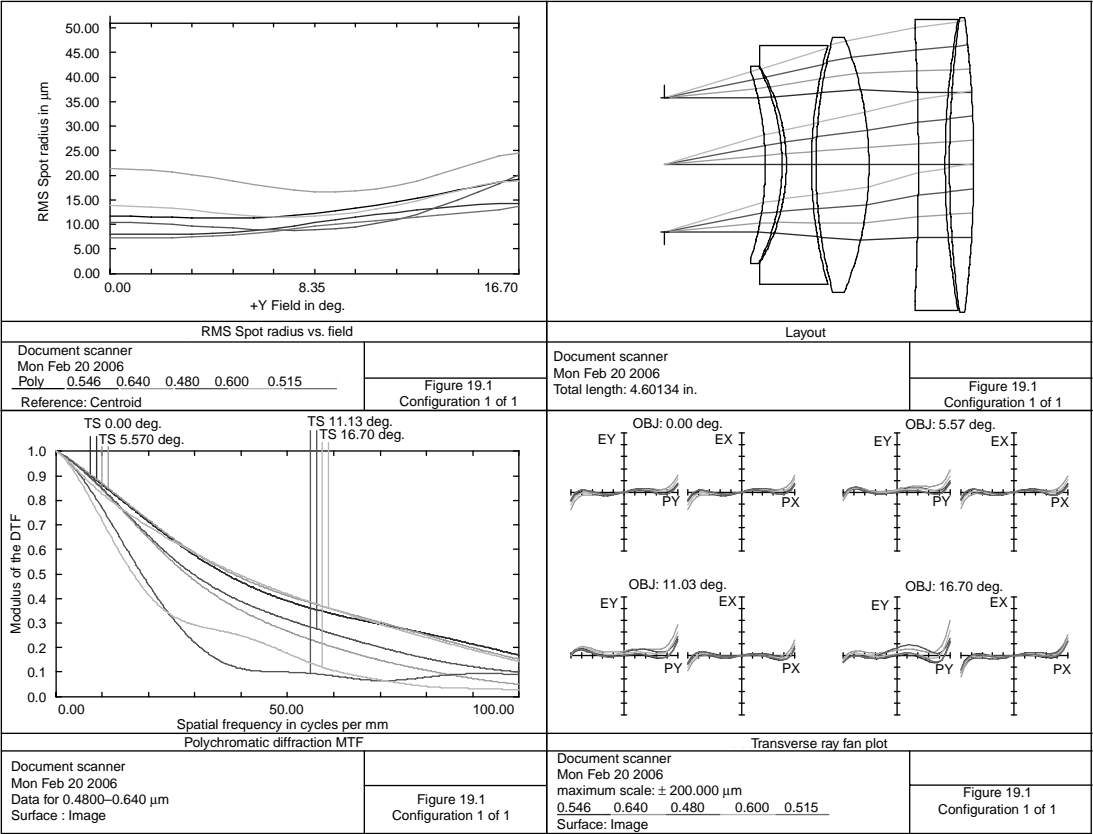


FIGURE 19.1 Document scanner.

---

**TABLE 19.1a**  
**Document Scanner**

Surface	Radius	Thickness	Material	Diameter
1	Stop	1.5000		2.000
2	−4.6415	0.2500	N-LAK22	2.840
3	−3.2759	0.0635		2.940
4	−2.9057	0.3732	N-ZK7	2.940
5	6.6019	0.0671		3.540
6	7.2933	0.7893	N-LAK22	3.780
7	−5.0900	0.7343		3.780
8	−40.7260	0.3978	SF1	4.160
9	12.1714	0.0645		4.320
10	15.9029	0.3617	N-LAK22	4.380
11	−17.7234	25.7694		4.380

Distance from entrance pupil to image = 30.371.

---



---

**TABLE 19.1b**  
**Image Heights vs. Scan Angle ( $\theta$ )**

$\theta$ (deg.)	Image Height
3.34	1.398
6.68	2.801
10.02	4.211
13.36	5.634
16.70	7.073

---

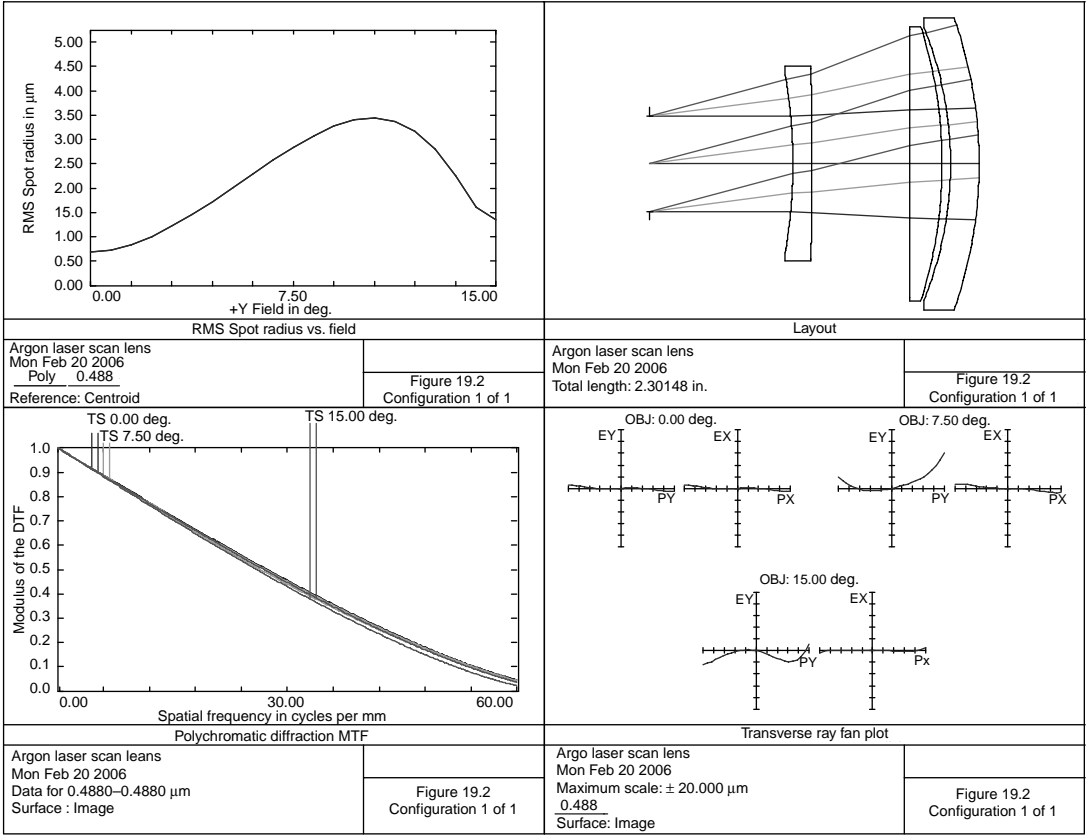


FIGURE 19.2 Argon laser scanner lens.



**TABLE 19.2a**  
**Argon Laser Scan Lens**

Surface	Radius	Thickness	Material	Diameter
1	Stop	1.0000		0.667
2	−3.5767	0.1300	F2	1.240
3	−68.8650	0.6884		1.360
4	0.0000	0.2242	SF1	1.920
5	−3.1420	0.0589		1.920
6	−2.5242	0.2000	SF1	1.900
7	−3.0566	23.4308		2.040

Distance from entrance pupil to image=25.732.

**TABLE 19.2b**  
**Image Heights vs. Scan Angle ( $\theta$ )**

$\theta$ (deg.)	Image Height
3.0	1.047
6.0	2.096
9.0	3.147
12.0	4.201
15.0	5.259

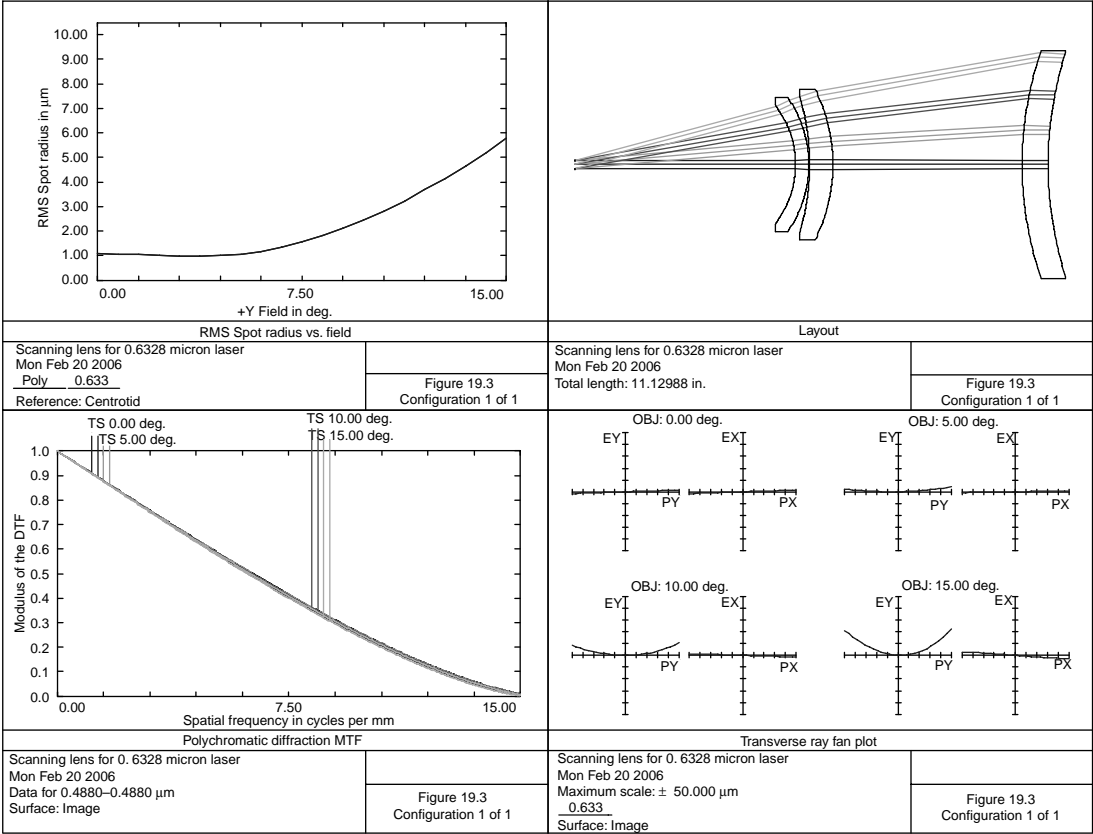


FIGURE 19.3 Scan lens 0.6328 μm.

**TABLE 19.3a**  
**Scanning Lens for 0.6328-μm Laser**

Surface	Radius	Thickness	Material	Diameter
1	Stop	5.0000		0.200
2	−2.2136	0.3000	SF57	2.720
3	−2.6575	0.0200		3.040
4	−5.5022	0.5292	SF57	3.160
5	−3.8129	4.2927		3.400
6	7.9951	0.5900	SF57	5.180
7	8.3654	18.0014		5.100

Distance from entrance pupil to image surface=28.733.

**TABLE 19.3b**  
**Image Heights vs. Scan Angle ( $\theta$ )**

$\theta$ (deg.)	Image Height
3.0	1.047
6.0	2.095
9.0	3.143
12.0	4.190
15.0	5.234

## REFERENCES

- Beiser, L. (1974) Laser scanning systems, In *Laser Applications*, Volume 2, Chapter 2, (M. Ross, ed.) Academic Press, New York.
- Beiser, L. (1992) *Laser Scanning Notebook*, SPIE Press, Bellingham, WA.
- Brixner, B. and Klein, M. M. (1992) Optimization to create a four-element laser scan lens from a five element design, *Optical Engineering*, 31: 1257–1258.
- Buzawa, M. J. and Hopkins, R. E. (1975) Optics for laser scanning, *Proceedings of SPIE*, 53: 9.
- Cobb, J. M., LaPlante, M. J., Long, D. C., and Topolovec, F. (1995) Telecentric and achromatic f-theta scan lens, US Patent #5404247.
- Fisli, T. (1981) High efficiency symmetrical scanning optics, US Patent #4274703.
- Gibbs, R. (2000) How to design a laser scanning system, *Laser Focus World*, 121.
- Griffith, J. D. and Wooley, B. (1997) High resolution 2-D scan lens, US Patent #5633736.
- Hopkins, R. (1987) Optical system requirements for laser scanning systems, *Optics News*, 11.
- Maeda, H. (1983) An f- $\theta$  lens system, US Patent #4401362.
- Maeda, H. (1984) An f- $\theta$  lens system, US Patent #4436383.
- Marshall, G. (1985) *Laser Beam Scanning*, Marcel Dekker, New York.
- Minami, S. (1987) Scanning optical system of the canon laser printer, *Proceedings of SPIE*, 741: 118.
- Murthy, E. K. (1992) Elimination of the thick meniscus element in high-resolution scan lenses, *Optical Engineering*, 31: 95–97.
- Sakuma, N. (1987) F- $\theta$  single lens, US Patent #4695132.
- Starkweather, G. (1980) High speed laser printing systems, In *Laser Applications*, Volume 4, (M. Ross, ed.) Academic Press, New York, p. 125.

---

# 20 Endoscope

Endoscopes are very long and narrow optical relay systems designed to probe interior parts of the body. The object medium is therefore water. Therefore, the front element is usually flat, thereby permitting the endoscope to view objects in air or in the body. Because endoscopes are used inside the body, they must be capable of being sterilized either by being placed in an autoclave or being immersed in a poisonous gas such as ethylene oxide. Because of their long and narrow arrangement, endoscopes are also used in industry as a means of inspecting the interior parts of deep bores. They are then called *borescopes*. A *laparoscope* is an endoscope fitted with instruments such that the surgeon may perform surgery while looking thru the endoscope.

In some systems, a front objective (the distal end of the probe) inside a small diameter stainless steel tube followed by a series of relay/field lenses is used to image the specimen onto a fiber optic bundle. This flexible bundle then transfers the image to its opposite end (the proximal end of the probe) where it is viewed with an eyepiece; alternatively, this image may be captured with a CCD to be conveniently viewed on a monitor. A separate fiber optic bundle is also used to provide illumination (Ouchi 2002). This provides a flexible system and is often preferred for medical examinations. To minimize trauma to the patient, diameters of the front rigid section are generally less than 3 mm (Remijan 2005).

In some medical applications it is desirable for the surgeon to be able to rotate the endoscope so that the field is scanned inside the patient's body. This is accomplished by means of a deviation prism placed in front of the objective (Lederer 2003).

Some of the earlier endoscopes were designed by separately designing the front objective and a relay. Several identical relay units were then assembled with the front objective to form a complete system. The problem with such a technique is that each relay is not completely corrected. When four or more such units are assembled, the aberrations are additive. All modern lens design programs have the ability to tie surfaces together. Thus, the entire system may be designed as a complete system. For example, in the following design, the curvature of surfaces 9, 15, and 21 were tied together. In this mode, the curvature of surface 9 is an independent variable; then curvatures 15 and 21 are set equal to it—likewise for surfaces 10, 16, and 22, as well as for 11, 17, and 23.

In [Figure 20.1](#) is shown an endoscope using rod lenses; data is provided in [Table 20.1](#). Such lens elements are very long in relation to their diameter. This helps in the mounting and assembly of the instrument. The thick lens feature also helps to reduce the Petzval sum (there is still an inward curving field) as well as spherical aberration. It has a field of view in water of  $50^\circ$  and is  $f/3$  (see Hopkins 1966).

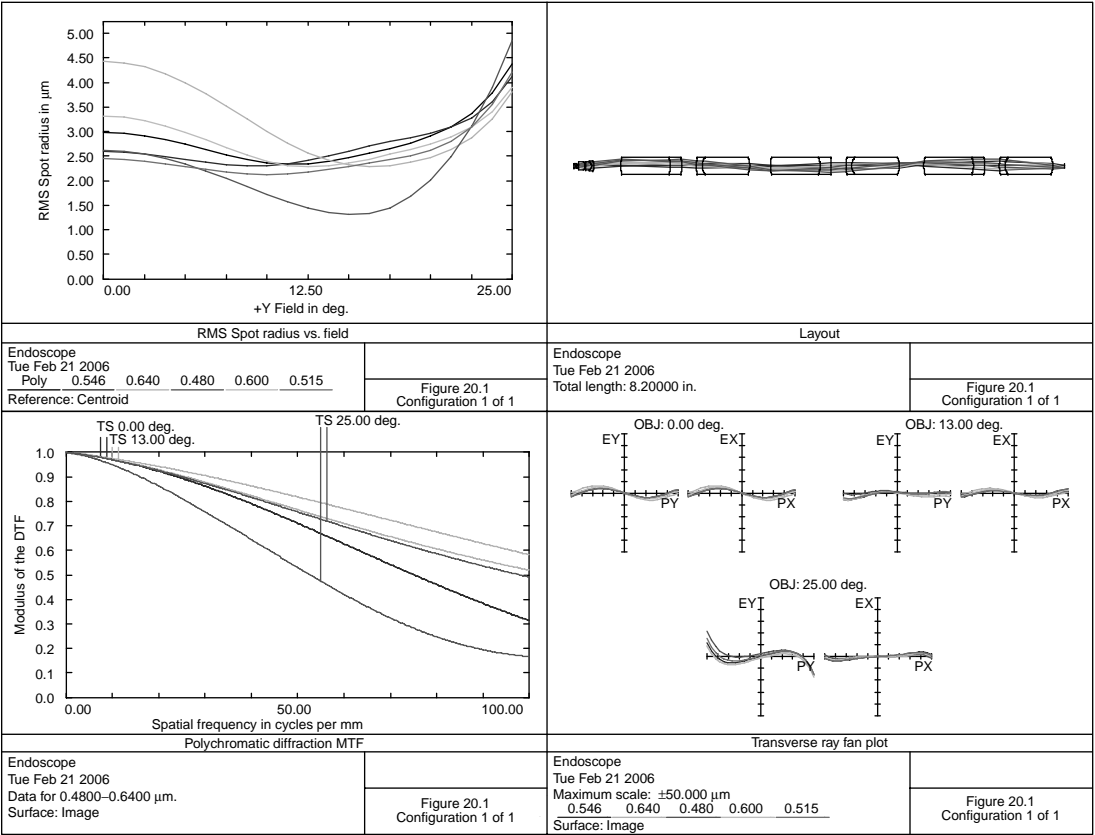


FIGURE 20.1 An  $f/3$  endoscope, rod lens.

**TABLE 20.1**  
**Endoscope, Rod Lens**

Surface	Radius	Thickness	Material	Diameter
0	0.0000	Infinity	Water	
1	0.0000	0.0310	N-BK7	0.080
2	0.0284	0.0334		0.050
3	Stop	0.0080		0.036
4	−0.3742	0.1139	N-LAK12	0.070
5	−0.0965	0.0050		0.140
6	0.7827	0.1050	SK16	0.140
7	−0.0842	0.0321	SF4	0.140
8	−0.3720	0.4515		0.166
9	0.5158	0.8304	N-LAF34	0.280
10	−0.3939	0.1884	SF4	0.280
11	−0.8018	0.2429		0.280
12	0.5380	0.0969	SF4	0.280
13	0.2073	0.7971	N-LAF34	0.280
14	−0.3509	0.3442		0.280
15	0.5158	0.8304	N-LAF34	0.280
16	−0.3939	0.1884	SF4	0.280
17	−0.8018	0.2429		0.280
18	0.5380	0.0969	SF4	0.280
19	0.2073	0.7971	N-LAF34	0.280
20	−0.3509	0.4087		0.280
21	0.5158	0.8304	N-LAF34	0.280
22	−0.3939	0.1884	SF4	0.280
23	−0.8018	0.2429		0.280
24	0.5380	0.0969	SF4	0.280
25	0.2073	0.7971	N-LAF34	0.280
26	−0.3509	0.2002		0.280

Distance from first lens surface to the image = 8.20, effective focal length = −0.067, distortion = 3.0%.

Note that the rear section, surfaces 9 thru 26, is divided into three identical modules: 9–14, 15–20, and 21–26. This is carried out in the optimization program by tying curvatures and thickness of the groups, 14–20 and 21–26 to the corresponding surfaces of the front section, surfaces 9–14. Also note the resemblance of the front objective, surfaces 1–8 to the Tachihara (1998) patent.

In [Figure 20.2](#) is shown an endoscope objective to image onto a 0.070 diameter fiber-optic bundle. The object distance is 0.2 and the object is in water, which is a close approximation to internal body fluids. The prescription is given in [Table 20.2](#).

Note from the MTF plot that this system is nearly diffraction limited. Effective focal length in air is 0.0658, with an f-number of 3.2; the overall length from object to the fiber bundle is 0.741. The distortion of 7.6% should not be a problem because the main function of this objective is the examination of the internal portions of the body.

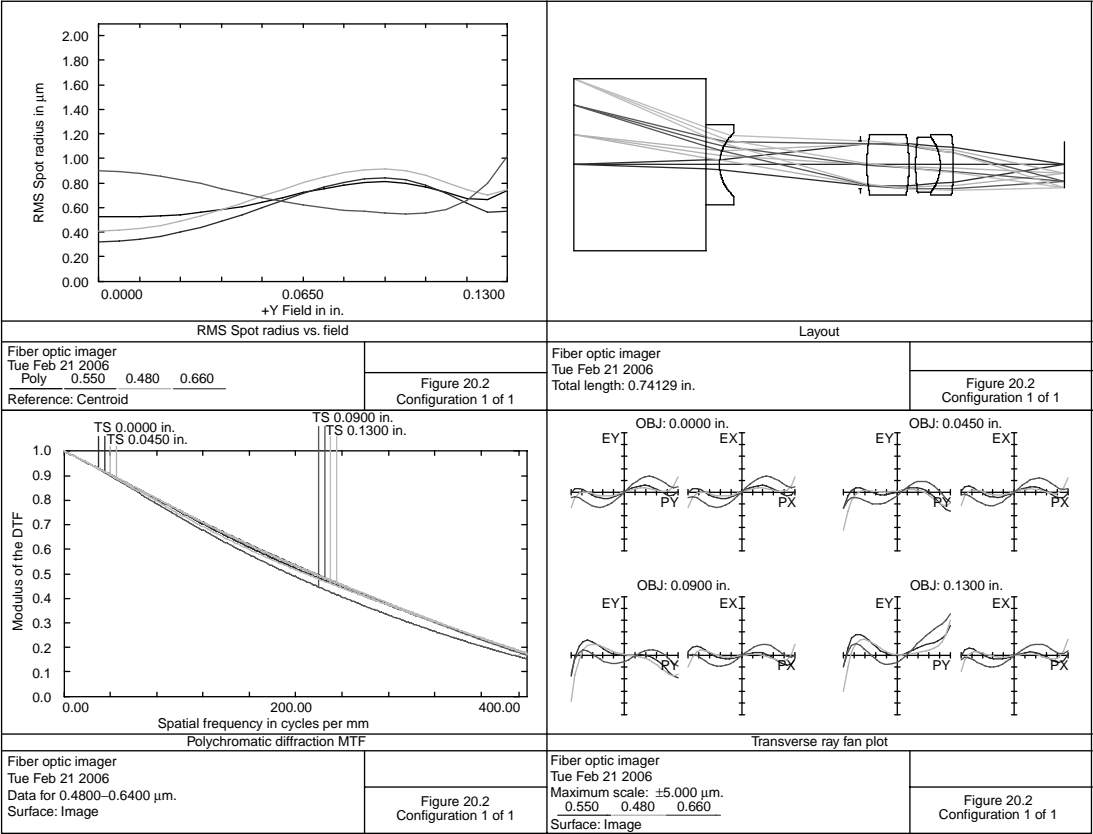


FIGURE 20.2 An endoscope, fiber-optic.



**TABLE 20.2**  
**Endoscope, Fiber Optic**

Surface	Radius	Thickness	Material	Diameter
0	0.0000	0.2000	Water	0.260
1	0.0000	0.0200	N-BK7	0.120
2	0.0642	0.2124		0.096
3	Stop	0.0100		0.073
4	0.2295	0.0637	N-LAK12	0.090
5	−0.2499	0.0100		0.090
6	0.2749	0.0372	N-SK16	0.084
7	−0.0690	0.0200	SF1	0.084
8	−0.3486	0.1680		0.090
9	0.0000	0.0000		0.070

Distortion = 7.6%.

Note that this is an inverted telephoto type design and is similar to the systems shown in Yamashita (1977, 1978).

## REFERENCES

- Hoogland, J. (1986) Flat field lenses, US Patent #4575195.
- Hopkins, H. H. (1966) Optical system having cylindrical rod-like lenses, US Patent #3257902.
- Lederer, F. (2003) Endoscope objective, US Patent #6635010.
- Nakahashi, K. (1981) Optical system for endoscopes, US Patent #4300812.
- Nakahashi, K. (1983) Objective for endoscope, US Patent #4403837.
- Ono, K. (1998) Image transmitting optical system, US Patent #5731916.
- Ouchi, T. (2002) Probe of endoscope, US Patent #6497653.
- Remijan, P. and McDonald, J. (2005) Miniature endoscope with imaging fiber system, US Patent #6863651.
- Rol, P., Jenny, R., Beck, D., Frankhauser, F., and Niederer, P. F. (1995) Optical properties of miniaturized endoscopes of ophthalmic use, *Optical Engineering*, 34: 2070.
- Tachihara, S. and Takahashi, K., (1998) Objective lens for endoscope, US Patent #5724190.
- Tomkinson, T. H., Bentley, J.L., Crawford, M. K., Harkrider, C. J., Moore, D. T., and Rouke, J. L. (1996) Ridgid endoscopic relay systems: A comparative study, *Applied Optics*, 35: 6674.
- Yamashita, N. (1977) Retrofocus type objective for endoscopes, US Patent #4042295.
- Yamashita, N. (1978) Optical system for endoscope, US Patent #4111529.



---

# 21 Enlarging and Copying Lenses

Enlarging and copying lenses all show some degree of symmetry and are used to project film onto sensitized paper (or other photosensitive medium). The enlarging lenses generally cover magnification ratios 2–8 or 8–16. The later case is for enlarging 35-mm single-lens reflex (SLR) film to 8×10 or 11×14 in. prints. F-numbers are usually  $f/2.8$  or larger.

Due to the sensitivity of many photographic papers to wavelengths shorter than 0.4  $\mu\text{m}$ , it is desirable to select glasses such that any energy below this wavelength is absorbed. (It is also very difficult to correct lens aberrations at these shorter wavelengths.) Conversely, the system must show high transmission at wavelengths longer than 0.4  $\mu\text{m}$ .

Figure 21.1 shows an enlarging lens designed for 10× magnification; details are given in Table 21.1. It is designed to cover a 44-mm diagonal image (35-mm SLR format). Focal length is 2.56.

This double-Gauss design would represent a “premium” lens for the professional photographer. Note that from the MTF plot, resolution is more than adequate at full aperture. A lower-priced lens would be a Tessar-type design (of the type shown in Figure 4.2) or, for even lower cost, a three-element  $f/5.6$ . This is the most popular type for amateur use. It yields best performance when stopped down to  $f/8$ . Most enlarging lenses have an iris with a maximum f-number of 32. Focal lengths longer than 150 mm generally have an iris to cover the range  $f/5.6$ – $f/45$ .

By using a completely symmetrical lens system, the transverse aberrations of distortion, coma, and lateral color may be completely eliminated.

Figure 21.2 shows a symmetric optical system. Due to symmetry, the chief ray—A, B, C, D—has a height at the object of  $H$  and a height at the image of  $H' = H$ . Because this is true for all obliquities and wavelengths, there is neither distortion nor lateral color.

Again, by symmetry, the upper and lower rim rays in image space are identical to their values in object space, thereby eliminating coma. Because each half of the system is not necessarily coma corrected, the chief ray is not parallel to the upper and lower rim rays at the aperture stop.

In Figure 21.3 is shown a copy lens for unit magnification; details are provided in Table 21.2. It is completely symmetrical about the stop, thus removing the transverse 14.1) aberrations of coma, distortion, and lateral color (see also the 1–1 relay of Figure 14.1).

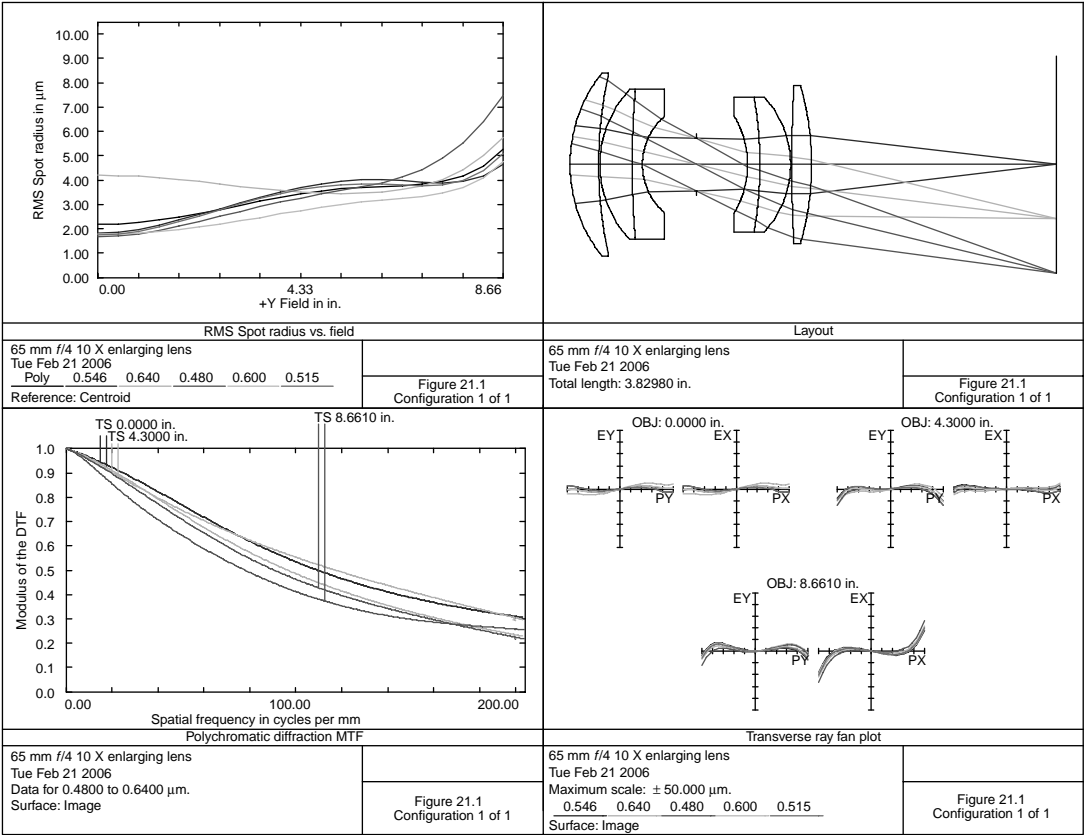
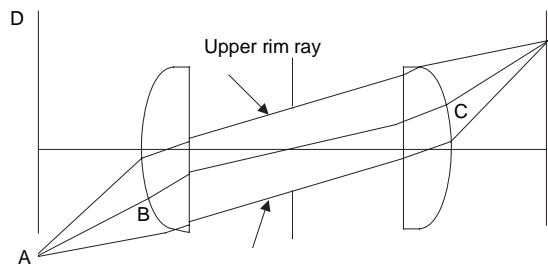


FIGURE 21.1 A 65-mm  $f/4$  10 $\times$  enlarging lens.

**TABLE 21.1**  
**A 10× Enlarging Lens**

Surface	Radius	Thickness	Material	Diameter
0	0.0000	26.5300		17.322
1	1.1627	0.2251	N-LAF2	1.440
2	3.3074	0.0100		1.380
3	0.8557	0.2544	N-BK7	1.180
4	7.2703	0.0800	F4	1.180
5	0.5018	0.4228		0.760
6	Stop	0.4051		0.410
7	−0.7320	0.0963	SF1	0.760
8	−3.1346	0.2416	N-LAK7	1.060
9	−0.7830	0.0100		1.060
10	12.3715	0.1557	N-LAF2	1.240
11	−2.2678	1.9288		1.240

Distance from first lens surface to image = 3.830, distortion at the edge = 0.5%.



**FIGURE 21.2** A symmetric optical system.

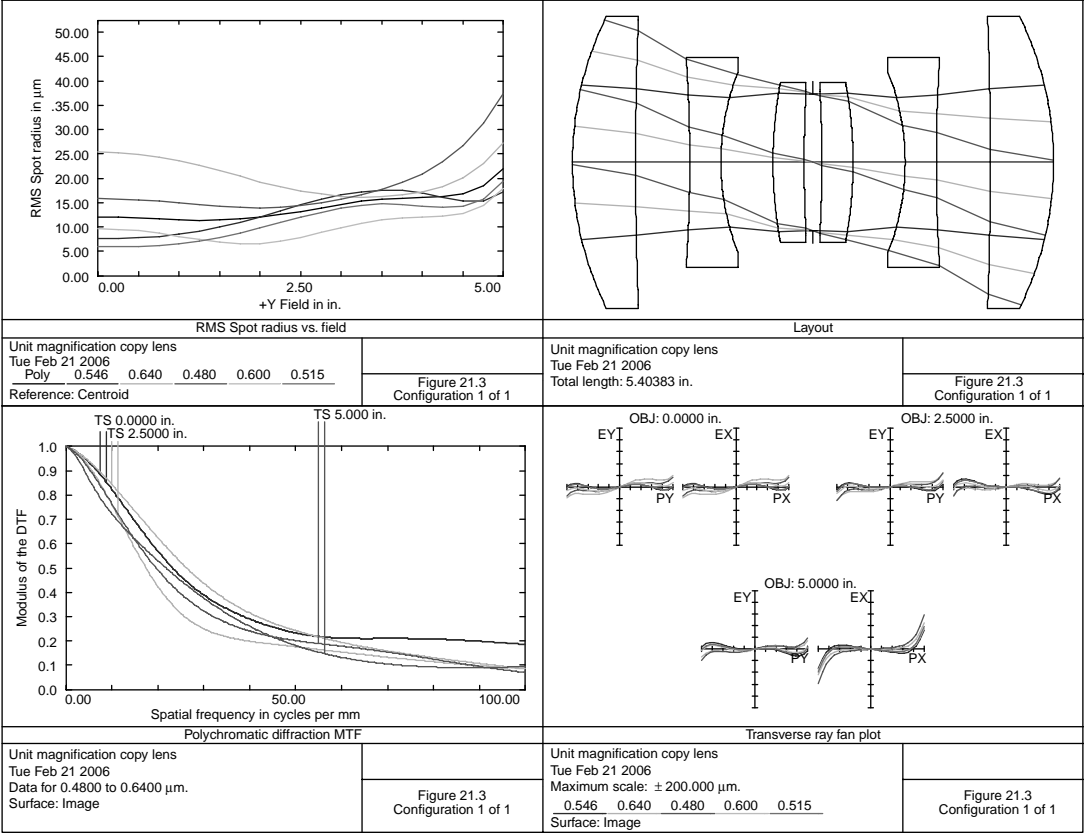


FIGURE 21.3 Unit magnification copy lens.

**TABLE 21.2**  
**Unit Magnification Copy Lens,  $f/4.58$**

Surface	Radius	Thickness	Material	Diameter
0	0.0000	15.7961		10.000
1	3.7078	0.7091	N-LAK33	3.280
2	42.2542	0.6081		3.280
3	−17.9061	0.3500	F4	2.360
4	2.7669	0.5847		2.020
5	4.7944	0.3500	N-LAK33	1.800
6	14.4922	0.1000		1.640
7	Stop	0.1000		1.543
8	−14.4922	0.3500	N-LAK33	1.640
9	−4.7944	0.5847		1.800
10	−2.7669	0.3500	F4	2.020
11	17.9061	0.6081		2.360
12	−42.2542	0.7091	N-LAK33	3.280
13	−3.7078	15.7961		3.280

Object to image distance = 36.996, focal length = 9.461.

## REFERENCES

- Kouthoofd, B. J. (1998) Enlarging lens with a large working distance, US Patent #5724191.  
 Lynch, G. B. (1965) Symmetrical copy lens of the inverse gauss type, US Patent #3439976.  
 Matsubara, M. (1977) Enlarging lens system, US Patent #4045127.  
 Matsubara, M. (1977) Enlarging lens system, US Patent #4057328.  
 Matsubara, M. (1977) Enlarging lens system, US Patent #4013346.  
 Velesik, S. (1975) Reproduction lens system, US Patent #3876292.





---

# 22 Projection Lenses

Although it is true that a camera lens can be used as a projection lens, a projection lens does have several differences from a camera lens:

1. They must be able to withstand the high power densities encountered in projection. (This assumes film projection. See discussion for [Figure 22.6](#), an liquid crystal display (LCD) projection lens.) This is particularly true when a high-wattage xenon arc is being used. There is usually no problem with coatings; the problem is with optical cements. Canada Balsam is totally unsuitable and, fortunately, this is rarely used today. “Lens Bond,” a thermosetting optical cement made by Summers Labs (Fort Washington, PA) works very well. It is a polyester resin. Versions are available for room-temperature curing, oven curing, and curing with a UV lamp. They meet the requirements of MIL-A-3920 with  $N_d=1.55$ . A similar material is made by Norland Optical (New Brunswick, NJ).

Epoxy cements are also sometimes used. These materials can withstand very high temperatures. A material that the author has found to be very useful is Hysol OSO-100. Parts must be cured overnight at 100 °C.  $N_d$  is 1.493. Lenses can withstand temperatures to 125 °C. Another useful material is TRA-BOND F114, Tracon Inc., Medford, Massachusetts. The  $N_d$  for this compound is 1.54. Useful over the temperature extremes –60°F to 130°F after a 24-h room-temperature cure.

2. An iris is not needed. These lenses have a fixed aperture stop.
3. Sufficient back focus must be provided to clear the film transport mechanism. This generally eliminates a field-flattening lens near the film plane ANSI (1982).
4. The lens exit pupil must correspond to a source image of the lamp. This is typically 4.0 in. from the film plane for xenon arc 70-mm projectors. About 2.2 in. are necessary for academy (35-mm) format projection.
5. Because the projection distance is always at least 100 focal lengths, projection lenses are frequently designed for infinite conjugates. This can sometimes be a dangerous mistake because, for wide-angle lenses with appreciable distortion, the lens aberrations are strongly influenced by conjugate distances. See comments regarding this in [Chapter 9](#). All designs in this section are presented for an infinite conjugate and the user is advised to check performance at the actual conjugate distance.
6. The screen is generally a cylinder and curved toward the audience. This radius is usually between 0.8 and 1.5 times the lens-to-screen distance. On a first-order basis, the film should be on a radius same as the screen radius.

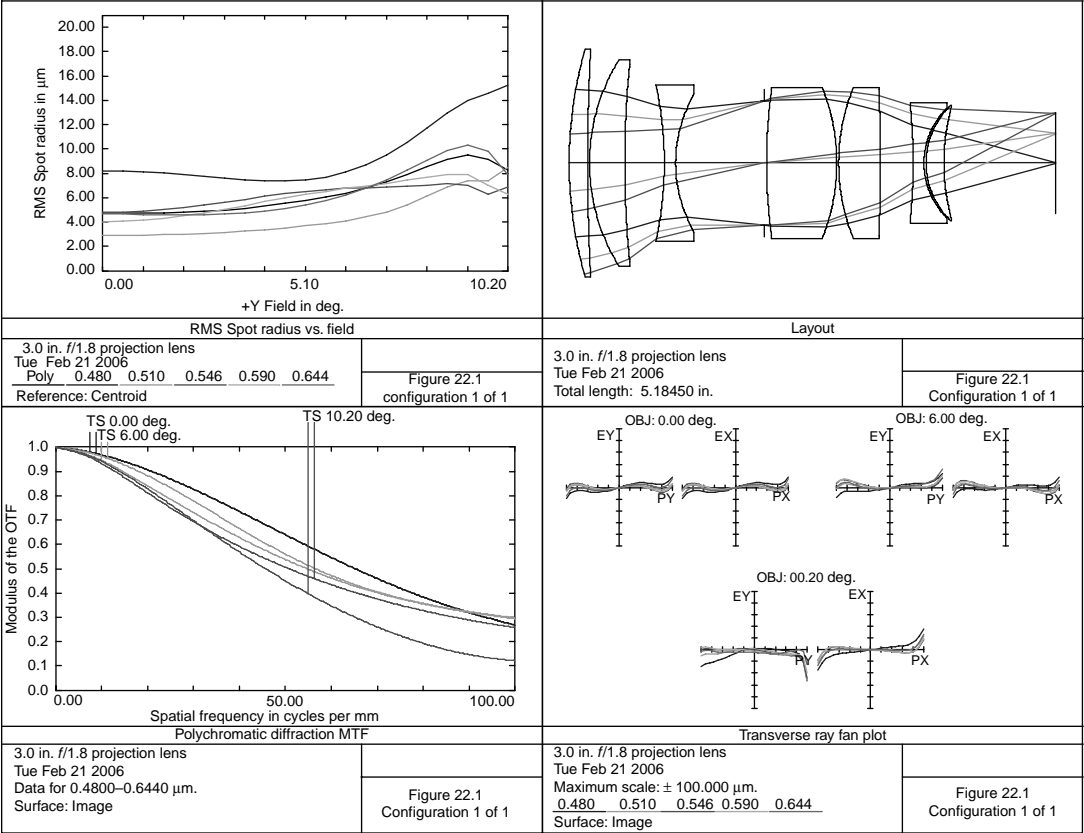


FIGURE 22.1 An  $f/1.8$  projection lens.

**TABLE 22.1**  
**A 3.0-in. *f*/1.8 Projection Lens**

Surface	Radius	Thickness	Material	Diameter
1	4.4446	0.1958	N-SK4	2.420
2	23.4433	0.0200		2.420
3	2.0828	0.3770	N-LAK7	2.200
4	11.1061	0.4202		2.100
5	−3.9104	0.1201	SF5	1.670
6	1.4530	0.9483		1.469
7	Stop	0.0206		1.331
8	5.6967	0.7482	N-LAK7	1.600
9	−2.1597	0.0200		1.600
10	2.1290	0.4441	N-LAK7	1.600
11	−20.2216	0.3497		1.600
12	−6.0474	0.1157	F2	1.276
13	0.8242	0.0223		1.177
14	0.8495	0.1892	N-SK4	1.220
15	2.2429	1.1932		1.180
16	0.0000	0.0000		1.067

Distance from first lens surface to film=5.185, distortion=1.1%.

However, because this radius is very long as compared to the film width, a flat film surface is generally used.

Projectors made by Pioneer have a 50-in. cylindrical radius (center of curvature is toward the arc). Likewise, the IMAX projector has a 18.78 cylindrical radius that requires a cylindrical field lens on the projection lens side. Strong–Ballantine projectors have a flat gate.

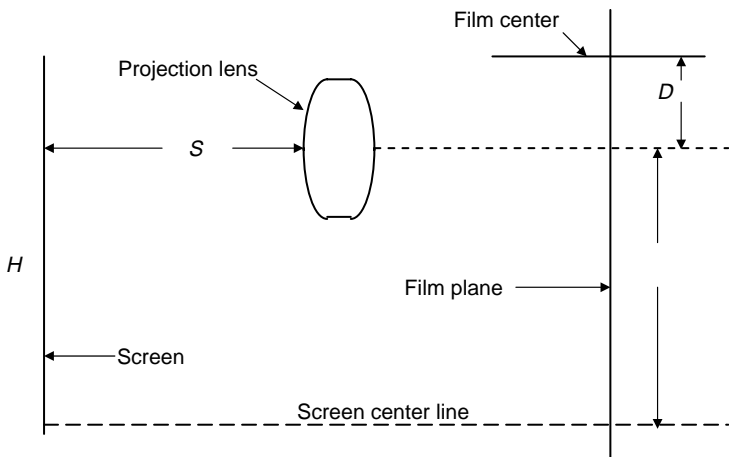


**FIGURE 22.2** Displaced projection lens.

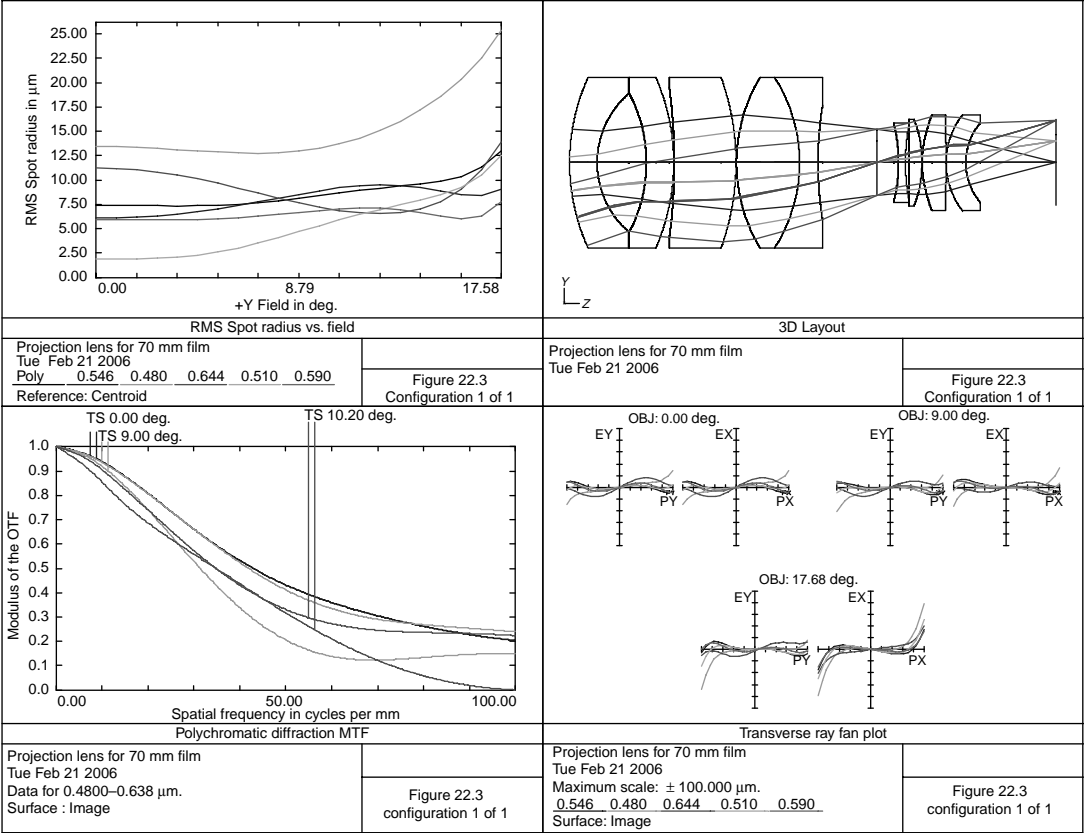


FIGURE 22.3 Projection lens, 70 mm film.

**TABLE 22.2**  
**Projection Lens for 70-mm Film**

Surface	Radius	Thickness	Material	Diameter
1	5.4309	0.7220	N-FK5	4.460
2	2.3942	1.2934		3.620
3	−3.8629	0.7140	SF5	3.620
4	−5.5409	0.0115		4.460
5	−16.0642	1.6219	N-LAK9	3.940
6	−6.5538	0.0134		4.460
7	4.3769	1.6521	N-LAK10	4.460
8	−4.1619	0.4850	F2	4.460
9	9.8038	1.5399		3.000
10	Stop	0.5755		1.732
11	−3.8829	0.1769	SF4	1.920
12	5.4280	0.0844		2.080
13	35.4552	0.3503	N-LAK10	2.280
14	−3.2140	0.0100		2.280
15	3.2160	0.6218	N-LAK9	2.520
16	−36.2242	0.0004		2.520
17	2.0680	0.5136	N-LAK9	2.520
18	1.6121	2.3729		2.100

Distance from first lens surface to image = 12.759, distortion = 1.4%.

7. ANSI 196M calls for 16 ft. Lamberts screen illuminance. Although the eye resolves 1 min arc at 100 ft. Lamberts, its resolution drops to 2 min arc at 16 ft. Lamberts screen illuminance. If an observer was in the rear of the theater (at the projector) his angular resolution,  $\theta$ , would be

$$\theta = \frac{1}{RF},$$

where  $R$  is the resolution at the film in lp/mm and  $F$  is the focal length of the projection lens (in mm). This applies to an observer at the rear. At the front of the theater, an observer will always see an aberrated image (if the lens was perfect, he would see the magnified image of the film grain). A compromise then is to achieve a resolution at the middle of the theater of 2 min of arc. This is equivalent to 1 min arc =  $1/RF$  at the center of the field of the projection lens. At 30° off-axis (as seen by an observer at the center of the theater), the resolution could be reduced to 5 min arc. See SMPTE (1994) as a guide to projected image quality.

A very useful program (Theater Design Pro 2.1b from Schneider Optics) is available as a download on the internet (<http://www.schneideroptics.com>).

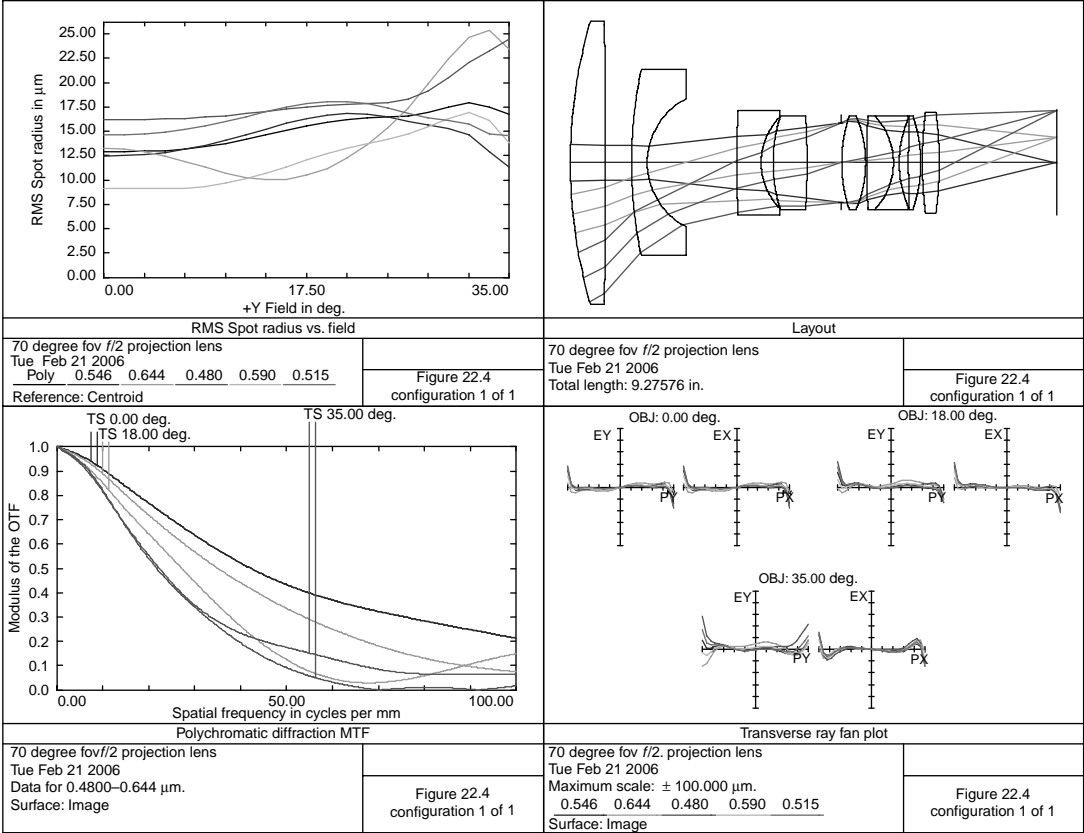


FIGURE 22.4 A 70° FOV projection lens, *f*/2.

**TABLE 22.3**  
**A 70° FOV, *f*/2 Projection Lens for 70-mm Film**

Surface	Radius	Thickness	Material	Diameter
1	9.7275	0.6688	N-SK14	5.400
2	−158.3779	0.4966		5.400
3	8.6145	0.2988		3.540
4	1.3766	1.7130	SF2	2.440
5	43.1382	0.4576		2.000
6	1.2346	0.2277		1.720
7	2.9000	0.6500	SF6	1.780
8	−13.0235	0.6425		1.780
9	Stop	0.0160		1.528
10	2.8503	0.4583	N-LAF2	1.780
11	−2.2679	0.0199		1.780
12	19.4831	0.5086		1.780
13	−1.2952	0.1100	SF6	1.780
14	2.1446	0.1754		1.660
15	25.7344	0.2334		1.780
16	−2.7763	0.0322	N-LAK9	1.780
17	7.8016	0.3218		1.920
18	−7.4907	2.2454		1.920

Distance from front lens surface to image=9.276, distortion=4.7% (at full field).

Figure 22.1 shows a 3-in. Focal length (FL) *f*/1.8 lens designed to project 35-mm motion-picture film (1.07-in. diagonal); details are given in Table 22.1. It is a modification of Mittal, Gupta, and Sharma (1990).

The exit pupil is located −2.204 in. from the image surface. Note that this is a seven-element lens whereas the lens shown in Figure 39.3 has similar performance with one less element but one of the elements is a gradient index material.

In most movie theaters, the projector is nearly at the screen centerline. However, there are times when the projector is substantially above the screen centerline. For certain situations, having the projector above the audience allows a more efficient theater design. Unfortunately, it causes keystone distortion: A square is projected as a trapezoid. For some cases this may not be objectionable. It may be eliminated by displacing the lens with respect to the film centerline. This is shown in Figure 22.2.

You will note that the lens is “dropped” a distance *D* below the film centerline:

$$D = \frac{FH}{S - F},$$

where *F* is the projection lens focal length.

This then images the film center into the screen center. Although this arrangement has the desirable effect of eliminating keystone distortion, it means

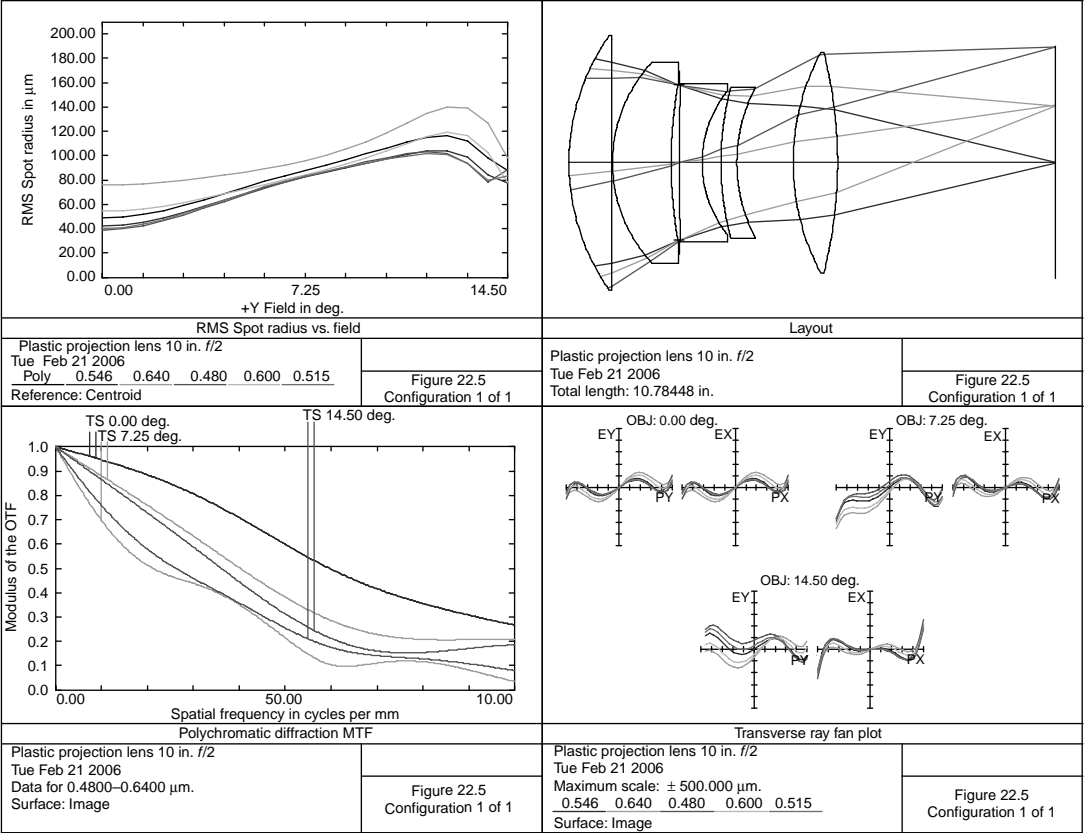


FIGURE 22.5 Plastic projection lens.



**TABLE 22.4**  
**Plastic Projection Lens**

Surface	Radius	Thickness	Material	Diameter
1	4.9281	0.9544	Acrylic	5.640
2	0.0000	0.0100		5.640
3	3.2798	1.3000	Acrylic	4.460
4	10.0724	0.1770		3.500
5	Stop	0.0100		3.445
6	151.2944	0.4995	Polystyrene	3.500
7	2.5623	0.4160		3.200
8	6.4575	0.3534	Polystyrene	3.360
9	3.5922	1.2481		3.320
10	5.1956	0.9839	Acrylic	4.880
11	-9.8660	4.8321		4.880

Distance from first lens surface to image = 10.784.

that the projection lens must be designed for a larger field of view (FOV) than normal. The Kodak 3D theater at the Epcot Center in Florida uses this principle. In this case, two projectors 5.5 ft. (horizontal) apart are used to project 70-mm film. Each projector has a Polaroid sheet in front of the lens and the viewers wear

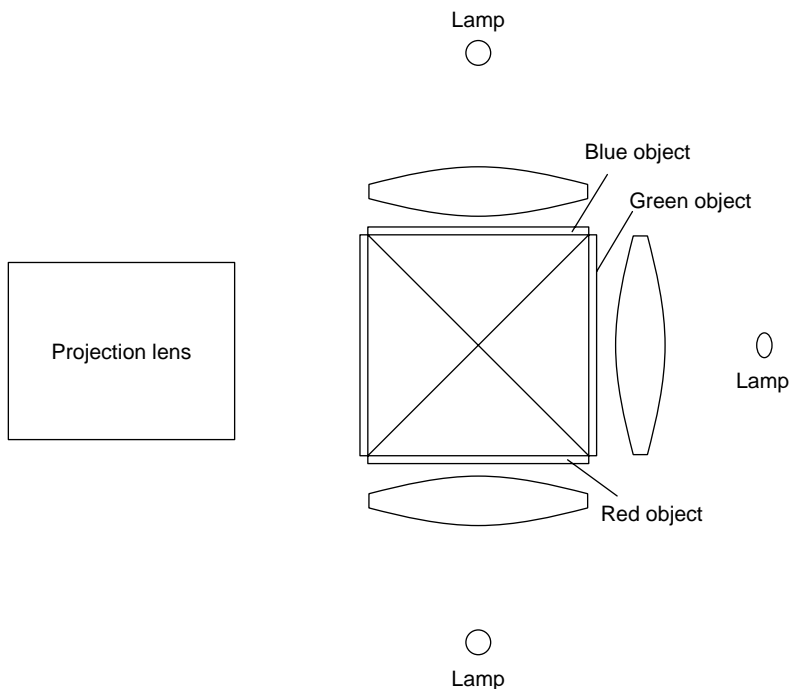


**FIGURE 22.6** LCD projection.

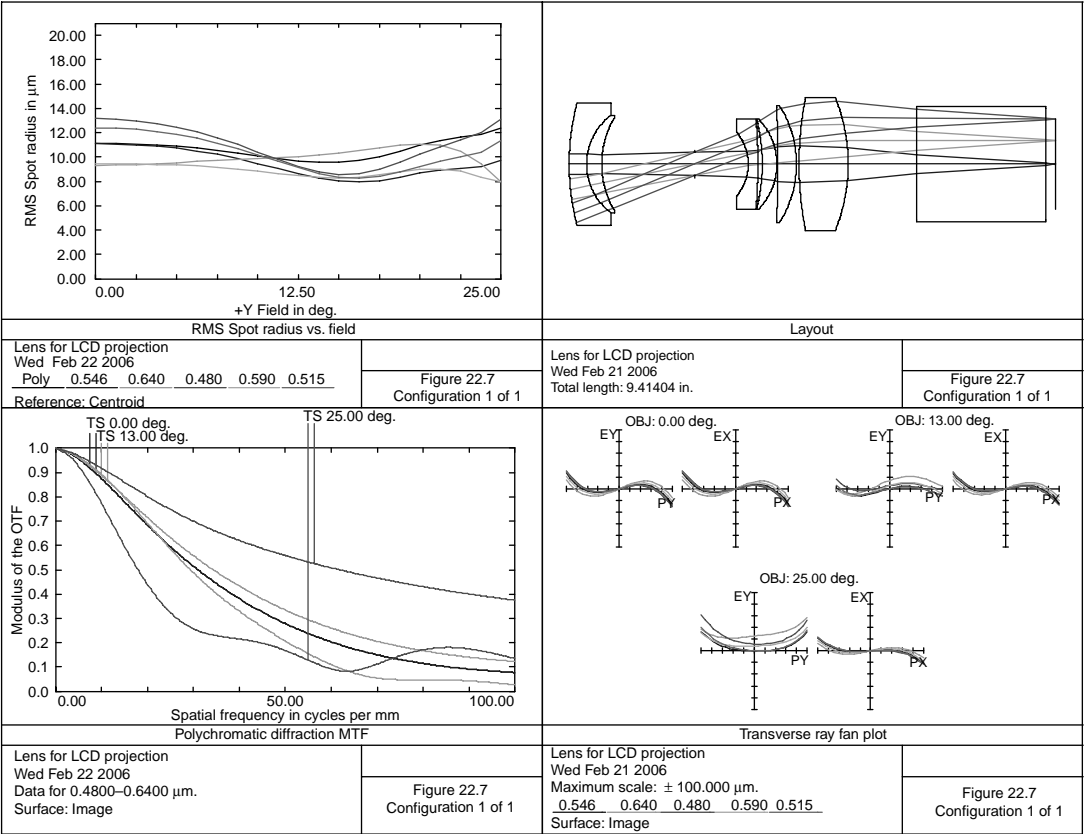


FIGURE 22.7 A 2-in. FL LCD projection lens.

**TABLE 22.5**  
**Lens for LCD Projection**

Surface	Radius	Thickness	Material	Diameter
1	4.7221	0.3368	N-PSK3	2.360
2	1.1775	0.2929	SF4	1.880
3	1.7742	1.8001		1.780
4	Stop	1.0330		0.449
5	−0.9642	0.1874	SF1	1.240
6	−10.7044	0.0858		1.740
7	−3.3891	0.2821	N-PSK53	1.680
8	−1.2436	0.0175		1.740
9	−26.6036	0.3617	N-PSK53	2.260
10	−2.0923	0.0486		2.260
11	6.4289	0.9514	N-PSK3	2.560
12	−3.4142	1.3166		2.560
13	0.0000	2.5000	N-BK7	2.220
14	0.0000	0.2000		2.220
15	0.0000	0.0000		1.751

Distortion = 6.4%.

polarizing glasses. Both images must be accurately registered over the entire screen. However, due to the projector separation, distortion at the edge of the field will be different for each projector (See [Figure 22.2](#)).

$$\begin{aligned} S &= 1236 \\ F &= 3.594 \\ H &= 33 \\ D &= 0.096. \end{aligned}$$

Referring to [Appendix A](#) the standard for 65-mm film is 1.912×0.870. Due to the lens displacement (in this case a horizontal displacement), the lens has to cover an additional horizontal amount of 2*D*. This corresponds to a diagonal of 2.277. This *f*/2 lens is shown in [Figure 22.3](#) and detailed in [Table 22.2](#).

The entrance pupil is 4.747 from the first lens surface. The exit pupil is −3.974 from the image (film) surface. Note that the diameters of the front lenses were made the same as this simplifies the lens housing design.

[Figure 22.4](#) shows a 70° FOV, *f*/2 projection lens for 70-mm film; details are provided in [Table 22.3](#). The effective focal length (EFL) is 1.5.

Exit pupil is −3.854 from the film. Referring to the root mean square (RMS) spot size plot in [Figure 22.4](#), note at 35° off-axis there is a RMS spot size of about

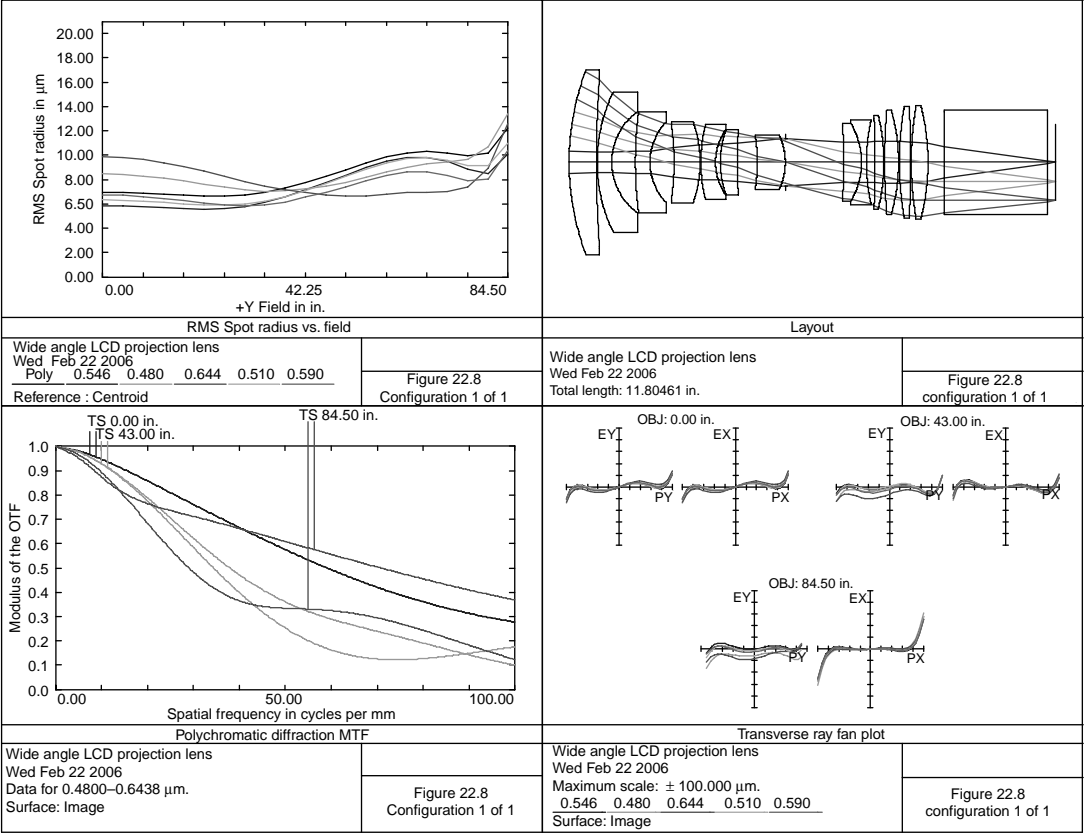


FIGURE 22.8 Wide-angle LCD projection lens.

**TABLE 22.6**  
**Wide-Angle LCD Projection Lens**

Surface	Radius	Thickness	Material	Diameter
0	0.0000	120.0000		169.000
1	6.3798	0.6603	N-PSK53	4.480
2	28.0523	0.0200		4.200
3	3.8816	0.3529	N-SK16	3.420
4	1.5168	0.5746		2.460
5	10.3990	0.3532	N-SK16	2.460
6	1.4210	0.5840		1.940
7	−6.3914	0.6299	N-LAK9	1.900
8	−2.9677	0.0200		1.960
9	3.7015	0.3541	N-LLF6	1.820
10	1.3587	0.1199		1.560
11	2.3754	0.4096	SF1	1.600
12	12.5928	0.4880		1.460
13	−3.7905	0.6745	N-PSK53	1.260
14	−1.6187	0.0200		1.320
15	Stop	1.3945		1.141
16	−18.6335	0.4372	N-PSK53	1.800
17	−1.8339	0.1180	SF4	1.880
18	4.5565	0.2057		2.060
19	−31.0074	0.2169	N-SK11	2.160
20	−4.8505	0.0200		2.280
21	15.7468	0.3374	N-PSK53	2.540
22	−4.6006	0.0200		2.540
23	7.6608	0.2685	F2	2.700
24	−39.0266	0.0200		2.700
25	8.1198	0.4054	N-PSK53	2.740
26	−5.5775	0.4000		2.740
27	0.0000	2.5000	N-BK7	2.520
28	0.0000	0.2000		2.520
29	0.0000	0.0000		1.852

Distance from first lens surface to image=11.805.

17 μm at the film. Someone in the rear of the theater would see an angular resolution at the corner of the screen of

$$\theta = \frac{0.017}{38.1} = 0.00045 = 1.5 \text{ min arc.}$$

As discussed above, a patron in the center of the theater would have an angular resolution of 3 min arc at the corner of the screen. This is adequate for most applications.

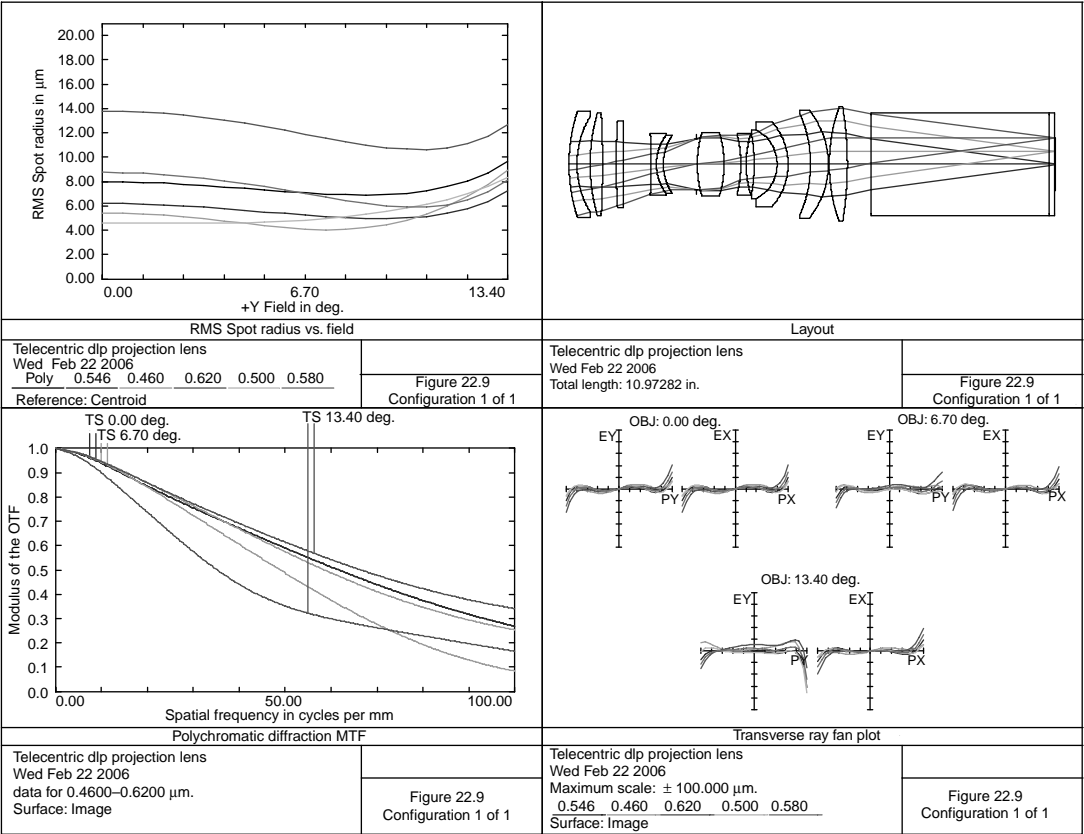


FIGURE 22.9 DLP projection lens.

**TABLE 22.7**  
**DLP Projection Lens**

Surface	Radius	Thickness	Material	Diameter
1	3.8544	0.1800	N-PSK53	2.400
2	2.1242	0.2966		2.200
3	4.1824	0.2798	N-LAF2	2.300
4	−22.2563	0.3072		2.300
5	15.4857	0.1577	N-LASF44	1.940
6	67.3299	0.6293		1.940
7	−14.8143	0.1200	N-PSK53	1.400
8	1.1074	0.1575	SF6	1.300
9	1.2006	0.7442		1.300
10	Stop	0.0200		1.158
11	2.5703	0.6034	N-LASF44	1.420
12	−2.4779	0.3775		1.420
13	−2.8356	0.1200	SF6	1.340
14	2.3240	0.1836		1.380
15	−3.5648	0.5151	N-FK51	1.380
16	−0.8775	0.2473	N-LASF44	1.560
17	−1.4332	0.5068		1.900
18	−2.8313	0.4021	N-PSK53	2.260
19	−1.9252	0.0200		2.440
20	3.8805	0.4084	N-PSK53	2.580
21	−7.9281	0.5226		2.580
22	0.0000	4.0354	N-BK7	2.300
23	0.0000	0.1181	N-ZK7	2.300
24	0.0000	0.0200		2.300
25	0.0000	0.0000		1.185

Distance from first lens surface to prism = 6.800, distortion = 0.61%.

Figure 22.5 shows a plastic projection lens (10-in. focal length,  $f/2$ ) designed to project images from a 5-in. diameter CRT tube. Details are given in Table 22.4. Plastic was chosen because the client wanted a lens that could be injection molded for high-volume, low-cost production. Because of the relatively low power densities, the use of plastics is not precluded.

The aperture stop is located between the second and third lenses. This is simply the spacer between these two lenses. Distortion is very low; a maximum of 0.27% at  $11^\circ$ , and nearly zero at full field. Note from the layout that there is vignetting of the lower rim ray at full field. This should cause only slight loss in illumination at full field.

The acrylic material is poly(methylmethacrylate) (PMMA) and is commercially available as Plexiglas<sup>®</sup> made by Rhom; an equivalent, Lucite<sup>®</sup>, is made by Lucite International. Both Plexiglas<sup>®</sup> and polystyrene are thermoplastic and are the most

common materials used in injection molding. As discussed earlier under aspheric surfaces, this type of injection-molded lens is an ideal candidate for aspheric surfaces.

Figure 22.6 shows an arrangement to project a LCD Watanabe (1999) and Meuret and De Visschere (2003) discusses other beam-splitting systems including a polarizing cube. The dielectric coatings selectively reflect (and transmit the complement) red, green, and blue images from the liquid crystal. Due to the properties of the dichroic coatings of the beam combiner, the lens should be nearly telecentric.

A lens suitable for LCD projection is shown in Figure 22.7 and detailed in Table 22.5. Focal length is 2.0 in. and the lens is  $f/5$ . It is a modification of Taylor (1980). It projects an image of 1.75" diameter. Length, first lens surface to image is 9.414 in.

Due to the fact that there are actually three light sources with their own object surfaces, one may compensate for color differences in the three primary colors (red, green, and blue) by moving the relative positions of these objects. In the above design and the following designs, this was not done.

Because this lens and the next two are often used to project images from a computer by projecting onto a screen, considerable keystone results. To prevent this, these lenses are designed to cover a format larger than required so that the lens may be shifted vertically and thus reduce the keystone effect. (See Figure 22.2 for a theater version of this principal.)

In Figure 22.8 is shown a wide-angle LCD projection lens; details are provided in Table 22.6. It uses the same glass block as the above lens, however in this optimization, a finite conjugate distance was chosen of 120 in. Distortion is a maximum at 0.8 field of 1.46% and drops to 1.03% at the edge of the field. It is  $f/2.5$  and has a focal length of 1.356.

Texas Instruments has developed a digital micromirror device (DMD) consisting of about a million small mirrors (each about  $15\ \mu\text{m}^2$ , and  $17\ \mu\text{m}$  center to center distance) on a semiconductor chip (Stupp and Brennesoltz 1999). Each mirror represents one pixel of screen resolution and can be tilted toward or away from the light to create a light or dark pixel. Because these pixels can be switched several thousand times a second, one gets the impression of a continuous image.

To convert the monochrome image into full color, a rapidly spinning color wheel is interposed between the light source and the chip. A more common method of obtaining a full color image is the use of a three chip system in which separate chips are used for each of the primary colors and combined together with a prism (Dewald 2000). A two-chip system is also used in which one chip is continuously illuminated with red light while the other chip is alternately illuminated with blue and green light (see the Caldwell reference in Chapter 35). These projectors are generally set on a table and projected upward; to avoid a keystone image, the lens is shifted in relation to the image center (see Figure 22.2).

In Figure 22.9 is shown such a projection lens. Details are given in Table 22.7. It has a focal length of 2.5 and is  $f/2.4$ . It is telecentric and has a FOV of  $26.8^\circ$ .



## REFERENCES

- ANSI (1982) *Dimensions for 35 and 70 mm Projection Lenses*, American National Standards Institute, 1430 Broadway, New York.
- ANSI (1986) *Screen Illuminance and Viewing Conditions*, American National Standards Institute, 1430 Broadway, New York.
- Betensky, B. (1982) Projection lens, US Patent #4348081.
- Buchroeder, R. A. (1978) Fisheye projection lens system for 35 mm motion pictures, US Patent #4070098.
- Caldwell, J. B. (1998) Compact wide-angle LCD projection lens, *International Optical Design Conference*, 1998, SPIE Volume 3482, p. 269.
- Clarke, J. A. (1988) Current trends in optics for projection TV, *Opt. Eng.*, 27: 16.
- Corbin, R. M. (1969) Motion picture equipment, In *Applied Optics and Optical Engineering*, Volume 5, (R. Kingslake ed.) Academic Press, New York, p. 305.
- Dewald, D. S. (2000) Using ZEMAX image analysis and userdefined surfaces for projection lens design and evaluation for DLP systems, *Opt. Eng.*, 39: 1802.
- Meuret, Y. and De Visschere, P. (2003) Optical engines for high performance liquid crystal on silicon projection systems, *Opt. Eng.*, 42: 3551.
- Mittal, M. K. and Gupta, B. (1994) Six element objective based on a new configuration, *Opt. Eng.*, 33: 1925.
- Mittal, M. K. and Gupta, B., and Sharma, K. D. (1990) 35 mm Cinema projection lens, *Appl. Opt.*, 29: 2446.
- Sharma, K. D. (1982) Better lenses for 35 mm projection, *Appl. Opt.*, 21: 4443.
- Sharma, K. D. (1983) Future lenses for 16 mm projection, *Appl. Opt.*, 22: 1188.
- Sharma, K. D. and Kumar, M. (1986), New lens for 35 mm cinematograph projector, *Appl. Opt.*, 25: 4609.
- Schneider Optics, (2000) Schneider Theater Design Pro 2.1b, [www.Schneideroptics.com](http://www.Schneideroptics.com).
- SMPTE (1994) *Engineering Guide EG 5-1994*, SMPTE 595 W. Hartsdale Ave, White Plains, NY, 10607.
- Stupp, E. H. and Brennesholtz, M. S. (1999) *Projection Displays*, John Wiley, New York.
- Taylor W. H. (1980) Wide angle telecentric projection lens, US Patent #4189211.
- Watanabe, F. (1999) Telecentric projection lens system, US Patent #5905596.
- Wheeler, L. J. (1969) *Principles of Cinematography*, Chapter 10, Fountain Press, Watford, England.



---

# 23 Telecentric Systems

A telecentric optical system is one that has its exit pupil at infinity (the chief ray emerges parallel to the optical axis). An example of use is in a contour projector where one wants to accurately measure screw threads. Because the chief ray is parallel to the optical axis, measurements are the same regardless of the image location. The object can be placed anywhere within its depth of field. Systems have also been developed that are telecentric in both object and image spaces. Another use is in liquid crystal display (LCD) and digital light projector (DLP) projection lenses where, due to the dichroic coatings, a telecentric system is required (see the lenses in [Figure 22.7](#) and [Figure 22.8](#) in the previous section).

The computer program should have the ability to control the exit-pupil distance from the last lens surface. However, for the telecentric feature, it is preferable to instead bound the reciprocal of the exit-pupil distance. This is because most bounded items are small numbers: lens thickness, refractive index, paraxial height ratios, etc. Bounding the pupil to an infinitely large number would force the program to obey this bound to the exclusion of all the other bounds. Reciprocal pupil distance solves this problem and thus keeps all the bounds within the same magnitude. Another method is to bound the chief ray angle for the various off-axis field angles after the last lens surface.

[Figure 23.1](#) shows a telecentric  $f/2.8$  lens used as a  $20\times$  profile projection lens. The data is given in [Table 23.1](#).

Several mirrors are placed between the lens and the screen to make a compact optical system. An erect image is obtained by the addition of a relay or prisms in conjunction with the mirrors.

[Figure 23.2](#) shows a variation of this lens; the object is now at infinity. The aperture stop is immediately behind the first lens. The effective focal length (EFL) is 4.0; field of view is  $20^\circ$ . The intercept ray plots show considerable flare at the edge of the pupil. Note the long back focal length in relation to the effective focal length. Details of this lens are provided in [Table 23.2](#).

[Figure 23.3](#) shows an  $f/2$ ,  $40^\circ$  field of view telecentric lens for which [Table 23.3](#) provides the details. The EFL is 1.0.

Cameras are now available with charge coupled devices (CCDs) rather than film. Following is a lens suitable for such a camera. It uses a prism system as described by Stoffels et al. (1978) with three,  $\frac{1}{3}$ -in. CCD chips ([Figure 23.4](#)). Each chip of 6-mm diagonal corresponds to one of the primary colors of red, green, or blue. The lens has a 10-mm focal length and is  $f/1.8$ . This lens is shown in [Figure 23.5](#); its prescription is given in [Table 23.4](#).

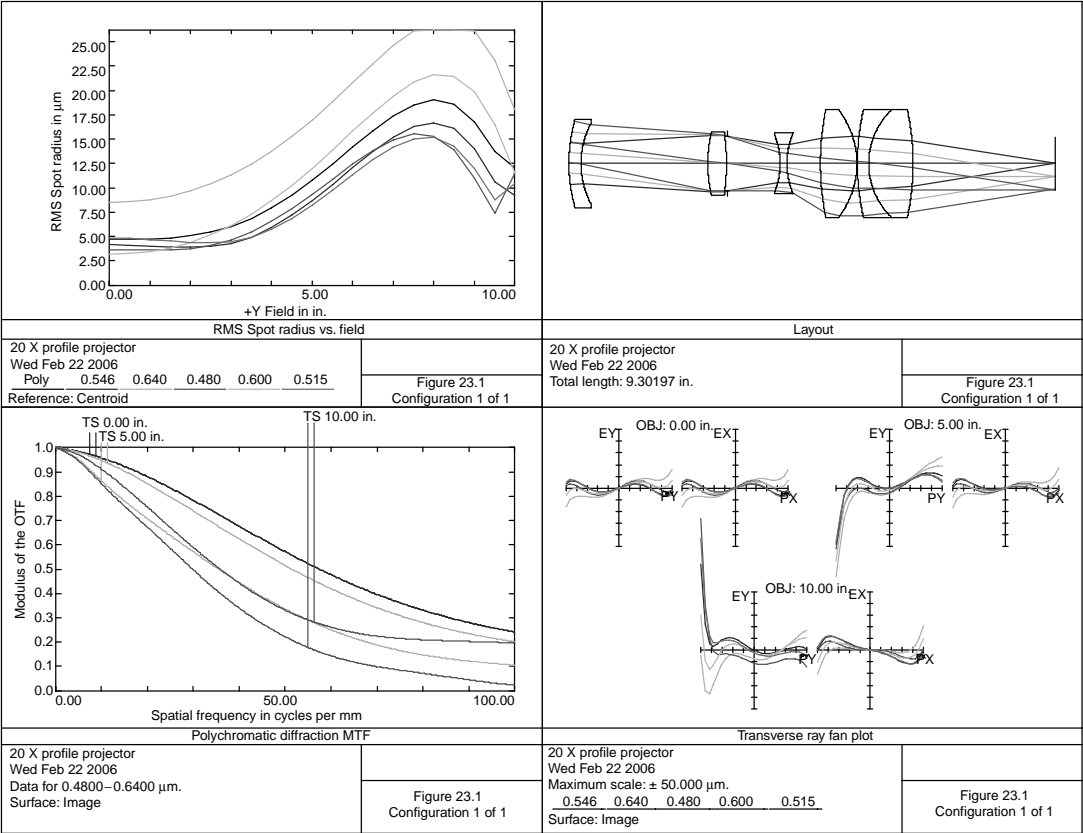


FIGURE 23.1 Profile projector, 20X.

**TABLE 23.1**  
**A 20× Profile Projector Lens**

Surface	Radius	Thickness	Material	Diameter
0	0.0000	50.0000		20.000
1	3.1273	0.2304	N-BK10	1.680
2	1.6504	2.4245		1.520
3	2.7310	0.3553	N-LAK12	1.220
4	−4.4936	0.0150		1.220
5	Stop	1.0126		1.051
6	−1.4680	0.1290	F5	1.060
7	1.4563	0.6409		1.160
8	5.2498	0.6963	N-SK5	2.060
9	−1.6901	0.0126		2.060
10	4.6960	0.2144	SF1	2.060
11	1.4284	0.8476	N-BALF4	2.060
12	−4.9196	2.7236		2.060
13	0.0000	0.0000		0.996

Object (projection screen) to first lens surface=50, first from lens surface to image=9.302, distortion=0.5%, image diameter=1.0.

**TABLE 23.2**  
**Telecentric Lens, f/2.8**

Surface	Radius	Thickness	Material	Diameter
1	−9.8950	0.1956	N-FK5	1.820
2	2.2296	0.9344		1.740
3	Stop	0.1272		1.799
4	−45.8969	0.4000	N-LAK33	1.940
5	−3.6443	3.4945		2.060
6	−23.2708	0.3451	N-LAK33	3.160
7	−3.8903	0.0150		3.200
8	0.0000	0.3389	SF1	3.100
9	2.8151	0.5361		3.000
10	3.7125	0.3000	SF1	3.400
11	2.6748	0.8362	N-LAK12	3.400
12	−7.3325	5.3365		3.400

Distance from first lens surface to image=12.860, distortion=1.1%.

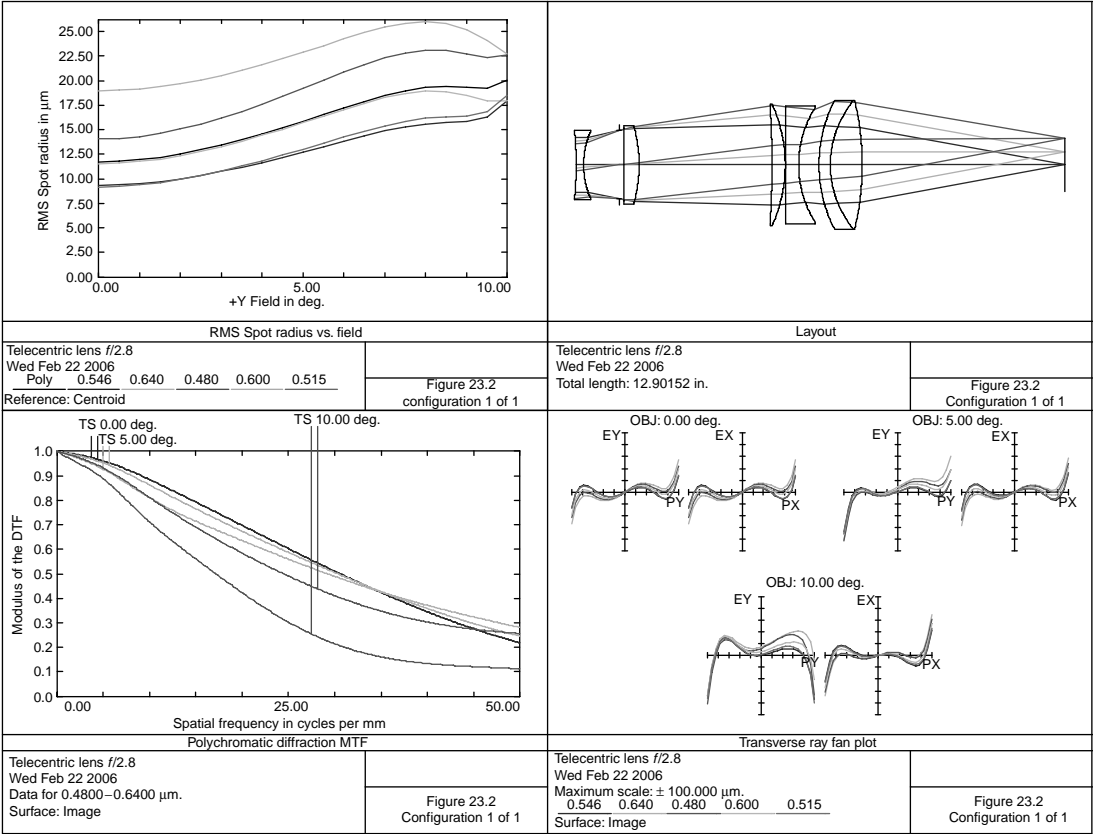


FIGURE 23.2 Telecentric lens,  $f/2.8$ .

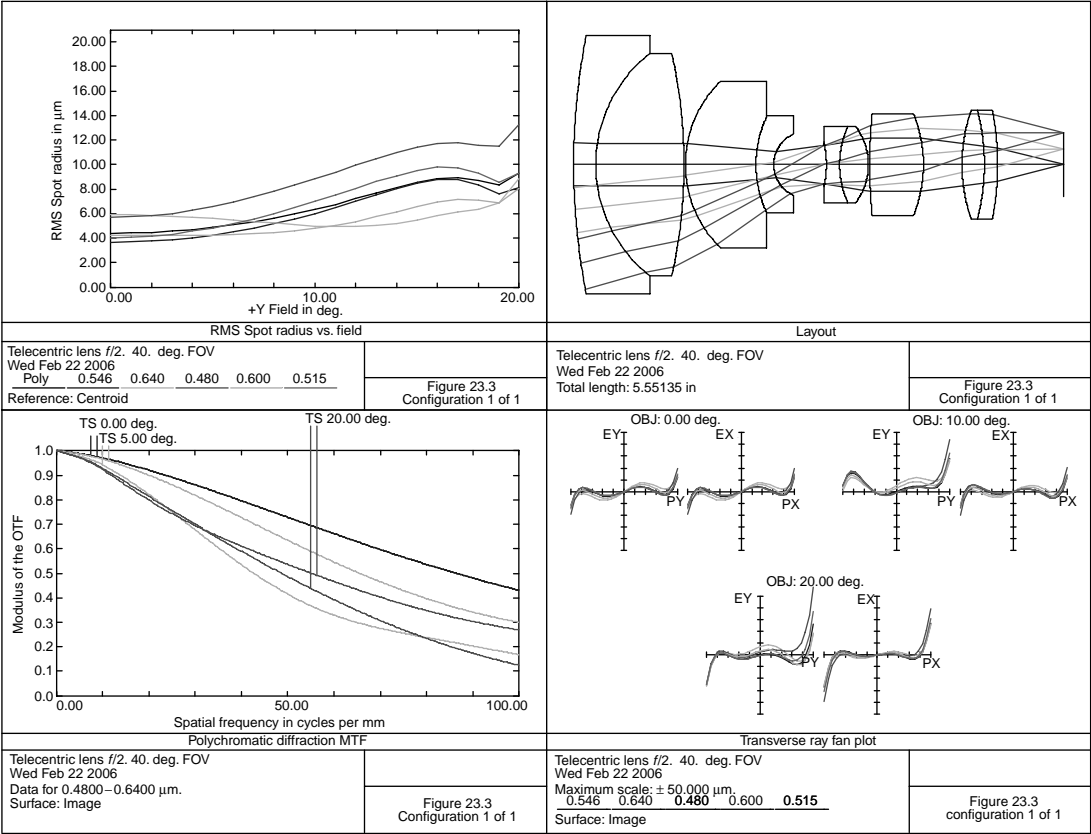
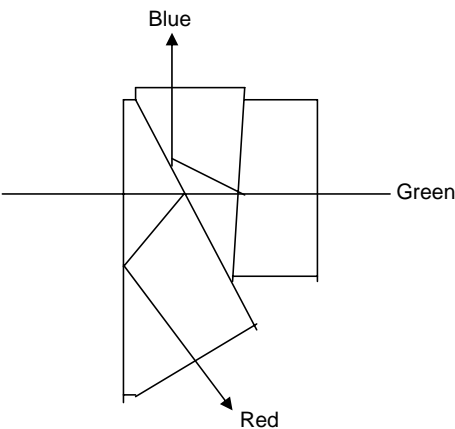


FIGURE 23.3 Telecentric lens,  $f/2$ .

**TABLE 23.3**  
**Telecentric Lens,  $f/2$  with 40.0° FOV**

Surface	Radius	Thickness	Material	Diameter
1	7.5636	0.2495	N-LAF21	2.920
2	1.5973	1.0000	N-BAF52	2.520
3	−5.7895	0.0150		2.520
4	1.3118	0.8000	SF4	1.880
5	1.2771	0.2006	N-BAF10	1.100
6	0.3826	0.5726		0.700
7	Stop	0.0239		0.432
8	−1.1379	0.1500	SF4	0.480
9	1.0502	0.3262	N-SK16	0.860
10	−0.7191	0.0150		0.860
11	6.3867	0.6082	N-LAK12	1.160
12	−1.5146	0.4365		1.160
13	1.8402	0.2538	N-SK16	1.240
14	−2.4770	0.1500	SF4	1.240
15	−3.1797	0.7500		1.240
16	0.0000	0.0000		0.725

Distance from first lens surface to image = 5.551, distortion = 1.0%.



**FIGURE 23.4** Prism assembly for three-chip camera.



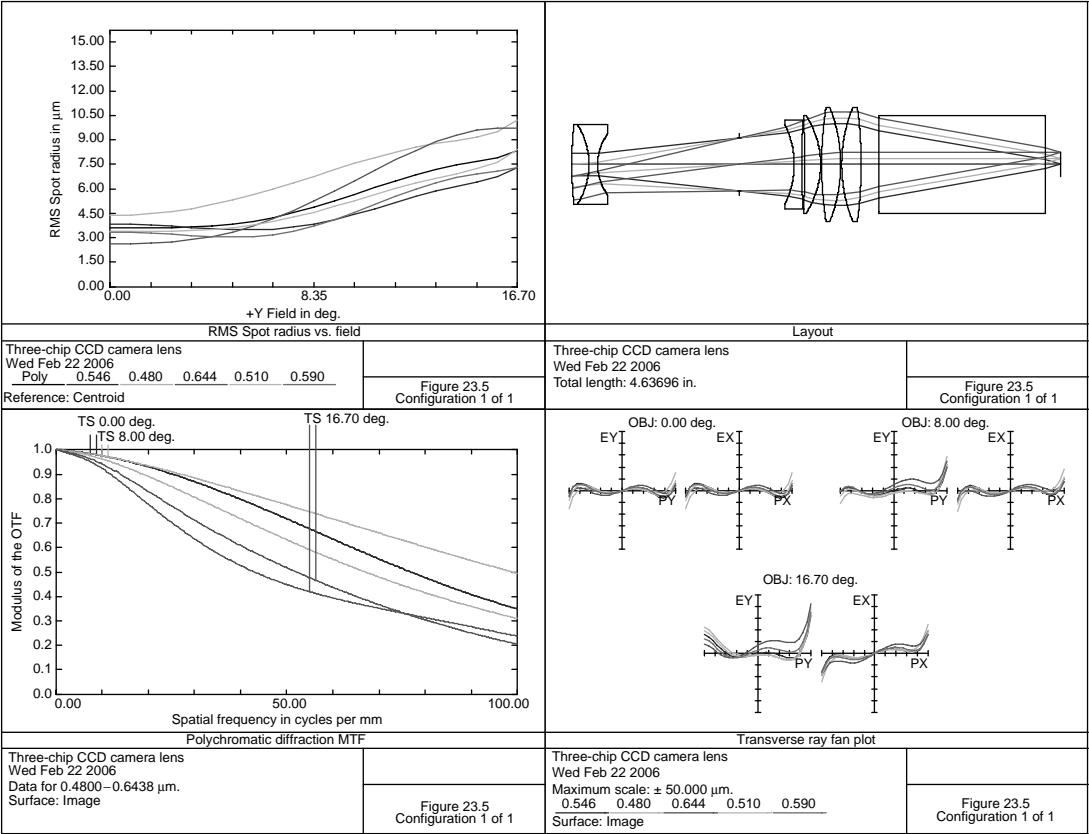


FIGURE 23.5 Three-chip CCD camera lens.

**TABLE 23.4**  
**Three-Chip CCD Camera Lens**

Surface	Radius	Thickness	Material	Diameter
1	4.0438	0.1621	SF1	0.760
2	−0.7013	0.0820	N-LAK21	0.760
3	0.4888	1.3452		0.580
4	Stop	0.5182		0.501
5	−0.8568	0.0700	SF4	0.760
6	5.3033	0.0315		0.850
7	−6.7302	0.1494	N-LAK21	0.860
8	−0.8513	0.0100		0.920
9	3.5699	0.1801	N-PSK53	1.080
10	−1.4808	0.0100		1.080
11	1.4419	0.1839	N-PSK53	1.080
12	−4.2564	0.1698		1.080
13	0.0000	1.5748	N-SK5	0.920
14	0.0000	0.1500		0.920
15	0.0000	0.0000		0.233

Distance from first lens surface to first surface of the prism = 2.912, distortion = 2.65%.

**REFERENCES**

Dilworth, D. (1971) Telecentric lens system, US Patent #3565511.  
Reiss, M. (1952) Telecentric objective of the reverse telephoto type, US Patent #2600805.  
Stoffels, J., Bluekens, A. J., Jacobus, P., and Peters, M. (1978) Color splitting prism assembly, US Patent #4084180.  
Tateoka, M. (1984) Telecentric projection lenses, US Patent #4441792.  
Young, A. W. (1967) Optical workshop instruments, *Applied Optics and Optical Engineering*, Vol. 4, Kingslake, R., ed., Academic Press, New York, p. 250.  
Zverev, V. A. and Shagal, A. M. (1976) Three component objective lens, *Sov. J. Opt. Tech.*, 43: 529.

---

# 24 Laser-Focusing Lenses (Optical Disc)

Lenses for video and optical disc use are small, high-numeric aperture lenses operating at a single laser wavelength. They cover a very small field, are diffraction limited, and are nearly aplanatic.

Figure 24.1 shows an  $f/1$  lens for video disc use for HeNe laser ( $0.6328\text{ }\mu\text{m}$ ). The details are provided in Table 24.1. The field of view (FOV) is  $1^\circ$ . Effective focal length (EFL) is 0.2. This design is based on the Minoura (1979) patent.

As can be seen from the MTF plot, it is diffraction limited for a FOV of  $1.0^\circ$ . A recent trend in the manufacture of these lenses is to injection mold in plastic or in glass (Fitch 1991). This has the advantage of

- Light weight
- Low cost
- An aspheric surface may be used

Another technique is to replicate a thin layer of plastic onto a molded glass lens (Saft 1994). It is true that mold costs are very high, but after these are made, lens cost in large volume is very low. It has the added advantage that the spacers and mounting means are molded into the lens.

Using conic sections, it is possible to have a single lens with zero spherical aberration. Referring to Figure 24.2, for the flat hyperbola case, a plane wave front is incident on the flat and is refracted at the hyperbolic surface such that a spherical wave front emerges. If the lens has an index of refraction  $N$ , paraxial radius  $R$ , and eccentricity  $\varepsilon$  ( $A_2 = -\varepsilon^2$  as used in the ZEMAX programs; see section on aspheric surfaces), then

$$R = -F(N - 1),$$

$$\varepsilon = N.$$

For the ellipse/sphere case,  $F = N + 1$ . For the ellipse,

$$R = \frac{N^2 - 1}{N},$$

$$\varepsilon = \frac{1}{N}.$$

For the sphere,  $R = \text{EFL} - T$ .

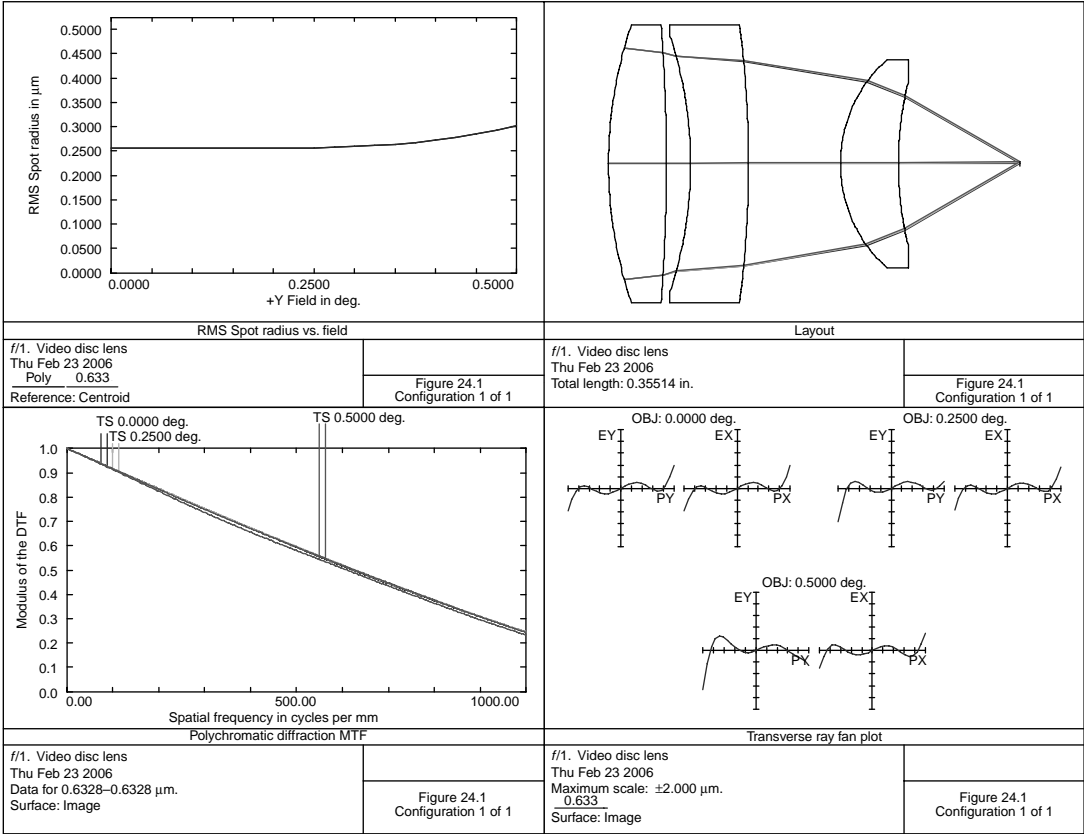
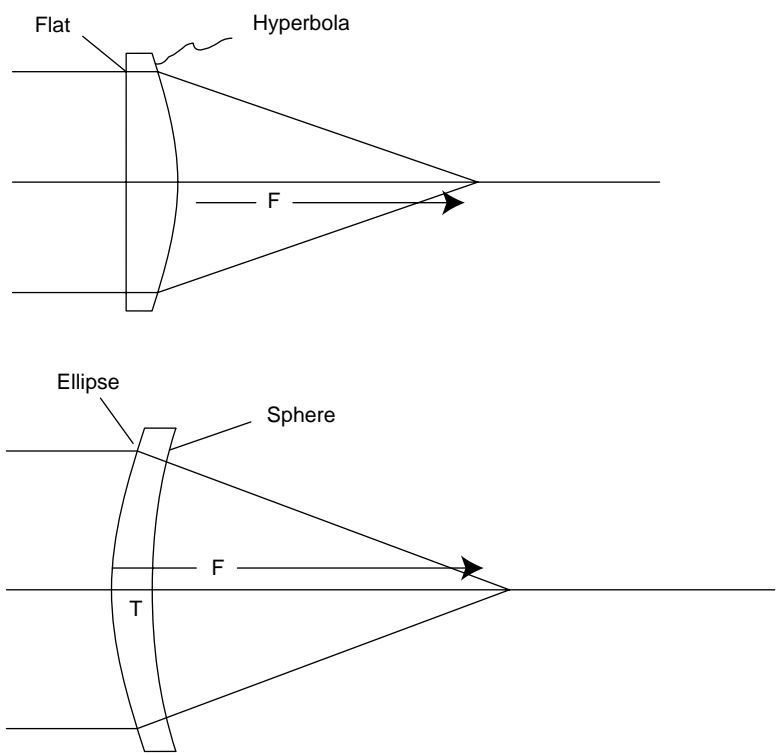


FIGURE 24.1 Video disc, f/1.

**TABLE 24.1**  
**An  $f/1$  Video Disc Lens**

Surface	Radius	Thickness	Material	Diameter
1	0.3752	0.0500	SF6	0.240 Stop
2	-1.5787	0.0209		0.240
3	-0.3499	0.0500	N-BK7	0.220
4	-0.9344	0.0793		0.240
5	0.1209	0.0500	SF6	0.180
6	0.2966	0.1050		0.140
7	0.0000	0.0000		0.003

Distance first lens surface to image=0.355, distortion=0.01%.



**FIGURE 24.2** A single lens with zero spherical aberration.

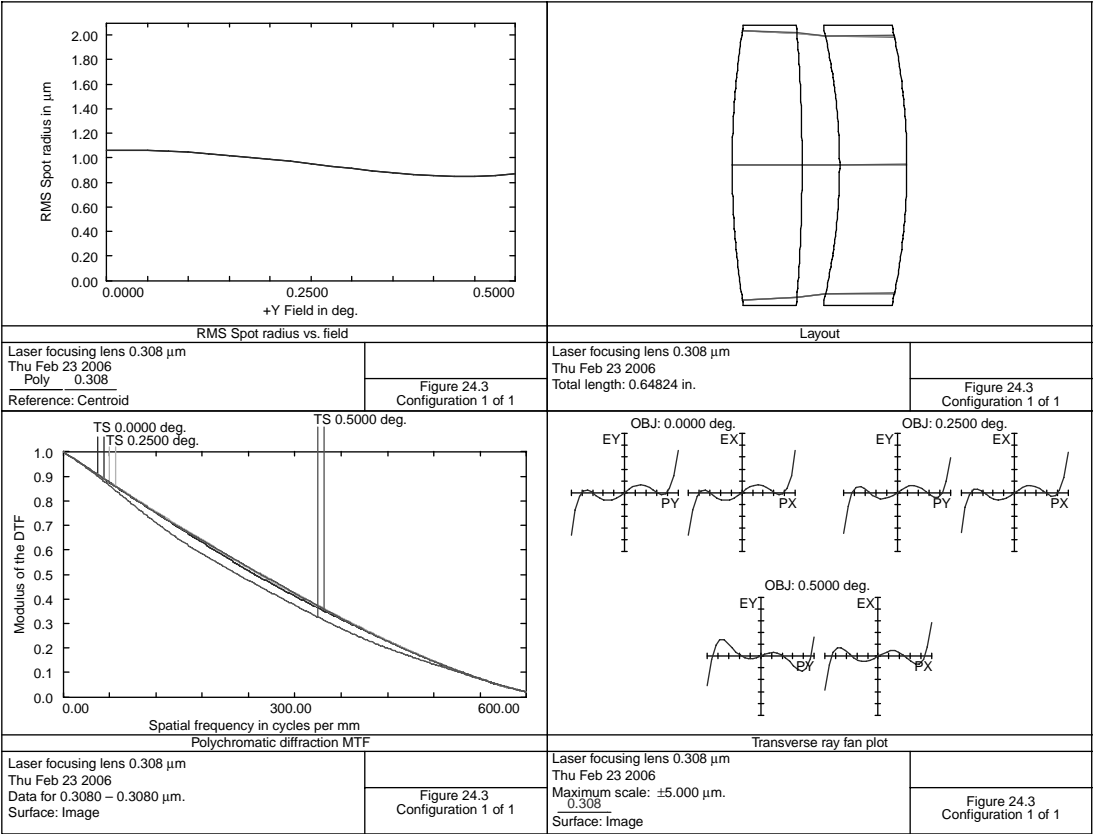


FIGURE 24.3 Laser focusing lens, 0.308 μm.

**TABLE 24.2**  
**Laser Focusing Lens, 0.308  $\mu\text{m}$**

Surface	Radius	Thickness	Material	Diameter
0	0.00000	1.00000E+7	Air	
1	3.17381	0.2592	Silica	1.100
2	−6.10489	0.1395	Air	1.100
3	−2.43609	0.2496	Silica	0.960
4	−2.88562	4.6691	Air	1.100

Distance from first lens surface to image=5.317.

Both cases show diffraction limited performance on axis. Due to excessive coma, performance is very poor, even  $0.5^\circ$  off-axis. For either of these cases to be effective, the beam would have to be aligned to the lens optical axis to within a few minutes of arc.

Figure 24.3 shows a lens used to focus an excimer laser (XeCl, 0.308  $\mu\text{m}$ ); lens details are given in Table 24.2. It has a focal length of 5.0 and a 1.0 diameter entrance pupil. The FOV is  $1.0^\circ$ . This correction of coma means that the laser beam does not have to be precisely aligned to the lens optical axis as with the above conic lenses.

Figure 24.4 shows a laser focusing lens to be used with a HeNe laser (0.6328  $\mu\text{m}$ ). Lens details are given in Table 24.3. It may be used as a bar-code-reader lens.

EFL is 0.4833 and the lens is  $f/1$ . It is nearly diffraction limited for a FOV of  $1.0^\circ$ . At 0.6328  $\mu\text{m}$ , the refractive index of polystyrene is 1.58662. The first surface is aspheric. Its equation is

$$X = \frac{3.316436Y^2}{1 + \sqrt{1 - 7.01341Y^2}} - 1.174228Y^4 - 10.87748Y^6 - 25.67630Y^8 - 721.13841Y^{10}.$$

Plastic lenses may be antireflection coated, but due to their low transition temperature as compared to glass, special techniques must be used (Bauer 2005; Schulz 2005).

With the improvement of production technology for light-emitting diodes (LEDs) at 0.405  $\mu\text{m}$ , the Blu-ray disk system has been developed. ZEONEX<sup>®</sup> 340R (Konishi 2005) has been developed as an ideal material for this application. It is a *cyclo*-olefin polymer and may be injection molded; it has high transmission at this short wavelength, with low water absorption and a stable refractive index.

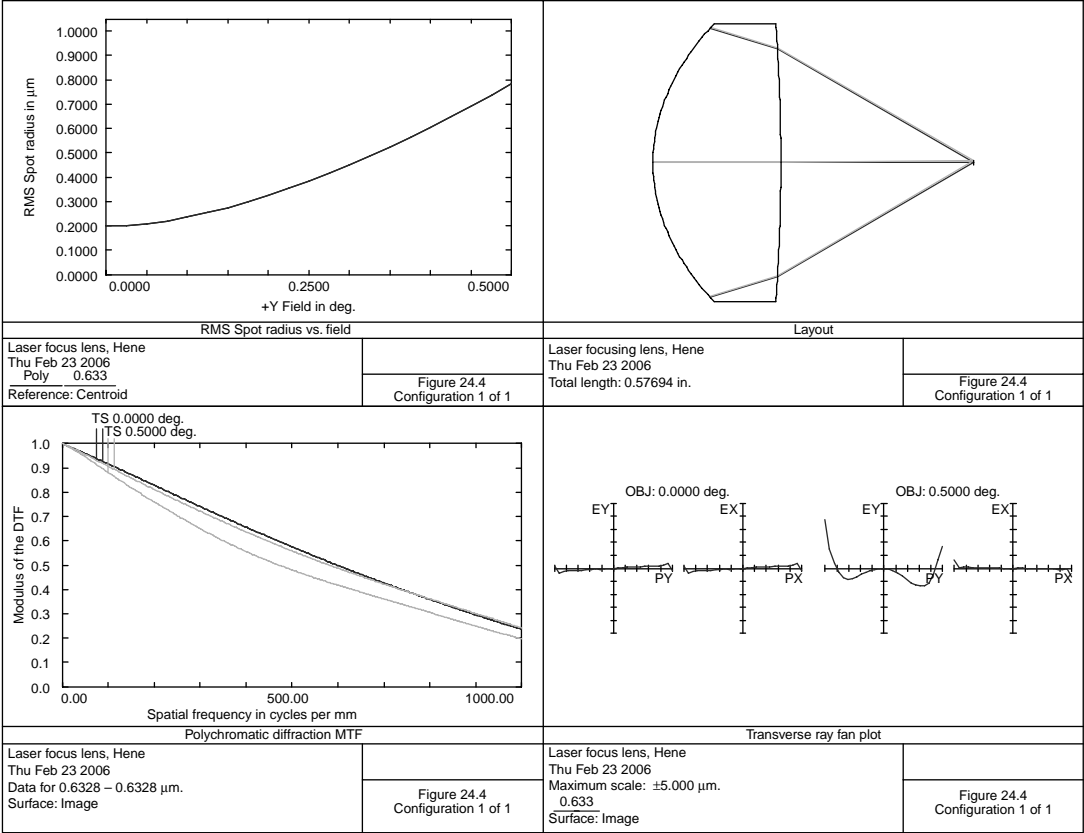


FIGURE 24.4 Laser focus lens, 0.6328 μm.



**TABLE 24.3**  
**Laser Focusing Lens, 0.6328  $\mu\text{m}$**

Surface	Radius	Thickness	Material	Diameter
0	0.0000	1.00000E+7	Air	
1	0.30153	0.2300	Polystyrene	0.500
2	− 3.4042	0.3469	Air	0.500

## REFERENCES

- Bauer, T. (2005) Optical coatings on polymers, *Proceeding of SPIE*, Vol. 5872, Goodman, T. D. ed., SPIE, 5872.
- Binnie, T. D. (1994) Fast imaging micro lenses, *Applied Optics*, 33: 1170–1175.
- Broome, B. G. (1992) *Proceeding of Lens Design Conference*, Vol. 3129, SPIE Press, Los Angeles, p. 235.
- Chirra, R. R. (1983) Wide aperture objective lens, US Patent #4368957.
- Fitch, M. A. (1991) Molded optics, *Photonics Spectra*, October 1991, p. 23.
- Isailovic, J. (1987) *Videodisc Systems*, Prentice Hall, Englewood Cliffs, NJ.
- Konishi, Y., Sawaguchi, T., Kubomura, K., and Minami, K. (2005) High performance cyclo olefin polymer ZEONEX<sup>®</sup>, *Proceedings of SPIE*, Vol. 5872, Goodman, T. D. ed., SPIE, 5872.
- Minoura, K. (1979) Lens having high resolving power, US Patent #4139267.
- Saft, H. W. (1994) Replicated optics, *Photonics Spectra*, February 1994.
- Schulz, S., Munzert, P., Kaless, A., Lau, K., and Kaiser, N. (2005) Procedures to reduce reflection on polymer surfaces, *Proceedings of SPIE*, Vol. 5872, Goodman, T. D. ed., SPIE, 587201.
- U.S. Precision Lens (1973) *The Handbook of Plastic Optics 3997*, Cincinnati, OH 45245.



---

# 25 Heads-Up Display Lenses

This type of lens is used in the cockpit of an aircraft to image a cathode ray tube (CRT) into the pilot's eyes. It is similar to a huge eyepiece, with the exit pupil being at the pilot's eyes. This pupil should be large enough to encompass both eyes and allow for some head movement. Typical specifications for such a system would be

Entrance pupil diameter	6 in.
Pupil distance to lens	25 in.
Angular resolution	
Center	1 min arc
Edge	3 min arc
Field of view	25°
Instantaneous field of view	20°
Maximum distortion	5%

Singh (1996) gives additional requirements. For this system, one can assume that there are two 8-mm-diameter pupils 65 mm apart. What one eye can see, without moving one's head, is referred to as "instantaneous field of view." Due to limitations on the size of the optics, one generally has to move one's head slightly to see the full CRT display.

Due to size limitations in the cockpit, an in-line system will not fit. The lens therefore must be "folded" to fit into the crowded cockpit. Figure 25.1 shows a typical heads-up display (see also Rogers 1980); details are given in Table 25.1a. Because it was designed to be used with a 4.25-in. diameter CRT and have a field of view of 25°, the focal length becomes 9.585.

The space between the first and second lenses allows the insertion of a mirror to fold the optical system for convenient packaging of the lens into the cockpit. The last element of N-K5 glass is the CRT face plate. Due to the difficulty of chromatic correction in these systems, they are generally designed to be used with a narrow-band CRT phosphor (for example, P53 phosphor). In this case, the central wavelength is 0.55  $\mu\text{m}$  with the half-power points being at 0.54 and 0.56  $\mu\text{m}$ . This narrow bandwidth also has another advantage. These systems are generally positioned such that the CRT image is reflected from the aircraft windshield into the pilot's eyes. To cause a minimum transmitted energy loss at the windshield, the windshield (or a beam splitter very close to this windshield) is coated with a narrow-band dielectric reflecting coating.

From the trace in Figure 25.1, notice that the 8-mm diameter pupil at the left eye position can view 5° to the left and 10° to the right, and likewise for the right eye. Therefore, the system is said to have an instantaneous field of view of 20°. By moving the head within a 6-in. diameter circle, the full 25° field will be visible.



**TABLE 25.1a**  
**Heads-Up Display**

Surface	Radius	Thickness	Material	Diameter
0	0.0000	0.100000E+11		0.00
1	Stop	25.0000		6.000
2	7.5799	2.1001	N-SK16	7.860
3	−11.7458	0.7000	SF6	7.860
4	160.7517	5.1618		7.860
5	10.4450	0.5592	N-SF6	5.960
6	212.3874	0.0200		5.960
7	4.8956	0.7300	N-LASF45	5.540
8	13.6943	0.3398		5.400
9	−67.4301	0.3500	SF6	5.360
10	5.3371	3.1451		4.820
11	0.0000	0.1890	N-K5	4.220
12	0.0000	0.0000		4.220

Distance from first lens surface to image=13.295.

**TABLE 25.1b**  
**Pupil Shift vs. Field Angle for a Heads-Up Display**

Field	Pupil Shift (from Center)	Angle (deg.)
1	2.8425	0.0
2	2.8425	2.0
3	2.8425	−6.0
4	2.8425	−12.5
5	1.279	0.0
6	1.279	5.0
7	1.279	−10.0
8	1.279	2.5 sagittal
9	1.279	5.0 sagittal

Distortion=2.2%.

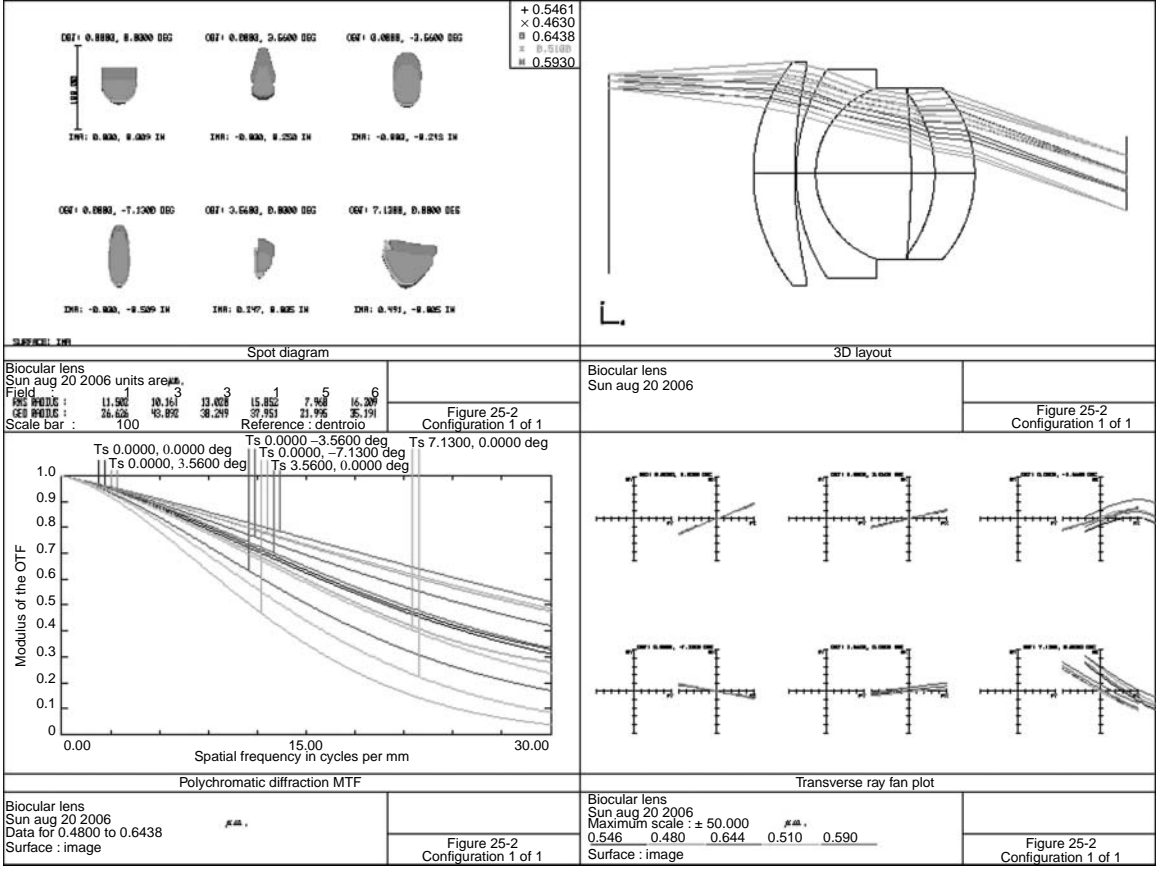


FIGURE 25.2 A biocular lens.

**TABLE 25.2a**  
**Biocular Lens**

Surface	Radius	Thickness	Material	Diameter
1	Stop	2.0000		2.757
2	2.4675	0.5716	N-PSK3	3.080
3	6.6708	0.0200		2.980
4	2.6344	0.2680	LAFN7	2.880
5	1.2475	1.3156	N-FK5	2.360
6	−11.3609	0.3275		2.360
7	−1.8260	0.5517	N-LLF6	2.200
8	−1.7963	2.0912		2.360
9	0.0000	0.0000		1.020

Distance first lens surface to image=5.146.

**TABLE 25.2b**  
**Field Angles for Biocular Lens**

Field	Angle Y (deg.)	Angle X (deg.)	Displacement
1	0.0	0.0	1.28
2	3.56	0.0	1.28
3	−3.56	0.0	1.28
4	−7.13	0.0	1.28
5	0.0	3.56	1.28
6	0.0	7.13	1.28

Maximum distortion=2.4%.

Because the pupil is displaced, not only must the computer program have the ability to displace the entrance pupil, but it must also be able to trace positive and negative field angles in addition to field angles in the sagittal plane. In the above example, nine field angles were used, seven in the tangential plane and two in the sagittal plane. These field angles are presented in [Table 25.1b](#).

Resolution in the central portion of the field is 1 min of arc. At the edge, resolution is reduced due to astigmatism.

A bi-ocular lens is similar in many respects to a heads-up display. However, in a bi-ocular system the user's eyes are much closer to the lens than in a heads up display. They are used in various types of viewing equipment where a relatively low power eyepiece is required, and the convenience of viewing thru both eyes is desired. As with the heads up display, the computer program must be able to shift the entrance pupil and trace from objects in both tangential and sagittal planes. [Figure 25.2](#) shows a bi-ocular lens of 4.0 focal length; data is given in [Table 25.2a](#) and [Table 25.2b](#). From the formula for magnification in [Chapter 10](#):

$$M = \frac{4 + 10}{4} = 3.5.$$

This lens has visual correction and covers an object diameter of 1.0. Rays were traced for a 5-mm diameter pupil, 32.5 mm from the lens center line. It is interesting that resolution off-axis is much better than the axial resolution.

## REFERENCES

- JEDEC Pub.# 16-C (1988) *Optical Characteristics of cathode Ray Tubes*, Electronic Industries Association, 2001 Eye St, NW, Washington, DC 2006.
- Rogers, P. J. (1980) Modified petzval lens, US Patent #4232943.
- Singh, I., Kumar, A., Singh, H. S., and Nijhawan, O. P. (1996) Optical design and performance evaluation of a dual beam combiner HUD, *Optical Engineering*, 35: 813–818.



---

# 26 The Achromatic Wedge

The achromatic wedge is a useful device to obtain a small angular deviation and still preserve an achromatic image. It is limited to small deviation angles for two reasons:

1. Individual prism angles become excessively large for large deviation angles.
2. Secondary color increases with deviation.

To prevent the introduction of coma and astigmatism into the axial image (see [Chapter 27](#)) it is important that these wedges be used only in a collimated light bundle.

Sometimes, prism deviation is measured by ophthalmic nomenclature:

$$1 \text{ Prism diopter} = \frac{1 \text{ cm deviation}}{1 \text{ m distance}}.$$

[Figure 26.1](#) shows an incident beam normal to the first prism surface. After refraction, the beam emerges with a deviation as shown. Smith (2000) gives useful first-order formulas for calculating the prism angles. The author wrote a program that traces a real ray through the prism assembly and, by a simple iterative scheme, calculates the prism angles for an achromatic condition and to obtain the desired deviation. (The deviation is calculated at the central wavelength; to be achromatic, the deviation is to be the same at the extreme wavelengths.)

Consider an achromatic prism in the visual region. N-BK7 glass is used for the first prism, and F2 is used for the second ([Table 26.1](#)).

*Secondary* refers to the angular difference between the deviation at the central wavelength and the deviation at the short wavelength.

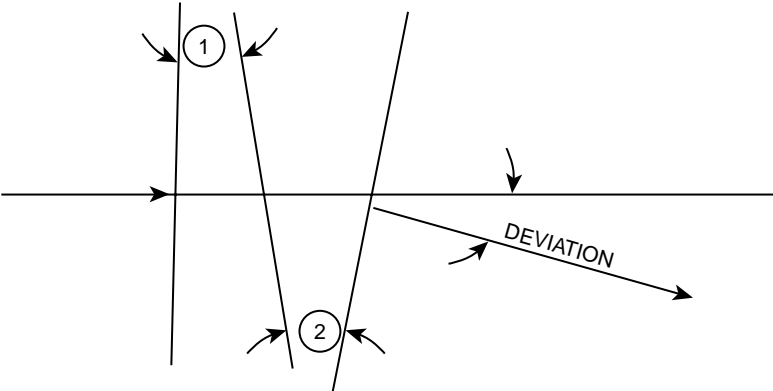


FIGURE 26.1 Achromatic prism.

TABLE 26.1 Achromatic Prism			
Deviation (deg)	Angle 1 (deg)	Angle 2 (deg)	Secondary (microradians)
1	4.419	2.071	10.0
2	8.781	4.098	19.0
3	13.031	6.040	29.0
4	17.127	7.865	38.0
5	21.032	9.546	48.0
6	24.719	11.070	58.0
7	28.176	12.430	68.0
8	31.393	13.625	78.0
9	34.374	14.663	89.0
10	37.124	15.554	99.0

## REFERENCES

- Goncharenko, E. N. and Repinskii, G. N. (1975) Design of achromatic wedges, *Sov. J. Opti. Tech.*, 42: 445.
- Sheinus, N. V. (1976) Design of a wedge scanner, *Sov. J. Opti. Tech.*, 43: 473.
- Smith, W. (2000) *Modern Optical Engineering*, McGraw Hill, New York.



---

# 27 Wedge-Plate and Rotary-Prism Cameras

It is frequently necessary to place a beam splitter in a convergent beam. If a plate is used, it will introduce coma and astigmatism into the axial image. This can be reduced or eliminated by:

1. Use a pellicle. This is equivalent to a plate of zero thickness. Pellicles are made by forming a nitrocellulose plastic over a flat frame. They are extremely thin, typically about 5  $\mu\text{m}$ . Limited types of coatings may be applied to this rather fragile part. Glass pellicles of perhaps 0.005-in. thick glass are also available. Although thicker than the plastic form, they are more durable and a large variety of coatings may be applied.
2. Use a cube beam splitter. This is equivalent to a plane plate in the system and they are easily accommodated in the optical design. They are bulky and sometimes there is no way to incorporate them into the mechanical package. In the IR region, a cube is out of the question.
3. Use a wedge plate. By this technique, axial coma and astigmatism may be substantially reduced.

As seen in [Figure 27.1](#), a plate of thickness  $T$  with a wedge angle of  $\theta$  is in a converging beam. It is a distance  $P$  to the image. The plate is at an angle  $\beta$  to a normal to the optical axis.

For zero astigmatism, De Lang (1957) gives the following value for the wedge angle,  $\theta$ , in radians:

$$\theta = \frac{\sin \beta (\cos^2 \beta) T}{2(N^2 - \sin^2 \beta) P}.$$

Coma is also substantially reduced.

The author once incorporated a beam-splitter into a 10 $\times$  microscope objective system. The beam splitter had the following parameters:

$$N = 1.51872(\text{N-BK7 glass})$$

$$B = 45^\circ$$

$$T = 0.04 \text{ in.}$$

$$P = 14.9473 \text{ in.}$$

Using these values in the above equation gives a wedge angle,  $\theta$  equal to 0.00026186 rad, or 54.0 sec. Using the ZEMAX optimization program,

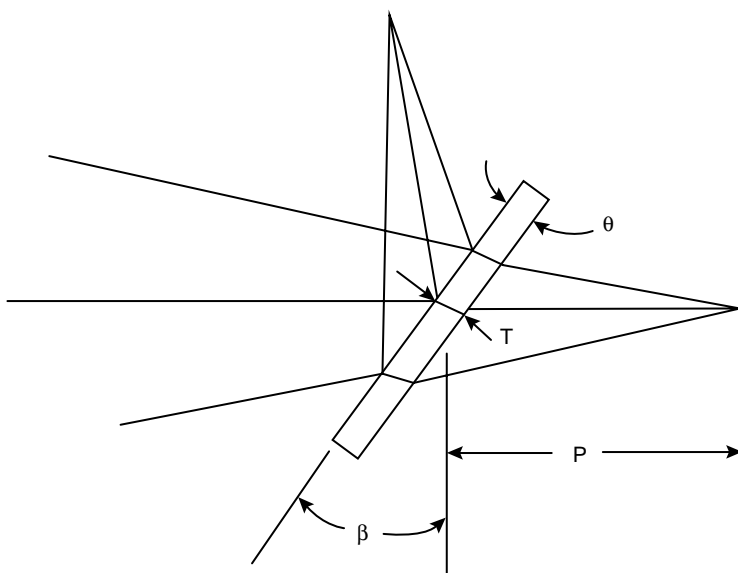


**FIGURE 27.1** A plate of thickness  $T$  with a wedge angle of  $\theta$  in a converging beam. It is a distance  $P$  to the image. The plate is at an angle  $\beta$  to a normal to the optical axis.

and with a perfect lens (a paraxial lens in ZEMAX) of  $f/4$  and effective focal length (EFL) of 20.0, gives a wedge angle of 36.7 sec. Figure 27.2 shows the results of this by means of the spot diagram of the axial image. For comparison, a spot diagram is also presented for a parallel plate. The difference between this computed value and that given by the De Lang formula is the formula is based on third-order theory, whereas the data shown in Figure 27.2 is based upon exact ray tracing.

4. Use two beam-splitters oriented  $90^\circ$  to each other. That is, if an observer looks along the optical axis, they will see two reflected beams at a  $90^\circ$  orientation to each other. A plane plate may be used to displace a beam and is the basis of rotary prism cameras. In this type of camera, a plate is coupled to the film movement such as to cause a displacement equal to the film movement. The problem, in addition to aberrations of the plate, is that this displacement is not a linear function of the plate rotation. Referring to Figure 27.3 that shows the displacement of a plane plate of thickness  $T$  and refractive index  $N$ ,

$$\sin I = \frac{\sin I'}{N},$$

$$D = \frac{T \sin(I - I')}{\cos I'}.$$

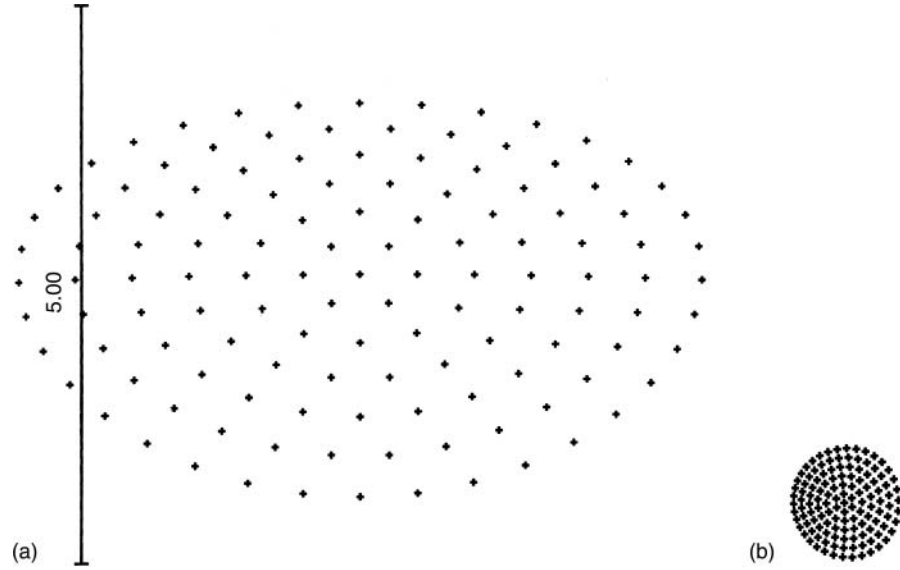
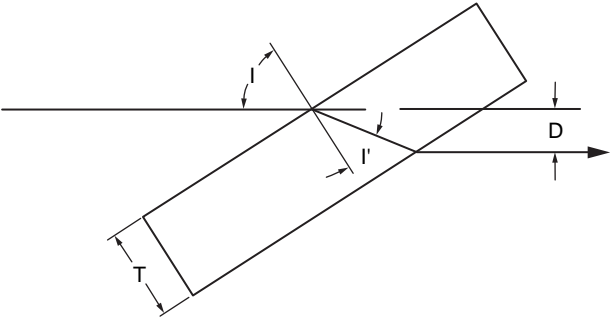


FIGURE 27.2 Wedge plate.



**FIGURE 27.3** The displacement of a plane plate of thickness  $T$  and refractive index  $N$ .

For small angles of incidence,

$$D = \frac{TI(N - 1)}{N}.$$

Increasing the refractive index of the prism rotator from N-K5 to N-LAK10 yields a thinner rotary prism, but with nearly the same nonlinear function of displacement vs. rotation. Due to the nonlinear displacement of the plate, a shutter is provided in rotary prism cameras to cutoff the beam to limit

**TABLE 27.1a**  
**A 35-mm  $f/2$  Lens for Rotary Prism Camera**

Surface	Radius	Thickness	Material	Diameter
1	0.6640	0.3017	SF1	1.080
2	0.4632	0.3151		0.760
3	0.6750	0.1870	LAF3	0.760
4	4.9569	0.0689	F2	0.760
5	0.5726	0.0846		0.560
6	Stop	0.1769		0.523
7	−0.8537	0.1509	F2	0.640
8	3.9727	0.3807	N-LAK33	0.980
9	−0.9634	0.2612		0.980
10	1.4883	0.3680	N-LAK12	1.100
11	−0.8926	0.1197	SF1	1.100
12	−2.8207	0.3500		1.100
13	0.0000	0.4510	N-LAK10	0.860
14	0.0000	0.4500		0.860
15	0.0000	0.0000		0.493

Distance from first lens surface to image = 3.666, distortion = 2.4%.



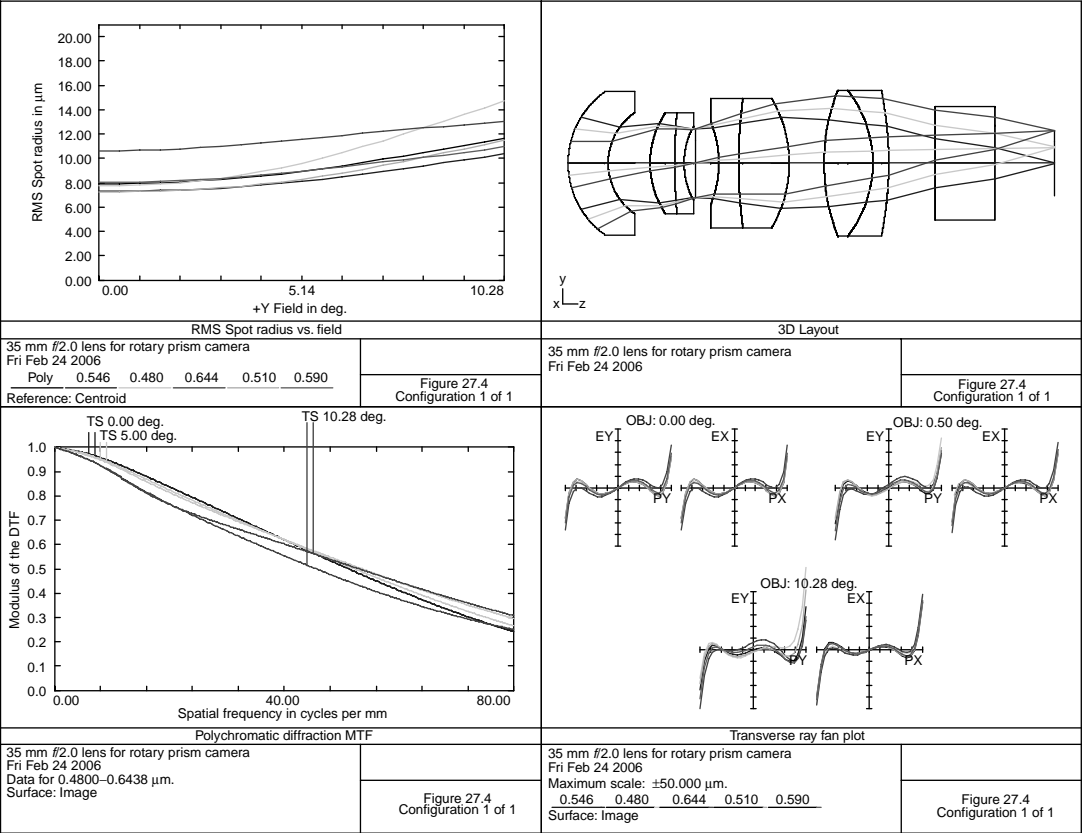


FIGURE 27.4 Lens for rotary camera.

**TABLE 27.1B**  
**Image Displacement vs. Film Movement**

Angle	Displacement	Film	Error
1	0.00330	0.00333	0.00003
2	0.00661	0.00667	0.00006
3	0.00992	0.01000	0.00008
4	0.01324	0.01333	0.00010
5	0.01656	0.01667	0.00011
6	0.01989	0.02000	0.00011
7	0.02323	0.02333	0.00010
8	0.02658	0.02667	0.00008
9	0.02995	0.03000	0.00005
10	0.03333	0.03333	0.00000
11	0.03674	0.03667	−0.00007
12	0.04016	0.04000	−0.00016
13	0.04360	0.04333	−0.00027
14	0.04706	0.04667	−0.00040
15	0.05055	0.05000	−0.00055
16	0.05407	0.05333	−0.00074
17	0.05762	0.05667	−0.00095
18	0.06119	0.06000	−0.00119
19	0.06480	0.06333	−0.00146
20	0.06844	0.06667	−0.00177

this displacement error. The example given is for a cube prism for a 16-mm film camera. Using the above formula for N-LAK10 glass and  $D$  equal to 0.3, one obtains a  $T$  value of 0.455.

Actual ray tracing indicates that the error is a monotonic increasing function. Making the cube a little thinner ( $T=0.451$ ) yields a better compensated system. A shutter is then provided that rotates with the cube and limits the angle of incidence to  $\pm 11^\circ$ . This of course, results in considerable light loss, but provides excellent image movement compensation.

In [Figure 27.4](#) is shown a lens for a rotary prism camera; the details are given in [Table 27.1a](#). To reduce the effects of astigmatism as the plate is rotated, the lens is made nearly telecentric (Buckroeder 1997). Focal length is 1.378 in. (35 mm); the lens is  $f/2$ , and will cover the 16-mm film format (see [Appendix A](#)). Table 27.1b shows the image displacement vs. the film movement for this system.

Note that the error between the image displacement due to the prism rotation and the film movement gets excessively large after  $11^\circ$ ; therefore, the camera is fitted with a shutter to cut off the light at this point. This is a rotating shutter attached to the prism.

## REFERENCES

- Buckroeder, R. A. (1997) Rotating prism compensators *Journal of SMPTE*, 86: 431–438.
- Howard, J. W. (1985) Formulas for the coma and astigmatism of wedge prisms in convergent light, *Applied Optics*, 24: 4265.
- De Lang, H. (1957) Compensation of aberrations caused by oblique plane parallel plates, *Philips Research Reports*, 12: 131.
- Sachteben, L. T., Parker, D. T., Allee, G. L., and Kornstein, E. (1952) Color television camera system, *RCA Review*, 8: 27.
- Shoberg, R. D. (1978) High speed movie camera, US Patent #4131343.
- Whitley, E. M., Boyd, A. K., and Larsen, E. J. (1996) High speed motion picture camera, US Patent #3259448.



---

# 28 Anamorphic Attachments

A recent trend in cinematography is to provide the audience with a wide field of view. This, of course, may be accomplished by using a wider film (70 mm rather than 35 mm). However, it is more economical and certainly more convenient to be able to photograph and project using 35-mm film. Chretien (1931) was perhaps the first to devise a process using anamorphic lenses.

Traditional 35 mm projection has a horizontal width-to-height ratio of 1.37. In the CinemaScope process, a  $2\times$  anamorphic afocal attachment is placed in front of the prime lens. This attachment has no effect in the vertical dimension but compresses the horizontal image on the film. Although standard 35-mm film is used, the vertical height on the film is slightly larger than standard (unsqueezed) cinematography. The net result is an aspect ratio of 2.35 (Wheeler 1969, 76). Projection is accomplished in the same manner: an afocal cylinder attachment is placed in front of a standard projection lens. This expands the horizontal field by a factor of two. SMPTE standard 195-2000 calls for a projected image area of  $0.825\times 0.690$  that results after the  $2\times$  horizontal expansion of an aspect ratio of 2.40 and is what is used here.

In [Figure 28.1](#), such a projection attachment is shown; the details of the attachment are given in [Table 28.1](#). It was meant to be used with a 3.0-in.  $f/2$  projection lens for 35-mm cinematography. This is an adaptation from Cook (1958). All surfaces are cylinders, and the view is in the cylinder axis power plane. This lens is a little too long; the large airspace should be reduced.

In [Figure 28.2](#) is shown a  $2\times$  anamorphic attachment for use with 70-mm film and a 4.0-in. focal length,  $f/2.4$  projection lens. (View is in the cylinder axis power plane, as for the above case.) Details are provided in [Table 28.2](#).

These attachments are made in such a manner as to permit adjusting the airspace for the actual lens to screen distance (usually 50–400 ft.). Because this is generally a large distance, this adjustment creates no problems. However, in the studio, at short close-up distances, the anamorphic ratio substantially changes and introduces astigmatism. This has the effect in projection of making the actors fatter than they actually are. This then proved to be a fatal flaw in the original CinemaScope system.

This was solved by Wallin and is now the basis of Panavision systems. Wallin (1959) introduced two weak cylinder lenses that are rotated in opposite directions as the attachment is focused. (Actually, the patent discusses astigmatism reduction.) Another method, but not as convenient, is to place the anamorphic device in convergent light between the prime lens and the image (Kingslake 1960). The prime lens is moved to focus on the object. Because the rear anamorphic device does not move, the anamorphic magnification remains constant.

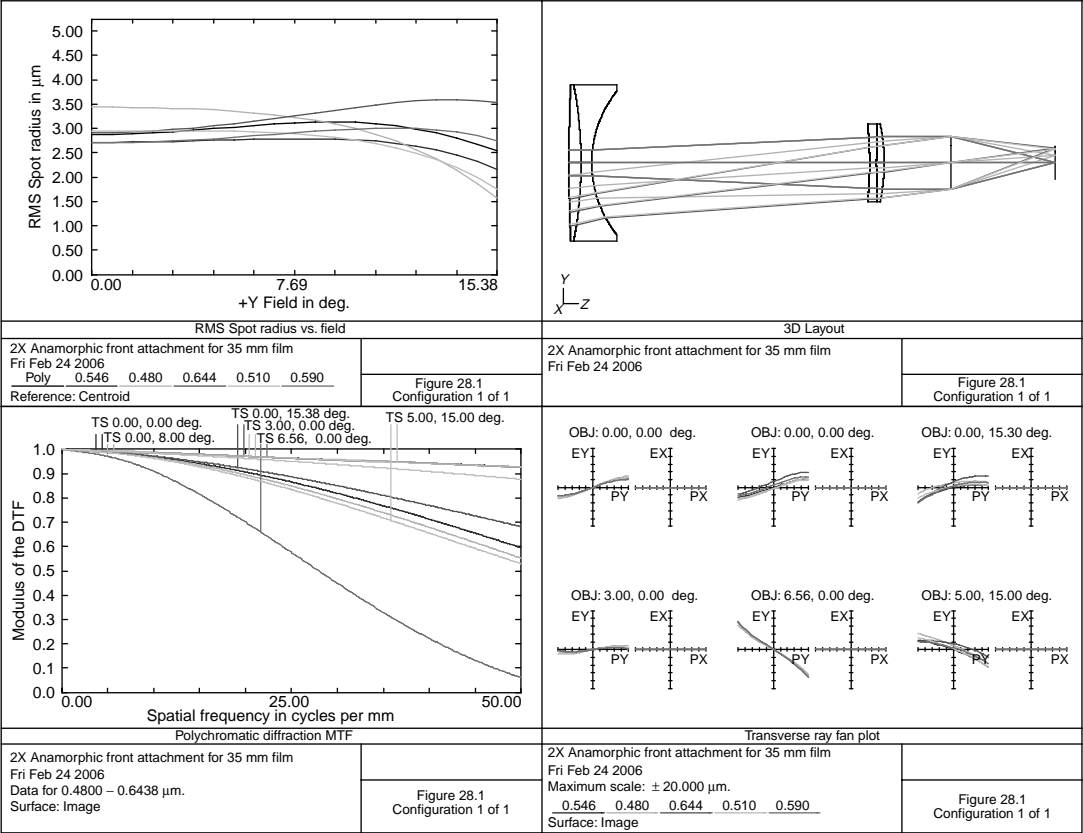


FIGURE 28.1 A 2× anamorphic attachment, 35-mm film.

**TABLE 28.1**  
**A 2× Anamorphic Front Attachment for Projection**

Surface	Radius	Thickness	Material	Diameter
1	46.7204	0.3551	SF1	4.460
2	−11.7061	0.3000	N-BK10	4.460
3	3.2802	7.9602		4.100
4	−11.9355	0.2006	SF5	2.240
5	83.4516	0.2246	N-SK5	2.240
6	−5.1488	1.9000		2.240
7	Stop	3.0000		1.500

Distance from vertex to vertex = 9.040, distortion in horizontal plane = 1.7%.

A system of this type, a rear expander, is shown in [Figure 28.3](#); details are provided in [Table 28.3](#). It was designed to be used with a camera lens that has an exit pupil of 1.2 and forms an image 4.8 from this exit pupil. The distance from the camera exit pupil (the aperture stop in this case) to the first lens surface is 1.5. Distortion in the corner of the image is 1.9%. The lens is plotted in the power plane (a vertical orientation). Note that this is a 1.5× expansion, not the usual 2× as in commercial cinematography.

**TABLE 28.2**  
**A 2× Anamorphic Attachment for 70 mm Projection**

Surface	Radius	Thickness	Material	Diameter
1	−112.0759	0.5598	N-SK14	6.660
2	−11.9655	0.0200		6.700
3	−17.5183	0.5930	N-SK14	6.240
4	3.7247	2.0541		5.080
5	−14.5527	1.1097	SF1	5.060
6	−6.5908	5.3111		5.240
7	−6.5937	0.5071	N-KF9	3.000
8	−2.6759	0.3655		3.060
9	−1.9715	0.3000	N-LAF3	2.600
10	−21.2689	0.5574	N-FK5	2.860
11	−2.1337	1.9320		2.860
12	Stop	4.0000		1.667
13	0.0000	0.0000		1.827

Distance from vertex to vertex = 11.378, distortion in tangential plane = 1.4%.

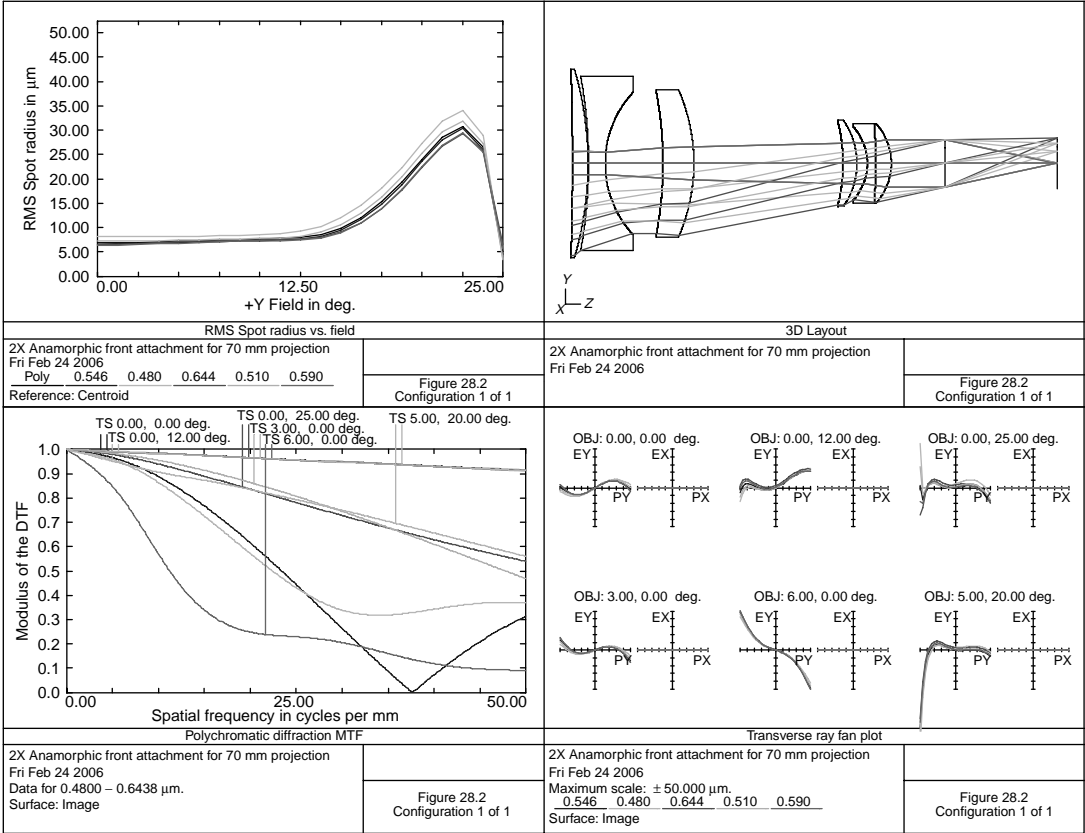


FIGURE 28.2 A 2× anamorphic attachment, 70-mm film.



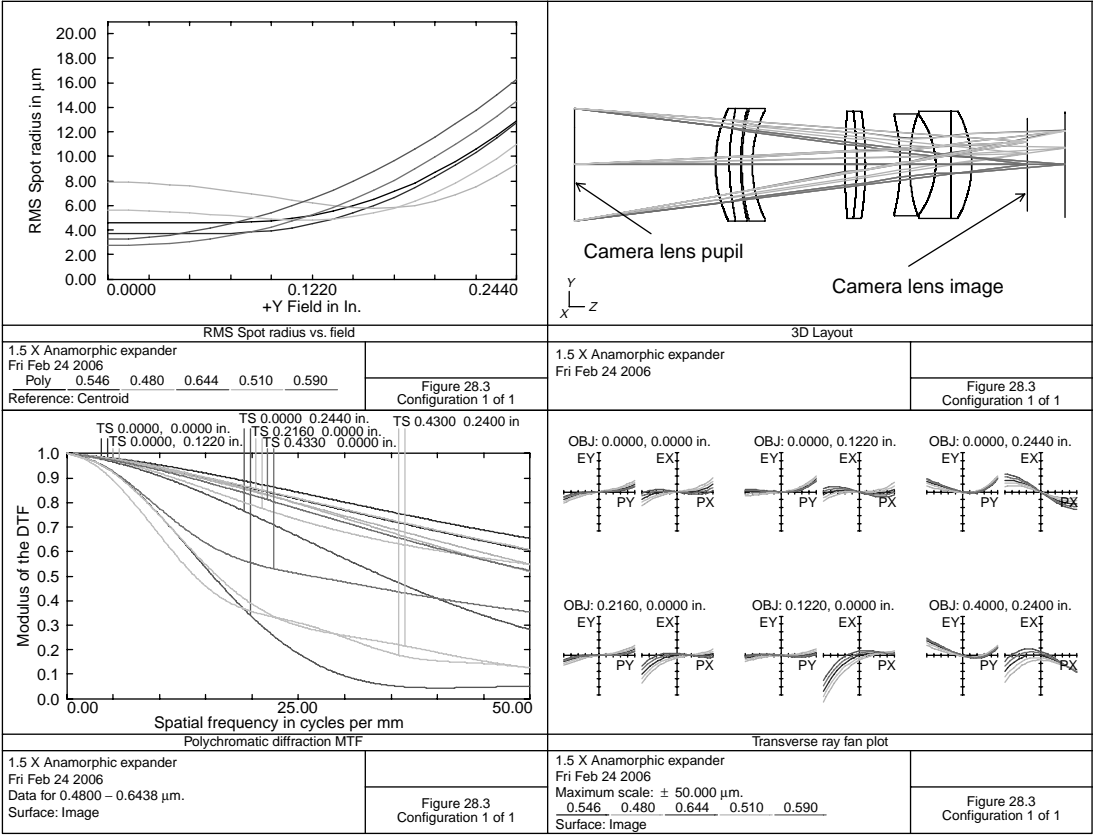
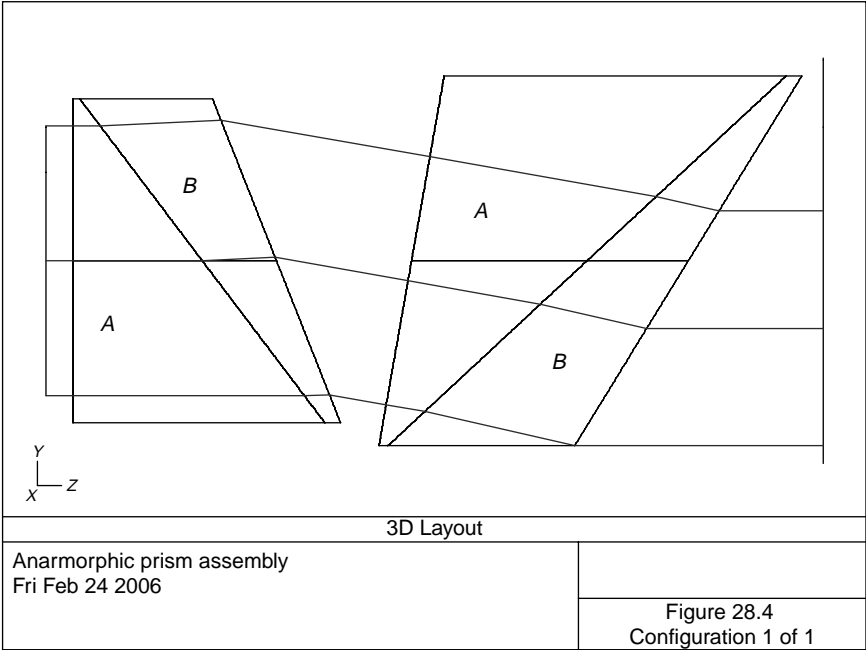


FIGURE 28.3 A 1.5× anamorphic expander.

**TABLE 28.3**  
**A 1.5× Rear Expander**

Surface	Radius	Thickness	Material	Diameter
0	0.0000	−4.8250		0.985
1	Stop	1.5000		1.200
2	1.3728	0.1486	N-FK5	1.200
3	2.7094	0.1180	SF1	1.200
4	2.4822	0.0150		1.140
5	2.3885	0.1111	N-PSK53	1.200
6	1.3056	0.9844		1.140
7	6.9781	0.1245	N-FK5	1.140
8	−4.8145	0.0924	SF1	1.140
9	−4.1143	0.3723		1.140
10	−2.2806	0.0999	N-FK5	1.080
11	1.7280	0.2756		1.080
12	−0.8902	0.1671	N-PSK53	1.080
13	94.2111	0.2172	N-BAF52	1.140
14	−1.1919	0.9989		1.140
15	0.0000	0.0000		

Distance first lens surface to image = 3.725.



**FIGURE 28.4** Anamorphic prism assembly.

Of course, one may also create anamorphic results by means of prisms (Newcomer 1933). However, they are awkward to mount and the beam is displaced from the lens axis.

In [Figure 28.4](#) is shown such an anamorphic prism assembly. It consists of two identical cemented prisms: prism angle  $A$  is  $37.1246^\circ$ ; prism angle  $B$  is  $15.554^\circ$ . The first prism assembly deviates the beam  $10^\circ$ . The second prism then has its first surface tilted  $10^\circ$ . As can be seen from the figure, the beam is displaced by 0.4991. For an input beam diameter of 2.0, the output beam diameter is 1.7367, giving a magnification of 1.15.

## REFERENCES

- American Cinematographer Manual (1993) American Society of Cinematographers, 1782 N Orange Dr., Hollywood, CA 90028.
- Betensky, E. I. (1977) Continuously variable anamorphic lens, US Patent #4017160.
- Chretien, H. (1931) Process for taking or projecting photographic or cinematographic panoramic views, US Patent #1829633.
- Cook, G. H. (1958) Anamorphic attachments for optical systems, US Patent #2821110.
- Kingslake, R. (1960) Anamorphic lens system for use in convergent light, US Patent #2933017.
- Larraburu, P. M. (1972) Anamorphic lens systems, US Patent #3644037.
- Newcomer, H. S. (1933) Anamorphising prism objectives, US Patent #1931992.
- Powell, J. (1983) Variable anamorphic lens, *Appl. Opt.*, 22: 3249.
- Raitiere, L. P. (1958) Wide angle optical system, US Patent #2822727.
- Rosin, S. (1960) Anamorphic lens system, US Patent #2944464.
- Schafter, P. (1961) Anamorphic attachment, US Patent #3002427.
- Vetter, R. H. (1972) Focusing anamorphic optical system, US Patent #3682533.
- Wallin, W. (1959) Anamorphosing system, US Patent #2890622.
- Wheeler, L. J. (1969) *Principles of Cinematography*, Fountain Press, Argus Books, 14 St James Rd., Watford, Herts, England.



---

# 29 Illumination Systems

A condensing lens transfers energy from the light source to the entrance pupil of the projection lens. It must also provide uniform illumination at the film (or other object that is to be illuminated). The assumption, of a circular uniformly illuminated pupil, is imbedded in the usual illumination formulas given in texts (Smith 2000:241). The illuminance produced at the image,  $E$ , is given by

$$E = \frac{T\pi B}{4[f^\#(m+1)]^2},$$

where  $T$  is system transmission,  $B$  is object brightness (luminance),  $f$  is the f-number of the projection lens, and  $m$  is its absolute value of magnification. If  $A$  is the area of the film, then for very large projection distances ( $M \gg 1$ ),

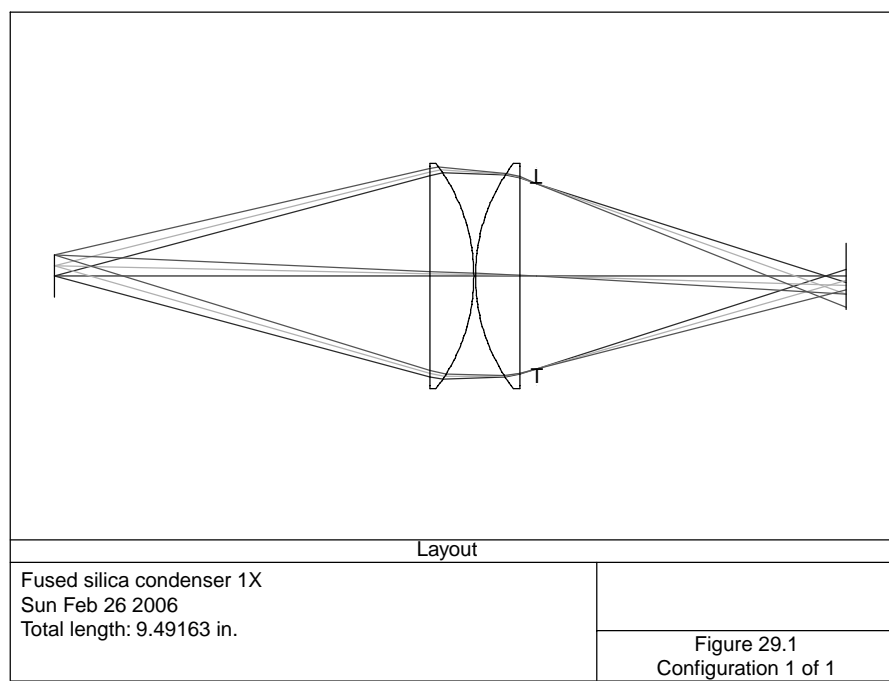
$$\text{Flux at the screen} = \frac{T\pi BA}{4(f^\#)^2} \text{ lumens.}$$

Therefore, for very large screen systems, the tendency is to use a large-format film (see [Appendix A](#) for the various film formats).

Although the usual lens optimization program was designed to minimize image aberrations, such a program may still be used in the design of a refractive condenser system. There are several points to consider:

1. Locate the aperture at the film plane.
2. Provide a system magnification such that the source will fill the entrance pupil of the projection lens.
3. Generally no vignetting.
4. Adjust the program for large emphasis on boundary violations and little on image errors.
5. Due to the generally small source, two field angles should be adequate.
6. In tracing from long conjugate to source, pincushion distortion is desirable. This is because an element of area at the edge of the entrance pupil that is being illuminated should be a proportionately larger area of the source than one in the center. Unfortunately, most sources have less brightness at the edge than at the center.
7. Rarely are these systems made achromatic.

Recently, various computer programs have been developed to specifically design illumination systems (Cassarly 2002). Most have the ability to model the light source.



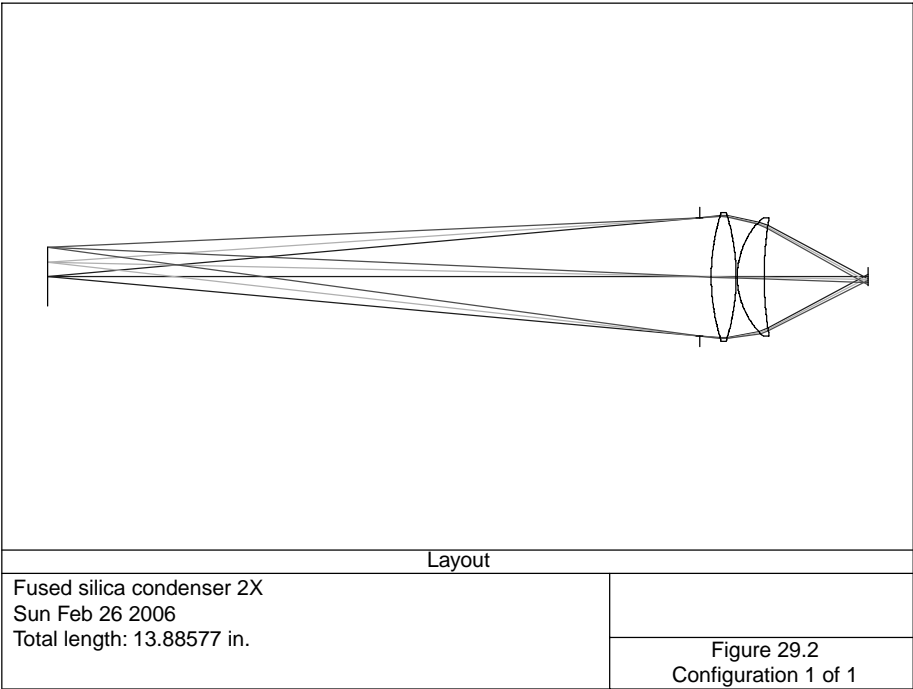
**FIGURE 29.1** Fused silica condenser, 1×.

Figure 29.1 shows a fused silica condenser at unit magnification. It fills a projection lens pupil of 0.5 in. Details are given in Table 29.1. It has a NA of 0.25 and will cover a film of 2.0-in. diameter. Although it shows considerable spherical aberration, it is a simple and effective condenser. Converting the spherical surfaces into parabolas will considerably improve this.

**TABLE 29.1**  
**Fused Silica Condenser, 1×**

Surface	Radius	Thickness	Material	Diameter
0	0.0000	4.5000		0.500
1	0.0000	0.5300	Silica	2.700
2	−2.2416	0.0200		2.700
3	2.2416	0.5300	Silica	2.700
4	0.0000	0.2000		2.700
5	Stop	3.7116		2.222
6	0.0000	0.0000		0.794

Distance from object (lamp) to first lens surface = 4.500, distance from object (projection lens pupil) to source = 9.492, effective focal length = 2.441.



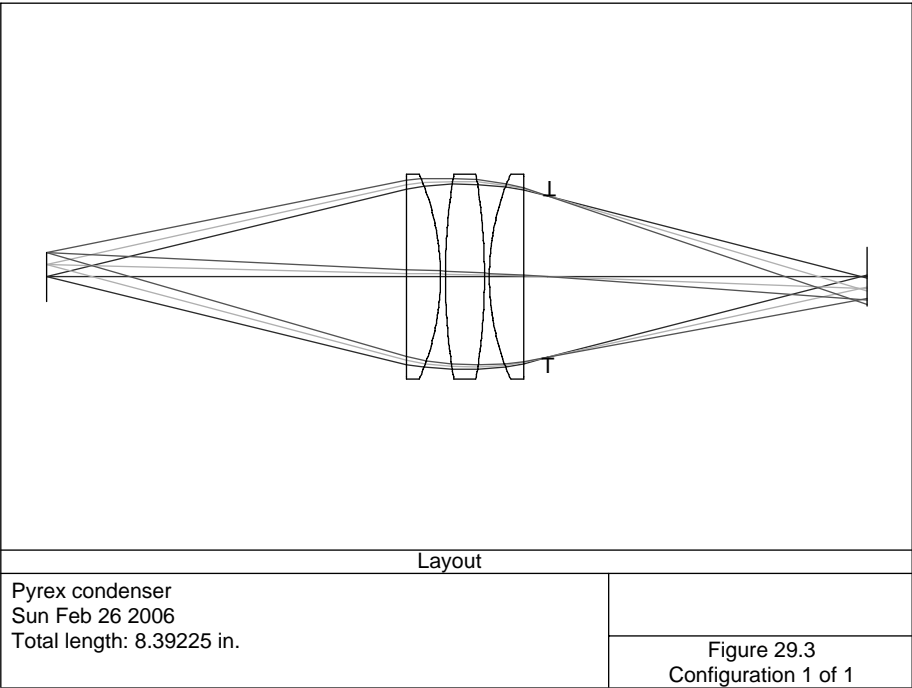
**FIGURE 29.2** Fused silica condenser, 0.2×.

Figure 29.2 shows a silica condenser at 0.2× magnification; details are given in Table 29.2. It is also  $f/1$  and will fill a 1.0-in. diameter projection lens entrance pupil. This has less spherical aberration than the previous system. Making surface 4 ( $R = 1.3573$ ) parabolic will reduce the spherical aberration.

**TABLE 29.2**  
**Fused Silica Condenser, 0.2×**

Surface	Radius	Thickness	Material	Diameter
0	0.0000	11.0330		1.000
1	Stop	0.2000		2.000
2	3.6166	0.4212	Silica	2.180
3	−3.6166	0.0200		2.180
4	1.3573	0.4541	Silica	2.000
5	5.9934	1.7575		1.880
6	0.0000	0.0000		0.302

Distance from object (projection lens pupil) to source = 13.886, effective focal length = 1.943.



**FIGURE 29.3** Pyrex condenser.

In Figure 29.3 is shown an  $f/0.833$  Pyrex<sup>™</sup> condenser consisting of three spherical elements; details are given in Table 29.3 It has unit magnification and will cover a film diameter of 1.8; adequate for a projector of 35 mm SLR film. Focal length is 2.055.

TABLE 29.3 Pyrex Condenser				
Surface	Radius	Thickness	Material	Diameter
0	0.0000	3.6800		0.500
1	0.0000	0.3500	Pyrex	2.100
2	−2.6470	0.0500		2.100
3	6.3189	0.4000	Pyrex	2.100
4	−6.3189	0.0500		2.100
5	2.6470	0.3500	Pyrex	2.100
6	0.0000	0.2500		2.100
7	Stop	3.2623		1.650
8	0.0000	0.0000		0.596

Distance from object (projection lens pupil) to source = 8.392.



Note from the optical schematic that this last system is better corrected than the previous two. Both of the unit magnification systems were traced from lamp to projection lens pupil, whereas the  $0.2\times$  magnification system was traced from projection lens to lamp filament.

Frequently, the lamp filament (or arc) is placed at the center of curvature of a spherical mirror. This redirects energy that never would be collected by the condenser back to the source. However, the author's experience indicates these mirrors only add a small amount to the illuminance. This is because in a modern tungsten halogen lamp the filament coils are very tightly packed together. This spherical mirror then images the filament onto itself; with little passing through.

Lamp number DYS is an example of a lamp with an open filament. It is a 600-W lamp on a two-pin pre-focus base. The mirror should be adjusted such that the filament image is a little above the lamp filament.

Some tungsten halogen lamps have these mirrors already built into the envelope. An example is ANSI code BCK. This is a 500-W lamp common in many slide projectors. It has a color temperature of 3250 K and a filament size of  $0.425\times 0.405$  in.<sup>2</sup>

Pyrex<sup>™</sup> is a trade name of Corning Glass Works. A similar material is made by Schott (Duran) and by Ohara (E-6). It is the preferred choice for condenser lenses for use with lamps of moderate power. To remove excess infrared radiation, a heat-absorbing filter is often placed between the condensing lenses and the lamp. (Some designs even split the lens system and place this heat absorber inside the lens group.) Common heat filters are Schott KG series or Corning 1-58, 1-59, or 1-75. A recent trend is to use a dichroic heat reflector between the lamp and the lens system in place of the heat absorber. With modern coating technology, it has proven to be a more efficient system. These heat reflectors are available as stock items on 0.125-in. thick Pyrex material. They are used at normal incidence, or at  $45^\circ$  incidence (a cold mirror). This latter case is generally more efficient and it has the advantage of reflecting the heat outside of the optical system.

Figure 29.4 shows a condenser system designed to illuminate a transparency of 7.16-in. diameter; details are given in Table 29.4. This transparency is then projected with a 9.54-in. focal length lens,  $f/8$ , at  $10\times$ . Because this condenser system has a magnification of  $2\times$ , the source diameter is then

$$\frac{9.54}{8(2)} = 0.596.$$

An ANSI number BCK lamp may thus be used here.

Given the focal length, the numerical aperture of this condenser then is 0.563 on the source side. The transparency to be projected is placed at the aperture stop of the condenser.

For heat resistance and economy, the rear elements are made of Pyrex. However, Pyrex (as well as Duran and other similar materials) has considerable striae, some bubbles and inclusions. The front two elements, due to their proximity to the

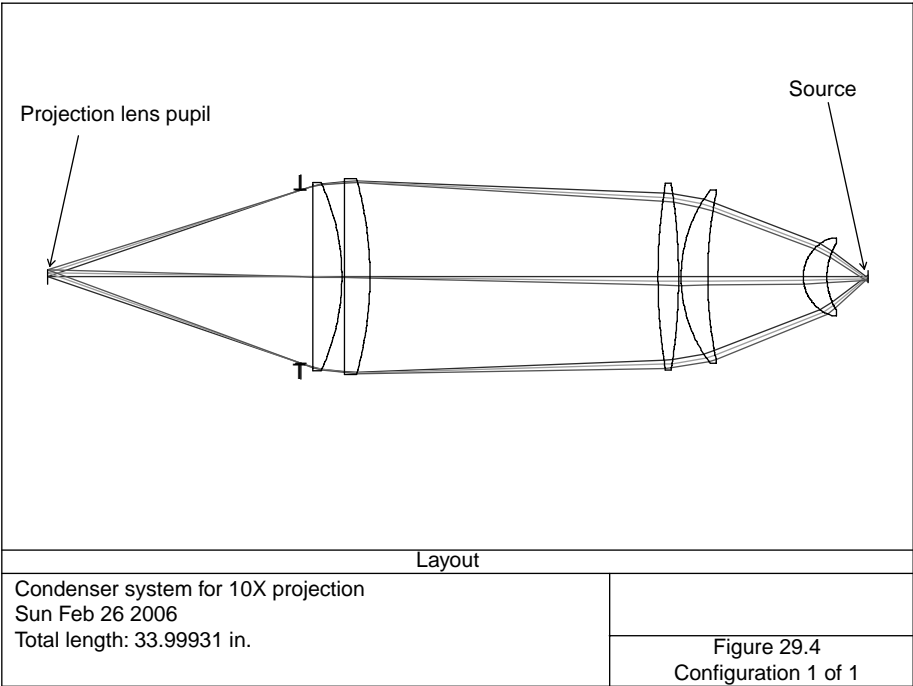
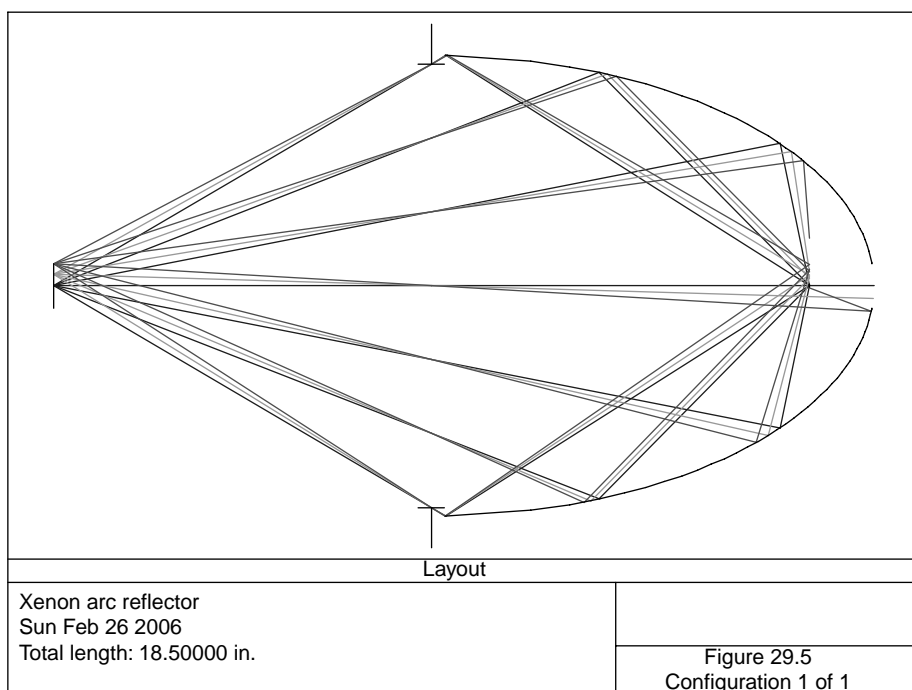


FIGURE 29.4 Condenser system for 10× projection.

TABLE 29.4  
Condenser System for 10× Projection

Surface	Radius	Thickness	Material	Diameter
0	0.0000	10.5000		0.596
1	Stop	0.5000		7.160
2	0.0000	1.2000	N-BK7	7.800
3	−9.2483	0.1100		7.800
4	0.0000	1.0500	N-BK7	8.120
5	−15.1872	11.9400		8.120
6	24.3817	0.8500	Pyrex	7.740
7	−24.3817	0.1100		7.740
8	5.9643	1.1000	Pyrex	7.180
9	17.2044	3.9593		6.980
10	1.6901	0.9800	Pyrex	3.220
11	2.6821	1.7000		2.760
12	0.0000	0.0000		0.489

Distance from the object (projection lens exit pupil) to source = 33.999, focal length = 69.613.



**FIGURE 29.5** Xenon arc reflector.

transparency, are made from N-BK7. The large air space between these elements and the rear Pyrex lenses contains a folding cold mirror.

For very large xenon arc lamps (as in movie picture projection), a far more efficient system uses a deep ellipsoidal mirror. The lamp is placed along the mirror axis, with the arc being at one of the ellipsoid's focii. Such a system is capable of collecting far more energy than the above described refractive devices. They have been made practical in recent years by the development of electroforming technology. In this process, a steel master is first made. It is then electroplated with nickel to perhaps a 2-mm thickness and then separated from the master. With proper controls, a low-stress part is produced. The inner concave surface then is aluminized.

Figure 29.5 shows an ellipsoidal reflector used with an arc source. Parameters for this reflector are

Axial radius	2.70641
Eccentricity ( $\epsilon$ )	0.853707, conic coefficient = $-\epsilon^2 = -0.728815$
Vertex to arc	1.46
Vertex to image	18.50
Magnification	12.67123

It should work well with a 7-kW xenon lamp. This has an arc size of  $1 \times 8$  mm. This same concept of the source being placed with its longitudinal axis along the axis of an elliptical-shaped reflector is also used with small tungsten halogen lamps (ANSI number ENH and number BHB). These lamps have a dichroic-coated reflector integral with the lamp; they are extensively used in consumer audio-visual products.

## REFERENCES

- Brueggemann, H. P. (1968) *Conic Mirrors*, Focal Press, New York.
- Cassarly, W. J. and Hayford, M. J. (2002) Illumination optimization: the revolution has begun, *International Optical Design Conference, 2002, SPIE*, Vol. 4832, Bellingham, WA, p. 258.
- Corning Glass Works (1984) Color filter glasses, Corning, NY 14831.
- DuPree, D. G. (1975) Electroformed metal optics, *Proc. SPIE*, 65: 103.
- General Electric (1988) Stage/studio lamps SS-123P, General Electric, Nela Park, Cleveland, OH 44112.
- GTE Sylvania (1977) *Sylvania Lighting Handbook*, Danvers, MA 01923.
- Hanovia (1988) Lamp Data, Hanovia, 100 Chestnut St., Newark, NJ 07105.
- Jackson, J. G. (1967) Light projection optical apparatus, US Patent #3318184.
- Koch, G. J. (1951) Illuminator for optical projectors, US Patent #2552184 and #2552185.
- Levin, R. E. (1968) Luminance, a tutorial paper, *SMPTE*, 77: 1005.
- Optical Radiation (1988) Lamp Data, Optical Radiation Corp., 1300 Optical Dr., Azusa, CA 91702.
- Sharma, K. D. (1983) Design of slide projector condenser, *Appl. Opt.*, 22: 3925.
- Smith, W. J. (2000) *Modern Optical Engineering*, McGraw Hill, New York.
- Wilkerson, J. (1973) Projection light source and optical system, US Patent #3720460.

---

# 30 Lenses for Aerial Photography

Aerial photography is used for a wide variety of applications, including military reconnaissance, aerial mapping, forest surveys, pollution monitoring, and various uses in oceanography. To record fine detail and to overcome the intrinsic grain size in film, long focal length lenses are combined with large format films. Standard widths of aerial films are 70 mm, 5.0 in., and 9.5 in. For dimensional stability, an ester-based film is preferred.

To reduce the effects of atmospheric haze, a filter is generally used. The purpose of this filter is to remove all short-wavelength radiation to which most films are very sensitive. Ultraviolet and blue radiation is scattered more than green and red radiation by water vapor and dust particles in the atmosphere. Typically used filters are

Wratten # 2A	Opaque to wavelengths shorter than 0.41 $\mu\text{m}$
3A	0.44 $\mu\text{m}$
4A	0.46 $\mu\text{m}$

Solid glass filters are also used. For a 3-mm thickness, the following apply:

GG420	Opaque to wavelengths shorter than 0.41 $\mu\text{m}$
GG455	0.44 $\mu\text{m}$
GG495	0.47 $\mu\text{m}$

To be useful for photogrammetry, these lenses have less than 0.1% distortion.

Figure 30.1 shows a 5-in. focal length,  $f/4$  wide-angle aerial camera lens. It is a modification of Rieche and Rische (1991). The distortion curve for this lens reaches a maximum value of  $-0.13\%$  at 0.7 of full field and has nearly zero distortion at full field (Table 30.1).

Figure 30.2 shows a 12-in. focal length,  $f/4$  aerial camera lens that covers a  $4\times 5$  in. film format (6.4 in. diagonal) (Table 30.2).

Figure 30.3 shows an 18-in. focal length  $f/3$  aerial lens of  $10^\circ$  field of view; details are given in Table 30.3. It covers a 2.25-in. square format (70-mm film). Axial secondary color is considerable in this design. It causes the best image surface to move about 50  $\mu\text{m}$  (away from the lens) from the image surface defined at 0.5461  $\mu\text{m}$ .

Figure 30.4 shows a 24-in. focal length  $f/6$  lens for use with the 9.5-in. wide film. Image size is  $9\times 4.5$  in. This corresponds to a field of view of  $23.66^\circ$  (Table 30.4).

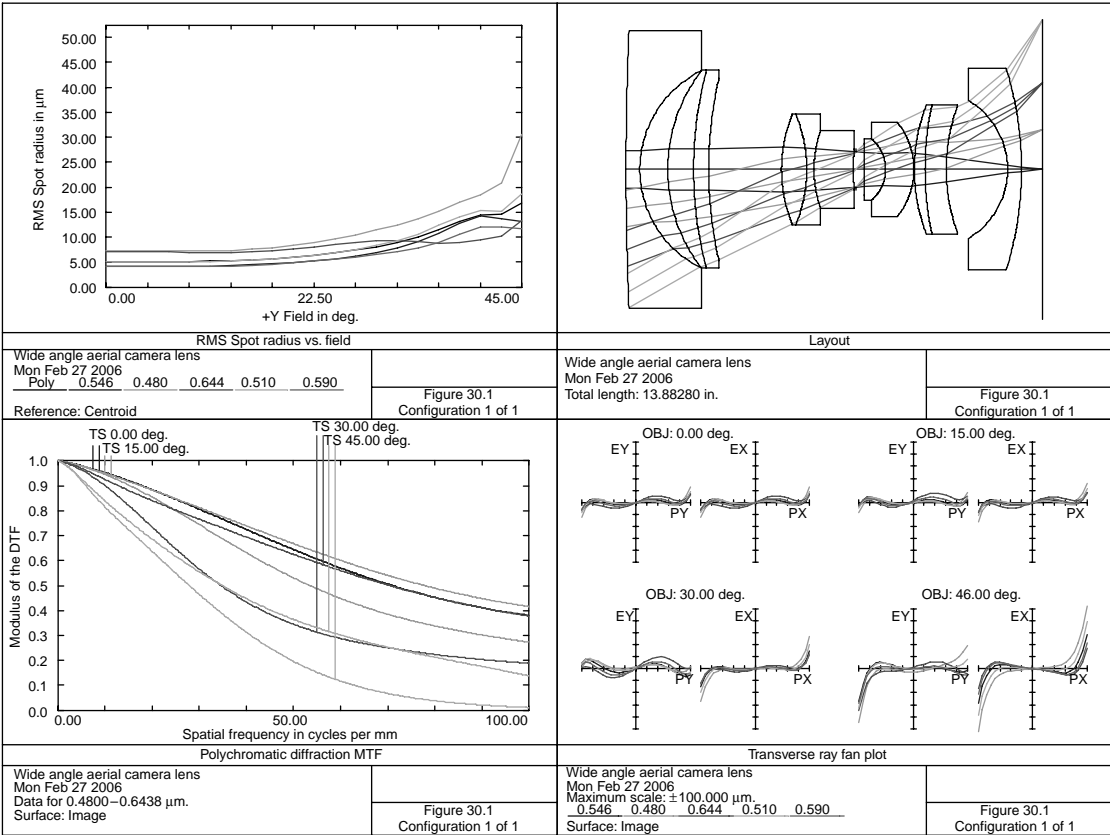


FIGURE 30.1 A 5-in.  $f/4$  aerial camera lens.

---

**TABLE 30.1**  
**Wide-Angle Aerial Camera Lens**

Surface	Radius	Thickness	Material	Diameter
1	110.0451	0.4604	N-FK5	9.260
2	3.6681	0.9308		6.580
3	5.3757	0.8631	N-LAF3	6.600
4	13.0828	0.4999	N-K5	6.600
5	13.5841	2.4301		0.100
6	4.8574	0.8373	LAKN13	3.690
7	−4.8943	0.2449	LLF1	3.690
8	3.8957	1.3133	LAKN13	2.620
9	7.8017	0.0886		1.360
10	Stop	0.2742		1.167
11	−37.7135	0.7134	N-FK51	1.720
12	−1.3462	0.9446	SF4	2.060
13	−2.5048	0.0125		3.140
14	5.9923	0.3546	SF4	4.300
15	10.2053	0.7098	N-LAK8	4.300
16	6.1582	2.0450		4.200
17	−2.6805	0.4604	N-SK5	4.620
18	−11.4269	0.7000		6.720
19	0.0000	0.0000		9.985

Distance from first lens surface to image = 13.883.

---

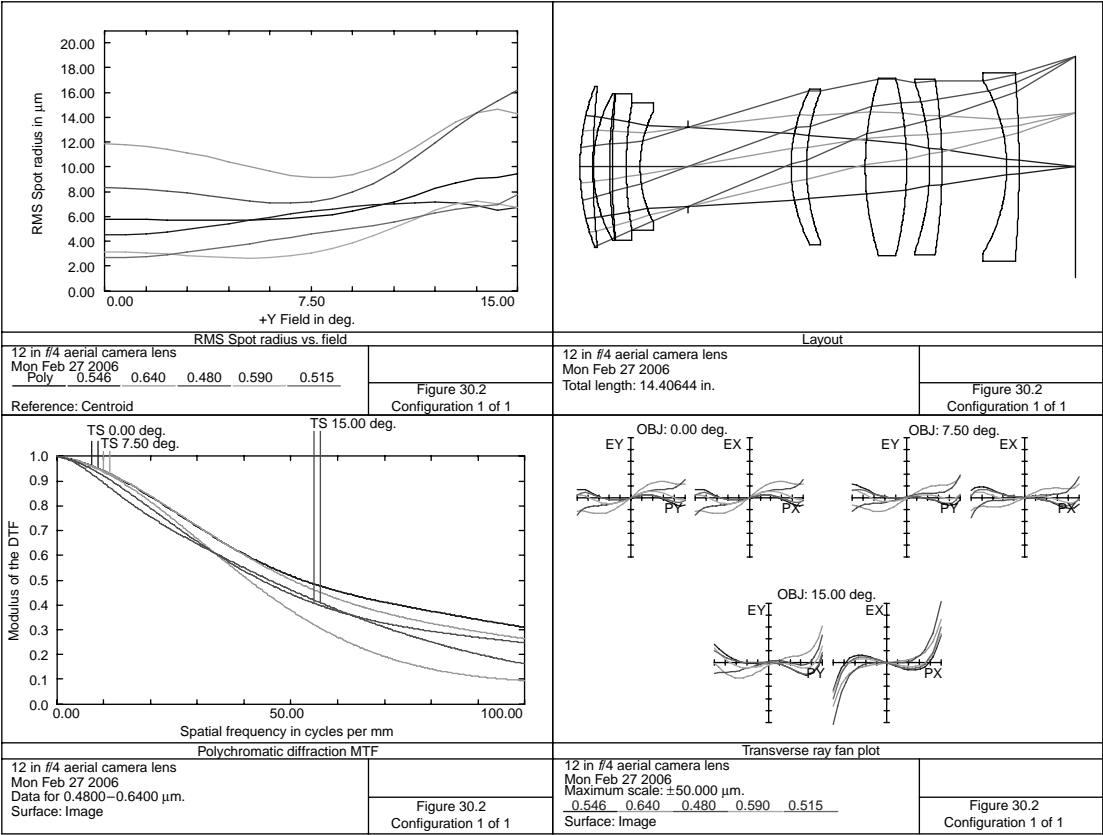


FIGURE 30.2 A 12-in. *f*/4 aerial lens.



**TABLE 30.2**  
**A 12-in.  $f/4$  Aerial Camera Lens**

Surface	Radius	Thickness	Material	Diameter
1	6.6030	0.3762	N-SK16	4.700
2	20.6605	0.0150		4.700
3	4.4208	0.4698	N-SK16	4.280
4	14.5008	0.0736		4.280
5	22.6257	0.4095	N-LAK21	4.280
6	10.4384	0.4028	SF5	3.700
7	3.5968	1.3792		3.200
8	Stop	3.0067		0.281
9	4.9032	0.4500	N-SK16	4.500
10	6.1144	1.7072		4.440
11	8.7324	1.2023	N-SK16	5.160
12	−10.5815	0.6659		5.160
13	−7.3027	0.3612	SF1	4.960
14	−15.8894	1.8786		5.080
15	−4.9302	0.3607	N-SK16	5.040
16	−33.9319	1.6480		5.460
17	0.0000	0.0000		6.433

Distance from first lens surface to image = 14.406, distortion = 0.13% (at 11.7°), field of view = 30°.

**TABLE 30.3**  
**An 18-in.  $f/3.0$  Aerial Lens**

Surface	Radius	Thickness	Material	Diameter
1	10.7516	2.2000	N-SSK2	7.600
2	40.5183	2.3449		7.200
3	5.6752	2.2364	N-SSK2	5.440
4	25.5110	0.5397	SF1	5.440
5	3.6865	0.4788		3.560
6	Stop	3.0863		3.487
7	−4.0816	0.8918	N-KZFS4	4.060
8	5.6748	1.5000	N-SSK2	5.340
9	−5.9607	0.4997		5.340
10	26.7675	0.7500	N-SSK2	5.700
11	−10.4439	10.6092		5.700
12	0.0000	0.0000		3.148

Distance from first lens surface to image = 25.137, distortion = 0.16%.

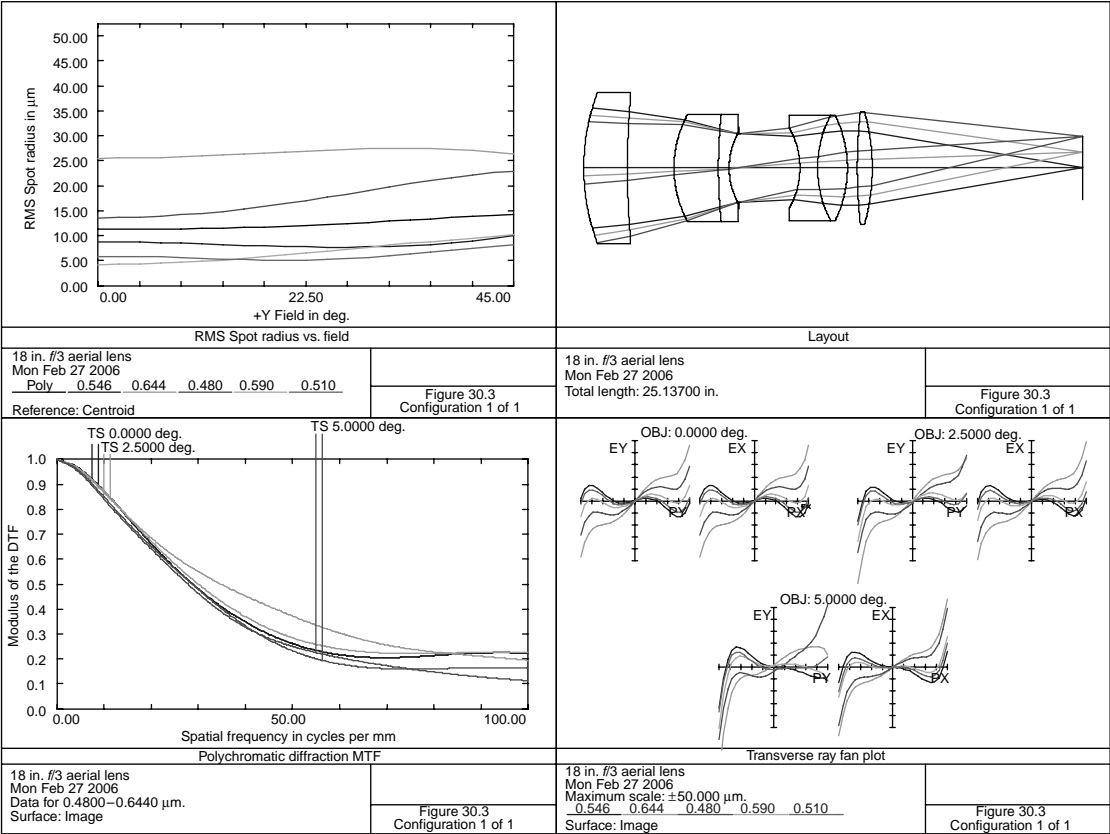


FIGURE 30.3 An 18-in. *f*/3 aerial lens.

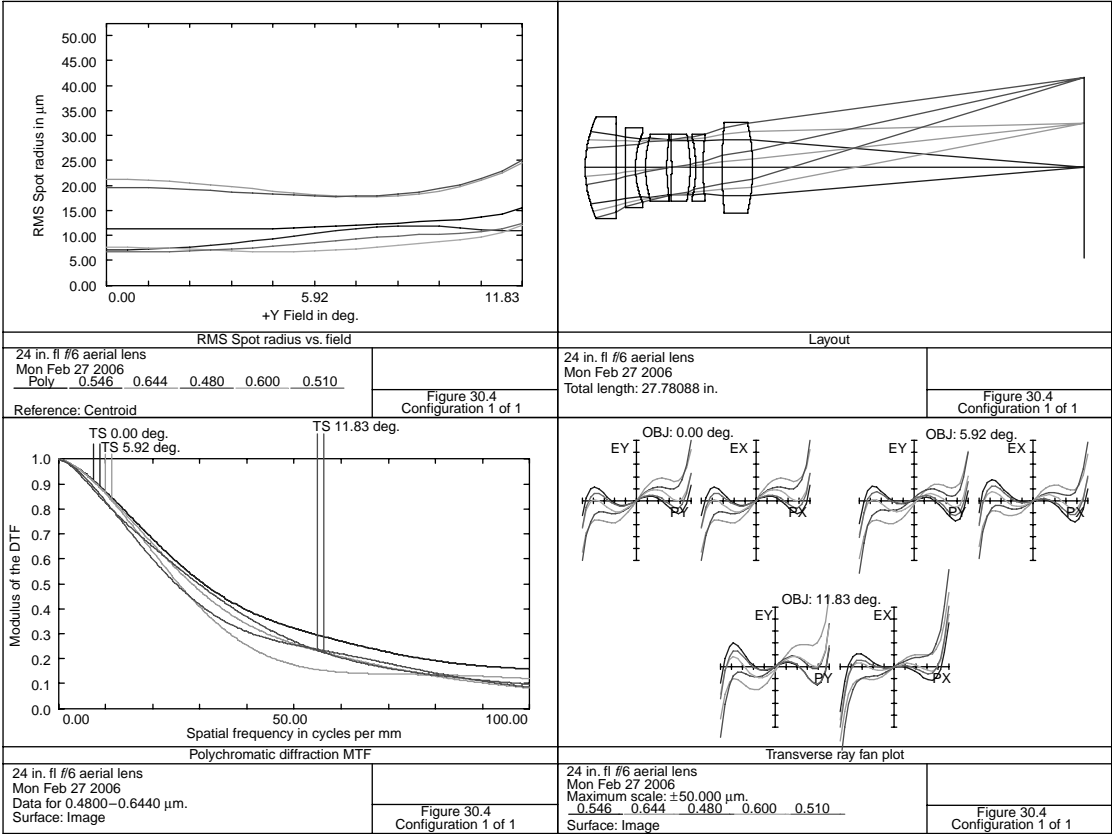


FIGURE 30.4 A 24-in. *f*/6 aerial lens.

**TABLE 30.4**  
**A 24-in.  $f/6$  Aerial Lens**

Surface	Radius	Thickness	Material	Diameter
1	6.8535	1.7210	N-LAK22	5.700
2	143.1421	0.5270		4.960
3	−194.9200	0.5500	LF5	4.440
4	4.8982	0.5611		3.900
5	6.3919	1.1796	N-LAF3	3.700
6	10.1724	0.1398		3.120
7	Stop	0.1265		3.062
8	−24.5739	1.0250	N-LAK33	3.140
9	−9.7198	0.3246		3.700
10	−7.1689	0.4000	LF5	3.480
11	13.7251	1.0629		3.760
12	24.6558	1.7000	N-LAK12	5.040
13	−11.1244	18.4633		5.040
14	0.0000	0.0000		10.049

Distance from first lens surface to image = 27.780, distortion = 0.056%.

Aerial cameras are quite large and expensive. They usually have the following features:

- Interchangeable lenses.
- Automatic exposure control.
- Means of recording CRT data in a corner of the frame.
- A focal plane shutter.

## REFERENCES

- Chicago Aerial Industries, (1960) *Data Sheets on Aerial Cameras*, Chicago Aerial Industries, Barrington, IL.
- Eastman Kodak Co., (1960) *Kodak Wratten Filters*, Pub. B-3, Eastman Kodak Co., Rochester, NY.
- Eastman Kodak Co., (1972) *Kodak Aerial Films*, Pub. M-57, Eastman Kodak Co., Rochester, NY, 1972.
- Eastman Kodak Co., (1974) *Properties of Kodak Materials for Aerial Photography*, Pub. M-61, M-62, and M-63, Eastman Kodak Co., Rochester, NY.
- Eastman Kodak Co., (1982) *Kodak Data for Aerial Photography*, Pub. M-29, Eastman Kodak Co., Rochester, NY.
- Hall, H. J. and Howell, H. K., eds., (1966) *Photographic Considerations for aerospace*, Itek Corp., Lexington, MA.
- Hoya Optics, (2004) *Hoya Color Filter Glass Catalog*, Hoya Optics, Fremont, CA.

- Rieche, G. and Rische, G., (1991) Wide angle objective, US Patent #5056901.
- Schott Glass Technologies, (1993) *Schott Optical Glass Filters*. Schott Glass Technologies, Duryea, PA.
- Thomas, W., ed, (1973) *SPSE Handbook of Photographic Science and Engineering*, Wiley, New York.



---

# 31 Radiation-Resistant Lenses

Most optical glasses will darken (sometimes called *browning*) when exposed to x-ray or gamma radiation. This darkening is due to the presence of free electrons in the glass matrix. The darkening is not stable in that it decreases with time. Raising the temperature and exposure to light accelerates this clearing process. Pure grades of fused silica (silicon dioxide) or quartz are very resistant to the effects of ionizing radiation.

Resistance to ionizing radiation may be increased in optical glasses by the addition of  $\text{CeO}_2$  to the glass formula. This causes considerable absorption at  $0.4\text{ }\mu\text{m}$ ; however, it substantially improves the glasses' radiation resistance. Most of the major optical glass manufacturers have stabilized some of their most common optical glasses with cerium. Unfortunately, variety is limited and delivery sometimes are slow.

Ceria-stabilized materials from Schott have a "G" in their designation and a number identifying the  $\text{CeO}_2$  concentration. The number represents  $10\times$ , in percent, the  $\text{CeO}_2$  concentration. Thus BAK1G12 contains 1.2%  $\text{CeO}_2$ .

Optical cements should not be used here. Most of the materials used for antireflection coatings are very resistant to radiation, so coatings should present no problems.

Figure 31.1 shows a 25-mm  $f/2.8$  triplet made from radiation-resistant glasses; details are provided in Table 31.1. It was designed to be used with a 1-in. vidicon or a 1-in. CCD (0.625-in. diagonal). It has the usual triplet form: high index crowns for the front and rear elements, and a low index of refraction for the middle elements which tends to reduce the Petzval sum.

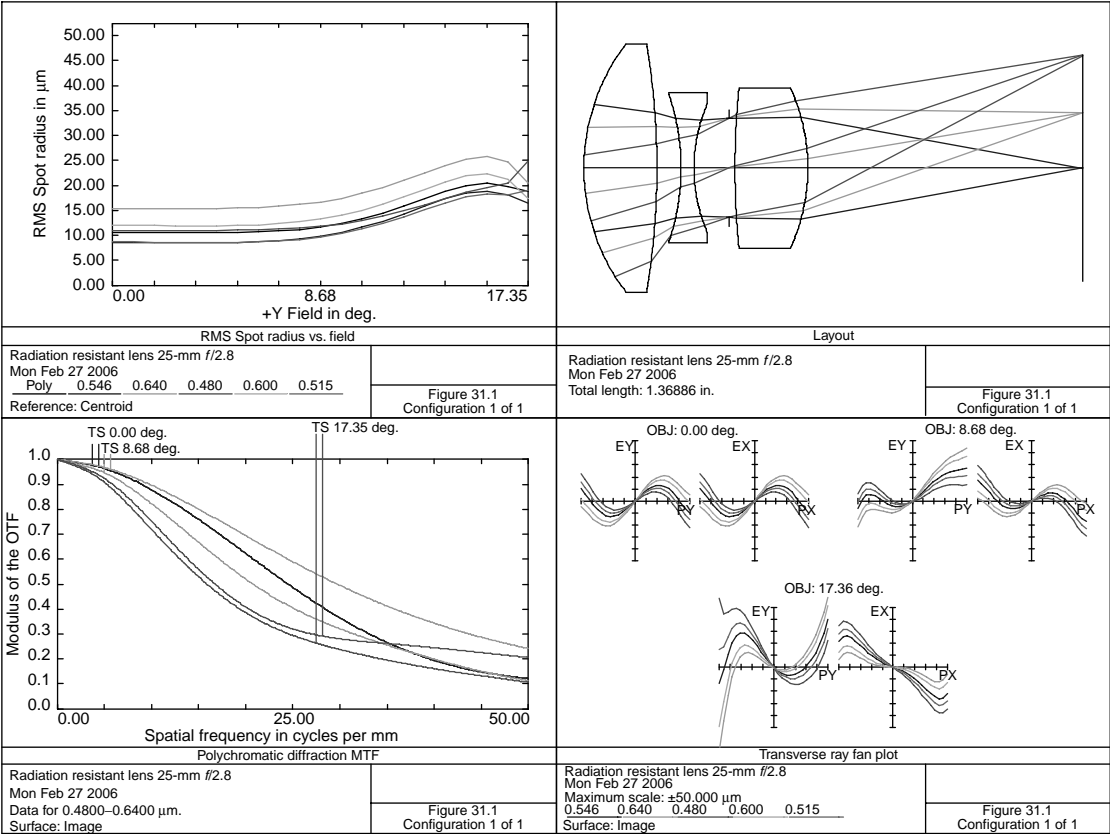


FIGURE 31.1 Radiation resistant lens, 25-mm, f/2.8.



**TABLE 31.1**  
**Radiation Resistant Lens**

Surface	Radius	Thickness	Material	Diameter
1	0.5593	0.2000	LAK9G15	0.680
2	−2.1032	0.0664		0.680
3	−0.6289	0.0355	F2G12	0.412
4	0.4459	0.0972		0.352
5	Stop	0.0150		0.271
6	2.1051	0.2000	LAK9G15	0.440
7	−0.5282	0.7547		0.440
8	0.0000	0.0000		0.623

Distance from first lens surface to image=1.369, maximum distortion=0.08% (at 14°).

**REFERENCES**

Kircher, J. and Bowman, R., eds., (1964) *Effects of Radiation on Materials and Components*, Reinhold Publishing Corp., New York.

Schott Glass (2003) *Radiation Resistant Optical Glass*, Schott Glass Technologies, Duryea, PA.



---

# 32 Lenses for Microprojection

Microprojection optical systems are used by banks to record checks and other financial data, by credit card companies to record transactions, by libraries to make available many less-used documents, by auto parts distributors to conveniently produce auto parts manuals, etc. The sensitive materials are either high-resolution diazo or conventional silver-based emulsions.

The projector contains a light source and condensing system, a projection lens that images the film onto a high-gain screen, and a film-transport mechanism. Some systems also have a pechan prism incorporated into the optical design to allow the user to rotate the image on the screen.

In [Figure 32.1](#) is shown a  $24\times$  microprojection lens; details are provided in [Table 32.1](#). Track length (object to image distance) is 40.0. It is  $f/2.8$  and the  $NA$  is 0.192. It was designed to be used for a microfiche system. This format consists of 60 images on a film  $5.826\times 4.134$  (Williams 1974) each image being  $0.5\times 0.395$  in. ( $0.637$  in. diagonal) which is then projected onto a screen (the object in this case)  $15.288$  diagonal. At the top portion of the film is a title. An alternate version uses 98 images on the same size film.

Rather than bounding the magnification in the merit function, magnification was held with a marginal ray angle solve. Object space  $NA$  was set to 0.00742 and so the marginal ray angle (to maintain the  $-24\times$  magnification) at surface 12 becomes  $0.00742\times(-24)=-0.17808$ .

Distortion reaches its maximum value of 0.04% at an object height of 6.0. Lens focal length is 1.542. Note that the next to the last element although of negative power, consists of a crown material (K10).

*Ultrafiche* is a system used with greater than  $100\times$  reduction (Grey 1970; Fleischman 1976b).

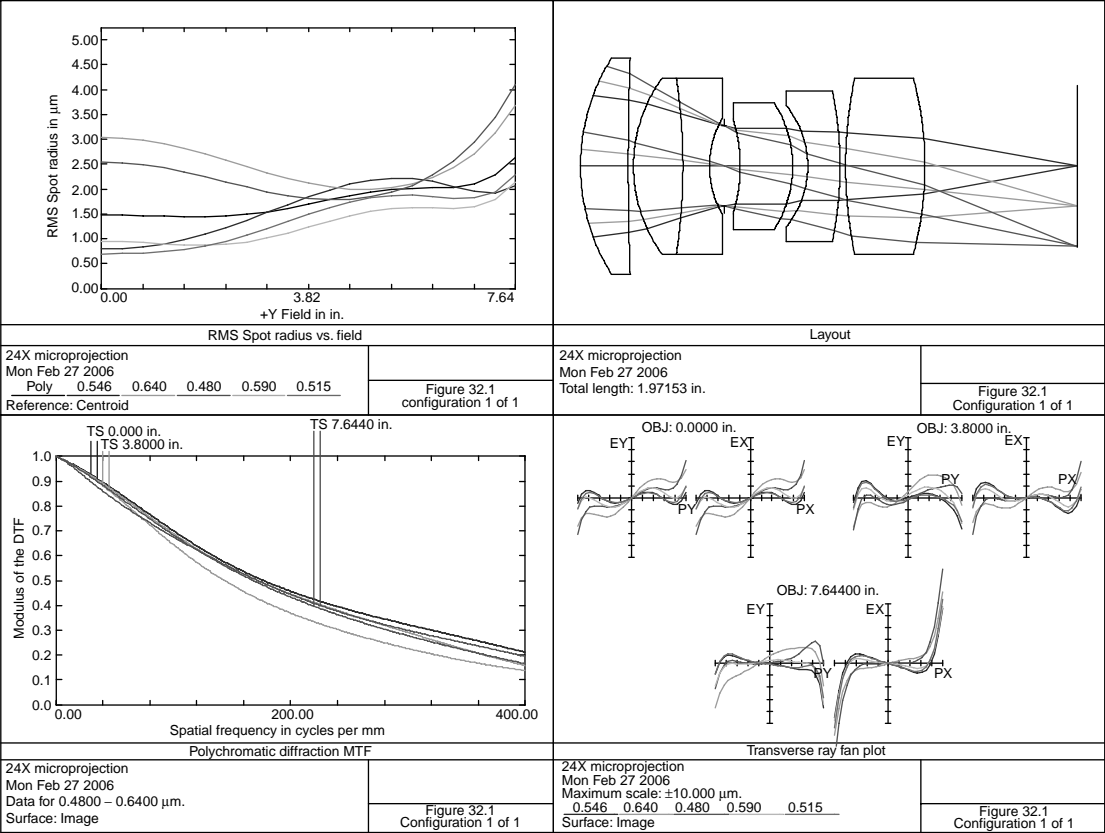


FIGURE 32.1 A 24× microprojection lens.

**TABLE 32.1**  
**A 24× Microprojection Lens**

Surface	Radius	Thickness	Material	Diameter
0	0.0000	38.0293		15.288
1	0.8117	0.1891	N-SSK2	0.860
2	12.3916	0.0209		0.860
3	0.5938	0.1959	N-SSK5	0.700
4	−2.3188	0.1055	SF1	0.700
5	0.3800	0.0576		0.380
6	Stop	0.0640		0.318
7	−0.6494	0.2081	N-LAK7	0.380
8	−0.4736	0.0601		0.500
9	−0.3811	0.1280	K10	0.480
10	−1.4774	0.0218		0.600
11	1.6919	0.3148	N-LAK7	0.700
12	−1.3624	0.6056		0.700
13	0.0000	0.0000		0.637

Object distance to first lens surface = 38.029, distance, first lens surface to image = 1.971.

## REFERENCES

- Fleischman, A. (1976a) Microfilm recorder lens, US Patent #3998529.  
 Fleischman, A. (1976b) 7 mm ultrafiche lens, US Patent #3998528.  
 Grey, D. S. (1970) High magnification high resolution projection lens, US Patent #3551031.  
 Olson, O. G. (1967) Microfilm equipment, *Applied Optics and Optical Engineering*, Vol. 4, Kingslake, R., ed., Academic press, New York, p. 167.  
 SPSE, (1968) Microphotography, fundamentals and applications, Symposium held in Wakefield, MA, April 1968.  
 Williams, B. J. S. and Broadhurst, R. N. (1974) Use of microfiche for scientific and technical reports, AGARD Report 198, NITS, Springfield, VA.



# 33 First-Order Theory, Mechanically Compensated Zoom

In the discussions that follow, a zoom lens is an optical system in which the focal length (or magnification) varies while the image plane remains stationary. For an excellent compendium of zoom lens papers, see Mann (1993). (Variable focal length lenses in which the image plane substantially moves are discussed in [Chapter 38](#).) All of these systems are rotationally symmetric.

It is desirable to divide the zoom region into logarithmically equal spaces: each succeeding focal length (or magnification) is obtained by multiplying the previous focal length by a constant. For example, for a  $10\times$  zoom lens and four positions, this multiplier becomes the cube root of 10 (2.15443). In the data presented, this is only approximately true because the desired value of focal length (or magnification) was entered into the optimization program as a bounded item.

In [Figure 33.1](#) is shown a four-component mechanically compensated zoom system. Lens group A is the front group. It only moves for focusing purposes. Therefore, the moving groups B and C always see a fixed virtual object for all conjugate distances. Group D is fixed. It generally contains the iris (the aperture stop) so that the image is always at a constant numerical aperture for all zoom positions.

For purposes of this discussion, two paraxial rays will be traced from the object to the image. For convenience, one ray is defined as emanating from an axial point; the height it makes on a surface is labeled as  $H$  and its angle with the optical axis is labeled  $U$ . The other ray will be a chief ray and has coordinates  $\bar{H}$  and  $\bar{U}$  (actually, any two paraxial rays will suffice). As shown in [Figure 33.1](#),  $\bar{U}_K$  is a negative number because the ray is falling.

The Invariant,  $\Psi$ , is given by

$$\Psi = \bar{H}NU - HN\bar{U}.$$

Because  $\Psi$  has the same value at each surface, it may be evaluated at the first lens surface. At this surface,  $\bar{H}$  is made zero; therefore, for a system in air,  $\Psi = -H_1\bar{U}_1$ .

As a further simplification, the paraxial rays are traced such that  $H_1=1$  and  $\bar{U}_1=1$ .

Therefore,  $\Psi = -1$ . The effective power of the B group is then given by (Hopkins 1962).

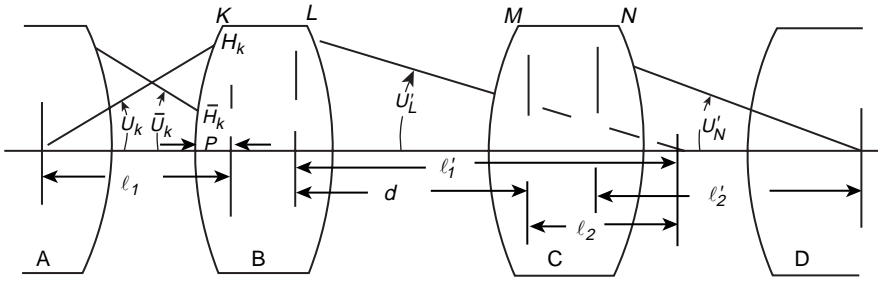


**FIGURE 33.1** A four-component mechanically compensated zoom system.

$$P_b = U_K \bar{U}' - \bar{U}_L U'_L$$

Hanav and Hopkins (1962).

Likewise for the C group,  $P_c$ , and the complete system,  $P$ .

As discussed above, the A group creates a virtual object for the B group. This distance from surface K is  $H_K/U_K$ . Likewise, the image distance after going through group C from surface N is  $H_N/U'_N$ .

The back focal length, BFL, of the B group is found by

$$\text{BFL}_b = \frac{-[\bar{H}_L U_K - H_L \bar{U}_K]}{P_b}.$$

The front focal length, FFL, of the B group is found by

$$\text{FFL}_b = -\frac{[\bar{H}_K U'_L - H_K \bar{U}'_L]}{P_b}.$$

And, of course, the same is true for the C group.

The distance  $P$  of the principal plane from surface K is

$$P = \frac{1}{P_b} + \text{FFL}_b.$$

( $\text{FFL}_b$  is negative if image is to the left.) Therefore,

$$l_1 = -[H_K/U_K + 1/P_b + \text{FFL}_b],$$

because  $l_1$  is a negative number as shown.

The magnification of the B and C groups is  $M = U_K/U'_N$ . The separation between the B and C groups,  $d$ , (measured between principal planes) is given by

$$d = \frac{P_b + P_c - P_{bc}}{P_b P_c} = T(L) + \frac{1}{P_b} - \text{BFL}_b - \frac{1}{P_c} + \text{FFL}_c.$$

where  $P_{BC}$  is the power of the B-C group.

Let  $S$  be the distance between object and image (minus the principal plane separations) of the B and C group.



$$S = d + l'_2 + l_1.$$

This is to remain constant as the lens is zoomed. Following the nomenclature of Clark (1973), the original positions are denoted by  $l$  and the new positions are denoted by  $L$ .

The B and C lens groups are now moved to new positions. Their separation is  $D$ .

$$L'_1 = L_1/(1 + P_b L_1); \quad (33.1)$$

$$L'_2 = L_2/(1 + P_c L_2); \quad (33.2)$$

$$M = \frac{L'_1 L'_2}{L_1 L_2} = \frac{1}{(1 + P_b L_1)(1 + P_c L_2)}; \quad (33.3)$$

$$S = -L_1 + L'_1 - L_2 + L'_2. \quad (33.4)$$

Substituting Equation 33.1 and Equation 33.2 into Equation 33.4 gives

$$S = \frac{-P_b L_1^2}{1 + P_b L_1} - \frac{P_c L_2^2}{1 + P_c L_2}. \quad (33.5)$$

From Equation 33.3,

$$\frac{1}{1 + P_c L_2} = M(1 + P_b L_1).$$

Substituting into Equation 33.5 results in

$$L_2 = \frac{1 - M(1 + P_b L_1)}{MP_c(1 + P_b L_1)} \quad (33.6)$$

Substituting Equation 33.6 into Equation 33.5 gives

$$S(1 + P_b L_1) = \frac{-P_b L_1^2 - [1 - M(1 + P_b L_1)]^2}{MP_c}.$$

Solving for  $L_1$ ,

$$L_1 = \frac{-b[b_2 - 4ac]^{1/2}}{2a}, \quad (33.7)$$

where

$$a = MP_b P_c + M^2 P_b^2,$$

$$b = SMP_b P_c - 2MP_b + 2M^2 P_b,$$

and

$$c = SMP_c + M^2 - 2M + 1.$$

The sign for the square root term in Equation 33.7 is so chosen that it would yield the starting solution values:  $L_1 = l_1$ . The value for the sign, then, is

$$\frac{2al_1 + b}{\sqrt{b^2 - 4ac}},$$

which takes on of a value of  $\pm 1$ .

From Equation 33.1, a new value of  $L'_1$  may be found, and from Equation 33.5, a new value of  $L_2$  may be found.

The separation between the B and C groups then becomes

$$D = L'_1 - L_2.$$

Again,  $D$  is measured between principal planes of the B and C groups. Because these principal planes do not change locations with respect to their groups as the lens assembly zooms, the new zoom spacers become

$$TH1 = T(K - 1) + l_1 - L_1,$$

$$TH2 = T(L) + D - d,$$

$$TH3 = T(K - 1) + T(L) + T(N) - TH1 - TH2,$$

where  $TH1$  is the zoom space between the A and B groups. Likewise,  $TH2$  corresponds to the B–C space and  $TH3$  is for the C–D space.

Clark (1973) gives a different thin-lens analysis for this mechanically compensated system. A great deal of effort has been made to reduce the size and weight of commercially made zoom lenses for cameras (Masumoto 1998). Particular emphasis has been placed upon the 35- to 105-mm zoom for single-lens reflex (SLR) cameras and recently for the CCD compact camera. This has been helped by the development of technology for the economic production of aspheric surfaces. All examples shown in [Chapter 35](#) are spherical solutions.

## REFERENCES

- Chunken, T. (1992) Design of a zoom system by the varifocal differential equation, *Applied Optics*, 31: 2265.
- Clark, A. D. (1973) *Zoom Lenses*, American Elsevier, New York.
- Grey, D. S. (1973) Zoom lens design, *Proceedings of SPIE*, Volume 39, p. 223.
- Hanau, R. and Hopkins, R. E. (1962) *Optical Design*, MIL-HDBK-141, Standardization Division, Defense Supply Agency, Washington, DC.
- Kingslake, R. (1960) the development of the zoom lens, *JSMPT*, 69: 534.
- Masumoto, H. (1982) Development of zoom lenses for cameras, *International Optical Design Conference, 1998, SPIE*, Volume 3482, p. 202.
- Yamaji, K. (1967) Design of Zoom Lenses, In *Progress in Optics*, Wolf, E., ed., Volume. 6, Academic Press, New York.

# 34 First Order Theory, Optically Compensated Zoom Lenses

In an optically compensated zoom lens, all of the moving lens groups, move in unison, as if they were linked together on a common shaft. This is shown in [Figure 34.1](#). It has the distinct advantage that no cam is required. However, such systems are generally longer than a comparable mechanically compensated system. Most important, the image plane moves slightly with zoom. An object of the designer is to make this movement less than the depth of focus.

Referring to Figure 34.1, lens groups A, C, and E are fixed while groups B and D are linked together. Tracing a paraxial, axial ray, it makes an angle with the optical axis after refraction at surface M of  $U'_M$  and emerges at the last surface, K with an angle  $U'_K$ . Tracing a paraxial chief ray through the system is denoted by  $U'_M$  etc. The axial space between surfaces M and M + 1 is  $T(M)$  Hanau and Hopkins (1962):

$$\frac{dU'_K}{dT(M)} = NU'_M \left[ \overline{U'_K} U'_M - U'_K \overline{U'_M} \right] / \psi,$$

where  $\psi$  is the invariant equal to  $N\overline{H}U - NH\overline{U} = -H_0\overline{U}$  for an object in air.

The zoom ratio, Z, given by

$$Z = \frac{[U'_K]_1}{[U'_K]_2},$$

where subscript 1 denotes the system at its initial position and subscript 2 denotes the system in its final zoom position. Since we are dealing with derivative changes, the total change in  $U'_K$  is the sum of these changes for all the variable air spaces.

As discussed above, the image moves with zoom. Wooters and Silvertooth (1965) have shown that the maximum number of positions where the longitudinal image motion is zero is equal to the number of moving air spaces. One must realize that for a distant object, if the first group moves, this is not considered a variable air space. Also this is the maximum number of crossing points; an actual system may very well have fewer.

As an extreme example, we may consider a zoom lens with only one moving element. [Figure 34.2](#) shows such a thin lens arrangement for a distant object. Paraxially, one obtains an effective focal length, EFL, and back focal length, BFL, of

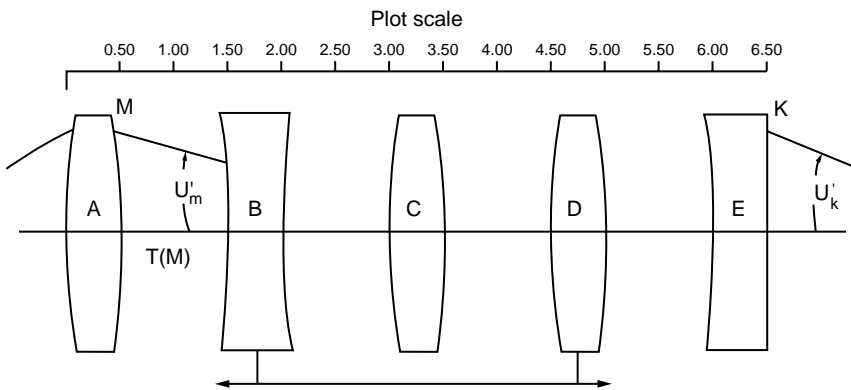


FIGURE 34.1 Optically compensated zoom lenses.

$$EFL = \frac{F_A F_B}{F_A + F_B - D},$$

$$BFL = \frac{(F_A - D) F_B}{F_A + F_B - D}.$$

For the image to be stationary,  $D + BFL$  is a constant.

If we move the B lens to a new position we obtain new values for EFL, BFL, and of course D. Let the new EFL be noted as  $Z(EFL)$  Where Z then is the zoom ratio.

For the sum of  $D + BFL$  to be the same as previous value,

$$Z = \frac{F_A^2}{EFL^2}.$$

The new value of D would be;

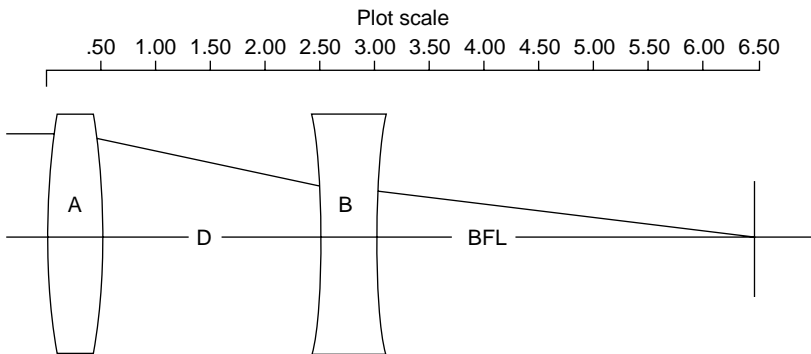


FIGURE 34.2 Zoom with one moving lens.

$$D_2 = F_A + F_B - \frac{F_A F_B}{Z(\text{EFL})}.$$

The image would be in the same location at these two positions.

Johnson and Feng (1992) discuss an afocal, infrared lens system with one moving group. They call it mechanically compensated. By this definition, it is optically compensated since the image remains exactly stationary at only two positions. However, if the cams are so arranged as to move both lens groups in relation to the image plane, then obviously the image will remain stationary. See [Chapter 38](#) for variable focal length lenses.

## REFERENCES

- Back, F. G. and Lowen, H. (1954) The basic theory of varifocal lenses with linear movement and optical compensation, *JOSA* 44: 684.
- Bergstern, L. (1958) General theory of optically compensated varifocal systems, *JOSA* 48: 154.
- Hanau, R. and Hopkins, R. E. (1962) *Optical Design, MIL-HDBK-141*, Defense Supply Agency, Washington, DC.
- Jamieson, T. H. (1970) Thin lens theory of zoom systems, *Optica Acta*, 17: 565.
- Johnson, R. B. and Feng, C. (1992) Mechanically compensated zoom lenses with a single moving element, *Applied Optics*, 31: 2274.
- Mann, A. (1993) Selector papers on zoom lenses, *SPIE MS85*. SPIE, Bellingham, WA.
- Pegis, R. J. and Peck, W. G. (1962) First-order design theory for linearly compensated zoom systems, *JOSA* 52: 905.
- Wooters, G. and Silvertooth, E. W. (1965) Optically compensated zoom lens, *JOSA* 55: 347.



---

# 35 Mechanically Compensated Zoom Lenses

In [Figure 35.1](#) is shown a  $10\times$  mechanically compensated zoom lens covering the range 0.59–5.9 (15–150 mm). The lens is  $f/2.4$  and has a 0.625 (16-mm) diameter image. The lens prescription (at the short focal length) is given in [Table 35.1a](#). It is designed for an object at infinity for a 1-in. vidicon or a 1-in. single-chip CCD.

This lens is of the form  $+, -, +, +, +$ , i.e., all the groups are positive except for the first moving group, surfaces 6 through 10. The variable air spaces are given in [Table 35.1b](#).

Note that in the short-focal-length position, surface 15 comes too close to the stop and so this should be increased to allow for the usual iris mechanism. In [Figure 35.1a](#), the lens is shown in its short-focal-length position.

[Figure 35.1b](#) shows the movement of the lens groups.  $T(5)$  and  $T(10)$  are large monotonic functions.  $T(15)$  is nearly linear but only has a small movement. MTF data for this lens is displayed in [Figure 35.1c](#). These correspond to the four focal positions of the above table. If this lens is used for 16-mm cinematography, the field of view will be slightly reduced. For example,

- 16-mm format has a 12.7-mm diagonal
- Super-16 format has a 14.5-mm diagonal

If used with a 1-in. vidicon (that has a 16-mm diagonal) then one should add the camera-tube face-plate glass to the lens prescription. This is generally a low-index-of-refraction crown glass (1.487) (see [Appendix A](#)). Most color TV cameras now use a prism beam splitter to separate the red, green, and blue images (Cook 1973). Reoptimization in this case would be required.

Many low-power microscopes, used in inspection, as surgical microscopes, for electronic assembly, etc., use an afocal pod as a means of obtaining the zoom. This has the advantage of forming modular components. That is, the objective, eyepiece, and prism assembly are the same as on the fixed-power microscopes. The afocal pod is inserted to zoom. [Table 35.2a](#) gives the prescription for such an afocal system. It has a zoom ratio of four.

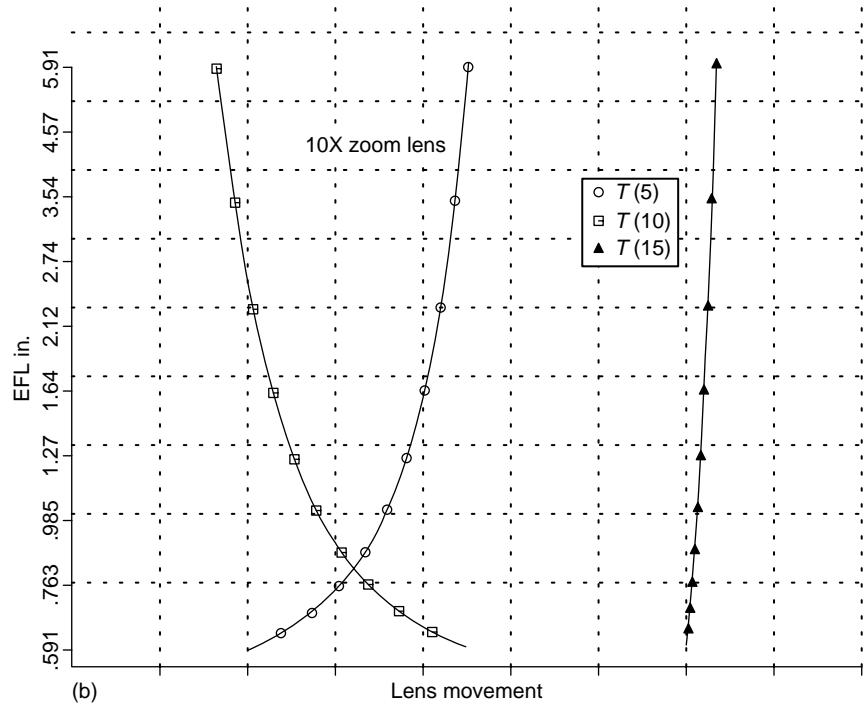
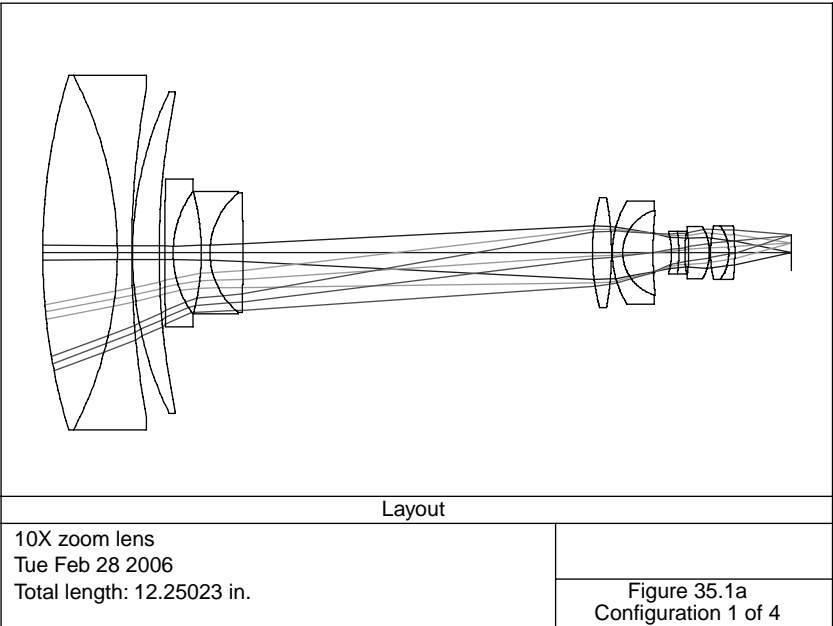


FIGURE 35.1 (a) Layout, (b) Lens movement, (c) MTF plots.



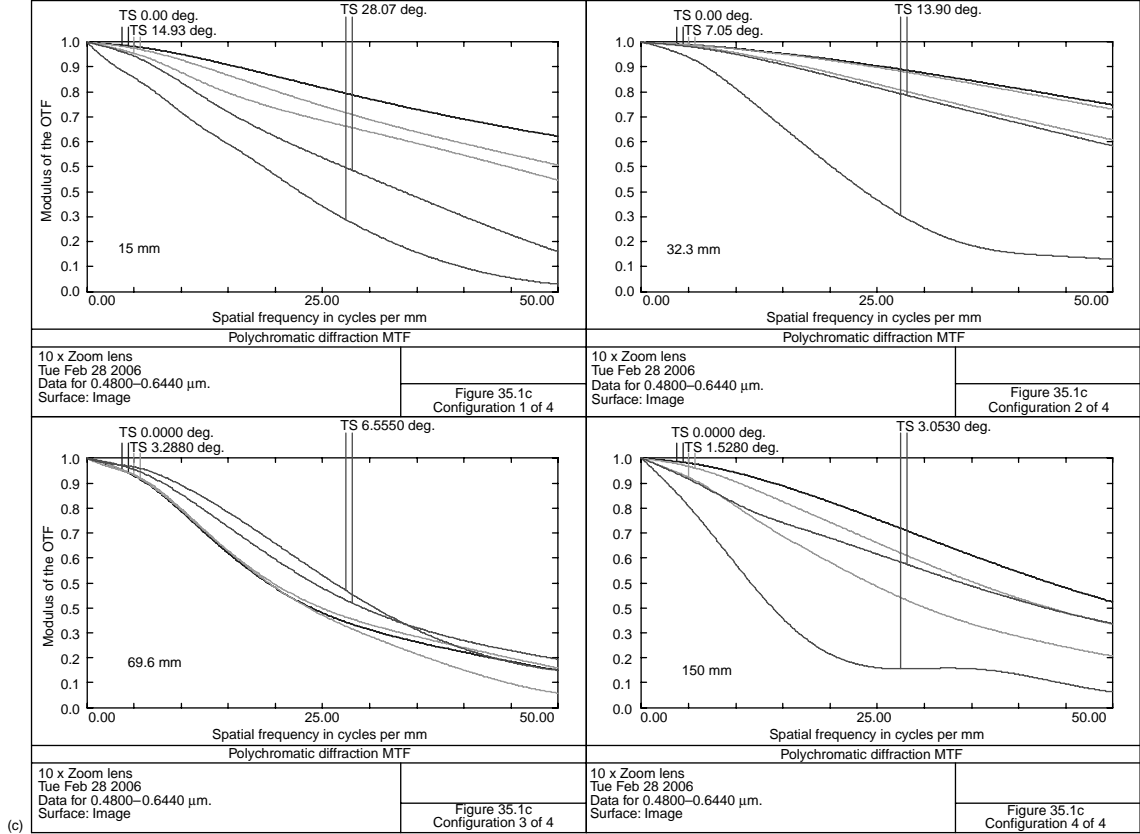


FIGURE 35.1 (continued)

**TABLE 35.1a**  
**A 10× Zoom Lens**

Surface	Radius	Thickness	Material	Diameter
1	10.0697	1.2211	N-LAK9	5.800
2	−6.2327	0.2360	SF5	5.800
3	15.1603	0.0150		5.380
4	6.0741	0.4336	N-LAF21	5.260
5	12.9033	0.0903		5.200
6	41.2877	0.1400	N-LAK9	2.420
7	1.7269	0.4613		2.000
8	−3.8953	0.1400	N-LAK9	2.000
9	1.2599	0.5386	SF5	1.960
10	−43.9995	5.7197		1.960
11	3.4298	0.3125	N-LAK9	1.800
12	−4.9794	0.0150		1.800
13	1.6004	0.1698	SF1	1.680
14	0.7220	0.4947	N-LAK9	1.380
15	6.9314	0.0090		1.380
16	Stop	0.2934		0.639
17	−1.2083	0.1191	N-LAK8	0.660
18	−2.8138	0.0984	SF1	0.700
19	1.9740	0.0659		0.700
20	−2.5527	0.3367	N-SF8	0.700
21	−0.8716	0.0200		0.860
22	1.9698	0.2970	N-BAK4	0.880
23	−0.7692	0.1000	SF1	0.880
24	−3.7908	0.9232		0.880
25	0.0000	0.0000		0.589

**TABLE 35.1b**  
**Focal Length, Spacings, and Distortion**

EFL	T(5)	T(10)	T(15)	Distortion (%)
0.591	0.0903	5.7197	0.0090	−8.5
1.272	2.4124	3.2501	0.1566	−0.6
2.741	4.0081	1.4376	0.3733	1.73
5.905	5.1199	0.0100	0.6891	2.95

Distance from first lens surface to image=12.250

**TABLE 35.2a**  
**Afocal Zoom for Microscope**

Surface	Radius	Thickness	Material	Diameter
1	Stop	−2.3622		0.400
2	1.2388	0.1504	K10	0.760
3	9.3542	0.0234		0.760
4	1.3062	0.0787	SF1	0.700
5	0.6690	0.1145	N-PSK3	0.700
6	2.4729	0.6310		0.600
7	2.6233	0.0709	N-SK16	0.460
8	0.2835	0.1794	N-SSK5	0.460
9	0.9740	0.3496		0.360
10	−0.6347	0.0606	N-SK16	0.320
11	3.7396	0.3475		0.320
12	−1.7308	0.0492	N-SK16	0.400
13	0.6212	0.1614	SF1	0.500
14	2.3140	0.1352		0.440
15	38.9045	0.0789	SF1	0.880
16	1.5054	0.1923	N-PSK3	0.880
17	−2.5537	0.0362		0.880
18	5.2888	0.2755	N-BK7	0.880
19	−1.7936	0.0000		0.880
20	0.0000	39.3700		0.785

The system is shown in [Figure 35.2a](#) in the  $M=2$  power position. Distance from the first to last surface is 2.935. MTF data is presented in [Figure 35.2b](#). Zoom movement and distortion data are presented in [Table 35.2b](#).

As discussed previously, the zoom region is divided into four equally spaced (logarithmically) divisions; the factor becomes  $\sqrt[3]{4}=1.5874$ .

Note that a paraxial trace of the above system yields an angular magnification of 1.955 at the first zoom position. The semi field angle is represented by  $\theta$ , measured in degrees of the entering beam. The above zoom movements are plotted in [Figure 35.2c](#). From this, we note that  $T(14)$  moves in a nearly linear fashion, whereas  $T(11)$  reverses direction at about 0.78 magnification.

In [Figure 35.3a](#) is shown an infrared Cassegrain zoom lens. It has an intermediate image inside the primary mirror. It was designed to cover the wavelength region of  $3.2\text{ }\mu\text{m}$ – $4.2\text{ }\mu\text{m}$ . The relative weightings are given in [Table 35.3a](#). The prescription is given in [Table 35.3b](#). [Table 35.3c](#) gives the focal lengths, spacings and distortion.

The entrance pupil has a constant 3.937 diameter and is located 23.164 to the right of the first lens surface. This places the aperture stop in contact with the secondary mirror that has the effect of minimizing the diameter required (and hence the obscuration) of the secondary mirror. Image diameter is 0.157 (4 mm).

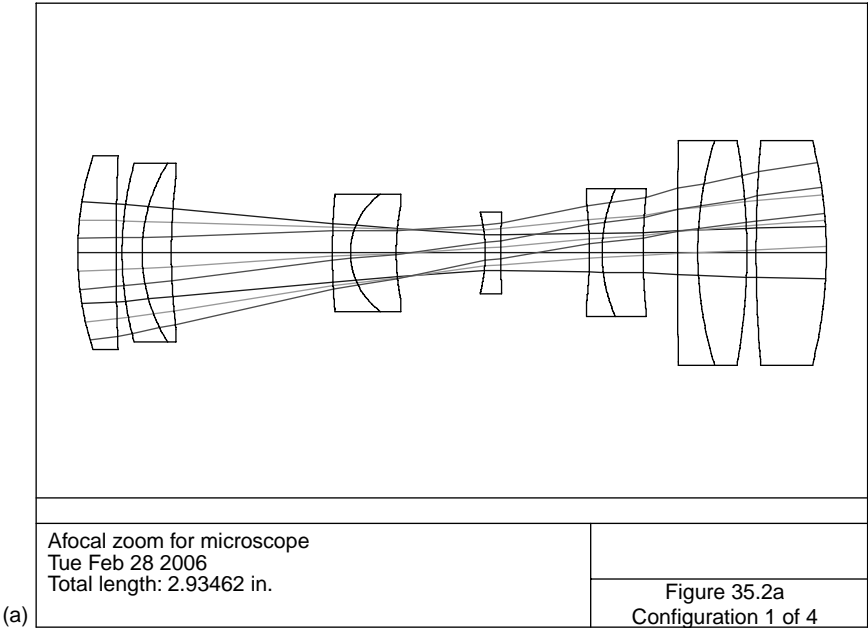


**FIGURE 35.2** (a) An afocal zoom for a microscope.

*Angle* in [Table 35.3c](#) is the semi-field angle for the full field corresponding to the image height of 0.0785. The movement of these lens groups is plotted in [Figure 35.3b](#). MTF data at the focal lengths indicated in the above table is plotted in [Figure 35.3c](#).

Rifle sights and binoculars are afocal devices. However, they differ from the afocal pods used in microscopy in that it is not a component, but rather the complete system. For use as a rifle sight, it must have very long eye relief to allow for the recoil of the rifle. Also, long length is desirable because this length allows easy mounting on the rifle.

In [Figure 35.4a](#), such a zoom rifle scope is shown in the low-magnification position; the prescription is provided in [Table 35.4a](#). The power will change from

**TABLE 35.2b**  
**Zoom Movement and Distortion Data**

Magnification	$\theta$	$T(6)$	$T(11)$	$T(14)$	Distortion (%)
2.0	3.500	0.6310	0.3475	0.1352	0.86
1.259	2.205	0.4967	0.1863	0.4306	0.005
0.7937	1.389	0.2548	0.2369	0.6219	−0.07
0.5	0.875	0.0083	0.4534	0.6520	−0.03

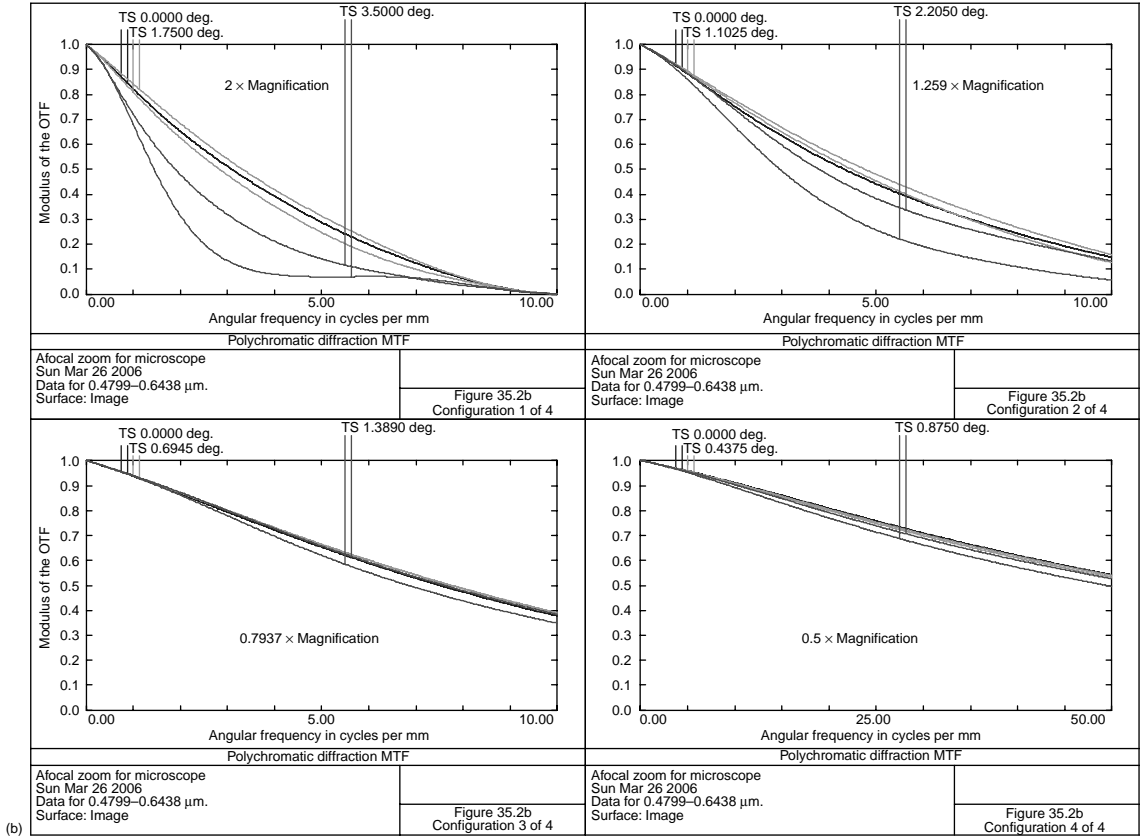


FIGURE 35.2 (continued)

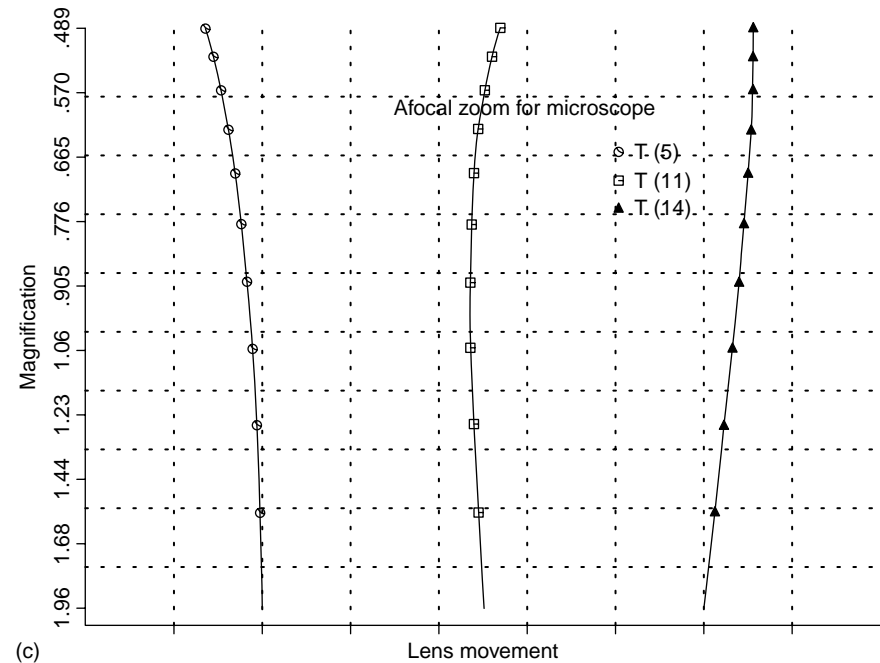


FIGURE 35.2 (continued)

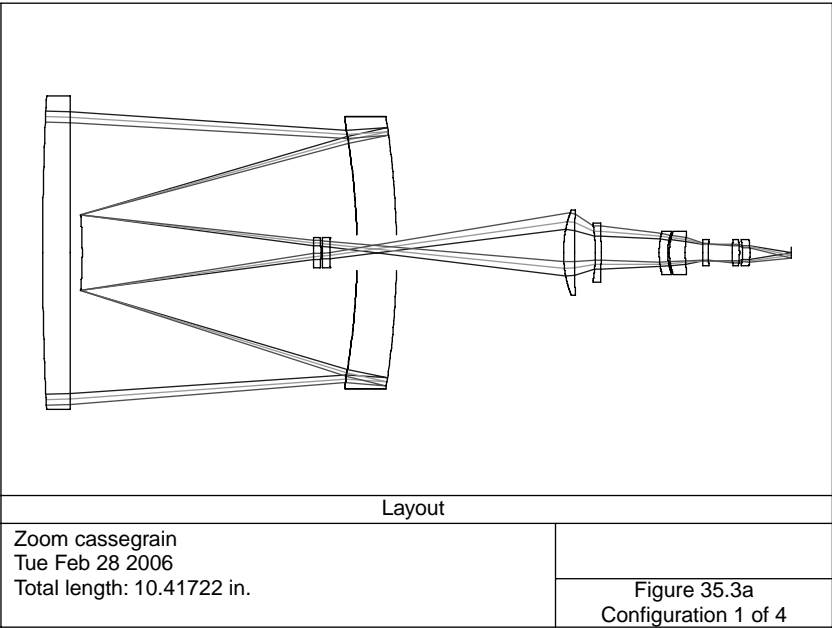
2.35 to 8.0. The entrance pupil is in contact with the first lens surface. Focusing for the individual shooter is accomplished by moving the eyepiece, and the front objective is moved to focus at various object distances. Eye relief is 3.543 (90 mm). This system suffers from considerable astigmatism, particularly in the low-magnification position.

The objective images the distant target onto the first surface of the reticle (surface 7) by means of a paraxial thickness solve on surface 6. This is often a tapered cross line and is adjusted to the boresight of the rifle. Because the zoom action occurs after the reticle, any misalignment as a result of the moving lenses will not affect the aiming accuracy.

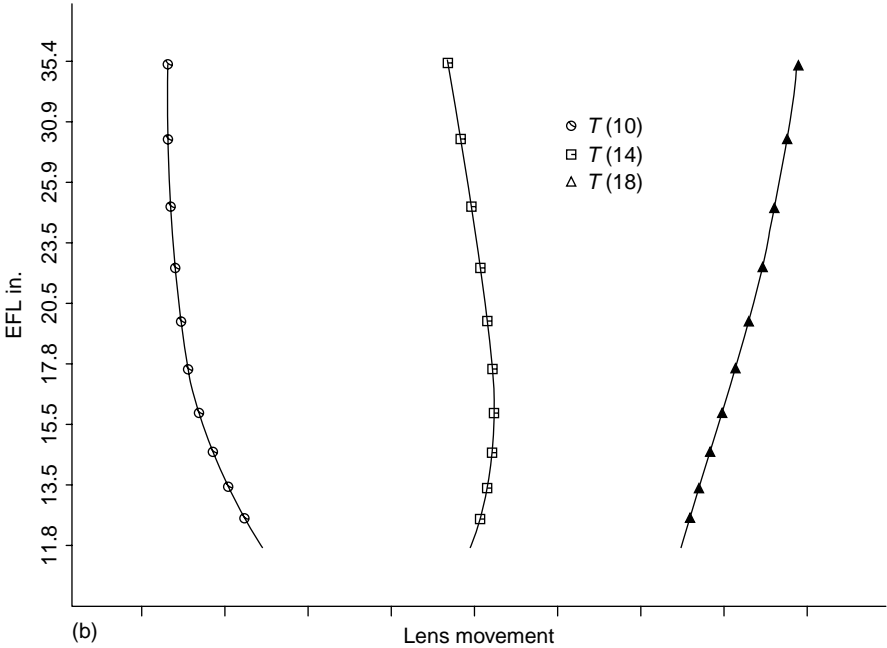
Zoom movements are plotted in [Figure 35.4b](#).

MTF data at the four zoom positions are given in [Figure 35.4c](#). Note that this data applies to the emerging ray bundle—what the eye sees. Thus, 3 cycles/milliradian corresponds to ray angles of  $1/3000=1$  min arc. Also note that resolution on-axis is more than adequate at all zoom positions. At the full field angle, resolution is seriously degraded for the sagittal component of the MTF. However, because the shooter's main interest is in the center of the field, this is not a significant defect.

In [Figure 35.5a](#) is shown (in the low magnification position) a system suitable as a stereo microscope. Zimmer (1998) illustrates the Greenough microscope as well as



(a)



(b)

FIGURE 35.3 (a) Layout, (b) Lens movement, (c) MTF plots.

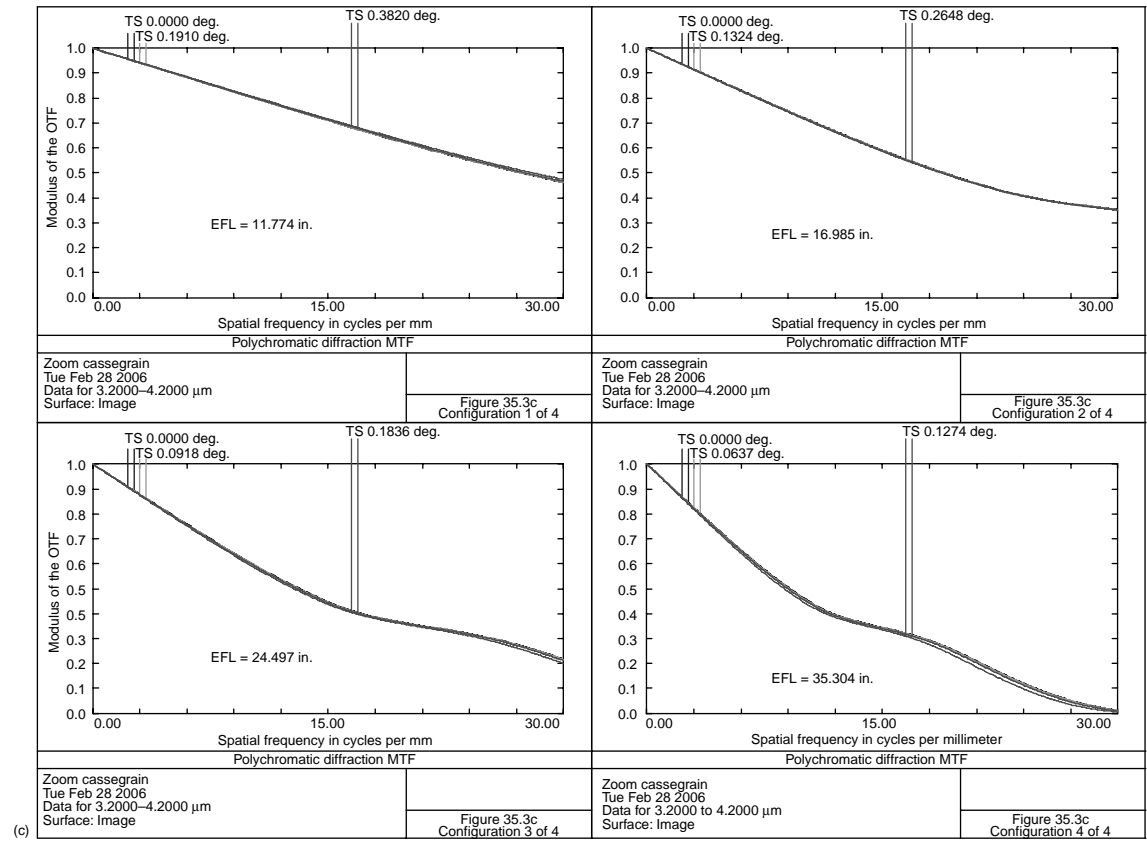


FIGURE 35.3 (continued)



**TABLE 35.3a**  
**Relative Weight vs. Wavelength**

Wavelength (μm)	Weight
3.2	0.3
3.4	0.6
3.63	1.0
3.89	0.6
4.2	0.3

**TABLE 35.3b**  
**Infrared Zoom Cassegrain**

Surface	Radius	Thickness	Material	Diameter
1	42.1589	0.3797	ZnSe	4.360
2	0.0000	3.9956		4.360
3	−9.9461	0.5500	ZnSe	3.660
4	−12.1094	−0.5500	Mirror	3.780
5	−9.9461	−3.8239		3.660
6	−6.7765	3.2207	Mirror	1.054 Stop
7	−5.7918	0.1000	Germanium	0.420
8	−1.8406	0.0225		0.420
9	−9.9278	0.1000	Silicon	0.420
10	2.1043	3.2548		0.420
11	1.7317	0.1514	Silicon	1.180
12	14.8150	0.2912		1.180
13	−2.4479	0.0800	Germanium	0.780
14	−15.8495	0.8080		0.820
15	1.1474	0.1181	Germanium	0.600
16	0.8076	0.0240		0.540
17	0.9050	0.2204	Silicon	0.600
18	1.8909	0.2410		0.480
19	0.0000	0.0788	Silicon	0.360
20	1.4949	0.3357		0.300
21	2.2105	0.1000	Silicon	0.360
22	−1.0808	0.0445		0.360
23	−0.6794	0.1000	Germanium	0.300
24	−1.2931	0.5747		0.360
25	0.0000	0.0000		0.156

Distance from front lens vertex to image = 10.417.

**TABLE 35.3c**  
**Focal Lengths, Spacings, and Distortion**

EFL	Angle	<i>T</i> (10)	<i>T</i> (14)	<i>T</i> (18)	Distortion (%)
−11.774	0.3820	3.2548	0.8080	0.2410	−1.04
−16.985	0.2648	2.6799	0.9496	0.6743	0.23
−24.497	0.1836	2.3033	0.7351	1.2654	0.89
−35.304	0.1274	2.1683	0.2936	1.8419	1.22

the common objective type of microscopes (shown in [Figure 35.6d](#)). It has a zoom range of three with the effective focal length varying from 0.591 to 1.773 (15–45 mm). [Table 35.5a](#) gives the prescription when in the long focal length (low magnification) position.

These first lenses (surfaces 1–6) are a Plossl eyepiece with a focal length of 0.836. It forms an intermediate image 0.684 from surface 6. A glass block of N-BK7 (surfaces 7–8) is actually a roof prism (Hopkins 1962) that inverts and reverts the image. It also deviates the beam so that the eyepiece assembly is 60° from the vertical axis. This makes for convenient viewing. A 60° deviation prism is shown in [Figure 35.5d](#). Surface 9 is the aperture and is fixed in location and so is part of the A group. This means that the eye position remains fixed as the lens is zoomed. Surfaces 10–12 are the B moving group and 13–15 are the C group. [Table 35.5b](#) provides data for the various zoom positions.

Magnification for the eyepiece portion is given by

$$\text{Magnification} = \frac{\text{EFL} + 10}{\text{EFL}} = 12.96.$$

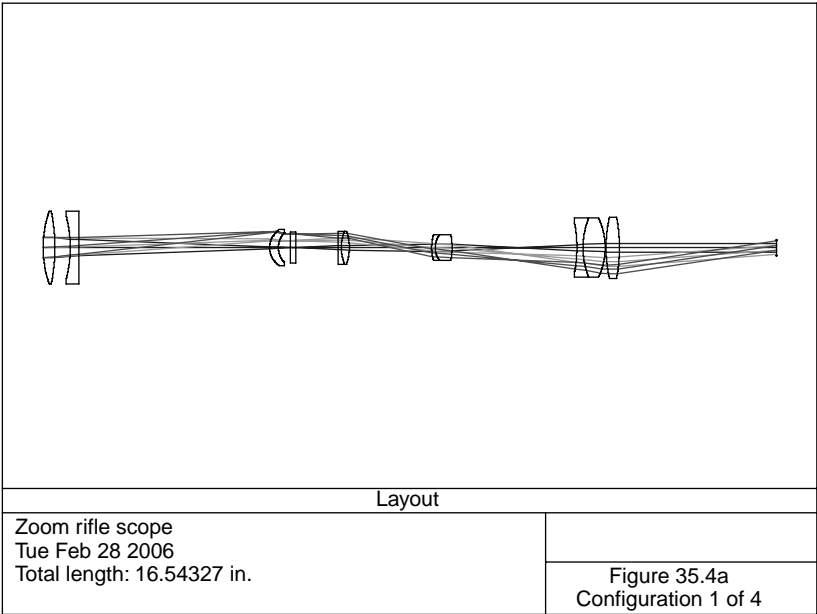
For the complete system, the magnification varies from 6.64 to 17.92. The zoom movements are plotted in [Figure 35.5b](#). MTF data at the various zoom settings is shown in [Figure 35.5c](#).

Determining the axial resolution from these graphs and then dividing by the focal length gives a nearly constant angular resolution, as seen by the eye, of 0.0005 rad over the field. This corresponds to about 1.6 min arc.

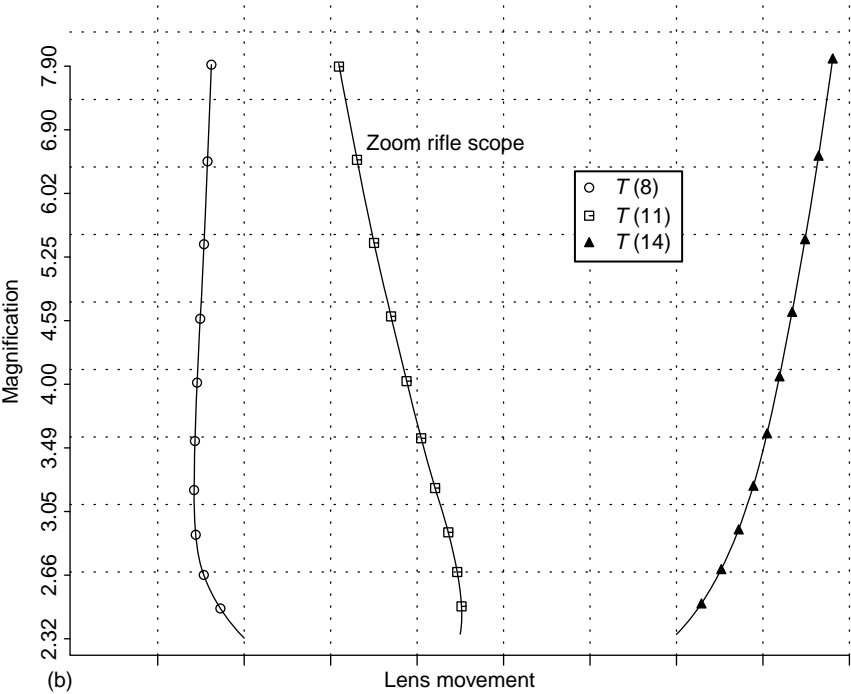
In [Figure 35.6a](#) is shown a zoom microscope with magnification changing from 11 to 51. It is shown in the low-magnification position. The prescription is given in [Table 35.6a](#). Data for the zoom positions is given in [Table 35.6b](#). These lens movements are plotted in [Figure 35.6b](#).

Notice that surface 13 is the aperture stop of the system which has a fixed diameter over the zoom region. Because it is part of a moving group, the entrance pupil moves slightly with zoom, and should not be objectionable. Surface 6 is a field stop. It has a fixed diameter of 0.397, which yields a fixed field of view for all zoom positions of 20°.

MTF data is shown in [Figure 35.6c](#).



(a)



(b)

FIGURE 35.4 (a) Layout, (b) Lens movement, (c) MTF plots.

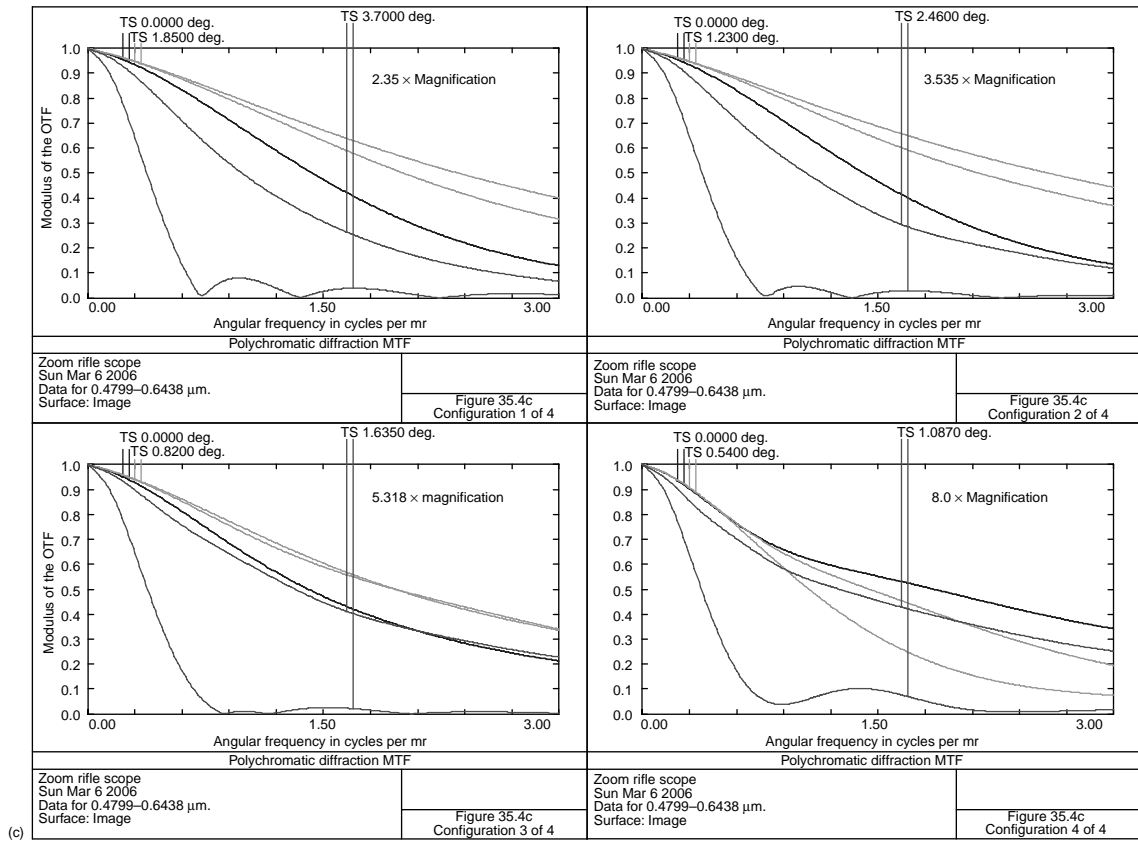
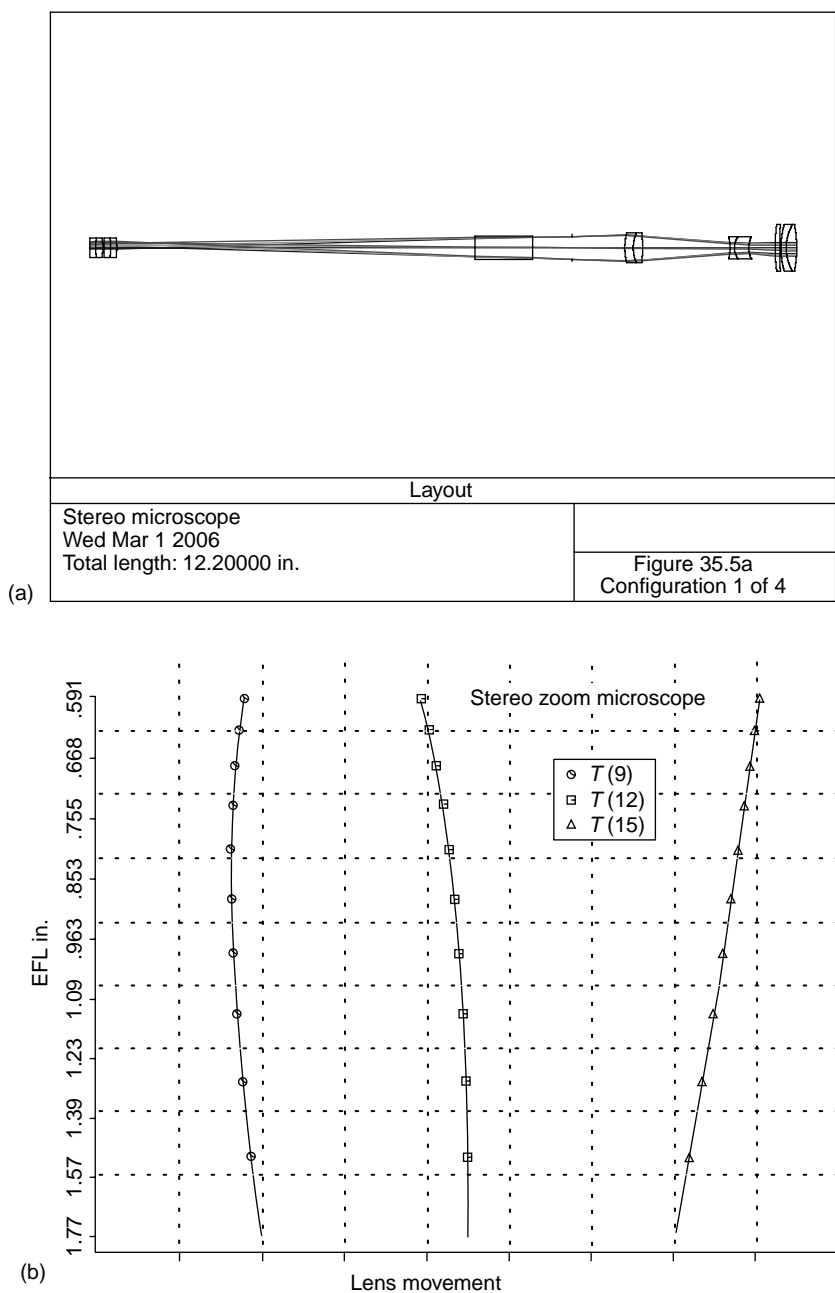


FIGURE 35.4 (continued)



**FIGURE 35.5** (a) Layout, (b) Lens movement, (c) MTF plots, (d) 60° deviation prism.

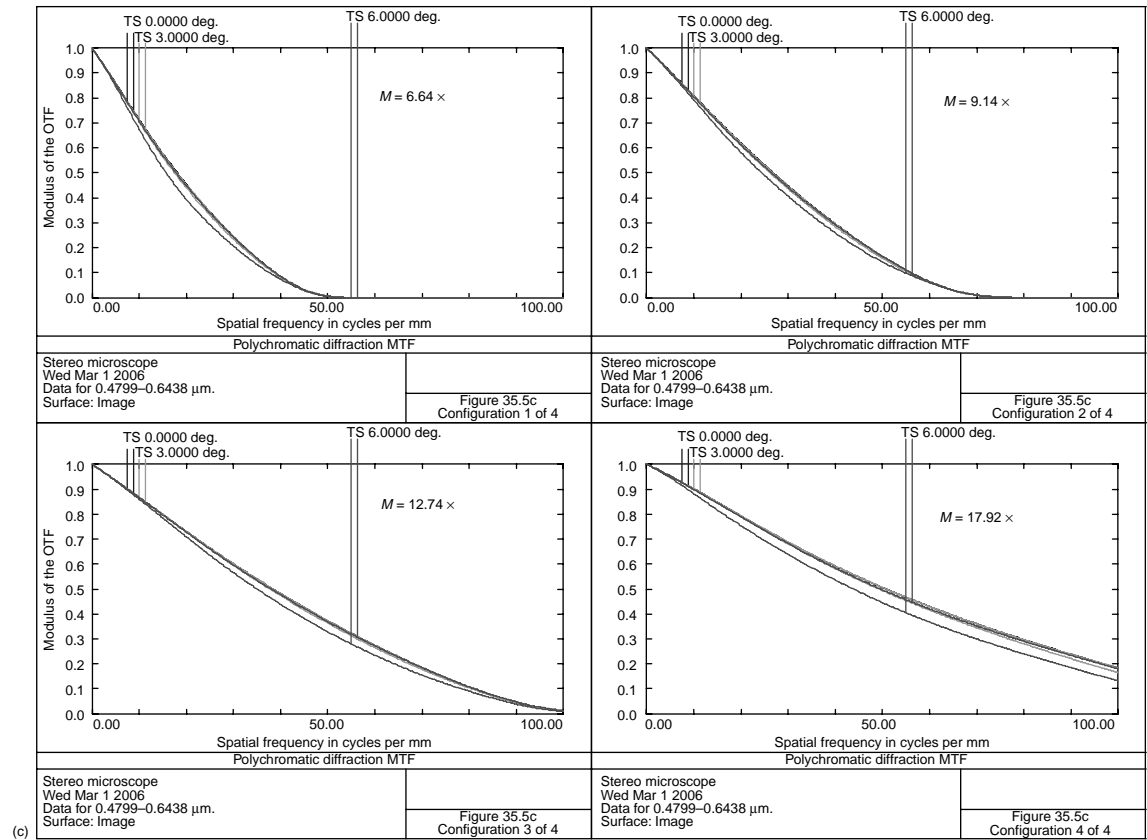


FIGURE 35.5 (continued)

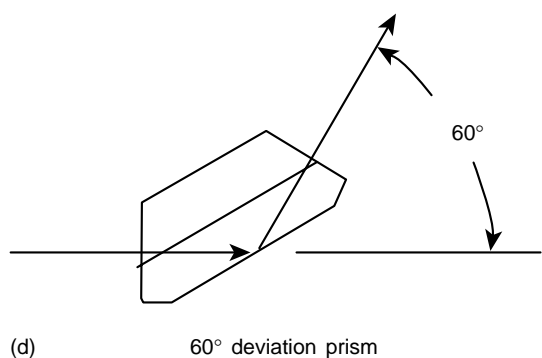


Figure 35.5 (continued)

Note that both of these zoom microscope systems use separate front objectives. This has the advantage of allowing each arm to be inclined to the work. Another method (Murty et al. 1997) uses a large front objective that is common to both sides. This has two advantages: construction is simpler and it may readily be

TABLE 35.4a  
Zoom Rifle Scope

Surface	Radius	Thickness	Material	Diameter
1	2.5318	0.2667	N-SK14	1.640 Stop
2	−4.0666	0.3455		1.640
3	−2.7909	0.2002	SF1	1.400
4	0.0000	4.2990		1.640
5	0.4969	0.1969	N-K5	0.820
6	0.4930	0.2708		0.680
7	0.0000	0.1181	N-K5	0.700
8	0.0000	0.9504		0.700
9	4.9915	0.0787	SF4	0.740
10	0.9644	0.1821	N-SSK2	0.740
11	−1.1026	1.8568		0.740
12	1.0412	0.0787	SF4	0.580
13	0.4661	0.3800	N-SSK2	0.580
14	−1.6318	2.8169		0.580
15	−3.0451	0.1378	SF4	1.100
16	1.7937	0.5002	N-SSK2	1.340
17	−1.5693	0.0200		1.340
18	3.1051	0.3013	N-PSK53	1.380
19	−3.8889	3.5433		1.380

Distance from first surface to last surface=13.0.

**TABLE 35.4b**  
**Zoom Movements for Rifle Scope**

Magnification <sup>a</sup>	Entrance Pupil	Angle <sup>b</sup> (deg.)	T(8)	T(11)	T(14)	Distortion (%)
2.350	0.4629	3.700	0.9504	1.8568	2.8169	−0.3
3.535	0.6964	2.460	0.3758	1.6389	3.6093	−1.0
5.318	1.0476	1.635	0.4361	1.0693	4.1186	0.4
8.000	1.5760	1.087	0.5843	0.4024	4.6373	0.9

<sup>a</sup> Angular magnification.  
<sup>b</sup> Full field semi-field angle.

**TABLE 35.5a**  
**Stereo Microscope**

Surface	Radius	Thickness	Material	Diameter
1	1.7902	0.1017	SF1	0.330
2	0.8492	0.1220	N-SK14	0.330
3	−1.6068	0.0200		0.330
4	1.6068	0.1220	N-SK14	0.330
5	−0.8492	0.1017	SF1	0.330
6	−1.7902	6.1873		0.330
7	0.0000	0.9843	N-BK7	0.400
8	0.0000	0.6890		0.400
9	Stop	0.9058		0.394
10	1.0343	0.1451	SF1	0.520
11	0.6173	0.1609	N-FK5	0.520
12	−3.2953	1.5102		0.520
13	−0.7848	0.0750	K7	0.350
14	0.3149	0.2500	SF4	0.380
15	0.4628	0.4542		0.380
16	3.3521	0.0800	N-FK5	0.800
17	8.3774	0.0200		0.760
18	1.4869	0.0906	SF4	0.800
19	0.8089	0.1803	K7	0.800
20	−2.1363	7.0000		0.800
21	0.0000	0.0000		0.371

Distance from the eye (the entrance pupil) to first lens surface = 0.787.



**TABLE 35.5b**  
**Zoom Positions and Distortion**

EFL	Object Dia.	T(9)	T(12)	T(15)	Distortion (%)
−1.773	0.363	0.9058	1.5102	0.4542	−0.60
−1.229	0.258	0.5403	1.3934	0.9366	−0.69
−0.852	0.179	0.4714	1.1783	1.2206	−0.75
−0.591	0.124	0.6080	0.8639	1.3984	−0.82

Distance from first lens surface to image = 19.20.

**TABLE 35.6a**  
**Zoom Microscope**

Surface	Radius	Thickness	Material	Diameter
1	−4.2467	0.1020	N-SK5	0.500
2	−0.6793	0.0200		0.500
3	1.1768	0.2000	N-SK5	0.500
4	−1.0717	0.0591	SF1	0.500
5	2.1570	0.8836		0.500
6	0.0000	3.6602		0.397
7	−49.0372	0.1200	SF1	1.020
8	−2.0457	0.1200	N-SK5	1.080
9	−1.9622	0.0200		1.080
10	3.6080	0.1049	SF1	1.080
11	0.8135	0.2000	N-SK5	1.080
12	10.0962	4.2320		0.960
13	Stop	0.0050		0.200
14	−2.4607	0.0601	SF1	0.220
15	−0.4319	0.0528	N-SK5	0.280
16	−0.3686	0.0200		0.280
17	−0.3401	0.0393	F5	0.240
18	2.0289	0.0222		0.240
19	18.9348	0.0787	F4	0.520
20	1.2857	0.2003	N-BK10	0.620
21	−1.1690	0.2000		0.620
22	1.1690	0.2003	N-BK10	0.620
23	−1.2857	0.0787	F4	0.620
24	−18.9348	2.0000		0.520
25	0.0000	0.0000		0.344

Distance from first lens surface to image = 12.679.

**TABLE 35.6b**  
**Zoom Positions and Distortion**

EFL	Entrance Pupil Dia. %	Eye Relief	T(6)	T(12)	T(18)	Distortion (%)
−0.9836	0.0912	0.8753	3.6602	4.2320	0.0222	−0.96
−0.5764	0.0766	0.9288	2.7529	4.1750	0.9865	−2.35
−0.3385	0.0566	0.8963	1.4706	5.0013	1.4425	−2.75
−0.1985	0.0352	0.9013	0.0204	6.3518	1.5422	−2.41

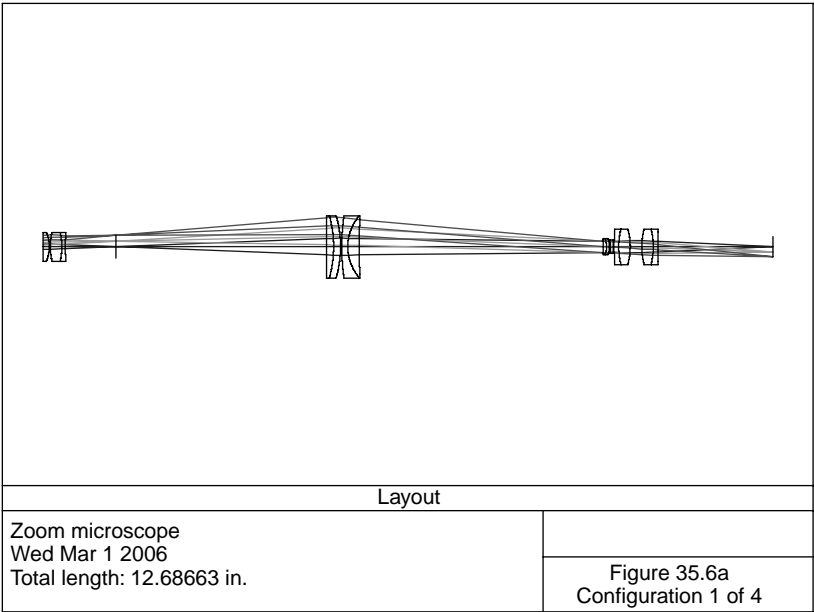
changed to change the overall magnification of the zoom system. This is shown in [Figure 35.6d](#).

In [Figure 35.7a](#), a zoom lens suitable for use with a vidicon, CCD, or 16-mm film camera (16-mm diameter image) is shown. It is  $f/2$  and varies in focal length from 0.787 to 4.33 (20–110 mm). This design is a modification of the Kato et al. (1989) patent. Note that for the usual video camera usage, a glass block should be added to the rear of the lens system (as in the patent). Unlike the above zoom camera lens designs, the iris is located between the two moving groups. Moving the iris into the forward portion of the lens tends to reduce the front lens diameters; this is particularly important at the wide-field position. The iris also moves, which causes an increased complexity in the mechanical construction. [Figure 35.7a](#) shows the lens in its 0.787-in. focal length position. Additional clearance between the iris and surface 12 should be added. The lens prescription (short focal length setting) is given in [Table 35.7a](#).

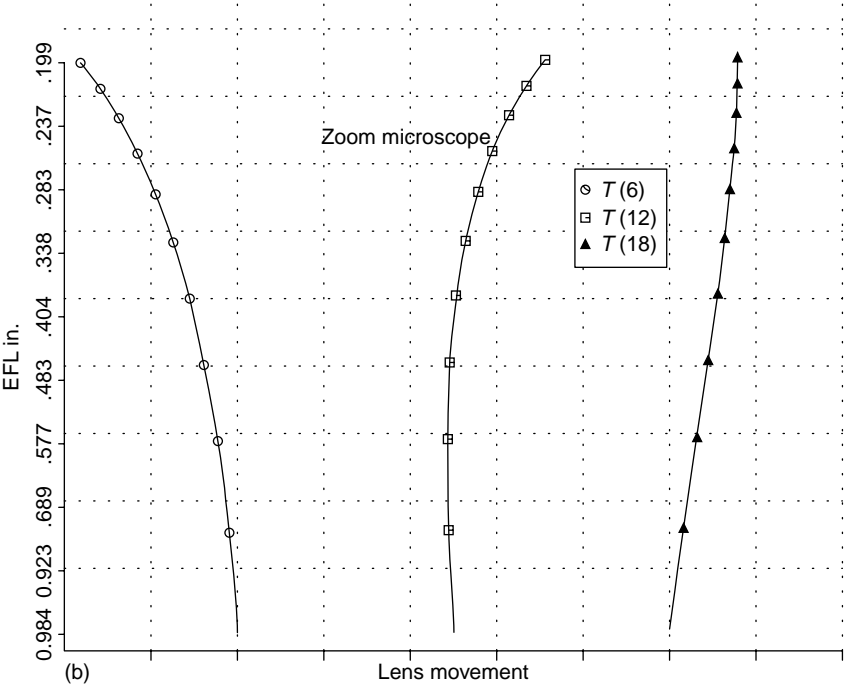
Movement of the lens groups is tabulated in [Table 35.7b](#). Note that the movement of the C group (surfaces 12–14) reverses direction. MTF data is plotted in [Figure 35.7c](#).

In [Figure 35.8a](#) is shown a 25- to 125-mm focal length zoom lens for 35-mm motion picture (Academy format, 1.069 diagonal) cinematography. The lens is  $f/4$ . This system differs from the previous examples in that it has three moving groups. Although only two moving groups are required to change focal length and maintain a fixed image plane, the additional moving group is used to for aberration control. This design is a modification of Cook’s and Laurent (1972) patent. As discussed in this patent, focusing is accomplished by moving the doublet and singlet (surfaces 5–9) following the front two singlets. The overall length of the lens then does not change with focus as it does in most zoom lenses. Another advantage with this system is that a nearly constant angular field of view is obtained as one focuses from distant to near objects. [Table 35.8a](#) lists the lens prescription for a distant object at the short focal length setting. To focus on near objects,  $T_4$  is decreased. [Table 35.8b](#) gives the zoom positions and distortion data.

MTF data is plotted in [Figure 35.8b](#).



(a)



(b)

**FIGURE 35.6** (a) Layout, (b) Lens movement, (c) MTF plots, (d) Stereo microscope with common front objective.

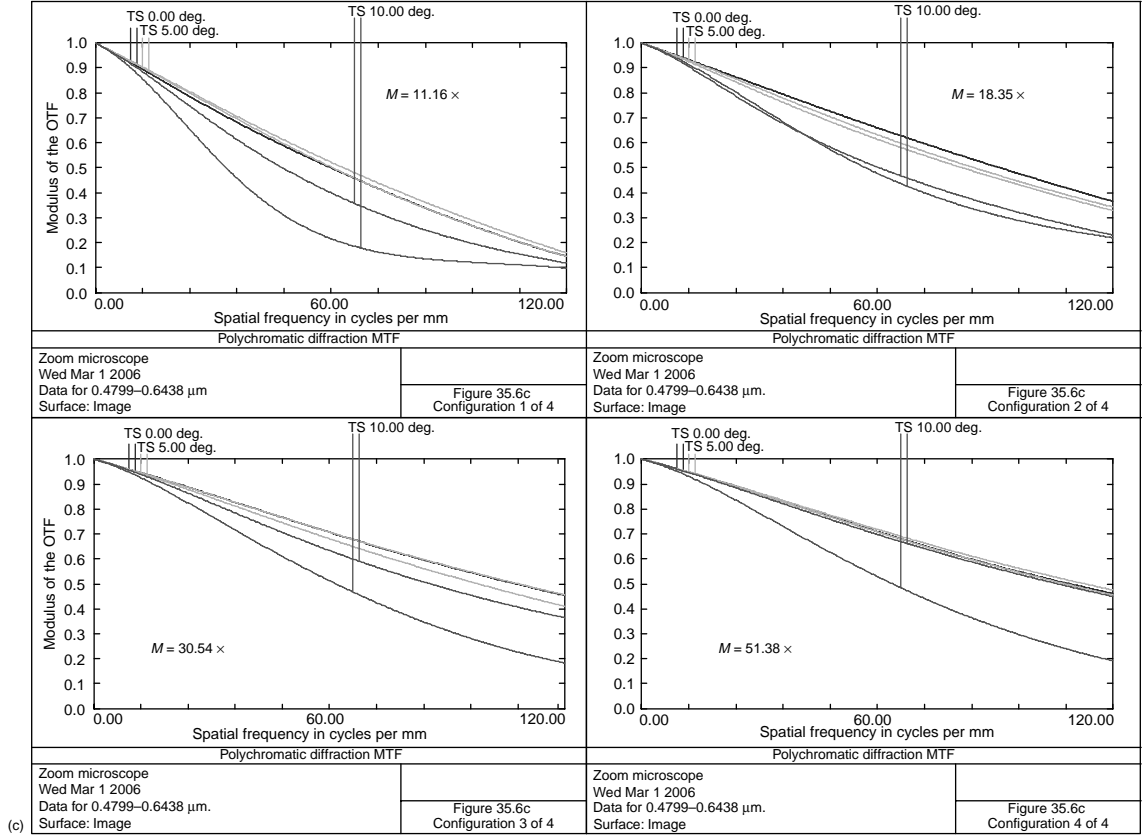
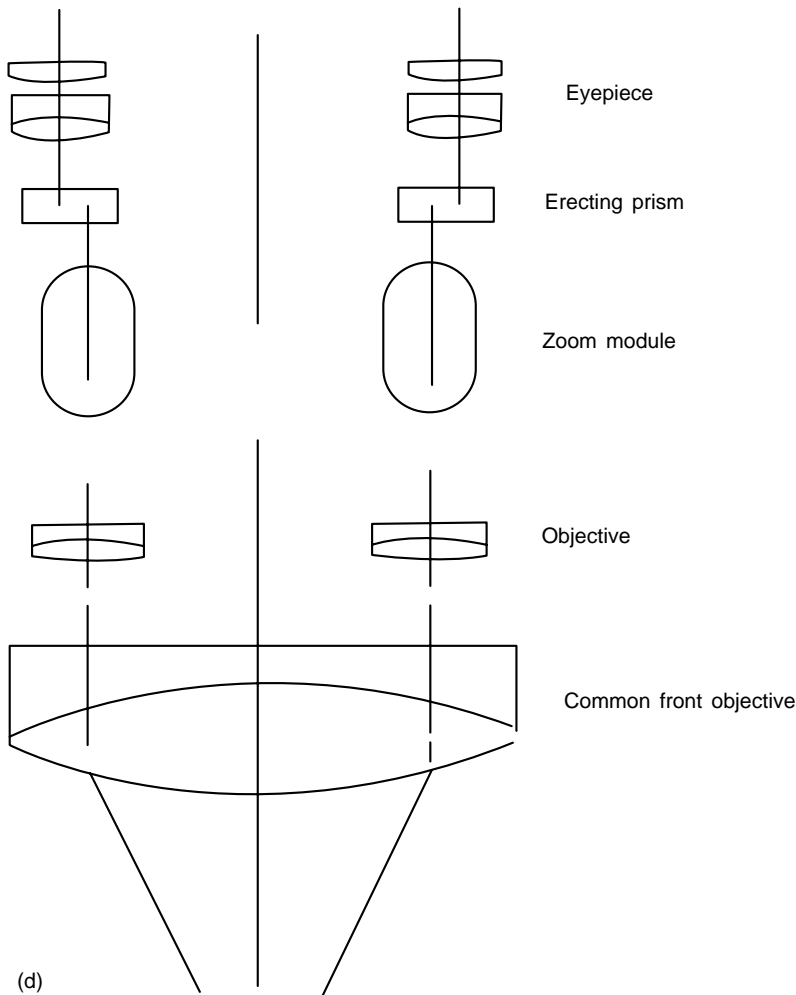


FIGURE 35.6 (continued)



**Figure 35.6** (continued)

In Figure 35.9a is plotted a  $2\times$  zoom lens designed for a single-lens reflex (SLR) camera (43-mm diagonal). The prescription data is given in Table 35.9a. Data for the focal length and zoom movements is given in Table 35.9b. The lens is  $f/2.8$  and zooms from 75 to 150 mm. Lens length from front surface to the image is 9.555, which is a little too long for a commercial product.

In Figure 35.10 is shown a lens suitable for TV usage. The focal length can be made to vary from 12 to 234 mm. It was designed for use with a 0.5-in. CCD ( $6.4 \times 4.8$  mm). The lens prescription in the short-focal-length configuration is given in Table 35.10a. Data on focal length and zoom movements are given in Table 35.10b.

**TABLE 35.7a**  
**A 20–110 mm Zoom**

Surface	Radius	Thickness	Material	Diameter
1	14.2226	0.2300	SF6	6.300
2	4.6570	1.0785	N-LAK33	5.840
3	0.0000	0.0200		5.840
4	4.1686	0.6582	N-LAK33	5.320
5	10.0881	0.0514		5.180
6	7.7040	0.1181	N-LAF3	2.640
7	1.4669	0.6133		2.140
8	−4.3993	0.1500	N-LAK33	2.120
9	1.7272	0.9000	SF6	2.140
10	0.0000	6.8756		2.140
11	Stop	0.0147		1.323
12	4.6496	0.4542	N-BAK2	2.140
13	−2.2132	0.1500	SF1	2.140
14	−7.4574	1.1543		2.220
15	4.3730	0.6820	N-LAK33	2.520
16	−6.9907	0.1600	SF6	2.520
17	0.0000	0.0200		2.520
18	1.6248	0.6112	N-PSK53	2.300
19	2.1437	0.4645		1.940
20	1.2756	0.1575	SF6	1.640
21	0.8345	0.1774		1.360
22	1.3775	0.1604	N-FK5	1.400
23	2.9995	0.0200		1.320
24	1.1583	0.2231	N-LAK14	1.300
25	1.4237	0.7800		1.140
26	0.0000	0.0000		0.619

Distance from first lens surface to image= 15.924.

**TABLE 35.7b**  
**Zoom Positions and Distortion**

EFL	T(5)	T(10)	T(11)	T(14)	Iris Dia.	Distortion (%)
0.787	0.0514	6.8756	0.0146	1.1543	1.3226	−2.02
1.411	1.7889	4.0586	2.2387	0.0098	1.0034	−1.01
2.404	2.5665	3.0433	2.1218	0.3644	1.0298	−0.77
4.331	3.0294	0.6762	2.4796	1.9108	1.0384	0.70

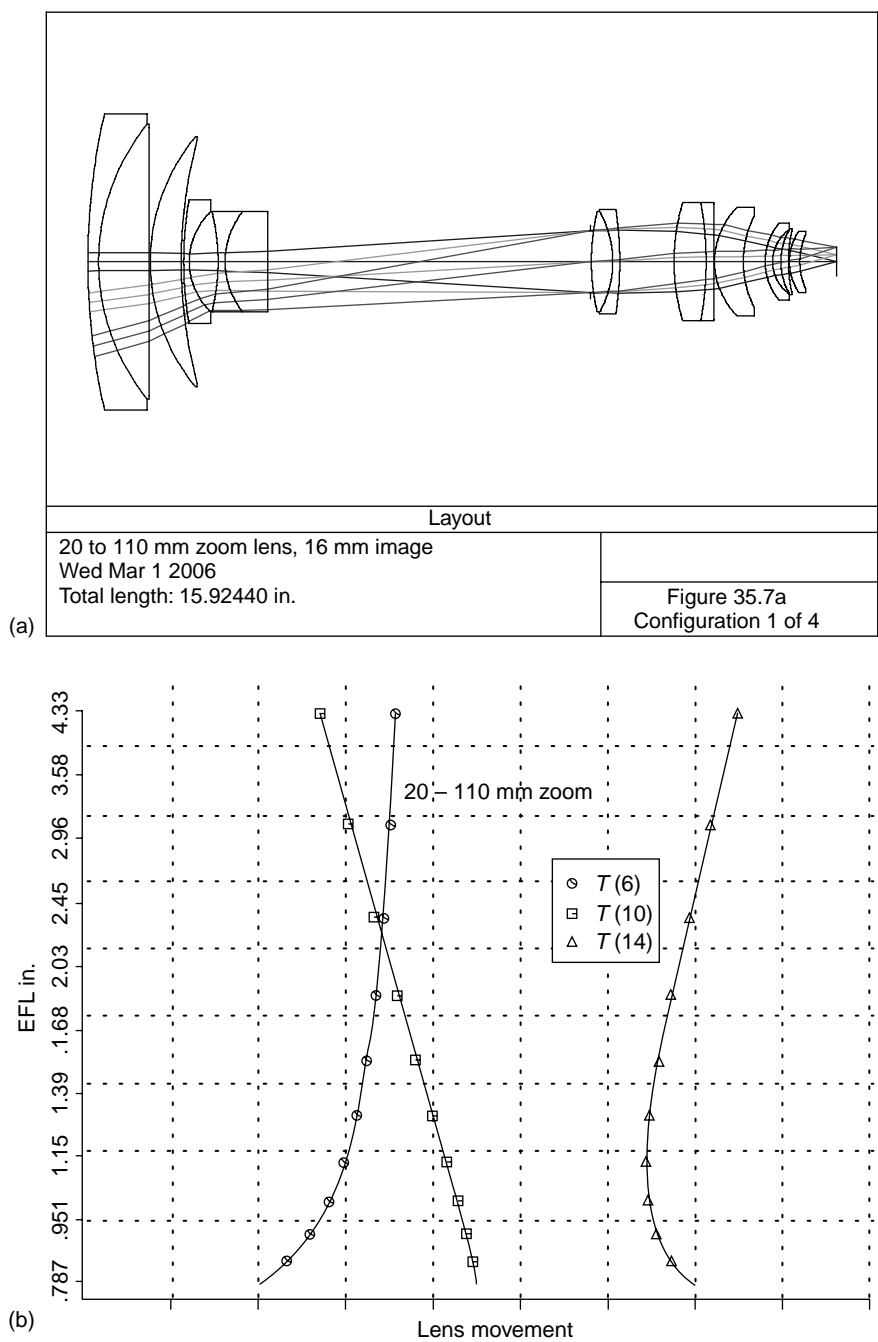
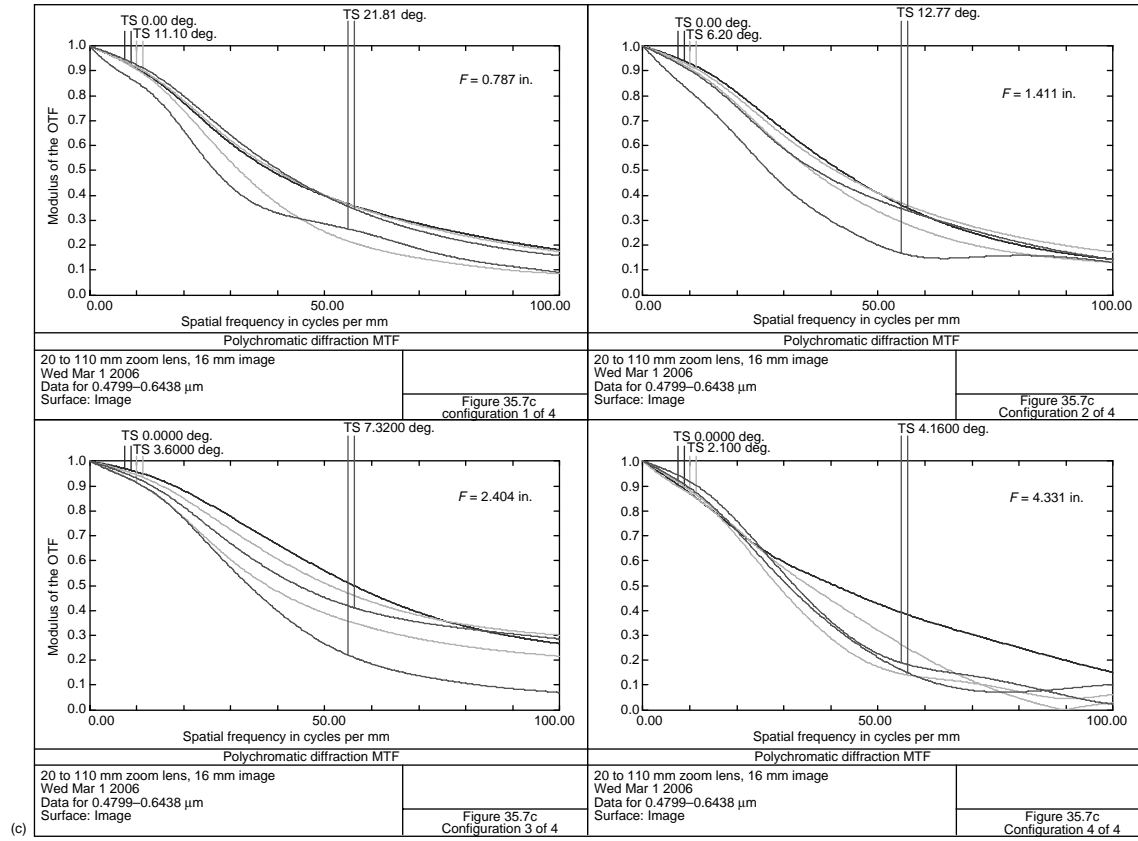


**FIGURE 35.7** (a) Layout, (b) Lens movement, (c) MTF plots.



(c)

FIGURE 35.7 (continued)



**TABLE 35.8a**  
**A 25- to 125-mm Zoom**

Surface	Radius	Thickness	Material	Diameter
1	5.5424	0.4481	N-LAK21	5.120
2	4.1535	0.5225		4.540
3	14.7730	0.3177	N-LAK21	4.560
4	5.9532	0.9787		4.160
5	−44.3038	0.7062	SF6	3.800
6	−5.8326	0.5362	F5	3.880
7	10.5241	0.5108		3.400
8	−5.3900	0.3000	N-LAK10	3.420
9	−12.0046	0.5744		3.660
10	0.0000	0.3000	SF6	3.920
11	9.4247	0.5950	N-SK16	3.920
12	−6.9815	0.0200		3.920
13	9.2390	0.2676	SF6	4.040
14	5.2032	0.6130	N-LAK21	4.040
15	−17.1406	0.0200		4.040
16	4.1080	0.5135	N-LAK21	3.940
17	28.2663	0.0295		3.840
18	9.1064	0.1600	N-LAK21	2.120
19	1.6703	1.0266		1.800
20	−2.3807	0.1500	N-LAF3	1.620
21	2.1988	0.6872	SF6	1.860
22	−22.1102	3.3140		1.860
23	24.5962	0.1500	SF6	1.920
24	2.3534	0.4365	N-SSK5	1.920
25	−2.8580	0.0200		1.920
26	2.7941	0.2955	N-FK5	1.860
27	−6.1514	0.0266		1.860
28	Stop	0.1053		0.950
29	−2.1692	0.1000	N-LAF3	0.980
30	1.4544	0.4000	SF6	1.100
31	27.2549	0.4372		1.060
32	−5.8483	0.2541	N-BK7	1.160
33	−2.1041	0.4358		1.260
34	10.8462	0.1000	SF6	1.280
35	1.3856	0.2850	N-SK5	1.280
36	−3.3962	3.1133		1.280
37	0.0000	0.0000		1.013

Distance from front surface to image = 18.750.

**TABLE 35.8b**  
**Zoom Positions and Distortion**

EFL	<i>T</i> (9)	<i>T</i> (17)	<i>T</i> (22)	<i>T</i> (27)	Distortion (%)
0.984	0.5744	0.2950	3.3140	0.0266	− 5.62
1.682	0.6175	1.0434	1.9653	0.3184	− 0.10
2.877	0.5005	1.8946	0.8880	0.6614	1.25
4.921	0.01213	2.7063	0.0200	1.1969	1.54

Note that the f-number increases as one zooms from short to long focal length, and consequently the stop diameter changes with zoom. This was done to reduce the size of the front group. The N-SK5 block at the rear of the lens is part of the CCD array (see [Figure 23.4](#) for details of this beam-splitting arrangement). To yield even illumination at the CCD array, this lens is nearly telecentric. (Exit pupil is located − 17.27 from the image.) It is a modification of the Enomoto and Ito (1998) patent. MTF data is plotted in [Figure 35.10c](#).

In [Figure 35.11a](#) is shown a zoom eyepiece which was designed to work with an *f*/5.0 objective of 80-in. effective focal length. The prescription information is given in [Table 35.11a](#); focal length and zoom movements are given in [Table 35.11b](#). With

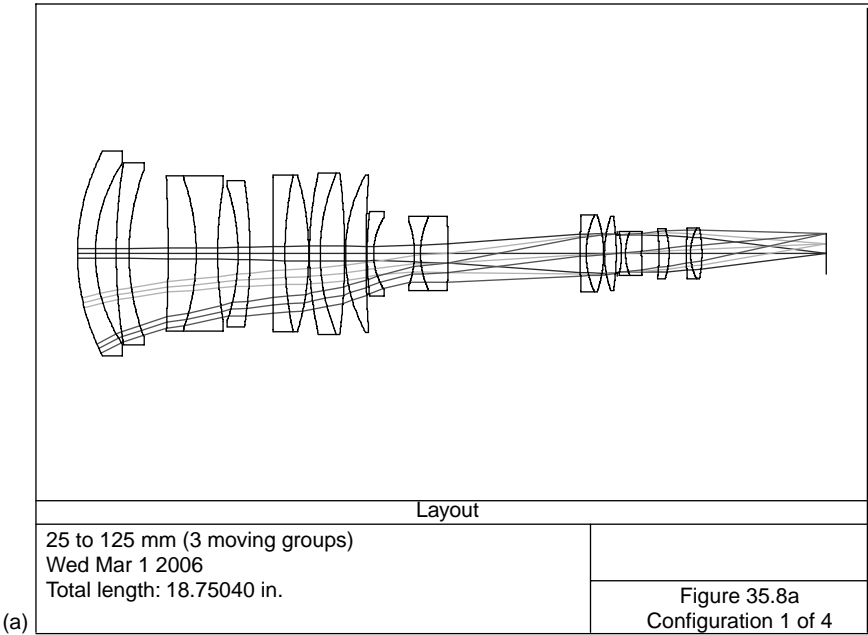


**FIGURE 35.8** (a) A 25- to 125-mm zoom lens with three moving groups, (b) 25 to 125mm zoom no plot of Lens movements.

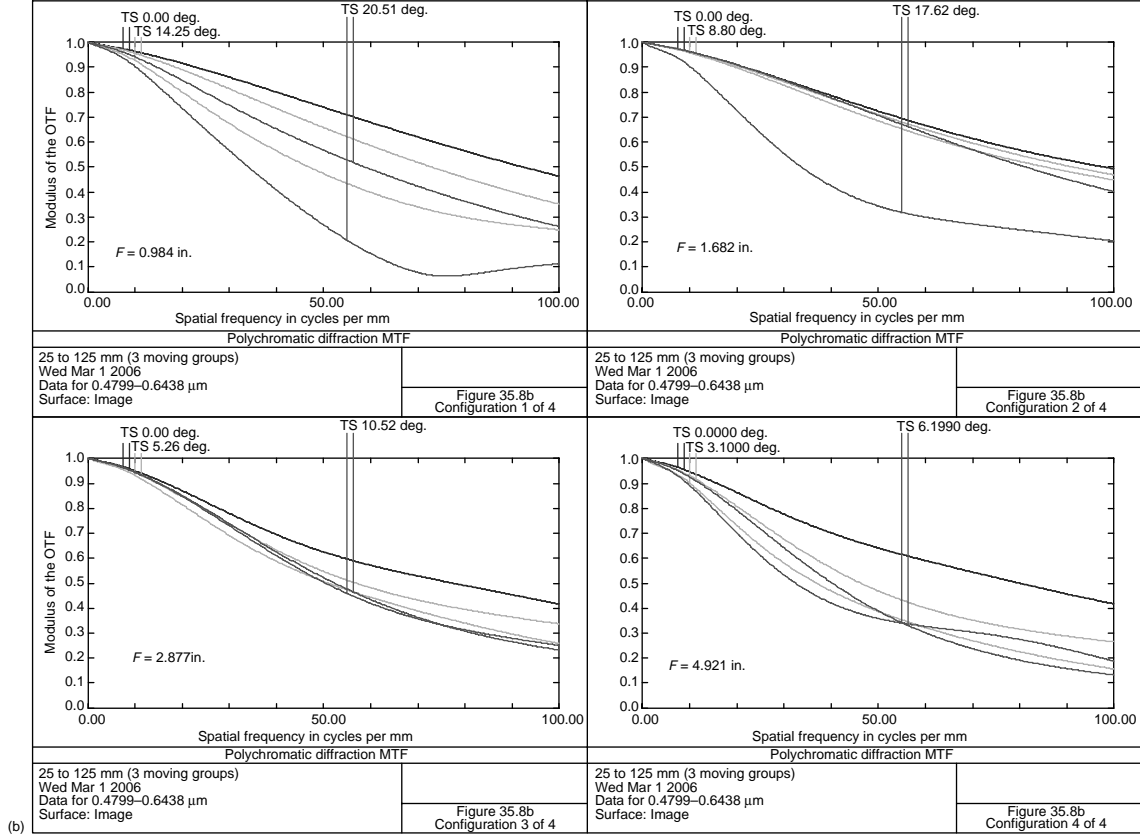
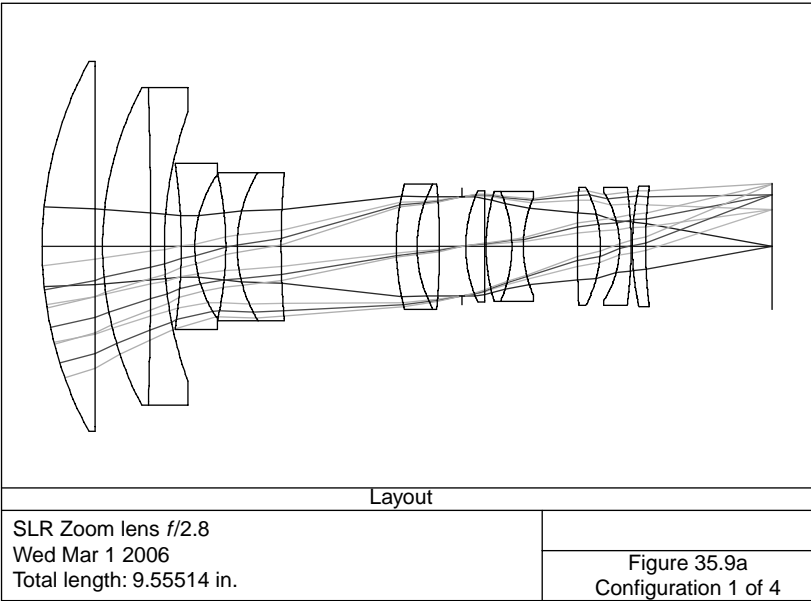
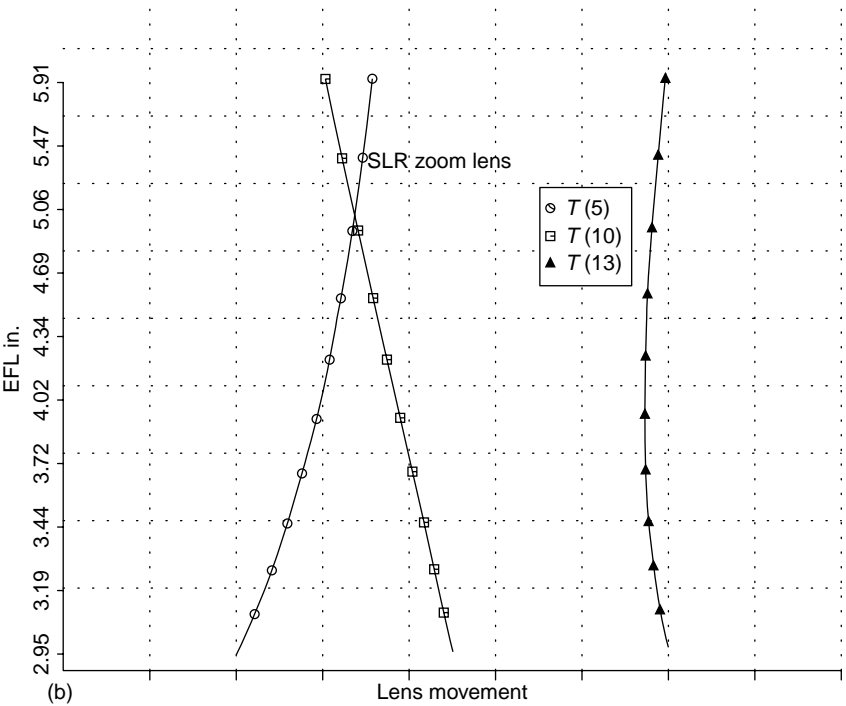


FIGURE 35.8 (continued)



(a)



(b)

FIGURE 35.9 (a) Layout, (b) Lens movement, (c) MTF plots.

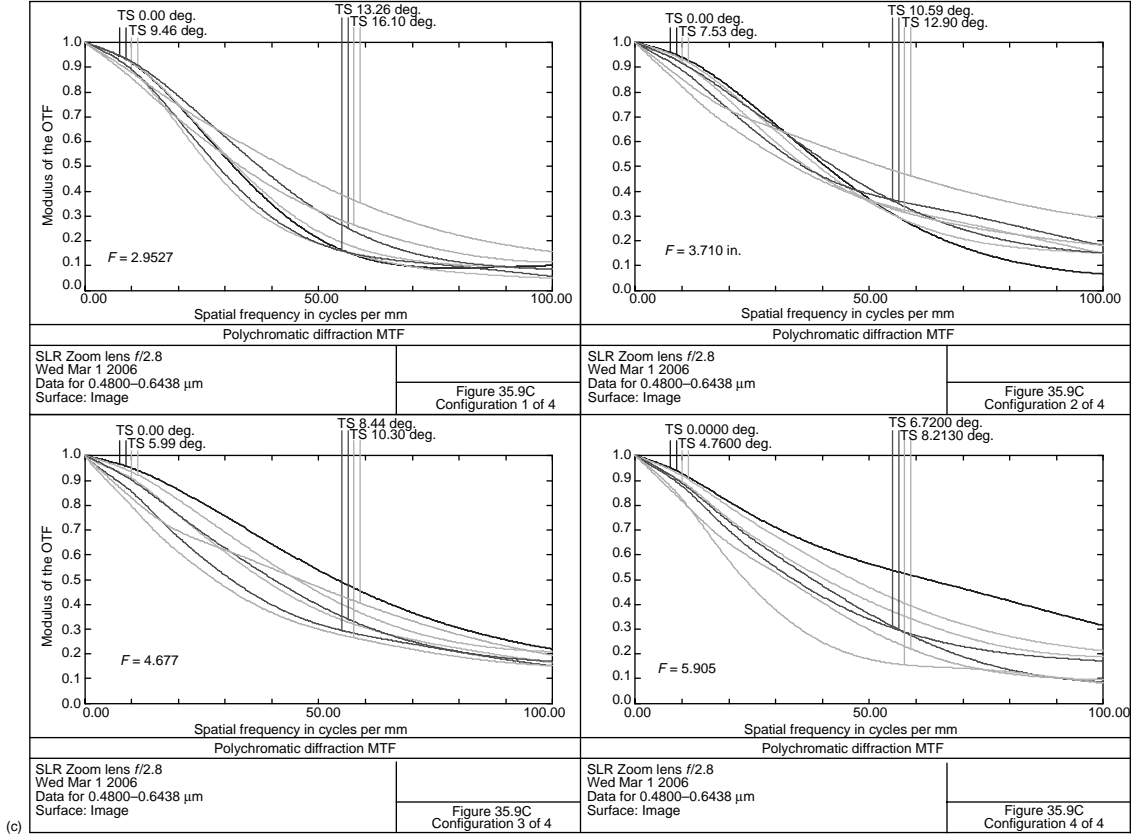
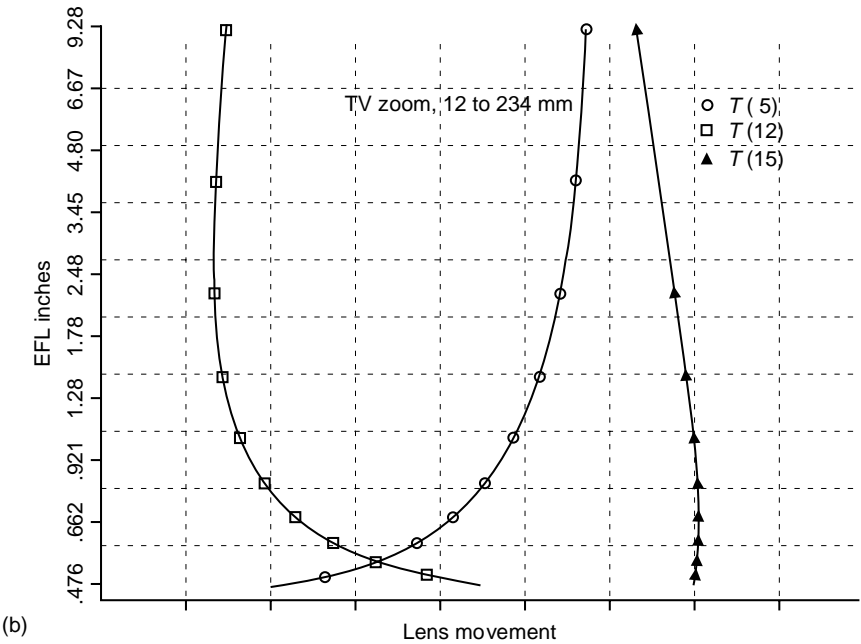
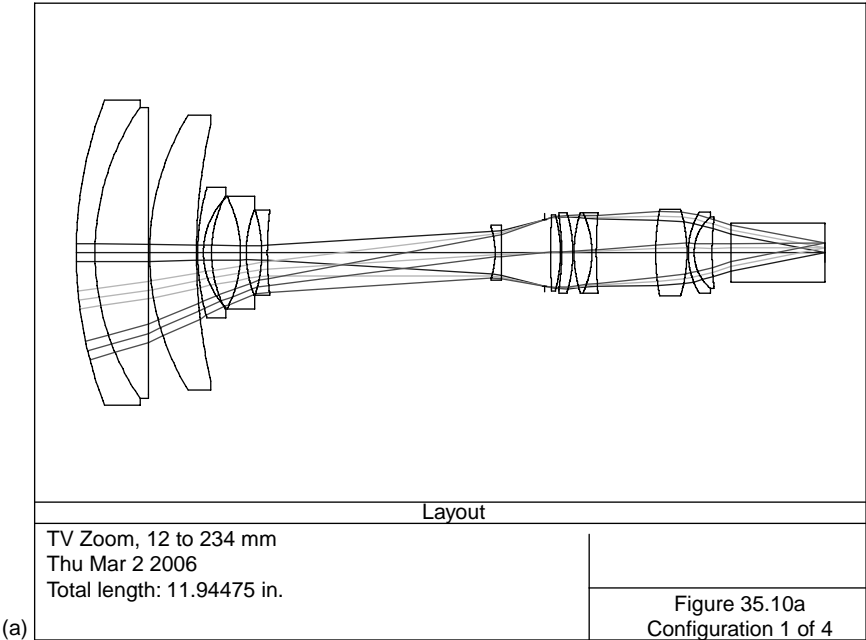


FIGURE 35.9 (continued)



**FIGURE 35.10** (a) A 12- to 234-mm TV zoom lens, (b) 12- to 234-mm TV zoom, (c) MTF plots.

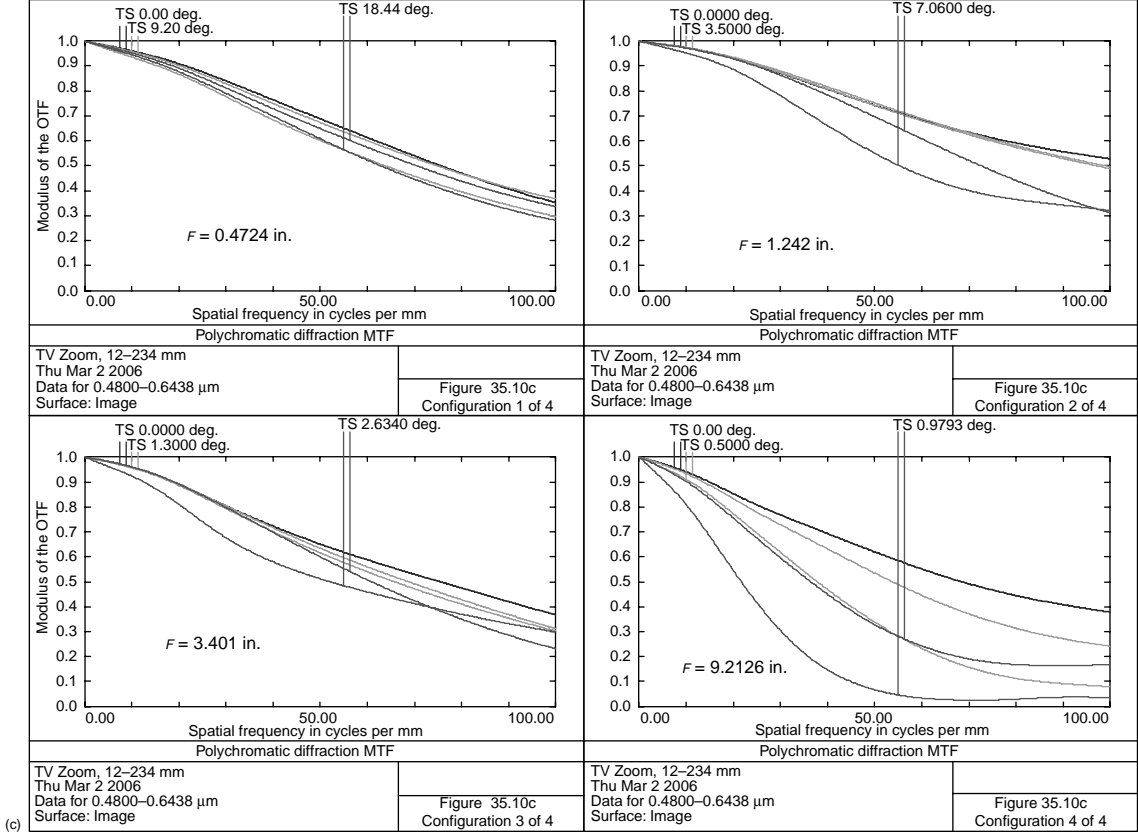


FIGURE 35.10 (continued)

**TABLE 35.9a**  
**Zoom Lens for SLR Camera**

Surface	Radius	Thickness	Material	Diameter
1	5.0954	0.6914	N-LAK7	4.840
2	0.0000	0.1013		4.840
3	4.4902	0.6299	N-LAK7	4.160
4	−69.5957	0.1772	SF4	4.160
5	5.1582	0.2229		3.520
6	−7.2570	0.1769	F5	2.180
7	1.6608	0.4048		1.880
8	−4.3110	0.1500	N-FK5	1.880
9	1.8731	0.5752	SF6	1.940
10	11.9465	1.5086		1.940
11	3.2456	0.2710	SF6	1.640
12	1.7322	0.2933	N-BALF4	1.640
13	−9.3690	0.2942		1.640
14	Stop	0.0500		1.295
15	1.7769	0.2471	N-SK14	1.460
16	0.0000	0.0185		1.460
17	2.4665	0.3370	N-SK14	1.440
18	−1.8183	0.1500	N-LAF2	1.440
19	1.6176	0.7093		1.300
20	17.8559	0.2993	N-LAK7	1.540
21	−1.6574	0.2518		1.540
22	−1.3171	0.1500	N-LAK7	1.420
23	−5.9934	0.0175		1.540
24	3.6479	0.1734	N-LAK9	1.580
25	6.3874	1.6543		1.540
26	0.0000	0.0000		1.648

**TABLE 35.9b**  
**Focal Length and Zoom Movements**

EFL	T5	T10	T13	Distortion (%)
2.953	0.2229	1.5086	0.2492	3.50
3.710	0.8699	1.1241	0.0318	1.52
4.677	1.3818	0.6358	0.0083	0.15
5.905	1.7839	0.0200	0.2219	1.53



**TABLE 35.10a**  
**A 12–234 mm TV Zoom Lens**

Surface	Radius	Thickness	Material	Diameter
1	6.7727	0.3000	SF6	4.860
2	4.1151	0.8508	N-PSK53	4.640
3	0.0000	0.0200		4.640
4	4.2186	0.7482	N-FK51	4.380
5	9.3181	0.0200		4.100
6	3.7889	0.0900	F2	2.080
7	1.2639	0.1296		1.760
8	1.9633	0.4635	SF6	1.800
9	−1.9633	0.0900	N-LAF2	1.800
10	1.8669	0.2466		1.380
11	−2.2435	0.0900	N-LAK8	1.360
12	5.7477	3.6347		1.320
13	−1.3500	0.1000	N-LAK33	0.840
14	−24.7601	0.6937		0.880
15	Stop	0.0946		1.060
16	17.5201	0.1538	SF6	1.220
17	−2.2770	0.0200		1.220
18	−3.8408	0.1781	N-LAK9	1.220
19	−2.2202	0.0200		1.280
20	2.1127	0.2842	N-FK5	1.280
21	−1.4969	0.0700	SF6	1.280
22	8.2419	0.9469		1.220
23	3.7216	0.4998	N-FK5	1.380
24	−2.3913	0.0200		1.380
25	1.2780	0.0945	LAFN7	1.300
26	0.7513	0.2856	N-PSK3	1.140
27	4.8498	0.3000		1.100
28	0.0000	1.5000	N-SK5	0.940
29	0.0000	0.0000		0.940
30	0.0000	0.0000		0.309

Distance from first surface to image = 11.945.

**TABLE 35.10b**  
**Focal Length and Zoom Movements**

EFL	T5	T12	T14	f#	Distortion (%)	Stop Dia.
0.4724	0.0200	3.6347	0.6937	1.6	−3.00	1.06
1.2420	2.0741	1.4353	0.8390	1.6	−1.00	1.06
3.4010	3.4211	0.1305	0.7967	2.0	−0.53	0.85
9.2126	4.1838	0.1206	0.0404	2.8	0.10	0.60

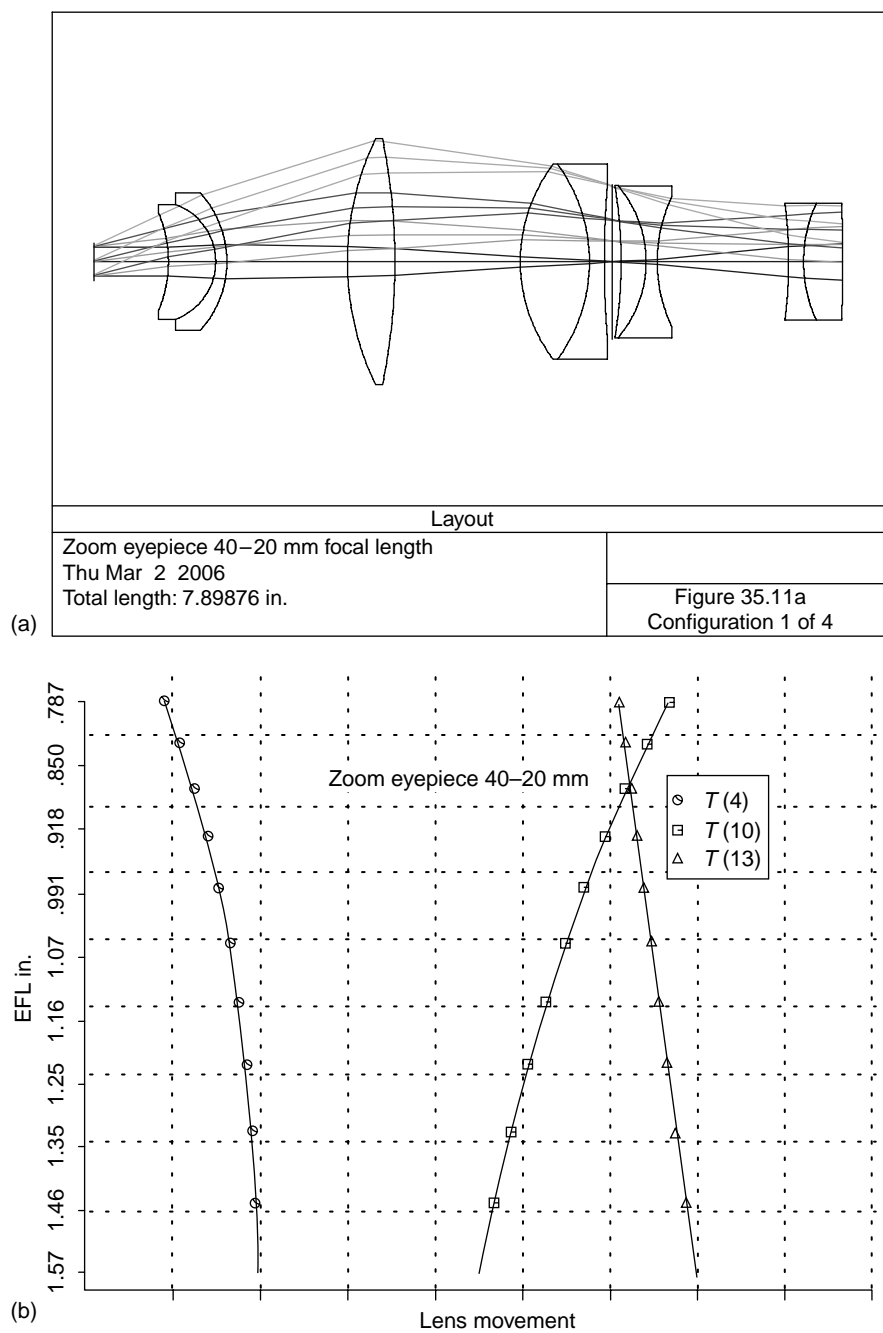


**FIGURE 35.11** A 40- to 20-mm zoom eyepiece, (b) zoom eyepiece enclosed, (c) MTF plots.

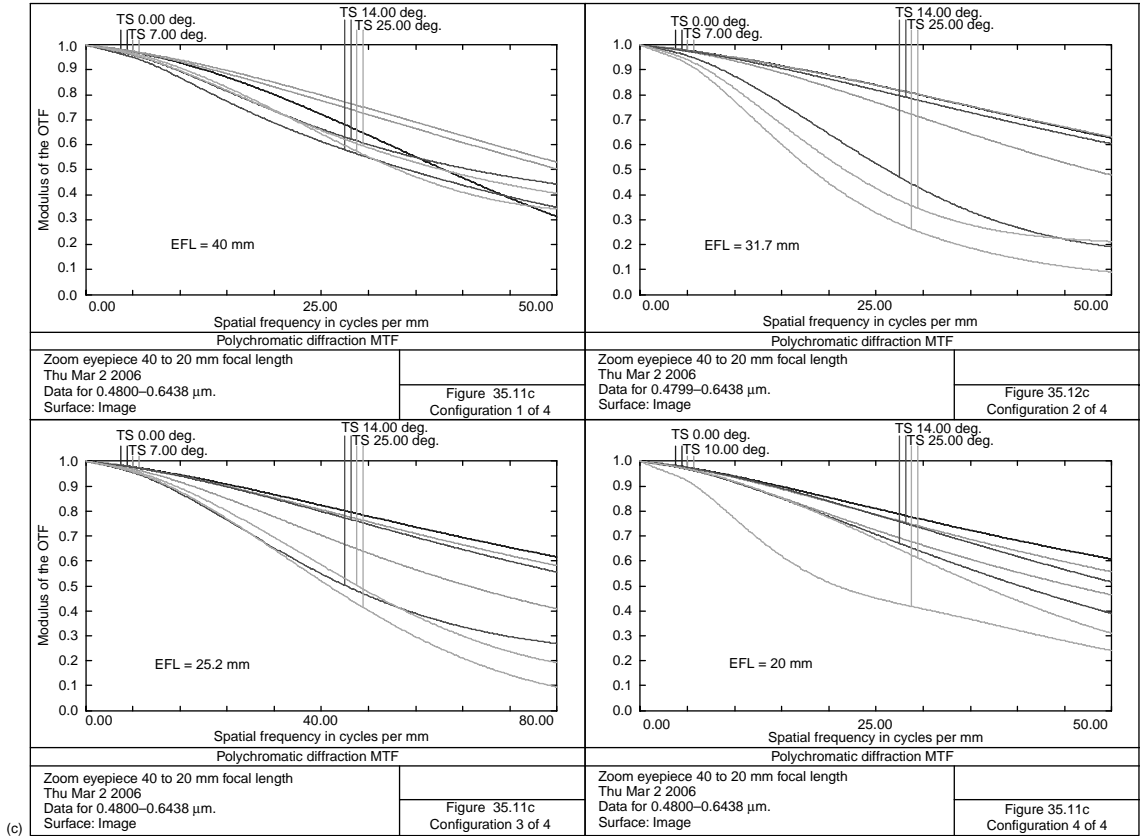
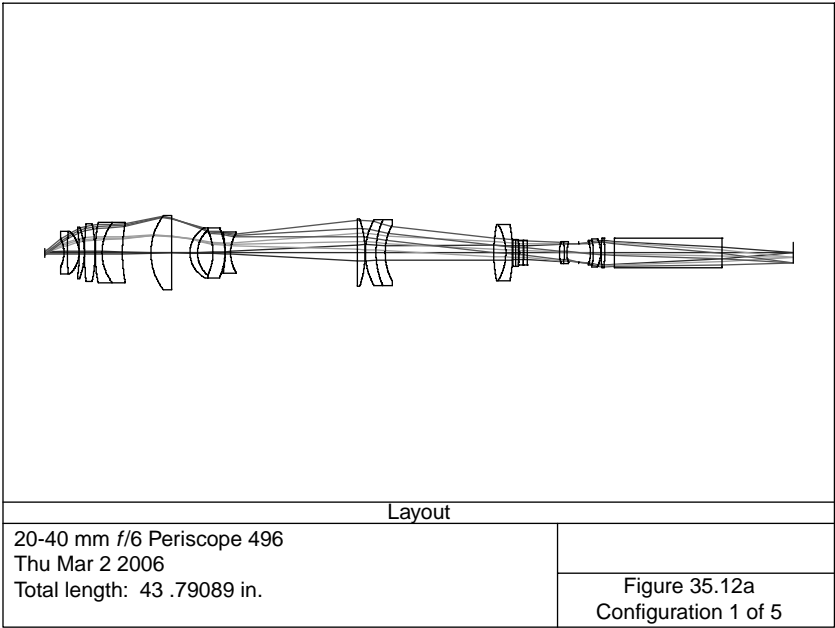


FIGURE 35.11 (continued)



(a)

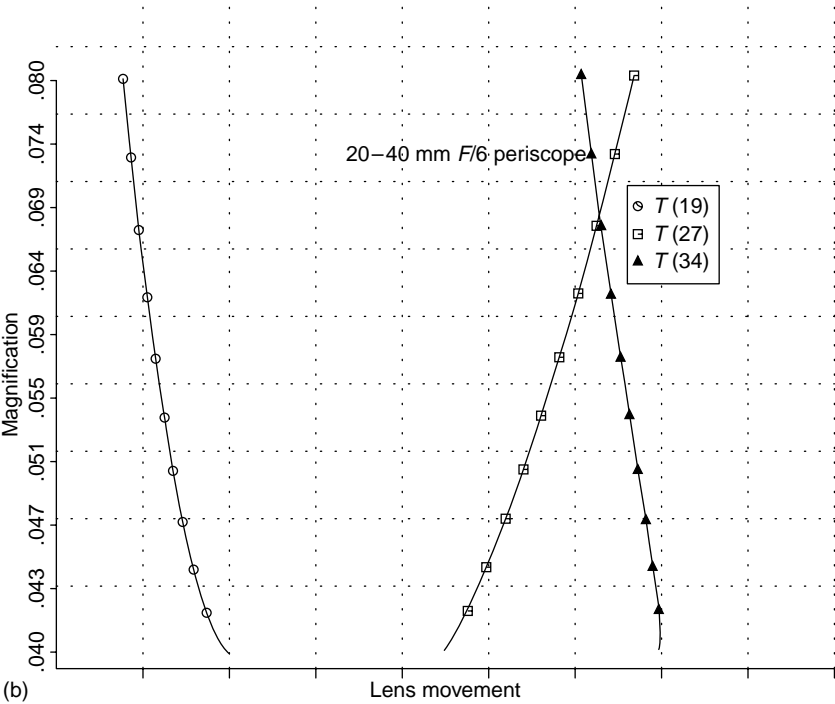


FIGURE 35.12 A 20- to 40-mm focal-length periscope.

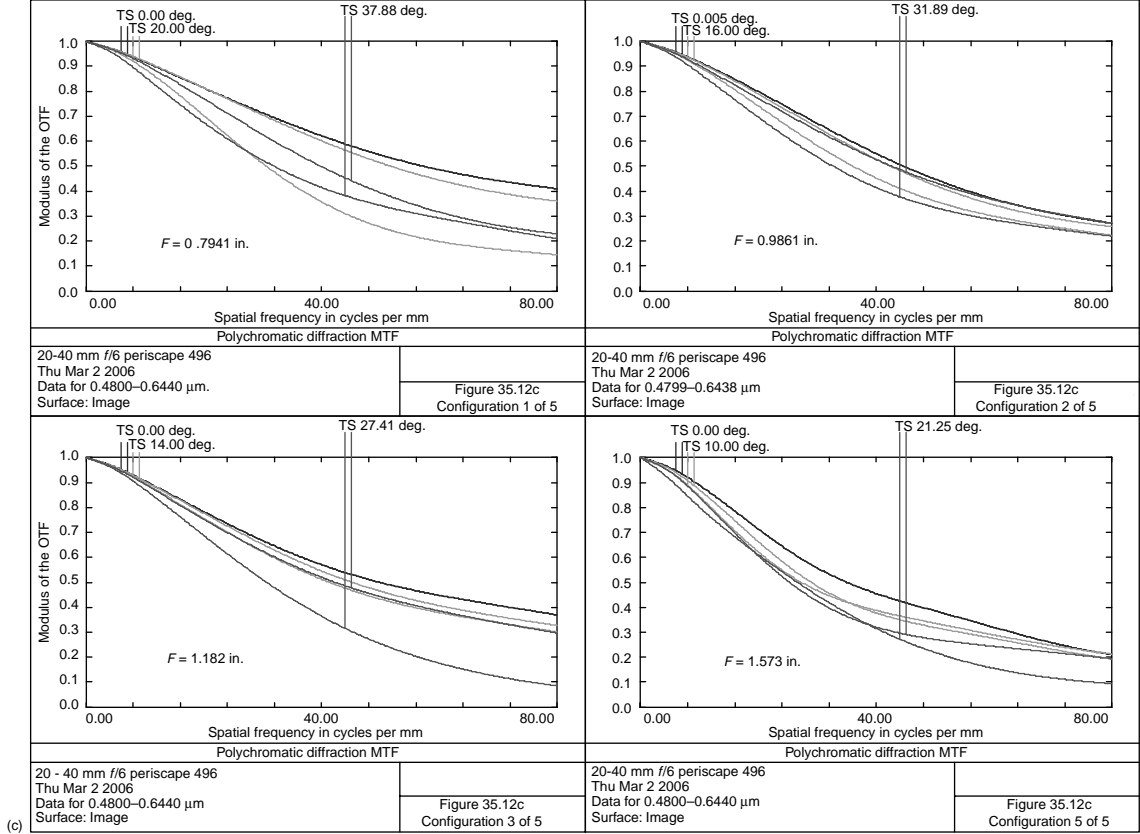


FIGURE 35.12 (continued)

**TABLE 35.11a**  
**A 40- to 20-mm Zoom Eyepiece**

Surface	Radius	Thickness	Material	Diameter
0	0.0000	$0.100000 \times 10^{11}$		0.00
1	0.0000	0.7874		0.375
2	−1.3231	0.4986	N-SK5	1.022
3	−0.6449	0.1181	SF1	1.213
4	−1.0733	1.2716		1.454
5	2.9747	0.5017	N-SK16	2.600
6	−6.4343	1.3233		2.600
7	1.7009	0.7283	N-LAK9	2.060
8	−1.7498	0.1575	SF4	2.060
9	10.4877	0.0836		1.682
10	0.0000	0.0939		1.633
11	−4.8561	0.2627	SF4	1.613
12	−1.2384	0.1181	N-BAF4	1.602
13	1.6068	1.3866		1.378
14	−4.8069	0.1575	N-BAF4	1.225
15	1.4821	0.4100	SF1	1.230
16	−34.0438	78.7402		1.230
17	Stop	−80.7087		15.748
18	0.0000	0.0000		1.369

only minor modifications it should work well with any *f*/5.0 telescope objective. It zooms from 40 to 20 mm effective focal length. It is shown for the 40 mm focal length case.

Notice that the entrance-pupil diameter changes with the zoom focal length. This is a result of system magnification and pupil magnification. Surface 17, the objective exit pupil, is the system stop; in the absence of pupil aberration, the

**TABLE 35.11b**  
**Focal Length and Zoom Movements**

EFL	T4	T10	T13	Distortion (%)	Entrance Pupil Dia.
1.575	1.2715	0.0939	1.3866	−6.8	0.375
1.248	1.0629	0.7109	0.9782	−5.4	0.398
0.992	0.6721	1.4100	0.6699	−5.5	0.326
0.787	0.1323	2.1833	0.4365	−5.3	0.240

**TABLE 35.12a**  
**A 20–40 mm  $f/6$  Periscope**

Surface	Radius	Thickness	Material	Diameter
0	0.0000	20.0000		30.830 Object
1	0.0000	1.1320		0.512 Mirror
2	−1.8490	0.1904	SF1	1.710
3	11.0597	0.6944	N-SSK5	2.480
4	−1.6883	0.0100		2.480
5	−10.2578	0.2979	N-LAK21	2.900
6	−4.1241	0.0100		3.020
7	16.8226	0.6167	N-LAK21	3.400
8	−8.2947	0.0100		3.400
9	9.3114	0.3984	N-LAF3	3.520
10	2.8763	1.1931	N-LAK21	3.520
11	9.0304	1.6682		3.480
12	3.6047	1.2066	SF1	4.340
13	0.0000	1.0742		4.340
14	1.6678	0.4471	SF4	2.940
15	1.7580	0.8985		2.640
16	−3.0143	0.7014	SF4	2.640
17	−3.4251	0.0100		2.940
18	−5.8472	0.3227	N-LAK21	2.440
19	2.2262	7.4314		2.220
20	0.0000	0.4368	N-SSK8	3.940
21	−6.2969	0.0101		3.940
22	3.8501	0.6269	SF4	3.840
23	4.8645	0.5309	N-LAK8	3.840
24	3.4260	6.3575		3.260
25	8.3274	0.7054	N-LAK21	3.300
26	−3.2017	0.3930	SF1	3.300
27	−9.0770	0.0200		3.300
28	38.2970	0.1516	N-LAK21	1.560
29	10.2122	0.1531	SF5	1.560
30	28.1989	0.0784		1.440
31	−3.7724	0.2059	N-LAK21	1.440
32	0.0000	0.0462		1.440
33	−6.7739	0.2210	SF5	1.420
34	−29.4443	1.8610		1.440
35	1.9608	0.2983	N-LAK21	1.260
36	−3.1032	0.1358	SF5	1.260
37	1.5418	0.7146		1.100
38	Stop	0.6720		1.082
39	−1.8725	0.1691	SF5	1.340
40	−3.1113	0.4325	N-LAK22	1.460
41	−1.7943	0.0166		1.640
42	5.8585	0.2077	LAFN7	1.740

(continued)

Table 35.12a (Continued)

Surface	Radius	Thickness	Material	Diameter
43	−14.0066	0.5525	N-SK16	1.740
44	0.0000	6.3074		1.740 Penta roof prism
45	0.0000	4.1740		1.740
46	0.0000	0.0000		1.219

TABLE 35.12b  
Focal Length and Zoom Movements

EFL	T19	T27	T34	Distortion (%)
0.794	7.4314	0.0200	1.8610	2.0
0.986	6.3863	1.4497	1.4763	0.86
1.182	5.8065	2.5390	0.9668	0.68
1.378	5.3657	3.4735	0.4732	0.65
1.573	5.0113	4.2939	0.0072	0.64

entrance-pupil diameter would be given by

$$\frac{D_1}{D_{17}} = \frac{F_{\text{eye}}}{F_{\text{obj}}} = \frac{1.5748}{80} = \frac{D_1}{15.748}.$$

and so the entrance pupil diameter,  $D_1$ , would vary from 0.310 in. diameter (the 40-mm focal length case) to 0.155 in. (the 20-mm focal length case).

In Figure 35.11c is shown the MTF for the four zoom positions, 40- to 20-mm focal lengths.

In Figure 35.12a is shown a zoom periscope, 20–40 mm focal length and is shown in the 20-mm focal-length setting. (See Figure 16.1 for a 25-mm focal-length periscope.) This was optimized for an object distance of 20 in. The lens prescription is given in Table 35.12a.

Surfaces 44–45 represent a penta-roof prism to deviate the beam 90°, whereas the first surface (the entrance pupil) consists of a mirror to deviate the incoming beam 90° nominal. Thus, the camera is facing forward and the camera operator sees in his viewfinder a normal, erect image. The f-number is 6 throughout the zoom.

The object distance was chosen to be 20 in. because it is to be used to photograph miniature objects. Focusing is accomplished by moving the D group, surfaces 35–43. Focal length and zoom movement data is given in Table 35.12b. A plot of these zoom movements is shown in Figure 35.12b.



## REFERENCES

- Betensky, E. (1992) Zoom lens principles and types, *Lens Design, SPIE Critical Review*, Volume. CR31, p. 88.
- Caldwell, J. B. and Betensky, E. I. (1998) Compact, wide range, telecentric zoom lens for DMD projectors, *International Optical Design Conference, 1998, SPIE*, Vol. 3482, p. 229.
- Cook, G. H. (1959) Television zoom lenses, *J. SMPTE*, 68: 25.
- Cook, G. H. (1973) Recent developments in television optics, *Royal Television Society Journal*, 158.
- Cook, G. H. and Laurent, F.R. (1972) Objectives of variable focal length, US Patent #3682534.
- Enomoto, T. and Ito, T. (1998) Zoom lens having a high zoom ratio, US Patent #5815322.
- Hopkins, R. E. (1962) *Optical Design*, Standardization Division, Defense Supply Agency, Washington, DC, MIL-HDBK-141, pp. 13–47.
- Jamerson, T. H. (1971) Zoom lenses for the 8–13 micron region, *Opt. Acta*, 18: 17.
- Johnson, R. B. (1990) All reflective four element zoom telescope, *International Lens Design Conference*, Monterey, p. 669.
- Kanai, M. (2004) Zoom eyepiece optical system, US Patent #6735019.
- Kato, M., Tsuji, S., Sugiura, M., and Tanaka, K. (1989) Compact zoom lens, US Patent #4854681.
- Kojima, T. (1970) Zoom objective lens system with highly reduced secondary chromatic aberration, US Patent #3547523.
- Kolzumi, N. (1997) Eyepiece zoom lens system, US Patent #5663834.
- Macher, K. (1970) High speed varifocal objective system, US Patent #3549235.
- Macher, K. (1974) High speed varifocal objective, US Patent #3827786.
- Mann, A. (1992) Infrared zoom lenses in the 1980's and beyond, *Opt. Eng.*, 31: 1064.
- Murty, A. S. et al. (1997) Design of a high resolution stereo zoom microscope, *Opt. Eng.*, 36: 201.
- Nothnagle, P. E. and Rosenberger, H. D. (1969) Zoom lens system for microscopy, US Patent #3421807.
- Rah, S. Y. and Lee, S. S. (1989) Spherical mirror zoom telescope satisfying the aplanatic condition, *Opt. Eng.*, 28: 1014.
- Schuma, R. F. (1962) Variable magnification optical system, US Patent #3057259.
- Yahagi, S. (2000) Zoom lens for a digital camera, US Patent #6014268.
- Zimmer, K.-P. (1998) Optical design of stereo microscopes, *International Optical Design Conference, 1998, SPIE*, Vol. 3482, p. 690.

---

# 36 Optically Compensated Zoom Lens

In Figure 36.1a is shown an optically compensated zoom lens with two moving groups. It zooms from 3.94 to 7.87 (100–200 mm) focal length and covers the full frame 35-mm motion-picture format (1.225 diagonal). It is shown in the long focal length position. Table 36.1a gives the lens prescription at this long focal length.

There are two moving lens groups: surfaces 4–6 and surfaces 12–16, which are tied together and move as a group. In the optimization program, this is accomplished by adjusting  $T(11)$  to maintain a constant value for all the zoom positions as measured from surface 6 and adjusting  $T(16)$  to maintain a constant value for all the zoom positions as measured from surface 3. Lens positions, focal lengths, and distortion are given in Table 36.1b.

In Figure 36.1b is plotted the zoom movement indicated as  $T(3)$  vs. the paraxial back focal length, BFL, shift, whereas the BFL values in the above table are actual values. Depth of focus is given by

$$d = \frac{2f^\#}{R},$$

where  $R$  is the resolution in line pairs/mm and  $f$  is the  $f$ -number. Assuming that for this system  $R$  is 150 lp/mm, then  $d$  is 0.0026 in. Therefore, the variation in BFL is well within the depth of focus. The system as shown has no vignetting and is  $f/5$  throughout the zoom. Distortion is fairly small.

Figure 36.1c shows the MTF for the above four focal settings. Note that although the paraxial BFL varies slightly with focal length, this MTF data is plotted on a common image surface as indicated in Table 36.1a.

In Figure 36.2a is shown an optically compensated zoom lens (shown in its short-focal-length position) suitable for use with a single-lens reflex (SLR) camera (43.3 mm diagonal). Focal length varies from 2.835 (72 mm) to 5.709 (145 mm). It is  $f/4.5$  throughout the zoom range. Table 36.2a details the lens prescription in the short-focal-length position. It is a modification of the design of Ikemori (1980). The distance from the first lens surface to the image varies from 9.704 (short-focal length position) to 11.431 (long-focal-length position). The focal lengths, spacings, and distortion are given in Table 36.2b.

MTF data is shown in Figure 36.2c. The lens movements and variation in back focal length is plotted in Figure 36.2b. Note that additional clearance should be allowed for the iris. Also, as a consumer product for a single lens reflex camera, most photographers would feel that this lens is too long. Mechanical compensation, although having the complexity of a cam, does provide a substantially more compact lens system.

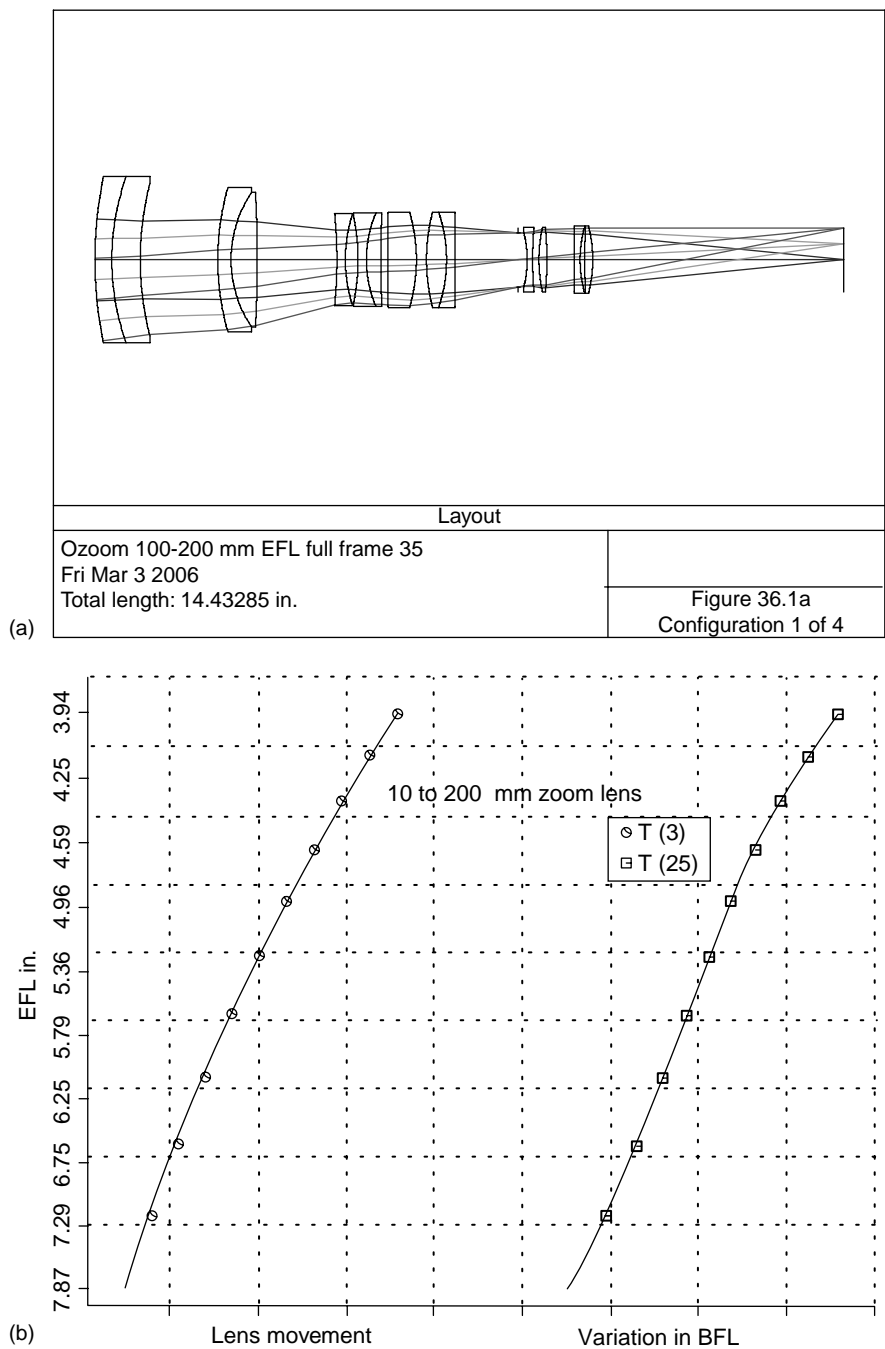
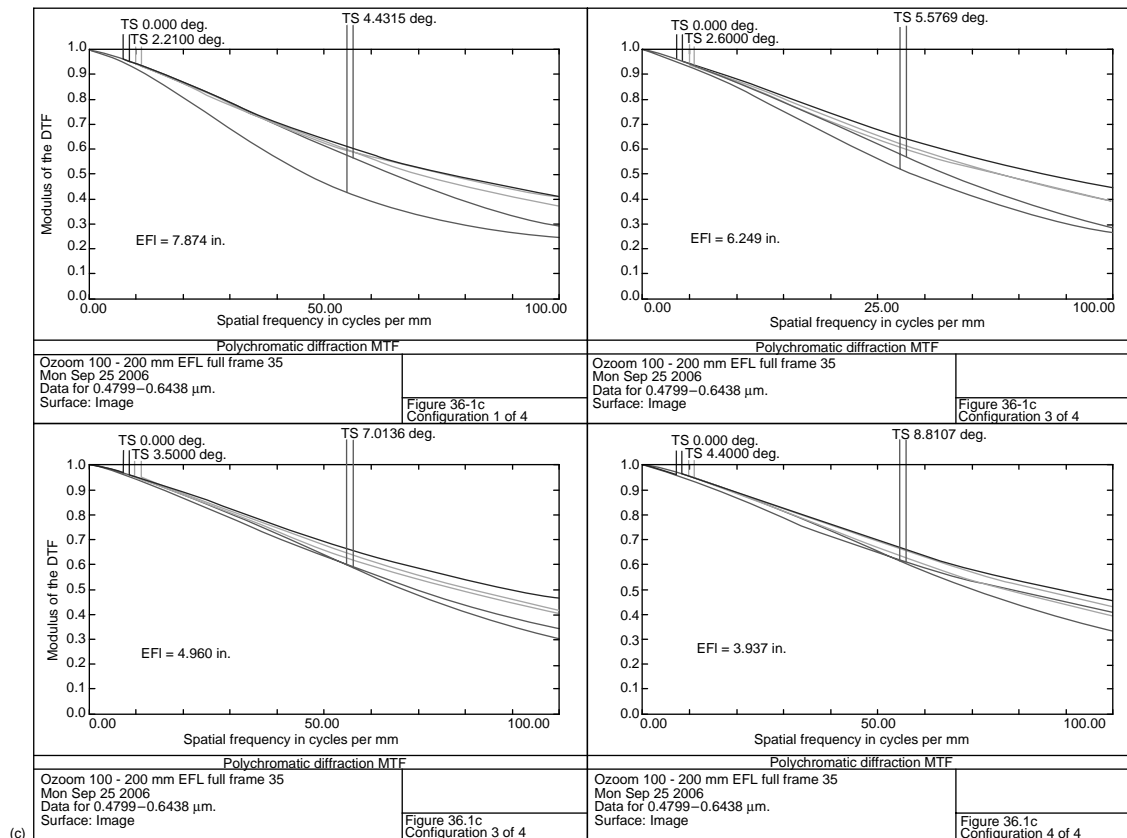


**FIGURE 36.1** (a) System layout, (b) zoom movements, and (c) MTF plots.



(c)

FIGURE 36.1 (continued)

**TABLE 36.1a**  
**Lens Prescription, 100–200-mm Focal Length, Optical Zoom**

Surface	Radius	Thickness	Material	Diameter
1	7.8887	0.3238	LF5	3.200
2	4.7233	0.5496	N-LAK8	3.200
3	5.9991	1.4933		2.940
4	5.0160	0.2568	SF4	2.780
5	2.3243	0.5055	N-BAF10	2.600
6	−24.2009	1.5342		2.600
7	−9.2215	0.1634	N-SK14	1.780
8	2.8425	0.2440		1.700
9	−4.1789	0.1633	N-SK14	1.700
10	2.3193	0.2800	SF4	1.800
11	31.6131	0.1318		1.800
12	54.0708	0.5507	N-SK14	1.840
13	−3.2619	0.1952		1.840
14	3.6571	0.3857	N-SK14	1.840
15	−2.9031	0.1619	SF4	1.840
16	0.0000	1.2227		1.840
17	Stop	0.1707		1.044
18	−2.1185	0.1053	N-BAF4	1.080
19	7.6501	0.1212		1.240
20	2.8668	0.1538	N-BASF2	1.240
21	−6.3400	0.5338		1.240
22	−27.9533	0.1053	SF2	1.240
23	2.3426	0.0881		1.300
24	11.1843	0.1569	N-LAK8	1.300
25	−2.5766	4.8360		1.300
26	0.0000	0.0000		1.234

Distance from first lens surface to image = 14.433.

**TABLE 36.1b**  
**Lens Positions, Focal Lengths, and Distortion**

EFL	T(3)	T(6)	T(11)	T(16)	BFL	Distortion %
3.937	2.6169	0.0500	1.6160	0.0991	4.8357	−0.65
4.960	2.2322	0.5583	1.1077	0.4838	4.8348	0.10
6.249	1.8431	1.0464	0.6195	0.8729	4.8341	0.60
7.874	1.4933	1.5342	0.1318	1.2227	4.8348	0.94

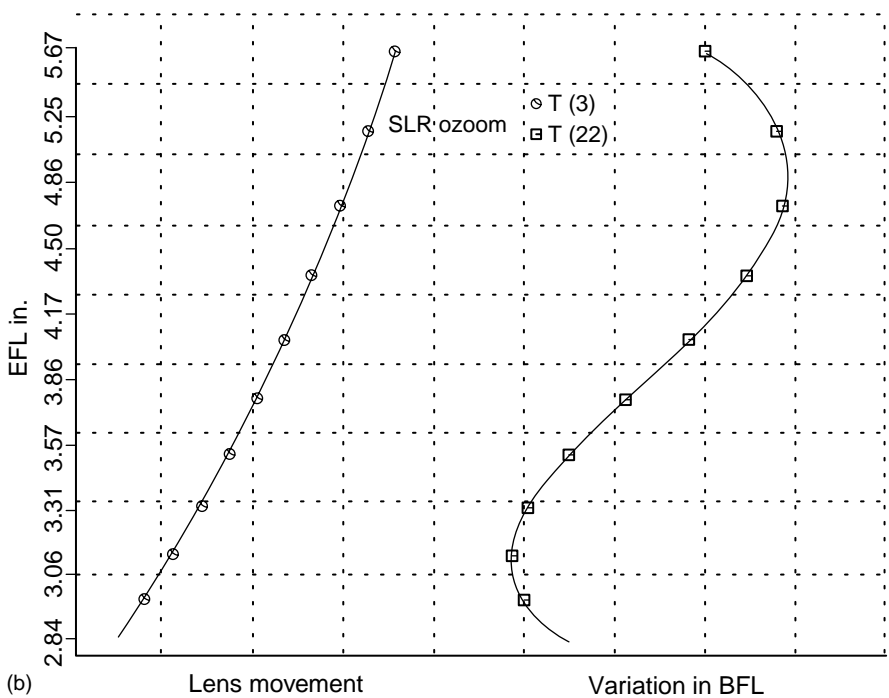
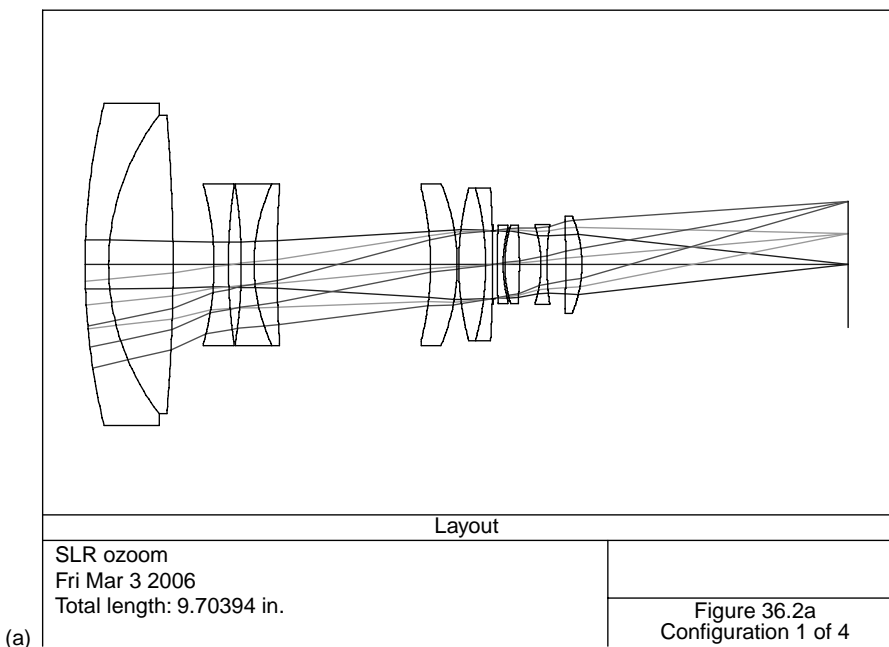


**FIGURE 36.2** (a) System layout, (b) zoom movements, and (c) MTF plots.

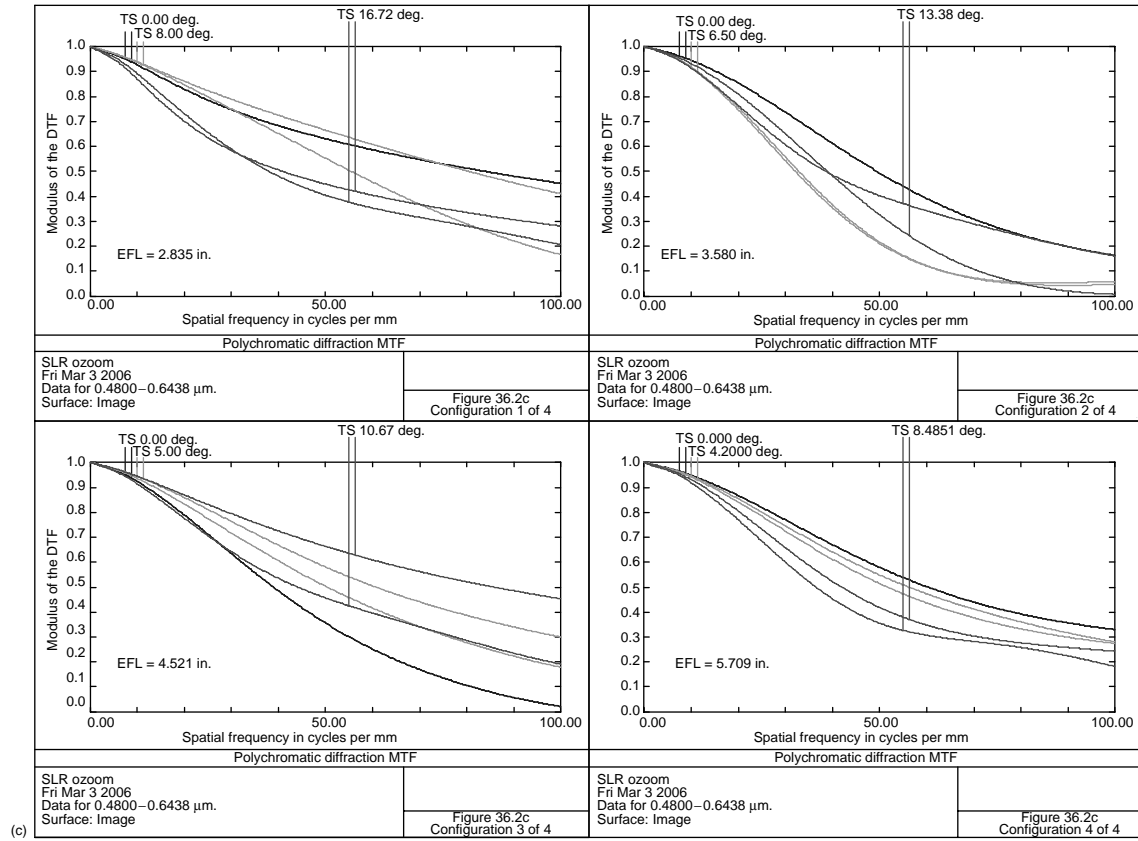


FIGURE 36.2 (continued)

**TABLE 36.2a**  
**Optically Compensated Zoom Lens for SLR Camera**

Surface	Radius	Thickness	Material	Diameter
1	8.7447	0.3000	SF4	4.100
2	3.1234	0.8196	N-LAF3	3.800
3	−22.7398	0.5217		3.800
4	−3.8212	0.1824	N-SK14	2.060
5	7.0240	0.1641		2.000
6	−6.5778	0.1614	N-SK14	2.000
7	2.4341	0.2930	SF4	2.060
8	15.3932	1.9516		2.060
9	−4.0346	0.3393	N-SK14	1.960
10	−2.6814	0.0200		2.060
11	3.7272	0.3415	N-SK14	1.940
12	−3.7272	0.0900	SF4	1.940
13	−18.0137	0.0080		1.940
14	Stop	0.0500		0.864
15	11.8022	0.0750	N-BAK2	1.000
16	1.7815	0.0203		0.950
17	1.6730	0.1870	N-LAK33	1.000
18	−6.9770	0.2743		1.000
19	−1.6225	0.0750	SF2	0.980
20	3.5322	0.2398		1.020
21	−14.6996	0.2054	N-LAK9	1.140
22	−1.6066	3.3846		1.240
23	0.0000	0.0000		1.603

**TABLE 36.2b**  
**Focal Length, Spacings, and Distortion for Zoom Lens for SLR Camera**

EFL	<i>T</i> (3)	<i>T</i> (8)	<i>T</i> (13)	Distortion %	Length
2.835	0.5217	1.9516	0.0080	−6.06	9.704
3.580	1.1110	1.3623	0.5973	−2.66	10.293
4.521	1.6839	0.7894	1.1702	−0.37	10.866
5.709	2.2491	0.2242	1.7354	1.16	11.431



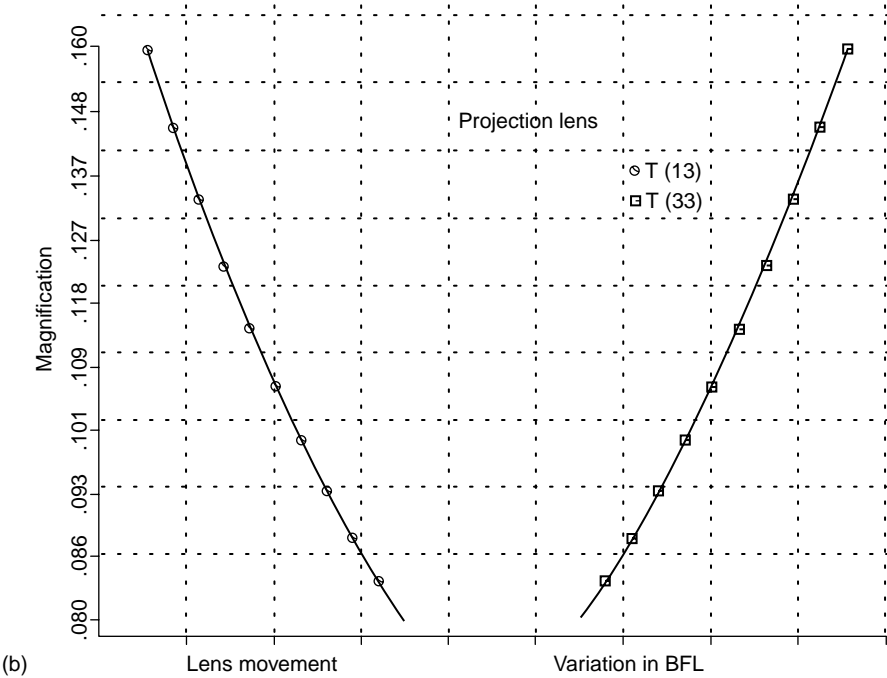
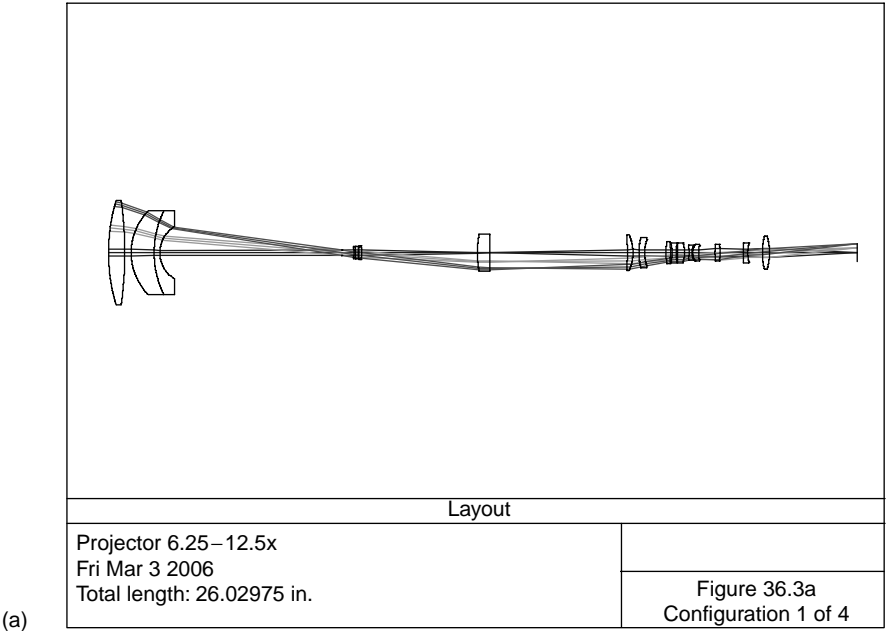


**FIGURE 36.3** (a) System layout, (b) zoom movements, and (c) MTF plots.

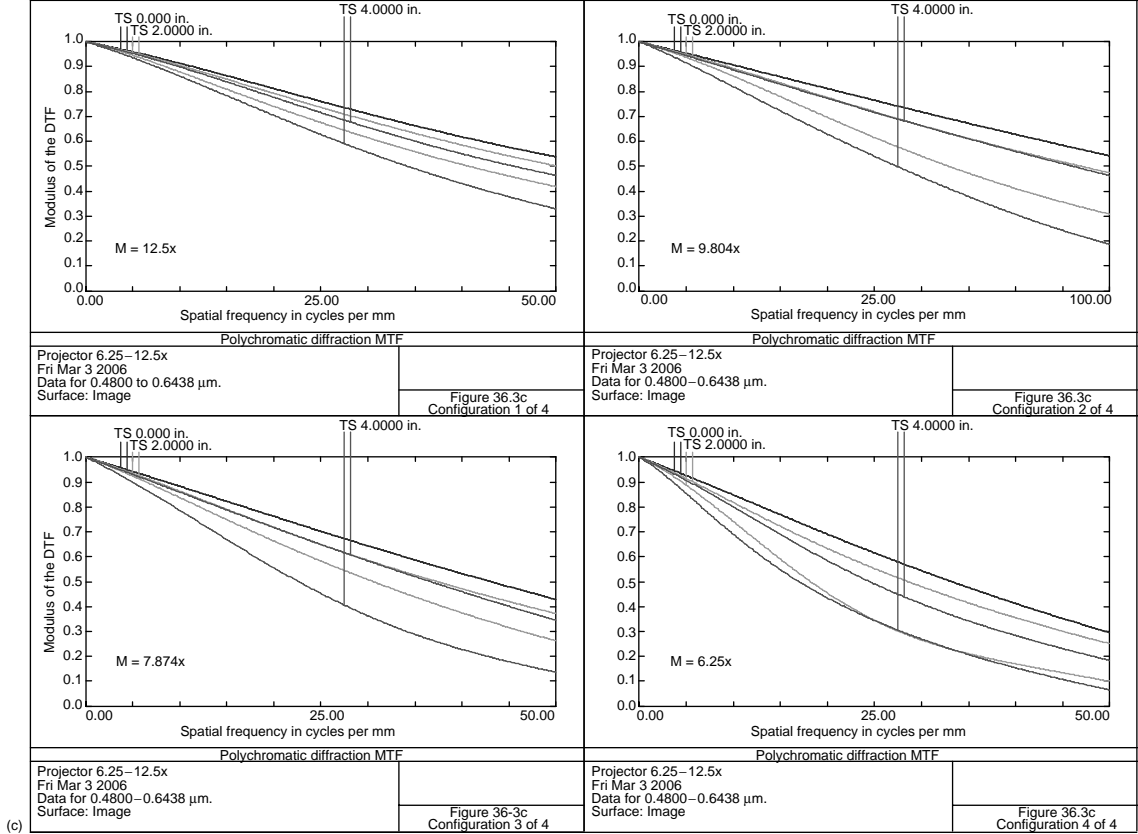


FIGURE 36.3 (continued)

**TABLE 36.3a**  
**Prescription for a 6.25–12.5 OZOOM Projector**

Surface	Radius	Thickness	Material	Diameter
0	0.0000	30.0000		8.000
3	6.4421	0.5639	N-LAK21	3.640
2	−13.2202	0.2251		3.640
3	2.1033	0.7964	N-LAK21	2.920
4	3.3309	0.2000	F2	2.920
5	1.0715	6.3259		1.820
6	Stop	0.4225		0.185
7	−0.9040	0.0500	F2	0.340
8	2.3249	0.0996	N-LAK21	0.440
9	−1.7977	0.0195		0.440
10	−4.3055	0.0993	N-LAK21	0.400
11	−0.9975	4.0246		0.480
12	3.7164	0.4401	N-LAK21	1.280
13	−12.7012	4.7729		1.280
14	−10.1125	0.1949	N-LAK21	1.240
15	−1.5456	0.2072		1.240
16	2.1324	0.2000	F2	1.060
17	1.3114	0.7434		0.920
18	2.5650	0.1561	N-LAK21	0.760
19	−3.4714	0.0556		0.760
20	−1.0916	0.1500	SF1	0.660
21	6.1375	0.0315		0.700
22	20.9579	0.2501	SF5	0.700
23	−1.0523	0.1564		0.700
24	−1.6450	0.1000	N-LAK14	0.540
25	0.4877	0.0289		0.520
26	0.5258	0.2107	N-LAK21	0.580
27	1.8312	0.5616		0.500
28	9.6178	0.1806	N-LAK21	0.580
29	−1.3403	0.8075		0.580
30	7.0546	0.1506	F2	0.700
31	1.0689	0.5067		0.660
32	2.2313	0.2519	N-LAK21	1.160
33	−1.9815	3.0460		1.160
34	0.0000	0.0000		0.629

Distance from first lens surface to image = 26.030.

In [Figure 36.3a](#) is shown an optically compensated lens used to project an image onto an 8-in. diameter screen. Distance from the screen to the first lens surface = 30 in. Table 36.3a gives the lens prescription when the lens is in the 12.5× magnification position. The zoom movements, distortion, and magnification are given in [Table 36.3b](#).

**TABLE 36.3b**  
**Zoom Movements, Distortion, and Magnification**

Magnification	<i>T</i> (13)	<i>T</i> (19)	<i>T</i> (27)	<i>T</i> (33)	Distortion (%)
12.50	4.7729	0.0556	0.5616	3.0460	−1.94
9.804	4.5801	0.2484	0.3688	3.2388	−0.66
7.874	4.4129	0.4156	0.2106	3.4060	0.26 at mid-field
6.250	4.2343	0.5942	0.0230	3.5846	−0.52 0.41 at mid-field

To maintain constant screen brightness over the zoom region, the system has a fixed NA at the screen of 0.004 (tracing from the screen to the “image”). MTF data is shown in Figure 36.3c. The main aberrations are color with coma dominating at the low magnification position.

Note that the main objection to the optically compensated zoom lens (as contrasted to the mechanically compensated) is its long length. As used in a projector, this extra length is not nearly as objectionable as it would be for a camera lens. Also note the considerable variation in back focal length with zoom, requiring some focus adjustment as one zooms.

## REFERENCES

- Back, F. (1963) Zoom projection lens, US Patent #3094581.  
 Grey, D. (1974) Compact eight element zoom lens with optical compensation, US Patent #3848968.  
 Hiroshi, T. (1983) Bright and compact optical compensation zoom, US Patent #4377325.  
 Ikemori, K. (1980) Optically compensated zoom lens, US Patent #4232942.  
 Macher, K. (1969) Optically compensated varifocal objective, US Patent #3451743.



---

# 37 Copy Lenses with Variable Magnification

In a xerographic copying machine and similar applications, the object and image is fixed and the lens is allowed to move to obtain various magnifications. Such a copy lens is shown (high-magnification position) in [Figure 37.1a](#). The aperture stop (surface 10) is just to the left of the next to the last lens. It was designed to cover an image size of 13.9 diagonal, corresponding to standard  $8.5 \times 11$  in. paper. Object to image distance is fixed at 54.134 in. Prescription data for this lens is given in [Table 37.1a](#). The variable spacing and distortion data is given in [Table 37.1b](#).

MTF data at the above magnifications is given in [Figure 37.1b](#).

This lens system has considerable longitudinal chromatic aberration. At the high magnification position, this is 1.49 mm (green to red). Note that this type of lens, although mechanically compensated in the sense that the moving groups operate under cam control, changes its overall length. However, object-to-image distance remains constant.

In [Figure 37.2](#) is shown a variable magnification copy lens. Prescription information is given in [Table 37.2a](#). Lens spacing and distortion data is given in [Table 37.2b](#). The lens has a fixed object-to-image distance of 46 in. and covers a 13.9 in. diameter object. The lens is symmetrical about the stop. It is a modification of the Yamakawa (1997) patent. MTF plots are shown in [Figure 37.2b](#).

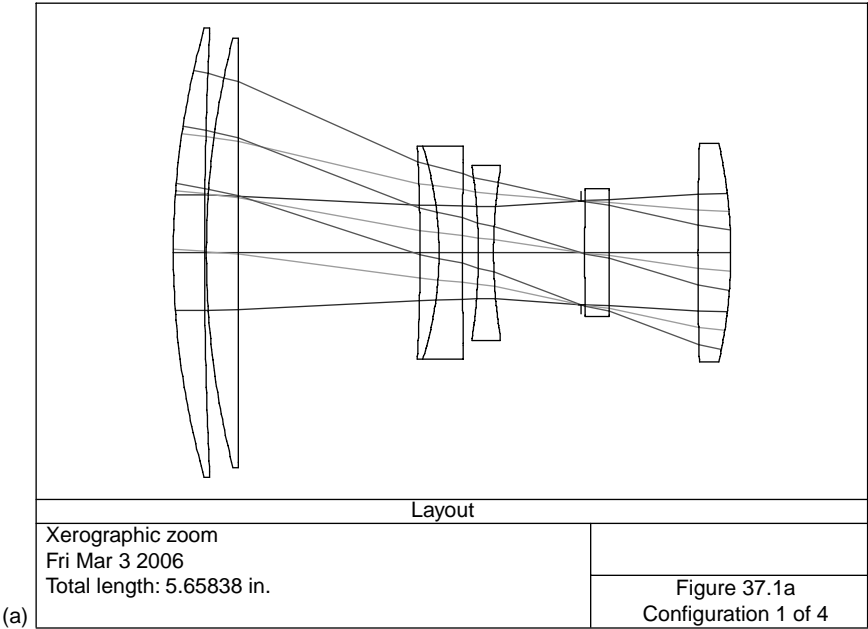


**FIGURE 37.1** Xerographic zoom (a) layout, (b) MTF plots.

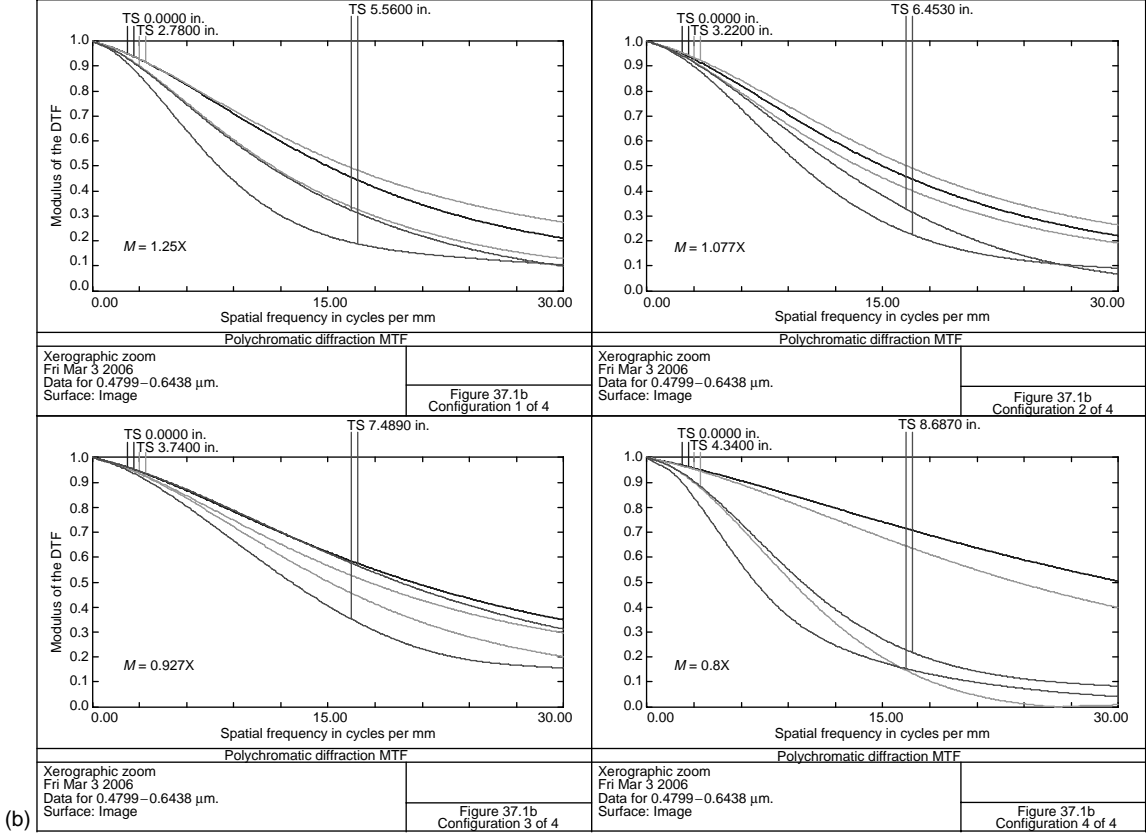


FIGURE 37.1 (continued)



**TABLE 37.1a**  
**Xerographic Zoom Copy Lens (High Magnification Position)**

Surface	Radius	Thickness	Material	Diameter
0	0.0000	21.2744		11.120
1	8.4626	0.3154	N-SK16	4.560
2	47.0276	0.0200		4.560
3	8.9304	0.3228	N-SK16	4.360
4	0.0000	1.8457		4.360
5	− 21.7334	0.1933	N-SK16	2.160
6	− 3.6312	0.2381	LF5	2.160
7	55.5291	0.1612		1.880
8	− 5.9960	0.1544	LF5	1.780
9	5.2889	0.8885		1.640
10	Stop	0.0372		1.051
11	99.3279	0.2502	N-SK16	1.300
12	0.0000	0.8984		1.300
13	40.0443	0.3333	N-SK16	2.220
14	− 5.1653	27.2012		2.220
15	0.0000	0.0000		13.905

**TABLE 37.1b**  
**Variable Spacings and Distortion vs. Magnification**

Mag	<i>T</i> (0)	<i>T</i> (4)	<i>T</i> (9)	<i>T</i> (14)	Distortion %
0.800	27.273	1.7890	0.9394	21.208	0.39
0.927	25.424	1.7463	0.8395	23.200	0.33
1.077	23.399	1.7640	0.8238	25.223	0.23
1.250	21.274	1.8457	0.8885	27.201	0.10

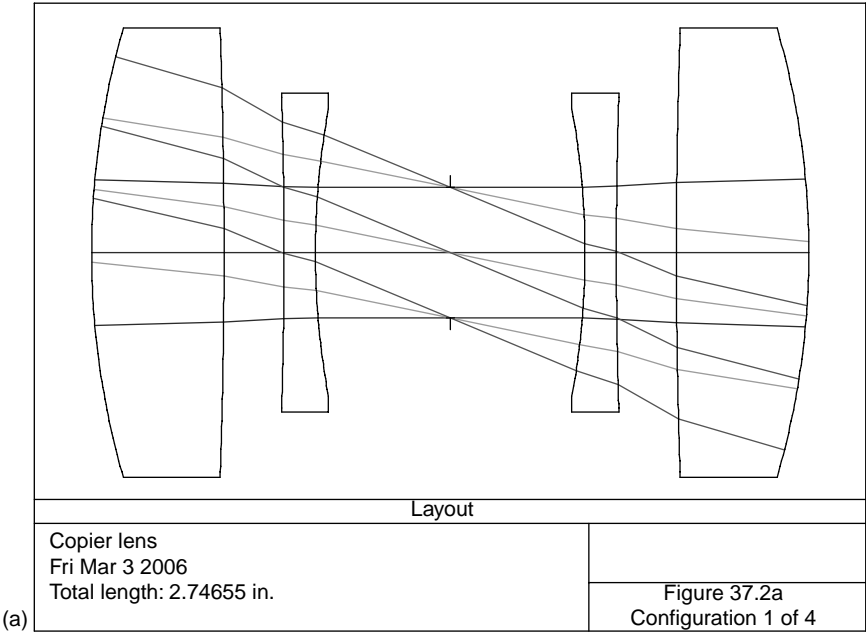


**FIGURE 37.2** Copy lens (a) layout, (b) MTF plots.

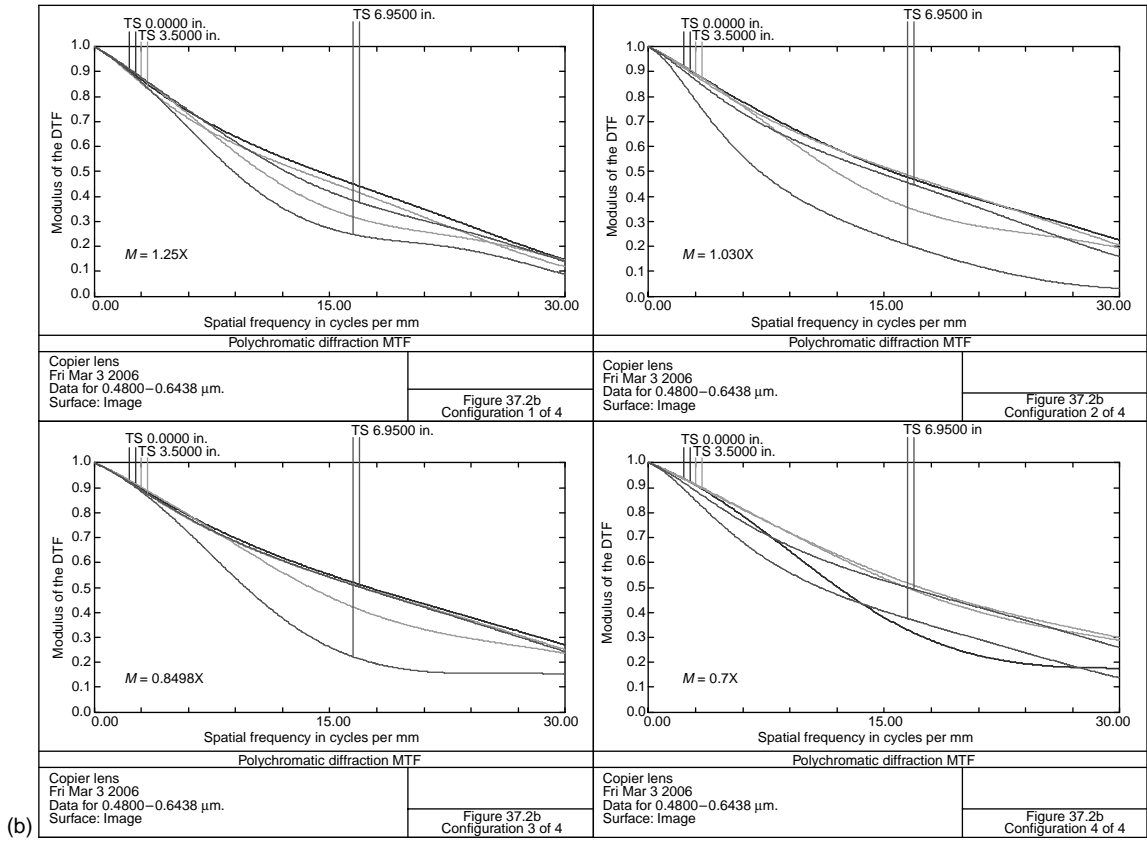


FIGURE 37.2 (continued)

## REFERENCES

- Arai, Y. and Minefuji, N. (1989) Zoom lens for copying, US Patent #4832465.
- Harper, D. C., McCrobie, G. L., and Ritter, J. A. (1975) Zoom lens for fixed conjugates, US Patent #3905685.
- Yamakawa, H. (1997) Zoom lens system in finite conjugate distance, US Patent #5671094.



---

# 38 Variable Focal Length Lenses

Variable focal length lenses pre-date true zoom lenses. It was realized some time ago that for a lens system consisting of positive and negative groups, varying the air space between these groups would change the effective focal length. For projection, this is a handy feature because by a simple adjustment and then refocusing, the image may be made to fit the screen.

In [Figure 38.1a](#) is shown a variable focal length lens suitable to project film from a 35-mm single-lens reflex (SLR) camera ( $18 \times 24$  mm format). [Table 38.1a](#) contains its lens prescription in the short-focal-length position, 1.417 (36.0 mm). The spacing and focal length data is given in [Table 38.2b](#).

[Figure 38.1b](#) displays the MTF at the above focal lengths. This lens system is a modification of the Sato (1988) patent. As with previous examples of projection lenses, an infinite object distance is used. It is recommended that a final computer run be made at a typical finite conjugate. Note that the exit pupil moves with the focal length changes and so the projection condenser system may have to be adjusted ([Table 38.1b](#)).

In [Figure 38.2a](#) is shown a variable focal length projection lens (see Angenieux 1958) to project 35-mm film (1.069 diagonal). The prescription is given in [Table 38.2a](#). [Table 38.2b](#) gives focal lengths vs. lens movements. Unlike the above example, the length of the lens does not change with changing focal length. The inner lens group moves to vary the focal length from 1.772 (45 mm) to 2.165 (55 mm). The lens is  $f/3.80$  at the short-focal-length position.

Note that the back focal length (BFL) increases with focal length. Also, for theatrical motion-picture projection, the f-number should be reduced to obtain sufficient screen illumination.

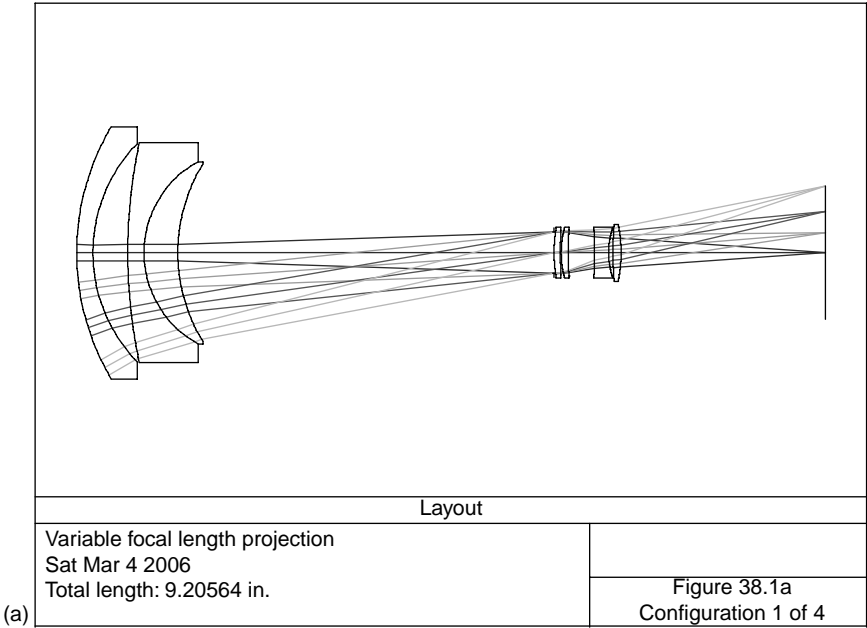


**FIGURE 38.1** Variable focal length projection for SLR camera (a) layout, (b) MTF plots.

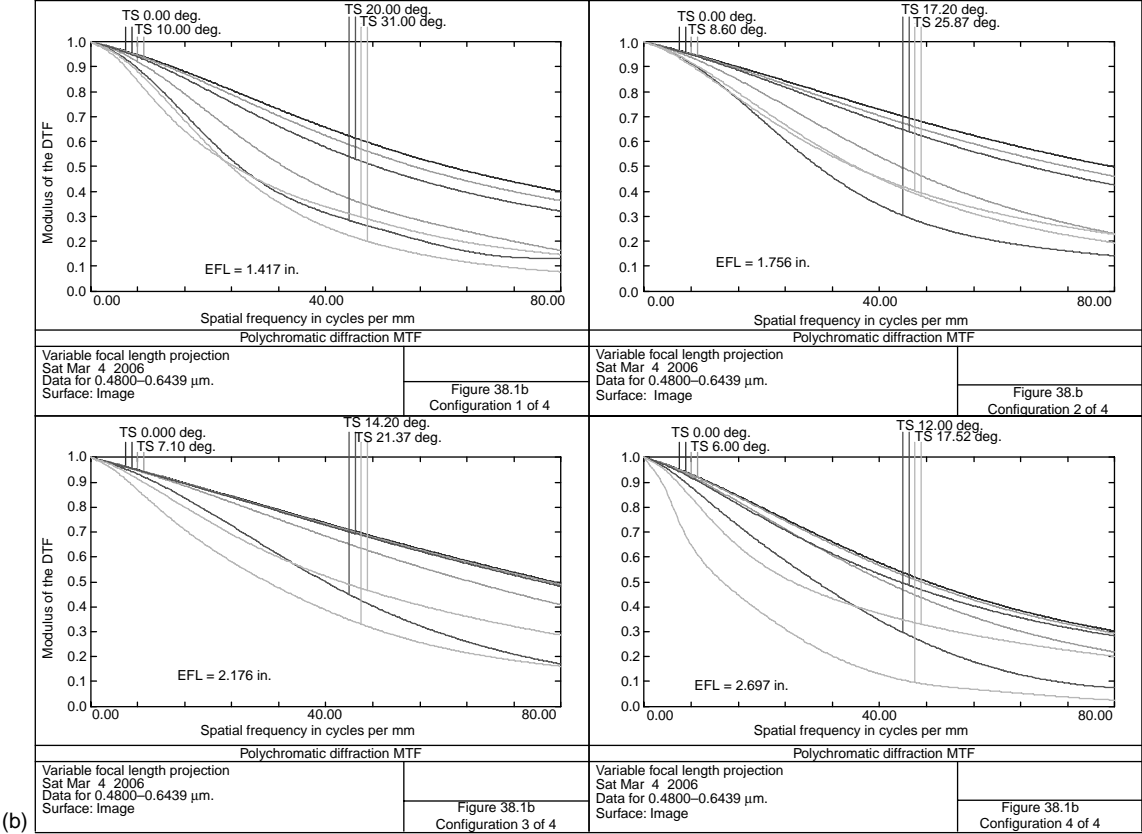


FIGURE 38.1 (continued)



**TABLE 38.1a**  
**Variable Focal Length Projection Lens**

Surface	Radius	Thickness	Material	Diameter
1	3.0383	0.2000	SF4	3.100
2	1.9289	0.4277		2.680
3	6.5000	0.2000	N-BAF10	2.700
4	1.2770	0.4162	SF4	2.240
5	2.0978	4.6266		2.180
6	Stop	0.0000		0.512
7	1.8348	0.0768	N-LAK33	0.620
8	6.4015	0.0095		0.560
9	1.1214	0.0864	N-SSK5	0.620
10	4.1292	0.3231		0.580
11	−7.5735	0.1743	SF4	0.600
12	0.9410	0.0535		0.620
13	4.1515	0.0994	N-BAF3	0.700
14	−1.8098	2.5122		0.700
15	0.0000	0.0000		1.638

**TABLE 38.1b**  
**Spacings vs. Focal Length**

Focal Length	$\theta^a$ (degrees)	Length <sup>b</sup>	Distortion <sup>c</sup> (%)	T(5)	BFL	f#	Exit Pupil
1.417	31.002	9.2056	−4.02	4.6266	2.5122	7.00	−3.11
1.756	25.869	8.4790	−1.83	3.6388	2.7734	7.58	−3.37
2.176	21.371	8.0182	−0.61	2.8594	3.0920	8.30	−3.69
2.697	17.522	7.7837	0.02	2.2210	3.4960	9.22	−4.09

<sup>a</sup> Full field semi-field angle.  
<sup>b</sup> Length of the lens system, from front lens vertex to image.  
<sup>c</sup> Distortion at full field.

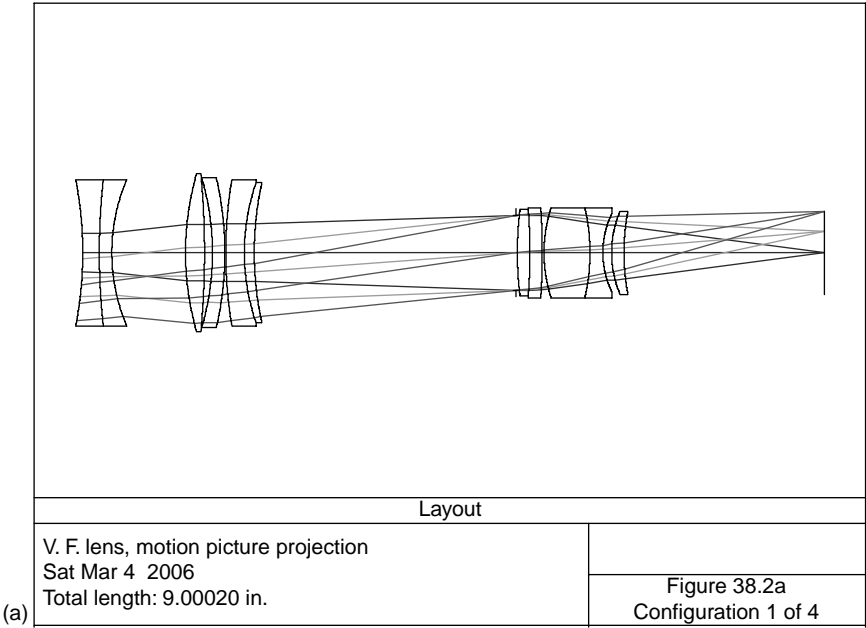


**FIGURE 38.2** Variable focal length motion picture projection lens (a) layout, (b) MTF plots.

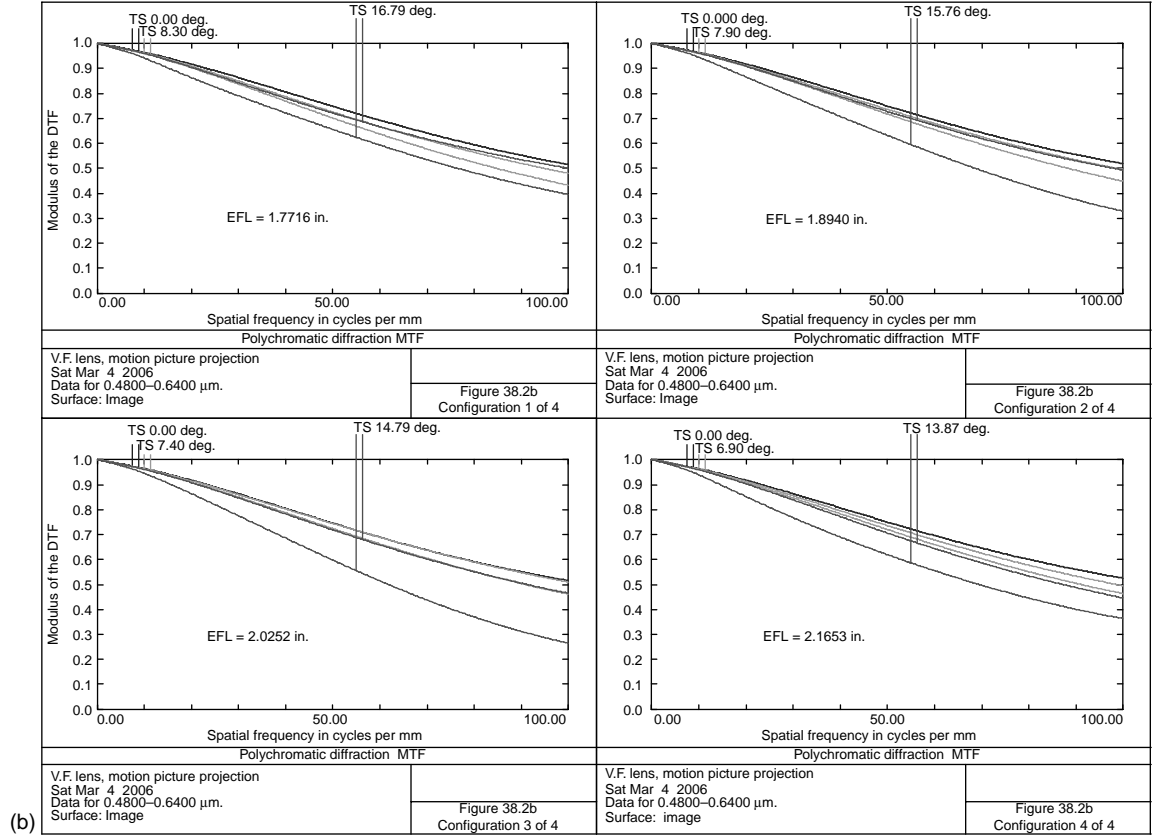


FIGURE 38.2 (continued)

**TABLE 38.2a**  
**Variable Focal Length Projection Lens**

Surface	Radius	Thickness	Material	Diameter
1	−4.6286	0.2000	N-LAK7	1.760
2	8.3461	0.1500	SF1	1.760
3	2.2419	0.8863		1.760
4	3.4666	0.2276	N-LAF2	1.900
5	−10.5167	0.0951		1.900
6	−3.2300	0.1500	F5	1.800
7	−3.9679	0.0100		1.760
8	5.2746	0.2247	N-LAK12	1.760
9	2.5992	0.1191	SF1	1.680
10	3.9967	3.1424		1.680
11	Stop	0.0200		0.900
12	4.2640	0.1500	N-BASF2	1.040
13	−7.4193	0.1500	N-LAK12	1.040
14	−7.7031	0.0200		1.080
15	1.7286	0.5532	N-LAK14	1.080
16	−2.3943	0.1547	SF1	1.080
17	1.0825	0.1053		0.940
18	1.2714	0.1500	N-LAK14	1.000
19	2.8182	2.4074		0.960
20	0.0000	0.0000		1.002

Distance from first lens surface to image = 8.916.

**TABLE 38.2b**  
**Focal Lengths vs. Lens Movements**

EFL	T(5)	T(10)	BFL	Distortion %	Exit Pupil
1.7716	0.0951	3.1424	2.4074	−6.58	−3.144
1.8940	1.0819	2.1555	2.4715	−5.77	−3.208
2.0252	1.9536	2.0252	2.5391	−5.00	−3.275
2.1653	2.7285	0.5090	2.6111	−4.27	−3.348

## REFERENCES

- Angenieux, P. (1958) Variable focal length objective, US Patent #2847907.
- Nasu, S., and Tada, E. (2004) Variable-focus lens system, US Patent #6683730.
- Sato, S. (1988) Zoom lens, US Patent #4792215.

---

# 39 Gradient-Index Lenses

In the previous chapters, it has been assumed that the refractive index and dispersion of the medium was the same for all locations in the lens. Here, lens systems are discussed in which the refractive index has been made to vary depending upon its location in the lens. There are basically two types to consider: axial gradients and radial gradients.

## AXIAL-GRADIENT LENSES

In a lens with an axial gradient, the refractive index varies according to its position along the optical axis. A typical equation describing this is (Marchand 1978)

$$n = n_0 + f(z)$$

where  $n_0$  is the refractive index at starting position  $Z_0$ , and  $f(z)$  is an index function referenced from this starting position. Ray tracing is accomplished by dividing up the lens into small slices ( $\Delta Z$ ). As the ray passes through the lens, the value of  $Z$  is determined at each slice, and the refractive index at that location computed. This is illustrated in [Figure 39.1](#). Large slices are taken for the preliminary system and reduced as the design progresses. Therefore, the designer has as a variable for any given material—the value of  $T$ —which is the distance of the lens vertex from  $Z_0$ .

This value of  $T$  must be indicated on the lens drawing. Unlike conventional glass blocks, this blank cannot be reversed by the optical shop. Hunter and Walters (1998) lists some of the items that should be specified on drawings for axial gradient lenses.

ZEMAX™, as well as most comprehensive lens design programs, provide the designer with several types of axial-gradient functions. One such type is the GRADIUM™ surface (Lightpath 1996; Hunter et al. 1989). [Figure 39.2](#) shows the index profile for one such material. In converting an existing design to one using a GRADIUM™ material, one should keep in mind that all of these materials are “flint” type materials—glasses with a high refractive index and large dispersion. Each type comes in two versions: P-type that goes from high refractive to low refractive, and N-type that goes from low to high. [Figure 39.2](#) is an example of N type.

The design procedure should be for the designer to first plot the ray intercept curves. Then, he or she should examine the existing design and decide which “flint” element should be converted to a gradient index material and whether it should be an N- or a P-type material. This is done by an examination of the ray intercepts and noting if the upper rim rays are above or below the optical axis. Wang and Moore (1990) present a systematic method for determining a starting solution.

In [Figure 39.3](#) is shown a 3.0-in.  $f/1.8$  projection lens containing an axial gradient material (GRADIUM G51SFN). The prescription information is given in

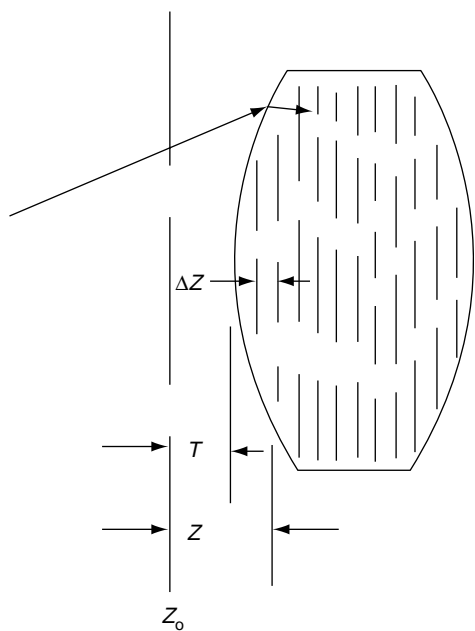


FIGURE 39.1 Tracing through a lens with an axial gradient.

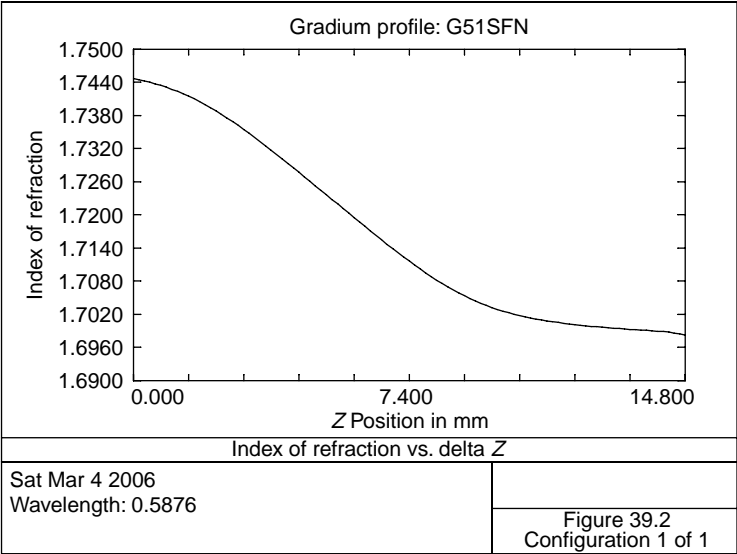


FIGURE 39.2 Index of refraction vs. delta Z.

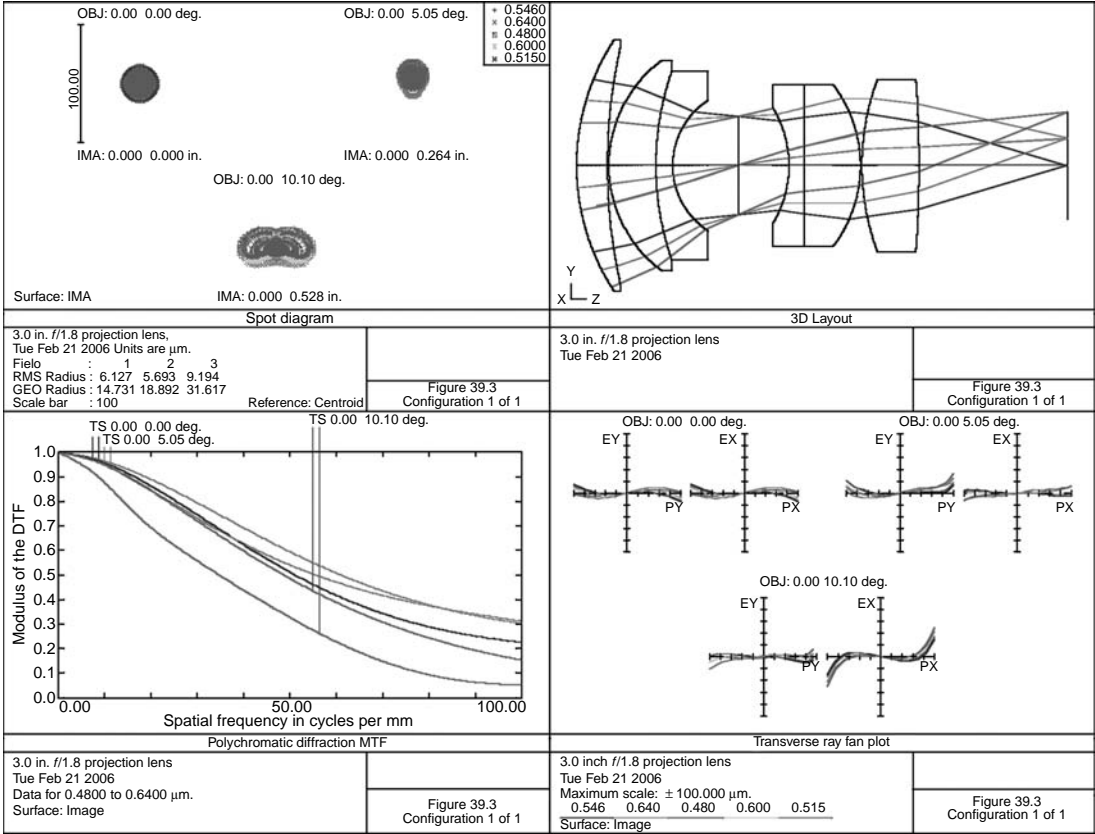


FIGURE 39.3 A 3.0-in. f/1.8 projection lens, axial gradient.



**TABLE 39.1**  
**A 3.0-in.  $f/1.8$  Projection Lens**

Surface	Radius	Thickness	Material	Diameter
1	2.2450	0.3014	N-LAK33	2.460
2	5.3001	0.0150		2.360
3	1.2863	0.4599	N-LAK33	2.060
4	2.8212	0.1641	SF5	1.840
5	0.7636	0.6442		1.280
6	Stop	0.4939		0.965
7	−1.0987	0.1486	G51SFN	1.140
8	0.0000	0.5506	N-LAK33	1.580
9	−1.3032	0.0150		1.580
10	2.4353	0.5579	N-LAK12	1.680
11	−11.8852	1.4577		1.680
12	0.0000	0.0000		1.058

Distance from first lens surface to image = 4.808, distortion = −1.19%.

Table 39.1.  $T$  is 0.13945, corresponding to a nominal refractive index of 1.7325. In comparison to the design of 22.1, note the comparable performance with one less element. Focal length,  $f$ -number, and field size are the same as in design 22.1. The exit pupil is located −4.592 from the film surface. Note that because there is adequate room for an iris in this design, it may also be used as a camera lens.

Figure 39.4 shows a lens of 6-in. focal length that is  $f/4$  and contains an axial gradient material. The prescription data is given in Table 39.2. The field of view is  $1.0^\circ$ . Note that positive, spherical lenses prepared from homogeneous glass have spherical aberrations such that rays at the margin are focused closer to the lens than paraxial rays. The axial gradient solves this problem with a negative gradient. This causes the refractive index to be less at the edge than at the center, thus reducing the spherical aberration.

$T$  is 0.0. The reference index of refraction, then, is 1.7758. The second surface should be set plane for manufacturing reasons. Wavelength is 0.6328  $\mu\text{m}$ .

## RADIAL GRADIENT

A typical radial gradient has an index profile given by

$$n = n_0 + n_{R2}R^2.$$

It is therefore possible to have a radial gradient material in the form of a plane plate and yet have power. Such a lens is listed in Table 39.3. Effective focal length

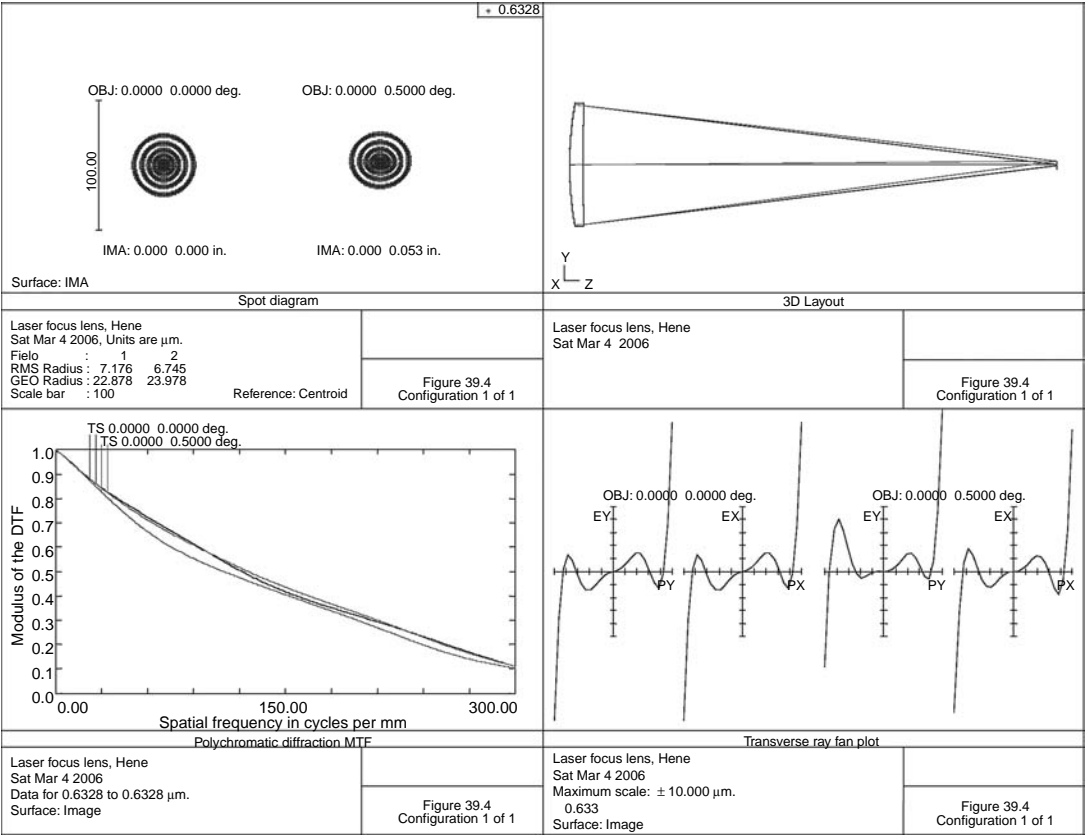


FIGURE 39.4 Laser focusing lens, axial gradient.

**TABLE 39.2**  
**6 Inch f/4, Laser Focus Lens**

Surface	Radius	Thickness	Material	Diameter
0	0.0000	$0.100000 \times 10^{11}$		0.00
1	4.4701	0.1705	G23SFN	1.500
2	123.6921	5.9069		1.485
3	0.0000	0.0000		0.107

(at 0.55  $\mu\text{m}$ ) is 50.0. The material (Radial) is per the above equation with  $N_0=1.7$  and  $N_{R2}=-0.05$ . The lens is shown in [Figure 39.5](#).

Long rod lenses, using a radial gradient index profile, may be made by an ion-exchange process. Such devices are used in making long and very small diameter borescopes for medical and industrial inspection purposes (Gradient Lens Corp., 1999). Such a device is shown in [Figure 39.6](#). This has eight intermediate images inside the scope. It may be combined with a front objective to obtain an erect image when viewed with an eyepiece ([Table 39.4](#)).

The radial gradient material is made by NSG America (1999). Its index profile is given by

$$n = n_0 \left[ 1.0 - \frac{A}{2} r^2 \right],$$

where  $A$  and  $N_0$  are functions of wavelength:

$$A(\lambda) = \left[ K_0 + \frac{K_1}{\lambda^2} + \frac{K_2}{\lambda^4} \right]^2,$$

**TABLE 39.3**  
**Data for 50-in. Focal Length Lens with Radial Gradient**

Surface	Radius	Thickness	Material	Diameter
0	0.0000	$0.100000 \times 10^{11}$		0.00
1	Stop	0.0000		2.000
2	0.0000	0.2000	Radial Grad., $N_0=1.7$ , $N_{R2}=-0.05$	2.000
3	0.0000	49.9592		2.000
4	0.0000	0.0000		0.874

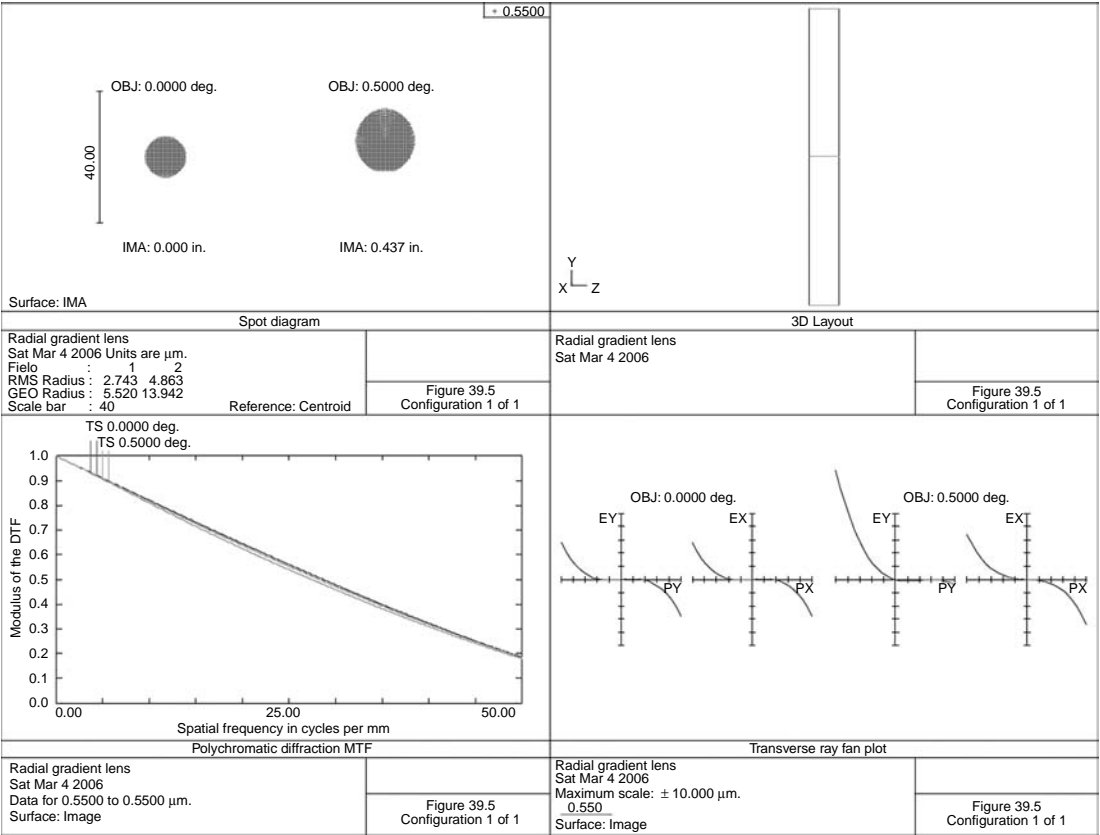


FIGURE 39.5 Radial gradient, 50-in. focal length.

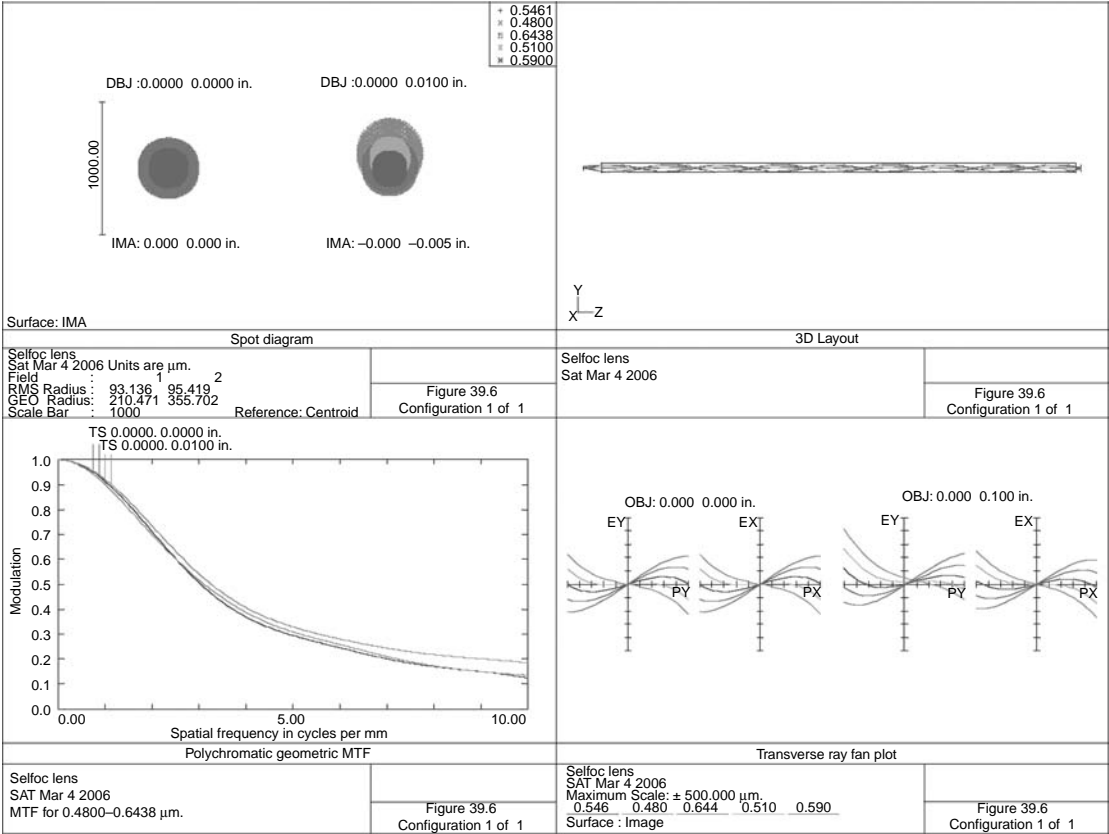


FIGURE 39.6 Selfoc lens.

**TABLE 39.4**  
**SELFOC Lens**

Surface	Radius	Thickness	Material	Diameter
0	0.0000	0.0800	SLS-1.0	0.020
1	Stop	2.0546		0.040
2	0.0000	0.0255		0.040
3	0.0000	0.0000		0.024

$$n_0 = B + \frac{C}{\lambda^2}.$$

Figure 39.6 shows the geometric MTF of this system (geometric MTF was used due to the relatively low resolution.) Changing the front surface from a plane to a curve improves performance slightly.

Corning has recently developed a line of radial gradient index lenses for use in fiber optics systems at 1.55  $\mu\text{m}$  featuring low chromatic dispersion (Corning 2003). This wavelength was chosen because glass fibers typically have their minimum loss at this wavelength and it is near the region of minimum dispersion (Hecht 1999). Also, the rare earth erbium laser may be used to amplify the signal for long-length fibers (Table 39.5).

A single mode fiber of 10- $\mu\text{m}$  diameter is placed 0.0053 in. from the lens. Figure 39.7 shows some of the aspects of this lens. In the upper left of the figure is a plot of refractive index as measured from the center ( $N=1.537$  at the center). The diffraction-encircled energy plot shows near-diffraction-limited performance with about 87% of the energy going into the 10- $\mu\text{m}$  fiber. The lens NA (numeric aperture) is 0.286.

**TABLE 39.5**  
**Corning-GRIN (Gradient Index Material) Laser Focusing Lens**

Surface	Radius	Thickness	Material	Diameter
0	0.0000	$0.100000 \times 10^{11}$	Corning-GRIN	0.00
1	0.0000	0.2000		0.050 Stop
2	0.0000	0.0053		0.002
3	0.0000	0.0000		0.001

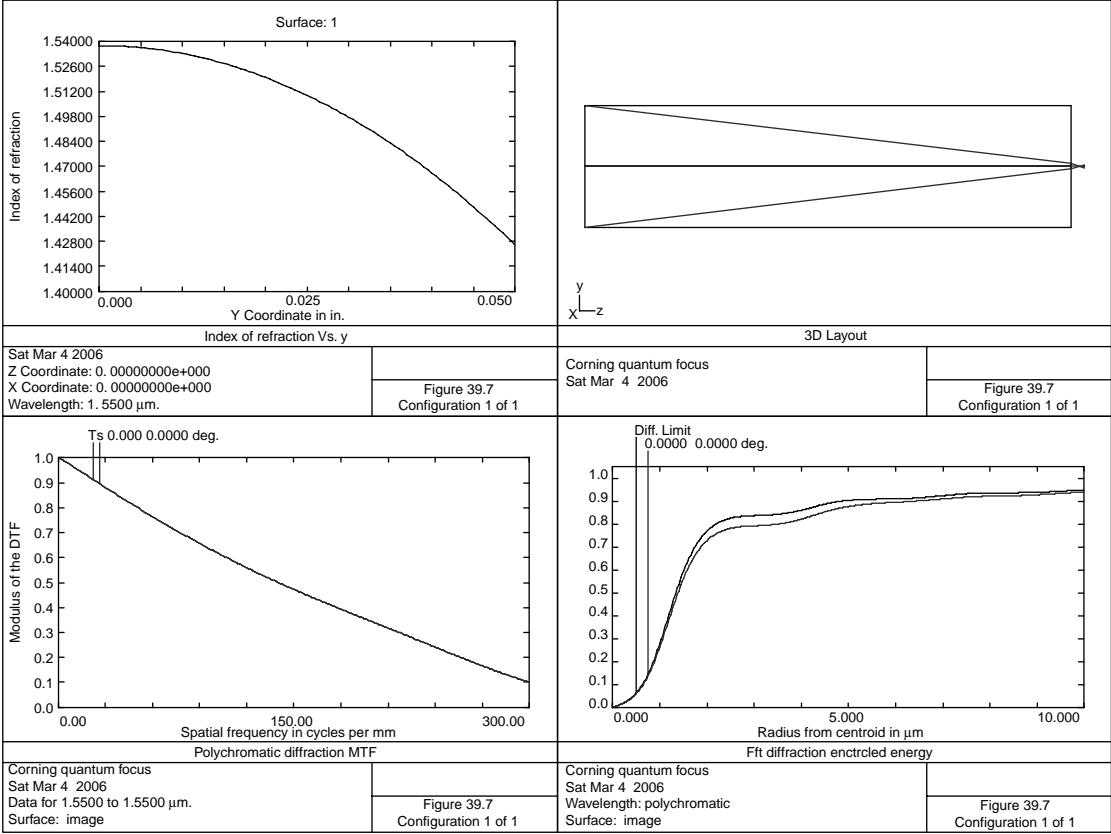


FIGURE 39.7 Corning-GRIN (Gradient Index Material) laser focusing lens.

## REFERENCES

- Corning (2003) *Low Chromatic Dispersion of Quantum focus  $\Theta$  Gradient Index Lens*, Corning Photonic Materials, Corning, NY.
- Gradient Lens Corp. (1999) *Data Sheet*. Gradient Lens Corp., Rochester, NY.
- Greisukh, G. I. and Stepanov, S. A. (1998) Design of a cemented, radial gradient-index triplet, *Applied Optics*, 37: 2687–2690.
- Greisukh, G. I., Bobrov, S. T., and Stepanov, S. A. (1997) *Optics of Diffractive and Gradient Index Elements and Systems*, SPIE Press, Bellingham, WA.
- Hecht, J. (1999) *Understanding Fiber Optics*, Prentice Hall, Upper Saddle river, NJ.
- Hunter, B. V. and Walters, B. (1998) How to design and tolerance with GRADIUM<sup>®</sup> glass, *International Optical Design Conference, 1998, SPIE*, Volume 3482, p. 801.
- Hunter, B. V., Tyagi, V., Tinch, D. A., and Fournier, P. (1989) Current developments in GRADIUM<sup>®</sup> glass technology, *International Optical Design Conference, 1989, SPIE*, Volume 3482, p. 789.
- Krishna, K. S. R. and Sharma, A. (1996a) Chromatic aberrations of radial gradient-index lenses I, *Applied Optics*, 35: 1032–1036.
- Krishna, K. S. R. and Sharma, A. (1996b) Chromatic aberrations of radial gradient-index lenses I, *Applied Optics*, 35: 1037–1040.
- Krishna, K. S. R. and Sharma, A. (1996c) Chromatic aberrations of radial gradient-index lenses I, *Applied Optics*, 35: 5636–5641.
- Lightpath Technologies *Data Sheet*, Lightpath Technologies, Albuquerque, NM.
- Manhart, P. K. (1997) Gradient refractive index lens elements, US Patent #5617252.
- Marchand, E. W. (1978) *Gradient index optics*. Academic Press, New York.
- NSG America *Data Sheet*, NSG America, Somerset, NJ. (1999).
- Rouke, J. L., Crawford, M. K., Fisher, D. J., Harkrider, C. J., Moore, D. T., and Tomkinson, T. H. (1998) Design of a three element night-vision goggle, *Applied Optics*, 37: 622–626.
- Wang, D. Y. H. and Moore, D. T. (1990) Systematic approach to axial gradient lens design, *International Lens Design Conference, 1990, SPIE*, Volume 1354, p. 599.





---

# 40 Stabilized Optical Systems

Sometimes it is desirable to prevent an image from moving due to the vibration of the optical system. This occurs, for example, in TV coverage of events from a helicopter, telescope (or a binocular at high magnifications) viewing from the deck of a boat, or action scenes where the cinematographer is moving. This stabilization of the image may be accomplished in several ways:

1. A liquid-filled wedge plate may be placed in front of the lens. One of the plates is tilted to keep the image fixed in relation to the case as the complete system is moved (De La Cierva 1965). A thin wedge prism will deviate the beam by an angle  $\theta = \phi(N - 1)$ , where  $N$  is the refractive index of the fluid,  $\theta$  is the deviation angle, and  $\phi$  is the wedge angle between the two plates. The liquid-filled wedge has the advantage of being able to be placed in front of a wide variety of optical systems. It generally has a higher bandwidth of frequency response than the other systems.
2. A group of lenses may be tilted or displaced to maintain the fixed image location (Furukawa 1976; Hayakawa 1998; Suzuki 1999).
3. An internal mirror (gyro stabilized) may be tilted to maintain the fixed image location (Kawasaki et al. 1976; Helm and Flogaus 1981).
4. An inertial prism (gyro stabilized) may be used to maintain the fixed image location (Humphrey 1969). This system is shown schematically in [Figure 40.1](#).  $M_1$  is the objective-relay assembly of focal length 10.0, whereas the gyro-stabilized prism is shown as  $M_2$ . The system is shown in [Figure 40.2](#) with the prism assembly in line with the objective. A concave mirror at the focus of the front objective is used as a field lens; however, the actual system tilts the beam with the concave mirror. A final objective images the collimated beam onto the image surface. The front objective is the same as shown in [Figure 2.3](#) whereas the other two objectives are simply are a 0.5 scale of this. The complete system has an effective focal length of 10.0 and so if not stabilized, a  $2^\circ$  tilt would correspond to an image displacement of 0.349, whereas with stabilization the displacement is only 0.000178 (chief ray values).

Referring to Figure 40.1,

$$M_1 = \frac{\theta_2}{\theta_1}.$$

For stabilization, the exiting ray must make an angle with the optical

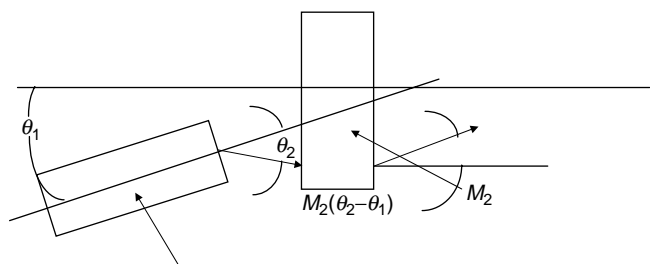


FIGURE 40.1 Case stabilization.

axis that is the same as before the tilt:

$$\theta_1 - M_2(\theta_2 - \theta_1) = 0.0$$

$$\theta_1 - M_2(\theta_1 M_1 - \theta_1) = 0.0$$

$$M_2(M_1 - 1.0) = 1.0$$

Because  $M_2$  has an odd number of reflections,  $M_2 = 1.0$  (as per the above sign convention) and  $M_1 = 2.0$ .

The following system is shown for an axial beam only (Table 40.1).

The significance of some of these surfaces is noted below:

- Surfaces 1, 9, and 19 are used to test the system for stabilization (rotate  $M_1$ ).
- Surfaces 2–4 have a front objective of focal length 10.0.

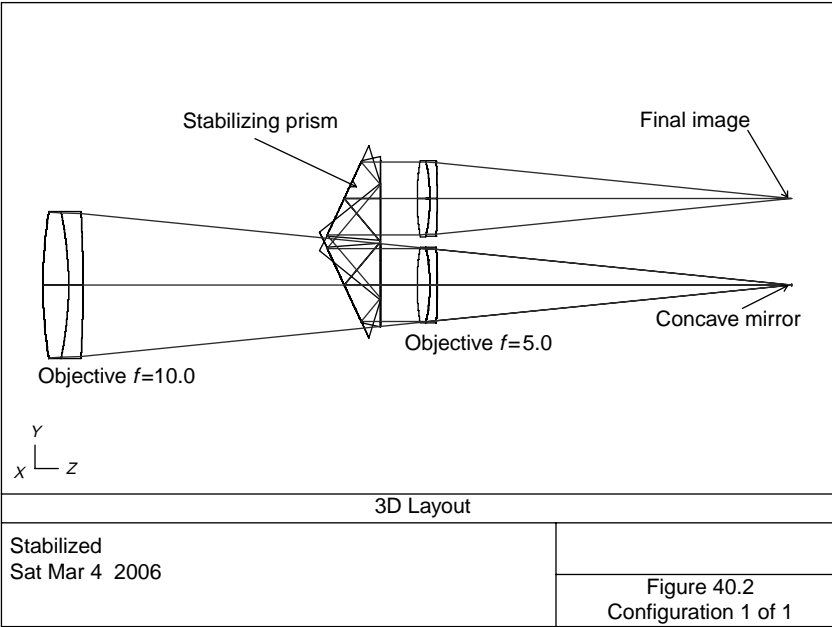


FIGURE 40.2 Stabilized lens system.

**TABLE 40.1**  
**Case-Stabilized System**

Surface	Radius	Thickness	Material	Diameter
0	0.0000	0.1000E+11		0.000
1	0.0000	0.0000		0.000
2	6.4971	0.3500	N-BAK1	2.000 Stop
3	-4.9645	0.2000	SF1	2.020
4	-17.2546	9.7267		2.002
5	-6.6660	-4.8663	Mirror	0.040
6	-8.6273	-0.1000	SF1	1.022
7	-2.4823	-0.1750	N-BAK1	1.031
8	3.2486	-0.5000		1.041
9	0.0000	0.0000		0.000
10	0.0000	-0.5000	N-BK7	1.040
11	0.0000	0.0000		0.000
12	0.0000	0.5517	Mirror	1.144
13	0.0000	0.0000		0.000
14	0.0000	-0.7779	Mirror	1.596
15	0.0000	0.0000		0.000
16	0.0000	0.5517	Mirror	1.144
17	0.0000	0.0000		0.000
18	0.0000	0.5000		1.046
19	0.0000	0.0000		0.000
20	3.2486	0.1750	N-BAK1	1.046
21	-2.4823	0.1000	SF1	1.036
22	-8.6273	4.8610		1.027
23	0.0000	0.0000		0.001

- Surface 5 is the concave mirror functioning as a field lens.
  - Surfaces 6–8 comprise a collimating lens of 5.0 focal length.
  - Surfaces 10–18 is the stabilized prism,  $M_2$ .
  - Surfaces 20–22 comprise the final imaging lens of 5.0 focal length.
  - Surface 23 is the final image that is then viewed with an eyepiece.
5. Hydrostatic compensation may be used (Humphrey 1970). In this method, the line of sight is reflected off of a plane mirror in a fluid-filled chamber that will not follow motions of the housing. The output beam then remains stable for accidental motion of the housing.

## REFERENCES

- De La Cierva, J. (1965) Image motion compensator, US Patent #3212420.  
 Furukawa, H. (1976) Image stabilizing optical element, US Patent #3953106.  
 Hayakawa, S. (1998) Design of image stabilizing optical systems, *Proceedings of SPIE*, Volume 3482, p. 240.

- Helm, D. B. and Flogaus, W. S. (1981) Optical scanning system using folding mirrors and with stabilization, US Patent #4249791.
- Humphrey, W. E. (1969) Accidental-motion compensation for optical devices, US Patent #3473861.
- Humphrey, W. E. (1970) Hydrostatically supported optical stabilizer, US Patent #3532409.
- Kawasaki, A. K., Machida, K. H., Furukawa, H., and Ichiyangi, T. (1976) Image stabilized zoom lens system, US Patent #3944324.
- Suzuki, K. (1999) Wide angle lens with image stabilizing function, US Patent #5917663.

---

# 41 The Human Emmetropic Eye

Following is a description of the most important optical device: our own eye. Because the eye is a fluid very similar to water, it is difficult to take one apart and measure its parameters. Various researchers have measured the curvature of the cornea in live people as well as measuring frozen sections of eyes from cadavers. Curvatures and positions of the internal surfaces of the eye also may be measured with a telescope and the image position of the surface in question may be noted. Making an assumption for the refractive index for the medium, the actual location of the surface is calculated. The most comprehensive work was done by Gullstrand (1924). This analysis is based on that data. This is also presented as Table 1 in Charman (1995) as well as in Emsley (1953).

Because most ophthalmic work is reported in millimeters, this section departs from the rest of the other designs in that all lens data is given in millimeters. Gullstrand's data was modified to include dispersion data for the lens, cornea, and aqueous to be similar to water. Also, the anterior cornea surface was modified to be aspheric (Lotmar 1971). This model is a little shorter than that presented by Blaker (1983) ([Table 41.1](#)).

This data is for an emmetropic eye—an eye focused at a distant object. Focusing at close objects is done by means of ciliary muscles that increase the curvature of the lens. Entrance-pupil diameter is controlled by muscle fibers of the iris. In total darkness, the iris is about 8 mm in diameter, whereas in bright light it is reduced to 2 mm in diameter ([Figure 41.1](#)).

The above plot is for a 3 mm diameter pupil.

Aspheric data for the cornea:

$$\begin{aligned}\text{Conic} &= -0.5917424 \\ A4 &= 1.10551 \times 10^{-4} \\ A6 &= -9.17369 \times 10^{-6} \\ A8 &= 1.000623 \times 10^{-6} \\ A10 &= -6.31872 \times 10^{-9}\end{aligned}$$

According to the Stiles–Crawford effect (Stiles 1933), rays passing through the outer portion of the entrance pupil are not as effective in retinal response as rays passing thru the center of the pupil. This is due to the rods and cones in the retina acting as fiber-optic conduits to the nerve endings. Accordingly, the entrance pupil was apodized according to the relation  $A(\rho) = e^{-G\rho^2}$ , where  $G$  is the apodization

**TABLE 41.1**  
**The Human Emmetropic Eye**

Surface	Radius	Thickness	Material	Diameter
0	0.0000	0.100000 E×10 <sup>11</sup>		
1	7.7000	0.5000	Cornea	8.200 Aspheric
2	6.8000	3.1000	Aqueous	7.600
3	10.0000	0.2730	Aqueous	6.000
4	10.0000	0.2730	Aqueous	5.000 Stop
5	7.9110	2.4190	Eyelens	7.000
6	−5.7600	0.6350	Aqueous	7.000
7	−6.0000	16.6424	Aqueous	7.000
8	−11.36431	0.0000	Aqueous	12.000

factor and  $\rho$  is the normalized pupil coordinate. A value for  $G$  of 0.34 was used to yield an intensity of 0.507 at the edge of an 8-mm pupil as compared to the center.

Because the index of refraction of the lens is 1.406 (at 0.5876  $\mu\text{m}$ ) in the central portion and reduces to 1.386 at the edge of the lens, a radial gradient (Blaker 1980) formula was used for this, listed as Eyelens in the above lens prescription. A photopic wavelength and weightings were used. The equation to account for dispersion in Eyelens is

$$N_{00} = 1.406 - 0.034 \times 10^{-8} \lambda^2,$$

where  $\lambda$  is in nanometers.

Because the refractive index for the vitreous material (between the lens and the retina) is nearly the same as that between the cornea and the lens, aqueous data was used for both materials. The refractive index for the cornea and the aqueous was fitted using a Conrady (1960) formula:

$$N = N_0 + A/\lambda + B/\lambda^{3.5}.$$

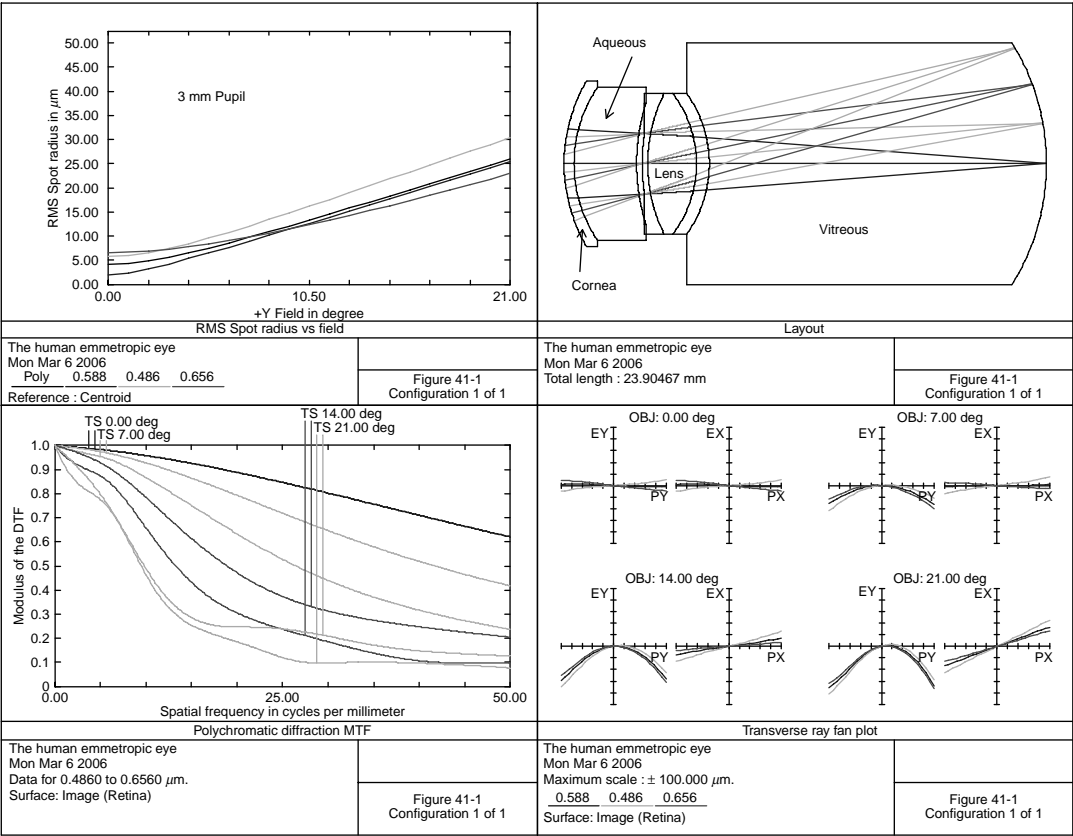


FIGURE 41.1 The human emmetropic eye.



This yields a value of 1.336 at 0.5876  $\mu\text{m}$  for the aqueous and 1.376 for the cornea.

Material	$N_0$	$A$	$B$
Aqueous	1.32420	0.0048714	0.00054201
Cornea	1.26536	0.0883011	−0.00616611

Effective focal length (EFL) is 16.63 mm. Goss (2002) lists a focal length of 16.5 mm. Note that from the root mean square (RMS) spot radius plot for a 3-mm pupil, the spot radius on axis is 5  $\mu\text{m}$ . Then

$$\tan \theta = \frac{0.005}{16.63} = 0.0003$$

and so  $\theta=1.0$  min arc, and at  $21^\circ$  off-axis, the spot radius increases to 25  $\mu\text{m}$ , yielding a resolution of  $\theta=5.0$  min arc.

Our eyes suffer from longitudinal chromatic aberration (see Figure 11 of Charman (1995)), the same as for a simple lens made of water. Correcting this chromatic aberration would not help because the limit is actually the diameters of the cones in the fovea.

REFERENCES

Blaker, J. W. (1980) Towards an adaptive model of the human eye, *JOSA*, 70: 220.  
Blaker, J. W. (1983) *Applied Optics and Optical Engineering*, Volume 9, Chapter 7, Ophthalmic Optics.  
Charman, W. N. (1995) Optics of the eye, *Handbook of Optics*, Volume 1, Chapter 24, McGraw Hill, New York.  
Conrady, A. E. (1960) *Applied Optics and Optical Design, Part 2*, Dover, New York, p. 659.  
Emsley, H. H. (1953) *Visual Optics, Volume 1: Optics of vision*, Butterworths, London.  
Goss, D. A. and West, R. W. (2002) *Introduction to the Optics of the Eye*. Butterworth-Heinemann, NY.  
Gullstrand, A. (1924) *Helmholtz's Treatise on Physiological Optics*, Optical Society of America, Washington, DC.  
Lotmar, W. (1971) Theoretical eye model with aspherics, *JOSA*, 61: 1522.  
Stiles, W. S. and Crawford, B. H. (1933) The luminous efficiency of rays entering the eye pupil at different points, *Proc. R. Soc. Lond., B*, 112: 428.

---

# 42 Spectrographic Systems

Spectrographic systems are used in a wide variety of applications, ranging from the analysis of atomic spectra, astronomy, blood and urine samples, forensic analysis, etc., (Harrison et al. 1948).

Figure 42.1 shows a prism used at minimum deviation and being illuminated with a circular beam of diameter  $A$  and at minimum deviation. This utilizes the maximum aperture of the prism; therefore, the beam travels parallel to the base.

For a prism of refractive index  $N$ , the angular dispersion of the prism is given by (Harrison et al. 1948):

$$\frac{d\theta}{d\lambda} = \frac{dN}{d\lambda} \left[ \frac{2 \tan I}{N} \right].$$

The resolving power of the prism is given by

$$\frac{\lambda}{d\lambda} = T \frac{dN}{d\lambda} \frac{1.22}{N} = A \frac{d\theta}{d\lambda}.$$

## 42.1 THE FERY PRISM

In Figure 42.2 is shown a system using a Fery prism (Miller et al. 1948, 1949; Warren et al. 1997). In this example, the source is considered as a point and is imaged as a line. The prescription information is given in Table 42.1.

Note that surface 2 in Figure 42.2 is a toroid. The slit images in the focal plane have the  $Y$  values at various wavelengths given in Table 42.2.

## 42.2 THE LITTROW PRISM

In Figure 42.3 is shown a Littrow prism system in which the angle of incidence on the prism is equal to the angle of refraction. In this case, the  $30^\circ$  prism is made of silica (crystal quartz also may be used because the reflected beam traveling nearly parallel to itself in the prism cancels the optical rotation) and is aluminized on the back face. Prescription information is given in Table 42.3.

Surface 2 is displaced by  $-0.75$  along the  $Y$  axis, whereas surface 5 is displaced  $-14.2663$  along the  $Y$  axis. The slit images in the focal plane have the  $Y$  values at the various wavelengths given in Table 42.4.

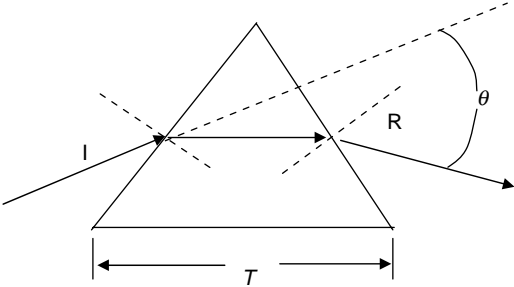


**FIGURE 42.1** Refraction at a minimum deviation prism.

Note that in this [Figure 42.3](#), the object and image are coincident. In actual practice, the object and image are slits one above the other at right angles to the plane of the paper.

Prisms generally have substantially less resolving power than a grating but do not have the problem of overlap of diffraction orders. The grating equation is (Palmer 2000),

$$m\lambda = d(\sin \alpha + \sin \beta),$$

where  $m$  is the diffraction order,  $d$  is the grating spacing,  $\alpha$  is the angle of the incident beam with respect to the grating normal,  $\beta$  is the angle of the diffracted beam with

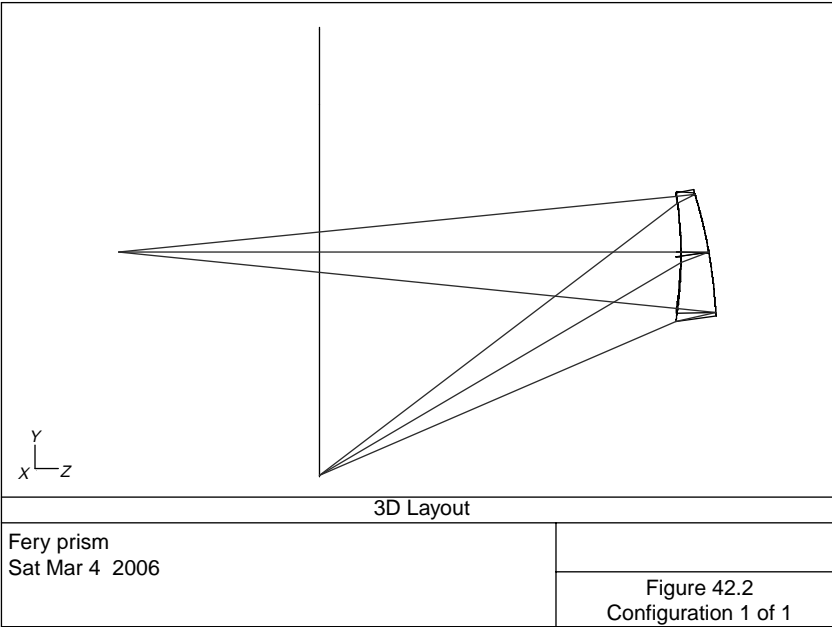


**FIGURE 42.2** Fery prism.

**TABLE 42.1**  
**Fery Prism System**

Surface	Radius	Thickness	Material	Diameter
0	0.0000	20.0000		0.000
1	−14.0335	1.0000	Silica	3.991 Stop
2	−17.4844	−1.0000	Mirror	4.327
3	−14.0335	−12.8739		4.579
4	0.0000	0.0000		15.977

R2 in X = −16.89774, surface 2 is tilted −10° to the optical axis.

respect to the grating normal. The above equation assumes that the incident beam is perpendicular the groove faces (Figure 42.4).

Differentiating the above equation with respect to  $\lambda$  gives the angular dispersion (Loewen 1997):

$$\frac{d\beta}{d\lambda} = \frac{\sin \alpha + \sin \beta}{\lambda \cos \beta} = \frac{m}{d \cos \beta}.$$

The resolving power,  $R$ , becomes

$$R = \frac{\lambda}{\Delta\lambda} = Nm.$$

For a Littrow configuration ( $\alpha = \beta$ ) (Figure 42.5), and Table 42.5.

$$\frac{d\beta}{d\lambda} = \frac{2 \tan \beta}{\lambda}, \quad (42.1)$$

$$2 \sin \alpha = \frac{m\lambda}{d}.$$

**TABLE 42.2**  
**Image Heights vs. Wavelengths for a Fery Prism**

Wavelength (μm)	Image Height
0.4	−7.987
0.5	−7.931
0.6	−7.900

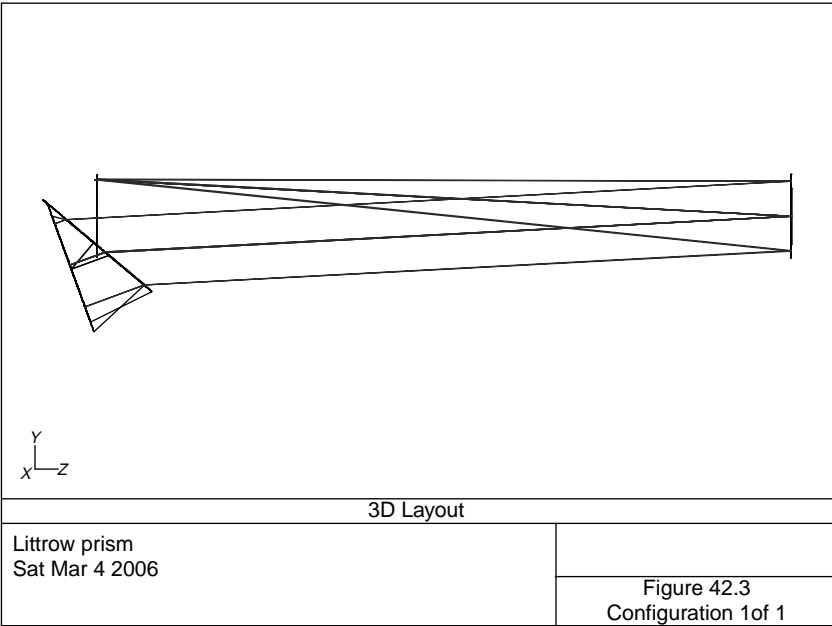


FIGURE 42.3 Littrow prism.

TABLE 42.3 Littrow Prism System					
Surface	Radius	Thickness	Material	Diameter	Tilt
0	0.0000	20.0000		0.000	
1	−40.0000	−20.0000	Mirror	2.000 Stop	−3.0
2	0.0000	−1.0000	Silica	3.790 Prism	−50.0
3	0.0000	1.1450	Mirror	2.784	30.0
4	0.0000	13.4387		3.216	−30.0
5	−40.0000	−19.9100	Mirror	2.414	50.0
6	0.0000	0.0000		2.369	
Tilt are values in degrees about the X axis.					

**TABLE 42.4**  
**Image Heights vs. Wavelengths for a Littrow Prism**

Wavelength ( $\mu\text{m}$ )	Image Height
0.4	1.1799
0.5	1.0546
0.6	0.8250

With respect to the above grating equation, note that there is an overlap of orders, i.e., at a wavelength of  $\lambda$  and order,  $m$ , of 1, there would be the same diffracted angle of  $\lambda/2$  at order 2. The free spectral range is given by (Loewen 1997)

$$\Delta\lambda = \frac{\lambda}{m}.$$

This overlap of orders may be eliminated with a prism as a pre-dispersion arrangement, or by the use of filters. Because the sample is often in a solvent, a double-beam system is sometimes used (Hollas 2005). In this case, the sample with its solvent is in one beam, and the other beam contains the solvent. Recording is the ratio of the two beams.

Referring to the angular dispersion equation given above Eq. (42.1), and noting that the diffracted ray angle at  $0.5 \mu\text{m}$  is 4.301 degrees, the angular dispersion then becomes 300.846/mm, or  $0.300846/\mu\text{m}$ . Because the concave mirror has a focal length of 20, and for a  $\Delta\lambda$  of  $0.1 \mu\text{m}$ , a difference in image height of 0.6017 is obtained, which agrees with the values in Table 42.6.

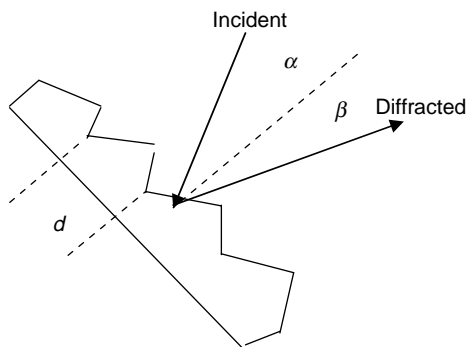


**FIGURE 42.4** Diffraction from a plane grating.

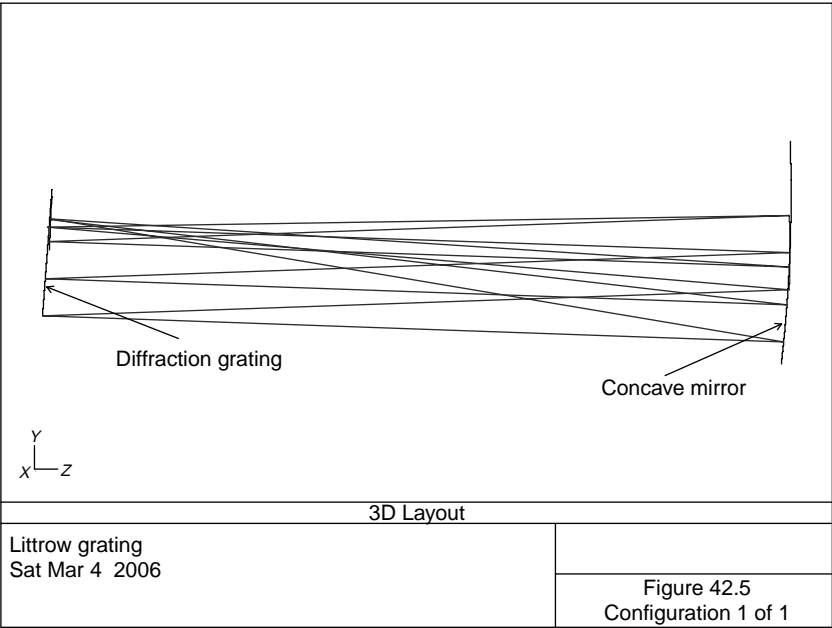


FIGURE 42.5 Littrow diffraction grating.

TABLE 42.5  
Littrow Grating System

Surface	Radius	Thickness	Material	Diameter	Tilt
0	0.0000	20.0000		0.000	
1	−40.0000	−20.0000	Mirror	2.000 Stop	−2.0
2	0.0000	20.0000	Mirror	3.410 Grating	4.301
3	−40.0000	−19.9328	Mirror	5.991	−2.0
4	0.0000	0.0000		1.421	

TABLE 42.6  
Image Heights vs. Wavelengths for a Littrow Diffraction Grating System

Wavelength (μm)	Image Height
0.4	−0.498
0.5	0.103
0.6	0.705

## REFERENCES

- Harrison, G. R., Lord, R. C., and Loofbourow, J. R. (1948) *Practical Spectroscopy*, Prentice Hall, New York.
- Hollas, J. M. (2005) *Modern Spectroscopy*, John Wiley, NY.
- Loewen, E. G. and Popov, E. (1997) *Diffraction Gratings and Applications*, Marcel Dekker, NY.
- Miller, W. C., Hare, G. G., George, K. P., Strain, D. C., and Stickney, N. E. (1948) A new spectrophotometer employing a glass Fery prism, *JOSA* 38: 1102.
- Miller, W. C., Hare, G. G., George, K. P., Strain, D. C., and Stickney, N. E. (1949) A new spectrophotometer employing a glass Fery prism, *JOSA* 39: 377.
- Palmer, C. (2000), *Diffraction Grating Handbook*, Richardson Grating Laboratory, Rochester, NY.
- Warren, D. and Hackwell, A. (1992) Compact prism spectrograph, US Patent #5127728.
- Warren, D., Hackwell, A., and Gutierrez, D. J. (1997) Compact prism spectrographs based on aplanatic principles, *Optical Engineering*, 36: 1174.





---

# 43 Diffractive Systems

A diffractive optical element can be considered as a very thin device that changes the phase of the emerging wavefront. The simplest type is a binary optic that has a discrete number of these phase altering steps. These steps either add zero or  $\pi$  phase difference to the wavefront. Such diffractive surfaces may be applied to a lens to aid in color and other aberration correction (O'Shea et al. 2004). The paraxial power of such surfaces is a linear function of wavelength, i.e.:

$$\nu = \frac{\lambda_0}{\lambda_{\text{short}} - \lambda_{\text{long}}};$$

consequently, this value is negative and its absolute value is much smaller than “flint” glasses (Buralli 1994). This, therefore, is very effective for correcting chromatic aberration. It also does not increase the Petzval sum.

In the ZEMAX computer program (Moore 2006), a binary optic diffractive surface is modeled by a polynomial expansion for the added phase to the surface:

$$\phi = M \sum_{i=1}^N A_i \rho^{2i},$$

where  $M$  is the diffraction order,  $N$  is the number of polynomial coefficients,  $A_i$  is the coefficient, and  $\rho$  is the normalized radial aperture coordinate.

In [Figure 43.1](#), a binary surface is applied to the rear surface of a simple positive lens to form an achromat; prescription data is given in [Table 43.1](#). Because this lens has a focal length of 20 in., is  $f/6$  and has a field of view of  $1.5^\circ$ , it may be compared to the cemented achromat doublet as shown in [Figure 2.2](#). Performance is nearly the same. If one compares the longitudinal chromatic aberration of these two designs, he or she will note that the cemented achromat exhibits the classic chromatic correction with the median wavelength focusing closest to the lens and the extreme wavelengths focusing farthest from the lens. However, this diffractive lens is just the opposite due to the extreme dispersion of the diffractive surface. The diffractive order,  $M$ , is 1.

The binary surface coefficients for a normalized radius of 1 are:

$$\begin{aligned} -400.01846 & \text{ for } P^{*2} \text{ term} \\ 9.6866789 & \text{ for } P^{*4} \text{ term} \\ -0.0514924 & \text{ for } P^{*6} \text{ term} \end{aligned}$$

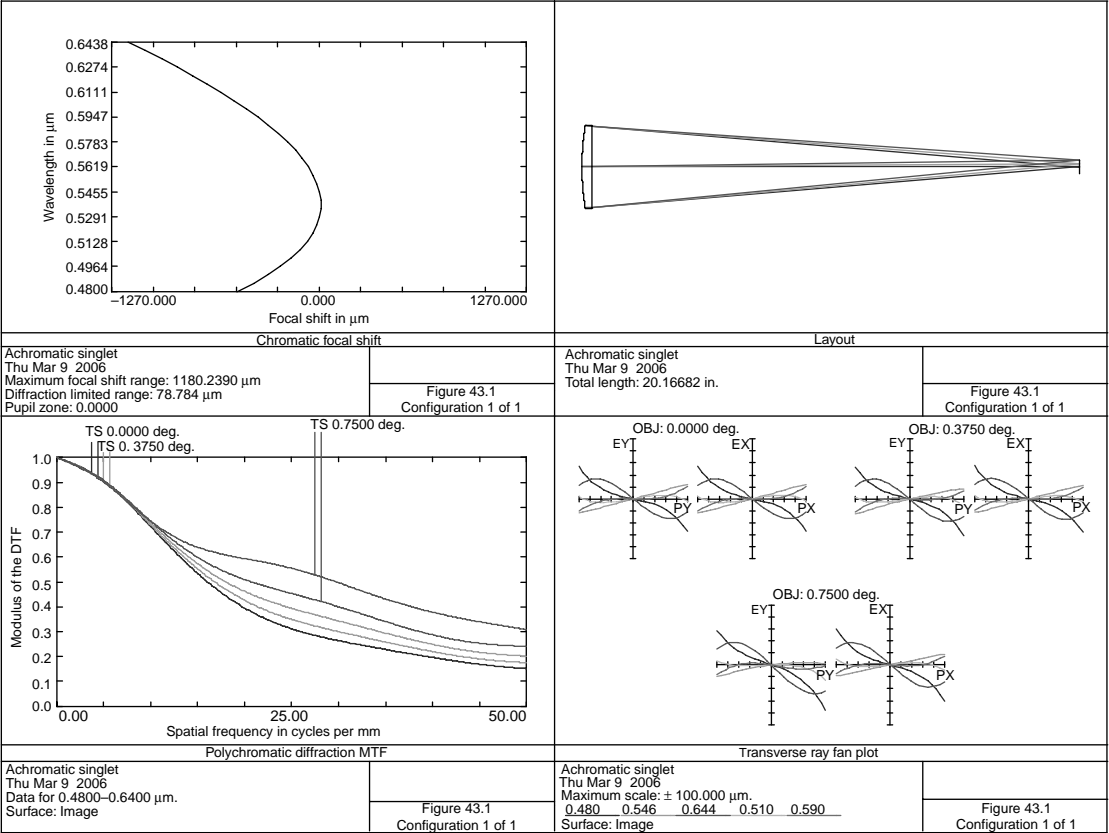


FIGURE 43.1 The achromatic singlet.

**TABLE 43.1**  
**Achromatic Singlet**

Surface	Radius	Thickness	Material	Diameter
0	0.0000	$0.100000 \times 10^{11}$		0.00
1	10.9831	0.4000	N-BK7	3.400 Stop
2	0.0000	19.7668		3.400
3	0.0000	0.0000	Diffractive	0.529

Due to this large dispersion, the positive lens should have a very large  $\nu$  value. However, the image is only slightly improved as one proceeds from N-BK7 to N-FK5 and finally to N-FK51.

In [Figure 43.2](#) is shown a Petzval-type lens used as a night vision objective; the prescription information is given in [Table 43.2](#). It is  $f/1.4$ , 6.39 in. focal length with a field of view of  $4^\circ$ . Because it is meant for night vision use, it covers the wavelength region from 0.48 to 0.863  $\mu\text{m}$ . It is a modification of a system described by Haixian (1998).

Coefficients for the binary surface are:

−437.57506 for  $P^{**2}$  term

14.675909 for  $P^{**4}$  term

5.153380 for  $P^{**6}$  term

−0.659243 for  $P^{**8}$  term

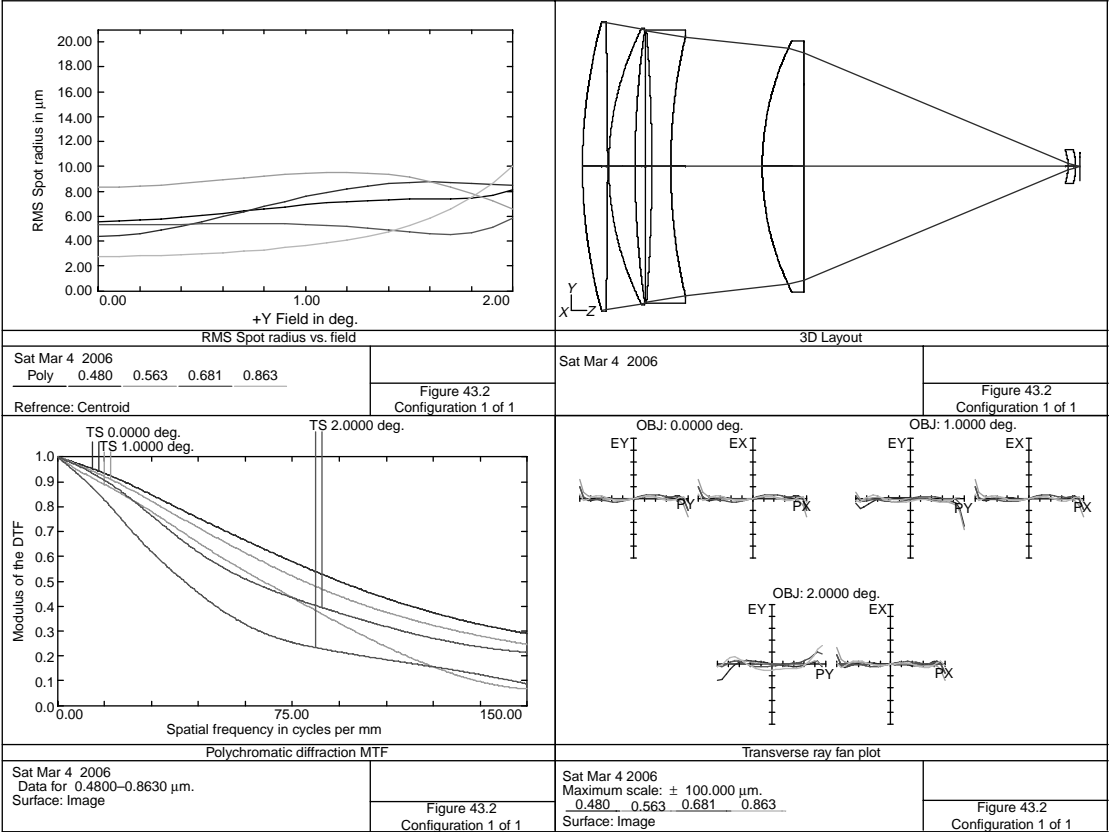


FIGURE 43.2 Hybrid night-vision lens.

**TABLE 43.2**  
**Hybrid Night-Vision Lens**

Surface	Radius	Thickness	Material	Diameter
0	0.0000	$0.100000 \times 10^{11}$		0.00
1	8.8747	0.3965	N-SK5	4.600
2	-111.4373	0.0200		4.600
3	4.8683	0.4181	N-PSK3	4.400
4	15.7334	0.1672		4.340
5	Stop	0.0970		4.338
6	-27.7053	0.3000	SF4	4.330
7	9.2624	1.4531		4.152
8	4.4627	0.6566	N-PSK53	4.000
9	0.0000	4.1999		4.000 Binary surface
10	-0.7670	0.1181	F5	0.534
11	-0.9983	0.0724		0.514
12	0.0000	0.0000		0.450

## REFERENCES

- Buralli, D. A. (1994) Using diffractive lenses in optical design, *Proceedings of the International Optical Design Conference*, Volume 22, OSA, Washington, DC.
- Greisukh, G. I., Bobrov, S. T., and Stepanov, S. A. (1997) *Optics of Diffractive and Gradient Index Elements and Systems*. SPIE Press, Bellingham, WA.
- Haixian, Z. (1998) Diffractive objective in night vision goggle, *International Optical Design Conference, 1998, SPIE*, Volume 3482, p. 887.
- Moore, K. (2006) *ZEMAX Optical Design Program, User's Guide*. Zemax development Corp., Bellevue, WA 98004.
- O'Shea, D. C., Suleski, T. J., Kathman, A. D., and Prather, D. W. (2004) *Diffractive Optics, Design Fabrication and Test*, TT62, SPIE Press, Bellingham, WA.

